



VNIVERSITAT  
DE VALÈNCIA



# **Dynamics of charmed and bottomed meson and baryon resonances**

Rafael Pereira Pires Pavão

Tesis doctoral, mayo 2020

Programa de Doctorat en Física

Directores

Juan M. Nieves Pamplona y Eulogio Oset Bágüena





VNIVERSITAT  
E VALÈNCIA



**Dr. Juan Miguel Nieves Pamplona**, Investigador Científico del Consejo Superior de Investigaciones Científicas y

**Dr. Eulogio Oset Báguena**, Catedrático de Física Teórica de la Universidad de Valencia,

CERTIFICAN: Que la presente memoria *Dynamics of charmed and bottomed meson and baryon resonances* ha sido realizada bajo su dirección en el Departamento de Física Teórica de la Universidad de Valencia por D. Rafael Pereira Pires Pavão como Tesis para obtener el grado de Doctor en Física.

Y para que así conste, en cumplimiento con la legislación vigente, presentan ante el Departamento de Física Teórica, la referida memoria, firmando el presente certificado.

Valencia, a 22 de mayo de 2020.

NIEVES  
PAMPLONA JUAN  
MIGUEL - DNI  
25386311S

Firmado digitalmente por  
NIEVES PAMPLONA JUAN  
MIGUEL - DNI 25386311S  
Fecha: 2020.05.23  
11:34:48 +02'00'

Juan Miguel Nieves Pamplona

Eulogio Oset Báguena



*“I’m not as sure, as when we started  
Then, I was inspired  
Now, I’m sad and tired  
Listen, surely I’ve exceeded expectations  
Tried for three years, seems like thirty  
Could you ask as much from any other man?”*

Gethsemane, Jesus Christ Superstar  
Andrew Lloyd Webber & Tim Rice



To my wife and my parents.





# Acknowledgements

Estos últimos años en Valencia fueron de los más inestimables e importantes de mi vida. En esta ciudad y país maravilloso mejoré como persona, cumplí un gran sueño de mi vida – hacer un doctorado en Física Teórica – publique muchos *papers*, di muchas charlas, etc. Pero no habría hecho nada de esto solo. Entonces, me gustaría aprovechar esta sección para agradecer a todas las personas que me ayudaron a llegar al final de este camino, más que de una manera profesional, de una manera personal. Las personas que siempre estuvieron allí para mí, en los momentos tristes, felices, deprimentes y alegres.

En primer lugar, me gustaría agradecer a mis directores de tesis, Juan y Eulogio. Sin su orientación nada de esto habría sido posible. Ellos siempre han estado disponibles para ayudar y explicar, y siempre han sido un ejemplo de seriedad y honestidad científica. El trabajo que he hecho en el doctorado, en cantidad y calidad, se debe a ellos, a su empeño y dedicación. También quiero agradecer a Laura Tolos, a quien considero mi directora no oficial, que me ha acogido en mi pequeña estancia en Barcelona, con quien he aprendido tanto y hecho trabajos tan interesantes, y quien ha sido una buena compañía en múltiples conferencias.

A Luis y Manolo por los cafés y los momentos placenteros en las pausas del trabajo, las cenas y las cervezas en Ambit.

To Philipp Gubler, I would like to thank for his hospitality. Being in such a different country as Japan is not easy. However, because of him, my stay there was remarkably fruitful, both in terms of scientific output and in terms of life experiences.

Quiero agradecer también a mis espléndidos amigos Pedro, Vinicius y Eduardo, con quien las idas a por agua se tornaban aventuras épicas. Gracias por todas las cenas, las idas al mercadona, al gimnasio, todos los cafés y las cervezas, el *data science*, la programación y también la física. Sin vuestra amistad estos tres años no hubieran sido una parte tan alegre de mi vida.

Ao meu grande amigo Ricardo Faleiro, com quem sempre pude discutir as minhas ideias e partilhar as minhas explicações, apesar de estarmos em áreas completamente diferentes. Tanto a um nível pessoal, como a um nível profissional, a sua pre-

sença tem constituído o eterno Juiz que nos obriga a ser sinceros connosco mesmos, ambos no positivo e negativo.

Aos meus pais, Adosinda Pires e Ângelo Pavão, pela sua eterna crença nas minhas habilidades. Sempre confiaram em mim e sempre me desafiaram a ir mais além. Agradeço também o seu apoio moral, já que me visitavam sempre que possível. Diz-se que o trabalho de um pai é primeiro proteger e educar os seus filhos, e depois libertá-los para o mundo, para prosseguirem o seu destino. Posso então dizer eles desempenharam esse trabalho de uma maneira exemplar.

Por último, quero agradecer à minha cara-metade, Liliana Pereira, por sempre se ter mantido ao meu lado, independentemente da situação. O seu apoio incondicional e a sua vontade de ferro ajudaram-me na (até agora) maior aventura da minha vida. Juntos durante este período evoluímos, testámo-nos e saímos vitoriosos. Posso dizer com toda a alegria que saio destes três anos não só com uma tese, mas também com uma maravilhosa noiva.

# Resumen

En la actualidad, el Modelo Estándar es el mejor marco teórico de que disponemos para describir multitud de fenómenos de física de partículas. Dentro del mismo, la Cromodinámica Cuántica (QCD) es la teoría que describe la interacción fuerte entre quarks y gluones, de los que están compuestos los hadrones. En este trabajo estudiamos diversos procesos hadrónicos donde se involucran bajas transferencias de energías y momentos. Al contrario que en otras teorías del Modelo Estándar, en este régimen, la aproximación perturbativa para QCD no resulta adecuada, porque la intensidad de la interacción fuerte aumenta al disminuir las escalas energéticas relevantes ( $q$ ), dando lugar a la propiedad de confinamiento para  $q \leq \Lambda_{\text{QCD}} \sim 200 - 250$  MeV. En la práctica, es necesario resolver no perturbativamente QCD utilizando técnicas Monte Carlo en un espacio-tiempo discretizado (*lattice* QCD), o formular teorías efectivas, que son aproximaciones de la teoría subyacente (QCD) basadas en ciertas de sus simetrías, exactas o aproximadas. En esta tesis describimos la dinámica de algunas resonancias, que interpretamos como moléculas, producto de la interacción entre dos hadrones. Para ello utilizamos una combinación de teorías efectivas y resumaciones no perturbativas.

El trabajo se estructura en cuatro partes. En la Parte I se presenta el formalismo físico-matemático necesario para obtener y analizar los resultados del resto de la tesis. Empezamos con un primer capítulo introductorio muy generico. A continuación, en el Capítulo 2 se describen brevemente QCD y la teoría quiral de perturbaciones ( $\chi PT$ ), la teoría efectiva que describe las interacciones entre bosones de Goldstone y de estos mesones con otras partículas (mesones vectoriales y bariones ligeros o hadrones con un quark pesado), también estudiadas en esta memoria. En este mismo capítulo se discute el formalismo del *local hidden gauge* (LHG), que propone una extensión de  $\chi PT$  para incluir las interacciones de los mesones vectoriales, y finalmente la simetría de espín de quarks pesados (HQSS). En este último caso, se presta una atención especial a las simplificaciones que se deducen, en el límite de masa de quark infinita, para la evaluación de elementos de matriz de transiciones que involucran estados iniciales y finales con hadrones pesados. En el Capítulo 3, se presenta una breve introducción a la teoría de dispersión de dos cuerpos, a los

conceptos de unitariedad, analiticidad, y a la definición de las hojas de Riemann de la amplitud extendida al plano complejo. A continuación, se extiende el formalismo para estudiar canales acoplados y presentamos el esquema quirral unitario (CUA), donde se restaura unitariedad en las amplitudes quirales del Capítulo 3 utilizando la ecuación de Bethe-Salpeter (BSE)<sup>1</sup>. Por último, utilizando los conceptos de unitariedad y analiticidad, en la última sección se detallan las condiciones para las que los *loops* con topología triangular, que pueden dar lugar a singularidades en el plano complejo de la matriz  $T$ , produzcan efectos visibles en los espectros experimentales.

En las Partes II, III y IV se presentan los resultados de esta tesis, todos publicados en revistas internacionales del primer tercil especializadas en física hadrónica [1–11].

En primer lugar (Parte II), abordamos diversos procesos en el sector ligero empleando las técnicas y los modelos presentados en la Parte I. En el Capítulo 4, estudiamos la desintegración  $\tau^- \rightarrow \nu_\tau M_1 M_2$ , con  $M_1, M_2$  mesones pseudoescalares (P) o vectoriales (V), usando álgebra de momento angular y evaluando los efectos debidos a la interacción fuerte de los mesones finales. Se relacionan los distintos modos de desintegración y se discute una interpretación diferente del papel que juega la simetría de  $G$ -paridad para estos procesos. Observamos que las anchuras de producción de mesones pseudoescalares (PP) en onda  $p$ , obtenidas dentro del esquema CUA, son compatibles con los resultados experimentales, mientras que comprobamos que no sucede lo mismo con la producción de pares pseudoescalar-vector (PV) y vector-vector (VV). Para estos dos últimos modos de desintegración, asumimos por tanto que la dinámica está dominada por la onda  $s$ . Comparamos nuestros resultados con los datos experimentales, y realizamos predicciones de otros modos para los que no existe información. Analizamos la distribución de masas  $M_1 M_2$  y demostramos su gran utilidad para estudiar la interacción mesón-mesón y la naturaleza de algunas resonancias generadas en dichas desintegraciones.

En el Capítulo 5 se examinan las propiedades de las resonancias  $N^*(1535)$  y  $N^*(1650)$  a partir de la distribuciones de masas para distintos estados  $MB$  en las desintegraciones  $\Lambda_c \rightarrow \bar{K}^0 MB$ , con  $MB = \pi N(I = 1/2), \eta p$  y  $K\Sigma(I = 1/2)$ . Se calculan las contribuciones a nivel árbol y a un *loop*, incluyendo mezclas entre canales pseudoescalar-barión y vector-barión usando el formalismo del LHG. Observamos que en la distribución de masas  $\pi\eta$ , sólo el estado  $N^*(1535)$  contribuye, mientras que en el caso de  $\pi N$  ambas  $N^*(1535)$  y  $N^*(1650)$  se aprecian claramente. También encontramos que la contribución del modo  $K\Sigma$  es menor que las correspondientes a los canales  $\pi N$  y  $\eta p$  en los procesos  $\Lambda_c^+ \rightarrow \bar{K}^0 \pi N$  y  $\Lambda_c^+ \rightarrow \bar{K}^0 \eta p$ , a pesar de que la

---

<sup>1</sup>En un abuso de notación, y por simplicidad, utilizaremos siempre la nomenclatura CUA para referirnos a esquemas donde se ha restaurado unitariedad en canales acoplados, aunque el *kernel* de la BSE no se haya obtenido a partir de Lagrangianos quirales.

constante de acoplamiento de la resonancia  $N^*(1650)$  al canal  $K\Sigma$  es muy grande. Demostramos que esto es debido a la supresión de la producción de  $K\Sigma$  en el primer paso de la desintegración débil de la  $\Lambda_c$ .

En la Parte III estudiamos las resonancias bariónicas  $\Lambda_{c(b)}^{(*)}$ ,  $\Omega_c^{(*)}$  y  $\Xi_{c(b)}^{(*)}$  utilizando las técnicas detalladas en las Partes I y II. En el Capítulo 6, estudiamos las implicaciones que se deducen de HQSS para las desintegraciones  $\Lambda_b \rightarrow \Lambda_c^* \ell \bar{\nu}_\ell$  y  $\Lambda_b \rightarrow \Lambda_c^* \pi^-$  [ $\Lambda_c^* = \Lambda_c(2595)$  y  $\Lambda_c(2625)$ ]. Identificando los estados de paridad negativa  $\Lambda_c(2595)$  y  $\Lambda_c(2625)$  como los miembros de un doblete de HQSS, con grados de libertad ligeros  $j_q^P = 1^-$ , encontramos que las razones  $\Gamma(\Lambda_b \rightarrow \Lambda_c(2595)\pi^-)/\Gamma(\Lambda_b \rightarrow \Lambda_c(2625)\pi^-)$  y  $\Gamma(\Lambda_b \rightarrow \Lambda_c(2595)\ell\bar{\nu}_\ell)/\Gamma(\Lambda_b \rightarrow \Lambda_c(2625)\ell\bar{\nu}_\ell)$  son compatibles con los valores experimentales recogidos en el *Review of Particle Physics*. En este capítulo también discutimos cómo una futura medida más precisa de estas anchuras de desintegración podría servir para dilucidar la estructura relacionada con HQSS de la resonancia  $\Lambda_c(2595)$ . En particular, mostramos cómo un análisis de este tipo permitiría determinar la posible existencia de una componente importante  $j_q^P = 0^-$  en su función de onda, y/o una estructura de dos polos, análoga a la de la resonancia  $\Lambda(1405)$ , tal y como predicen la mayoría de estudios que interpretan el estado  $\Lambda_c(2595)$  como una molécula hadrónica. Por último, investigamos las razones de universalidad de sabor leptónico  $R[\Lambda_c^*] = \Gamma(\Lambda_b \rightarrow \Lambda_c^* \tau \bar{\nu}_\tau)/\Gamma(\Lambda_b \rightarrow \Lambda_c^* \mu \bar{\nu}_\mu)$ , y discutimos cómo la interpretación de los datos de  $R[\Lambda_c(2595)]$  puede verse afectada por un importante error sistemático, si existiera un patrón de dos polos para la  $\Lambda_c(2595)$ .

En el Capítulo 7, estudiamos en detalle la estructura de las resonancias  $\Lambda_c(2595)$  y  $\Lambda_c(2625)$  utilizando un formalismo de teorías efectivas consistente con HQSS y simetría quiral, que incorpora la interacción de los grados de libertad mesón-barión  $\Sigma_c^{(*)} \pi - ND^{(*)}$  con estados modelo quark  $c\bar{u}d$  en onda  $p$ . Concluimos que estas resonancias puede que no formen un doblete de HQSS. Así, damos argumentos para asignar la resonancia  $\Lambda_c(2625)$  ( $J^P = 3/2^-$ ) a un estado genuino de tres quarks, ligeramente modificado por efectos debidos a su interacción con pares mesón-barión. Sin embargo, la resonancia  $\Lambda_c(2595)$  ( $J^P = 1/2^-$ ) presentaría una estructura predominantemente molecular, existiendo dos posibles escenarios. En el primero, la resonancia resultaría ser dinámicamente generada por la interacción quiral  $\Sigma_c \pi$ , cuyo umbral de producción se encuentra mucho más cerca de su posición que la masa desnuda del estado de tres quarks. En este contexto los grados de libertad ligeros tendrían números cuánticos  $j_q^P = 1^-$ . En el segundo escenario, los grados de libertad ligeros de la estructura interna de la  $\Lambda_c(2595)$  se acoplarían a  $j_q^P = 0^-$ , y su dinámica molecular quedaría determinada por las interacciones  $ND$  y  $ND^*$ . Analizamos la dependencia de los resultados del esquema de renormalización (RS) y demostramos cómo los escenarios mencionados ocurren dependiendo del RS utilizado. Además, predecimos algunos estados adicionales, pero en general resulta complicado clasi-

ficar el espectro en términos de HQSS, a pesar de haber utilizado una interacción consistente con esta simetría. Esto se debe a que el estado desnudo de tres quarks y el umbral  $\Sigma_c\pi$  se encuentran muy cerca de la masa nominal de las resonancias  $\Lambda_c(2625)$  y  $\Lambda_c(2595)$ , respectivamente, y por tanto, juegan un papel totalmente diferente en cada sector. En el Capítulo 8 utilizamos una extensión del formalismo de canales acoplados del LHG, que incluye sabores pesados, para estudiar la generación dinámica de las resonancias  $\Xi_c$  y  $\Xi_b$ . Estos estados moleculares aparecen como polos en las amplitudes de dispersión, y varios de ellos pueden identificarse con los estados  $\Xi_c(2790)$ ,  $\Xi_c(2930)$ ,  $\Xi_c(2970)$ ,  $\Xi_c(3055)$  y  $\Xi_c(3080)$  observados experimentalmente. Además, para la resonancia  $\Xi_b(6227)$ , recientemente detectada, encontramos dos polos con masas y anchuras muy próximas a los valores experimentales en los sectores  $J^P = 1/2^-$  y  $J^P = 3/2^-$ .

En el Capítulo 9 utilizamos el modelo completo del Capítulo 7, amplitudes de Weinberg–Tomozawa (WT) derivadas del Lagrangiano quiral extendido al grupo de simetría  $SU(6)_{\text{light-spin-flavor}} \times \text{HQSS}$  y unitarizadas resolviendo la BSE en canales acoplados, para estudiar el impacto del RS empleado en el sector  $C = 1$ ,  $S = -2$  y  $I = 0$ . Realizamos este estudio en este sector, porque la colaboración LHCb ha observado recientemente cinco estados  $\Omega_c^{(*)}$ , cuyas propiedades pueden servir para fijar las constantes de substracción indeterminadas que aparecen en los diferentes esquemas. La interacción mesón–barión es consistente con simetría quiral y HQSS, y conduce a una descripción plausible de las resonancias más ligeras de paridad negativa  $\Lambda_c(2595)$ ,  $\Lambda_c(2625)$ ,  $\Lambda_b(5912)$  y  $\Lambda_b(5920)$ . La conclusión del trabajo es que algunos de los estados  $\Omega_c^{(*)}$  detectados por LHCb (al menos tres) también tendrían paridad negativa y  $J = 1/2$  ó  $J = 3/2$ , y dos de ellos pertenecerían al mismo multiplete  $SU(6)_{l_{sf}} \times \text{HQSS}$  que los bariones  $\Lambda_{c(b)}$  mencionados.

Por otro lado, también analizamos con el formalismo WT– $SU(6)_{l_{sf}} \times \text{HQSS}$  de nuevo los estados  $\Xi_c^{(*)}$  y  $\Xi_b^{(*)}$ . Estos estados fueron previamente estudiados en el Capítulo 8, pero utilizando el marco del LHG extendido para incluir un quark pesado. De esta forma se pueden cuantificar las incertidumbres sistemáticas derivadas de la utilización de diversos modelos para la interacción entre mesones pseudoescalares y vectoriales con bariones de espín–paridad  $J^P = 1/2^+$  y  $J^P = 3/2^+$ , involucrando tres quarks ligeros y uno pesado ( $c$  ó  $b$ ). Dentro del modelo WT– $SU(6)_{l_{sf}} \times \text{HQSS}$ , predcimos una componente molecular  $\Lambda_c\bar{K}$  muy grande para el estado  $\Xi_c(2790)$ , con una configuración dominante de espín  $j_q^P = 0^-$  para los grados de libertad ligeros. Discutimos las diferencias entre los estados  $J^P = 3/2^-$   $\Lambda_c(2625)$  y  $\Xi_c(2815)$  en este contexto, y concluimos que parece plausible que pudieran no pertenecer al mismo multiplete de  $SU(3)$ . Por otra parte, se predice la existencia de otros estados tipo  $\Xi_c$ , dos de ellos relacionados con la posible estructura de dos polos de la  $\Lambda_c(2595)$ . Es especialmente interesante el caso de un par de resonancias con  $J = 1/2$  y  $J = 3/2$ , que forman un

doblete HQSS y que asociamos a los estados  $\Xi_c(2930)$  y  $\Xi_c(2970)$ , respectivamente. Además, la resonancia  $\Xi_c(2930)$  sería miembro de un sextete de SU(3), del cual también formaría parte la  $\Omega_c(3090)$  ó la  $\Omega_c(3119)$ , y que se completaría con el estado  $\Sigma_c(2800)$ . En el sector del quark  $b$ , identificamos un sextete con  $J = 1/2$  que incluiría los estados  $\Xi_b(6227)$  y  $\Sigma_b(6097)$ , este último también descubierto muy recientemente. Asumiendo la *equal spacing rule* para completar el multiplete, predecimos la existencia de un estado  $\Omega_b$  con paridad negativa y espín  $J = 1/2$ , y una masa cercana a 6360 MeV y que debería observarse en el canal  $\Xi_b\bar{K}$ .

En el Capítulo 10, calculamos las desintegraciones  $\Xi_b^- \rightarrow \pi^- \Xi_c^0(2790)$  ( $J^P = 1/2^-$ ),  $\Xi_b^- \rightarrow \pi^- \Xi_c^0(2815)$  ( $J^P = 3/2^-$ ) y las mismas reacciones reemplazando el  $\pi^-$  por un mesón  $D_s^-$ . También evaluamos las transiciones semileptónicas  $\Xi_b^- \rightarrow \Xi_c^0(2790)\ell\bar{\nu}_\ell$  y  $\Xi_b^- \rightarrow \Xi_c^0(2815)\ell\bar{\nu}_\ell$ . Es un estudio similar al realizado en el Capítulo 6, pero en este caso para el sector con extrañeza y encanto. Mientras que en el Capítulo 6 hicimos hincapié en las relaciones/restricciones que se derivaban de HQSS para las transiciones, aquí adoptamos la perspectiva de que las resonancias  $\Xi_c^0(2790)$  y  $\Xi_c^0(2815)$  forman un doblete de HQSS y que son generadas dinámicamente por la interacción pseudoescalar-barión y vector-barión. Prestamos una atención especial a las razones de las anchuras de desintegración con  $\Xi_c^0(2790)$  ó  $\Xi_c^0(2815)$  en el estado final y demostramos que los resultados dependen bastante del acoplamiento entre las resonancias  $\Xi_c^*$  y las componentes  $\Sigma D^*$  y  $\Lambda D^*$  del espacio de canales acoplados. Nuestras predicciones para estos cocientes de anchuras podrán compararse con futuros experimentos, y proporcionarán una información valiosa, tal y como ya concluimos en el Capítulo 6, para entender la estructura de las resonancias bariónicas de mas baja energía y paridad negativa.

En la Parte IV estudiamos el efecto de las singularidades triangulares, haciendo uso de las técnicas presentadas y desarrolladas a lo largo de esta tesis, en varias reacciones que involucran hadrones ligeros y pesados. En el Capítulo 11 investigamos el papel desempeñado por el mecanismo triangular en las desintegraciones  $B^- \rightarrow D^{*0}\pi^-\pi^0\eta$  y  $B^- \rightarrow D^{*0}\pi^-\pi^+\pi^-$ . En ambos procesos la singularidad aparece en la reacción  $B^- \rightarrow D^{*0}K^-K^{*0}$ , seguida de  $K^{*0} \rightarrow \pi^-K^+$  y la interacción de estados finales  $K^+K^-$ , que forma los estados  $a_0(980)$  ó  $f_0(980)$  y que finalmente se desintegran en  $\pi^0\eta$  o  $\pi^+\pi^-$ , respectivamente. El diagrama triangular del *loop*  $\bar{K}^*K\bar{K}$  genera un pico visible en la masa invariante de  $\pi^-a_0$  ó  $\pi^-f_0$  alrededor de 1420 MeV, y da lugar a las anchuras parciales  $\text{Br}(B^- \rightarrow D^{*0}\pi^-a_0; a_0 \rightarrow \pi^0\eta) = (1.66 \pm 0.45) \times 10^{-6}$  y  $\text{Br}(B^- \rightarrow D^{*0}\pi^-f_0; f_0 \rightarrow \pi^+\pi^-) = (2.82 \pm 0.75) \times 10^{-6}$ . En el Capítulo 12 investigamos las secciones eficaces de los procesos  $\pi^-p \rightarrow K^0\pi\Sigma$  y  $pp \rightarrow pK^+\pi\Sigma$  prestando atención a los mecanismos que generan singularidades triangulares. El exceso de sucesos debidos a la singularidad triangular se produce partiendo de la desintegración de una resonancia  $N^*$  en un par  $K^*\Sigma$ , seguida de  $K^* \rightarrow \pi K$ , y finalmente incluyendo la in-

teracción fuerte de los estados finales  $\pi\Sigma$ , que generan dinámicamente la  $\Lambda(1405)$ . Encontramos que este mecanismo, cuando se considera la excitación de la resonancia  $N^*(2030)$  que se acopla de forma importante a  $K^*\Sigma$ , produce un pico en la masa invariante del par  $K\Lambda(1405)$  en la región de 2100 MeV, unos 40 MeV por debajo del valor donde se esperaría la posición de la singularidad triangular para este proceso. Además, y en buen acuerdo con los resultados del experimento HADES, el mecanismo que hemos estudiado produce la señal de la resonancia  $\Lambda(1405)$  alrededor de 1400 MeV.

En el Capítulo 13 analizamos la contribución de un diagrama triangular para la desintegración  $\Lambda_c^+ \rightarrow \pi^+\pi^0\Lambda(1405)$ , con  $\Lambda(1405) \rightarrow \pi^0\Sigma^0$ . Este proceso se inicia con  $\Lambda_c^+ \rightarrow \pi^+\bar{K}^*N$ , seguido de  $\bar{K}^* \rightarrow \bar{K}\pi$ , y finalmente la interacción de estados finales  $\bar{K}N$  genera dinámicamente la resonancia  $\Lambda(1405)$ . El mecanismo se produce a través de un *loop* triangular que contiene  $K^*NK$  y que induce una singularidad para masas invariantes  $\pi^0\Lambda(1405)$  de alrededor de 1890 MeV. Esta reacción viola la simetría de isospín, pero se ve favorecida por la presencia de la singularidad triangular, que es muy sensible a la masa de las partículas internas. Encontramos un pico muy estrecho en la masa invariante de  $\pi^0\Sigma^0$ , que se origina por la amplitud de producción de la  $\Lambda(1405)$ , pero que se debe a la diferencia de masas entre los estados cargados y neutros  $\bar{K}N$ . La futura observación de este pico asociado a esta singularidad en la producción de la resonancia  $\Lambda(1405)$ , en esta reacción que viola isospín, daría indudablemente un gran soporte a la interpretación molecular de la  $\Lambda(1405)$ , y proporcionaría una información muy valiosa sobre los detalles de la interacción  $\bar{K}N$ .

Finalmente, en la Parte V se resumen los resultados principales y conclusiones de esta tesis.



# Abstract

Particle Physics is currently best described by the Standard Model. Within this framework, the interaction between quarks and gluons is characterized by the theory of Quantum Chromodynamics (QCD). Hadrons can be formed by combining quarks and gluons through strong interaction. However, these interactions happen typically at low energies and, unlike the other theories in the Standard Model, QCD can be only calculated perturbatively at high energies. As a consequence, to describe this non-perturbative regime one has to apply other approaches, like lattice QCD (LQCD), scattering theory, effective theories... In this thesis, special attention will be given to molecular resonances that result from the interaction between two hadrons, which will be described using a combination of non-perturbative resummations and effective theories.

The work is divided into four parts. Part I deals with the mathematical and physical formalism necessary to understand the results shown in Parts II to IV. After a first introductory chapter, in Chapter 2 we briefly present QCD and continue with a review of different effective approaches used through this thesis. We begin with chiral perturbation theory ( $\chi$ PT), which systematically describes the low energy dynamics of Goldstone bosons and the interactions of these mesons with other matter fields. The local hidden gauge (LHG) formalism to account for vector meson interactions is presented in Section 2.3. Finally, the chapter ends by introducing heavy quark spin symmetry (HQSS), which is an exact symmetry of QCD in the infinite quark mass limit. We pay a special attention to the evaluation of matrix elements for transitions involving hadrons with one heavy quark, and the constraints/simplifications that can be deduced from HQSS. In Chapter 3, we review the concepts of analyticity, unitarity and Riemann sheets of scattering amplitudes, starting with a brief introduction to elastic two body scattering theory (Subsecs. 3.1.1 and 3.1.2). Then we discuss the extension to the coupled channel case (Sec. 3.2) and present the chiral unitary approach (CUA), where the amplitudes obtained from the chiral effective Lagrangians of Chapter 3 are unitarized using the Bethe-Salpeter equation (BSE)<sup>2</sup> In this section

---

<sup>2</sup> For simplicity, although abusing notation, we will systematically refer to CUA as any unitary scheme in coupled channels, regardless of whether  $\chi$ PT is not used to calculate the BSE kernel.

we also review some general features of resonances that are dynamically generated using the CUA (Sec. 3.2.3) and relate them with the analytic properties discussed in Sec. 3.1.2. Next, in Sec. 3.2.2, we introduce several ways to regularize the loop function used in the BSE. Finally in Sec. 3.3, we explain under which conditions triangle loops can give rise to singularities that can be experimentally observed. Such study uses the concepts of analyticity and unitarity discussed at the beginning of the chapter.

In Parts II, III and IV we present the results of this dissertation, that were obtained using the techniques outlined in Part I. These contents of the thesis are based on the references: [1–11].

In Part II, the behavior of hadrons in the light sector is explored, using the techniques and models presented in the previous chapters, such as the CUA in coupled channels and the study of dynamically generated resonances. In Chapter 4, a calculation is performed of the  $\tau^- \rightarrow \nu_\tau M_1 M_2$  decays, with  $M_1, M_2$  either pseudoscalar or vector mesons, using the basic weak interaction and angular momentum algebra to relate the different processes. This formalism also leads to a different interpretation of the role played by G-parity in these decays. It is also observed that, while pseudoscalar-pseudoscalar (PP) meson  $p$ -wave production is clearly compatible with  $\chi$ PT and experiment, pseudoscalar-vector (PV) meson and vector-vector (VV) meson  $p$ -wave production is incompatible with data and a scheme is developed in this case, producing the PV or VV pairs in  $s$ -wave. A comparison of our results with experiment is made as well as predictions for unmeasured decays. A special attention is paid to the  $M_1 M_2$  mass distribution, which is shown to be a powerful tool to learn about the meson-meson interaction and the nature of some resonances produced in such decays.

In Chapter 5, the mass distributions of  $MB$  in the  $\Lambda_c \rightarrow \bar{K}^0 MB$  decay ( $MB = \pi N(I = 1/2), \eta p$ , and  $K\Sigma(I = 1/2)$ ) are evaluated, and used to study the properties of the  $N^*(1535)$  and  $N^*(1650)$ . This is achieved by calculating the tree-level and loop contributions, mixing pseudoscalar-baryon and vector-baryon channels using the LHG formalism. We observed that in the  $\eta N$  mass distribution only the  $N^*(1535)$  is seen, with the  $N^*(1650)$  contributing to the width of the curve, while for the  $\pi N$  mass distribution both resonances are clearly visible. In the case of  $MB = K\Sigma$ , we found that the strength of the  $K\Sigma$  mass distribution is smaller than that of the mass distributions of the  $\pi N$  and  $\eta p$  in the  $\Lambda_c^+ \rightarrow \bar{K}^0 \pi N$  and  $\Lambda_c^+ \rightarrow \bar{K}^0 \eta p$  processes, in spite of this channel having a large coupling to the  $N^*(1650)$ . This is because the  $K\Sigma$  pair production is suppressed in the primary production from the  $\Lambda_c$  decay.

In Part III, baryon resonance states with heavy quarks, such as the  $\Lambda_{c(b)}^{(*)}$ ,  $\Omega_c^{(*)}$  and  $\Xi_{c(b)}^{(*)}$ , are studied using the various techniques presented in Parts I and II. First, in Chapter 6, an exhaustive study of the HQSS implications for  $\Lambda_b \rightarrow \Lambda_c^* \ell \bar{\nu}_\ell$

and  $\Lambda_b \rightarrow \Lambda_c^* \pi^-$  [ $\Lambda_c^* = \Lambda_c(2595)$  and  $\Lambda_c(2625)$ ] decays is conducted. Identifying the odd parity  $\Lambda_c(2595)$  and  $\Lambda_c(2625)$  resonances as HQSS partners, with total angular momentum–parity  $j_q^P = 1^-$  for the light degrees of freedom, we find that the ratios  $\Gamma(\Lambda_b \rightarrow \Lambda_c(2595)\pi^-)/\Gamma(\Lambda_b \rightarrow \Lambda_c(2625)\pi^-)$  and  $\Gamma(\Lambda_b \rightarrow \Lambda_c(2595)\ell\bar{\nu}_\ell)/\Gamma(\Lambda_b \rightarrow \Lambda_c(2625)\ell\bar{\nu}_\ell)$  agree, within errors, with the experimental values given in the Review of Particle Physics. A discussion is given of how future, and more precise, measurements of the above branching fractions could be used to shed light into the inner HQSS structure of the narrow  $\Lambda_c(2595)$  odd-parity resonance. Namely, it is shown that such studies would constrain the existence of a sizable  $j_q^P = 0^-$  component in its wave-function, and/or of a two-pole pattern, in analogy to the case of the similar  $\Lambda(1405)$  resonance in the strange sector, as suggested by most of the approaches that describe the  $\Lambda_c(2595)$  as a hadron molecule. Also, the lepton flavour universality ratios  $R[\Lambda_c^*] = \Gamma(\Lambda_b \rightarrow \Lambda_c^* \tau \bar{\nu}_\tau)/\Gamma(\Lambda_b \rightarrow \Lambda_c^* \mu \bar{\nu}_\mu)$  are investigated, and it is discussed how  $R[\Lambda_c(2595)]$  may be affected by a new source of potentially large systematic errors if there are two  $\Lambda_c(2595)$  poles. In Chapter 7, we study the structure of the  $\Lambda_c(2595)$  and  $\Lambda_c(2625)$  resonances in the framework of an effective model consistent with heavy quark spin and chiral symmetries, which incorporates the interplay between  $\Sigma_c^{(*)}\pi - ND^{(*)}$  baryon-meson degrees of freedom and bare  $p$ -wave  $c\bar{u}d$  quark-model states. We show that these two resonances might not be HQSS partners. The  $J^P = 3/2^-$   $\Lambda_c(2625)$  should be viewed mostly as a dressed three quark state, whose origin is determined by a bare state, predicted to lie very close to the mass of the resonance. The  $J^P = 1/2^-$   $\Lambda_c(2595)$  seems to have, however, a predominant molecular structure. This is because, it is either the result of the chiral  $\Sigma_c\pi$  interaction, which threshold is located much closer than the mass of the bare three-quark state, or a  $ND - ND^{(*)}$  hadron molecule, where the light degrees of freedom in its inner structure are coupled to the unnatural  $j_q^P = 0^-$  quantum-numbers. We show that both situations can occur depending on the used renormalization procedure. We find some additional states, but the classification of the spectrum in terms of HQSS is difficult, despite having used interactions that respect this symmetry. This is because the bare quark-model state and the  $\Sigma_c\pi$  threshold are located extraordinarily close to the  $\Lambda_c(2625)$  and  $\Lambda_c(2595)$ , respectively, and hence they play totally different roles in each sector.

In Chapter 8, several  $\Xi_c$  and  $\Xi_b$  states, dynamically generated from the meson-baryon interaction in coupled channels, are studied using an extension to SU(4) of the LHG approach unitarized in the BSE. These molecular states appear as poles of the scattering amplitudes, and several of them can be identified with the experimentally observed  $\Xi_c$  states, including the  $\Xi_c(2790)$ ,  $\Xi_c(2930)$ ,  $\Xi_c(2970)$ ,  $\Xi_c(3055)$  and  $\Xi_c(3080)$ . Also, for the recently reported  $\Xi_b(6227)$  state, two poles with masses and widths remarkably close to the experimental data are found, for both the  $J^P = 1/2^-$  and  $J^P = 3/2^-$  sectors. Next, in Chapter 9, we use again the meson-baryon model of

Chapter 7 (Weinberg-Tomozawa amplitudes derived from the chiral Lagrangian extended to the symmetry group  $SU(6)_{\text{light-spin-flavor}} \times \text{HQSS}$  and unitarized by solving the BSE in coupled channels) to study the impact of the renormalization scheme in the  $C = 1$ ,  $S = -2$ , and  $I = 0$  sector, where five  $\Omega_c^{(*)}$  states have been recently observed by the LHCb Collaboration. The meson-baryon interactions used in the model are consistent with both chiral and heavy-quark spin symmetries, and lead to a plausible description of the observed lowest-lying odd parity resonances  $\Lambda_c(2595)$  and  $\Lambda_c(2625)$ , and  $\Lambda_b(5912)$  and  $\Lambda_b(5920)$  resonances. It is shown that some (probably at least three) of the states observed by LHCb will also have odd parity and  $J = 1/2$  or  $J = 3/2$ , belonging two of them to the same  $SU(6)_{\text{lsf}} \times \text{HQSS}$  multiplets as the latter charmed and beauty  $\Lambda$  baryons. In addition, we revisit the  $\Xi_c$  and  $\Xi_b$  excited states within this  $SU(6)_{\text{lsf}} \times \text{HQSS}$ -extended Weinberg-Tomozawa framework. These states were previously studied in Chapter 8, but using the extended LHG framework to include vector meson and heavy quark degrees of freedom. In this way, we try to quantify systematic uncertainties arising from the use of various models for the interaction between charmed pseudoscalar and vector mesons with  $J^P = 1/2^+$  and  $J^P = 3/2^+$  baryons in this sector. Within the  $SU(6)_{\text{light-spin-flavor}} \times \text{HQSS}$  scheme, we predict a large molecular  $\Lambda_c \bar{K}$  component for the  $\Xi_c(2790)$  with a dominant  $j_q^P = 0^-$  light-degree-of-freedom spin configuration. We discuss the differences between the  $3/2^-$   $\Lambda_c(2625)$  and  $\Xi_c(2815)$  states, and conclude that they cannot be  $SU(3)$  siblings, whereas we predict the existence of other  $\Xi_c$ -states, two of them related to the two-pole structure of the  $\Lambda_c(2595)$ . It is of particular interest a pair of  $J = 1/2$  and  $J = 3/2$  poles, which form a HQSS doublet and that we tentatively assign to the  $\Xi_c(2930)$  and  $\Xi_c(2970)$ , respectively. Within this picture, the  $\Xi_c(2930)$  would be part of a  $SU(3)$  sextet, containing either the  $\Omega_c(3090)$  or the  $\Omega_c(3119)$ , and that would be completed by the  $\Sigma_c(2800)$ . Moreover, we identify a  $J = 1/2$  sextet with the  $\Xi_b(6227)$  state and the recently discovered  $\Sigma_b(6097)$ . Assuming the *equal spacing rule* and to complete this multiplet, we predict the existence of a  $J = 1/2$   $\Omega_b$  odd parity state, with a mass of 6360 MeV and that should be seen in the  $\Xi_b \bar{K}$  channel.

In Chapter 10, calculations are performed for the nonleptonic  $\Xi_b^- \rightarrow \pi^- \Xi_c^0(2790)$  ( $J = \frac{1}{2}$ ) and  $\Xi_b^- \rightarrow \pi^- \Xi_c^0(2815)$  ( $J = \frac{3}{2}$ ) decays and the same reactions replacing the  $\pi^-$  by a  $D_s^-$ . At the same time the semileptonic rates for  $\Xi_b^- \rightarrow \bar{\nu}_l l \Xi_c^0(2790)$  and  $\Xi_b^- \rightarrow \bar{\nu}_l l \Xi_c^0(2815)$  are evaluated. It is a study similar to the one carried out in Chapter 6, but in this case for the sector with strangeness and charm. While in Chapter 6 we emphasized the constraints that were derived from HQSS for these transitions, here we take the perspective that the  $\Xi_c^0(2790)$  and  $\Xi_c^0(2815)$  resonances form a HQSS doublet and are dynamically generated from the pseudoscalar-baryon and vector-baryon interactions. The ratios of the rates of these processes are evaluated and predictions made that can be tested in future experiments. Finally, it is found that

the results are rather sensitive to the coupling of the  $\Xi_c^*$  resonances to the  $D^*\Sigma$  and  $D^*\Lambda$  components.

In Part IV we study the effect of triangle singularities in several reactions involving both light and heavy hadrons, making use also of the techniques explored and developed so far in this thesis. In Chapter 11, the possible role of the triangle mechanism in the  $B^-$  decay into  $D^{*0}\pi^-\pi^0\eta$  and  $D^{*0}\pi^-\pi^+\pi^-$  is investigated. In this process, the triangle singularity appears from the decay of  $B^-$  into  $D^{*0}K^-K^{*0}$  followed by the decay of  $K^{*0}$  into  $\pi^-K^+$  and the fusion of the  $K^+K^-$ , which forms the  $a_0(980)$  or  $f_0(980)$ , that finally decay into  $\pi^0\eta$  or  $\pi^+\pi^-$ , respectively. The triangle mechanism from the  $\bar{K}^*K\bar{K}$  loop generates a peak around 1420 MeV in the invariant mass of  $\pi^-a_0$  or  $\pi^-f_0$ , and gives sizable branching fractions  $\text{Br}(B^- \rightarrow D^{*0}\pi^-a_0; a_0 \rightarrow \pi^0\eta) = (1.66 \pm 0.45) \times 10^{-6}$  and  $\text{Br}(B^- \rightarrow D^{*0}\pi^-f_0; f_0 \rightarrow \pi^+\pi^-) = (2.82 \pm 0.75) \times 10^{-6}$ . In Chapter 12, the cross sections for the  $\pi^-p \rightarrow K^0\pi\Sigma$  and  $pp \rightarrow pK^+\pi\Sigma$  reactions are investigated paying attention to a diagram that develops a triangle singularity. The triangle diagram is realized by the decay of a  $N^*$  to  $K^*\Sigma$  and the  $K^*$  decay into  $\pi K$ , and the  $\pi\Sigma$  finally merges into  $\Lambda(1405)$ . The mechanism is expected to produce a peak around 2140 MeV in the  $K\Lambda(1405)$  invariant mass. It is found that a clear peak appears around 2100 MeV, about 40 MeV lower than the expectation, and that is due to the mass distribution of the  $N^*(2030)$  resonance, which plays a crucial role in the  $K^*\Sigma$  production. The mechanism studied produces the peak of the  $\Lambda(1405)$  around or below 1400 MeV, as it is seen in the  $pp \rightarrow pK^+\pi\Sigma$  HADES experiment.

In Chapter 13, the decay of  $\Lambda_c^+$  into  $\pi^+\pi^0\Lambda(1405)$  with the  $\Lambda(1405)$  decay into  $\pi^0\Sigma^0$  through a triangle diagram is studied. This process is initiated by  $\Lambda_c^+ \rightarrow \pi^+\bar{K}^*N$ , and then the  $\bar{K}^*$  decays into  $\bar{K}\pi$  and  $\bar{K}N$  produce the  $\Lambda(1405)$  through a triangle loop containing  $\bar{K}^*N\bar{K}$ , which develops a singularity around 1890 MeV in the  $\pi^0\Lambda(1405)$  invariant mass distribution. This process is prohibited by the isospin symmetry, but the decay into this channel is enhanced by the contribution of the triangle diagram, which is sensitive to the mass of the internal particles. A narrow peak is found in the  $\pi^0\Sigma^0$  invariant mass distribution, which originates from the  $\Lambda(1405)$  amplitude, but is tied to the mass differences between the charged and neutral  $\bar{K}$  or  $N$  states. The observation of the unavoidable peak of the triangle singularity in the isospin-violating  $\Lambda(1405)$  production would provide further support for the hadronic molecular picture of the  $\Lambda(1405)$  and further information on the  $\bar{K}N$  interaction.

Finally, in Part V, a summary of the main results and conclusions obtained in this thesis is given.



# Contents

<b>Resumen</b>	<b>v</b>
<b>Abstract</b>	<b>xi</b>
<b>1 Introduction</b>	<b>1</b>
1.1 Quantum Chromodynamics and Hadrons . . . . .	1
1.1.1 The case of the $\Lambda(1405)$ . . . . .	5
1.1.2 Heavy Baryon Resonances . . . . .	6
1.2 Kinematical effects: Triangle Singularities . . . . .	7
<b>I Theory Elements</b>	<b>9</b>
<b>2 Effective Field Theories</b>	<b>11</b>
2.1 QCD Lagrangian . . . . .	12
2.2 Chiral Symmetry . . . . .	13
2.3 Local Hidden Gauge Approach . . . . .	15
2.4 Chiral SU(3) Meson-Baryon Interaction . . . . .	17
2.5 Heavy Quark Symmetries . . . . .	18
2.5.1 Heavy Quark Symmetries In Semileptonic Decays . . . . .	21
<b>3 Analyticity &amp; <math>T</math>-matrix</b>	<b>27</b>
3.1 Scattering Theory . . . . .	27
3.1.1 Partial Wave Amplitudes . . . . .	30
3.1.2 Analyticity and Riemann Sheets . . . . .	33
3.2 Unitarity in Coupled Channels . . . . .	40
3.2.1 Bethe-Salpeter equation and the chiral unitary approach . . . . .	40
3.2.2 Regularizing the loop function . . . . .	43
3.2.3 Dynamically Generated Resonances . . . . .	46
3.3 Triangle Singularities . . . . .	49

<b>II</b>	<b>Hadrons In The Light Sector</b>	<b>55</b>
<b>4</b>	<b>Decays of <math>\tau^-</math> to <math>PP, PV</math> and <math>VV</math> meson pairs</b>	<b>57</b>
4.1	Introduction . . . . .	57
4.2	Formalism . . . . .	58
4.2.1	Weak interaction . . . . .	61
4.2.2	$G$ -parity considerations . . . . .	67
4.3	Evaluation of $\overline{\Sigma}\Sigma t ^2$ for the different processes . . . . .	70
4.4	$s$ -wave decays . . . . .	72
4.5	Results . . . . .	74
4.6	Discussion and perspective . . . . .	82
4.7	Comparison with other approaches . . . . .	88
4.8	Conclusions . . . . .	91
<b>5</b>	<b><math>N^*</math> production in <math>\Lambda_c</math> decays</b>	<b>93</b>
5.1	Introduction . . . . .	93
5.2	Formalism . . . . .	95
5.3	Results . . . . .	102
5.4	Conclusions . . . . .	105
<b>III</b>	<b>Hadrons In The Heavy Sector</b>	<b>107</b>
<b>6</b>	<b><math>\Lambda_b \rightarrow \Lambda_c^*</math> decays and heavy quark spin symmetry</b>	<b>109</b>
6.1	Introduction . . . . .	109
6.2	HQSS structure of the $\Lambda_c(2595)$ and $\Lambda_c(2625)$ states in hadron-molecular approaches. . . . .	112
6.3	Molecular models . . . . .	113
6.4	HQSS structure of the $\Lambda_c(2595)$ and $\Lambda_c(2625)$ hadron-molecules . . . . .	115
6.4.1	$SU(6)_{\text{lsf}} \times SU(2)_{\text{HQSS}}$ . . . . .	116
6.4.2	Extended local hidden gauge (ELHG) . . . . .	120
6.4.3	$SU(4)$ flavor $t$ -channel exchange of vector mesons . . . . .	121
6.4.4	Chiral isoscalar $\pi\Sigma_c^{(*)}$ molecules . . . . .	122
6.5	Weinberg compositeness condition . . . . .	123
6.6	Semileptonic $\Lambda_b \rightarrow \Lambda_c^* \ell \bar{\nu}_\ell$ decays . . . . .	123
6.7	Infinite heavy quark mass limit . . . . .	126
6.8	$\mathcal{O}(\Lambda_{\text{QCD}}/m_c)$ corrections . . . . .	128
6.9	Decays to molecular $\Lambda_c^{\text{MOL}}$ states . . . . .	130
6.10	$\Lambda_b \rightarrow \Lambda_c^* \pi^-$ decay . . . . .	132
6.11	Results . . . . .	133
6.12	Semileptonic ( $\mu^- \bar{\nu}_\mu$ or $e^- \bar{\nu}_e$ ) and pion $\Lambda_b \rightarrow \Lambda_c^*$ decays . . . . .	133



6.13	$\Lambda_b \rightarrow \Lambda_c(2595)\tau \bar{\nu}_\tau$ and $\Lambda_b \rightarrow \Lambda_c(2625)\tau \bar{\nu}_\tau$ decays . . . . .	138
6.14	Conclusions . . . . .	139
<b>7</b>	<b>The nature of the <math>\Lambda_c(2595)</math> and <math>\Lambda_c(2625)</math> resonances</b>	<b>143</b>
7.1	Introduction . . . . .	143
7.2	Formalism . . . . .	146
7.2.1	$SU(6)_{\text{lsf}} \times \text{HQSS}$ amplitudes and renormalization . . . . .	146
7.2.2	Interplay between bare CQM and baryon-meson degrees of freedom . . . . .	148
7.2.3	The $\Lambda_c^*(1/2^-, 3/2^-) \rightarrow \Lambda_c(1/2^+) \pi \pi$ three-body decays through the $\pi \Sigma_c^{(*)}$ intermediate state . . . . .	149
7.3	Results and discussion . . . . .	154
7.3.1	$SU(6)_{\text{lsf}} \times \text{HQSS}$ hadron molecules: dependence on the renormalization scheme . . . . .	154
7.3.2	CQM and baryon-meson degrees of freedom . . . . .	158
7.3.3	Further comments . . . . .	165
7.4	Conclusions . . . . .	167
<b>8</b>	<b><math>\Xi_b</math> and <math>\Xi_c</math> as molecular states from extended Local Hidden Gauge</b>	<b>169</b>
8.1	Introduction . . . . .	169
8.2	Formalism . . . . .	170
8.3	Results . . . . .	179
8.3.1	Molecular $\Xi_c$ states generated from meson-baryon states . . . . .	179
8.3.2	Molecular states for $\Xi_b$ generated from meson-baryon states . . . . .	181
8.4	Conclusions . . . . .	188
<b>9</b>	<b><math>\Omega_c, \Xi_c</math> and <math>\Xi_b</math> molecular states within a <math>SU(6)_{\text{lsf}} \times \text{HQSS}</math> model</b>	<b>189</b>
9.1	Introduction . . . . .	189
9.2	Formalism . . . . .	192
9.3	Results . . . . .	193
9.3.1	$\Omega_c$ excited states . . . . .	193
9.3.2	$\Xi_c$ excited states . . . . .	200
9.3.3	$\Xi_b$ excited states . . . . .	206
9.4	Conclusions . . . . .	217
<b>10</b>	<b>Predictions for <math>\Xi_b^- \rightarrow \pi^- (D_s^-) \Xi_c^*</math> and <math>\Xi_b^- \rightarrow \bar{\nu}_l l \Xi_c^*</math> decays, with <math>\Xi_c^* = \Xi_c^0(2790)</math> and <math>\Xi_c^0(2815)</math></b>	<b>219</b>
10.1	Introduction . . . . .	219
10.2	Formalism . . . . .	220
10.3	The weak vertex . . . . .	223

10.4 The spin structure in the hadronization . . . . .	224
10.5 Semileptonic decay . . . . .	227
10.6 Results . . . . .	230
10.7 Relativistic Effects . . . . .	232
10.8 Estimation of absolute values for the rates and uncertainties . . . . .	235
10.9 Conclusion . . . . .	238

## **IV Triangle Singularities 241**

<b>11 Triangle Singularities in non-leptonic <math>B^- \rightarrow D^{*0}</math> decays</b>	<b>243</b>
11.1 Introduction . . . . .	243
11.2 Formalism . . . . .	244
11.3 Results . . . . .	251
11.4 Conclusions . . . . .	254
<b>12 Triangle Singularities in <math>\Lambda(1405)</math> production in <math>\pi p</math> and <math>pp</math> reactions</b>	<b>255</b>
12.1 Introduction . . . . .	255
12.2 Formalism . . . . .	256
12.2.1 $\pi^- \mathbf{p} \rightarrow \mathbf{K}^0 \pi \Sigma$ . . . . .	256
12.2.2 $pp \rightarrow p \mathbf{K}^+ \pi \Sigma$ . . . . .	261
12.3 Results . . . . .	265
12.4 Further considerations . . . . .	272
12.5 Conclusions . . . . .	274
<b>13 Triangle Singularity and enhancement of the isospin-violating decay</b>	
$\Lambda_c^+ \rightarrow \pi^+ \pi^0 \pi^0 \Sigma^0$	<b>275</b>
13.1 Introduction . . . . .	275
13.2 Formalism . . . . .	276
13.3 Decay mechanism at quark level . . . . .	278
13.4 Calculation of the three vertices . . . . .	279
13.4.1 First vertex . . . . .	279
13.4.2 Second vertex . . . . .	279
13.4.3 Third vertex . . . . .	280
13.5 The total amplitude . . . . .	280
13.6 Isospin-breaking effect . . . . .	281
13.7 Results . . . . .	282
13.8 Conclusions . . . . .	285

<b>V</b>	<b>Conclusions and Summary</b>	<b>287</b>
<b>VI</b>	<b>Appendices</b>	<b>295</b>
<b>A</b>	<b>Some additional details for the study of the <math>\tau^- \rightarrow \nu_\tau M_1 M_2</math> decays</b>	<b>297</b>
	A.1 Evaluation of the matrix elements for the operators "1" and $\sigma_i$ . . . . .	297
	A.2 Evaluation of $\overline{\Sigma} \Sigma  t ^2$ . . . . .	302
<b>B</b>	<b>Spin 1/2 and 3/2 <math>N^*</math> contributions to the <math>K^* \Sigma \rightarrow K^* \Sigma</math> and <math>\pi N \rightarrow K^* \Sigma</math> reactions</b>	<b>309</b>



# Chapter 1

## Introduction

### 1.1 Quantum Chromodynamics and Hadrons

The theory of Quantum Chromodynamics (QCD) describes the (strong) interaction between quarks and gluons. It has an analogous property to the electric charge, called the color, that the particles should have to experience the interaction. The difference in this case, compared with Quantum Electrodynamics, is that the quarks can be in three different color states. In fact, QCD obeys the non-abelian  $SU(3)$  color symmetry, where the gluons are the gauge fields of the theory, and have color content, in clear contrast to photons, which do not carry electric charge. Two very important properties of QCD are:

- Color confinement,
- Asymptotic freedom.

Color confinement results from the fact that the potential between two color charges increases linearly with the distance between them. Thus, one can never isolate non-singlet color particles. Asymptotic freedom comes from the fact that the interaction between color particles decreases with increasing energy and increases with a decrease in the energy scale. Thus, QCD only allows for perturbative calculations at high energies, unlike the other theories of the Standard Model. Because of this, to study low energy QCD one has to apply other approaches like lattice QCD (LQCD), effective field theories (Chapter 2) [12–14] or the use of non-perturbative techniques from scattering theory (Chapter 3). Constituent quark model (CQM) calculations are also quite popular. In those models, hadrons are composed of some effective (constituent) quarks of valencia and, though they cannot systematically approach QCD, in some cases capture in an easy way some global aspects of the complex QCD dynamics. The success of the constituent quark models in the low-lying hadron

spectrum gives us an interpretation of the baryons as a composite of three quarks, and the mesons as that of quark and anti-quark [15, 16]. Meanwhile, the possibility of non conventional hadrons called exotics, which are not prohibited by QCD, have been intensively studied [17]. The light sector of hadron spectrum is made of baryons and mesons that one can construct using the three lightest quarks: up, down and strange. Since their masses are very close to zero (compared to the typical hadronic masses), they will obey the approximate SU(3) flavor symmetry. In the sixties it was discovered [18–20] that one could organize the (many) hadron states found in the light sector according to the irreducible representations (irreps) that one gets from this symmetry. In the case of lowest-lying mesons we have,

$$3 \otimes 3^* = 1 \oplus 8, \quad (1.1)$$

which means we will have eight states from the octet irrep and one from the singlet, with total angular momentum  $J^P = 0^-$ . For baryons we have, in principle, 27 possible states<sup>1</sup>,

$$3 \otimes 3 \otimes 3 = 1 \oplus 8 \oplus 8 \oplus 10, \quad (1.2)$$

which will have  $J^P = 1/2^+$  and  $J^P = 3/2^+$  total angular momenta.

The lowest-lying states belonging to these irreps can be found in Fig. 1.1.

Aside from the ground states, one can have excited states with higher angular momentum or different parity. They will be unstable particles (resonances) that can decay to the ground states.

From the Schrödinger equation we get that the probability density that a particle,  $R$ , will decay at any given time,  $t$ , is given by,

$$|\psi(t)|^2 = |\psi(0)|^2 e^{-\Gamma t}, \quad (1.3)$$

where  $\Gamma$  is the decay width of the particle. From Eq. (1.3) we have that the time dependent wave function of particle  $R$  will behave like

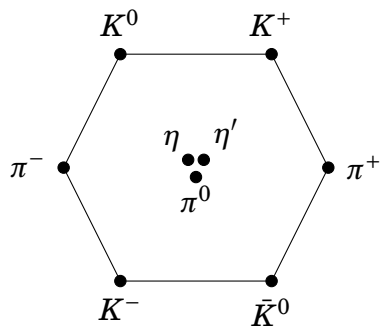
$$\psi(t) = \psi(0) e^{-iE_0 t} e^{-\Gamma/2 t}, \quad (1.4)$$

with  $E_0$  a constant with dimensions of energy. We can get the energy distribution of that particle by performing the Fourier transform,

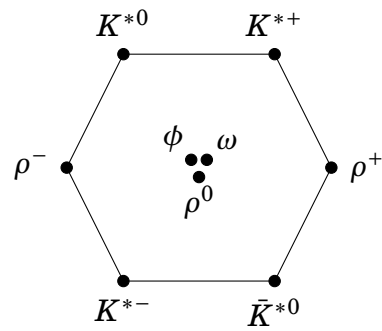
$$\psi(E) = \int dt \psi(0) e^{i(E-E_0+i\Gamma/2)t} \propto \frac{1}{E-E_0+i\frac{\Gamma}{2}}. \quad (1.5)$$

---

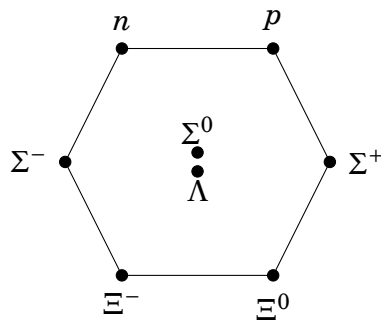
<sup>1</sup>The number is reduced when one demands symmetry of the flavor-spin wave function (color brings the antisymmetry).



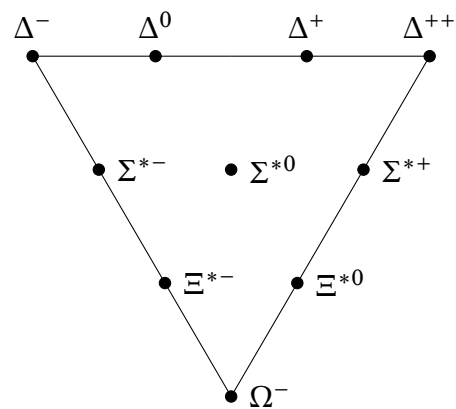
(a) Pseudoscalar meson octet



(b) Vector meson octet

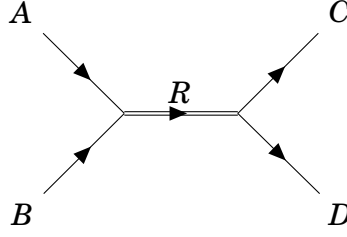


(c) Baryon octet



(d) Baryon decuplet

Figure 1.1: Graphic representation of meson and baryon irreps.

Figure 1.2: Feynman diagram of a resonance appearing in a scattering  $A B \rightarrow C D$ .

For a stable particle ( $\Gamma = 0$ ),  $E_0$  is the mass. For an unstable particle, we can interpret its mass as a continuous distribution around  $E_0$ , instead of a fixed value. Alternatively, one can see the mass of such particle as having a "imaginary component" given by  $-i\Gamma/2$ .

In general, unstable particles, or resonances, will appear as peaks in the spectrum of physical reactions, either in collisions like [21]

$$A + B \rightarrow R \rightarrow C_1 + C_2 + \cdots + C_n, \quad (1.6)$$

or in decays,

$$A \rightarrow R + B \rightarrow C_1 + \cdots + C_n + B. \quad (1.7)$$

Eq. (1.5) is called the Breit-Wigner distribution, and it can be used to parametrize resonance amplitudes. For baryonic resonances we use the same formula [6],

$$T_{BW} = \frac{g_i g_f}{\sqrt{s} - M_R + i \frac{\Gamma_R}{2}}, \quad (1.8)$$

while for mesonic resonances is common to use [21, 22],

$$T_{BW} = \frac{g_i g_f}{s - \left(M_R - i \frac{\Gamma_R}{2}\right)^2} \rightarrow \frac{g_i g_f}{s - M_R^2 + i M_R \Gamma_R}, \quad (1.9)$$

which one obtains by substituting  $M_R \rightarrow M_R - i \frac{\Gamma_R}{2}$  in the boson propagator and neglecting  $(\Gamma_R/2M_R)^2$ . Here  $g_i$  and  $g_f$  are couplings to the initial and final states (see Fig. 1.2), respectively, and as such, will change with the reaction being parametrized.  $M_R$  and  $\Gamma_R$  are the mass and width of the resonance, and ideally should remain constant across reactions. From the Breit-Wigner amplitude we see that resonances can appear as poles in the complex plane of the energy, in the position  $E = M_R - i \frac{\Gamma_R}{2}$  if  $\Gamma_R$  is considered constant. Yet, when  $\Gamma_R$  has the right energy dependence one must go to the second Riemann sheet to find the poles.



In general this parametrization of resonance amplitudes is accurate only if a single resonance exists, and if that resonance is far away from any relevant thresholds [21]. There are ways of dealing with more resonances, and there exist other distributions, such as that associated to the Flatté parametrization [23]. Typically a spectrum is observed in an experiment and one has to try to get its characteristics by using one of these parameterizations.

Some states that are observed cannot be described by the constituent quark model [13, 24]. To describe those resonances one needs other degrees of freedom, such as the interaction of two hadrons, that can lead to the production of a hadronic molecule (see the case of the  $\Lambda(1405)$  next section), or tetra/penta quark states, glueballs, etc [25]. A resonance may even be a combination of different components with several degrees of freedom, for example:

$$|R\rangle = N_{3q} |q_1 q_2 q_3\rangle + N_{5q} |q_1 q_2 q_3 q \bar{q}\rangle + N_h |\text{hadrons}\rangle + \dots, \quad (1.10)$$

### 1.1.1 The case of the $\Lambda(1405)$

The nature of the  $\Lambda(1405)$ , the lowest excitation of the  $\Lambda$ -hyperon with  $J^P = 1/2^-$ , has been given much attention for a long time. The quark model predicts the mass at higher energy than the observed peak [26], and a description of the  $\Lambda(1405)$  as a  $\bar{K}N$  molecular state shows a good agreement with the experimental result, as originally pointed out in Refs. [27–29]. The studies of the  $\bar{K}N$  system based on SU(3) chiral symmetry with the implementation of unitarity and coupled channels suggest that the  $\Lambda(1405)$  is generated as a  $\bar{K}N$  quasi-bound state [30–41]. The recent analysis of the lattice QCD simulation supports the molecular picture of the  $\Lambda(1405)$  [42, 43]. Furthermore, the analysis of the compositeness [44–46], which is a measure of the hadronic molecular component, and the root mean square radius [47, 48], also support the picture of the  $\Lambda(1405)$  as a  $\bar{K}N$  molecule. Other than these works, many studies for the  $\Lambda(1405)$  production induced by photons [49–54], pions [55], kaon [56–60], proton-proton collision [61, 62], and in heavy meson decay [63] were carried out to clarify the nature of the  $\Lambda(1405)$  resonance. The studies related to the  $\bar{K}N$  system are summarized in Refs. [24, 64] (see also note in the PDG [65]).

In addition to the essential coupling to  $\bar{K}N$ , it was also found that the  $\Lambda(1405)$  has a large coupling to the  $\pi\Sigma$  channel [66–68]. If the  $\Lambda(1405)$  is a molecular state of meson-baryon pairs that respect the chiral vector SU(3) symmetry, then  $\Lambda(1405)$  will be formed from the interaction of two octets, which will have the following irreps,

$$8 \otimes 8 = 1 \oplus 8_S \oplus 8_A \oplus 10 \oplus \bar{10} \oplus 27, \quad (1.11)$$

where the attraction occurs in the singlet and the octets [35]. Assuming perfect SU(3) symmetry, all the states belonging to each irrep will be degenerate. However, because

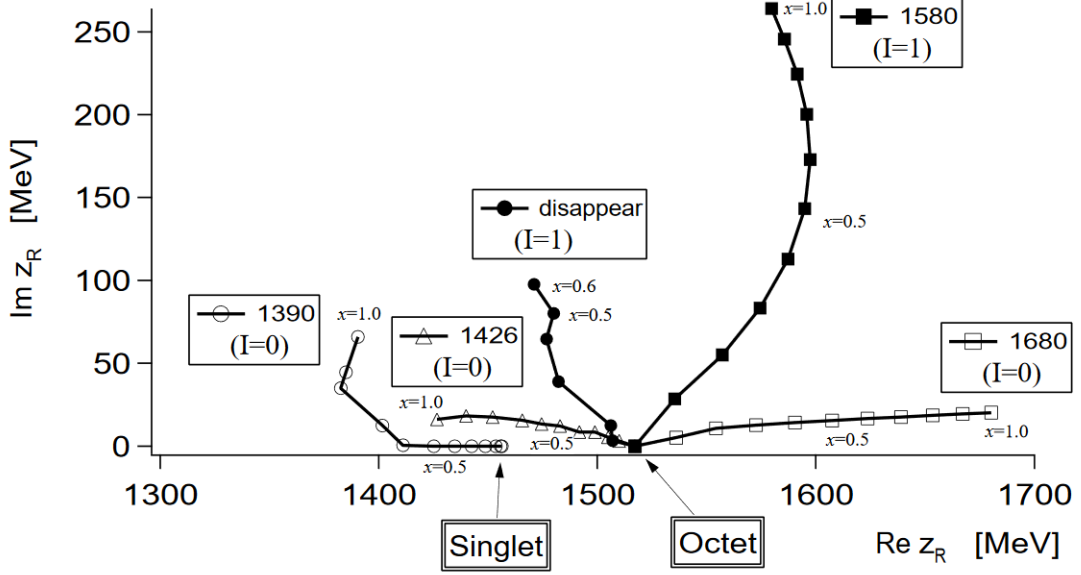


Figure 1.3: Trajectories of poles in scattering amplitudes, obtained when adiabatically breaking SU(3) symmetry. Near the mass of the  $\Lambda(1405)$ , in the physical limit, there are two poles, one broad (singlet) and one narrow (octet). Graph taken from Ref. [35].

the light quarks (u,d,s) have different masses, SU(3) is only an approximate symmetry and in this case the states stop being degenerate. One can see the evolution of these states if one introduces in the CUA of Ref. [35] the masses of the light quarks adiabatically (see Fig. 1.3). Doing this, in this reference and later in Refs. [32, 69] it was shown that the observed  $\Lambda(1405)$  resonance is the result of two poles coming from two different irreps of the SU(3) symmetry: one from the two octets, that couples mostly to  $\bar{K}N$ , and one from the singlet, which couples mostly to  $\pi\Sigma$  (see Fig. 1.3). In the physical limit both poles will be close in energy, but the singlet will have a large width, while the octet will have a smaller one [32, 35, 69].

## 1.1.2 Heavy Baryon Resonances

Nowadays much attention is paid to the spectroscopy of heavy hadrons in order to investigate the symmetries of QCD. As pointed out in Refs. [70–72], in the infinite quark mass limit ( $m_Q \rightarrow \infty$ ), the spectrum of hadrons containing a heavy quark should show a SU(2)-pattern, because of the symmetry that QCD acquires in that limit under arbitrary rotations of the spin of the heavy quark. This is known as heavy quark spin symmetry (HQSS) in the literature. In that case, the total angular

momentum  $j$  of the brown muck, which is the subsystem of the hadron apart from the heavy quark, is conserved and hadrons with  $J = j \pm 1/2$  form a degenerate doublet. This is because the one gluon exchange chromomagnetic interaction between the heavy quark and the brown muck is suppressed by the infinitely large mass of the quark.

In particular, heavy baryons containing one  $c$  or  $b$  quark have been the subject of intense study. Starting from early quark models [16], work along this line has been rather extensive and fruitful [73–79]. Lattice QCD has also contributed to this area [80–82] and dynamical models building molecular states in coupled meson-baryon channels [83–95] have also brought their share to this intense research. There are also many review papers on the subject to which we refer the reader [13, 96–102].

A review of the physics involving hadrons with heavy quarks will be given in Sec. 2.5 of Chapter 2.

## 1.2 Kinematical effects: Triangle Singularities

Not all peaks are resonances. An example of that are the Triangle Singularities (TS). These type of singularities were first studied by Landau in Ref. [103], where he explored what singularities could arise from different type of loop diagrams – but here we shall focus only on triangle loops. A TS can occur when we have a triangle diagram, like the one shown in Fig. 1.4, if certain conditions, known as the Landau equations, are fulfilled. This singularity appears as a peak in the (B,C) mass distribution (initial particle A). In Ref. [104], a physical interpretation of the Landau equations, known as the Coleman-Norton theorem, was presented. In that paper, the authors state that in order for a singularity to exist, the following must be true in the corresponding loop diagram:

*“...each vertex interaction occurs as an instantaneous event in space-time, and the internal particles propagate on the mass shell with the momenta  $q_i$ , forward in time, for just the correct distances and times to « tie together » the entire graph and allow it to be visualized as an ordered sequence of successive interactions.” [104].*

In other words, a loop diagram (in our case a triangle diagram) will have a singularity as long as the reaction happening in the loop can happen classically, with all the particles on-shell. A full mathematical description of the TS will be given in Sec. 3.3 of Chapter 3.

We shall now look at the example of the “ $a_1(1420)$ ”. In Ref. [105], the COMPASS Collaboration, in a collision of a pion with a hydrogen stationary target, observed a peak in the invariant mass of the  $\pi^-\pi^-\pi^+$  final state, at around 1.4 GeV, that they

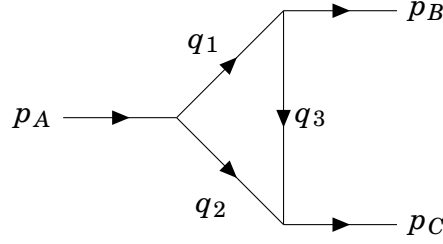


Figure 1.4: Feynman diagram corresponding to a triangle loop, where a particle  $A$  decays into particles 1 and 2. Then, particle 1 decays into 3 and  $B$ , and particles 2 and 3 fuse to form particle  $C$ .

classified as being an axial-vector meson resonance which they called  $a_1(1420)$ . However, the possibility of this peak being originated by a TS was explored in Refs. [106–108]. There, a contribution from the reaction  $\pi^+ p \rightarrow p a_1^-(1260) \rightarrow p \pi^- \pi^- \pi^+$  with a triangle loop was analyzed, and they found a TS associated with this diagram which appears at around  $m_{3\pi} \simeq 1420$  MeV and can explain the observed peak. In a subsequent publication by the COMPASS Collaboration, in Ref. [109], they mention that the triangle diagram can describe the data equally as well as a Breit-Wigner amplitude, and in a recent review of “Hadronic molecules” [13], the TS is considered a “*natural explanation*” for the  $a_1(1420)$ , thus signaling the acceptance of the validity of these studies by the scientific community, as well as the importance of keeping TS in mind when analyzing the hadronic resonances spectrum. Other than the “ $a_1(1420)$ ”, the interpretation of the “ $f_1(1420)$ ” and “ $f_2(1810)$ ” in the PDG [110] as a peak of the triangle singularity was proposed in Refs. [111] and [112], respectively.

Other examples are the studies in Refs. [106, 113, 114] which suggest the possible explanation of  $Z_c(3900)$  with the triangle mechanism. Also for the decay of  $\eta(1405)$  into  $\pi^0 \pi^0 \eta$  via  $\pi^0 a_0$  and  $\pi^0 \pi^+ \pi^-$  via  $\pi^0 f_0$ , the triangle mechanism gives a good explanation [115–117]. The  $K^* \bar{K} K$  loop generates the triangle singularity in this process, and the anomalously large branching fraction of the isospin-violating  $\pi^0 f_0$  channel reported by BESIII [118] is well explained with the mechanism. The study of the singularity is also potentially a useful tool to study some baryonic molecular states. Regarding the pentaquark  $P_c$  peak, discovered in the  $J/\psi p$  invariant mass distribution of the  $\Lambda_b$  decay [119, 120], the possibility of the interpretation as a triangle singularity was pointed out in Refs. [121, 122]. However, in Ref. [123] it was noted that if the  $P_c$  quantum numbers were  $\frac{1}{2}^+$  or  $\frac{3}{2}^+$  the triangle mechanism could provide an interpretation of the narrow experimental peak, but not if the quantum numbers are  $\frac{3}{2}^-$ ,  $\frac{5}{2}^+$ , as preferred by experiment. Furthermore, the possible manifestations of the TS in the heavy sector were investigated in Refs. [9, 106, 124–128].

**Part I**  
**Theory Elements**



# Chapter 2

## Effective Field Theories

Effective field approaches have shown to be powerful tools for the study of processes, far below from the typical energy scale where the original theories are formulated. If one is interested only in a particular energy scale, then one can “ignore” much bigger scales contained in the underlying theory, thus obtaining what we call an effective theory [129]. For example, in the case of hadron physics, if one is only interested in the lowest-lying pseudo-scalar mesons ( $\pi^\pm, \pi^0, K^\pm, K^0, \bar{K}^0, \eta_8$ ), and their interactions, then one can ignore the degrees of freedom above a typical hadronic mass scale  $\Lambda \simeq 1$  GeV (the lightest vector meson and baryon masses are  $m_\rho = 770$  MeV and  $m_p = 938$  MeV, respectively). Since all these pseudo-scalar meson masses are below that scale, the heavier degrees of freedom should not affect the system too strongly and thus can be integrated out. In a more formal way, if one has a theory with light  $l_i$  and heavy  $H_j$  degrees of freedom, and if

$$m_{l_i} \ll \Lambda \lesssim m_{H_j}, \quad (2.1)$$

with  $\Lambda$  the typical “heavy” energy scale, then the heavy fields can be integrated out of the theory, leaving an effective Lagrangian [130]

$$\mathcal{L}(l_i, H_j) \rightarrow \mathcal{L}_{\text{eff}}(l_i). \quad (2.2)$$

The heavy degrees of freedom are not actually fully forgotten, since their information will appear as renormalization effects in effective coupling constants, or as suppressed higher order operators [130].

In the next sections, we will briefly introduce effective Lagrangians for Goldstone-boson and vector-meson interactions (chiral and local hidden gauge Lagrangians) and for other processes, where HQSS provides useful constraints. With the exception of those based on HQSS, the effective interactions shown here are valid in the light sector (for SU(3) symmetry). However, in Chapters 6 to 8 we will extend these interactions to other symmetry groups, to account for an extra (heavy) quark.

## 2.1 QCD Lagrangian

Before starting with the effective interactions relevant for this thesis, one should first introduce the QCD Lagrangian<sup>1</sup>,

$$\mathcal{L}_{QCD} = \bar{q}_\alpha (i\mathcal{D} - M)_\beta^\alpha q^\beta - \frac{1}{4} G_{\mu\nu}^\alpha G_{\alpha}^{\mu\nu}, \quad \alpha, \beta = 1, \dots, 8 \quad (2.3)$$

for  $N_c = 3$  colors. In addition  $q_\alpha^T = (u_\alpha, d_\alpha, \dots)$  the quark fields,  $M = \text{diag}(m_u, m_d, \dots)$  the quark mass matrix,

$$(D_\mu)_\beta^\alpha = \partial_\mu \delta_\beta^\alpha - ig \left( A_\mu^\gamma \frac{\lambda_\gamma}{2} \right)_\beta^\alpha, \quad \gamma = 1, \dots, 8 \quad (2.4)$$

the covariant derivative, with  $A_\mu^\alpha$  the gluon fields,  $\lambda_\alpha$  the Gell-Mann matrices, and

$$G_{\mu\nu}^\alpha = \partial_\mu A_\nu^\alpha - \partial_\nu A_\mu^\alpha + gf^{\alpha\beta\gamma} A_\mu^\beta A_\nu^\gamma, \quad (2.5)$$

the gluon field strength tensor, with  $f^{\alpha\beta\gamma}$  the color SU(3) structure constants.

If one ignores the quark masses then the Lagrangian in Eq. (2.3) will be invariant under  $G = SU(N_f)_L \otimes SU(N_f)_R$  transformations<sup>2</sup> (with  $N_f$  the number of flavors). Defining the left- and right-handed fields,

$$q_{L,R} = \frac{1}{2}(1 \mp \gamma_5)q = P_{L,R} q, \quad (2.6)$$

one gets

$$\mathcal{L}_{QCD}^0 = \bar{q} i\mathcal{D}q - \frac{1}{4} G_{\mu\nu}^\alpha G_{\alpha}^{\mu\nu} = (\bar{q}_L i\mathcal{D}q_L + \bar{q}_R i\mathcal{D}q_R) - \frac{1}{4} G_{\mu\nu}^\alpha G_{\alpha}^{\mu\nu}. \quad (2.7)$$

Then, for a chiral transformation  $g = (g_L, g_R) \in G$ , the fields transform as

$$q_L \xrightarrow{G} g_L q_L, \quad q_R \xrightarrow{G} g_R q_R, \quad (2.8)$$

which have the following associated Noether currents,

$$J_{L,R}^{\alpha\mu} = \bar{q}_{L,R} \gamma^\mu T^\alpha q_{L,R}, \quad \alpha = 1, \dots, (N_f^2 - 1), \quad (2.9)$$

where here  $T^\alpha$  are the generators of  $SU(N_f)$  in the fundamental representation (i.e.  $T^\alpha = \lambda^\alpha/2$  for  $N_f = 3$ ). Another way to write the symmetry is with vector and axial

<sup>1</sup>We do not pay here full attention to the color transformation of the Lagrangian, which is designed to remain invariant under local gauge transformations of color [131]

<sup>2</sup>The complete symmetry would be  $SU(N_f)_L \otimes SU(N_f)_R \otimes U(1)_V$ , with  $V = R + L$ , but  $U(1)_V$  which gives the quark number/baryon number is trivial in the meson sector.



transformations,  $G = SU(N_f)_V \otimes SU(N_f)_A$ , with  $V = L + R$  and  $A = R - L$ , and the following Noether currents,

$$V^{a\mu} = \bar{q}\gamma^\mu T^a q, \quad (2.10a)$$

$$A^{a\mu} = \bar{q}\gamma^\mu \gamma_5 T^a q, \quad a = 1, \dots, (N_f^2 - 1). \quad (2.10b)$$

## 2.2 Chiral Perturbation Theory

If one takes into account all flavors, up to the top quark, then chiral symmetry is heavily broken. However, if one takes into account only the lightest quarks,  $q^T = (u, d, s)$ , then their masses are light enough to consider chiral symmetry [now  $G = SU(3)_L \otimes SU(3)_R$ ] an approximate symmetry of QCD. Experimentally, however, one does not observe the  $G$  symmetry in the hadronic spectrum, but instead only the subgroup  $SU(3)_V$  [12]. We say there is spontaneous chiral symmetry breaking (SCSB), from  $G$  to  $SU(3)_V$ . As a consequence of the spontaneous symmetry breaking of chiral symmetry eight pseudoscalar Goldstone bosons will be produced, since there are eight axial currents being broken, which are  $(\pi^\pm, \pi^0, K^\pm, K^0, \bar{K}^0, \eta_8)$ . These will be the degrees of freedom of our effective theory. Let's call the vector symmetry  $H = SU(3)_V$ , such that  $G \xrightarrow{SCSB} H$ . Let  $\vec{\phi} = (\phi_1, \dots, \phi_8)$  be the Goldstone fields. It can be proven that the Goldstone bosons can be identified with elements,  $\xi(\vec{\phi}) = (\xi_L(\vec{\phi}), \xi_R(\vec{\phi})) \in G$ , of the left coset  $G/H$  [130, 132], since there is an isomorphic mapping between the  $G/H$  space and the Goldstone boson fields. The left coset of a subgroup  $H \subseteq G$  with respect to a group element  $g \in G$  is given by the set

$$gH = \{gh : \forall h \in H\}. \quad (2.11)$$

Then,  $G/H$  is the set of all  $gH$  cosets,

$$G/H = \{gH : \forall g \in G\} \quad (2.12)$$

Then, a chiral transformation  $g = (g_L, g_R)$  will act on the Goldstone bosons as

$$\xi_{L,R} \xrightarrow{G} g_{L,R} \xi_{L,R}(\vec{\phi}) h^\dagger(\vec{\phi}, g), \quad (2.13)$$

with  $h(\vec{\phi}, g) \in H$  and it is required to return to the given choice of coset representative. Since an element  $g$  of  $G$  can be written as  $g = (g_L, g_R) = (1, g_R g_L^\dagger)(g_L, g_L)$ , and  $gh = (1, g_R g_L^\dagger)(g_L, g_L)h = (1, g_R g_L^\dagger)h$ , one may represent each element of the coset as  $g_R g_L^\dagger$ . Thus, Goldstone bosons can also be represented by

$$U(\vec{\phi}) = \xi_R(\vec{\phi}) \xi_L^\dagger(\vec{\phi}). \quad (2.14)$$

This way, a  $g$  transformation will act as

$$U(\vec{\phi}) \xrightarrow{G} g_R U(\vec{\phi}) g_L^\dagger. \quad (2.15)$$

Moreover, without loss of generality, we can take a canonical choice of coset representative such that  $\xi_R(\vec{\phi}) = \xi_L^\dagger(\vec{\phi}) = u(\vec{\phi})$ . In addition, Lie Algebra tells us that a group element  $E$ , depending on a continuous variable  $x$ , can be represented by using the group generators,  $g$ , as,

$$E(x) = e^{igx}. \quad (2.16)$$

In our case, the generators are the Gell-Mann matrices, and the continuous variables are given by the Goldstone fields  $\vec{\phi}$ , such that

$$U(\vec{\phi}) = u(\vec{\phi})^2 = e^{i\sqrt{2}\Phi/f}, \quad (2.17)$$

with

$$\Phi(x) = \frac{\vec{\lambda}}{\sqrt{2}} \vec{\phi} = \begin{pmatrix} \frac{\pi^0}{\sqrt{2}} + \frac{\eta}{\sqrt{3}} + \frac{\eta'}{\sqrt{6}} & \pi^+ & K^+ \\ \pi^- & -\frac{\pi^0}{\sqrt{2}} + \frac{\eta}{\sqrt{3}} + \frac{\eta'}{\sqrt{6}} & K^0 \\ K^- & \bar{K}^0 & -\frac{\eta}{\sqrt{3}} + \sqrt{\frac{2}{6}}\eta' \end{pmatrix}, \quad (2.18)$$

where the standard  $\eta, \eta'$  mixing is assumed [133], and  $f$  is the Goldstone-boson decay constant, given by

$$\langle 0 | A_a^\mu | \phi_b(p) \rangle = i p^\mu \delta_{ab} f. \quad (2.19)$$

If we allow for some  $SU(3)_V$  symmetry breaking, then  $f_a$  will be different for each Goldstone boson, otherwise,  $f \simeq f_\pi = 92.4$  MeV in the chiral limit.

The usefulness of working with  $U(\vec{\phi})$ , instead of  $\vec{\phi}$ , comes from the fact that the group transformations on  $U(\vec{\phi})$  are linear, while on  $\vec{\phi}$  they are not [132]. This way, it is easier to construct an effective Lagrangian which is symmetric under  $G$ . Such a Lagrangian will only have even powers of derivatives (momentum) to conserve the right parity. Then,

$$\mathcal{L}_{\text{eff}} = \sum_n \mathcal{L}_{2n} \quad (2.20)$$

For mesons, the lowest (non-trivial) order is given by,

$$\begin{aligned} \mathcal{L}_2 &= \frac{f^2}{4} \text{Tr} \left( \partial_\mu U \partial^\mu U^\dagger \right) = \frac{1}{2} \text{Tr} \left( \partial_\mu \Phi \partial^\mu \Phi \right) \\ &+ \frac{1}{12f^2} \text{Tr} \left[ \left( \Phi \overleftrightarrow{\partial}_\mu \Phi \right) \left( \Phi \overleftrightarrow{\partial}^\mu \Phi \right) \right] + \mathcal{O}(\Phi^6/f^4), \end{aligned} \quad (2.21)$$

where in the last part of the equation, we have expanded  $U(\vec{\phi})$  in Taylor series. Then, the lowest order  $\Phi$  term is given by,

$$\mathcal{L}_{PP} = \frac{1}{2} \text{Tr} (\partial_\mu \Phi \partial^\mu \Phi). \quad (2.22)$$

In addition, there will be mass terms which explicitly break the symmetry.

## 2.3 Local Hidden Gauge Approach

So far, we have studied interactions involving pseudo-scalar mesons (PP). In this section we shall describe interactions between pseudo-scalar mesons and vector mesons (PV), and vector mesons with vector mesons (VV), using the local hidden gauge (LHG) model. [134–138]. The LHG Lagrangian will be symmetric under  $H = SU(3)_V$  transformations, with elements  $h(\vec{\phi}, g) \in H$  that have an implicit dependence on the coordinates  $x$  through  $\vec{\phi}$  and hence,  $H$  will be a local symmetry. Instead of building an effective Lagrangian that respects the global symmetry  $G$ , as we did in the previous section, we can now explicitly use the symmetry  $S = G_{\text{global}} \times H_{\text{local}}$ . Here, we are still going to use the  $U(\vec{\phi}) = \xi_R \xi_L^\dagger$  field representation for the Goldstone bosons, but we will also have an additional gauge vector field,  $V^\mu(x)$ , associated with  $H_{\text{local}}$ , which is used to define the covariant derivative,

$$D_\mu \xi_X(x) = \partial_\mu \xi_X(x) - ig V_\mu(x) \xi_X(x), \quad (2.23)$$

with  $g$  a coupling-constant and  $X = L, R$ . This vector field transforms under the full symmetry as [134–138]

$$V_\mu(x) \xrightarrow{S} h(x) V_\mu(x) h^\dagger(x) - i \partial_\mu h(x) h^\dagger(x), \quad (2.24)$$

where we have written  $h(\vec{\phi}, g)$  as  $h(x)$  for simplicity. This new vector field can be written as a vector meson nonet [137, 139],

$$V_\mu = \begin{pmatrix} \frac{1}{\sqrt{2}} \rho_\mu^0 + \frac{1}{\sqrt{2}} \omega_\mu & \rho_\mu^+ & K_\mu^{*+} \\ \rho_\mu^- & -\frac{1}{\sqrt{2}} \rho_\mu^0 - \frac{1}{\sqrt{2}} \omega_\mu & K_\mu^{*0} \\ K_\mu^{*-} & \bar{K}_\mu^{*+} & \phi_\mu \end{pmatrix}, \quad (2.25)$$

where the ideal mixing of the isospin-singlet mesons is assumed.

One can construct two axial and vector quantities, symmetric under  $G_{\text{global}} \times H_{\text{local}}$ , using the Maurer-Cartan 1-forms [134–138],

$$\alpha_\perp^\mu = \frac{1}{2i} \left( \partial^\mu \xi_R \xi_R^\dagger - \partial^\mu \xi_L \xi_L^\dagger \right), \quad (2.26a)$$

$$\alpha_\parallel^\mu = \frac{1}{2i} \left( \partial^\mu \xi_R \xi_R^\dagger + \partial^\mu \xi_L \xi_L^\dagger \right), \quad (2.26b)$$

which transform as [134–138],

$$\alpha_{\perp}^{\mu} \rightarrow h(x)\alpha_{\perp}^{\mu}h^{\dagger}(x), \quad (2.27a)$$

$$\alpha_{\parallel}^{\mu} \rightarrow h(x)\alpha_{\parallel}^{\mu}h^{\dagger}(x) - i\partial_{\mu}h(x)h^{\dagger}(x). \quad (2.27b)$$

The invariant version of these quantities, if we substitute  $\partial_{\mu}$  by  $D_{\mu}$ , is given by [137]

$$\hat{\alpha}_{\perp}^{\mu} = \alpha_{\perp}^{\mu}, \quad (2.28a)$$

$$\hat{\alpha}_{\parallel}^{\mu} = \alpha_{\parallel}^{\mu} - V^{\mu}. \quad (2.28b)$$

Two invariant Lagrangians can be constructed with these quantities [137],

$$\mathcal{L}_A = f_{\pi}^2 \text{Tr}(\hat{\alpha}_{\perp\mu}\hat{\alpha}_{\perp}^{\mu}), \quad (2.29a)$$

$$\mathcal{L}_V = C \text{Tr}(\hat{\alpha}_{\parallel\mu}\hat{\alpha}_{\parallel}^{\mu}), \quad (2.29b)$$

$$(2.29c)$$

where the most general Lagrangian, involving only the lowest derivatives, is constructed using a linear combination of the previous two [137],

$$\mathcal{L}_{\chi} = \mathcal{L}_A + a\mathcal{L}_V, \quad (2.30)$$

with  $a$  a constant.

As anticipated in Sec. 2.2, the gauge can be fixed by requiring that  $\xi_L^{\dagger} = \xi_R = u = e^{i\frac{\Phi}{\sqrt{2}f}}$  (called the unitary gauge) [12, 137], where  $u(\vec{\phi})^2 = U(\vec{\phi})$ .

Then, the 1-forms can be expanded as [137],

$$\hat{\alpha}_{\perp}^{\mu} = \frac{1}{\sqrt{2}f_{\pi}}\partial^{\mu}\Phi + \frac{1}{12\sqrt{2}f_{\pi}^3}[[\Phi, \partial^{\mu}\Phi], \Phi] + \dots, \quad (2.31a)$$

$$\hat{\alpha}_{\parallel}^{\mu} = -gV^{\mu} + \frac{i}{4f_{\pi}^2}[\Phi, \partial^{\mu}\Phi] + \dots, \quad (2.31b)$$

and,

$$\mathcal{L}_{\chi} = \frac{1}{2}\text{Tr}(\partial_{\mu}\Phi\partial^{\mu}\Phi) + aCg^2 \text{Tr}(V_{\mu}V^{\mu}) - \frac{iaCg}{2f_{\pi}^2} \text{Tr}([\Phi, \partial_{\mu}\Phi]V^{\mu}) + \dots, \quad (2.32)$$

where the first term in the left hand side of the equation is equivalent to Eq. (2.22). The lowest order term which has at least one  $V^{\mu}$  field and at least one  $\Phi$  field is given by,

$$\mathcal{L}_{VPP} = -ig\text{Tr}([\Phi, \partial_{\mu}\Phi]V^{\mu}), \quad (2.33)$$

with  $C = f_\pi^2$ ,  $a = 2$  and  $g = m_V/(2f_\pi)$ , with  $m_V \simeq 800$  MeV [134–138]. In this way, the  $t$ -channel exchange of vector mesons between Goldstone bosons implements chiral symmetry, incorporating the universal vector meson coupling hypothesis [Kawarabayashi, Suzuki, Fayyazuddin, Riazuddin (KSFR) [140, 141]].

Now to get the interaction between vector fields, one can build the gauge field strength tensor,

$$V_{\mu\nu} = \partial_\mu V_\nu - \partial_\nu V_\mu - ig[V_\mu, V_\nu], \quad (2.34)$$

and then construct the kinetic term of the Lagrangian for the vector field,

$$\mathcal{L}_{\text{kin}} = -\frac{1}{4} \text{Tr}(V_{\mu\nu} V^{\mu\nu}). \quad (2.35)$$

The lowest order interaction term is then given by,

$$\mathcal{L}_{VVV} = ig \text{Tr}[(\partial_\mu V_\nu - \partial_\nu V_\mu) V^\mu V^\nu]. \quad (2.36)$$

## 2.4 Chiral SU(3) Meson-Baryon Interaction

The introduction of baryons into the theory is similar to the introduction of vector mesons [12]. The octet of baryon fields is collected in the matrix field

$$B = \frac{\lambda^a B_a}{\sqrt{2}} = \begin{pmatrix} \frac{1}{\sqrt{2}}\Sigma^0 + \frac{1}{\sqrt{6}}\Lambda & \Sigma^+ & p \\ \Sigma^- & -\frac{1}{\sqrt{2}}\Sigma^0 + \frac{1}{\sqrt{6}}\Lambda & n \\ \Xi^- & \Xi^0 & -\frac{2}{\sqrt{6}}\Lambda \end{pmatrix}, \quad (2.37)$$

which contains all the ground state  $J^P = 1/2^+$  baryons that one can construct with the three light quarks. The matrix  $B$  transforms non-linearly as an  $H = SU(3)_V$  octet,

$$B \xrightarrow{G} h(\vec{\phi}, g) B h^\dagger(\vec{\phi}, g). \quad (2.38)$$

Again using the unitary gauge, we have that  $u(\vec{\phi})$  transforms as

$$u(\vec{\phi}) \xrightarrow{G} K u(\vec{\phi}) g_L^\dagger = g_R u(\vec{\phi}) K^\dagger, \quad (2.39)$$

The matrix  $K$  is a unitary matrix which is not only a function of the  $g_L$  and  $g_R$  matrices, but also of the fields in  $\vec{\phi}(x)$ , consequently it is also space-time dependent: it is local, and comparing with Eq. (2.15), we get

$$K(\vec{\phi}, g) = (g_R U(\vec{\phi}) g_L^\dagger)^{-1/2} g_R u(\vec{\phi}). \quad (2.40)$$

In order for the interaction between  $B$  and  $u$  to preserve the right symmetry, the easiest choice of transformation for  $B$  will be given by [12, 132],

$$B \xrightarrow{G} K(\vec{\phi}, g) B K^\dagger(\vec{\phi}, g). \quad (2.41)$$

By convention we shall write the 1-forms in Eq (2.26) as

$$\Gamma^\mu = -i\alpha_\parallel^\mu, \quad (2.42a)$$

$$u^\mu = 2\alpha_\perp^\mu. \quad (2.42b)$$

The covariant derivatives will then be of the form [132, 137]

$$D_\mu B = \partial_\mu B + [\Gamma_\mu, B], \quad (2.43)$$

Then, the lowest order effective Lagrangian is given by [142, 143]<sup>3</sup>

$$\mathcal{L}_{MB}^{(1)} = \text{Tr} [\bar{B} (iD - M) B] + \frac{D}{2} \text{Tr} (\bar{B} \gamma^\mu \gamma_5 \{u_\mu, B\}) + \frac{F}{2} \text{Tr} (\bar{B} \gamma^\mu \gamma_5 [u_\mu, B]), \quad (2.44)$$

with  $D = 0.85 \pm 0.06$  and  $F = 0.52 \pm 0.04$  constants of the interaction [144]. At lowest order momentum, the interaction will come only from the  $\Gamma_\mu$  term [31]. Then, expanding  $u$  and taking lower order terms, one gets,

$$\mathcal{L}_{MB}^{(1)} = \text{Tr} \left( B i \gamma^\mu \frac{1}{4f^2} [[\Phi, \partial_\mu \Phi], B] \right). \quad (2.45)$$

## 2.5 Heavy Quark Symmetries

Let us consider a baryon containing a heavy quark (the discussion for heavy mesons runs in parallel). The single heavy baryon and heavy quark velocities are equal in the  $m_Q \rightarrow \infty$  limit. The heavy baryon can be viewed as a freely propagating point-like color source (the heavy quark), dressed by a strongly interacting brown muck bearing appropriate color, flavour, baryon number, energy, angular momentum and parity to make up the observed physical state. Since an infinitely massive heavy quark does not recoil from the emission and absorption of soft ( $E \sim \Lambda_{\text{QCD}}$ ) gluons, and since chromomagnetic interactions of such a quark are suppressed as  $1/m_Q$ , neither its mass (flavour) nor its spin affect the state of the light degrees of freedom.

These symmetries of the heavy hadron system with regards to the flavour and the spin of the heavy quark are called, respectively, heavy quark flavour symmetry (HQFS) and heavy quark spin symmetry (HQSS), and in this section we shall see

<sup>3</sup>Note here that the masses of the baryons, given by  $M$ , do not break  $G$  symmetry.

how they arise from QCD. In the heavy quark limit, the momentum of the hadron ( $P_H$ ) is the same as the momentum of the heavy quark ( $p_Q$ ), such that

$$P_H^\mu = m_H v^\mu = p_Q^\mu + q^\mu \xrightarrow{m_Q \rightarrow \infty} p_Q^\mu = m_Q v^\mu, \quad (2.46)$$

with  $q^\mu$  a residual momentum from low energy QCD [145].

For a mass  $m_Q \gg \Lambda_{QCD}$  but not infinite, the four-velocities of the heavy quark and the heavy hadron are not the same,  $v^\mu = v_H^\mu \neq v_Q^\mu$ , although they are still approximately the same. Then, the momentum of the heavy quark can be written as

$$p_Q^\mu = m_Q v^\mu + k^\mu, \quad (2.47)$$

with  $k^\mu$  related to  $q^\mu$  through Eq. (2.46)

$$k^\mu = (m_H - m_Q)v^\mu - q^\mu, \quad (2.48)$$

and the velocity of the heavy quark given by

$$v_Q^\mu = v^\mu + \frac{k^\mu}{m_Q}. \quad (2.49)$$

With these properties we can construct an effective Lagrangian for the heavy quark. From QCD we have,

$$\mathcal{L}_{\text{QCD}}^Q = \bar{\Psi}_Q(x) (i\mathcal{D} - m_Q) \Psi_Q(x), \quad (2.50)$$

with  $\Psi_Q(x)$  the heavy quark field and, in the heavy quark limit, the free propagator becomes,

$$\Delta^0 = \frac{i(\not{p}_Q + m_Q)}{p_Q^2 - m_Q^2 + i\epsilon} \rightarrow \frac{i(1 + \psi)}{2v \cdot k + i\epsilon}. \quad (2.51)$$

One can also define the following projection operators:

$$\Lambda_\pm \equiv \frac{(1 \pm \psi)}{2}, \quad (2.52)$$

with the following properties,

$$\Lambda_\pm \Lambda_\pm = \Lambda_\pm, \quad (2.53a)$$

$$\Lambda_\pm \Lambda_\mp = 0. \quad (2.53b)$$

The heavy quark field can be further decomposed into the large ( $Q_v$ ) and small components ( $\mathcal{Q}_v$ )

$$\Psi_Q(x) = e^{-im_Q v \cdot x} [Q_v(x) + \mathcal{Q}_v(x)], \quad (2.54)$$

where,

$$Q_v(x) = e^{im_Q v \cdot x} \Lambda_+ \Psi_Q(x), \quad (2.55a)$$

$$\mathcal{Q}_v(x) = e^{im_Q v \cdot x} \Lambda_- \Psi_Q(x). \quad (2.55b)$$

Then, Eq. (2.50) becomes,

$$\begin{aligned} \mathcal{L}_{\text{QCD}}^Q &= \bar{Q}_v(x) i v \cdot D Q_v(x) - \bar{\mathcal{Q}}_v(x) i v \cdot D \mathcal{Q}_v(x) - 2m_Q \bar{\mathcal{Q}}_v(x) \mathcal{Q}_v(x) \\ &\quad + \bar{\mathcal{Q}}_v(x) i D Q_v(x) + \bar{Q}_v(x) i D \mathcal{Q}_v(x). \end{aligned} \quad (2.56)$$

The first term of the Lagrangian is invariant under both spin (HQSS) and flavour (HQFS) transformations. The small component can be integrated out of the Lagrangian by using the following equations of motion [146, 147],

$$\begin{aligned} (iD - m_Q) \Psi_Q(x) = 0 &= (iD - m_Q) e^{-im_Q v \cdot x} [Q_v(x) + \mathcal{Q}_v(x)] \\ &= e^{-im_Q v \cdot x} (iD Q_v(x) + [iD - 2m_Q] \mathcal{Q}_v(x)). \end{aligned} \quad (2.57)$$

Then,

$$\mathcal{Q}_v(x) \simeq \frac{1}{2m_Q} iD Q_v(x) + \mathcal{O}\left(\frac{1}{4m_Q^2}\right). \quad (2.58)$$

Putting Eq. (2.58) into Eq. (2.56), we get,

$$\mathcal{L}_{\text{QCD}}^Q = \bar{Q}_v(x) i v \cdot D Q_v(x) - \frac{1}{2m_Q} \bar{Q}_v(x) D^2 Q_v(x) + \mathcal{O}\left(\frac{1}{4m_Q^2}\right), \quad (2.59)$$

where, from Eqs. (2.4) and (2.5), we get

$$D^2 = D^2 + g \frac{\sigma^{\mu\nu}}{2} G_{\mu\nu}, \quad (2.60)$$

with

$$\sigma^{\mu\nu} = i \frac{[\gamma^\mu, \gamma^\nu]}{2}. \quad (2.61)$$

From Eq. (2.59) we see that the leading order term is invariant under both flavour and spin transformations while the second term in the Lagrangian breaks both HQFS and HQSS. HQFS is broken because of the  $m_Q$  dependence and HQSS because of the term proportional to  $\sigma^{\mu\nu}$ . This means that heavy quark symmetries can be regarded as approximate symmetries of QCD, that become exact in the limit of infinite heavy quark mass.



## 2.5.1 Heavy Quark Symmetries In Semileptonic Decays

Heavy quark symmetries can provide remarkable simplifications to the description of transitions in which a hadron containing a heavy quark, with velocity  $v^\mu$ , decays into another hadron containing a heavy quark of a different flavour. To the heavy quark, this looks like a free decay (up to perturbative QCD corrections), in which the light dressing plays no role. The brown muck, on the other hand, knows only that its point-like source of color is now recoiling at a new velocity  $v'^\mu$ , and it must rearrange itself about it in some configuration [148]. Hence, in the  $m_Q \rightarrow \infty$  limit, the weak matrix elements must become invariant under independent spin rotations of the heavy quarks. This is easily shown in the brick wall frame ( $\vec{v} = -\vec{v}'$ ,  $v^0 = v'^0$ ) by quantizing the angular momentum of the light degrees of freedom (*ldof*) - (brown muck)- about the spatial axis defined by  $\vec{v}$ . It follows that neither the initial and final heavy baryons, nor the initial and final quarks have orbital angular momentum about this decay axis. Thus, in the Isgur-Wise (IW) limit, the spins of the heavy quarks are decoupled from the light quanta, and the component of the *ldof* total angular momentum along the decay axis is conserved [148, 149].

The quantum state of a heavy hadron,  $|\Psi_J(v)\rangle$ , will be given by,

$$|\Psi_J(v)\rangle \simeq |u_Q(v); \pm 1/2\rangle |\text{light}; v, j, m_j\rangle, \quad (2.62)$$

where the light and heavy degrees of freedom decouple. A consequence of the decoupling of the spins is that since  $J = j \pm 1/2$  when  $j \neq 0$ , a hadron with a total angular momentum  $J = j - 1/2$  will always have a partner (called the heavy quark partner) with  $J = j + 1/2$  that must have the same properties in the heavy quark limit.

A transition from one heavy hadron  $H_\alpha$  to another  $H_\beta$ ,  $\Psi_{\alpha J}(v) \rightarrow \Psi_{\beta J'}(v')$ , through a general current  $j_C$ , will be given by a matrix element of the form,

$$\langle \Psi_{\beta J'}(v') | j_C | \Psi_{\alpha J}(v) \rangle = \langle u_{Q_\beta}(v'); s'_Q | j_C | u_{Q_\alpha}(v); s_Q \rangle_\beta \langle \text{light}; v', j', m_{j'} | \text{light}; v, j, m_j \rangle_\alpha. \quad (2.63)$$

If we take the vector current

$$j_V^\mu = \bar{u}_Q \gamma^\mu u_Q, \quad (2.64)$$

as an example, and we calculate the matrix element for the case of a meson with  $j = 1/2$ , we get

$$\begin{aligned} \langle \Psi_{J'}(v') | \bar{u}_Q \gamma^\mu u_Q | \Psi_J(v) \rangle &= \langle u_Q(v'); s'_Q | \bar{u}_Q \gamma^\mu u_Q | u_Q(v); s_Q \rangle \langle \text{light}; v', m_{j'} | \text{light}; v, m_j \rangle = \\ &= 2m_H \delta_{s'_Q s_Q} \langle \text{light}; v', m_{j'} | \text{light}; v, m_j \rangle = 2m_H \delta_{s'_Q s_Q} \delta_{m'_j m_j} \left( \xi(\omega) + \mathcal{O}\left(\frac{1}{m_Q}\right) \right), \end{aligned} \quad (2.65)$$

where  $\omega = v' \cdot v$  and  $\xi(\omega)$  is the Isgur-Wise function which encodes the non-perturbative dynamics of the interaction. For  $v' = v$  (zero recoil),  $\xi(1) = 1$  [145] and we get the transition amplitude entirely from HQSS arguments. For  $v' \neq v$ , the Isgur-Wise function does not depend on the heavy quark degrees of freedom, as it will only depend on the quantum numbers of the  $ldof$  and thus will be the same for heavy quark partners.

### Heavy Baryon States

In this thesis we are interested in the study of baryons with one heavy quark and light degrees of freedom with  $j = 0, 1, \dots$ . Then, we must generalize the procedure used in Eq. (2.65).

From Eq. (2.50) one gets that the free Dirac equation for a heavy quark is given,

$$(i\partial - m_Q)\Psi_Q(x) = 0, \quad (2.66)$$

or, for a Dirac spinor,

$$(\not{p}_Q - m_Q)u_Q(v) = 0 \Leftrightarrow \psi u_Q(v) = u_Q(v) - \frac{\not{k}}{m_Q}u_Q(v) \xrightarrow{m_Q \rightarrow \infty} u_Q(v). \quad (2.67)$$

Then, in the HQSS limit, the Dirac equation for a heavy quark can be written as

$$\psi u_Q(v) = u_Q(v) + \mathcal{O}\left(\frac{1}{m_Q}\right), \quad (2.68)$$

where  $u_Q(v)$  is the positive energy spinor.

For a heavy baryon with  $j = 0$  and  $J = 1/2$ , all the system will be described by a simple spinor  $\psi = u(v)$  that obeys Eq. (2.68)<sup>4</sup>

$$\psi u(v) = u(v). \quad (2.69)$$

For  $j = 1$ , we will have two heavy quark partners with  $J = 1/2$  and  $J = 3/2$ . The  $J = 3/2$  baryon will no longer be described by a simple spinor, but a Rarita-Schwinger spinor,  $\psi^\mu(x)$ , which obeys the Rarita-Schwinger equations,

$$(i\partial - M)\Psi^\mu(x) = 0, \quad (2.70a)$$

$$\gamma_\mu \Psi^\mu(x) = 0, \quad (2.70b)$$

which give a third condition

$$\partial_\mu \Psi^\mu(x) = 0. \quad (2.71)$$

---

<sup>4</sup>We drop the terms  $\mathcal{O}\left(\frac{1}{m_Q}\right)$  for the rest of the section, for simplicity.

Then, in momentum space, the Rarita-Schwinger (RS) spinors obey,

$$(\not{p} - M)u^\mu = 0, \quad (2.72a)$$

$$p_\mu u^\mu = \gamma_\mu u^\mu = 0. \quad (2.72b)$$

These spinors can be obtained by combining a Dirac spinor [ $u(p, s)$ ] and spin-1 vector [ $\epsilon^\mu(p, \lambda)$ ],

$$u_\mu(p, s_R) = \sum C \left( 1 \lambda \frac{1}{2} s \left| \frac{3}{2} s_R \right. \right) \epsilon_\mu(p, \lambda) u(p, s), \quad (2.73)$$

with  $s = \pm 1/2$  the third component of the  $1/2$  spin and  $\lambda$  the polarization of the vector  $\epsilon^\mu(p, \lambda)$ .

For a heavy quark spinor with  $j = 1$ ,  $\psi_{3/2}^\mu$ , Eqs. (2.72) become

$$\psi \psi_{3/2}^\mu = \psi_{3/2}^\mu, \quad (2.74a)$$

$$v_\mu \psi_{3/2}^\mu = \gamma_\mu \psi_{3/2}^\mu = 0, \quad (2.74b)$$

A heavy quark spinor, with  $J = 1/2$  and  $3/2$  components, will have a form like [148]

$$\psi^\mu = A^\mu u, \quad (2.75)$$

with  $A^\mu$  the  $j = 1$  part and  $u$  a Dirac spinor, with the following spin sums

$$\sum_{i=1,2} u^{(i)} \bar{u}^{(i)} = \frac{1 + \not{v}}{2} = \Lambda_+, \quad (2.76a)$$

$$\sum_{i=1,2,3} A_\mu^{*(i)} A_\nu^{(i)} = -g_{\mu\nu} + v_\mu v_\nu. \quad (2.76b)$$

Furthermore,  $\psi^\mu$  can be decomposed into  $1/2$  and  $3/2$  components,

$$\psi^\mu = \psi_{1/2}^\mu + \psi_{3/2}^\mu. \quad (2.77)$$

Then, by writing [148],

$$\psi_{3/2}^\mu = \left[ \delta_\nu^\mu - \frac{1}{3} (\gamma^\mu + v^\mu) \gamma_\nu \right] \psi^\nu, \quad (2.78a)$$

$$\psi_{1/2}^\mu = \frac{1}{3} (\gamma^\mu + v^\mu) \gamma_\nu \psi^\nu, \quad (2.78b)$$

Eqs. (2.74) and (2.77) are fulfilled. The spin- $1/2$  component can also be written in terms of the positive energy Dirac spinor  $\tilde{\psi}$ ,

$$\psi_{1/2}^\mu = \sqrt{\frac{1}{3}} (\gamma^\mu + v^\mu) \gamma_5 \tilde{\psi}, \quad (2.79)$$

with

$$\tilde{\psi} = \sqrt{\frac{1}{3}} \gamma_5 \gamma_\nu \psi_{1/2}^\nu. \quad (2.80)$$

Finally, from Eqs. (2.76), one gets

$$\sum_{i=1,2} \psi_{1/2}^\mu \bar{\psi}_{1/2}^\nu = -\frac{1}{3} \Lambda_+ (\gamma^\mu - v^\mu) (\gamma^\nu - v^\nu), \quad (2.81a)$$

$$\sum_{i=1,2,3} \psi_{3/2}^\mu \bar{\psi}_{3/2}^\nu = \Lambda_+ \left[ -g^{\mu\nu} + v^\mu v^\nu + \frac{1}{3} (\gamma^\mu - v^\mu) (\gamma^\nu - v^\nu) \right]. \quad (2.81b)$$

For the general case for arbitrary integer  $j$ , we will have the spinor [148],

$$\psi^{\mu_1 \dots \mu_j} = A^{\mu_1 \dots \mu_j} u, \quad (2.82)$$

which can also be separated into heavy quark partners,

$$\psi^{\mu_1 \dots \mu_j} = \psi_{j-1/2}^{\mu_1 \dots \mu_j} + \psi_{j+1/2}^{\mu_1 \dots \mu_j}. \quad (2.83)$$

The  $j - 1/2$  component can be written as,

$$\psi_{j-1/2}^{\mu_1 \dots \mu_j} = \frac{1}{2j+1} \left[ (\gamma^{\mu_1} + v^{\mu_1}) \gamma_{\nu_1} \delta_{\nu_2}^{\mu_2} \dots \delta_{\nu_j}^{\mu_j} + \dots + \delta_{\nu_1}^{\mu_1} \dots \delta_{\nu_{j-1}}^{\mu_{j-1}} (\gamma^{\mu_j} + v^{\mu_j}) \gamma_{\nu_j} \right] \psi^{\nu_1 \dots \nu_j}, \quad (2.84)$$

or, in terms of lower dimension spinors,

$$\begin{aligned} \psi_{j-1/2}^{\mu_1 \dots \mu_j} = & \sqrt{\frac{1}{2j+1}} \left[ (\gamma^{\mu_1} + v^{\mu_1}) \gamma_5 \tilde{\psi}^{\mu_2 \dots \mu_j} + (\gamma^{\mu_2} + v^{\mu_2}) \gamma_5 \tilde{\psi}^{\mu_1 \mu_3 \dots \mu_j} + \dots \right. \\ & \left. + (\gamma^{\mu_j} + v^{\mu_j}) \gamma_5 \tilde{\psi}^{\mu_1 \dots \mu_{j-1}} \right], \end{aligned} \quad (2.85)$$

with

$$\tilde{\psi}^{\mu_1 \dots \mu_{i-1} \mu_{i+1} \dots \mu_j} = \sqrt{\frac{j}{2j+1}} \gamma_5 \gamma_{\mu_i} \psi_{j-1/2}^{\mu_1 \dots \mu_j}. \quad (2.86)$$

As in the  $j = 1$  case,  $\psi_{j+1/2}^{\mu_1 \dots \mu_j}$  can be written in terms of the partner.

### Matrix Elements

The light part of the matrix element in Eq. (2.63) can be written as,

$$\beta \langle \text{light}; v', j', m_{j'} | \text{light}; v, j, m_j \rangle_\alpha = A^{i\nu_1 \dots \nu_{j'}} A^{\mu_1 \dots \mu_j} \zeta_{\nu_1 \dots \nu_{j'}; \mu_1 \dots \mu_j}^{\alpha\beta}, \quad (2.87)$$

where  $\zeta_{v_1 \dots v_{j'}; \mu_1 \dots \mu_j}^{\alpha\beta}$  is a tensor that contains all the possible Isgur-Wise functions,  $\xi(\omega)$ , and is given by [148]

$$\zeta_{v_1 \dots v_{j'}; \mu_1 \dots \mu_j}^{\alpha\beta} = (-1)^j \Delta_{v_{j+1}} \dots \Delta_{v_{j'}} \left[ \xi_0^{(j',j)}(\omega) g_{v_1 \mu_1} \dots g_{v_j \mu_j} + \xi_1^{(j',j)}(\omega) \Delta_{v_1} \Delta_{\mu_1} \times \right. \\ \left. g_{v_2 \mu_2} \dots g_{v_j \mu_j} + \dots + \xi_j^{(j',j)}(\omega) \Delta_{\mu_1} \Delta_{v_1} \dots \Delta_{v_j} \Delta_{\mu_j} \right], \quad (2.88)$$

with  $\Delta_\mu = (v'_\mu - v_\mu)$ . Then, using a general current,

$$j_C = \bar{u}_{Q_\beta} \Gamma u_{Q_\alpha}, \quad (2.89)$$

the matrix element for a general  $j$  to  $j'$  transition becomes,

$$\langle \psi_{\beta j'}(v') | j_C | \psi_{\alpha j}(v) \rangle = -\sqrt{4MM'} A^{v_1 \dots v_{j'}} \bar{u}_\beta \Gamma u_\alpha A^{\mu_1 \dots \mu_j} \zeta_{v_1 \dots v_{j'}; \mu_1 \dots \mu_j}^{\alpha\beta}. \quad (2.90)$$

Then, using Eq.(2.83), Eq. (2.63) becomes

$$\langle \psi_{\beta j' \pm 1/2}(v') | j_C | \psi_{\alpha j \pm 1/2}(v) \rangle = -\sqrt{4MM'} \bar{\psi}_{j' \pm 1/2}^{v_1 \dots v_{j'}} \Gamma \psi_{j \pm 1/2}^{\mu_1 \dots \mu_j} \zeta_{v_1 \dots v_{j'}; \mu_1 \dots \mu_j}^{\alpha\beta} \quad (2.91)$$

This formalism can also be extended to half-integer  $j$  (mesons). However, this case is not relevant for this thesis and so we will not show it here. For more information the reader is referred to Ref. [148].

In this section we have explored what we could find out about matrix elements involving heavy hadrons using HQSS. For the purpose of this thesis, this discussion limited to HQSS is enough. However, effective Lagrangians can also be constructed for heavy mesons and heavy baryon interactions. For more information about these theories the reader is referred to Refs. [145, 146, 150].



# Chapter 3

## Analytic Structure Of Scattering Amplitudes

### 3.1 Scattering Theory

If we have a system in an initial state  $|i\rangle$ , then the amplitude of probability that the system will be found in a final state  $|f\rangle$  will be given by

$$S_{fi} = \langle f|S|i\rangle, \quad (3.1)$$

where  $S$  is the  $S$ -matrix of the system, also known as the scattering operator. The  $S$ -matrix can be separated like

$$S = 1 - iT, \quad (3.2)$$

where 1 represents the amplitude of the system remaining unchanged by the interaction, and  $T$  the amplitude when it changes. From probability conservation (unitarity), we have that

$$S^\dagger S = 1 \Leftrightarrow (T^\dagger - T) = iT^\dagger T. \quad (3.3)$$

Since the total four momentum  $P$  of the system is conserved, then we can define an  $S$ -matrix,  $S_P$ , with a specific momentum, such that,

$$\langle f|S|i\rangle = (2\pi)^4 \delta^4(P_f - P_i) \langle f|S_P|i\rangle. \quad (3.4)$$

For a system of a single particle, its state can be written as

$$|m, j; \vec{p}, \mu\rangle, \quad (3.5)$$

with  $m$  the mass,  $j$  the spin,  $\mu$  the third spin component<sup>1</sup> and  $\vec{p}$  the three-momentum of the particle. The normalization of these states will be given by

$$\langle m, j; \vec{p}', \mu' | m, j; \vec{p}, \mu \rangle = 2E(2\pi)^3 \delta^3(\vec{p}' - \vec{p}) \delta_{\mu'\mu}, \quad (3.6)$$

with  $E = (m^2 + \vec{p}^2)^{\frac{1}{2}}$  the energy of the particle. The third component of the spin,  $\mu$ , can be related to a physical direction. For a particle at rest, the  $\mu$  represents the spin component along the  $z$ -direction. By making a boost along the  $z$ -axis, such that,

$$|m, j; \vec{0}, \mu\rangle \xrightarrow{\text{boost}} |m, j; q\hat{e}_z, \mu\rangle, \quad (3.7)$$

with  $\hat{e}_z = (0, 0, 1)$  and  $q = |\vec{p}|$  then, in this new reference frame,  $\mu$  becomes the spin component along the direction of movement, which is the definition of the helicity. Furthermore, if we now make an arbitrary rotation in the three-momentum, such that the direction of motion is no longer the  $z$ -axis,

$$|m, j; q\hat{e}_z, \mu\rangle \xrightarrow{\text{rotation}} |m, j; \vec{p}, \mu\rangle, \quad (3.8)$$

the helicity will still be given by  $\mu$ , since it is unaffected by rotations [151]. This way the state in Eq. (3.5) is defined by its helicity, and is thus an helicity state.

Using the helicity formalism is very useful for several reasons. First, even if a particle has angular momentum  $\vec{L}$ , because it is given by  $\vec{L} = \vec{r} \times \vec{p}$ , its projection along the direction of movement will always be zero. Thus,  $\mu$  will be both the spin and the total angular momentum projections. Also, as was mentioned already, helicity is invariant under rotations. It is also defined for massless particles, which means that the formalism can be used for both massive and massless particles.

The state in Eq. (3.5) can be written in a more relativistically friendly manner if one uses the four momentum of the particle,  $p_\mu = (E, \vec{p})$ ,

$$|m, j; \vec{p}, \mu\rangle \rightarrow |p_\mu, j; \mu\rangle. \quad (3.9)$$

From now on we will drop the index  $\mu$  of the four-momenta in the scattering states for the sake of clarity.

If we now consider two particle scattering, we can write a non-interaction scattering state as

$$|p_1 p_2; \mu_1 \mu_2; \gamma\rangle = |p_1, j_1; \mu_1\rangle \otimes |p_2, j_2; \mu_2\rangle, \quad (3.10)$$

where the  $\gamma$  label includes  $j_1, j_2$  and other possible quantum numbers (e.g. baryon number, strangeness, etc.). These states will have the the following normalization

<sup>1</sup>Considering the generators,  $J_i$ ,  $i = 1, 2, 3$ , of the three dimensional rotation group, the eigenvalues of  $\vec{J}^2$  will be given by  $j(j+1)$  and of  $J_3$  by  $\mu$ .



rules:

$$\langle p'_1 p'_2; \mu'_1 \mu'_2; \gamma' | p_1 p_2; \mu_1 \mu_2; \gamma \rangle = 2E_1 2E_2 (2\pi)^6 \delta^3(\vec{p}'_1 - \vec{p}_1) \delta^3(\vec{p}'_2 - \vec{p}_2) \delta_{\mu'_1 \mu_1} \delta_{\mu'_2 \mu_2} \delta_{\gamma' \gamma}. \quad (3.11)$$

Then, the initial and final states of the system can be written as,

$$|i\rangle = |p_1 p_2; \mu_1 \mu_2; \gamma\rangle, \quad (3.12a)$$

$$|f\rangle = |p'_1 p'_2; \mu'_1 \mu'_2; \gamma'\rangle. \quad (3.12b)$$

One can also write  $|i\rangle$  and  $|f\rangle$  in terms of the total four-momentum of the system,  $P = p_1 + p_2$ , such that

$$|i\rangle = |P\rangle |\alpha\rangle, \quad (3.13a)$$

$$|f\rangle = |P'\rangle |\alpha'\rangle, \quad (3.13b)$$

where  $\alpha, \alpha'$  depend on the rest of the quantum numbers, and

$$\langle P' | P \rangle = (2\pi)^4 \delta(P' - P), \quad (3.14a)$$

$$\langle \alpha' | \alpha \rangle = (2\pi)^2 \frac{4\sqrt{s}}{q} \delta(\Omega' - \Omega) \delta_{\mu'_1 \mu_1} \delta_{\mu'_2 \mu_2} \delta_{\gamma' \gamma}, \quad (3.14b)$$

with  $q = |\vec{p}_1| = |\vec{p}_2|$  in the C.M. frame. The explicit dependence of  $|\alpha\rangle$  on the angles  $\Omega = (\theta, \phi)$  and the parameters  $\mu_1, \mu_2, \gamma$  is given by [151]

$$|\alpha\rangle = \left( \frac{4\sqrt{s}}{q} \right)^{1/2} |\theta, \phi; \mu_1 \mu_2; \gamma\rangle. \quad (3.15)$$

Because of momentum conservation, we can always write the  $S$ -matrix as

$$S = 1 \otimes S_P, \quad (3.16)$$

where the identity 1 acts on the  $|P\rangle$  states, and  $S_P$  on the  $|\alpha\rangle$  states. We can also define  $T_P$  in the same way. For the two particle scattering, Eq. (3.1) becomes

$$S_{fi} = (2\pi)^4 \delta^4(P_f - P_i) \langle \alpha_f | S_P | \alpha_i \rangle, \quad (3.17)$$

and the  $T$ -matrix is given by

$$T_{fi} = (2\pi)^4 \delta^4(P_f - P_i) \langle \alpha_f | T_P | \alpha_i \rangle. \quad (3.18)$$

One can define the following function of the Mandelstam variables  $s$  and  $t$ ,

$$T(s, t) \equiv \langle \alpha_f | T_P | \alpha_i \rangle = 4 \sqrt{\frac{s}{qq'}} \langle \theta, \phi; \mu_1 \mu_2; \gamma | T_P | \theta', \phi'; \mu'_1 \mu'_2; \gamma' \rangle, \quad (3.19)$$

with  $q' = |\vec{p}'_1| = |\vec{p}'_2|$  the momentum of the final state particles in the C.M. frame.

With these tools, we can write Eq. (3.3) as

$$\langle f|T^\dagger|i\rangle - \langle f|T|i\rangle = i \sum_{\lambda_\beta} \int \frac{dQ d\Omega}{(2\pi)^6} \frac{q}{4\sqrt{s}} \langle f|T^\dagger|Q, \beta\rangle \langle Q, \beta|T|i\rangle, \quad (3.20)$$

where we used the projection operator for the states in Eq. (3.13),

$$1 = \sum_{\lambda_\beta} \int \frac{dQ d\Omega}{(2\pi)^6} \frac{q}{4\sqrt{s}} |Q, \beta\rangle \langle Q, \beta|, \quad (3.21)$$

with  $\sum_{\lambda_\beta}$ , the sum over the quantum numbers of  $|\beta\rangle$  and  $Q$  the total momentum of the  $|Q, \beta\rangle$  states. Using Eqs. (3.13) and (3.14a), we get

$$T^*(s, t) - T(s, t) = i \frac{q}{4\sqrt{s}} \sum_{\lambda_\beta} \int \frac{d\Omega}{(2\pi)^2} \langle \alpha_f|T^\dagger|\beta\rangle \langle \beta|T|\alpha_i\rangle. \quad (3.22)$$

### 3.1.1 Partial Wave Amplitudes

Because of conservation of total angular momentum, a scattering amplitude  $T(s, t)$  can always be written as an expansion of partial scattering amplitudes that depend only on a specific angular momentum [151]. For initial and final scattering states  $|p_1 p_2; \mu_1 \mu_2; \gamma\rangle$  and  $|p'_1 p'_2; \mu'_1 \mu'_2; \gamma'\rangle$  (respectively) with non-zero spin, the partial wave expansion of the amplitude can be written as

$$T(s, t) = \sum_j (2j+1) T_j(s) d_{\mu\mu'}^j(\theta), \quad (3.23)$$

where  $\mu = \mu_1 - \mu_2$ ,  $\mu' = \mu'_1 - \mu'_2$ , and

$$\begin{aligned} d_{\mu'\mu}^j(\theta) &= \langle j\mu'|e^{-i\theta J_y}|j\mu\rangle \\ &= \sum_n \frac{(-1)^n \sqrt{(j+\mu)!(j-\mu)!(j+\mu')!(j-\mu')!}}{(j-\mu'-n)!(j+\mu-n)!(n+\mu'-\mu)!n!} \\ &\quad \times [\cos(\theta/2)]^{2j+\mu-\mu'-2n} [-\sin(\theta/2)]^{\mu'-\mu+2n}, \end{aligned} \quad (3.24)$$

the Wigner small  $d$ -matrix.

At lot of properties relating to the analyticity of the partial wave amplitudes can be studied for zero spin which remain valid for higher spins [151]. Thus, it is useful to study this specific case. For scalar particles we have that  $\mu' = \mu = 0$ , and  $d_{00}^j = P_j(\cos\theta)$ , and the partial wave expansion can be written as

$$T(s, t) = \sum_{l=0}^{\infty} (2l+1) T_l(s) P_l(\cos\theta). \quad (3.25)$$

Redefining the partial wave amplitude, such that

$$T_l(s) = -8\pi\sqrt{s} f_l(s), \quad (3.26)$$

then Eq. (3.25) becomes

$$T(s, t) = -8\pi\sqrt{s} \sum_{l=0}^{\infty} (2l+1) f_l(s) P_l(\cos\theta), \quad (3.27)$$

The unitary condition in Eq. (3.22) for partial waves becomes

$$\begin{aligned} \sum_{l=0}^{\infty} (2l+1) P_l(\cos\theta) [f_l^*(s) - f_l(s)] &= i \frac{q}{4\sqrt{s}} \sum_{l'} (2l'+1) f_{l'}(s) \int \frac{d\Omega}{(2\pi)^2} T^*(s, \cos\beta) \\ &\times P_{l'}(\cos\beta) = i \frac{q}{4\sqrt{s}} \sum_{l'} (2l'+1) f_{l'}(s) \int_{-1}^1 \frac{dx'}{(2\pi)} T^*(s, x') P_{l'}(x) = \\ &= -2iq \sum_{l'} (2l'+1) f_{l'}(s) f_{l'}^*(s), \end{aligned} \quad (3.28)$$

where we have used the fact that

$$T^*(s, t) = -8\pi\sqrt{s} \sum_l (2l+1) f_l^*(s) P_l(\cos\theta). \quad (3.29)$$

Then, Eq. (3.28) becomes

$$f_l^*(s) - f_l(s) = -2i \operatorname{Im} f_l(s) = -2iq |f_l(s)|^2. \quad (3.30)$$

Or, using the inverse of the amplitudes,

$$\operatorname{Im} f_l^{-1}(s) = -q, \quad \operatorname{Im} T_l^{-1}(s) = \rho(s) \quad (3.31)$$

with

$$\rho(s) = \frac{q}{8\pi\sqrt{s}}, \quad (3.32)$$

the phase space factor.<sup>2</sup>

From Eq. (3.23) one can also write the boson-fermion partial wave scattering amplitudes, which are useful to describe meson-baryon interactions. Separating the

---

<sup>2</sup>Note that, below the threshold of the interacting particles, the phase space of the reaction is zero. So, there is an implicit Heaviside function  $\Theta(s - (m_1 + m_2)^2)$  multiplying in the left side of the phase space equation above.

contributions from  $J = l + \frac{1}{2}$  and  $J = l - \frac{1}{2}$ , the operator amplitude  $T(s, t)$  can be written as<sup>3</sup> [151, 152],

$$T(s, t) = \sum_l (2l + 1) [f_{l+}(s) \hat{Q}_{l+} + f_{l-}(s) \hat{Q}_{l-}] P_l(\cos \theta), \quad (3.33)$$

with  $\hat{Q}_{l\pm}$  and  $f_{l\pm}$  the projection operators and partial wave amplitudes for  $J = l \pm \frac{1}{2}$ , respectively. The projection operators are given by [152]

$$\hat{Q}_{l+} = \frac{l + 1 + \vec{l} \cdot \vec{\sigma}}{2l + 1}, \quad (3.34a)$$

$$\hat{Q}_{l-} = \frac{l - \vec{l} \cdot \vec{\sigma}}{2l + 1}, \quad (3.34b)$$

with  $\vec{\sigma}$  the spin vectors. The amplitude of the interaction can also be separated into spin-flip ( $h(s, t)$ ) and spin non-flip parts ( $g(s, t)$ ) [151, 152],

$$T(s, t) = g(s, t) + ih(s, t) \vec{\sigma} \cdot \hat{n}, \quad (3.35)$$

with

$$\hat{n} = \frac{\vec{p}'_2 \times \vec{p}_2}{|\vec{p}'_2 \times \vec{p}_2|}, \quad (3.36)$$

and  $\vec{p}_2, \vec{p}'_2$  the momentum of the initial and final bosons. The functions  $g$  and  $h$  have partial wave expansions of the form [151, 152]

$$g(s, t) = \sum_l [(l + 1)f_{l+}(s) + lf_{l-}(s)] P_l(\cos \theta), \quad (3.37a)$$

$$h(s, t) = \sin \theta \sum_l [f_{l+}(s) - f_{l-}(s)] P'_l(\cos \theta). \quad (3.37b)$$

For  $s$ -wave ( $l = 0$ ), only the  $g(s, t)$  term will survive, because of the derivative in the  $h(s, t)$  expansion. Then,

$$T(s, t)|_{l=0} = g(s, t)|_{l=0} = f_{0+}(s). \quad (3.38)$$

The projection of the full amplitude into  $s$ -wave can then be done as in the spinless case,

$$f_+(s) = \frac{1}{2} \int_{-1}^1 d \cos \theta T(s, t) P_0(\cos \theta). \quad (3.39)$$

<sup>3</sup>It is important to remember here that  $T(s, t)$  describes the scattering of two particles and as such is defined between both states.

### Chiral lowest order $s$ -wave Goldstone boson-octet baryon amplitude

This  $s$ -wave meson-baryon amplitude will be the most used throughout this thesis. From the density Lagrangian in Eq. (2.45), one can calculate the tree-level Goldstone-boson-octet baryon amplitude, which is given by [24]

$$V_{ij}(\sqrt{s}, \Omega, \vec{\sigma}_i, \vec{\sigma}_j) = -\frac{C_{ij}}{4f^2} \sqrt{\frac{E_i + M_i}{2M_i}} \sqrt{\frac{E_j + M_j}{2M_j}} \chi_{\sigma_i}^T \left[ 2\sqrt{s} - M_i - M_j \right. \\ \left. + (2\sqrt{s} + M_i + M_j) \frac{\vec{q}_i \cdot \vec{q}_j + i(\vec{q}_i \times \vec{q}_j) \cdot \vec{\sigma}}{(E_i + M_i)(E_j + M_j)} \right] \chi_{\sigma_j}, \quad (3.40)$$

where  $E_i$ ,  $M_i$ ,  $\chi_{\sigma_i}$  and  $\sigma_i$  are the energy, mass, two component Pauli spinor ( $\chi_{\sigma_i}$  and  $\chi_{\sigma_i}^T$  for its transposed) and the spin of baryon in channel  $i$ , respectively. As expected, the structure of this amplitude is indeed equal to Eq. (3.35).

The  $s$ -wave projection of the meson-baryon amplitude is given by the Weinberg-Tomozawa term,

$$V_{ij}(s) = -\frac{C_{ij}}{4f^2} (2\sqrt{s} - M_i - M_j) \sqrt{\frac{E_i + M_i}{2M_i}} \sqrt{\frac{E_j + M_j}{2M_j}} \quad (3.41)$$

$$\simeq -\frac{C_{ij}}{2f^2} (k_i^0 + k_j^0), \quad (3.42)$$

with  $k_i^0$  the energy of the meson in channel  $i$ ,

$$k_i^0 = \frac{s + m_i^2 - M_i^2}{2\sqrt{s}}. \quad (3.43)$$

The  $C_{ij}$  coefficients for SU(3) can be found in Refs. [153, 154]. In Chapters 7 and 9, we will use an extension of the Weinberg-Tomozawa term for SU(6)<sub>lsf</sub> × SU(2)<sub>HQSS</sub> symmetry, while in Chapter 8 we will use an extension within the local hidden gauge approach to account for an extra (heavy) quark, both of which will result in different  $C_{ij}$  factors.

### 3.1.2 Analyticity and Riemann Sheets

To understand why the unitarity and analyticity of the  $T$ -matrix are relevant to the study of resonances, let us look at a simple example [155]. Consider an elastic  $2 \rightarrow 2$  interaction of two identical spinless bosons with mass  $m$ . Then,

$$\rho(s) = \frac{1}{16\pi} \sqrt{\frac{s - 4m^2}{s}}, \quad (3.44)$$

and we get

$$\text{Im}T_l^{-1}(s) = \frac{1}{16\pi} \sqrt{\frac{s-4m^2}{s}}, \quad (3.45)$$

as the unitarity condition. If we write  $t_l(s)$  in the following way

$$t_l(s) = -\frac{e^{i\delta_l}}{\rho} \sin \delta_l = (-\rho \cot \delta_l + i\rho)^{-1}, \quad (3.46)$$

where  $\delta_l$  is the phase shift, we see that Eq. (3.31) is automatically fulfilled. For resonances, the amplitude is given by Eq. (1.9)

$$t_l(s) = \frac{g^2}{s - s_R + i\rho(s)g^2}, \quad (3.47)$$

where, in this case  $M_R\Gamma = g^2\rho$ , and by comparing this with Eq. (3.46), we get that,

$$\delta_l = \tan^{-1} [\rho g^2 / (s_R - s)]. \quad (3.48)$$

An interesting idea is to analyze the singularities present in Eq. (3.47), since the mass and width of a resonance can be obtained from the position of the singularities in the complex plane of  $s$ . For simplicity, let us approximate, close to the resonance mass position,  $\rho$  by  $q/(8\pi\sqrt{s_R})$ . Then,

$$t_l(s) = \frac{g^2}{s - s_R + i\frac{qg^2}{8\pi\sqrt{s_R}}} = \frac{g^2}{8A} \left[ \frac{1}{q - q_R} - \frac{1}{q + q_R^*} \right], \quad (3.49)$$

with  $q_R = A - i\gamma$ , where  $A$  is a constant defined such that  $s_R = 4(A^2 + \gamma^2 + m^2)$ , and  $\gamma = \frac{g^2}{64\pi\sqrt{s_R}}$ . As we can see in Eq. (3.49),  $t_l(s)$  will have two singularities, one in  $q = -q_R^*$  and another in  $q = q_R$ . Both singularities have a negative imaginary part, which means that if we make an analytical continuation of Eq. (3.49) into complex values of  $q$ , both singularities will appear in the lower part of the complex plane of  $q$  (see Fig. 3.1). To explain why this is important, let us explore a bit the nature of complex variables and analytic continuations.

### Riemann Sheets

Given a complex number  $z \in \mathcal{C}$ , one can write it as either,

$$z = x + iy, \quad (3.50)$$

with  $x$  and  $y \in \mathcal{R}$ , or, alternatively,

$$z = \rho e^{i\theta}, \quad (3.51)$$

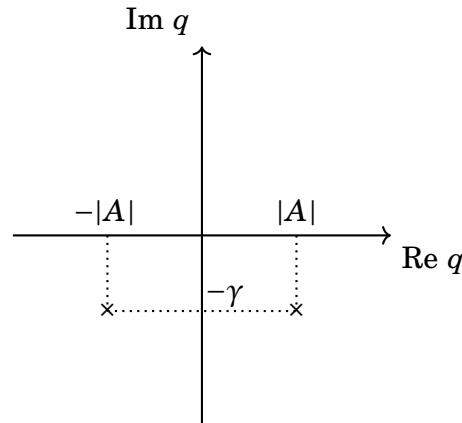


Figure 3.1: Position of the two poles of  $t_l(s)$ ,  $q_R$  and  $q_R^*$ . Note that they appear below the real axis for resonances (and on the real axis for bound states).

with  $\rho = \sqrt{x^2 + y^2}$  and  $\theta = \arctan(y/x)$ . The phase  $\theta$  is called the principal argument of the complex number  $z$ . Then, it is straightforward to see that adding a phase equal to  $2\pi$  to  $\theta$  does not change the value of  $z$ .

From  $z$ , we can also define the square root,

$$w = \sqrt{z} = \sqrt{\rho} e^{i\frac{\theta}{2}}. \quad (3.52)$$

Now, if we add  $2\pi$  to the principal argument  $\theta$  in Eq. (3.51), although  $z$  still remains the same,  $w$  changes

$$w_I = \sqrt{z} \rightarrow w_{II} = \sqrt{\rho} e^{i\frac{\theta}{2} + i\pi} = -\sqrt{z}. \quad (3.53)$$

This is by no means a unique behavior of the square root of complex numbers. Take, for example, the case of the logarithm:

$$w = \log(z) = \log(\rho) + i\theta \quad (3.54)$$

Here the situation is even more extreme, since we can have infinite different values for the same  $z$  if we add an arbitrary number  $n$  of  $2\pi$  phases,

$$w \rightarrow w_n = \log(\rho) + i\theta + 2in\pi, \quad (3.55)$$

with  $n \in \mathcal{N}$ .

This behavior is all the more interesting if we look at the square root (or the logarithm) of  $z$ , as a complex function,  $f$ , such that

$$f: \mathcal{C} \rightarrow \mathcal{C}, z \rightarrow \sqrt{z} = w. \quad (3.56)$$

From Eq. (3.53) one can see that  $f$  is a multi-valued function, that is, it can have several values for the same point  $z$ . Let us look at this problem more carefully. Take  $z = \rho + i\epsilon$ , with  $\rho, \epsilon \in \mathcal{R}$ . Then,

$$\lim_{\epsilon \rightarrow 0^+} f(\rho + i\epsilon) = \sqrt{\rho}, \quad (3.57a)$$

$$\lim_{\epsilon \rightarrow 0^-} f(\rho + i\epsilon) = \lim_{\epsilon \rightarrow 0^+} f(\rho - i\epsilon) = -\sqrt{\rho}, \quad (3.57b)$$

where the principal arguments are taken between 0 and  $2\pi$ . Or in other words, whether one approaches  $\rho$  from above or below the real axis will affect the value of the function.

One way to solve this problem is to define a branch cut, which basically means, a line where a given function is not continuous. More precisely, a branch cut is a line that connects two branch points, and a branch point is a point where  $f$  is discontinuous if we go through a small circuit around the point [156]. Our function  $f$  will have two branch points, one at  $z = 0$  and another one at  $z = \infty$ , and thus we can define the branch cut for  $z \in [0, +\infty[$ . By doing this we disconnect the space above and below this curve, and, by not being able to travel between these two spaces, we impose the desired behavior into the function – it will not be multi-valued. Our function  $f$  will not have two values for  $z \in [0, +\infty[$ , because that line is no longer part of the space where the argument  $z$  is mapped to. For values of  $z$  defined in  $\theta \in [0, 2\pi[$ , all points of  $f(z)$  will be either in  $\text{Im}(w) > 0$  or in the real axis  $\text{Re}(w) > 0$  for  $\text{Im}(w) = 0$  (see Fig. 3.2). Then, by allowing for a branch cut in the  $z$  space, we are effectively separating the region  $[\text{Im}(w) < 0 \vee (\text{Im}(w) = 0 \wedge \text{Re}(w) < 0)]$  and the region  $[\text{Im}(w) > 0 \vee (\text{Im}(w) = 0 \wedge \text{Re}(w) > 0)]$  in the  $w$  space (see Fig. 3.2b). Thus, the function cannot have two different values for a given  $z$ , and in Eq. (3.57),  $f(\rho - i\epsilon)$  will no longer be defined.

What we define as a branch cut is somewhat arbitrary, provided it connects two branch points [156, 157]. For example, we have  $[0, +\infty[$  if we use  $\theta \in [0, 2\pi[$ , but if one were to define the domain of  $\theta$  as  $[-\pi, \pi[$ , the branch cut would be defined as  $z \in ]-\infty, 0]$ .

There is another way of describing these types of multi-valued functions. In Eq. (3.56), instead of starting from a general complex plane  $\mathcal{C}$  and going to a space defined through a branch cut, one can divide the original space into subspaces  $C_n$ , such that for each  $C_n$  no two values of  $z$  give the same  $w$ . For example, in the case of the square root function, we only need two subspaces:

$$C_I = \{z \in \mathcal{C} : \text{Arg}(z) \in [0, 2\pi]\}, \quad (3.58a)$$

$$C_{II} = \{z \in \mathcal{C} : \text{Arg}(z) \in [2\pi, 4\pi]\}, \quad (3.58b)$$

since adding another  $2\pi$  to the domain of  $\theta$  takes us back to  $C_I$ . Because of this, it is no longer sufficient to define a function  $f$  that accepts an argument  $z$ , one also has



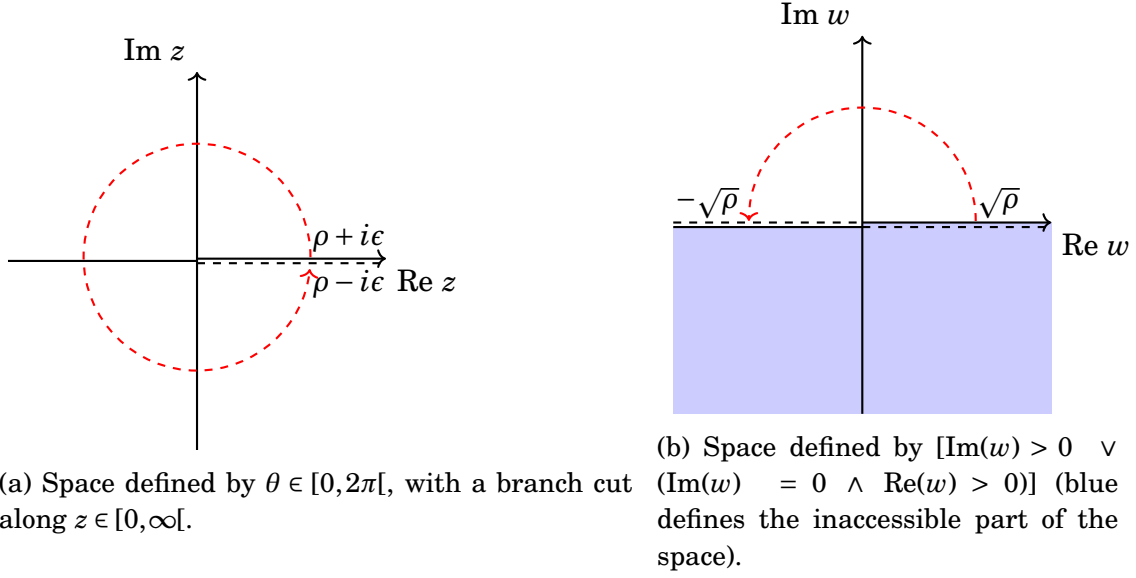


Figure 3.2: Subspaces in the complex plane of  $z$  (a) and  $w$  (b). Here, we no longer have a two valued function defined in all of  $w$ -plane, a function defined only in one of the subspaces that originate from the existence of a branch cut along  $z \in [0, \infty[$ .

to define in which subspace our argument lives. Then, we define a parameter  $n$  that we use to specify the space, which works almost like a second argument, alongside  $z$ . Thus,

$$f_n : \mathcal{C}_n \rightarrow \mathcal{C}, z \rightarrow \sqrt{z} = w. \quad (3.59)$$

This solves the discontinuity problem because now we define  $f = f_I$  above the real axis and  $f = f_{II}$  below,

$$f_I(\rho + i\epsilon) = \sqrt{\rho} e^{i\epsilon/2} \simeq \sqrt{\rho} \simeq f_{II}(\rho - i\epsilon) = \sqrt{\rho} e^{2i\pi - i\epsilon/2}, \quad (3.60)$$

and

$$f_I(\rho - i\epsilon) = \sqrt{\rho} e^{i\pi - i\epsilon/2} \simeq -\sqrt{\rho} \simeq f_{II}(\rho + i\epsilon) = \sqrt{\rho} e^{i\pi + i\epsilon/2}. \quad (3.61)$$

Functions in physics are defined in the first Riemann sheet (FRS),  $C_I$  in this case, and to take them to the second Riemann sheet (SRS) we must do an analytic continuation. We know that,

$$f_{II}(\rho - i\epsilon) = f_I(\rho + i\epsilon). \quad (3.62)$$

and, by making some manipulations, we get

$$f_{II}(\rho + i\epsilon) = f_I(\rho - i\epsilon) = f_I(\rho - i\epsilon) - f_I(\rho + i\epsilon) + f_I(\rho + i\epsilon) \Leftrightarrow \quad (3.63)$$

$$f_{II}(\rho + i\epsilon) = -\text{Disc}[f_I(\rho)] + f_I(\rho + i\epsilon) \quad (3.64)$$

We can extend the real variable in that equation to a complex one,  $\rho \rightarrow z$ . Then, the above equation becomes,

$$f_{II}(z) = -\text{Disc}[f_I(z)] + f_I(z). \quad (3.65)$$

### Poles and Resonances

Now we can look again at Eqs. (3.46) and (3.49). We see that the amplitude of the resonance depends on the function  $\rho(s)$ , which contains a square root. Hence, everything we have talked about so far is relevant here. The amplitude  $t_l(s)$  will have a branch cut in the real axis, for  $\text{Re}(s) \in [4m^2, +\infty[$  and, in Eq. (3.49), we see that the poles associated to the resonance are in the lower half of the complex plane in the  $q \propto \rho(s)$  space. Also, in the previous section, we have seen that the lower half of the complex plane in the  $w = \sqrt{z}$  space corresponds to the SRS in the  $z$  space. Thus, we can see that the singularities associated with the resonance of Eq. (3.49) will be found in the SRS [155].

One can define the amplitude  $t_l$  in the SRS by using Eqs. (3.64) and (3.31), together with the Hermitian analyticity condition,  $t_l^*(s) = t_l(s^*)$ , and we get

$$t_{II}^{-1}(s) = -2i\rho(s) + t_{II}^{-1}(s). \quad (3.66)$$

From Eq. (3.46) and since the partial wave  $S$ -matrix for an elastic interaction is given by  $S_l = e^{2i\delta_l}$  [151], one can see that

$$t_{II}^{-1}(s) = t_{II}^{-1}(s)S_l, \quad (3.67)$$

which means that the poles found in the SRS correspond to zeros of the  $S_l$  matrix plus the poles of  $t_{II}$  [14].

The first Riemann sheet (FRS) is known as the physical sheet, and the amplitudes that we typically use in physics are defined there.

A general amplitude will depend on the Mandelstam variables. Typically, one assumes that  $T(s, t, u)$  will permit an analytical continuation over the complex planes of  $s$ ,  $t$  and  $u$ , apart from certain singularities of “physical origin”. This is known as the Mandelstam Hypothesis. While constructing amplitudes, usually it is taken as a postulate that they must have as little singularities as possible [151] (typically the ones required by unitarity) which appear in the real axis. However, as we have seen in Eq. (3.67), the amplitudes in the SRS will have extra singularities in the complex plane, which can correspond to resonances. Even though these poles are in the non-physical sheet, since both sheets are connected for  $\text{Re}(s) \in [4m^2, +\infty[$ , these poles can still influence the real axis, which is the region that we observe in experiments.

In Fig. 3.3 we show an example of an amplitude in both sheets. Notice how both sheets connect in the real axis.

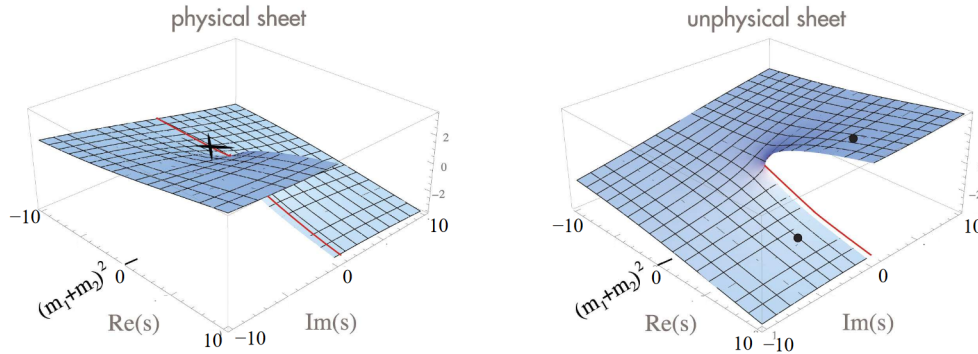


Figure 3.3: Plot of an hypothetical amplitude (z-axis) in terms of the real and imaginary part of  $s$ . Picture taken from Ref.'s [110] review of “Resonances”.

This direct analysis between the case of  $f(z) = \sqrt{z}$  and  $\rho(s) \propto \sqrt{s - 4m^2}$  rests on the fact that we have made the substitution  $\rho = \frac{q}{8\pi\sqrt{s}} \rightarrow \frac{q}{8\pi\sqrt{s_R}}$ . The real  $\rho(s)$  is a bit more complicated, since besides the branch cut for  $\text{Re}(s) \in [4m^2, +\infty[$ , because of the  $\sqrt{s}$  in the denominator, we would have another branch cut for  $\text{Re}(s) \in ]-\infty, 0]$ .<sup>4</sup> It is typical while studying hadronic resonances to neglect the left-hand cut [32, 158, 159]. If one wants to take it into account, the usual way is to use the N/D method. In this method  $t_l(s)$  is defined as a quotient of two functions,

$$t_l(s) = \frac{N_l(s)}{D_l(s)}, \quad (3.68)$$

where  $N_l(s)$  contains the left-hand cut, and  $D_l(s)$  contains the right-hand cut. Any other singularities that could be found in one of these functions can always be redefined as zeros of the other function. This way, the study of each of these branch cuts can be done using separate functions. An interesting result that comes from the N/D method, as shown in Refs. [32, 158–160], is that one can express the amplitude  $t_l(s)$  as

$$t_l^{-1}(s) = v_l^{-1}(s) - g_l(s), \quad (3.69)$$

with  $g_l(s)$  a function that has the right-hand cut, and  $v_l^{-1}(s)$  a function that has the contributions from other pole terms and crossed channel dynamics, but not the right-hand cut. The function  $g_l(s)$  is given by the scalar loop function [32, 158, 159]

$$g_l(s) \propto G(s) = i \int \frac{d^4q}{(2\pi)^4} \frac{1}{(P-q)^2 - m_1^2 + i\epsilon} \frac{1}{q^2 - m_2^2 + i\epsilon}, \quad (3.70)$$

<sup>4</sup>For scattering of particles with different masses there can also be a circular cut in the complex  $s$ -plane, defined by  $|s| = |m_2^2 - m_1^2|$ , however we shall consider only the right- and left-hand cuts, as was done in Ref. [158].

in case of two mesons interacting and,

$$G(s) = i \int \frac{d^4 q}{(2\pi)^4} \frac{2M_1}{(P-q)^2 - M_1^2 + i\epsilon} \frac{1}{q^2 - m_2^2 + i\epsilon}, \quad (3.71)$$

in case of meson-baryon interaction. Here,  $P$  is the total momentum of the system.

As we will see in the following section, the function  $v_l(s)$  can be related to the amplitudes of the effective fields studied in Chapter 2.

## 3.2 Unitarity in Coupled Channels

The equations studied in the previous sections were deduced for elastic scattering. However, they can be generalized to inelastic multichannel scattering in a straightforward way. In this case, for  $N$  channels, the unitary condition becomes

$$\text{Im} [t_l]_{ij} = - \sum_{k=1}^N [t_l^*]_{ik} \rho_k [t_l]_{kj} \theta(s - s_k), \quad (3.72)$$

with  $s_k$  and  $\rho_k$  the threshold and phase space of the  $k$ th channel, respectively (from now on and for simplicity, the partial wave label  $l$  will be left implicit). In matrix notation

$$\text{Im} t = -t^\dagger \rho t, \quad (3.73)$$

where  $\rho = \text{Diag}\{\rho_1 \theta(s - s_1), \dots, \rho_N \theta(s - s_N)\}$ . Then Eq. (3.31) becomes

$$\text{Im} t^{-1} = \rho. \quad (3.74)$$

### 3.2.1 Bethe-Salpeter equation and the chiral unitary approach

Consider the elastic scattering of two particles  $A$  and  $B$ . One can calculate perturbatively this amplitude,  $T(p, k; p', k')$ , using the effective theories discussed in Chapter 2, which we shall represent as

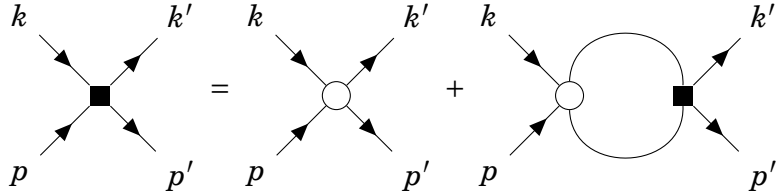
$$, \quad (3.75)$$

where  $p$  and  $k$  are the initial momenta, and  $p'$ ,  $k'$  the final momenta, respectively, of  $A$  and  $B$ . Given one perturbative order, one can re-sum some higher order to restore

unitarity by solving the Bethe-Salpeter equation (BSE) [161],

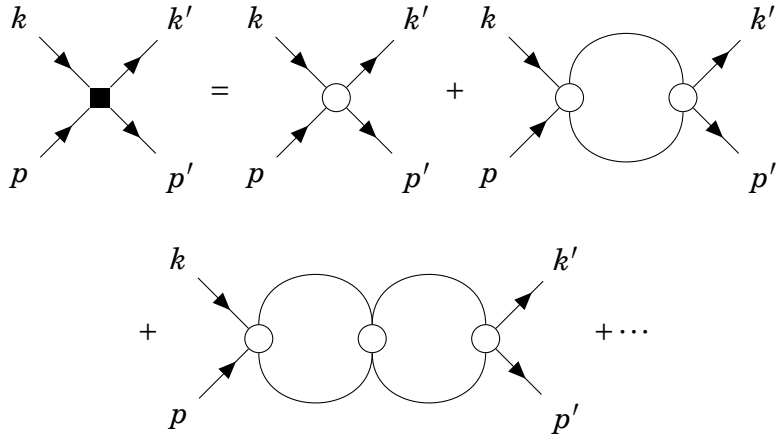
$$T(p, k; p', k') = V(p, k; p', k') + i \int \frac{d^4 q}{(2\pi)^4} V(p, k; q, p + k - q) \Delta_A(q) \times \Delta_B(p + k - q) T(q, p + k - q; p', k') \quad (3.76)$$

with  $V(p, k; p', k')$  and  $\Delta_i$ , the perturbative two particle irreducible amplitude and particles  $A$  and  $B$  propagators, respectively. The amplitude  $V(p, k; p', k')$  in this equation is typically called the kernel. The BSE fulfills the two particle unitary condition (Eq. (3.3)) [161], while, at the same time, taking into account the symmetries of our (effective) field theory through the kernel. In terms of Feynman diagrams, the new BSE amplitude is represented as,



$$\quad (3.77)$$

which we can expand as



$$\quad (3.78)$$

The unitarized amplitude will contain the original kernel, plus the rescattering amplitudes of  $A$  and  $B$ .

At lowest order, in addition to considering the kernel at tree level, the particle propagators are approximated by the free ones [161, 162]

$$V(p, k; p', k') \simeq V_0(p, k; p', k'), \quad (3.79a)$$

$$\Delta_i(q) \simeq \Delta_{i0} = [q^2 - m^2 + i\epsilon]^{-1}, \quad (3.79b)$$

from where one gets,

$$G(p, k) = i \int \frac{d^4 q}{(2\pi)^4} \Delta_{A0}(q) \Delta_{B0}(p + k - q), \quad (3.80)$$

which is equal to the loop function in Eq.(3.70). In the case of the meson-baryon interaction, the loop function needs to be multiplied by two times the mass of the baryon, within our normalizations.

It is common to take the  $s$ -wave projection of the amplitudes, which we write as  $T(p, k; p', k') \rightarrow t(s)$  and  $V(p, k; p', k') \rightarrow V(s)$ . Another common simplification is to take only into account the on-shell contribution of the kernel, where  $q^2 = m^2$ , which means that the kernel and the  $T$ -matrix can be factored out of the integral in Eq. (3.76). For an  $s$ -wave Weinberg-Tomozawa (WT) type kernel and a cutoff regularization scheme, it was shown in Refs. [31, 122, 163] that the off-shell contributions will be reabsorbed in the lowest order Lagrangians by a suitable renormalization. In general, as it was proven in Ref. [161] for  $\pi\pi$  scattering, the off-shell terms will be reabsorbed by a suitable renormalization of the effective theory involving higher perturbative orders. Then, from now on, we will use the on-shell approximation and take into account only the on-shell part of the kernel. In this way, Eq. (3.76) becomes

$$t(s) = V(s) + V(s) G(s) t(s). \quad (3.81)$$

Then, if we develop the geometric series, we get,

$$t(s) = \frac{V(s)}{1 - V(s) G(s)}. \quad (3.82)$$

We can extend these equations to multiple channels by defining the matrices,

$$t_{ij} = t(p_i, k_i; p'_j, k'_j); \quad V_{ij} = V(p_i, k_i; p'_j, k'_j); \quad G_{ij} = \delta_{ij} G(p_i, k_i), \quad (3.83)$$

and, again for  $s$ -wave, we get

$$t(s) = [1 - V(s)G(s)]^{-1}V(s). \quad (3.84)$$

If we take the inverse of  $t$ , we get

$$t^{-1}(s) = V^{-1}(s) - G(s), \quad (3.85)$$

which is equal to Eq. (3.69) for  $V(s) = v_l(s)$ , ( $l = 0$ ).

The chiral unitary approach (CUA) is defined by the scheme outlined in this subsection. Within this approach, the amplitudes obtained from the chiral effective Lagrangians are unitarized using the BSE. This non-perturbative resummed amplitudes,

in some cases, give rise to dynamically generated resonances or bound states, after they are properly renormalized, as we will discuss in the next Secs. 3.2.3 and 3.2.2.

For simplicity, although abusing notation, we will systematically refer to CUA as any unitary scheme in coupled channels, regardless of whether  $\chi$ PT is not used to calculate the BSE kernel.

### 3.2.2 Regularizing the loop function

For the sake of simplicity, we shall only write here the expressions for the meson-baryon loop function, keeping in mind that for the meson-meson case one needs to remove the extra factor  $2M$  multiplying the loop function.

The loop function defined in Eq. (3.80) is ultraviolet (UV) divergent and it needs to be regularized. Usually, this is accomplished in one of two ways: either by using dimensional regularization or a cutoff in the three momenta. Using dimensional regularization, one introduces a subtraction constant  $a(\mu)$  that depends on an energy scale  $\mu$ , such that for free propagators one gets<sup>5</sup>

$$G_i^R(s) = \frac{2M_i}{16\pi^2} \left[ a_i(\mu) + \log \frac{M_i^2}{\mu^2} + \frac{s + m_i^2 - M_i^2}{2s} \log \frac{m_i^2}{M_i^2} + \frac{|\vec{k}_i|}{\sqrt{s}} \times \left\{ \log \frac{-s - \Delta_i + 2\sqrt{s}q_i}{s - \Delta_i + 2\sqrt{s}q_i} + \log \frac{-s + \Delta_i + 2\sqrt{s}q_i}{s + \Delta_i + 2\sqrt{s}q_i} \right\} \right], \quad (3.86)$$

with,

$$|\vec{k}_i| = \frac{\lambda^{1/2}(s, M_i^2, m_i^2)}{2\sqrt{s}}, \quad (3.87)$$

$\Delta_i = M_i^2 - m_i^2$  and  $M_i$  ( $m_i$ ) the baryon (meson) mass, and  $\lambda(x, y, z)$  the ordinary Källén function. In general, this regularization scheme does not depend on the energy scale  $\mu$ , since any changes on the scale can be reabsorbed into the subtraction constant  $a(\mu)$  [164].

Alternatively, one can use a cutoff in the three momentum. Integrating out the  $q^0$  component in Eq. (3.80), the loop function is given by [165],

$$G_i(s) = 2M_i \int \frac{d^3q}{(2\pi)^3} \frac{\Omega_i(\vec{q})}{s - (\omega_i(\vec{q}) + E_i(\vec{q}))^2 + i\epsilon}, \quad (3.88)$$

with  $\omega_i(\vec{q}) = \sqrt{\vec{q}^2 - m_i^2}$ ,  $E_i(\vec{q}) = \sqrt{\vec{q}^2 - M_i^2}$  and

$$\Omega_i(\vec{q}) = \frac{E_i(\vec{q}) + \omega_i(\vec{q})}{2E_i(\vec{q})\omega_i(\vec{q})}. \quad (3.89)$$

<sup>5</sup>Since we will be discussing several regularization methods, it is useful to add the  $R$  label to the loop function in Eq.(3.86), although outside of this section, no such distinction will be made.

To regularize this function using a cutoff, one can introduce a factor  $f(|\vec{q}|, \Lambda_i)$ , such that for  $|\vec{q}| > \Lambda$  the factor tends to zero in such a way that these terms do not contribute to the integral in Eq.(3.88). Then,  $\Lambda_i$  will be our cutoff, which *a priori* does not have to be the same for all channels (hence the subscript  $i$ ). The loop function becomes,

$$G_i^\Lambda(s) = 2M_i \int \frac{d^3q}{(2\pi)^3} \frac{\Omega_i(\vec{q})f(|\vec{q}|, \Lambda_i)}{s - (\omega_i(\vec{q}) + E_i(\vec{q}))^2 + i\epsilon}. \quad (3.90)$$

The two most common factors correspond to a Gaussian-cutoff and a sharp-cutoff,

$$f(|\vec{q}|, \Lambda_i)|_{\text{gaussian}} = e^{-2(|\vec{q}|^2 - |\vec{k}|^2)/\Lambda_i^2}, \quad (3.91a)$$

$$f(|\vec{q}|, \Lambda_i)|_{\text{sharp}} = \Theta(\Lambda_i - |\vec{q}|), \quad (3.91b)$$

with  $\Theta(x)$  the Heaviside function. In this thesis, we will use the sharp-cutoff. Then, the loop function becomes [166],

$$G_i^\Lambda(s) = \frac{2M_i}{16\pi^2} \left[ \frac{|\vec{k}_i|}{\sqrt{s}} \left\{ \log \frac{s - \Delta_i + 2\sqrt{s}|\vec{k}_i|\sqrt{1 + \frac{m_i^2}{\Lambda_i^2}}}{-s + \Delta_i + 2\sqrt{s}|\vec{k}_i|\sqrt{1 + \frac{m_i^2}{\Lambda_i^2}}} + \log \frac{s + \Delta_i + 2\sqrt{s}|\vec{k}_i|\sqrt{1 + \frac{M_i^2}{\Lambda_i^2}}}{-s - \Delta_i + 2\sqrt{s}|\vec{k}_i|\sqrt{1 + \frac{M_i^2}{\Lambda_i^2}}} \right\} \right. \\ \left. + \log \frac{m_i M_i}{\Lambda_i^2} - \frac{\Delta_i}{s} \log \frac{m_i}{M_i} - \log \left[ \left( 1 + \sqrt{1 + \frac{m_i^2}{\Lambda_i^2}} \right) \left( 1 + \sqrt{1 + \frac{M_i^2}{\Lambda_i^2}} \right) \right] + \frac{\Delta_i}{s} \log \frac{1 + \sqrt{1 + \frac{m_i^2}{\Lambda_i^2}}}{1 + \sqrt{1 + \frac{M_i^2}{\Lambda_i^2}}} \right]. \quad (3.92)$$

It is also common to find in the literature [31, 164] calculations of the loop function using a sharp-cutoff while neglecting the negative energy term of the baryon propagator in the loop function. In this case, after integrating  $q^0$ , the loop function is given by

$$G_i^\Lambda(s) = \int \frac{d^3q}{(2\pi)^3} \frac{M_i}{2E_i(\vec{q})\omega_i(\vec{q})} \frac{\Theta(\Lambda_i - |\vec{q}|)}{\sqrt{s} - \omega_i(\vec{q}) - E_i(\vec{q}) + i\epsilon}. \quad (3.93)$$

In Ref. [32], by comparing both the cutoff and subtraction constant schemes, and taking  $\Lambda = \mu$ , it was found that a cutoff near the energy region of the mass of  $\rho(770)$  (the first meson resonance) gives a “natural” value for the subtraction constant, around  $a \simeq -2$ .

In Refs. [33, 167–169] the chiral “low energy theorem”, which requires that

$$T(\mu_m^2) = V(\mu_m^2), \quad (3.94)$$



at some low energy scale  $\mu_m$  (called the subtraction scale), is used to constrain the values of the subtraction constant  $a(\mu)$ . The condition above implies that there is a value of  $\sqrt{s}$  where

$$G(\mu_m^2) = 0, \quad (3.95)$$

and since in both the right and left hand cuts,  $G(s)$  is complex, one has that [168,169]

$$M - m \leq \mu_m \leq M + m. \quad (3.96)$$

In Refs. [170,171] the subtraction scale is taken to be the same for all channels and given by

$$\mu_m = \sqrt{m_{th}^2 + M_{th}^2}, \quad (3.97)$$

with  $m_{th} + M_{th}$  the smallest threshold energy among all the channels being considered. With this prescription, which we shall call Lutz's prescription, the loop function is given by

$$G_i^L(s) = \bar{G}_i(s) - \bar{G}_i(\mu_m^2), \quad (3.98)$$

where the function  $\bar{G}(s)$  is given by the finite part of the loop function

$$G_i(s) = \bar{G}_i(s) + G_i(s_{i+}), \quad (3.99)$$

with  $s_{i\pm} = (m_i \pm M_i)^2$  and, using Eq. (3.86), we get that

$$\bar{G}_i(s) = \frac{2M_i}{16\pi^2} \left\{ \left[ \frac{M_i^2 - m_i^2}{s} - \frac{M_i - m_i}{M_i + m_i} \right] \log \frac{M_i}{m_i} + \frac{2|\vec{k}_i|}{\sqrt{s}} \left[ \log \frac{1 + \sqrt{\frac{s-s_{i+}}{s-s_{i-}}}}{1 - \sqrt{\frac{s-s_{i+}}{s-s_{i-}}}} - i\pi \right] \right\}, \quad (3.100)$$

We can relate this latter scheme with the cutoff if we regularize the divergent part of the loop function,  $G_i(s_{i+})$ , with a sharp-cutoff. Then, from Eq. (3.92), we get

$$G_i^\Lambda(s_{i+}) = \frac{1}{8\pi^2} \frac{2M_i}{m_i + M_i} \left\{ m_i \log \frac{m_i}{\Lambda_i + \sqrt{\Lambda_i^2 + m_i^2}} + M_i \log \frac{M_i}{\Lambda_i + \sqrt{\Lambda_i^2 + M_i^2}} \right\}, \quad (3.101)$$

and

$$G_i^{\Lambda_i}(s_{i+}) = -\bar{G}_i(\mu_m^2). \quad (3.102)$$

Then,

$$G_i^\Lambda(s) = \bar{G}_i(s) + G_i^{\Lambda_i}(s_{i+}). \quad (3.103)$$

Note that, in order for this equation to be fulfilled, one is obligated to use a different cutoff for each channel. If a common UV cutoff is employed for all channels within a given sector characterized by some quantum numbers, both schemes are independent and will lead to different results.

### 3.2.3 Dynamically Generated Resonances

One of the most powerful features of unitarizing the amplitudes using the Bethe-Salpeter equation is that resonances can be dynamically generated through this process. In other words, even though our original kernel does not have any explicit information about any resonance, the re-summation of these amplitudes can generate resonances. This because the full BSE amplitude obeys the unitarity properties of two particle scattering amplitudes. A famous example, already discussed in the Introduction, is the case of the  $\Lambda(1405)$ , which is a molecular state, composed mostly of  $\bar{K}N$  and  $\pi\Sigma$ , which can be dynamically generated using the BSE with a WT particle irreducible amplitude. Also, as we have seen in section 3.1.2, resonances will appear as poles in the SRS. From Eq. (3.64), we see that the SRS is defined through the equation

$$t_{II}^{-1}(s) = t_I^{-1}(s) - \text{Disc}[t_I^{-1}(s)]. \quad (3.104)$$

From Eq. (3.85) we have that

$$\text{Disc}[t_I^{-1}(s)] = \text{Disc}[V^{-1}(s)] - \text{Disc}[G(s)]. \quad (3.105)$$

The kernels we use in this thesis do not have a discontinuity in  $s > s_+$  and thus

$$\text{Disc}[t_I^{-1}(s)] = -\text{Disc}[G(s)] = -2i \text{Im } G(s). \quad (3.106)$$

Then, applying the Sokhotski–Plemelj theorem to Eq. (3.88), we get that

$$\text{Im } G(s) = -2M \frac{k(s)}{8\pi\sqrt{s}}, \quad (3.107)$$

and we can redefine the loop function such that,

$$G(s, n) = G_I(s) + i2M \frac{nk(s)}{4\pi\sqrt{s}}, \quad (3.108)$$

with  $n$  a factor that is 0 for the FRS and 1 for the SRS. Now we have a way of going from  $t_I^{-1}$  to  $t_{II}^{-1}$ .

Generalizing this for more than one channel, we can first define the vector

$$\vec{n} = (n_1, n_2, \dots, n_N), \quad (3.109)$$

with,

$$n_i = \begin{cases} 0 & \text{if } FRS \\ 1 & \text{if } SRS \end{cases}. \quad (3.110)$$

Then, one defines the loop matrix in Eq. (3.83) for  $N$  channels as  $G(s) \rightarrow G(s, \vec{n}) = \text{Diag}\{G_1(s, n_1), \dots, G_N(s, n_N)\}$ . Typically, for each channel  $i$ , one will want  $G_i$  to be in the FRS for  $s < s_{+i}$ , and in the SRS for  $s > s_{+i}$ .

Since some poles can couple only to certain channels, a useful way to see all the poles of one given sector at the same time is by defining the function [172]

$$\tilde{T}(s) = \max_j \sum_i |t_{ij}(s)|. \quad (3.111)$$

This function will be used throughout the thesis to plot pole positions.

To calculate the coupling,  $g_i$ , of a resonance to the different channels  $i$  we use the fact that, near a pole, the amplitudes for meson-baryon become,

$$t_{ij}(s) \simeq \frac{g_i g_j}{\sqrt{s} - \sqrt{s_R}},$$

with  $s_R = (M_R - i\Gamma_R/2)^2$ . Since the couplings  $g_i$  can be complex, the relative signs between the real and imaginary parts of the couplings are very important. The method we use to obtain the complex couplings is as follows: First we assign an arbitrary sign to one of the non-zero couplings,  $g_a$ , such that  $g_a = |g_a|$ . Then, we have, that

$$g_a^2 = \lim_{\sqrt{s} \rightarrow \sqrt{s_R}} (\sqrt{s} - \sqrt{s_R}) t_{aa}(s), \quad (3.112)$$

and, to obtain the other couplings we use

$$g_j = g_a \lim_{\sqrt{s} \rightarrow \sqrt{s_R}} (\sqrt{s} - \sqrt{s_R}) \frac{t_{aj}(s)}{t_{aa}(s)}. \quad (3.113)$$

In the case of meson-meson interactions, we proceed in the similar way, just substituting  $(\sqrt{s} - \sqrt{s_R}) \rightarrow (s - s_R)$  in both the amplitude near the pole and in the calculation of the couplings.

### Structure of Hadron Resonances

As we have seen in the Introduction, a resonance can have components from different degrees of freedom. A certain resonance may be mostly a molecular state of a certain channel, or it may be mostly a quark model state, etc. In this thesis, in order to determine the importance of a given channel for a resonance  $R$ , two measures were used, which we detail in this section.

In recent years, the compositeness condition, first proposed by Weinberg to explain the deuteron as a neutron-proton bound state [173, 174], has been advocated as a model independent way to determine the relevance of hadron-hadron components in a molecular state. With renewed interests in hadron spectroscopy, this method has been extended to more deeply bound states, resonances, and higher partial waves [44, 175–185].

From Ref. [183], we have that, for a state  $|R\rangle$ , the probability of scattering states in the description of  $R$  is given by

$$X = 1 - Z = -g^2 \left. \frac{dG(s)}{d\sqrt{s}} \right|_{\sqrt{s} \rightarrow \sqrt{s_R}}, \quad (3.114)$$

with  $Z$  the measure of the probability of bare bound state contributions to  $|R\rangle$ , given by,

$$Z = -g^2 G^2(s) \left. \frac{dV(s)}{d\sqrt{s}} \right|_{\sqrt{s} \rightarrow \sqrt{s_R}}, \quad (3.115)$$

and  $\sqrt{s_R}$  the position of the state in the complex plane. Typically our scattering states are the hadronic channels of the theory, thus  $X$  can measure the importance of hadronic degrees of freedom. For more than one channel, we have that

$$X_i = -\sum_j g_i g_j \left. \frac{dG_i(s)}{d\sqrt{s}} \right|_{\sqrt{s} \rightarrow \sqrt{s_R}} \delta_{ij}, \quad (3.116a)$$

$$Z = -\sum_{ij} g_i g_j G_i(s) G_j(s) \left. \frac{dV_{ij}(s)}{d\sqrt{s}} \right|_{\sqrt{s} \rightarrow \sqrt{s_R}} \quad (3.116b)$$

with  $X_i$  giving the probability of each individual channel. However, we should mention that this analysis is only valid for bound states. For resonances, it involves complex numbers and, therefore, a strict probabilistic interpretation is lost as pointed out in Ref. [180]. A possible solution for this problem, when dealing with resonances, is to take into account only the real part of the quantities in Eqs. (3.116a) and (3.116b) [185],

$$\tilde{X}_i = -\sum_j \text{Re} \left\{ g_i g_j \left. \frac{dG_{i,SRS}(s)}{d\sqrt{s}} \right|_{\sqrt{s} \rightarrow \sqrt{s_R}} \delta_{ij} \right\}, \quad (3.117a)$$

$$\tilde{Z} = -\sum_{ij} \text{Re} \left\{ g_i g_j G_i(s) G_j(s) \left. \frac{dV_{ij}(s)}{d\sqrt{s}} \right|_{\sqrt{s} \rightarrow \sqrt{s_R}} \right\}. \quad (3.117b)$$

Another method consists on using  $g_i G_i(s_R)$ , which is proportional to the wave function of each channel at the origin of the coordinate space [177],

$$g_i G_i(s_R) = (2\pi)^{3/2} \psi(0), \quad (3.118)$$

thus also giving a measure of the importance of the  $i$ th channel.

A precise interpretation of the meaning of  $X$  when one has open channels is given in [180]. The magnitude  $X$  measures the integral of the square (not the modulus squared) of the wave function with a given phase convention, which gets most of its contribution from distances before the channel becomes asymptotic.

### 3.3 Triangle Singularities

Triangle Singularities (TS) have already been introduced in Sec. 1.2. In this section we shall analyze how a triangle diagram can originate a TS, as well as how one can predict their position in the invariant mass of the final state particles in Fig. 1.4.

In Ref. [103], the existence of singularities in generalized loops of the form

$$I = \int \frac{B dk_1 dk_2 \cdots}{A_1 A_2 A_3 \cdots} \quad (3.119)$$

was studied, where  $A_i = q_i^2 - m_i^2$  with  $q_i$  a certain four-momentum,  $B$  a certain polynomial of the four vectors  $q_i$  and  $k_j$  the momentum associated with the  $j$ th closed loop. Then, by using the Feynman method,

$$\frac{1}{A_1 A_2 A_3 \cdots} = (n-1)! \prod_{i=1}^n \int_0^1 d\alpha_i \frac{\delta\left(\sum_{j=1}^n \alpha_j - 1\right)}{\left(\sum_{k=1}^n \alpha_k A_k\right)^n}, \quad (3.120)$$

to parametrize the generalized loop function, Landau argued that the integral in Eq. (3.119) is regular everywhere except when the Landau equations [103, 104, 186],

$$q_i^2 = m_i^2 \quad \text{or} \quad \alpha_i = 0, \quad (3.121a)$$

$$\sum \alpha_i q_i = 0, \quad (3.121b)$$

are fulfilled.

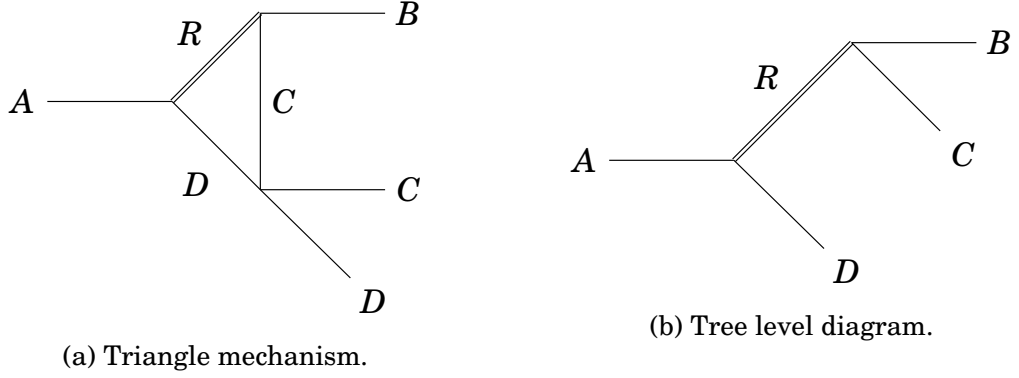
As already mentioned in Section 1.2, the Coleman-Norton theorem gives a physical interpretation to these equations, specifically that there is only a singularity in Eq. (3.119) if and only if one can interpret the corresponding loop diagram as a physical process with all particles in the loop on-shell and moving forward in time [104].

One should introduce now the Schmid theorem, developed in Ref. [187]. The Schmid theorem states that if there is a triangle diagram like the one shown in Fig. 3.4a, where the scattering,  $CD \rightarrow CD$ , is an elastic one, then, if there is a corresponding tree-level diagram (like the one in Fig. 3.4b) the TS will not appear in the mass distribution of  $CD$ . If  $f_l^{\text{tree}}$  is a partial wave amplitude of the tree-level diagram and  $f_l^{\text{ts}}$  a partial wave amplitude of the triangle diagram, then, at the position of the TS,  $m_{CD} = \sqrt{s_{ts}}$ , according to Ref. [187],

$$f_l^{\text{tree}}(s_{ts}) + f_l^{\text{ts}}(s_{ts}) = S_l f_l^{\text{tree}}(s_{ts}), \quad (3.122)$$

with  $S_l$  the  $S$ -matrix of the elastic scattering process  $CD \rightarrow CD$ . This equation means that, since [187]

$$|f_l(s_{ts})|^2 = |f_l^{\text{tree}}(s_{ts}) + f_l^{\text{ts}}(s_{ts})|^2 = |f_l^{\text{tree}}(s_{ts})|^2, \quad (3.123)$$

Figure 3.4: Two possible diagrams for the  $A \rightarrow BCD$  decay.

the presence of a TS would not be seen in the final observable – the singularity originated by the triangle mechanism is already contained in the tree level diagram [187].

A more recent analysis of the theorem was made in Ref. [188]. There the authors find that the theorem is exact only when  $\Gamma_R \rightarrow 0$ . For values different from zero, the system still has memory of the theorem, but a peak associated with the TS can be visible in the mass distribution. In any case, within the context of this thesis, the Schmid theorem does not apply, since for us the intermediate scattering will always be inelastic<sup>6</sup>, and the relative strengths between the tree level and the triangle mechanism will have to be judged in a case by case basis.

In Ref. [123] a different method of analyzing TS, without the use of Feynman parameters, was developed. Let us look at a triangle mechanism of the type of Fig. 3.5 (which will be the mechanism used throughout this thesis) where the scattering  $23 \rightarrow CD$  is inelastic (and typically will happen through a resonance). The amplitude associated to the triangle loop will contain

$$t_T = i \int \frac{d^4 q}{(2\pi)^4} \frac{1}{(q^2 - m_2^2 + i\epsilon) [(P - q)^2 - m_1^2 + i\epsilon] [(P - q - k)^2 - m_3^2 + i\epsilon]}, \quad (3.124)$$

with  $p_A = P$ ,  $q_2 = q$ ,  $q_1 = P - q$ ,  $q_3 = P - q - k$  and  $p_B = k$ . For the cases that interest us, we will typically be in the energy region where resonance 1 (labelled as  $R$  in the figure) may be treated non-relativistically. Thus, one can integrate over  $q^0$  while neglecting the negative energy pole of particle 1 and one gets:

$$t_T = \int \frac{d\vec{q}}{(2\pi)^3} \frac{1}{[P^0 - \omega_2(\vec{q}) - E_3(\vec{k} + \vec{q}) - k^0 + i\epsilon] [P^0 - E_1(\vec{q}) - \omega_2(\vec{q}) + i\epsilon]} \quad (3.125)$$

<sup>6</sup>In the examples studied in this thesis, the intermediate scattering ( $CD \rightarrow CD$  in the example of Fig. 3.4b) will always have an intermediate resonance, which usually magnifies the effects of the TS in the final mass distribution [188].

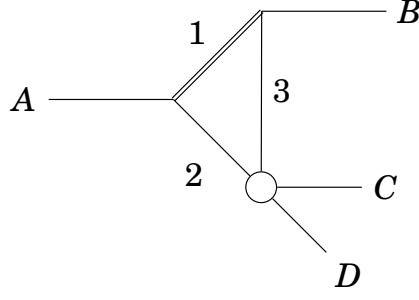


Figure 3.5: Triangle diagram for the  $A \rightarrow BCD$  decay, through inelastic scattering.

$$\times \frac{P^0 \omega_2(\vec{q}) + k^0 E_3(\vec{k} + \vec{q}) - [\omega_2(\vec{q}) + E_3(\vec{k} + \vec{q})] [\omega_2(\vec{q}) + E_3(\vec{k} + \vec{q}) + E_1(\vec{q})]}{(4 \omega_2(\vec{q}) E_1(\vec{q}) E_3(\vec{k} + \vec{q})) [k^0 - E_3(\vec{k} + \vec{q}) - E_1(\vec{q})] [P^0 + \omega_2(\vec{q}) + E_3(\vec{k} + \vec{q}) - k^0]},$$

where  $\omega_2(\vec{q}) = \sqrt{m_2^2 + \vec{q}^2}$ ,  $E_1(\vec{q}) = \sqrt{m_1^2 + \vec{q}^2}$ ,  $E_3(\vec{k} + \vec{q}) = \sqrt{m_3^2 + (\vec{k} + \vec{q})^2}$ ,  $P^0 = m_A$ , and  $k^0 = \sqrt{m_B^2 + \vec{k}^2}$ .

As we have seen from the Coleman-Norton theorem, a TS will develop if all three intermediate particles are on-shell which is equivalent to,

$$P^0 - E_1(\vec{q}) - \omega_2(\vec{q}) + i\epsilon = 0, \quad (3.126a)$$

$$P^0 - \omega_2(\vec{q}) - E_3(\vec{k} + \vec{q}) - k^0 + i\epsilon = 0, \quad (3.126b)$$

since the other propagators do not lead to singularities. Then, one just needs to analyze the poles in the following simplified loop amplitude [123]

$$I(m_{23}) = \int \frac{d\vec{q}}{(2\pi)^3} \frac{1}{[P^0 - \omega_2(\vec{q}) - E_3(\vec{k} + \vec{q}) - k^0 + i\epsilon] [P^0 - E_1(\vec{q}) - \omega_2(\vec{q}) + i\epsilon]} \quad (3.127)$$

$$= 2\pi \int_0^\infty dq \frac{q^2}{P^0 - E_1(q) - \omega_2(q) + i\epsilon} \int_{-1}^1 dz \frac{1}{E_{23} - \omega_2(q) - \sqrt{m_3^2 + q^2 + k^2 + 2qkz} + i\epsilon}, \quad (3.128)$$

with  $q = |\vec{q}|$ ,  $k = |\vec{k}|$ ,  $E_{23} = P^0 - k^0$ , and  $z = \cos\theta$  with  $\theta$  the angle between  $\vec{q}$  and  $\vec{k}$ . There are two integrals and so we must analyze the singularities in both of them. There are two cases where a singularity in the integrand will be a singularity in the integral: end point singularities and when two poles pinch at the real axis. In the case of end point singularities, one cannot deform the contour around them since they are at the limit of the domain of integration. In the case of two poles pinching, two

singularities approach the contour (in this case the real axis) from different direction and we cannot deform the contour in order to avoid both of them. For a triangle mechanism, a TS will appear if there is a pair of singularities that pinch the contour with one of them being an end point singularity [104]. Inspecting Eq. (3.128), one can see that an end point singularity can appear for  $z = \pm 1$ , since  $-1 \leq \cos\theta \leq 1$ . This is because for  $z = \pm 1$  the principal part of the integration over  $\cos\theta$  does not get cancelled since there is no contribution above  $z = 1$  or below  $z = -1$ . Now, one can look again at Eqs. (3.126), substituting  $z = \pm 1$ , such that

$$P^0 - E_1(\vec{q}) - \omega_2(\vec{q}) + i\epsilon = 0, \quad (3.129a)$$

$$E_{23} - \omega_2(q) - \sqrt{m_3^2 + q^2 + k^2 \pm 2qk} + i\epsilon = 0, \quad (3.129b)$$

We shall call the momentum that satisfies Eq. (3.129a),  $q_{on+}$ , and the solution will be

$$q_{on+} = \frac{\lambda^{1/2}(m_A^2, m_1^2, m_2^2)}{2m_A} + i\epsilon. \quad (3.130)$$

Eq. (3.129b) will have two solutions for each value of  $z$ . Then, for  $z = +1$  we will have,

$$q_{b+} = \gamma(-vE_2^* + p_2^*) + i\epsilon, \quad (3.131a)$$

$$q_{b-} = -\gamma(vE_2^* + p_2^*) - i\epsilon, \quad (3.131b)$$

while for  $z = -1$ ,

$$q_{a+} = \gamma(vE_2^* + p_2^*) + i\epsilon, \quad (3.132a)$$

$$q_{a-} = \gamma(vE_2^* - p_2^*) - i\epsilon, \quad (3.132b)$$

with

$$p_2^* = \frac{\lambda^{1/2}(m_{23}^2, m_2^2, m_3^2)}{2m_{23}}, \quad v = \frac{k}{E_{23}}, \quad (3.133a)$$

$$E_2^* = \frac{(m_{23}^2 + m_2^2 - m_3^2)}{2m_{23}}, \quad \gamma = \frac{1}{\sqrt{1-v^2}}, \quad (3.133b)$$

and  $m_{23}$  the invariant mass of the (23) [or (CD)] pair.

Note that  $q_{b-}$  is already negative and since the modulus of  $q$  in the integration is positive this pole has no influence in the results. The pole at  $q_{b+}$  is equally inoperative because it is in the same upper side of the complex plane as  $q_{on+}$  and one can deform the contour integration to avoid both poles (see Fig. 3.6). So is the case in a situation like in Fig. 3.7 (a). However, there are two situations where the singularities are unavoidable which correspond to Figs. 3.7 (b) and (c). In the first case  $p_2^* = 0$



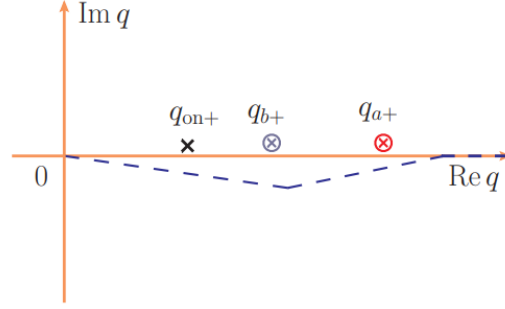


Figure 3.6: Case where all the poles are in the same size of the complex plane and thus no pinching is possible. Image taken from Ref. [123].

(see Eqs. (3.132a) and (3.132b)) and we have a threshold singularity. In the case of Fig. 3.7 (c) we have a different singularity which is the triangle singularity. Hence the triangle singularity is given by the equation,

$$\lim_{\epsilon \rightarrow 0} (q_{on+} - q_{a-}) = 0. \quad (3.134)$$

This equation not only tells us if there is a triangle singularity, but also for which values of the invariant masses  $m_{11}$  and  $m_{23}$ . Indeed, for given  $m_2$ ,  $m_3$ ,  $m_A$  and  $m_B$  the range of  $m_1$  where the triangle singularity shows up is given by [123]

$$m_1^2 \in \left[ \frac{m_A^2 m_3 + m_B^2 m_2}{m_2 + m_3} - m_2 m_3, (m_A - m_2)^2 \right], \quad (3.135)$$

and the triangle singularity in  $I(m_{23})$  is within the range

$$m_{23}^2 \in \left[ (m_2 + m_3)^2, \frac{m_A m_3^2 - m_B^2 m_2}{m_A - m_2} + m_A m_2 \right]. \quad (3.136)$$

Finally, it is worth noting that no actual infinity will appear in the final mass distribution because, since particle 1 is by definition a resonance (it decays at least into  $B$  and  $3$ ), it will have width, and then, in Eq. (3.126), one needs to add  $i\Gamma_1/2$  to the mass of  $m_1$  in order to take it into account, and the infinite peak of the singularity becomes a finite broader peak.

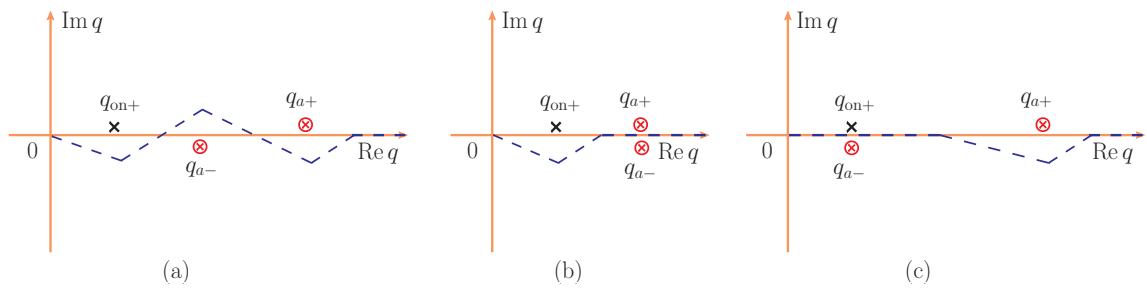


Figure 3.7: (a) Case where there is no pinching. (b) Case where there is pinching of  $q_{a-}$  and  $q_{a+}$ , which corresponds to a threshold singularity. (c) Case where there is pinching of  $q_{a-}$  and  $q_{on+}$ , which corresponds to a TS. Notice how, when two poles pinch, one cannot deform the contour to avoid them, which means that the singularity will remain after we integrate over  $q$ . Image taken from Ref. [123].

**Part II**

**Hadrons In The Light Sector**



# Chapter 4

## Decays of $\tau^-$ to $PP$ , $PV$ and $VV$ meson pairs

### 4.1 Introduction

Tau decays have been instrumental to learn about weak interaction as well as strong interaction affecting the hadrons produced on  $\tau^-$  hadronic decay [189–196].  $\tau^-$  decays into  $\nu_\tau$  and a pair of mesons make up for a sizable fraction of the  $\tau^-$  decay width [110]. Several modes are well measured, as  $\tau^- \rightarrow \nu_\tau K^0 K^-$  [197]<sup>1</sup>,  $\tau^- \rightarrow \nu_\tau \pi^- \bar{K}^0$  [197],  $\tau^- \rightarrow \nu_\tau \pi^- \omega$  [198, 199],  $\tau^- \rightarrow \nu_\tau K^{*0} K^-$  [200],  $\tau^- \rightarrow \nu_\tau \eta K^{*-}$  [201],  $\tau^- \rightarrow \nu_\tau K^- \omega$  [202],  $\tau^- \rightarrow \nu_\tau \pi^0 \rho^-$  [200],  $\tau^- \rightarrow \nu_\tau \pi^- K^{*0}$  [200],  $\tau^- \rightarrow \nu_\tau \pi^- \phi$  [203],  $\tau^- \rightarrow \nu_\tau K^- \phi$  [203],  $\tau^- \rightarrow \nu_\tau \eta K^-$  [204]. As we can see, there are modes with two pseudoscalar mesons and also modes with pseudoscalar-vector. Surprisingly, there are no vector-vector modes reported in the PDG [110]. Certainly the large mass of the vector mesons leaves small phase space for the decay, but modes like  $\rho^0 \rho^-$ ,  $\rho^- \omega$ ,  $K^{*-} \rho^0$ ,  $K^{*-} \omega$ ,  $\bar{K}^{*0} \rho^-$  are kinematically possible, and even  $K^{*0} K^{*-}$  considering the width of  $K^*$ . One may wonder whether there is some fundamental reason for this experimental fact. Actually, in as much as the pseudoscalar and vector mesons differ only by the spin arrangement of the quarks, it should be possible to relate the rates of decay for two pseudoscalar mesons and the related pseudoscalar-vector or vector modes, for instance,  $\tau^- \rightarrow \nu_\tau K^0 K^-$ ,  $\nu_\tau K^0 K^{*-}$ ,  $\nu_\tau K^{*0} K^-$ ,  $\nu_\tau K^{*0} K^{*-}$ .

Many of the works on  $\tau$  decay into two mesons rely upon vector meson dominance producing a vector meson that decays into two pseudoscalars, or a pseudoscalar and a vector [195]. One approach often used [196] upon production of a  $q\bar{q}$  pair that posteriorly hadronizes into two hadrons, and the Nambu–Jona-Lasinio (NJL) model

---

<sup>1</sup>We mention explicitly the most recent experiments. The full information can be obtained in Ref. [110].

[205] is used for this purpose.

In the present chapter we use the basic dynamics of the weak interaction at the quark level, producing a primary  $q\bar{q}$  pair. The hadronization of this pair into two mesons is done using the  ${}^3P_0$  model [206–208]. The method allows us to correlate many different processes. To make that possible we carry out an elaborate and detailed angular momentum algebra that allows us to write amplitudes analytically in a very simple form.

One interesting point concerning  $\tau^-$  mesonic decays is the issue of charge symmetry discussed in Ref. [209] and the classification of the weak interaction into first and second class currents. The issue, with suggestions of experiments, is retaken in Ref. [210]. One of the interesting reactions is the  $\tau^- \rightarrow \nu_\tau \pi^- \eta(\eta')$ , which according to that classification is forbidden by  $G$ -parity.

The  $G$ -parity plays indeed an important role in these reactions and in this paper we offer a new perspective into this issue. We shall see that  $G$ -parity for the non strange mesons plays an important role and the rules are different for pseudoscalar-pseudoscalar ( $PP$ ) pseudoscalar-vector ( $PV$ ) or vector-vector ( $VV$ ) production. Interestingly, an extension of these rules appears also in the strange sector for the  $\tau^- \rightarrow \nu_\tau K^- \eta(\eta'), \nu_\tau K^{*-} \eta(\eta')$  reactions.

This chapter is based on the findings of Ref. [1]. We make a thorough study of all possible Cabibbo-favored and Cabibbo-suppressed reactions and compare with present available data and with results of other theoretical approaches.

## 4.2 Formalism

The first step is to look at the  $\tau^- \rightarrow \nu_\tau q\bar{q}$  decay depicted in Fig. 4.1 for the Cabibbo-favored  $d\bar{u}$  production. We obtain the Cabibbo-suppressed mode substituting the  $d$  quark by an  $s$  quark. However, we are interested in the production of two mesons, not just one, as it would come from the mechanism of Fig. 4.1 when  $q\bar{q}$  merge into a meson. The procedure to produce two mesons is hadronization by creating a new  $q\bar{q}$  pair with the quantum numbers of the vacuum. This is depicted in Fig. 4.2.

It is easy and important to see how two mesons appear, and in which order, to see the relevance of the  $G$ -parity in the reactions. For this purpose, and looking only at the flavor components, we proceed as follows [211–213]: we introduce the SU(3) matrix  $M$

$$M = \begin{pmatrix} u\bar{u} & u\bar{d} & u\bar{s} \\ d\bar{u} & d\bar{d} & d\bar{s} \\ s\bar{u} & s\bar{d} & s\bar{s} \end{pmatrix}, \quad (4.1)$$

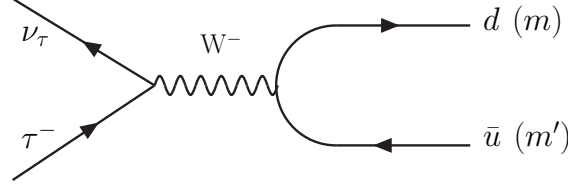


Figure 4.1: Elementary  $\tau^- \rightarrow \nu_\tau d \bar{u}$  diagram. The labels  $m, m'$  stand for the third component of spin of the quarks.

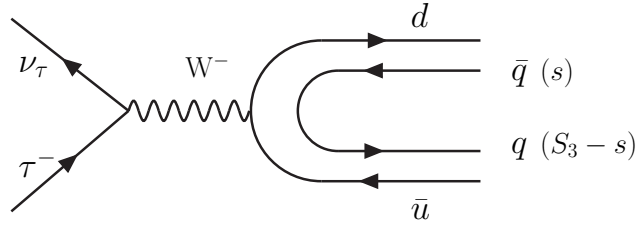


Figure 4.2: Hadronization of the primary  $d \bar{u}$  pair to produce two mesons,  $s$  is the third component of the spin of  $\bar{q}$  propagating as a particle, while  $S_3 - s$  is the third component of the spin of  $q$ , where  $S_3$  is the third component of the total spin  $S$  of  $\bar{q}q$ .

and when we do the hadronization of  $d \bar{u}$  we get

$$d \bar{u} \rightarrow \sum_{i=1}^3 d \bar{q}_i q_i \bar{u} = M_{2i} M_{i1} = (M \cdot M)_{21}. \quad (4.2)$$

And now we write the  $M$  matrix in terms of pseudoscalar ( $\Phi$  in Eq. (2.18)) or vector mesons ( $V_\mu$  in Eq. (2.25)). Then  $M^2$  becomes  $\Phi \cdot \Phi, \Phi \cdot V, V \cdot \Phi, V \cdot V$  and it is important to keep the order of the mesons. Thus we get

$$\begin{aligned} (\Phi \cdot \Phi)_{21} &= \pi^- \left( \frac{\pi^0}{\sqrt{2}} + \frac{\eta}{\sqrt{3}} + \frac{\eta'}{\sqrt{6}} \right) + \left( -\frac{\pi^0}{\sqrt{2}} + \frac{\eta}{\sqrt{3}} + \frac{\eta'}{\sqrt{6}} \right) \pi^- + K^0 K^- \\ &= \left( \pi^- \frac{\pi^0}{\sqrt{2}} - \frac{\pi^0}{\sqrt{2}} \pi^- \right) + \pi^- \left( \frac{\eta}{\sqrt{3}} + \frac{\eta'}{\sqrt{6}} \right) + \left( \frac{\eta}{\sqrt{3}} + \frac{\eta'}{\sqrt{6}} \right) \pi^- + K^0 K^-. \end{aligned} \quad (4.3)$$

We shall see later that it is precisely the combination of  $\pi^- \eta(\eta')$  and  $\eta(\eta') \pi^-$  that appears in Eq. (4.3) what makes the  $\tau^- \rightarrow \nu_\tau \pi^- \eta$  decay  $G$ -parity forbidden, while the  $\pi^- \pi^0, \pi^0 \pi^-$  combination gets reinforced by the relative sign in Eq. (4.3).

Similarly, we obtain

$$(\Phi \cdot V)_{21} = \pi^- \left( \frac{\rho^0}{\sqrt{2}} + \frac{\omega}{\sqrt{2}} \right) + \left( -\frac{\pi^0}{\sqrt{2}} + \frac{\eta}{\sqrt{3}} + \frac{\eta'}{\sqrt{6}} \right) \rho^- + K^0 K^{*-}, \quad (4.4)$$

$$(V \cdot \Phi)_{21} = \rho^- \left( \frac{\pi^0}{\sqrt{2}} + \frac{\eta}{\sqrt{3}} + \frac{\eta'}{\sqrt{6}} \right) + \left( -\frac{\rho^0}{\sqrt{2}} + \frac{\omega}{\sqrt{2}} \right) \pi^- + K^{*0} K^- . \quad (4.5)$$

We see again that  $\pi^- \rho^0$  appears as  $\pi^- \rho^0$  or  $-\rho^0 \pi^-$ ,  $\pi^- \omega$  and  $\omega \pi^-$  and  $(\frac{\eta}{\sqrt{3}} + \frac{\eta'}{\sqrt{6}}) \rho^-$  with  $\rho^- (\frac{\eta}{\sqrt{3}} + \frac{\eta'}{\sqrt{6}})$ . Once again, we shall see that the order matters in the  $G$ -parity conservation.

Thirdly, for the  $VV$  combination we get

$$(V \cdot V)_{21} = \left( \rho^- \frac{\rho^0}{\sqrt{2}} - \frac{\rho^0}{\sqrt{2}} \rho^- \right) + \left( \rho^- \frac{\omega}{\sqrt{2}} + \frac{\omega}{\sqrt{2}} \rho^- \right) + K^{*0} K^{*-}, \quad (4.6)$$

with, again, relevant signs between the  $\rho^- \rho^0$ ,  $\rho^0 \rho^-$  and  $\rho^- \omega$ ,  $\omega \rho^-$  components.

Replacing the  $d$  quark by an  $s$  quark we get the Cabibbo-suppressed modes. The hadronization leads to

$$s\bar{u} \rightarrow \sum_{i=1}^3 s \bar{q}_i q_i \bar{u} = M_{3i} M_{i1} = (M \cdot M)_{31},$$

with the results

$$(\Phi \cdot \Phi)_{31} = K^- \frac{\pi^0}{\sqrt{2}} + \bar{K}^0 \pi^- + \left( K^- \frac{\eta}{\sqrt{3}} - \frac{\eta}{\sqrt{3}} K^- \right) + \left( K^- \frac{\eta'}{\sqrt{6}} + \frac{2\eta'}{\sqrt{6}} K^- \right), \quad (4.7)$$

$$(\Phi \cdot V)_{31} = K^- \left( \frac{\rho^0}{\sqrt{2}} + \frac{\omega}{\sqrt{2}} \right) + \bar{K}^0 \rho^- + \left( -\frac{\eta}{\sqrt{3}} + \frac{2\eta'}{\sqrt{6}} \right) K^{*-}, \quad (4.8)$$

$$(V \cdot \Phi)_{31} = K^{*-} \left( \frac{\pi^0}{\sqrt{2}} + \frac{\eta}{\sqrt{3}} + \frac{\eta'}{\sqrt{6}} \right) + \bar{K}^{*0} \pi^- + \phi K^-, \quad (4.9)$$

$$(V \cdot V)_{31} = K^{*-} \left( \frac{\rho^0}{\sqrt{2}} + \frac{\omega}{\sqrt{2}} \right) + \bar{K}^{*0} \rho^- + \phi K^{*-}. \quad (4.10)$$

Interestingly, even if here we do not have  $G$ -parity states, we have also some states appearing in different order, as  $K^- \eta$ ,  $\eta K^-$  and  $K^- \eta'$ ,  $\eta' K^-$  in  $PP$  and  $\eta K^{*-}$ ,  $K^{*-} \eta$ ,  $\eta' K^{*-}$ ,  $K^{*-} \eta'$  in  $PV$ ,  $VP$ . This has also consequences, similar to those leading to  $G$ -parity selection rules, as we shall see.



### 4.2.1 Weak interaction

We shall not worry about the global normalization and concentrate only on the relationship of the different decay modes discussed before. Then the weak interaction is given by

$$H = \mathcal{C} L^\mu Q_\mu, \quad (4.11)$$

with  $\mathcal{C}$  containing weak interaction constants and radial matrix elements that we shall see later on, where  $L^\mu$  is the leptonic current

$$L^\mu = \langle \bar{u}_\nu | \gamma^\mu - \gamma^\mu \gamma_5 | u_\tau \rangle, \quad (4.12)$$

and  $Q_\mu$  the quark current

$$Q^\mu = \langle \bar{u}_d | \gamma^\mu - \gamma^\mu \gamma_5 | v_{\bar{u}} \rangle. \quad (4.13)$$

As is usual in the evaluation of decay widths to three final particles, we evaluate the matrix elements in the frame where the two mesons system is at rest. For the evaluation of the matrix element  $Q_\mu$  we assume that the quark spinors are at rest in that frame and we have in the Itzykson-Zuber normalization [214]

$$u_r = \begin{pmatrix} \chi_r \\ 0 \end{pmatrix}, v_r = \begin{pmatrix} 0 \\ \chi_r \end{pmatrix}, \chi_1 = \begin{pmatrix} 1 \\ 0 \end{pmatrix}, \chi_2 = \begin{pmatrix} 0 \\ 1 \end{pmatrix}, \quad (4.14)$$

with the  $\gamma^\mu$  matrices,

$$\gamma^0 = \begin{pmatrix} I & 0 \\ 0 & -I \end{pmatrix}; \gamma_5 = \begin{pmatrix} 0 & I \\ I & 0 \end{pmatrix}; \gamma^i = \begin{pmatrix} 0 & \sigma^i \\ -\sigma^i & 0 \end{pmatrix}. \quad (4.15)$$

For the spinors at rest we have

$$\gamma_5 v_r = u_r,$$

and then

$$\begin{aligned} Q^\mu &= \langle \bar{u} | \gamma^\mu - \gamma^\mu \gamma_5 | v \rangle = \langle \bar{u} | \gamma^\mu - \gamma^\mu \gamma_5 | \gamma_5 u \rangle = \langle \bar{u} | \gamma^\mu \gamma_5 - \gamma^\mu | u \rangle, \\ &= -\langle \bar{u} | \gamma^\mu - \gamma^\mu \gamma_5 | u \rangle. \end{aligned} \quad (4.16)$$

Thus, apart from a global sign we can work with the  $u$  spinors all the time.

Next we must care about how to combine the spins of the quark-antiquark to states of given angular momentum. Indeed, in the  $Wq\bar{q}$  vertex of Fig. 4.1, we shall have the matrix element

$$ME = \langle m | Operator | m' \rangle, \quad (4.17)$$

but we want to combine the spins to total angular momentum and for this we use for the antiparticles the rule of particle-hole conjugation [215], where the hole with  $m'$  behaves as a particle state according to

$$|hole, m'\rangle \rightarrow (-1)^{\frac{1}{2}-m'} \left| \frac{1}{2}, -m' \right\rangle. \quad (4.18)$$

We can include the minus sign of Eq. (4.16) and then we will implement the rule

$$|hole, m'\rangle \rightarrow (-1)^{\frac{1}{2}+m'} \left| \frac{1}{2}, -m' \right\rangle. \quad (4.19)$$

We shall, then, carry on the former phase and change the sign of  $m'$  to combine spins in what follows.

The next step is to realize that for the spinors at rest and  $\gamma^\mu$  matrices, Eqs. (4.14) and Eq. (4.15),  $\bar{u}\gamma^0 u \rightarrow \langle \chi' | \chi \rangle$ ,

$$\bar{u}\gamma^0 u \rightarrow \langle \chi' | \chi \rangle,$$

which means,  $\gamma^0$  becomes the operator 1 with bispinors, and

$$\bar{u}\gamma^i \gamma_5 u \rightarrow \langle \chi' | \sigma_i | \chi \rangle,$$

hence, replacing  $\gamma^i \gamma_5$  by  $\sigma_i$ , the Pauli matrices, with bispinors. The rest of matrix elements are zero. Then

$$\begin{aligned} Q_0 &= \langle \chi' | 1 | \chi \rangle \equiv M_0, \\ Q_i &= \langle \chi' | \sigma_i | \chi \rangle \equiv N_i, \end{aligned} \quad (4.20)$$

Denoting for simplicity,

$$\bar{L}^{\mu\nu} = \overline{\sum} \sum L^\mu L^{\nu\dagger}, \quad (4.21)$$

we can write

$$\overline{\sum} \sum L^\mu L^{\nu\dagger} Q_\mu Q_\nu^* = \bar{L}^{00} M_0 M_0^* + \bar{L}^{0i} M_0 N_i^* + \bar{L}^{i0} N_i M_0^* + \bar{L}^{ij} N_i N_j^*, \quad (4.22)$$

where in  $M_0 M_0^*$ ,  $M_0 N_i^*$ ,  $N_i M_0^*$ ,  $N_i N_j^*$  we shall sum over the final polarizations of the mesons produced.  $\overline{\sum} \sum L^\mu L^{\nu\dagger}$  is easily evaluated and we have

$$\overline{\sum} \sum L^\mu L^{\nu\dagger} = \frac{1}{m_\nu m_\tau} \left( p'^\mu p^\nu + p'^\nu p^\mu - g^{\mu\nu} p' \cdot p + i\epsilon^{\alpha\mu\beta\nu} p'_\alpha p_\beta \right), \quad (4.23)$$

where  $p, p'$  are the momenta of the  $\tau$  and  $\nu_\tau$  respectively and we use the field normalization for fermions of Ref. [216]. These techniques have also been used successfully in the evaluation of weak decays  $M_1 \rightarrow M_2 M_3$  [217] and semileptonic decays of  $B^{(*)}$ ,  $D^{(*)}$  into  $\nu l$  and pseudoscalar or vector mesons [218].

Next we must evaluate  $M_0$  and  $N_i$  for the different  $PP$ ,  $PV$ ,  $VP$  and  $VV$  combinations. In order to implement the hadronization of Fig. 4.2 we use the  ${}^3P_0$  model [206–208]. The  ${}^3P_0$  model has been widely used in the literature and recently it has been found very instrumental to address different problems in hadron physics. A few of the most recent examples include the study of selfenergies of baryons from the coupling to the meson-baryon continuum [219], or meson coupling to the meson-meson continuum [220], the unquenching of the quark model to account for sea quarks [221], the strong and electromagnetic decays of mesons [222], the strong decay of charmed states into open charm meson pairs [223], the weak decays of  $\Lambda_b$ ,  $\Xi_b$  into open charmed baryons and mesons [8, 224], the strong decays of higher isovector scalar mesons [225], the strong decays of  $1P$  and  $2D$  double charmed states [226], or to mix  $q\bar{q}$  bare meson states with meson-meson components [227]. The essence of this model is that a  $\bar{q}q$  state is introduced with parity + and zero total angular momentum. Since  $\bar{q}$  has negative parity we need  $L = 1$  to restore parity, which forces the  $\bar{q}q$  to couple to spin  $S = 1$  and then  $L, S$  couple to  $J = 0$ . We take the contribution of spin

$$|1S_3\rangle = \sum_s \mathcal{C}(\frac{1}{2} \frac{1}{2} 1; s, S_3 - s) | \frac{1}{2}, s \rangle | \frac{1}{2}, S_3 - s \rangle, \quad (4.24)$$

where  $| \frac{1}{2}, S_3 - s \rangle$  corresponds to the antiparticle  $\bar{q}$  with sign and phase implicitly included and is considered as a normal particle state. This is now coupled to  $Y_{1, M_3}$  to give  $J = 0$ . Thus

$$|00\rangle = \sum_{M_3} \mathcal{C}(110; M_3, S_3) Y_{1, M_3}(\hat{\mathbf{r}}) |1, S_3\rangle = \sum_{S_3} \mathcal{C}(110; -S_3, S_3) Y_{1, -S_3}(\hat{\mathbf{r}}) |1, S_3\rangle. \quad (4.25)$$

Next we must look at the spatial matrix element. We assume that for this low energy problem all the quark states are in their ground state. This assumption leads naturally to the weak chiral Lagrangians [228, 229]. Then we have

$$ME(\mathbf{q}) = \int d^3\mathbf{r} \varphi_{\bar{u}}(r) \varphi_d(r) \varphi_q(r) \varphi_{\bar{q}}(r) e^{i\mathbf{q}\cdot\mathbf{r}} Y_{1, -S_3}(\hat{\mathbf{r}}) \quad (4.26)$$

with  $\mathbf{q} = \mathbf{p}_1 - \mathbf{p}_2$ , where  $\mathbf{p}_1, \mathbf{p}_2$  are the momenta of the mesons produced. By means of

$$e^{i\mathbf{q}\cdot\mathbf{r}} = 4\pi \sum_l i^l j_l(qr) \sum_{\mu} Y_{l\mu}(\hat{\mathbf{q}}) Y_{l\mu}^*(\hat{\mathbf{r}}) \quad (4.27)$$

we obtain

$$ME(\mathbf{q}) = i4\pi Y_{1, -S_3}(\hat{\mathbf{q}}) \int r^2 dr \varphi_{\bar{u}}(r) \varphi_d(r) \varphi_q(r) \varphi_{\bar{q}}(r) j_1(qr). \quad (4.28)$$

As we have commented, we do not wish to evaluate this matrix element which involves large uncertainties, but rather establish relationships between different decays based exclusively on the flavor-spin structure. However, due to the fact that

$j_1(qr)$  goes as  $qr$ , hence  $q$ , for low values of  $qr$ , and the fact that  $q$  is very different for different decays, due to their different masses, the appropriate procedure is to write

$$ME(\mathbf{q}) = i4\pi q Y_{1,-S_3}(\hat{\mathbf{q}}) \frac{1}{3} \int r^2 dr \prod_i \varphi_i(r) \frac{3j_1(qr)}{qr} r \equiv q Y_{1,-S_3}(\hat{\mathbf{q}}) F(q). \quad (4.29)$$

where in the evaluation of  $F(q)$  we use the factor  $\frac{3j_1(qr)}{qr}$  in the integrand which goes to 1 as  $qr \rightarrow 0$  and is a smooth function over the range of  $\prod_i \varphi_i(r)$ . This allows for a better comparison of rates for different decays, assuming  $F(q)$  the same for all of them since the quark wave functions refer to the ground state in all cases that we study. This factor  $q Y_{1,-S_3}(\hat{\mathbf{q}}) = \sqrt{\frac{3}{4\pi}} q_{-S_3}$  (in spherical basis) leads to the WPP coupling of chiral perturbation theory [228, 229].

Once the integral over  $d^3r$  is done, and assuming  $F(q)$  the same in all the decays, the  $|00\rangle$  state of Eq. (4.25) leads to

$$|00\rangle_q = \sum_{S_3} (-1)^{1+S_3} \frac{1}{\sqrt{3}} Y_{1,-S_3}(\hat{\mathbf{q}}) |1S_3\rangle, \quad (4.30)$$

where we have permuted indices in  $\mathcal{C}(110; -S_3, S_3)$  to obtain this Clebsch-Gordan coefficient (CGC) (we follow Rose conventions and formulas for all the coming Racah algebra in Ref. [230]).

Next we must combine  $|00\rangle_q$  with the  $d, \bar{u}$  spins to obtain the final  $JM, J'M'$  angular momenta of the two mesons produced. This is accomplished by means of the CGC and we have

$$\begin{aligned} |JM\rangle &= \sum_m \mathcal{C}\left(\frac{1}{2} \frac{1}{2} J; m, s, M\right) \left| \frac{1}{2} m \right\rangle \left| \frac{1}{2} s \right\rangle, \\ |J'M'\rangle &= \sum_{m'} \mathcal{C}\left(\frac{1}{2} \frac{1}{2} J'; S_3 - s, -m', M'\right) (-1)^{\frac{1}{2}+m'} \left| \frac{1}{2}, S_3 - s \right\rangle \left| \frac{1}{2}, -m' \right\rangle, \end{aligned} \quad (4.31)$$

which requires  $m = M - s, m' = S_3 - s - M'$ , and combined with  $|00\rangle_q$  of Eqs. (4.30) and (4.24) lead to the matrix elements

$$\begin{aligned} ME &= -\frac{1}{\sqrt{3}} \sum_{S_3} \sum_s \mathcal{C}\left(\frac{1}{2} \frac{1}{2} 1; s, S_3 - s, S_3\right) (-1)^{\frac{1}{2}-s-M'} q Y_{1,-S_3}(\hat{\mathbf{q}}) \mathcal{C}\left(\frac{1}{2} \frac{1}{2} J; M - s, s, M\right) \\ &\times \mathcal{C}\left(\frac{1}{2} \frac{1}{2} J'; S_3 - s, M' - S_3 + s, M'\right) \left\{ \begin{array}{ll} \langle m | 1 | m' \rangle & \text{(i)} \\ \langle m | \sigma_i | m' \rangle & \text{(ii)} \end{array} \right. . \end{aligned} \quad (4.32)$$

- (i) In the case of the operator 1 leading to  $M_0$  of Eq. (4.20) we have the extra constraint  $m = m' = M - s$  and then  $S_3 = M + M'$ .

- (ii) We shall work in spherical basis and evaluate  $\langle m|\sigma_\mu|m'\rangle$  ( $\mu = \pm 1, 0$ ). We have  $\langle m|\sigma_\mu|m'\rangle = \sqrt{3}\mathcal{C}(\frac{1}{2}1\frac{1}{2}; m', \mu, m)$ , which induces the constraint  $m' + \mu = m$ ,  $\mu = M - S_3 + M'$ . We call  $N_\mu$  the matrix element resulting from Eq. (4.32) in this case.

In Appendix A.1 we evaluate these matrix elements explicitly for  $PP$ ,  $PV$ ,  $VP$ ,  $VV$  and we quote here the results. For convenience, in the final formulas we take as  $z$  axis of quantization the direction of the  $v_\tau$  in the  $\tau^- \rightarrow v_\tau M_1 M_2$  decay, which is the direction of  $\tau^-$  and  $v_\tau$  when we make a boost to have the  $M_1 M_2$  system at rest.

- (i)  $M_0$

- (a)  $PP: J = 0, J' = 0$

$$M_0 = 0 \quad (4.33)$$

- (b)  $PV: J = 0, J' = 1$

$$M_0 = (-1)^{-M-M'} \frac{1}{\sqrt{6}} q Y_{1, -(M+M')}(\hat{\mathbf{q}}) \delta_{M0} \quad (4.34)$$

- (c)  $VP: J = 1, J' = 0$

$$M_0 = (-1)^{-M-M'} \frac{1}{\sqrt{6}} q Y_{1, -(M+M')}(\hat{\mathbf{q}}) \delta_{M'0} \quad (4.35)$$

- (d)  $VV: J = 1, J' = 1$

$$M_0 = (-1)^{-M-M'} \frac{1}{\sqrt{3}} \mathcal{C}(111; M, M', M+M') q Y_{1, -(M+M')}(\hat{\mathbf{q}}) \quad (4.36)$$

- (ii)  $N_\mu$

- (a)  $PP: J = 0, J' = 0$

$$N_\mu = \frac{1}{\sqrt{6}} q Y_{1, \mu}(\hat{\mathbf{q}}) \delta_{M0} \delta_{M'0} \quad (4.37)$$

- (b)  $PV: J = 0, J' = 1$

$$N_\mu = (-1)^{1-M'} \frac{1}{\sqrt{3}} q Y_{1, \mu-M'}(\hat{\mathbf{q}}) \mathcal{C}(111; M', -\mu, M'-\mu) \delta_{M0} \quad (4.38)$$

(c)  $VP: J = 1, J' = 0$ 

$$N_\mu = (-1)^{-M} \frac{1}{\sqrt{3}} q Y_{1,\mu-M}(\hat{\mathbf{q}}) \mathcal{C}(111; M, -\mu, M - \mu) \delta_{M'0} \quad (4.39)$$

(d)  $VV: J = 1, J' = 1$ 

$$\begin{aligned} N_\mu &= \frac{1}{\sqrt{6}} q Y_{1,\mu-M-M'}(\hat{\mathbf{q}}) \{ (-1)^{-M'} \delta_{\mu M} + 2(-1)^{-M} \mathcal{C}(111; M, -\mu, M - \mu) \\ &\times \mathcal{C}(111; M', -M - M' + \mu, -M + \mu) \} \end{aligned} \quad (4.40)$$

The formulas obtained allow us to exploit selection rules for  $G$ -parity. Let us see how it proceeds. By inspecting the change when we permute particle 1 and 2, taking into account that in this permutation  $Y_{1,\nu}(\hat{\mathbf{q}}) = Y_{1,\nu}(\widehat{\mathbf{p}_1 - \mathbf{p}_2})$  goes to  $Y_{1,\nu}(\widehat{\mathbf{p}_2 - \mathbf{p}_1}) = (-1)^\nu Y_{1,\nu}(\widehat{\mathbf{p}_1 - \mathbf{p}_2})$ , we find the results of Table 4.1.

	$PP$	$PV$	$VP$	$VV$
$M_0$	0	-	-	+
$N_\mu$	-	+	+	-

Table 4.1: Signs resulting in the  $M_0$ , and  $N_\mu$  amplitudes by permuting the order of the mesons.

In the signs of Table 4.1 we have taken into account that when exchanging particle 1 and 2 in the  $PV$  case we go to the  $VP$  case. For the case of the  $M_0$  amplitude there is no sign change (apart from  $Y_{1,-(M-M')}(\hat{\mathbf{q}})$ ) in the formula to go from  $PV$  to  $VP$ , but for the case of  $VV$  we have  $\mathcal{C}(111; M, M', M + M') = (-1)^{1+1-1} \mathcal{C}(111; M', M, M + M')$  and hence a change of sign. On the other hand, the situation in the  $N_\mu$  amplitude is opposite. For  $PP$  there is no change of sign, apart from  $Y_{1,\mu}(\hat{\mathbf{q}})$ . However, in the  $PV$  to  $VP$  exchange we see a change of sign from the phase of CGC, apart from  $Y_{1,\mu-M}(\hat{\mathbf{q}})$ . Finally the case of  $VV$  is more complicated but taking the  $z$  axis such that  $\sigma_i$  becomes  $\sigma_z$ , only  $\mu = 0$  contributes and one can explicitly see by inspection of all possible cases that the amplitude does not change by exchanging the two particles, except for the  $Y_{1,\mu-M-M'}(\hat{\mathbf{q}})$ . Interestingly, in some cases the role of the first and second terms in Eq. (4.40) are exchanged, but the sum remains the same.

Let us use the result of Table 4.1 to see the contribution of the channels shown in Eqs. (4.3), (4.4), (4.5) and Eqs. (4.7), (4.8), (4.9), (4.10). If we take the  $\pi^- \pi^0$  channel it comes with the combination  $\pi^- \pi^0 - \pi^0 \pi^-$ . As a consequence  $N_\mu$  adds for the two terms and we have a weight  $2 \frac{1}{\sqrt{2}}$  for the  $\pi^- \pi^0$  channel. On the other hand if we take  $\pi^- \eta, \pi^- \eta'$  they come with the combinations  $\pi^- \eta + \eta \pi^-, \pi^- \eta' + \eta' \pi^-$  and then the combination of the two terms cancels and we do not have  $\pi^- \eta, \pi^- \eta'$  production. In

the next subsection we shall see the relationship of this to  $G$ -parity. We can proceed like that for the  $\pi^- \rho^0$ ,  $\rho^0 \pi^-$  where the two terms add in  $M_0$  and cancel in  $N_\mu$ . The opposite happens to the  $\pi^- \omega$  channel and so on. A consequence of that, although there is no  $G$ -parity in this case, is that the terms  $K^- \eta$ ,  $\eta K^-$  also add in  $N_\mu$  to give a weight of  $\frac{2}{\sqrt{3}}$  for the  $K^- \eta$  channel, and  $K^- \eta'$ ,  $\eta' K^-$  also lead to a weight  $-\frac{1}{\sqrt{6}}$  for  $N_\mu$  for the  $K^- \eta'$  channel. For the same reasons the contribution of  $\eta K^{*-}$ ,  $K^{*-} \eta$  leads to a weight  $-\frac{2}{\sqrt{3}}$  in  $M_0$  for  $\eta K^{*-}$  and zero in  $N_\mu$ , while  $\eta' K^{*-}$  and  $K^{*-} \eta'$  combine to give a weight  $\frac{1}{\sqrt{6}}$  in  $M_0$  and  $\frac{3}{\sqrt{6}}$  in  $N_\mu$  for  $\eta' K^{*-}$ . Altogether we find the weight of  $M_0$ ,  $h_i$ , and  $N_\mu$ ,  $\bar{h}_i$ , for the different channels in Table 4.2. Since we want to evaluate ratios, the Cabibbo suppressed modes go with  $\frac{\sin \theta_c}{\cos \theta_c} = \tan \theta_c$  with respect to the allowed modes, with  $\theta_c$  the Cabibbo angle,  $\cos \theta_c = 0.97427$ .

### 4.2.2 $G$ -parity considerations

Taking into account the  $G$ -parity of the mesons,  $\pi(-)$ ,  $\eta(+)$ ,  $\eta'(+)$ ,  $\rho(+)$ ,  $\omega(-)$ ,  $\phi(-)$  we can associate a  $G$ -parity to all non-strange  $M_1 M_2$  pairs. On the other hand, the  $G$ -parity can already be established from the original  $d\bar{u}$  pair and the operator producing them, 1 or  $\sigma_i$ . We know that the  $G$ -parity for quarks belonging to the same isospin multiplet is given in Ref. [208],

$$G = (-1)^{L+S+I}, \quad (4.41)$$

but here  $L = 0, I = 1$  and  $S = 0$  for the 1 operator and  $S = 1$  for the  $\sigma_i$  operator. Thus we have  $G$ -parity negative for the 1 operator and positive parity for the  $\sigma_i$  operator. As a consequence we find the result of Table 4.3 for the different channels.

We can see, comparing with Table 4.2, that the  $G$ -parity rules of Table 4.3 coincide with what we obtained in Table 4.2 considering the order of the  $M_1 M_2$  pairs in the hadronization and the explicit formulas for  $M_0$  and  $N_\mu$ , with their properties under the exchange of  $M_1$  and  $M_2$ . We can see that the matrix elements are all zero for  $\pi^- \eta$ ,  $\pi^- \eta'$  cases, which shows from a different perspective that it is the value of  $M_0 = 0$  for  $PP$  and  $G$ -parity what makes the matrix elements zero, in coincidence with results obtained through different methods [210]. Note, however, that the  $G$ -parity restrictions have clear repercussions on which of the  $M_0$  or  $N_\mu$  terms contribute to the process.

Channels	$h_i$ (for $M_0$ )	$\bar{h}_i$ (for $N_\mu$ )
$\pi^0\pi^-$	0	$\sqrt{2}$
$\pi^-\eta$	0	0
$\pi^-\eta'$	0	0
$\pi^-\rho^0$	$\sqrt{2}$	0
$\pi^-\omega$	0	$\sqrt{2}$
$\pi^0\rho^-$	$-\sqrt{2}$	0
$\eta\rho^-$	0	$\frac{2}{\sqrt{3}}$
$\eta'\rho^-$	0	$\frac{2}{\sqrt{6}}$
$\rho^-\rho^0$	0	$\sqrt{2}$
$\rho^-\omega$	$\sqrt{2}$	0
$K^-\eta'$	0	$-\frac{1}{\sqrt{6}}\tan\theta_c$
$K^0K^-$	0	1
$K^0K^{*-}$	1	1
$K^{*0}K^-$	1	1
$K^{*0}K^{*-}$	1	1
$K^-\pi^0$	0	$\frac{1}{\sqrt{2}}\tan\theta_c$
$\bar{K}^0\pi^-$	0	$\tan\theta_c$
$K^-\rho^0$	$\frac{1}{\sqrt{2}}\tan\theta_c$	$\frac{1}{\sqrt{2}}\tan\theta_c$
$K^-\omega$	$\frac{1}{\sqrt{2}}\tan\theta_c$	$\frac{1}{\sqrt{2}}\tan\theta_c$
$\bar{K}^0\rho^-$	$\tan\theta_c$	$\tan\theta_c$
$\eta K^{*-}$	$-\frac{2}{\sqrt{3}}\tan\theta_c$	0
$\eta'K^{*-}$	$\frac{1}{\sqrt{6}}\tan\theta_c$	$\frac{3}{\sqrt{6}}\tan\theta_c$
$K^{*-}\pi^0$	$\frac{1}{\sqrt{2}}\tan\theta_c$	$\frac{1}{\sqrt{2}}\tan\theta_c$
$K^{*0}\pi^-$	$\tan\theta_c$	$\tan\theta_c$
$\phi K^-$	$\tan\theta_c$	$\tan\theta_c$
$K^{*-}\rho^0$	$\frac{1}{\sqrt{2}}\tan\theta_c$	$\frac{1}{\sqrt{2}}\tan\theta_c$
$K^{*-}\omega$	$\frac{1}{\sqrt{2}}\tan\theta_c$	$\frac{1}{\sqrt{2}}\tan\theta_c$
$\bar{K}^{*0}\rho^-$	$\tan\theta_c$	$\tan\theta_c$
$\phi K^{*-}$	$\tan\theta_c$	$\tan\theta_c$

Table 4.2: Weight for the different channels after taking into account the  $M_1M_2$  and  $M_2M_1$  components as they appear in the hadronization.



Channels	G-parity	$M_0$	$N_\mu$
$\pi^- \pi^0$	+	0	×
$\pi^- \eta$	-	0	0
$\pi^- \eta'$	-	0	0
$\pi^- \rho^0$	-	×	0
$\pi^- \omega$	+	0	×
$\pi^0 \rho^-$	-	×	0
$\eta \rho^-$	+	0	×
$\eta' \rho^-$	+	0	×
$\rho^- \rho^0$	+	0	×
$\rho^- \omega$	-	×	0

Table 4.3: Contributions of the different non-strange  $M_1 M_2$  pairs. The cross indicates non zero contribution.

### 4.3 Evaluation of $\bar{\sum} \sum |t|^2$ for the different processes

Following the nomenclature adopted in Eq. (4.21) we must evaluate

$$\bar{\sum} \sum |t|^2 = \bar{L}^{00} M_0 M_0^* + \bar{L}^{0i} M_0 N_i^* + \bar{L}^{i0} N_i M_0^* + \bar{L}^{ij} N_i N_j^* \quad (4.42)$$

and in this equation we must sum over  $M, M'$  the spin third components of  $J, J'$ . This is done in Appendix A.2 and here we summarize the results.

1)  $PP, J = 0, J' = 0$

Only the term  $N_\mu$  contributes and we obtain

$$\bar{\sum} \sum |t|^2 = \frac{1}{m_\tau m_\nu} \frac{1}{2\pi} \tilde{p}_1^2 \left( E_\tau E_\nu - \frac{\mathbf{p}^2}{3} \right), \quad (4.43)$$

which, as discussed previously, is evaluated in the frame where the system  $M_1, M_2$  is at rest,  $p$  is the momentum of the  $\tau$ , or  $\nu$ , in that frame, given by

$$p = \frac{\lambda^{1/2}(m_\tau^2, m_\nu^2, M_{\text{inv}}^2(M_1 M_2))}{2M_{\text{inv}}(M_1 M_2)}, \quad (4.44)$$

$E_\tau = \sqrt{m_\tau^2 + p^2}$ ,  $E_\nu = p$  and  $\bar{L}^{\mu\nu}$  of Eq. (4.23) is evaluated in this frame too. In Eq. (4.43)  $\tilde{p}_1$  is the momentum of the meson  $M_1$  in the same frame where the system  $M_1 M_2$  is at rest,

$$\tilde{p}_1 = \frac{\lambda^{1/2}(M_{\text{inv}}^2(M_1 M_2), m_{M_1}^2, m_{M_2}^2)}{2M_{\text{inv}}(M_1 M_2)}. \quad (4.45)$$

2)  $PV, J = 0, J' = 1; VP, J = 1, J' = 0$

a) The  $\bar{L}^{00} M_0 M_0^*$  contribution, summed over  $M, M'$  gives

$$\bar{\sum} \sum |t_a|^2 = \frac{1}{m_\tau m_\nu} \frac{1}{2\pi} \tilde{p}_1^2 (E_\tau E_\nu + \mathbf{p}^2). \quad (4.46)$$

b) The  $M_0 N_i^*$  and  $N_i M_0^*$  combinations give zero.

c) The  $N_i N_j^*$  term of Eq. (4.42) gives

$$\bar{\sum} \sum |t_c|^2 = \frac{1}{m_\tau m_\nu} \frac{1}{\pi} \tilde{p}_1^2 \left( E_\tau E_\nu - \frac{\mathbf{p}^2}{3} \right). \quad (4.47)$$

3)  $VV, J = 1, J' = 1$

(a) The  $\bar{L}^{00} M_0 M_0^*$  term gives

$$\bar{\sum} \sum |t_a|^2 = \frac{1}{m_\tau m_\nu} \frac{1}{\pi} \tilde{p}_1^2 (E_\tau E_\nu + \mathbf{p}^2). \quad (4.48)$$

(b) The  $\bar{L}^{0i} M_0 N_i^*, \bar{L}^{i0} N_i M_0^*$  terms give zero.

(c) The  $\bar{L}^{ij} N_i N_j^*$  term gives the result

$$\bar{\sum} \sum |t_c|^2 = \frac{1}{m_\tau m_\nu} \frac{1}{\pi} \tilde{p}_1^2 \frac{7}{2} \left( E_\tau E_\nu - \frac{\mathbf{p}^2}{3} \right). \quad (4.49)$$

Taking into account the weights  $h_i, \bar{h}_i$  of Table 4.2, we get finally the following result

1)  $PP, J=0, J'=0$

$$\bar{\sum} \sum |t|^2 = \bar{h}_i^2 \frac{1}{m_\tau m_\nu} \frac{1}{2\pi} \tilde{p}_1^2 \left( E_\tau E_\nu - \frac{\mathbf{p}^2}{3} \right). \quad (4.50)$$

2)  $PV, J=0, J'=1; VP, J=1, J'=0$

$$\bar{\sum} \sum |t|^2 = \frac{1}{m_\tau m_\nu} \frac{1}{2\pi} \tilde{p}_1^2 \left[ h_i^2 (E_\tau E_\nu + \mathbf{p}^2) + 2\bar{h}_i^2 \left( E_\tau E_\nu - \frac{\mathbf{p}^2}{3} \right) \right]. \quad (4.51)$$

3)  $VV, J=1, J'=1$

$$\bar{\sum} \sum |t|^2 = \frac{1}{m_\tau m_\nu} \frac{1}{\pi} \tilde{p}_1^2 \left[ h_i^2 (E_\tau E_\nu + \mathbf{p}^2) + \frac{7}{2} \bar{h}_i^2 \left( E_\tau E_\nu - \frac{\mathbf{p}^2}{3} \right) \right]. \quad (4.52)$$

In the former equations the angle integrations are already done in a way that finally we must take into account the full phase space with the angle independent expressions obtained in the former equations and we obtain

$$\frac{d\Gamma}{dM_{\text{inv}}(M_1 M_2)} = \frac{2m_\tau 2m_\nu}{(2\pi)^3} \frac{1}{4m_\tau^2} p_\nu \tilde{p}_1 \bar{\sum} \sum |t|^2, \quad (4.53)$$

where  $p_\nu$  is the neutrino momentum in the  $\tau$  rest frame

$$p_\nu = \frac{\lambda^{1/2}(m_\tau^2, m_\nu^2, M_{\text{inv}}^2(M_1 M_2))}{2M_\tau}, \quad (4.54)$$

and  $\tilde{p}_1$  the momentum of  $M_1$  in the  $M_1, M_2$  rest frame given in Eq. (4.45). The mass distribution of Eq. (4.53) is then integrated over the  $M_1 M_2$  invariant mass in order to obtain the width.

channels	$h_i$ (for $M_0$ )	$\bar{h}_i$ (for $N_\mu$ )
$\pi^- \rho^0$	0	$\sqrt{2}$
$\pi^- \omega$	$\sqrt{2}$	0
$\pi^0 \rho^-$	0	$-\sqrt{2}$
$\eta \rho^-$	$\frac{2}{\sqrt{3}}$	0
$\eta' \rho^-$	$\frac{2}{\sqrt{6}}$	0
$\rho^- \rho^0$	$\sqrt{2}$	0
$\rho^- \omega$	0	$\sqrt{2}$
$\eta K^{*-}$	0	$-\frac{2}{\sqrt{3}} \tan \theta_c$
$\eta' K^{*-}$	$\frac{3}{\sqrt{6}} \tan \theta_c$	$\frac{1}{\sqrt{6}} \tan \theta_c$

Table 4.4:  $h_i$  and  $\bar{h}_i$  coefficient for different channels with the two final mesons in  $s$ -wave.

## 4.4 $s$ -wave decays

In the previous sections we have assumed that the quarks  $d, \bar{u}$  of Fig. 4.1 are produced in their ground state. This leads to a negative parity  $q\bar{q}$  state, which makes the pair of mesons after the hadronization to be produced in  $p$ -wave and this is in agreement with the results of chiral perturbation theory for  $\tau^-$  decay into  $\nu_\tau$  and a pair of pseudoscalar mesons.

We shall extrapolate the scheme to pseudoscalar-vector and vector-vector production, but we can anticipate that, since the masses of these mesons are larger, the resulting momenta for the mesons are much smaller and the  $p$ -wave mechanism will lead to very small widths. Certainly, in this case,  $s$ -wave production shall be preferable. There is just one inconvenience. Two mesons with negative parity and  $s$ -wave have positive parity. This means that the  $d\bar{u}$  must be produced in an  $L' = 1$  state. This is accomplished creating one quark in  $L' = 1$  state.

The formalism in this case proceeds in total analogy to what we have done before. There is only one difference. Since a  $Y(L', M'_3, 1)$  is introduced, we have now two spherical harmonics: this one and the one from the  ${}^3P_0$  model, and they must combine to a final  $s$ -wave. Hence

$$Y_{1M_3} Y_{1M'_3} = \sum_l \left[ \frac{3 \cdot 3}{4\pi(2l+1)} \right] \mathcal{C}(11l; M_3, M'_3) \mathcal{C}(11l; 0, 0, 0) Y_{l, M_3+M'_3} \quad (4.55)$$

which can have  $l = 0, 2$  for parity reasons and we then choose  $l = 0$ . Evaluating explicitly the CGC we obtain

$$Y_{1M_3} Y_{1M'_3} \rightarrow \frac{1}{4\pi} (-1)^{M_3} \delta_{M_3, -M'_3} \quad (4.56)$$

And the rest of calculations proceed as in the case of  $p$ -wave, only the  $Y_{1,\mu}(\hat{\mathbf{q}})$  does not appear. Also the form factor now implies  $j_0(qr)$  in the integrand instead of  $\frac{3j_1(qr)}{qr}$  and the factor  $q$  outside the integral of Eq. (4.29) does not appear now. We obtain the results:

1)  $M_0$

a)  $PP, J = 0, J' = 0$

$$M_0 = 0 \quad (4.57)$$

b)  $PV, J = 0, J' = 1$

$$M_0 = \frac{1}{\sqrt{6}} \frac{1}{4\pi} \quad (4.58)$$

c)  $VP, J = 1, J' = 0$

$$M_0 = \frac{1}{\sqrt{6}} \frac{1}{4\pi} \quad (4.59)$$

d)  $VV, J = 1, J' = 1$

$$M_0 = \frac{1}{\sqrt{3}} \frac{1}{4\pi} \mathcal{C}(111; M, M', M + M') \quad (4.60)$$

2)  $N_\mu$

a)  $PP, J = 0, J' = 0$

$$N_\mu = \frac{1}{\sqrt{6}} \frac{1}{4\pi} \delta_{M0} \delta_{M'0} (-1)^{-\mu} \quad (4.61)$$

b)  $PV, J = 0, J' = 1$

$$N_\mu = -(-1)^{-\mu} \frac{1}{\sqrt{3}} \frac{1}{4\pi} \mathcal{C}(111; M', -\mu, M' - \mu) \delta_{M0} \quad (4.62)$$

c)  $VP, J = 1, J' = 0$

$$N_\mu = (-1)^{-\mu} \frac{1}{\sqrt{3}} \frac{1}{4\pi} \mathcal{C}(111; M, -\mu, M - \mu) \delta_{M'0} \quad (4.63)$$

d)  $VV, J = 1, J' = 1$

$$\begin{aligned} N_\mu &= \frac{1}{\sqrt{6}} \frac{1}{4\pi} \left\{ \delta_{M\mu} + 2(-1)^{-\mu-M'} \mathcal{C}(111; M, -\mu, M - \mu) \right. \\ &\quad \left. \times \mathcal{C}(111; M', -M - M' + \mu, -M + \mu) \right\} \quad (4.64) \end{aligned}$$

In this case table 4.1 is changed and under the exchange of the two mesons we obtain opposite signs than in this table because we do not have the  $Y_{1,\mu}(\hat{\mathbf{q}})$  factor. As a consequence, the weights of some channels, particularly those of defined  $G$ -parity, are changed. Note that now the rule  $(-1)^{L+S+I}$  for the  $G$ -parity implies positive  $G$ -parity for the operator "1" and negative  $G$ -parity for the operator  $\sigma_i$ . As a consequence, we get the results of table 4.4 for the new weights of the channels involved. The rest do not change. The final formulas for  $\overline{\sum} \sum |t|^2$ , up to a global normalization, are the same for  $p$ -wave removing the factor  $\tilde{p}_1^2$ , concretely:

1)  $PP, J = 0, J' = 0$

$$\overline{\sum} \sum |t|^2 = \frac{1}{m_\tau m_\nu} \left( \frac{1}{4\pi} \right)^2 \left( E_\tau E_\nu - \frac{\mathbf{p}^2}{3} \right) \frac{1}{2} \bar{h}_i^{-2} \quad (4.65)$$

2)  $PV, J = 0, J' = 1; VP, J = 1, J' = 0$

$$\overline{\sum} \sum |t|^2 = \frac{1}{m_\tau m_\nu} \left( \frac{1}{4\pi} \right)^2 \left[ (E_\tau E_\nu + \mathbf{p}^2) \frac{1}{2} h_i^2 + \left( E_\tau E_\nu - \frac{\mathbf{p}^2}{3} \right) \bar{h}_i^{-2} \right] \quad (4.66)$$

3)  $VV, J = 1, J' = 1$

$$\overline{\sum} \sum |t|^2 = \frac{1}{m_\tau m_\nu} \left( \frac{1}{4\pi} \right)^2 \left[ (E_\tau E_\nu + \mathbf{p}^2) h_i^2 + \frac{7}{2} \left( E_\tau E_\nu - \frac{\mathbf{p}^2}{3} \right) \bar{h}_i^{-2} \right] \quad (4.67)$$

## 4.5 Results

In Table 4.5 we show the results for the decays in Table 4.2 assuming the mesons are in  $p$ -wave. We should be careful selecting the data because in some cases a strong resonance can appear. This is the case of  $\tau^- \rightarrow \nu_\tau \pi^0 \pi^-$ , where the  $\rho^-(770)$  can be formed and decay to  $\pi^0 \pi^-$ . We should note that the  $\tau^- \rightarrow \nu_\tau \rho^-$  decay does not require the hadronization since a  $q\bar{q}$  can already produce the  $\rho^-$  [231]. In this case the rate of  $\rho^-$  production should be bigger than the non-resonant  $\nu_\tau \pi^0 \pi^-$  which is actually the case experimentally. We calculate only the non-resonant part of the decay, which involves the hadronization and we compare with the "non-resonant" results of the PDG [110]. The same can be said about the  $\nu_\tau \pi^- \bar{K}^0$  and  $\nu_\tau \pi^0 K^-$ . In fact, for  $\nu_\tau \pi^- \bar{K}^0$  the whole branching ratio is  $8.4 \times 10^{-3}$  while the "non-resonant" part is  $5.4 \times 10^{-4}$ . In this case the resonant part comes from  $\tau^- \rightarrow \nu_\tau K^{*-}$ . For the  $\nu_\tau \pi^0 K^-$  the PDG only quotes the whole branching ratio. We have estimated the non-resonant part as explained in the footnote of Table 4.5.

If we look at the Table 4.5 for decay to two pseudoscalars, we find that fixing our normalization to  $\nu_\tau K^- K^0$  the rates obtained in the other cases are close to experiment within a factor of two or less. The rates obtained for  $\nu_\tau \eta \pi^-$  and  $\nu_\tau \eta' \pi^-$  are zero

in our case, and experimentally the upper bounds are very small. For the case of  $\nu_\tau \eta' K^-$  we also get a value of the branching ratio which is smaller than the experimental upper bound. The exception to the rule is the  $\tau^- \rightarrow \nu_\tau \pi^0 \pi^-$  that in our case is about one order of magnitude bigger than experiment. This already indicates that the form factor of Eq. (4.29), with  $q$  quite big and  $\frac{3j_1(qr)}{qr}$  in the integrand, which we have assumed equal for all decays, should be smaller in the case of  $\nu_\tau \pi^0 \pi^-$  production. We should also note that we are taking a pion as a simple  $q\bar{q}$ , but this light Goldstone boson should be more complicated. Our results, and the discrepancies found, could serve as a tool of comparison for theoretical models of this form factor.

There is another consideration that we must do. If we take  $\tau^- \rightarrow \nu_\tau \pi^0 \pi^-$ , the  $\pi^0 \pi^-$  pair is in  $I = 1$ , but for identical spin zero particles within the same isospin multiplet this implies  $L = 1$ ,  $p$ -wave. However, in the case that we have different mesons in the final state this requirement does not hold and one could have some  $s$ -wave contribution in cases like  $\tau^- \rightarrow \nu_\tau \pi^0 K^-$ ,  $\tau^- \rightarrow \nu_\tau K^- K^0$ , etc. Note that we have related all the processes in Table 4.5 using the SU(3) results of Eq. (4.7). Dynamically we have assumed that the  $d\bar{u}$  pair ( $s\bar{u}$  pair) is produced in  $L = 0$  in all these cases, but this is not necessarily the case when we have two different pseudoscalars in the final state. Since the form factors in these two cases are different, we cannot relate the two mechanisms and this brings an extra uncertainty to our non-resonant pseudoscalar pair production. Since the  $s$ -wave requires  $L = 1$  primary quark pair production, the matrix element in Eq. (4.28) will be somewhat suppressed relative to  $L = 0$ . The contribution from  $s$ -wave in  $\tau^- \rightarrow \nu_\tau \pi \bar{K}$  is found small in [232, 233], and is shown to contribute only at very low  $\pi \bar{K}$  invariant masses in the  $\pi \bar{K}$  spectrum of the experiment [197]. The integrated contribution is estimated in [232] to be of the order of  $BR[\tau^- \rightarrow \nu_\tau (K\pi)_{s\text{-wave}}] = (3.88 \pm 0.19) \times 10^{-4}$ , or about one half of the sum of the non-resonant  $\tau^- \rightarrow \nu_\tau \pi^0 K^-$  and  $\tau^- \rightarrow \nu_\tau \pi^- \bar{K}^0$  contributions in Table 4.5.

The discrepancies with experiment that we find are in line with all the uncertainties that we have discussed. On the contrary the  $VP$ ,  $PV$  and  $VV$  cases, which are much less studied both theoretically and experimentally, proceeding all in  $s$ -wave, can be better related and there is where our approach is more useful. Also, because these reactions also allow to study the  $VP$  and  $VV$  interaction where some dynamically generated resonance appear. We turn now to this sector.

In Table 4.6, for  $PV$ , and  $VV$  decay, what we observe is that the assumption of  $p$ -wave in the mesons leads systematically to very small results compared to the experiment. There are two cases where the discrepancies are larger than in the other cases. This occurs for  $\tau^- \rightarrow \nu_\tau K^- \rho^0$  and  $\tau^- \rightarrow \nu_\tau \bar{K}^0 \rho^-$ . This has to be understood as a large contribution from the resonance  $K_1(1270)$  decaying into  $\bar{K} \rho$ , as found in [234], while we only calculate the non-resonant contributions. Yet, the findings of that work are illustrative because the  $K_1(1270)$  couples to  $\bar{K} \rho$  in  $s$ -wave [167, 235, 236], which

clearly indicate that  $PV$  and  $VV$  proceed via  $s$ -wave meson-meson production, not  $p$ -wave. We also take into account the mass distributions for the particles that have a width, but this leads to effects of the order of 10 – 20% for the cases where there are data, and do not improve the large discrepancies found.

As mentioned, the experimental data for  $\tau^- \rightarrow PV$  or  $\tau^- \rightarrow VV$  indicate that  $p$ -wave is not adequate and instead the decays proceed with the two mesons in  $s$ -wave. In Tables 4.7, 4.8, we show the results for the  $\tau^- \rightarrow \nu_\tau PV$  or  $\tau^- \rightarrow \nu_\tau VV$  with and without the convolution to take into account the mass distribution of the vector mesons that have a width. This has been done according to the following formulas. In the case of only one vector we make the convolution

$$\Gamma_{\tau^- \rightarrow \nu_\tau M_1 M_2} = \frac{1}{N} \int_{(M_1-2\Gamma_1)^2}^{(M_1+2\Gamma_1)^2} dm_1^2 \left( -\frac{1}{\pi} \right) \text{Im} D_{M_1}(m_1) \int dM_{\text{inv}} \frac{d\Gamma(m_1, m_2)}{dM_{\text{inv}}(12)}, \quad (4.68)$$

where  $D(m_1)$  is the vector propagator,

$$D(m_1) = \frac{1}{m_1^2 - m_R^2 + i\Gamma_R m_R}. \quad (4.69)$$

and  $N$  is the normalization factor

$$N = \int_{(M_1-2\Gamma_1)^2}^{(M_1+2\Gamma_1)^2} dm_1^2 \left( -\frac{1}{\pi} \right) \text{Im} D_{M_1}(m_1). \quad (4.70)$$

For the case of two vectors we make a double convolution as

$$\begin{aligned} \Gamma_{\tau^- \rightarrow \nu_\tau M_1 M_2} &= \frac{1}{N'} \int_{(M_1-2\Gamma_1)^2}^{(M_1+2\Gamma_1)^2} dm_1^2 \left( -\frac{1}{\pi} \right) \text{Im} D_{M_1}(m_1) \int_{(M_2-2\Gamma_2)^2}^{(M_2+2\Gamma_2)^2} dm_2^2 \left( -\frac{1}{\pi} \right) \\ &\times \text{Im} D_{M_2}(m_2) \int dM_{\text{inv}} \frac{d\Gamma(m_1, m_2)}{dM_{\text{inv}}(12)}, \end{aligned} \quad (4.71)$$

where

$$N' = \int_{(M_1-2\Gamma_1)^2}^{(M_1+2\Gamma_1)^2} dm_1^2 \left( -\frac{1}{\pi} \right) \text{Im} D_{M_1}(m_1) \int_{(M_2-2\Gamma_2)^2}^{(M_2+2\Gamma_2)^2} dm_2^2 \left( -\frac{1}{\pi} \right) \text{Im} D_{M_2}(m_2). \quad (4.72)$$

When performing the convolution, some of the decays forbidden in Table 4.7, as  $\tau^- \rightarrow \nu_\tau \eta' K^{*-}$  and  $\tau^- \rightarrow \nu_\tau K^{*0} K^{*-}$ , are now allowed, and finite results arise in Table 4.8, although with very small rates. By looking at Table 4.8 and normalizing the results to the  $\tau^- \rightarrow \nu_\tau \eta K^{*-}$  branching ratio, we obtain fair results compared to experiment within a factor of about two, with two exceptions:  $\tau^- \rightarrow \nu_\tau K^- \rho^0$  and  $\tau^- \rightarrow \nu_\tau \bar{K}^0 \rho^-$ . As discussed previously, these two decays have a large contribution



from the  $K_1(1270)$  resonance [234] and thus, with the non-resonant part that we calculate we underestimate the experimental results by about a factor three or more. This can be used in an opposite direction: a gross underestimation of the rates that we have calculated compared with future experiments would be indicative of substantial resonance contribution, which can stimulate the research for such resonance in the mass distribution.

It is also worth mentioning that in the work of Refs. [235, 236] two  $K_1(1270)$  resonances were found coupling mostly to  $\pi K^*$  and  $K\rho$ . The fair agreement with the data of  $\tau^- \rightarrow \nu_\tau \bar{K}^{*0} \pi^-$  should be looked with caution, because we expect some overestimation due to the light pion mass, which indicates that there is room for a resonant contribution, in this case one of the two  $K_1(1270)$ . Something similar could be said about the  $\tau^- \rightarrow \nu_\tau \pi^- \rho^0$  and  $\tau^- \rightarrow \nu_\tau \pi^0 \rho^-$  decays. We should also expect an overestimation due to the small pion mass but we instead underestimate the data by about a factor of two. This again has to be looked with the perspective that the  $\pi\rho$  couples strongly to the  $h_1(1170)$  and  $a_1(1260)$  resonances [235].

An interesting and clean case is the decay  $\tau^- \rightarrow \nu_\tau \phi K^-$ , where the agreement with experiment is fair. In this case the coupling of  $\phi K^-$  to the two  $K_1(1270)$  resonances found in Ref. [235] is quite weak. Also in the  $\tau^- \rightarrow \nu_\tau \eta K^{*-}$  decay, taken as reference, the coupling of  $\eta K^{*-}$  to one  $K_1(1270)$  resonance is negligible and the coupling to the second  $K_1(1270)$  is also smaller than to the  $\rho K$  dominant channel [235]. This makes the comparison of these two modes fair.

For vector-vector there is also work leading to dynamically generated resonance from the  $VV$  interaction [236–238]. However we do not have data for  $\tau^-$  decay into  $\nu_\tau$  and  $VV$ , something that could change in the future. In that case the comparison of the measured decay rates with our predictions would be of interest.

Finally, we should also mention that the formalism discussed here can be considered as a starting point to study the final state interaction of  $M_1 M_2$ , eventually leading to dynamically generated resonances. It would be most interesting to study experimentally in detail invariant mass distributions in the  $\tau^- \rightarrow \nu_\tau M_1 M_2$  decays. One case that has deserved some attention from this perspective is the  $\tau^- \rightarrow \nu_\tau \pi \rho$  via the  $a_1(1260)$  [239]. In Ref. [240] this decay is done via  $\tau^- \rightarrow \nu_\tau PV$ , with  $PV$  coupled channels that generate the  $a_1(1260)$ , which decays into  $\pi\rho$ . In the approach [240] one would take the amplitudes evaluated here for  $\tau^- \rightarrow \nu_\tau \widetilde{M}_1 \widetilde{M}_2$  with all possible coupled channels that lead to a given resonance, then propagate  $\widetilde{M}_1 \widetilde{M}_2$  as they would do in scattering theory, and later these  $\widetilde{M}_1 \widetilde{M}_2$  mesons would be coupled to  $M_1 M_2$ , which are the observed mesons. The transition of  $\widetilde{M}_1 \widetilde{M}_2$  to  $M_1 M_2$  is given by the  $MM \rightarrow MM$  matrix that contains information on the resonance [235, 236]. Work along these lines has already been done studying the  $\tau^-$  decay into a pseudoscalar and an axial-vector meson [241], or into  $\pi^-$  and the  $f_0(980)$ ,  $a_0(980)$  resonances [242].

We have used a novel formalism with the explicit  ${}^3P_0$  model for hadronization

and the necessary angular momentum algebra to relate the different processes, and we have shown that only one form factor is needed for  $p$ -wave production and another one for  $s$ -wave production. It is interesting to relate our formalism with a more conventional one used in the related semileptonic  $M_1 \rightarrow \bar{\nu}lM_2$  process which involves several form factors. This comparison is done in Section 5 of [243]. Indeed, taking the  $P \rightarrow \bar{\nu}lV$  reaction to compare, one can see in [244–246] that four form factors are needed. Equivalently, four other form factors are proposed in [241, 247],  $V(q^2)$ ,  $A_0(q^2)$ ,  $A_1(q^2)$ ,  $A_2(q^2)$ . In [243] it was found that close to the end point,  $\omega = 1$  ( $M_{\text{inv}}(\nu l)$  maximum) the two formalisms, the one used here and the one of [241, 247] gave practically identical results for ratios of rates. This limit corresponds to having the two mesons at rest, and this is the approximation that we have used in Section 4.2.1, which allows us to use only one form factor for this reaction. In [243] it was shown that at the end point,  $M_{\text{inv}}(\nu l)$  maximum, only the form factor  $A_1(q^2)$  contributes, which shows in a different way that only one form factor is needed in this limit. In [248] the application of the formalism of [241, 247] to  $\tau^-$  decay was done, showing that, indeed, the range of  $M_{\text{inv}}$  of the mesons in  $\tau^-$  decays falls well within the range where the single form factor  $A_1(q^2)$  dominates. Our approach allows to extrapolate the results to the  $\tau^- \rightarrow \nu_\tau VV$  case without extra form factors.

Decay process	$BR$ (Theo.)	$BR$ (Exp.)
$^1\tau^- \rightarrow \nu_\tau \pi^0 \pi^-$ <sup>a</sup>	$2.48 \times 10^{-2}$	$(3.0 \pm 3.2) \times 10^{-3}$
$^1\tau^- \rightarrow \nu_\tau \eta \pi^-$	0	$< 9.9 \times 10^{-5}$
$^1\tau^- \rightarrow \nu_\tau \eta' \pi^-$	0	$< 4.0 \times 10^{-6}$
$^2\tau^- \rightarrow \nu_\tau \eta K^-$ <sup>b</sup>	$8.17 \times 10^{-5}$	$(1.55 \pm 0.08) \times 10^{-4}$
$^2\tau^- \rightarrow \nu_\tau \eta' K^-$	$3.26 \times 10^{-7}$	$< 2.4 \times 10^{-6}$
$^2\tau^- \rightarrow \nu_\tau \pi^0 K^-$ <sup>c</sup>	$1.29 \times 10^{-4}$	$(2.7 \pm 1.1) \times 10^{-4}$
$^1\tau^- \rightarrow \nu_\tau K^- K^0$	fit to the Exp.	$(1.48 \pm 0.05) \times 10^{-3}$
$^2\tau^- \rightarrow \nu_\tau \pi^- \bar{K}^0$	$2.52 \times 10^{-4}$	$(5.4 \pm 2.1) \times 10^{-4}$

Table 4.5: Branching ratios for  $PP$  case in  $p$ -wave normalized by  $\tau^- \rightarrow \nu_\tau K^- K^0$ .

<sup>a</sup> Means Cabibbo-allowed

<sup>b</sup> Means Cabibbo-suppressed

<sup>c</sup> The PDG has only the whole contribution including  $K^{*-}$  production. We evaluate the rates in two ways:  $\frac{1}{2}$  of the rate of  $\tau^- \rightarrow \nu_\tau \pi^- \bar{K}^0$  (non-resonant) and taking the whole range times the ratio of  $\frac{BR(\tau^- \rightarrow \nu_\tau \pi^- \bar{K}^0)(\text{non-resonant})}{BR(\tau^- \rightarrow \nu_\tau \pi^- \bar{K}^0)(\text{whole})}$ . Both ways give the same result. The error is taken from  $\tau^- \rightarrow \nu_\tau \pi^- \bar{K}^0$  in the table.

Decay process	$BR$ (Theo.)	$BR$ (Exp.)
${}^1\tau^- \rightarrow \nu_\tau \pi^- \rho^0$	$3.90 \times 10^{-3}$	—
${}^1\tau^- \rightarrow \nu_\tau \pi^- \omega$	$5.31 \times 10^{-3}$	$(1.95 \pm 0.06)\%$
${}^1\tau^- \rightarrow \nu_\tau \pi^0 \rho^-$	$3.95 \times 10^{-3}$	—
${}^1\tau^- \rightarrow \nu_\tau \eta \rho^-$	$4.32 \times 10^{-4}$	—
${}^1\tau^- \rightarrow \nu_\tau \eta' \rho^-$	$8.25 \times 10^{-9}$	—
${}^1\tau^- \rightarrow \nu_\tau K^0 K^{*-}$	$2.51 \times 10^{-4}$	—
${}^1\tau^- \rightarrow \nu_\tau K^{*0} K^-$	$2.49 \times 10^{-4}$	$(2.1 \pm 0.4) \times 10^{-3}$
${}^2\tau^- \rightarrow \nu_\tau K^- \rho^0$	$2.18 \times 10^{-5}$	$(1.4 \pm 0.5) \times 10^{-3}$
${}^2\tau^- \rightarrow \nu_\tau K^- \omega$	$2.04 \times 10^{-5}$	$(4.1 \pm 0.9) \times 10^{-4}$
${}^2\tau^- \rightarrow \nu_\tau \bar{K}^0 \rho^-$	$4.22 \times 10^{-5}$	$(2.2 \pm 0.5) \times 10^{-3}$
${}^2\tau^- \rightarrow \nu_\tau \eta K^{*-}$	$3.70 \times 10^{-6}$	$(1.38 \pm 0.15) \times 10^{-4}$
${}^2\tau^- \rightarrow \nu_\tau \eta' K^{*-}$	0	—
${}^2\tau^- \rightarrow \nu_\tau \pi^0 K^{*-}$	$6.37 \times 10^{-5}$	—
${}^2\tau^- \rightarrow \nu_\tau \bar{K}^{*0} \pi^-$	$1.22 \times 10^{-4}$	$(2.2 \pm 0.5) \times 10^{-3}$
${}^2\tau^- \rightarrow \nu_\tau \phi K^-$	$2.40 \times 10^{-6}$	$(4.4 \pm 1.6) \times 10^{-5}$
${}^2\tau^- \rightarrow \nu_\tau \rho^- \rho^0$	$1.24 \times 10^{-4}$	—
${}^2\tau^- \rightarrow \nu_\tau \rho^- \omega$	$3.35 \times 10^{-5}$	—
${}^2\tau^- \rightarrow \nu_\tau K^{*0} K^{*-}$	0	—
${}^2\tau^- \rightarrow \nu_\tau K^{*-} \rho^0$	$9.04 \times 10^{-8}$	—
${}^2\tau^- \rightarrow \nu_\tau K^{*-} \omega$	$6.65 \times 10^{-8}$	—
${}^2\tau^- \rightarrow \nu_\tau \bar{K}^{*0} \rho^-$	$1.54 \times 10^{-7}$	—
${}^2\tau^- \rightarrow \nu_\tau K^{*-} \phi$	0	—

Table 4.6: The same as Table 4.5 but for  $PV$  and  $VV$  cases. The results here in  $p$ -wave are only to support that they are in clear contradiction with experiment. Our real predictions for these cases are in Table 4.7 and 4.8.

Decay process	$BR$ (Theo.)	$BR$ (Exp.)
$\tau^- \rightarrow \nu_\tau \pi^- \rho^0$	$7.68 \times 10^{-2}$	—
$\tau^- \rightarrow \nu_\tau \pi^- \omega$	$5.80 \times 10^{-2}$	$(1.95 \pm 0.06)\%$
$\tau^- \rightarrow \nu_\tau \pi^0 \rho^-$	$7.78 \times 10^{-2}$	—
$\tau^- \rightarrow \nu_\tau \eta \rho^-$	$4.50 \times 10^{-3}$	—
$\tau^- \rightarrow \nu_\tau \eta' \rho^-$	$5.89 \times 10^{-7}$	—
$\tau^- \rightarrow \nu_\tau K^0 K^{*-}$	$4.95 \times 10^{-3}$	—
$\tau^- \rightarrow \nu_\tau K^{*0} K^-$	$4.93 \times 10^{-3}$	$(2.1 \pm 0.4) \times 10^{-3}$
$\tau^- \rightarrow \nu_\tau K^- \rho^0$	$3.41 \times 10^{-4}$	$(1.4 \pm 0.5) \times 10^{-3}$
$\tau^- \rightarrow \nu_\tau K^- \omega$	$3.24 \times 10^{-4}$	$(4.1 \pm 0.9) \times 10^{-4}$
$\tau^- \rightarrow \nu_\tau \bar{K}^0 \rho^-$	$6.64 \times 10^{-4}$	$(2.2 \pm 0.5) \times 10^{-3}$
$\tau^- \rightarrow \nu_\tau \eta K^{*-}$	fit to the exp.	$(1.38 \pm 0.15) \times 10^{-4}$
$\tau^- \rightarrow \nu_\tau \eta' K^{*-}$	0	—
$\tau^- \rightarrow \nu_\tau \pi^0 K^{*-}$	$1.07 \times 10^{-3}$	—
$\tau^- \rightarrow \nu_\tau \bar{K}^{*0} \pi^-$	$2.05 \times 10^{-3}$	$(2.2 \pm 0.5) \times 10^{-3}$
$\tau^- \rightarrow \nu_\tau \phi K^-$	$6.82 \times 10^{-5}$	$(4.4 \pm 1.6) \times 10^{-5}$
$\tau^- \rightarrow \nu_\tau \rho^- \rho^0$	$1.15 \times 10^{-3}$	—
$\tau^- \rightarrow \nu_\tau \rho^- \omega$	$3.19 \times 10^{-3}$	—
$\tau^- \rightarrow \nu_\tau K^{*0} K^{*-}$	0	—
$\tau^- \rightarrow \nu_\tau K^{*-} \rho^0$	$5.15 \times 10^{-6}$	—
$\tau^- \rightarrow \nu_\tau K^{*-} \omega$	$4.05 \times 10^{-6}$	—
$\tau^- \rightarrow \nu_\tau \bar{K}^{*0} \rho^-$	$9.09 \times 10^{-6}$	—
$\tau^- \rightarrow \nu_\tau K^{*-} \phi$	0	—

Table 4.7: Branching ratios for  $PV$  and  $VV$  cases in  $s$ -wave normalized by  $\tau^- \rightarrow \nu_\tau \eta K^{*-}$

Decay process	$BR$ (Theo.)	$BR$ (Exp.)
$\tau^- \rightarrow \nu_\tau \pi^- \rho^0$	$7.81 \times 10^{-2}$	—
$\tau^- \rightarrow \nu_\tau \pi^- \omega$	$5.56 \times 10^{-2}$	$(1.95 \pm 0.06)\%$
$\tau^- \rightarrow \nu_\tau \pi^0 \rho^-$	$7.91 \times 10^{-2}$	—
$\tau^- \rightarrow \nu_\tau \eta \rho^-$	$5.34 \times 10^{-3}$	—
$\tau^- \rightarrow \nu_\tau \eta' \rho^-$	$2.96 \times 10^{-5}$	—
$\tau^- \rightarrow \nu_\tau K^0 K^{*-}$	$4.91 \times 10^{-3}$	—
$\tau^- \rightarrow \nu_\tau K^{*0} K^-$	$4.87 \times 10^{-3}$	$(2.1 \pm 0.4) \times 10^{-3}$
$\tau^- \rightarrow \nu_\tau K^- \rho^0$	$3.82 \times 10^{-4}$	$(1.4 \pm 0.5) \times 10^{-3}$
$\tau^- \rightarrow \nu_\tau K^- \omega$	$3.10 \times 10^{-4}$	$(4.1 \pm 0.9) \times 10^{-4}$
$\tau^- \rightarrow \nu_\tau \bar{K}^0 \rho^-$	$7.44 \times 10^{-4}$	$(2.2 \pm 0.5) \times 10^{-3}$
$\tau^- \rightarrow \eta K^{*-} \nu_\tau$	fit to the Exp.	$(1.38 \pm 0.15) \times 10^{-4}$
$\tau^- \rightarrow \nu_\tau \eta' K^{*-}$	$1.21 \times 10^{-10}$	—
$\tau^- \rightarrow \nu_\tau \pi^0 K^{*-}$	$1.03 \times 10^{-3}$	—
$\tau^- \rightarrow \nu_\tau \bar{K}^{*0} \pi^-$	$1.99 \times 10^{-3}$	$(2.2 \pm 0.5) \times 10^{-3}$
$\tau^- \rightarrow \nu_\tau \phi K^-$	$6.54 \times 10^{-5}$	$(4.4 \pm 1.6) \times 10^{-5}$
$\tau^- \rightarrow \nu_\tau \rho^- \rho^0$	$3.31 \times 10^{-3}$	—
$\tau^- \rightarrow \nu_\tau \rho^- \omega$	$5.82 \times 10^{-3}$	—
$\tau^- \rightarrow \nu_\tau K^{*0} K^{*-}$	$8.18 \times 10^{-6}$	—
$\tau^- \rightarrow \nu_\tau K^{*-} \rho^0$	$2.96 \times 10^{-5}$	—
$\tau^- \rightarrow \nu_\tau K^{*-} \omega$	$6.0 \times 10^{-6}$	—
$\tau^- \rightarrow \nu_\tau \bar{K}^{*0} \rho^-$	$5.46 \times 10^{-5}$	—
$\tau^- \rightarrow \nu_\tau K^{*-} \phi$	0	—

Table 4.8: The same as Table 4.7 but with convolution.

## 4.6 Discussion and perspective

The present paper brings some novelties and the results are useful for predictions of new decay modes, as well as a means to find out resonances that couple to certain meson-meson channels. We briefly discuss below the novelties of the present work:

1. Although the sums over CGC can be done numerically nowadays, the laborious but useful work reported in the appendix allowed us to get finally extremely simple matrix elements for all possible transitions to  $PP$ ,  $PV$ ,  $VP$ ,  $VV$ . This allows a qualitative understanding of the different rates obtained.
2. Another useful output of these analytical calculations is the fact that we could see explicitly the role of  $G$ -parity in the different reactions, and how it affects different  $PP$  or  $PV$ ,  $VV$  decay modes. This was done from a very different perspective to the conventional one, based on the order in which the  $M_1M_2$  components are produced in the hadronization and the expressions of our amplitudes for  $M_1M_2$  and  $M_2M_1$  production. Also, it was interesting to find the extrapolation of these constraints to the strange sector, even if  $G$ -parity is not a good quantum number there, something that is pointed out for the first time.
3. The study done here also convinced us that the  $VP$ ,  $PV$  and  $VV$  modes proceed in the  $s$ -wave meson-meson channel, unlike the  $PP$  mode that requires  $p$ -wave, although for  $PP$  corresponding to different particles a contribution from  $s$ -wave is also possible. Experimental data in some reactions support this finding.
4. For the case of  $PP$  production we indicated that we did not consider the direct vector production followed by  $V \rightarrow PP$ . This is a part that has been calculated in many approaches and is simpler and more accurate to evaluate because the original  $q\bar{q}$  produced can directly produce the vector meson [195,196]. Instead, we calculated the non-resonant part, which requires the hadronization of the initial  $q\bar{q}$  pair and is subject to larger uncertainty, also in the experimental extraction. Our agreement with experiment for this non-resonant part within a factor of two is fair.
5. For the  $PV$  and  $VP$  decay modes there is no experimental separation between the resonant and non-resonant parts. In this case we turn the discrepancies found between our results and experiment into an advantage. Indeed, the results of [167, 235, 236] indicate that resonances in this sector stem from the interaction of  $VP$  components in coupled channels. Hence, the discrepancies found indicate the need for final state interaction of coupled channels that couple to the final  $VP$ . In other words, these cases constitute clear examples where one can learn much about meson meson interaction and hadron dynamics. The

same could be said in case of  $VV$ , which also produces dynamically generated resonances [236–238], but there are no data so far.

6. We also value that by means of the simple formulas that we obtained we could correlate many reactions and we did the calculations for eventually all possible  $\tau \rightarrow \nu_\tau M_1 M_2$  decays.
7. As a new path to continue with this problem, starting from the findings of the present work, we can suggest the test of quark models by implementing the form factor

$$\left\{ \begin{array}{ll} \int r^3 dr \frac{3j_1(qr)}{qr} \prod_i \varphi_i(r), & \text{for } PP \text{ case;} \\ \int r^2 dr j_0(qr) \prod_i \varphi_i(r), & \text{for } PV \text{ and } VV \text{ cases,} \end{array} \right. \quad (4.73)$$

and using them together with the amplitudes obtained here. Quark models like those in Refs. [219, 227] and [249] would be most suited for this work.

8. There is another benefit from the present formulation. We provide directly the amplitudes in terms of  $JM, J'M'$ . Recently the power of polarization measurements to provide information of models beyond the standard model in the related semileptonic decay of  $B$  mesons has been stressed [250, 251]. The present formalism provides accurate ratios of differential widths for different  $M, M'$  since in these ratios the missing form factor cancels. Steps in this direction are given within the present formalism in [218] for semileptonic reactions. Similar steps could be done for  $\tau$  decays into the different channels that we have studied. Steps in this direction are given in [248]. Actually, the polarization issue in  $\tau$  decays has already been addressed, concretely in the  $\tau^- \rightarrow \nu_\tau K^- \pi^0$  reaction, but only looking at the  $\tau$  polarization [252].
9. Another path worth undertaking would be the consideration of final state interaction of the meson pair produced. As mentioned above, the rates evaluated by us correspond to non-resonant contribution of the meson pairs. In some cases of  $PP$  there is a clear contribution from vector mesons, which does not come from final state interaction but from the direct production of  $q\bar{q}$  that forms the vector mesons. Note that the dominance of the  $q\bar{q}$  component for the vector mesons has been thoroughly checked [231]. Conversely, the meson-meson interaction in  $s$ -wave gives rise to many dynamically generated resonances, and the  $M_1 M_2$  invariant mass distribution would reveal this. Steps in this direction for other reactions have been done in Refs. [8, 224]. This is a promising source of information which should be accompanied by a parallel experimental

study of invariant mass distributions. Our work provides the  $M_1M_2$  mass distributions at tree level (non-resonant part). Any experimental diversion from these predictions is a signal of a resonance as a strong final state interaction of the pair of mesons. To help in this direction we plot three mass distributions to the  $PP$ ,  $PV$  and  $VV$  cases, concretely the  $\tau^- \rightarrow \nu_\tau K^- K^0$ ,  $\tau^- \rightarrow \nu_\tau \eta K^{*-}$ , and  $\tau^- \rightarrow \nu_\tau \rho^- \omega$  in Figs. 4.3, 4.4 and 4.5, respectively.

We have chosen cases where one expects very small final state interaction, according to the findings of Refs. [236,238,253], and we expect them to agree well with experiments. It is rewarding that there are data for two of these reactions, the  $\tau^- \rightarrow K^- K^0 \nu_\tau$  and the  $\tau^- \rightarrow \eta K^{*-} \nu_\tau$ .

We should note that the shapes of the  $PP$  (Fig.4.3) and  $PV$ ,  $VV$  (Figs.4.4, 4.5) distributions are quite different.

In Fig.4.3 we show our predictions for the  $K^- K^0$  mass distribution for the  $\tau^- \rightarrow K^- K^0 \nu_\tau$  decay. We show experimental data from the experiments [254–256], the most recent one [256] providing a very precise spectrum. We can see that the agreement of our mass distribution with experiments is relatively good, particularly taking into account the very different shape of the mass distribution compared to the  $VP$  and  $VV$  cases. Our results and the data of [255] are normalized to the area of the integrated experimental  $d\Gamma/dM_{\text{inv}}$  of the other two experiments.

In Fig.4.4 we also show our results compared to the experimental data for the  $\eta K^{*-}$  invariant mass distribution from the  $\tau^- \rightarrow \eta K^{*-} \nu_\tau$  decay [201]. The experimental mass distribution is for  $\pi \bar{K}_S \eta$ , but in the same paper one can see that  $\pi K$  comes from  $K^*$ . We see again that the agreement with experiment is good, and the shape of the distribution is very different to the one of  $K^- K^0$  in Fig.4.3. This supports our conclusion that the  $PV$  pair is produced in  $s$ -wave.

In Fig.4.5 we show our predictions for the  $\rho^- \omega$  mass distribution in  $\tau^- \rightarrow \nu_\tau \rho^- \omega$  decay. There are no data for this reaction, but we predict a shape similar to the one of Fig.4.4, which is tied to the  $s$ -wave character of the  $VV$  pair produced.

It is interesting to mention that in [201] there is also a mass distribution for  $\eta K$  coming from  $\tau^- \rightarrow \nu_\tau \eta K$  decay. The shape is not symmetrical like the one of Fig. 4.3, but more similar to the one of Fig.4.4. However, one should not conclude that this proceeds in  $s$ -wave, rather the reason for it is that the  $\eta K$  channel couples very strongly to  $K^*$  (stronger than  $\pi K$  to  $K^*$ ), and the  $K^*$  mass is below the threshold of  $\eta K$ . As a consequence, the strength of the distribution tends to pile up close to threshold. One may wonder why this does not happen in Fig.4.3, since  $K \bar{K}$  also couples to the  $\rho$ . However, in studies of coupled channels with unitarity for the  $\rho$  including  $\pi\pi$  and  $K \bar{K}$ , the role of  $K \bar{K}$  is found small



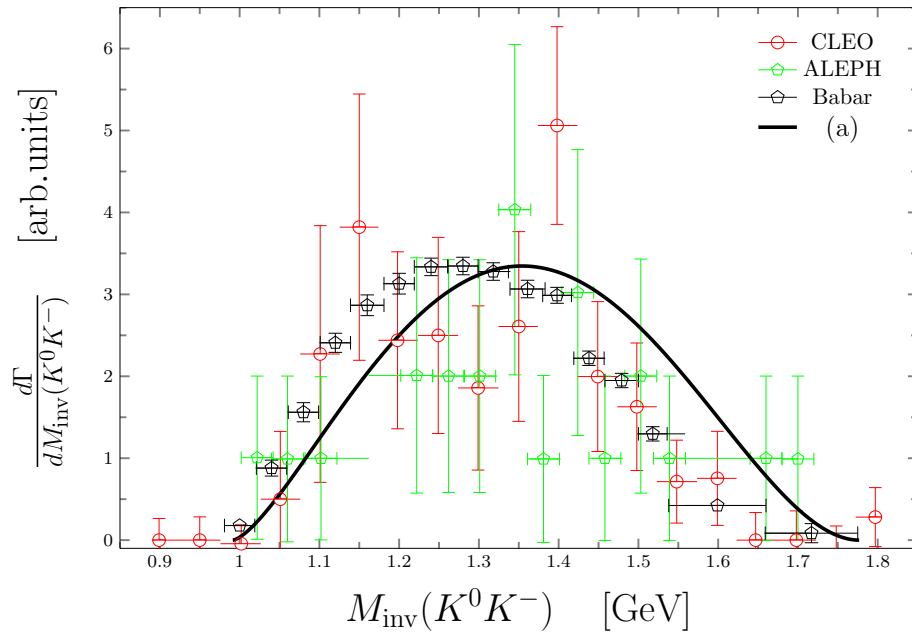


Figure 4.3: Invariant mass distribution for  $\tau^- \rightarrow \nu_\tau K_S^0 K^-$  decay. Data of CLEO, ALEPH, and BaBar Collaborations are from Refs. [254–256], respectively, and line (a) shows the results evaluated with Eq. (4.50).

[158, 257]. Yet, this could be responsible for the small diversion of our results with the very precise recent data of BaBar [256].

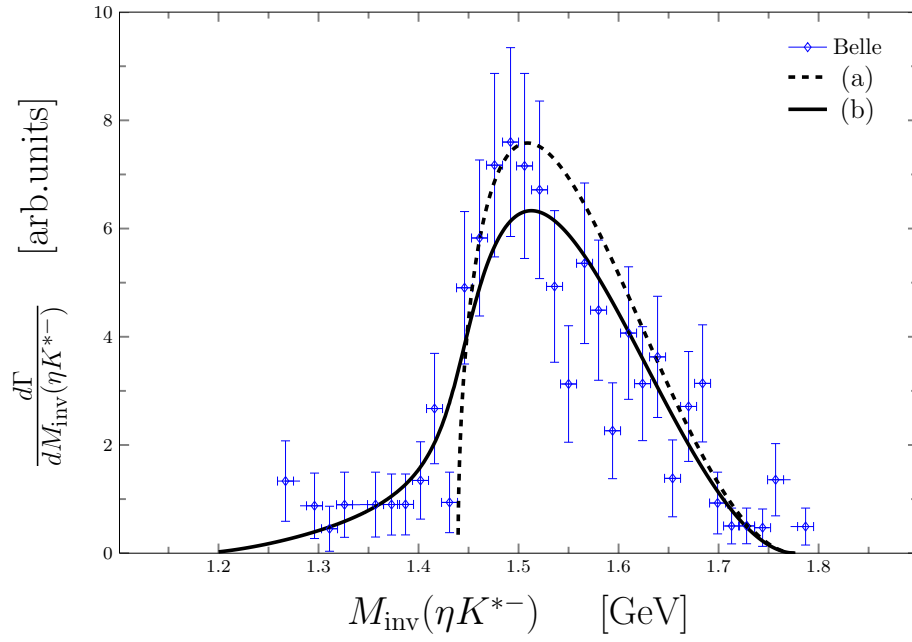


Figure 4.4: invariant mass distribution for  $\tau^- \rightarrow \nu_\tau \eta K^{*-}$  decay. The experimental data is taken from Belle Collaboration Ref. [201]. The line (a) shows the result without a convolution, and line (b) takes into account the width of the  $K^*$ , evaluated with a convolution with the  $K^*$  spectral function, as in Eqs. (4.68) and (4.70) but putting the limits of  $m^2$  as given by phase space (not  $M_1 - 2\Gamma_1$ ,  $M_1 + 2\Gamma_1$ ).

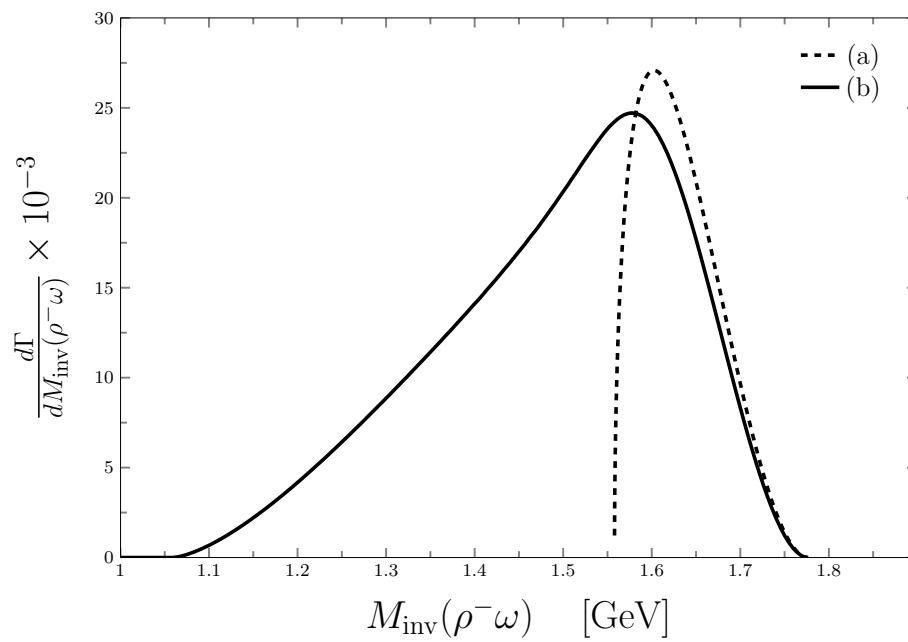


Figure 4.5: invariant mass distribution for  $\tau^- \rightarrow \nu_\tau \rho^- \omega$  decay. The results are normalized by fitting the data of  $\tau^- \rightarrow \nu_\tau \eta K^{*-}$  decay, and line (a) with fixed  $m_\rho$  mass and (b) taking the  $m_\rho$  mass distribution over the full phase space as in Fig. 4.4.

## 4.7 Comparison with other approaches

In this section we take advantage to compare our results with other ones obtained in different approaches. The example most studied is  $\tau^- \rightarrow \pi^- \pi^0 \nu_\tau$  [191, 192, 195, 258]. In Ref. [195] vector meson dominance is addressed in  $\tau^- \rightarrow \nu_\tau \rho^-$  with the  $\rho$  decaying into  $\pi^- \pi^0$ . In Ref. [191] vector form factors are considered and the  $\rho$ ,  $\rho'$ , contributions are evaluated. One model that has proved rather adequate to study these reactions is the NJL model, which is used in [258]. The model for this and related reactions is based on the mechanism of Fig.4.6 (a) and (b).

In the diagram of Fig.4.6 (a) the  $W$  couples to a  $q\bar{q}$  state and by means of a triangle mechanism, exchanging a quark  $q'$ , the  $q\bar{q}'$  and  $q'\bar{q}$  pairs give rise to two pions with the Lagrangians of the NJL model [205]. In the diagram of Fig.4.6 (b) the  $W$  also couples to  $q\bar{q}$  but this  $q\bar{q}$  couples later to a vector meson which again decays into  $\pi^- \pi^0$ , for which the NJL model is used again. Eventually all models give fair results for this mode where the  $\rho$  production is largely dominant.

As we discussed in the results section, for this mode we only calculated the non-resonant part and furthermore it relies on form factors implicitly evaluated from the  $\tau^- \rightarrow \nu_\tau K^- K^0$  (our reference decay width). Since there are larger momentum transfers for the case of the  $\pi$  production, the reduction should be bigger, and this is the reason why we overestimate the experimental rate in at least a factor of four (note also the large experimental errors). This is the largest disagreement of our results for  $PP$  compared to the corresponding data. In all other  $PP$  cases the agreement is much better, always within a factor of two, which we should accept as the intrinsic uncertainty for our model, trying to correlate such diverse data.

It is interesting to observe that although the NJL model and our way of hadronization using the  ${}^3P_0$  model and quark wave functions look so different, they are not. Indeed, loops with intermediate particles (quarks or nucleons) are the alternative way in Field Theory to take into account wave functions of a conventional Quantum Mechanical approach [259, 260].

Another channel worth discussing is the  $\tau^- \rightarrow \nu_\tau \eta (\eta') \pi^-$ . Our formalism, with the  ${}^3P_0$  model for hadronization, produces amplitudes which clearly show why  $G$ -parity is conserved in these decays and other ones, but in  $\tau^- \rightarrow \nu_\tau \eta (\eta') \pi^-$  there is  $G$ -parity violation and the amplitude vanishes in our approach. Certainly there are corrections when  $G$ -parity is broken, and again, within the NJL model, by taking different  $u, d$  quark masses, a finite value for the width can be obtained [261], which is consistent with the present experimental bounds.

The Cabibbo-suppressed  $\tau^- \rightarrow \nu_\tau \eta K^-$  reaction is also studied within the extended NJL model in [262] and a width of  $1.45 \times 10^{-4}$  is obtained, which compares well with experiment. Our rate in Table 4.6 is 0.56 times this value. As we have mentioned above, this kind of qualitative agreement is what we expect from our approach in

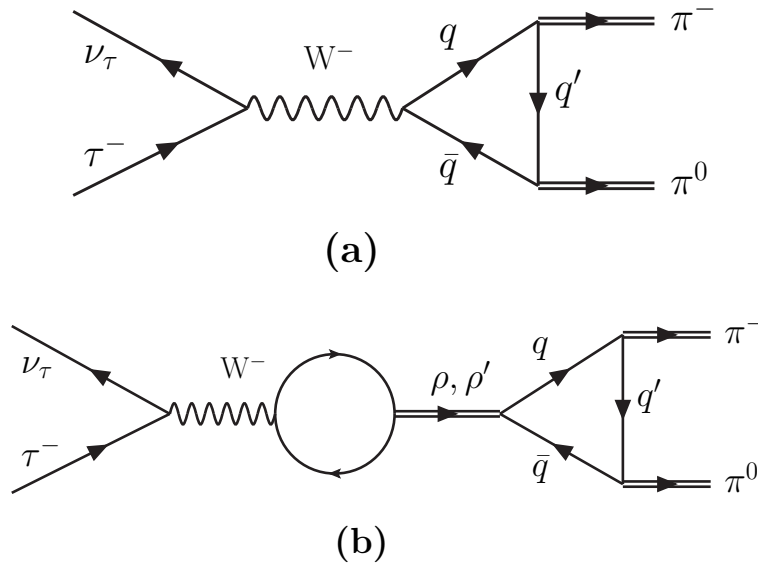


Figure 4.6: The diagram of the  $\tau^- \rightarrow \nu_\tau \pi^- \pi^0$  decay, (a) contact term; (b) vector meson production from Ref. [258].

which we have no free parameters (up to the fit to one particular rate).

The  $\tau^- \rightarrow \nu_\tau \pi^0 K^-$  decay is also addressed in [263] with the extended NJL model. We cannot compare with the results of [263] because the full width is calculated which is dominated by  $K^{*-}$  production. We compare with results of the experimental non-resonant contribution and we find a rate about one half smaller, like in the  $\eta K^-$  case. The same occurs with the  $\pi^- K^0$  non-resonant width, where we also get about one half the rate of the experiment. Actually, within the framework of [263] it is possible to calculate the non-resonant contribution, removing the  $K^{*-}$  pole. Although some numbers are given in [263] for different options, it would be most interesting to address this individual problem from that perspective to the light of the existing experimental data.

One example worth discussing is the  $\tau^- \rightarrow \nu_\tau K^- K^0$ . We used this reaction to get the normalization for the rest of the reactions. So we cannot say anything about the width, but we can comment on the invariant mass distribution of Fig. 4.3. There are some theoretical works that provide rates for this reaction. Models based on the vector meson dominance and form factors provide branching ratios of  $27 \times 10^{-4}$  [195],  $12.5 \times 10^{-4}$  [264],  $13.5 \times 10^{-4}$  [265],  $16 \times 10^{-4}$  [266], and using the extended NJL model  $12.7 \times 10^{-4}$  is obtained in [267]. Results are also available from [268] using vector meson dominance with a branching rate  $\Gamma = 27 \times 10^{-4}$ . In [267] the  $K^- K^0$

invariant mass distribution is provided (see Fig.4.3 of [267]) and a large contribution is obtained from the  $\rho'(1450)$ , providing a big peak in this energy region, although uncertainties on this contribution are acknowledged. It also contains another peak at lower invariant masses. The recent accurate measure of this amplitude in [256] does not show any peak in the mass distribution. We plotted our results in Fig.4.3 and we find a fair agreement with experiment, relating the small shift to lower invariant mass of the experiment to the role of the moderate coupling of  $K\bar{K}$  to  $\rho$ .

For the case of  $\tau^- \rightarrow \nu_\tau PV$  decays we compare results with other ones for the cases of  $\tau^- \rightarrow \nu_\tau \rho \eta$ ,  $\tau^- \rightarrow \nu_\tau K^* \bar{K}$  and  $\tau^- \rightarrow \nu_\tau \omega \pi^-$ .

For the reaction  $\tau^- \rightarrow \nu_\tau \rho \eta$  a branching ratio of  $1.44 \times 10^{-3}$  is obtained in [269] using the extended NJL model. We get for this ratio  $4.5 \times 10^{-3}$  with no convolution of the  $\rho$  and  $5.34 \times 10^{-3}$  considering the  $\rho$  convolution to account for the  $\rho$  mass distribution. This is a rate which in our case is related to the similar  $\tau^- \rightarrow \nu_\tau \eta K^{*-}$  reaction (used as reference, see Tables 4.7,4.8) and should be rather reliable. We do not expect diversions of more than a factor two from the experiment. Unfortunately there are no data for this reaction, but it is clear that its measurement will provide helpful information to get more insight into hadron physics from  $\tau$  decay reactions.

The  $\tau^- \rightarrow \nu_\tau K^* \bar{K}$  branching ratio is evaluated in [195], using vector meson dominance, with a result of  $3.92 \times 10^{-3}$ . Our result in Table 4.8 is  $4.87 \times 10^{-3}$ , very close to the result of [195] and both of them within approximately a factor two from experiment.

In the case of  $\tau^- \rightarrow \nu_\tau \omega \pi^-$  there are results in [195] with a branching ratio of  $1.2 \times 10^{-2}$ , compared to  $1.95 \times 10^{-2}$  from experiment. Our result from Table 4.8 exceeds the experiment by about a factor of two, following the usual trend. There are also results of  $1.85 \times 10^{-2}$  using the extended NJL model in [270] and  $(1.22 \pm 0.56) \times 10^{-2}$  from [268].

There are calculations from other models that we can compare with. From Ref. [195] we find  $BR[\tau^- \rightarrow \nu_\tau (\bar{K}^0 \rho^- + K^- \rho^0)] = 7.5 \times 10^{-4}$  versus  $11.26 \times 10^{-4}$  from our results. Note however, that as mentioned earlier, this result would be enhanced in both approaches when final state interaction of the  $\bar{K} \rho$  is allowed. In [195] one finds another rate which is  $BR[\tau^- \rightarrow \nu_\tau K^- \omega] = 2.5 \times 10^{-4}$  for which we obtain  $3.1 \times 10^{-4}$  and the experiment is  $(4.1 \pm 0.9) \times 10^{-4}$ . Finally, in [195] the rate for  $\tau^- \rightarrow \nu_\tau K^* \eta$  is also evaluated with the result  $BR[\tau^- \rightarrow \nu_\tau K^* \eta] = 1.1 \times 10^{-4}$  versus  $(1.38 \pm 0.15) \times 10^{-4}$  for the experiment. Here we cannot compare because this is the mode used by us for normalization of the rest of the results.

The discussion above served to put our results in perspective and see that, once we normalize to one datum, the branching ratios obtained for other reactions are in line with the results of other approaches, usually a bit less accurate, but this is the price to pay to obtain so many ratios with our approach with no parameters, while all theories with which we compare have a fair amount of parameters that are fitted to

different observables. As discussed earlier, these results constitute a basis to begin with, using this different formalism, which can be improved with the use of form factors calculated for example from existing quarks models, and the implementation of final state interaction of the mesons, for which the use of the chiral unitary approach would be most suited.

## 4.8 Conclusions

We have performed a study of the  $\tau^-$  decay into  $\nu_\tau$  and two mesons, with the aim of establishing a relationship between production of two pseudoscalars, a pseudoscalar and a vector and two vectors. For this we have used the dynamics of the weak interaction and worked out all the angular momentum-spin algebra to relate these processes, provided the form factors stemming from the radial wave functions are the same in the different cases.

The calculations done allow us to present a new perspective of the role played by  $G$ -parity in these reactions, involving  $u, d$  quarks. However, we also find that the selection rules of  $G$ -parity have repercussion in the matrix elements of  $\tau^- \rightarrow \nu_\tau K^- \eta$ ,  $\tau^- \rightarrow \nu_\tau K^- \eta'$ ,  $\tau^- \rightarrow \nu_\tau K^{*-} \eta$ ,  $\tau^- \rightarrow \nu_\tau K^{*-} \eta'$ , where  $G$ -parity does not apply.

We compare our results with experiment. For  $\tau^-$  decays into  $\nu_\tau$  and two pseudoscalars we assume that the two mesons are produced with  $p$ -wave. This is in agreement with the formalism of chiral perturbation theory. In our case the two mesons are produced from an initial  $q\bar{q}$  formation by the  $W$ , followed by the hadronization of  $q\bar{q}$  into two mesons, which is done using the  ${}^3P_0$  model. For the case that the two pseudoscalars are not identical particles,  $s$ -wave production is also possible, although somewhat suppressed since it involves producing the primary  $d\bar{u}$  system in  $L = 1$  rather than in its ground state.

However, we observe that assuming also  $p$ -wave for the pseudoscalar-vector and vector-vector production one obtains results clearly incompatible with experimental data. This fact and experimental evidence that in such cases the mesons are produced in  $s$ -wave, leads us to redo the formalism for production of the two mesons in  $s$ -wave.

Comparison with the experimental results shows that our predictions are fair, in spite of the large differences in the rates for different cases. We also compare our results with other approaches and make predictions for unmeasured decays.

We have also compared our mass distributions with some available data and the agreement found is relatively good. We also see a very different shape, both theoretically and experimentally for  $PP$  production or  $PV, VV$  production.

Another point in the results is that sometimes there are larger discrepancies from the data, and in these cases we could identify the reason of the discrepancies to

large resonance contribution, with the resonance decaying finally into the two meson observed.

We also emphasize that our formalism can be directly used to take into account final state interaction of the mesons that in some cases lead to dynamically generated resonances.

Finally we also emphasize the value of these decays to study the meson-meson interaction and the nature of some resonances, which should stimulate experimentalists to measure the two-meson mass distributions with precision in these decays, as recently done in the  $\tau^- \rightarrow \nu_\tau K^- K^0$  decay in Ref. [256].



# Chapter 5

## $N^*$ production in $\Lambda_c$ decays

### 5.1 Introduction

The nature of the  $N^*(1535)$  ( $J^P = 1/2^-$ ) remains to be well understood [99, 271]. Its properties have been studied within the context of the constituent quark model [110, 272] where the mass of the lowest excitation of the nucleon with a negative parity is found smaller than its positive-parity counterpart, contrary to what is observed in experiment, namely, the  $N^*(1535)$  and  $N^*(1440)$  resonances. This is known as the mass reverse problem. Also it seems to be difficult to explain the fact that the  $N^*(1535)$  could couple to channels with strangeness, such as  $\eta N$  and  $K\Lambda$  [110, 273], within the formalism of the quark model with a naive  $qqq$  configuration where the  $\bar{s}s$  component is not contained.

Studies, such as the ones found in Refs. [274–278], attempt to solve some difficulties in the description of the  $N^*(1535)$  properties with some extension of the conventional quark model, and the possible role of the  $N^*(1535)$  resonance in some reactions is explored in Refs. [279–286].

On the other hand, by using the chiral Lagrangians within the framework of the unitary coupled channels approach, some previously unexplained baryonic resonances could be understood as meson-baryon molecular states. A well-known example of this are the studies of the  $\Lambda(1405)$  that were carried out in Refs. [24, 30–32, 34, 35, 64, 287–289]. In the same way, the  $N^*(1535)$  resonance is studied including the  $\eta N$ ,  $\pi N$ ,  $K\Lambda$  and  $K\Sigma$  channels. The mass and width of the  $N^*(1535)$  could be obtained by calculating the position of the poles of the  $T$  matrix on the second (unphysical) Riemann sheet [160, 290–294], and were found to be in good agreement with experiment. Using this formalism, the  $N^*(1535)$  was also found to couple strongly to  $\eta N$ ,  $K\Sigma$  and  $K\Lambda$ , as well as less strongly to  $\pi N$ . In Refs. [287, 290, 295] in particular, where the  $N^*(1535)$  was dynamically generated through pseudoscalar meson–

baryon ( $PB$ ) interactions. The loop functions were renormalized using the cutoff (in Refs. [287, 295]) and dimensional (in Ref. [290]) regularization schemes, and the cutoffs/subtraction constants were required to have different values for each of the coupled channels in order to get a good agreement with experiment. This is quite different from the case of the  $\Lambda(1405)$ , where only a single global cutoff was needed [31]. In the case of the dimensional regularization [290], the values of the subtraction constants are different from the “natural” size which is related to the mass of the first resonance (the  $\rho$  meson in this case) [32]. On the other hand, from the consideration of the Castillejo-Dalitz-Dyson pole contribution, the study of Ref. [168] suggests that some contribution other than the meson–baryon component would also be important for the  $N^*(1535)$ .

In the vector meson-baryon system, the  $N^*(1650)$  was firstly obtained as a degenerate state of  $J^P = 1/2^-$  and  $3/2^-$  in the study of the vector octet-baryon octet system with the chiral unitary approach [139]. The  $J^P = 3/2^-$  case was studied in Ref. [296] with the  $\rho N(s$  wave),  $\pi\Delta(s$  wave),  $\pi N(d$  wave) and  $\pi\Delta(d$  wave) channels, and there a pole was found which can be associated with the  $N^*(1700)$  resonance, having a sizable coupling to  $\rho N$ . The mixing effects of the  $PB$  channels with vector meson–baryon ( $VB$ ) channels with  $J^P = 1/2^-$  were explored in Refs. [293, 297–299] and they were found to be quite significant. In Ref. [294], the possibility that the missing component in Refs. [290, 295] corresponds to  $VB$  channels was explored by introducing the  $\rho N(s$  wave) and  $\pi\Delta(d$  wave) states in the model of Ref. [290] using the local hidden gauge formalism. Doing this, both the  $N^*(1535)$  and  $N^*(1650)$  ( $J^P = 1/2^-$ ) resonances were dynamically generated, and the masses and widths obtained were very close to their experimental values. Also the subtraction constants used in that study, although still different for each channel, were now very close to a “natural” value. A similar work to this was done in Ref. [293]. The two resonances were also generated in Refs. [160, 291] using only  $PB$  channels with an off-shell approach that is equivalent to considering different subtraction constants from those in Ref. [294].

Nonleptonic weak decays have been widely explored with the objective of studying and testing the properties of baryonic resonances [63, 101, 300–304], thus allowing for a way to distinguish between the different models used to generate them. For example, in Ref. [301] the decay  $\Lambda_c^+ \rightarrow \pi^+ \pi \Sigma$  was studied in order to get the  $\pi \Sigma$  scattering lengths. In Ref. [63] the  $\Lambda_c^+ \rightarrow \pi^+ MB$  decay, with the  $M$  a meson and  $B$  a baryon, for  $MB = \pi \Sigma, \bar{K} N$ , and  $\eta \Lambda$  was studied to better understand the  $\Lambda(1405)$  and  $\Lambda(1670)$  properties, and in Ref. [302] the  $\Lambda_c^+ \rightarrow \eta \pi^+ \Lambda$  was used to investigate the  $a_0(980)$  and  $\Lambda(1670)$  resonances. With this in mind, in Ref. [304] the  $\Lambda_c^+ \rightarrow \bar{K}^0 \eta p$  decay was used to study the nature of the  $N^*(1535)$  by comparing different models, including the one in Ref. [290]. In that study, only  $PB$  channels were considered in this process, which corresponds to ignoring the influence that the  $VB$  channels can have in the nonleptonic decay through a large coupling of the  $N^*(1535)$  to the  $\rho N$  channel, as found in

Ref. [294]. Indeed, the effect of the  $VB$  channel can be quite large in some reactions as was shown in Refs. [8, 224].

In this chapter we extend the calculations done in Ref. [304] to take into account the  $VB$  channels, and the effects of the  $N^*(1650)$  resonance, using the model developed in Ref. [294]. Using this we calculate the mass distribution of  $\eta N$  in the  $\Lambda_c^+ \rightarrow \bar{K}^0 \eta p$  decay and the mass distribution of  $\pi N$  and  $K\Sigma$  in the  $\Lambda_c^+ \rightarrow \bar{K}^0 \pi N$ ,  $\Lambda_c^+ \rightarrow \bar{K}^0 K\Sigma$  decays. In this way we hope to shed some light on the nature of the  $N^*(1535)$  as well as the  $N^*(1650)$ .

This chapter is based on the findings of Ref. [2] and it is organized as follows. The theoretical framework of this study, the weak process of  $\Lambda_c^+ \rightarrow \bar{K}^0 MB$  and the meson-baryon scattering amplitude, is given in Sec. 5.2. Section 5.3 is devoted to the results, the mass distribution of the  $\Lambda_c^+ \rightarrow \bar{K}^0 MB$  [ $MB = \pi N(I = 1/2), \eta p$  and  $K\Sigma(I = 1/2)$ ]. The conclusions of this chapter are outlined in Sec. 5.4.

## 5.2 Formalism

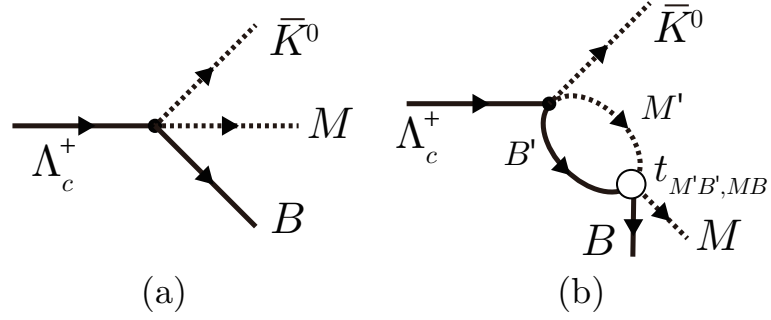
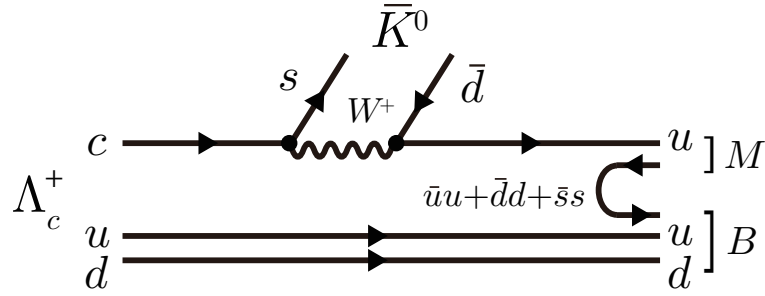
The diagrams for the  $\Lambda_c^+$  decay into  $\bar{K}^0 MB$  which we take into account in this study are depicted in Fig. 5.1. The primary  $\bar{K}^0 MB$  production in the  $\Lambda_c^+$  decay occurs in the weak process and it is followed by the rescattering of the meson-baryon pair  $MB$  where, as studied in Ref. [294], the resonances  $N^*(1535)$  and  $N^*(1650)$  are generated through the dynamics of hadrons.

First we discuss the primary vertex of the  $\Lambda_c^+$  decay into  $\bar{K}^0 MB$ . In this process, we use the same approach as done in Ref. [304], but now we have an additional  $\rho N$  channel. We consider the diagram shown in Fig. 5.2 for the weak transition and the hadronization at the quark level. The reaction can occur with the intermediate  $W^+$  exchange with the Cabibbo-allowed coupling of  $W^+$  to  $cs$  and  $\bar{d}u$  [305], with a sequential pair creation of the light quark from the vacuum. The  $\bar{d}s$  pair forms the  $\bar{K}^0$ , and the remaining  $uud$  quarks with a  $\bar{q}q$  from the vacuum hadronize into the meson-baryon pair. In this approach, the  $ud$  pair in  $\Lambda_c^+$  with the spin  $S = 0$  and isospin  $I = 0$  acts as a spectator. Then, at the quark level we can write the final state as

$$u(\bar{u}u + \bar{d}d + \bar{s}s) \frac{1}{\sqrt{2}}(ud - du) = \sum_i M_{1i} q_i \frac{1}{\sqrt{2}}(ud - du). \quad (5.1)$$

and, at the hadronic level, we obtain

$$\begin{aligned} \sum_i M_{1i} q_i \frac{1}{\sqrt{2}}(ud - du) &= \left( \frac{\pi^0}{\sqrt{2}} + \frac{\eta}{\sqrt{3}} \right) u \frac{1}{\sqrt{2}}(ud - du) \\ &+ \pi^+ d \frac{1}{\sqrt{2}}(ud - du) + K^+ s \frac{1}{\sqrt{2}}(ud - du). \end{aligned} \quad (5.2)$$


 Figure 5.1: The diagrams for the  $\Lambda_c^+ \rightarrow \bar{K}^0 MB$  decay.

 Figure 5.2: The quark-level diagram for the  $\Lambda_c^+ \rightarrow \bar{K}^0 MB$  process.

Referring to Ref. [306] for the quark representation of the baryons (see also footnote 1 in Chapter 10),

$$p = \frac{u(ud - du)}{\sqrt{2}}, \quad (5.3)$$

$$n = \frac{d(ud - du)}{\sqrt{2}}, \quad (5.4)$$

$$\Lambda = \frac{u(ds - sd) + d(su - us) - 2s(ud - du)}{2\sqrt{3}}, \quad (5.5)$$

we can write the final state of the pseudoscalar meson and baryon  $|PB\rangle$ , apart from the  $\bar{K}^0$  meson, as

$$\begin{aligned} |PB\rangle &= \frac{1}{\sqrt{2}}|\pi^0 p\rangle + \frac{1}{\sqrt{3}}|\eta p\rangle + |\pi^+ n\rangle - \sqrt{\frac{2}{3}}|K^+ \Lambda\rangle \\ &= -\sqrt{\frac{3}{2}}|\pi N(I = 1/2)\rangle + \frac{1}{\sqrt{3}}|\eta p\rangle - \sqrt{\frac{2}{3}}|K^+ \Lambda\rangle, \end{aligned} \quad (5.6)$$

where the  $\pi N$  channel is written in terms of the isospin basis ( $|\pi^+\rangle = -|I = 1, I_z = 1\rangle$  in this convention). Here, we have omitted the  $\eta' p$  channel because the threshold is far above the energy of the  $N^*(1535)$  and  $N^*(1650)$  that we focus on in this study. In the same way, replacing the matrix  $M$  with  $V$  from Eq. (2.25), we can obtain the final state with a vector meson  $|VB\rangle$  as

$$|VB\rangle = -\sqrt{\frac{3}{2}}|\rho N(I = 1/2)\rangle. \quad (5.7)$$

Here, the irrelevant channels containing the  $\omega$ ,  $\phi$ ,  $K^*$  and  $\bar{K}^*$  mesons are omitted and the phase convention  $|\rho^+\rangle = -|I = 1, I_z = 1\rangle$  should be understood.

Combining these two cases in Eqs. (5.6) and (5.7), we can write the hadronic final state except for the  $\bar{K}^0$  meson  $|MB\rangle$  as

$$\begin{aligned} |MB\rangle &= -\sqrt{\frac{3}{2}}|\pi N(I = 1/2)\rangle + \frac{1}{\sqrt{3}}|\eta p\rangle - \sqrt{\frac{2}{3}}|K^+\Lambda\rangle \\ &\quad - \sqrt{\frac{3}{2}}|\rho N(I = 1/2)\rangle \\ &\equiv \sum_{MB} h_{MB}|MB\rangle, \end{aligned} \quad (5.8)$$

where the coefficient of each channel  $h_{MB}$  stands for the relative production weight from the  $\Lambda_c^+$  and is summarized in Table 5.1. The weight of the  $\rho N$  channel in

	$\pi N(I = 1/2)$	$\eta N$	$K\Lambda$	$\rho N(I = 1/2)$
$h_{MB}$	$-\sqrt{\frac{3}{2}}$	$\frac{1}{\sqrt{3}}$	$-\sqrt{\frac{2}{3}}$	$-\sqrt{\frac{3}{2}}$
$f_{MB}$	$\frac{1}{4\pi} \frac{1}{2}$	$\frac{1}{4\pi} \frac{1}{2}$	$\frac{1}{4\pi} \frac{1}{2}$	$\frac{1}{4\pi} \frac{1}{2\sqrt{3}}$

Table 5.1: The table for the coefficients  $h_{MB}$  and  $f_{MB}$  in Eq. (5.11).

Eq. (5.8) is only due to flavor. In addition a different spin structure of the pseudoscalar and vector meson leads to a different factor for the production weight in the decay process, as was studied in Refs. [8, 224] based on the  ${}^3P_0$  model for the hadronization. Now, we only need to see the  $J = 1/2$  case because the resonances  $N^*(1535)$  and  $N^*(1650)$  have  $J^P = 1/2^-$ . Because the  $q\bar{q}$  should have  $J^P = 0^+$  which are the same quantum numbers as those of the vacuum, the total angular momentum after the hadronization should come from that of the  $u$  quark from the weak vertex that is denoted by  $|J, M; u\rangle$ . The  $ud$  pair in the  $\Lambda_c^+$ , or equivalently in the final state baryon, has spin  $J = 0$  and isospin  $I = 0$ , and is written as  $|0, 0; ud\rangle_{\text{spectator}}$ . Following the works of Refs. [8, 224] and using the  ${}^3P_0$  model introduced in Section 4.2.1, one

can write the relative angular momentum between the produced  $u$  quark from the weak vertex and  $\bar{q}$  of the  $\bar{q}q$  from the vacuum in the final state as  $j$ , and the spin structure of the system can be rewritten as

$$\begin{aligned} & |J, M; u\rangle |0, 0; \bar{q}q\rangle_{3P_0} |0, 0; ud\rangle_{\text{spectator}} \\ &= \sum_j \mathcal{C}(j, J) |J, M, j\rangle, \end{aligned} \quad (5.9)$$

where the  $\bar{q}q$  state is written as  $|0, 0; \bar{q}q\rangle_{3P_0}$  (see Eq. (4.25)).

Now, the  $j = 0$  and  $1$  cases correspond to the pseudoscalar and vector meson production, respectively. Then, since we are only interested in the  $J = 1/2$  case, we can write

$$\begin{aligned} & |\frac{1}{2}, \pm\frac{1}{2}; u\rangle |0, 0; \bar{q}q\rangle_{3P_0} |0, 0; ud\rangle_{\text{spectator}} \\ &= \sum_{MB} f_{MB} |\frac{1}{2}, \pm\frac{1}{2}; MB\rangle, \end{aligned} \quad (5.10)$$

where the factor  $f_{MB}$  is  $\frac{1}{4\pi} \frac{1}{2}$  and  $\frac{1}{4\pi} \frac{1}{2\sqrt{3}}$  for the cases with  $M$  the pseudoscalar meson and the vector meson, respectively, and we show it in Table 5.1.

Then, we can write the decay amplitude of the tree-level diagram given in Fig. 5.1(a) as

$$t_{\Lambda_c \rightarrow \bar{K}^0 MB} = V_P h_{MB} f_{MB}, \quad (5.11)$$

where  $V_P$  is a common constant for the strength of the production and the coefficients  $h_{MB}$  and  $f_{MB}$  are the factors originating from the flavor and spin structures given in Eqs. (5.8) and (5.10) (see Table 5.1). In this study, we omit the possible energy dependence of the amplitude because the reaction proceeds in  $s$  wave and, as we will see later, only a small energy range around the  $N^*(1535)$  and  $N^*(1650)$  resonances is of our interest.

In this approach, the  $\pi\Delta$  and  $K\Sigma$  productions are suppressed because the  $ud$  pair in  $\Lambda_c^+$ , which has spin  $S = 0$  and isospin  $I = 0$ , is a spectator, *i.e.*, the spin and isospin structure of the  $ud$  pair is not changed throughout the hadronization process. While there are other possibilities for the creation of the quark pair which enable us to have the  $K\Sigma$  or  $\pi\Delta$  production, the study of Ref. [307] suggests that in the case of  $\Lambda_b^0 \rightarrow J/\psi \pi^- p$ , which has the same topology as the diagram of the weak process studied here, the spectator treatment gives a good description for the experimental data of Ref. [308]. Then, we expect that this treatment also works well in the present case.

For the meson-baryon amplitude  $t_{MB, M'B'}$  in Fig. 5.1(b) which is responsible for the rescattering after the hadronization, we follow the study of Ref. [294]. In the

study, the meson-baryon amplitude was evaluated by using the chiral unitary approach with the  $\pi N$ ,  $\eta N$ ,  $K\Lambda$ ,  $K\Sigma$ ,  $\rho N$ , and  $\pi\Delta$  ( $d$  wave) channels, and it was found that the  $N^*(1535)$  and  $N^*(1650)$  resonances are dynamically generated. The interaction kernel of  $PB$  to  $PB$  and  $VB$  to  $VB$  is given by the leading order of the chiral Lagrangian, or equivalently the vector meson exchange [139,290], and the transition of  $PB$  to  $VB$  is taken into account through the one pion exchange and the Kroll-Ruderman term [296,297]<sup>1</sup>

In this section, the meson-baryon loop function will be evaluated using dimensional regularization (Eq. (3.86)).

Finally, the decay amplitude of the  $\Lambda_c^+ \rightarrow \bar{K}^0 MB$  process from the diagrams in Fig. 5.1(a) and (b) is given by

$$t_{\Lambda_c^+ \rightarrow \bar{K}^0 MB} = V_P h_{MB} f_{MB} + \sum_{M'B'} V_P h_{M'B'} f_{M'B'} G_{M'B'}(M_{M'B'}) t_{M'B', MB}(M_{MB}), \quad (5.12)$$

where  $M_{MB}$  denotes the invariant mass of the meson  $M$  and baryon  $B$  (now  $M_{MB} = M_{M'B'}$ ). Regarding the meson-baryon loop function  $G_{MB}$  following the tree-level amplitude for  $\Lambda_c^+ \rightarrow \bar{K}^0 M'B'$  and before  $t_{M'B', MB}$  in Fig. 5.1(b), we use the same subtraction constants as those in the meson-baryon amplitude  $t_{MB, M'B'}$  given in Ref. [294]. In the same way as done in Refs. [294,296], and in Eq. (4.68) for the differential decay width, we use the  $\rho N$  loop function  $\tilde{G}_{\rho N}$  which is obtained by smearing the loop function  $G_{\rho N}(\sqrt{s}, m_\rho, M_N)$  given by Eq. (3.86) with the  $\rho$ -meson spectral function to take account of the width of the  $\rho$  meson<sup>2</sup>,

$$\tilde{G}_{\rho N}(\sqrt{s}) = \frac{1}{N} \int_{m_\rho - 2\Gamma_\rho}^{m_\rho + 2\Gamma_\rho} 2\tilde{m} d\tilde{m} \left( -\frac{1}{\pi} \right) \times \text{Im} \left[ \frac{1}{\tilde{m}^2 - m_\rho^2 + i\tilde{m}\Gamma_\rho(\tilde{m})} \right] G_{\rho N}(\sqrt{s}, \tilde{m}, M_N) \quad (5.13)$$

with

$$\Gamma_\rho(\tilde{m}) = \Gamma_\rho \frac{|\vec{q}|^3}{|\vec{q}|_{\text{on}}^3} \theta(\tilde{m} - 2m_\pi), \quad (5.14)$$

$$|\vec{q}| = \frac{\lambda^{1/2}(\tilde{m}^2, m_\pi^2, m_\pi^2)}{2\tilde{m}}, \quad (5.15)$$

<sup>1</sup>In practice to obtain the same result of Ref. [294], we add the contact and Born terms to the diagonal  $\rho N$  channel of the interaction kernel as in Ref. [299], and the energy transfer in the one pion exchange diagram is omitted in this calculation.

<sup>2</sup>We note that the real part of the  $\rho N$  loop function becomes positive below the  $\rho N$  threshold with the subtraction constant in Ref. [294].

$$|\vec{q}|_{\text{on}} = \frac{\lambda^{1/2}(m_\rho^2, m_\pi^2, m_\pi^2)}{2m_\rho}, \quad (5.16)$$

$$N = \int_{m_\rho - 2\Gamma_\rho}^{m_\rho + 2\Gamma_\rho} 2\tilde{m} d\tilde{m} \left( -\frac{1}{\pi} \right) \times \text{Im} \left[ \frac{1}{\tilde{m}^2 - m_\rho^2 + i\tilde{m}\Gamma_\rho(\tilde{m})} \right]. \quad (5.17)$$

Here, we note that the  $K\Sigma$  and  $\pi\Delta$  channels are not included in the sum of  $M'B'$  in Eq. (5.12) because there is no direct production from  $\Lambda_c^+$  in our approach in Eq. (5.8), while these channels appear in the meson-baryon amplitude  $t_{MB, M'B'}$ .

With an appropriate phase-space factor, the mass distribution  $d\Gamma_{\Lambda_c^+ \rightarrow \bar{K}^0 MB} / dM_{MB}$  as a function of  $M_{MB}$  is given by

$$\frac{d\Gamma_{\Lambda_c^+ \rightarrow \bar{K}^0 MB}}{dM_{MB}} = \frac{1}{(2\pi)^3} \frac{M_B}{M_{\Lambda_c^+}} |\vec{p}_{\bar{K}^0}| |\vec{p}_M| |t_{\Lambda_c^+ \rightarrow \bar{K}^0 MB}|^2, \quad (5.18)$$

where  $p_{\bar{K}^0}$  and  $\tilde{p}_M$  are the momentum of  $\bar{K}^0$  in the  $\Lambda_c^+$  rest frame and that of the meson  $M$  in the  $MB$  CM frame, respectively, with

$$|\vec{p}_{\bar{K}^0}| = \frac{\lambda^{1/2}(M_{\Lambda_c^+}^2, m_{\bar{K}^0}^2, M_{MB}^2)}{2M_{\Lambda_c^+}}, \quad (5.19)$$

$$|\vec{p}_M| = \frac{\lambda^{1/2}(M_{MB}^2, m_M^2, M_B^2)}{2M_{MB}}. \quad (5.20)$$

Here, we give a comment on the possible modification of the mass distribution by the rescattering of  $\bar{K}^0$  with the meson  $M$  or baryon  $B$  in the final state, which are not taken into account in this study. The  $\bar{K}^0 p$  in the  $\Lambda_c^+ \rightarrow \bar{K}^0 \eta p$  decay can couple to some  $\Sigma^*$  resonances, but as pointed out in Ref. [304], these resonances would not give a large modification to the mass distribution because of the small overlap with the phase space and the  $p$ -wave coupling of the  $\Sigma^*$  to the  $\bar{K}^0 p$  channel. Another possibility is the coupling of  $K\bar{K}$  with the  $a_0(980)$  or  $f_0(980)$  states in the  $\Lambda_c^+ \rightarrow \bar{K}^0 K \Lambda$  or  $\bar{K}^0 K \Sigma$  decays. In this case, the invariant mass of the  $\bar{K}^0 K$  pair spreads up in a range of invariant masses above 1050 MeV, and then, the overlap of the  $a_0(980)$  and  $f_0(980)$  resonances with the  $\Lambda_c^+ \rightarrow \bar{K}^0 K \Lambda$  or  $\bar{K}^0 K \Sigma$  phase space is small. Though some  $\Lambda^*$  resonances can also contribute in the  $\Lambda_c^+ \rightarrow \bar{K}^0 \pi N$  process through the  $\bar{K}^0 N$  rescattering, it does not matter in our case because now we are interested in the mass distribution as a function of  $M_{\pi N}$ , not  $M_{\bar{K}^0 N}$ , where the  $\Lambda^*$  distributes its strength. Then, a resonance such as  $\Lambda(1800)$  [110] which can have a certain overlap with the phase space in  $d^2\Gamma_{\Lambda_c^+ \rightarrow \bar{K}^0 \pi N} / dM_{\pi N} dM_{\bar{K}^0 N}$  is integrated over in  $M_{\bar{K}^0 N}$ , and gives just a broad background in the  $M_{\pi N}$  mass distribution.



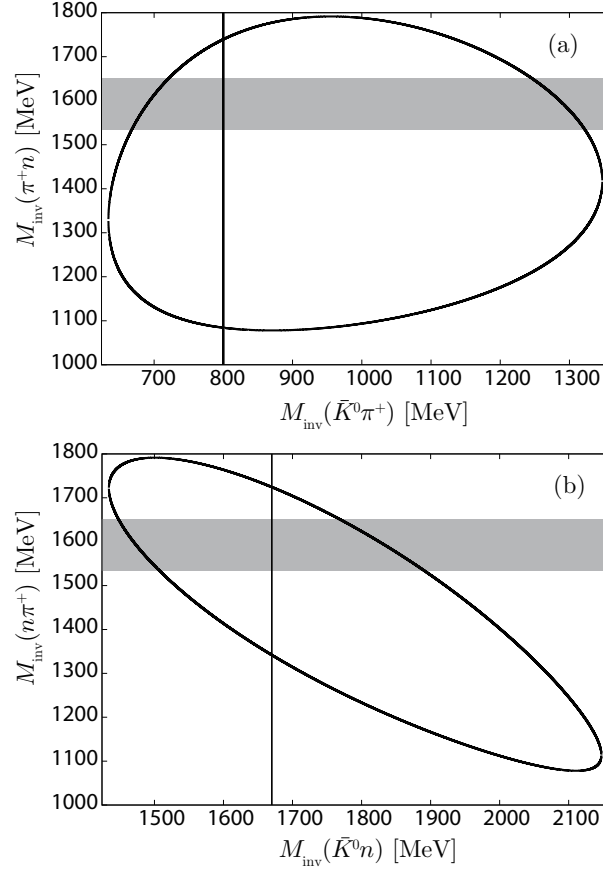


Figure 5.3: Dalitz plots for  $\bar{K}^0\pi^+n$  showing  $M_{\text{inv}}(\pi^+n)$  versus  $M_{\text{inv}}(\bar{K}^0\pi^+)$  for the case (a) and  $M_{\text{inv}}(n\pi^+)$  versus  $M_{\text{inv}}(\bar{K}^0n)$  for the case (b). The shaded areas are the energies of  $N^*(1535)$  and  $N^*(1650)$  which we are interested in. The vertical lines in (a) and (b) correspond to the masses of  $\kappa(800)$  and  $\Lambda(1670)$ , respectively.

To clarify further this issue, we show in Fig. 5.3 two examples of what happens to the interaction of  $\bar{K}^0\pi$  or  $\bar{K}^0N$  in the  $\Lambda_c^+ \rightarrow \bar{K}^0\pi^+n$  reaction (we take the  $\Lambda_c^+ \rightarrow \bar{K}^0\pi^+n$  reaction, as an example). In Fig. 5.3, we show two Dalitz plots for this reaction, one showing  $M_{\text{inv}}(\pi^+n)$  versus  $M_{\text{inv}}(\bar{K}^0\pi^+)$  and another one showing  $M_{\text{inv}}(n\pi^+)$  versus  $M_{\text{inv}}(\bar{K}^0n)$ . In the first case, the  $\bar{K}^0\pi^+$  can lead to the  $\kappa(800)$  resonance in  $s$  wave. This resonance is very broad, and furthermore, as can be seen in Fig. 5.3 (a), the strength of this resonance is spread out in a range of values of  $M_{\text{inv}}(\pi^+n)$  from 1100 MeV to about 1750 MeV. Then the effect of this resonance in the  $\bar{K}^0\pi^+$  channel is spread out over 650 MeV of  $M_{\text{inv}}(\pi^+n)$  and its effects are totally diluted, contributing with a small and smooth background to the  $M_{\text{inv}}(\pi^+n)$  distribution. The case in Fig. 5.3 (b) is similar. Here, we plot  $M_{\text{inv}}(n\pi^+)$  versus  $M_{\text{inv}}(\bar{K}^0n)$ . Now in  $s$  wave we

can have three resonances of  $\bar{K}^0 n$ , either of the two  $\Lambda(1405)$  and the  $\Lambda(1670)$ . The two  $\Lambda(1405)$  resonances are below the  $\bar{K}N$  threshold, but the  $\Lambda(1670)$  could in principle contribute. Once again we see that for this value of the  $\bar{K}^0 n$  invariant mass the values of  $M_{\text{inv}}(n\pi^+)$  range from about 1350 MeV to 1730 MeV, nearly 400 MeV span where the effect of the  $\Lambda(1670)$  (relatively weak) would be also spread out, leading to a smooth background below the  $\pi N$  resonance peaks of  $N^*(1535)$  and  $N^*(1650)$ .

### 5.3 Results

The mass distributions  $d\Gamma_{\Lambda_c^+ \rightarrow \bar{K}^0 MB}/dM_{MB}$  with  $MB = \pi N(I = 1/2), \eta p$ , and  $K\Sigma(I = 1/2)$  as functions of  $M_{MB}$  are given in Fig. 5.4. In these figures, we show the results with  $V_P = 1 \text{ MeV}^{-1}$  because of our lack of the knowledge to fix the value of  $V_P$ . This is not a problem since we only want to focus on the qualitative behavior of the mass distribution.

For the  $\pi N$  mass distribution of the  $\Lambda_c^+ \rightarrow \bar{K}^0 \pi N$  decay, we can see two peaks; the peak located in the lower energy, which is associated with the  $N^*(1535)$  resonance, has larger strength than the one in the higher energy which comes from the  $N^*(1650)$ . On the other hand in the scattering amplitude of the diagonal  $\pi N$  channel in Ref. [294], the magnitude of the higher peak is larger than that of the lower peak. We can understand this difference from the coupling of the resonances with the meson-baryon states given in Ref. [294]. Indeed,  $g_{N^*(1535), \pi N} = 1.03 + i0.21$  versus  $g_{N^*(1650), \pi N} = 1.37 + i0.54$ . Then, the Breit-Wigner amplitude  $g_{R, \pi N}^2 / (\sqrt{s} - M_R + i\Gamma_R/2)$  has larger strength in the case of the  $N^*(1650)$ . On the other hand, if we write the meson-baryon amplitude with the Breit-Wigner amplitude (see Fig. 5.5 for the diagram), the  $\Lambda_c^+ \rightarrow \bar{K}^0 MB$  amplitude  $T_{BW}$  is given by

$$T_{BW} = \sum_{N^*} \sum_{M'B'} V_P h_{M'B'} f_{M'B'} G_{M'B'}(M_{M'B'}) \times \frac{g_{N^*, M'B'} g_{N^*, MB}}{M_{MB} - M_{N^*} + i\Gamma_{N^*}/2}, \quad (5.21)$$

where the sum of  $N^*$  runs over  $N^*(1535)$  and  $N^*(1650)$ . Then, the difference of the intermediate states appears in the combination of  $g_{N^*, M'B'} G_{M'B'}$  around the resonance peak. We compare the absolute values of  $g_{N^*, M'B'} G_{M'B'}$ , given here in Table 5.2, to get a rough understanding. The value of  $g_{N^*, MB} G_{MB}$  for the  $\eta N$  and  $K\Lambda$  channels is larger for  $N^*(1535)$  than  $N^*(1650)$  while the magnitude of the coupling of the  $\pi N$  channel to  $N^*(1650)$  is larger than the coupling to  $N^*(1535)$ . Furthermore, in the primary vertex the  $K\Sigma$  channel which has a larger coupling to  $N^*(1650)$  than  $N^*(1535)$  is not produced. As the result, the peak of the  $N^*(1535)$  resonance is larger than that of the  $N^*(1650)$  in the mass distribution of  $\Lambda_c^+$  decay into  $\bar{K}^0 \pi N$ .

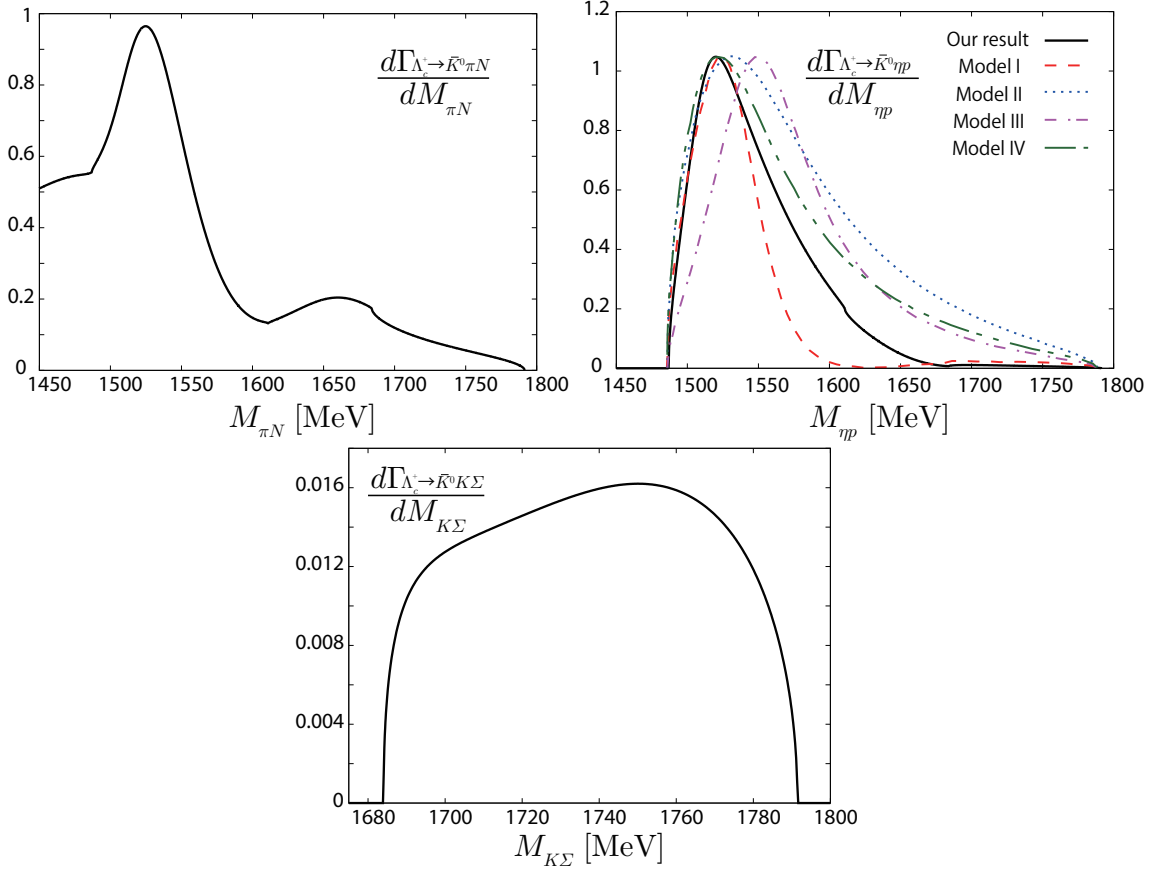
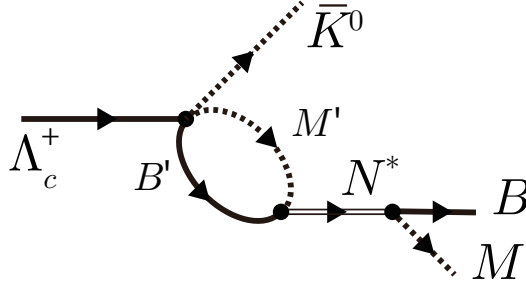


Figure 5.4: The mass distributions for  $\Lambda_c^+$  decay into  $\bar{K}^0 \pi N$  with  $I = 1/2$  (top),  $\bar{K}^0 \eta p$  (middle), and  $\bar{K}^0 K \Sigma$  with  $I = 1/2$  (bottom) as functions of  $M_{MB}$ . In the middle figure, the lines other than the solid one are the results given in Ref. [304] with the height scaled to agree with the result of this study.

At the middle of Fig. 5.4, we show the  $\eta p$  invariant mass distribution in the  $\Lambda_c^+ \rightarrow \bar{K}^0 \eta p$  process with the result of Ref. [304] for comparison. In this case, we can see only a single peak. Compared with the mass distribution of Model I in Ref. [304], the mass distribution has a larger width. This would be attributed to the effect of the  $N^*(1650)$ , analogously to the amplitude of the  $\pi N$  to  $\eta N$  reaction in Ref. [294] where a single peak is observed in the cross section and its larger width than in Ref. [290] is ascribed to the  $N^*(1650)$ . On the other hand, the contribution from the  $N^*(1650)$  is more suppressed than that in the  $\Lambda_c^+ \rightarrow \bar{K}^0 \pi N$  process because of the stronger coupling of the  $\eta N$  channel to the  $N^*(1535)$  than  $N^*(1650)$ . In addition, the absence of the  $K \Sigma$  channel in the initial production process (see Eq. (5.8)), also weakens the strength of the  $N^*(1650)$  because, while  $gG$  for this channel is stronger for  $N^*(1650)$  than for  $N^*(1535)$  (see Table 5.2), the present process cannot be initiated by the  $K \Sigma$

	$\pi N$	$\eta N$	$K\Lambda$	$K\Sigma$	$\rho N$	$\pi\Delta$
$N^*(1535)$	25.2	42.2	40.7	3.2	17.9	8.8
$N^*(1650)$	36.6	34.0	20.3	31.6	8.1	9.0

Table 5.2: The absolute values of  $g_{N^*,M'B'}G_{M'B'}$  (in MeV) at the resonance pole, taken from Ref. [294].Figure 5.5: The diagram from the resonance for the  $\Lambda_c^+ \rightarrow \bar{K}^0 MB$ .

channel. However, the mass distribution in Fig. 5.4 still has a larger width compared to the mass distribution of the Model I in Ref. [304], where only the  $N^*(1535)$  is included following the work of Ref. [290], using the chiral unitary approach without the  $\rho N(I = 1/2)$  and  $\pi\Delta(d \text{ wave})$  channels. Meanwhile, the width of the mass distribution of the  $\Lambda_c^+ \rightarrow \bar{K}^0 \eta p$  is smaller than those of Models II, III and IV in Ref. [304]. In these models, the  $N^*(1535)$  is treated as a Breit-Wigner amplitude and its width is larger than that obtained in Refs. [290, 294] or has energy dependence which makes the width effectively large at higher energy.

For completeness, the  $K\Sigma$  mass distribution of the  $\Lambda_c^+ \rightarrow \bar{K}^0 K\Sigma$  decay is shown at the bottom of Fig. 5.4. In Ref. [294], the value of  $g_{N^*,K\Sigma}G_{K\Sigma}$  is larger for the  $N^*(1650)$  resonance than the  $N^*(1535)$  resonance, and the  $N^*(1535)$  energy is about 200 MeV below the  $K\Sigma$  threshold. Then, we can expect that the  $K\Sigma$  production is mainly driven by the  $N^*(1650)$  resonance. However, as given in Eq. (5.8) the  $K\Sigma$  pair is not produced directly from the  $\Lambda_c$  decay. Then, the  $K\Sigma$  pair is produced only through the coupled channel effect of the meson-baryon amplitude  $t_{MB,M'B'}$  in our approach, and the magnitude of the mass distribution is much smaller compared with that of  $\pi N$  or  $\eta N$ .

In Fig. 5.6, we show the mass distribution omitting the  $\rho N$  channel in the sum of  $M'B'$  in Eq. (5.12). The  $\rho N$  channel contributes in a destructive way to the mass distribution. In the  $\pi N$  case, the effect of the  $\rho N$  channel looks more significant for the lower peak. This is because, as shown in Ref. [294], the  $\rho N$  channel has a larger value of  $g_{N^*,\rho N}G_{\rho N}$  for the  $N^*(1535)$  resonance than for the  $N^*(1650)$  resonance.

Thus, in the  $\Lambda_c^+$  decay into  $\bar{K}^0 MB$  [ $MB = \pi N(I = 1/2), \eta p$  and  $K\Sigma(I = 1/2)$ ] the res-

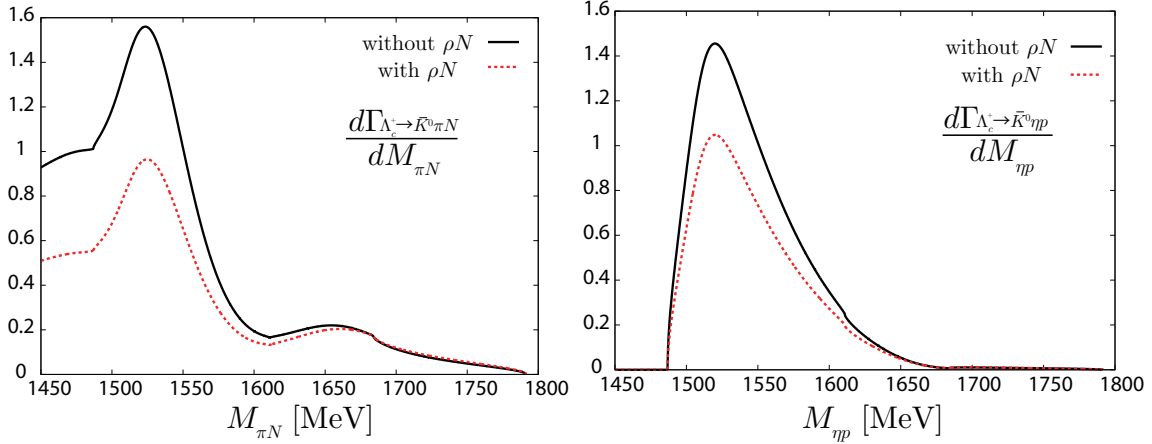


Figure 5.6: The mass distribution for  $\Lambda_c^+ \rightarrow \bar{K}^0 \pi N$  with  $I = 1/2$  (top) and  $\bar{K}^0 \eta p$  (bottom) without  $\rho N$  channel. The mass distributions with the  $\rho N$  channel are shown with the dotted lines.

onances  $N^*(1535)$  and  $N^*(1650)$  appear in a different way than in the meson-baryon amplitude in Ref. [294]. In addition, we found a difference from the models which do not contain the  $N^*(1650)$ , or with respect the five-quark models of the  $N^*(1535)$  that were discussed in Ref. [304]. Then, the production of the  $N^*(1535)$  and  $N^*(1650)$  from the  $\Lambda_c^+$  decay is a good process to clarify the properties of the  $N^*(1535)$  and  $N^*(1650)$  resonances.

## 5.4 Conclusions

We have studied the mass distribution of the  $\Lambda_c^+ \rightarrow \bar{K}^0 MB$  [ $MB = \pi N (I = 1/2), \eta p$ , and  $K\Sigma (I = 1/2)$ ] including the effect of the  $N^*(1535)$  and  $N^*(1650)$  resonances, which are generated by the hadron dynamics with the  $\pi N, \eta N, K\Lambda, K\Sigma, \rho N$ , and  $\pi\Delta$  ( $d$  wave) channels, as investigated in Ref. [294]. While both effects of the  $N^*(1535)$  and  $N^*(1650)$  are seen in the mass distributions, we found that their manifestation is different from that in the meson-baryon amplitude given in Ref. [294]. In our mass distribution for  $\Lambda_c^+ \rightarrow \bar{K}^0 \pi p (I = 1/2)$  and  $\bar{K}^0 \eta p$ , the peak from  $N^*(1535)$  is larger than that from  $N^*(1650)$ , while two peaks with a comparable magnitude are seen in the amplitude of the  $\pi N$  to  $\pi N$  channel in Ref. [294], as well as in data. This is because the  $K\Sigma$  channel which couples more strongly to  $N^*(1650)$  than  $N^*(1535)$  is suppressed in the primary production from  $\Lambda_c^+$  in our treatment of the weak and hadronization processes and the  $\rho N (I = 1/2)$  and  $K\Lambda$  channels have larger couplings to the  $N^*(1535)$  resonance than to the  $N^*(1650)$  resonance.

Furthermore, we find differences from the treatment of the  $N^*(1535)$  made in Ref. [304], where a five-quark component is included using a Breit-Wigner amplitude.

In the case of  $MB = K\Sigma(I = 1/2)$ , the  $N^*(1650)$  resonance is expected to give a dominant contribution to the production amplitude, but we found that the magnitude of the mass distribution of the  $\Lambda_c^+ \rightarrow \bar{K}^0 K\Sigma(I = 1/2)$  is much smaller than for the other processes, like  $\Lambda_c^+ \rightarrow \bar{K}^0 \eta p$ , because the production of the  $K\Sigma$  is suppressed in the weak and hadronization process.

The subtleties and results in the different channels in the reactions studied here are tied to the nature of the  $N^*(1535)$  and  $N^*(1650)$  resonances as dynamically generated from the hadron interaction in coupled channels, and the experimental observation of these decay modes should bring new information concerning the nature of these states.

**Part III**

**Hadrons In The Heavy Sector**





# Chapter 6

## $\Lambda_b \rightarrow \Lambda_c^*$ decays and heavy quark spin symmetry

### 6.1 Introduction

Constituent quark models (CQMs) predict a nearly degenerate pair of  $p$ -wave  $\Lambda_c^*$  excited states, with spin-parity  $J^P = 1/2^-$  and  $3/2^-$ , whose masses are similar to those of the isoscalar odd-parity  $\Lambda_c(2595)$  and  $\Lambda_c(2625)$  resonances [74, 309–312]. In the most recent of these CQM studies [312], two different types of excitation-modes are considered: The first one,  $\lambda$ -mode, accounts for excitations between the heavy quark and the brown muck as a whole, while the second one,  $\rho$ -mode, considers excitations inside the brown muck. When all quark masses are equal,  $\lambda$ - and  $\rho$ -modes are degenerate [312]. However for singly-heavy baryons, the typical excitation energies of the  $\lambda$ -mode are smaller than those of the  $\rho$ -mode. This is because for singly charm or bottom baryons, the interactions between the heavy quark and the brown muck are more suppressed than between the light quarks [312, 313]. Thus, one should expect the  $\lambda$  excitation modes to become dominant for low-lying states of singly heavy-quark baryons. Within this picture, the  $\Lambda_c^{\text{CQM}}(2595)$  and  $\Lambda_c^{\text{CQM}}(2625)$  resonances would correspond to the members of the HQSS-doublet associated to  $(\ell_\lambda = 1, \ell_\rho = 0)$ , with total spin  $S_q = 0$  for the light degrees of freedom (*ldof*), leading to a spin-flavor-spatial symmetric wave-function for the light isoscalar diquark subsystem inside of the  $\Lambda_c^*$  baryon. The total spins of these states are the result of coupling the orbital-angular momentum  $\ell_\lambda$  of the brown muck –with respect to the heavy quark– with the spin ( $S_Q$ ) of the latter. Thus both  $\Lambda_c^{\text{CQM}}(2595)$  and  $\Lambda_c^{\text{CQM}}(2625)$  states are connected by a simple rotation of the heavy-quark spin, and these resonances will be

degenerate in the heavy-quark limit<sup>1</sup>.

Since the total angular momentum and parity of the *ldof* in the *s*-wave  $\pi\Sigma_c$  and  $\pi\Sigma_c^*$  pairs are  $1^-$ , as in the CQM  $\Lambda_c(2595)$  and  $\Lambda_c(2625)$  resonances, the  $\Lambda_c^{\text{CQM}}(2595) \rightarrow \pi\Sigma_c \rightarrow \pi\pi\Lambda_c$  and  $\Lambda_c^{\text{CQM}}(2625) \rightarrow \pi\Sigma_c^* \rightarrow \pi\pi\Lambda_c$  decays respect HQSS, and hence one should expect sizable widths for these resonances, unless these transitions are kinematically suppressed. This scenario seems plausible, as can be inferred from the masses and thresholds compiled in Table 6.1. Indeed, the recent works of Refs. [314, 315] find widths for the CQM ( $\ell_\lambda = 1, \ell_\rho = 0$ ) states ( $j_q^P = 1^-$ ) predicted in [312] consistent with data.

A different mechanism to explain the small width of the  $\Lambda_c(2595)$  would be that its wave-function had a large  $j_q^P = 0^-$  *ldof* component<sup>2</sup>. This is because the transition of this  $j_q^P = 0^-$  term of the  $\Lambda_c(2595)$  to the final  $\pi\Sigma_c$  state will be suppressed by HQSS. This new mechanism will act in addition to any possible kinematical suppression. As we will see in the next section, it turns out that some of the approaches that describe the  $\Lambda_c(2595)$  as a hadron-molecule predict precisely a significant  $j_q^P = 0^-$  component for the inner HQSS structure of this resonance. These models generate also the existence of a second, broad, resonance in the region of the  $\Lambda_c(2595)$ , with a large  $j_q^P = 1^-$  *ldof* component, that could be naturally identified to the HQSS partner of the  $\Lambda_c(2625)$ , since both states will have the same brown muck configuration in the heavy-quark limit<sup>3</sup>.

In this chapter, we will derive HQSS relations between the  $\Lambda_b$  decays into  $\Lambda_c^*\pi^-$

<sup>1</sup>The lowest-lying  $\rho$ -mode, ( $\ell_\lambda = 0, \ell_\rho = 1$ ) gives rise to two  $\frac{1}{2}^-$  and also two  $\frac{3}{2}^-$  multiplets of  $\Lambda_c^*$ 's, together with an additional  $\frac{5}{2}^-$   $\Lambda_c$ -excited state, significantly higher in the spectrum [312]. Note that the isoscalar light diquark could have  $0^-, 1^-$  and  $2^-$  quantum-numbers, resulting from the coupling of the spin,  $S_q = 1$ , and the orbital-angular momentum,  $\ell_\rho = 1$ , of the light quarks. In the heavy quark limit all the baryons with the same light diquark  $j_q^P$  configuration will be degenerate [313].

<sup>2</sup>Note that, in principle, both  $j_q = 0^-$  and  $j_q = 1^-$  configurations can couple with the spin ( $S_Q = \frac{1}{2}$ ) of the charm quark to give a total  $J^P = \frac{1}{2}^-$  for the  $\Lambda_c(2595)$ .

<sup>3</sup>Since the spin-parity of the  $\Lambda_c(2625)$  is  $\frac{3}{2}^-$  and it is the lowest-lying state with these quantum numbers, one should expect the total angular momentum and parity of the *ldof* in the  $\Lambda_c(2625)$  to be  $1^-$ .

	$M$	$\Gamma$	$M(\Sigma_c^{(*)+} + \pi^0)$	$M(\Sigma_c^{(*)0} + \pi^+)$	$M(\Sigma_c^{(*)++} + \pi^-)$
$\Lambda_c(2595)$	$2592.25 \pm 0.28$	$2.6 \pm 0.6$	$2587.9 \pm 0.4$	$2593.32 \pm 0.14$	$2593.54 \pm 0.14$
$\Lambda_c(2625)$	$2628.11 \pm 0.19$	$< 0.97$	$2652.5 \pm 2.3$	$2658.05 \pm 0.20$	$2657.98 \pm 0.20$

Table 6.1: Masses and widths of the  $\Lambda_c(2595)$  and  $\Lambda_c(2625)$  resonances (MeV units). Thresholds (MeV) of some possible *s*-wave decay channels are also given. In addition, the thresholds of the three-body channels, after the *p*-wave decay of the  $\Sigma_c^{(*)}$  resonances, are  $M(\Lambda_c + \pi^+ + \pi^-) = 2565.60 \pm 0.14$  MeV and  $M(\Lambda_c + \pi^0 + \pi^0) = 2566.41 \pm 0.14$  MeV. Data taken from the Review of Particle Physics (RPP) [21].

and  $\Lambda_c^* \ell \bar{\nu}_\ell$  [ $\Lambda_c^* = \Lambda_c(2595)$  and  $\Lambda_c(2625)$ ], supposing firstly that the  $\Lambda_c(2595)$  and  $\Lambda_c(2625)$  form the lowest-lying  $j_q^P = 1^-$  HQSS doublet. We will also discuss how measurements of the ratio of branching fractions  $\Gamma[\Lambda_b \rightarrow \Lambda_c(2595)]/\Gamma[\Lambda_b \rightarrow \Lambda_c(2625)]$  can be used to constrain the existence of a sizable  $j_q^P = 0^-$  *ldof* component in the  $\Lambda_c(2595)$  wave-function, and/or of a second pole, in analogy to the case of the similar  $\Lambda(1405)$  resonance.

Exclusive semileptonic  $\Lambda_b$  decays into excited charmed  $\Lambda_c(2595)$  and  $\Lambda_c(2625)$  baryons have been studied using heavy quark effective theory (HQET), including order  $\Lambda_{QCD}/m_Q$  corrections [316, 317], and non-relativistic and semi-relativistic CQMs [318], always assuming a single pole structure for the first of these resonances and a dominant  $j_q^P = 1^-$  configuration. Recently, it has also been suggested that measurements of these decays by LHCb could be used to perform precise lepton flavor universality (LFU) tests [319, 320], comparing branching fractions with  $\tau$ - or  $\mu$ -leptons in the final state. The analyses of Refs. [319] and [320] assumed that both excited charmed baryons form a doublet under HQSS, and therefore it neither contemplated the possibility that the narrow  $\Lambda_c(2595)$  might not be the HQSS partner of the  $\Lambda_c(2625)$ , nor that it could contain a non-negligible  $j_q^P = 0^-$  component, as it occurs in most of the molecular descriptions of this resonance. It is therefore timely and of the utmost interest to test the HQSS doublet assumption for the  $\Lambda_c(2595)$  and  $\Lambda_c(2625)$  with the available data.

A first step in that direction was given in Refs. [224, 321]. In these two works, the semileptonic  $\Lambda_b \rightarrow \Lambda_c^*$  transitions, together with the  $\Lambda_b$  decays into  $\Lambda_c^* \pi^-$  and  $\Lambda_c^* D_s^-$  were studied. It was found that the ratios of the rates obtained for  $\Lambda_c(2595)$  and  $\Lambda_c(2625)$  final states are very sensitive to the couplings of these resonances to the  $D^* N$  channel, which also becomes essential to obtain agreement with the available data. Following the claims of Refs. [224, 321], these results seem to give strong support to the molecular picture of the two  $\Lambda_c^*$  states, and the important role of the  $D^* N$  component in their dynamics<sup>4</sup>. As we will discuss in the next section, the  $\Lambda_c(2595) D^* N$  and  $\Lambda_c(2625) D^* N$  couplings, together with those to the  $DN$  and  $\pi \Sigma_c^{(*)}$  pairs, can also be used to obtain valuable information on the inner HQSS structure of these resonances.

Within a manifest Lorentz and HQSS invariant formalism [148, 322, 323], we will re-examine here some of the results obtained in Refs. [224, 321], and will connect the findings of these two works with the quantum numbers of the *ldof* in the  $\Lambda_c(2595)$  wave function. Specifically, we will discuss how future accurate measurements of the different ratios of branching fractions proposed in [224, 321] may be used to constrain or discard i) a sizable  $j_q^P = 0^-$  component in the  $\Lambda_c(2595)$  wave-function, and ii) the

<sup>4</sup>The same type of ideas were extended in Ref. [8] to the semileptonic and one pion decays of the  $\Xi_b^-$  baryons into  $\Xi_c^*$  resonances, analogs of the  $\Lambda_c(2595)$  and  $\Lambda_c(2625)$  states in the charm-strange sector.

existence of a second pole, analog to the second (broad)  $\Lambda(1405)$  resonance [21]. The study will also shed some light on the validity of some of the most popular hadron-molecular interpretations of the odd-parity lowest-lying  $\Lambda_c^*$  states.

This chapter is based on the findings of Ref. [3] and it is structured as follows. After this introduction, in Sec. 6.2 we critically review different molecular descriptions of the  $\Lambda_c(2595)$  and  $\Lambda_c(2625)$  baryons, and discuss in detail the main features of those models that predict a two-pole pattern for the  $\Lambda_c(2595)$ . Next in Sec. 6.6, we study the semileptonic  $\Lambda_b \rightarrow \Lambda_c^* \ell \bar{\nu}_\ell$  decays and the constraints imposed by HQSS to these processes. We derive a scheme that preserves spin-symmetry in the  $b$ -quark sector and that leads to simple and accurate expressions for the differential widths, including  $\mathcal{O}(1/m_c)$  corrections and full finite-lepton mass contributions that are necessary for testing LFU. Semileptonic decays to molecular  $\Lambda_c^{\text{MOL}}$  states are addressed in Subsec. 6.9, and the pion mode is examined in Sec. 6.10. The numerical results of this work are presented in Sec. 6.11. First in Subsec. 6.12, we discuss the semileptonic ( $\mu^- \bar{\nu}_\mu$  or  $e^- \bar{\nu}_e$ ) and pion  $\Lambda_b \rightarrow \Lambda_c^*$  decays, and present  $m_Q \rightarrow \infty$ ,  $\mathcal{O}(1/m_Q)$  HQET and molecular-model predictions for the ratios of branching fractions studied in [224,321]. Next in Subsec. 6.13, we show results for  $\Lambda_b$  semileptonic decays with a  $\tau$  lepton in the final state that can be of interest for LFU tests. Finally, we outline the main conclusions of this work in Sec. 6.14.

## 6.2 HQSS structure of the $\Lambda_c(2595)$ and $\Lambda_c(2625)$ states in hadron-molecular approaches.

In this section, we will discuss the most important common features and results obtained from approaches where the  $\Lambda_c(2595)$  and  $\Lambda_c(2625)$  are described as hadron-molecules. These studies are motivated by the appealing similitude of these resonances to the  $\Lambda(1405)$  and  $\Lambda(1520)$  in the strange sector. In particular the two isoscalar  $s$ -wave  $\Lambda(1405)$  and  $\Lambda_c(2595)$  resonances have several features in common. The mass of the former lies in between the  $\pi\Sigma$  and  $\bar{K}N$  channel thresholds, to which it couples strongly [27–29]. In turn, the  $\Lambda_c(2595)$  lies below the  $DN$  and just slightly above the  $\pi\Sigma_c$  thresholds, and substituting the  $c$  quark by a  $s$  quark, one might expect the interaction of  $DN$  to play a role in the dynamics of the  $\Lambda_c(2595)$  similar to that played by  $\bar{K}N$  in the strange sector.

The hadronic molecular interpretation of the  $\Lambda(1405)$  provides a good description of its properties. Actually, the dynamics of this resonance is mostly governed by the leading order (LO) SU(3) chiral WT meson-baryon interaction. One of the distinctive features of this resonance is its two-pole structure [24,32,34,35,64,69,324], that have found experimental confirmation [325, 326] as discussed in Ref. [56]. This two-pole

pattern<sup>5</sup> is by now widely accepted by the community (see f.i. the mini review on this issue in the RPP by the Particle Data Group [21]).

On the other hand, many works have been also devoted to the study of dynamically generated  $J^P = 3/2^-$  states in the SU(3) sector [139, 164, 292, 327–335]. Early works considered only the chiral interaction of pseudoscalar  $0^-$  mesons with the baryons of the  $3/2^+$  decuplet, but more recently, vector-mesons degrees of freedom have also been incorporated in the coupled-channel approach, using different schemes (see for instance the discussion in [292]). In these approaches, the  $\Lambda(1520)$  is dynamically generated mostly from the  $s$ -wave  $\pi\Sigma^* - \bar{K}^*N$  coupled-channels dynamics, appearing it slightly above the  $\pi\Sigma^*$  threshold. It has a non-vanishing width, since the  $\pi\Sigma^*$  channel is open. In clear analogy, one might naturally think of a similar mechanism to generate the  $\Lambda_c(2625)$  from the  $\pi\Sigma_c^* - D^*N$  dynamics, though the major difference is that the charm-resonance is located around 30-25 MeV below the  $\pi\Sigma_c^*$  threshold.

### 6.3 Molecular models

The general scheme consists of taking some  $s$ -wave interactions as kernel of a BSE, conveniently ultraviolet (UV) renormalized, and whose solutions fulfill exact elastic unitarity in coupled-channels. In this context, bound and resonant states appear as poles in the appropriate Riemann-sheets<sup>6</sup>, and the residues provide the coupling of the dynamically generated states to the different channels considered in the approach.

The resemblance of the physics in the odd-parity charm  $C = 1$  baryon sector to the phenomenology seen in  $\bar{K}N - \pi\Sigma$  dynamics was first exploited in the works of Refs. [336, 337]. These first two works had some clear limitations. In the first one, the  $J^P = 1/2^-$  sector is studied using the scattering of Goldstone bosons off  $1/2^+$  heavy-light baryon resonances. Despite the interactions were fully consistent with chiral symmetry, neither the  $DN$ , nor the  $D^*N$  channels were considered [336]. The work of Ref. [337] also studied the  $\Lambda_c(2595)$  and there, the interactions were obtained from chirally motivated Lagrangians upon replacing the  $s$  quark by the  $c$  quark. Though in this way, the  $DN$  channel was accounted for, the HQSS counterpart  $D^*N$  was not considered.

The subsequent works of Refs. [170, 338] and [171] for the  $J^P = 3/2^-$  sector, introduced some improvements on the schemes of Refs. [336, 337]. Namely, the BSE

<sup>5</sup>One narrow state situated below the  $\bar{K}N$  threshold and with a small coupling to the open  $\pi\Sigma$  channel, and a second state much wider because its large coupling to the open  $\pi\Sigma$  channel.

<sup>6</sup>This is in gross features also the scheme used in the previous works on the  $\Lambda(1405)$  and  $\Lambda(1520)$ , and in most of the studies leading to hadron-molecular interpretations of many other resonances.

interaction kernels were obtained from  $t$ -channel exchange of vector mesons between pseudoscalar mesons and baryons, in such a way that chiral symmetry is preserved in the light meson sector. Besides, the universal vector meson coupling hypothesis [Kawarabayashi-Suzuki-Fayyazuddin-Riazuddin (KSFR) [140, 141]] was modified to take into account the reduction of the interaction strength provoked by the mass of the  $t$ -channel exchanged meson. In this way, some SU(4) flavor-symmetry breaking corrections, additional to those induced by the use of the physical masses, were considered. Similar qualitative findings were obtained in the work of Ref. [339], where some finite range effects were explored.

A detailed treatment of the interactions between the ground-state singly charmed and bottomed baryons and the pseudo-Nambu-Goldstone bosons, discussing also the effects of the next-to-leading-order chiral potentials, was carried out in [340]. However, channels not involving Goldstone bosons, like  $DN$  or  $D^*N$ , were again not considered. In this reference, several aspects related to the renormalization procedure were also critically discussed<sup>7</sup>.

In all cases, the  $\Lambda_c(2595)$ , or the  $\Lambda_c(2625)$  if studied, could be dynamically generated after a convenient tuning of the renormalization constants. However, none of these works were consistent with HQSS since none of them considered the  $D^*N$  [172]. Heavy pseudoscalar and vector mesons should be treated on equal footing, since they are degenerated in the heavy quark limit, and are connected by a spin-rotation of the heavy quark that leaves unaltered the QCD Hamiltonian in that limit. This is to say the  $D$  and  $D^*$  mesons form a HQSS-doublet.

The first molecular description of the  $\Lambda_c(2595)$  and  $\Lambda_c(2625)$  resonances, using interactions fully consistent with HQSS, was derived in Refs. [86, 172]. In these works a consistent  $SU(6)_{\text{lsf}} \times SU(2)_{\text{HQSS}}$  extension of the WT  $\pi N$  Lagrangian –where “lsf” stands for light-spin-flavor symmetry–, is implemented, although the adopted renormalization scheme (RS) [170, 171] might not respect HQSS (see the discussion below). Within such scheme, two states are dynamically generated in the region of 2595 MeV. The first one, identified with the  $\Lambda_c(2595)$  resonance, is narrow and it strongly couples to  $DN$  and especially to  $D^*N$ , with a small coupling to the open  $\pi\Sigma_c$  channel. The second state is quite broad since it has a sizable coupling to this latter channel. On the other hand, a  $J^P = 3/2^-$  state is generated mainly by the  $(D^*N - \pi\Sigma_c^*)$  coupled-channel dynamics. It would be the charm counterpart of the  $\Lambda(1520)$ , and could be identified with the  $\Lambda_c(2625)$  resonance. The same  $SU(6)_{\text{lsf}} \times SU(2)_{\text{HQSS}}$  scheme also dynamically generates the  $\Lambda_b(5912)$  and  $\Lambda_b(5920)$  narrow resonances, discovered by LHCb in 2012 [346], which turn out to be HQSS partners, naturally explaining in

<sup>7</sup>It is also worth mentioning Ref. [341], where the properties of the  $\Lambda_c(2595)$  are discussed in the limit of large number of colors ( $N_c$ ), within several schemes. The  $N_c \gg 3$  behaviour of the resonance properties (mass, width, couplings, etc.) puts constraints on its possible dynamical origin, since the importance of the unitary loops involving Goldstone bosons decreases as  $N_c$  grows [342–345].

this way their approximate mass degeneracy [83]. The extension of the model to the hidden charm sector was carried out in [347], and more recently, it was shown [6] that some (probably at least three) of the narrow  $\Omega_c^*$  states recently observed by LHCb [348] in the  $\Xi_c^+ K^-$  spectrum in  $pp$  collisions can be also dynamically generated within the same scheme.

Several  $\Lambda_c^*$  poles were also obtained in the approach followed in Ref. [85]. There, the interaction of  $DN$  and  $D^*N$  states, together with their coupled channels are considered by using an extension to four flavours of the SU(3) local hidden gauge formalism from the light meson sector [134–136]. The scheme also respects LO HQSS constraints [349] and, as in Refs. [86, 172], a two-pole structure for the  $\Lambda_c(2595)$  was also found, with the  $D^*N$  channel playing a crucial role in its dynamics. This is a notable difference to the situation in the strange sector, where the analog  $\bar{K}^*N$  channel is not even considered in most of the studies of the  $\Lambda(1405)$ , because of the large  $\bar{K}^* - \bar{K}$  mass splitting. (See also the discussion carried out in Ref. [298].)

The beauty  $\Lambda_b(5912)$  and  $\Lambda_b(5920)$  states were also studied in the extended local hidden gauge (ELHG) approach in Ref. [84], while the predictions of this scheme referred to the LHCb  $\Omega_c^*$  states can be found in [350]. These latter states were also addressed in Ref. [351] using a model constructed out of the SU(4)-flavor  $t$ -channel exchange of vector mesons. There, the original model of Ref. [170] is revisited, and after taking an appropriate regularization scheme with physically sound parameters, two of the LHCb  $\Omega_c^*$  resonances could be accommodated.

## 6.4 HQSS structure of the $\Lambda_c(2595)$ and $\Lambda_c(2625)$ hadron-molecules

To make more transparent the inner HQSS structure of the  $\Lambda_{c(n)}^{\text{MOL}}(2595)$ ,  $\Lambda_{c(b)}^{\text{MOL}}(2595)$  and  $\Lambda_c^{\text{MOL}}(2625)$  states found in molecular (MOL) scenarios [( $n$ ) and ( $b$ ) refer to the narrow and broad resonances that form the two-pole structure of the  $\Lambda_c(2595)$  in these schemes], we perform a change of basis. We pass from  $s$ -wave states where the meson and baryon spins are defined, to other ones, where the total angular momentum of the  $ldof$  is well determined. In both sets of states, the total angular momentum of the meson-baryon pair is defined. The two basis are related by a Racah rotation [349], which is straightforward to obtain in the present case, where the discussion is restricted to  $s$ -wave meson-baryon pairs. Thus for instance, we find (the rotation is independent of the isospin of the meson-baryon pair)

$$|S_Q^P = 1/2^+ j_q^P = 1^-; J^P = 3/2^-\rangle_1 = |\pi\Sigma_c^*; J^P = 3/2^-\rangle \quad (6.1)$$

$$|S_Q^P = 1/2^+ j_q^P = 1^-; J^P = 3/2^-\rangle_2 = |D^*N; J^P = 3/2^-\rangle \quad (6.2)$$

$$|S_Q^P = 1/2^+ j_q^P = 1^-; J^P = 1/2^-\rangle_1 = |\pi\Sigma_c; J^P = 1/2^-\rangle \quad (6.3)$$

$$|S_Q^P = 1/2^+ j_q^P = 1^-; J^P = 1/2^-\rangle_2 = \frac{\sqrt{3}}{2}|DN; J^P = 1/2^-\rangle + \frac{1}{2}|D^*N; J^P = 1/2^-\rangle \quad (6.4)$$

$$|S_Q^P = 1/2^+ j_q^P = 0^-; J^P = 1/2^-\rangle_2 = -\frac{1}{2}|DN; J^P = 1/2^-\rangle + \frac{\sqrt{3}}{2}|D^*N; J^P = 1/2^-\rangle \quad (6.5)$$

where we have used that the total angular momentum and parity of the *ldof* in the  $\Sigma_c^{(*)}$  and  $D^{(*)}$  ground states are  $j_q^P = 1^+$  and  $1/2^-$ , respectively. Besides, the sub-indices 1 and 2 on the states in the left-hand side of the equations distinguish if the meson is a Goldstone or a charmed heavy-light boson. In this context, the approximate HQSS of QCD leads to meson-baryon interactions  $V$  satisfying (kinetic terms respect HQSS)

$$\alpha \langle S_Q^P = 1/2^+ j_q^P; J^P | V | S_Q^P = 1/2^+ \hat{j}_q^{P'}; \hat{J}^{P'} \rangle_\beta = \delta_{j_q^P j_q^{P'}} \delta_{J^P J^{P'}} \langle \alpha || V || \beta \rangle_{j_q^P}, \quad \alpha, \beta = 1, 2 \quad (6.6)$$

where  $\mathcal{O}(\Lambda_{\text{QCD}}/m_Q)$  corrections have been neglected. The reduced matrix elements depend only on the configuration of the *ldof*, because QCD dynamics is invariant under spin rotations of the heavy quark in the infinite mass limit. Note that quantum numbers like isospin or strangeness ..., are conserved by QCD, and that for simplicity, such trivial dependencies are not explicitly shown in Eq. (6.6), though the  $\langle \alpha || V || \beta \rangle_{j_q^P}$  elements obviously depend on these additional properties needed to define the *ldof*. Finally, just mention that, in principle, the orthogonal  $|j_q^P = 1^-; J^P\rangle_1$  and  $|j_q^P = 1^-; J^P\rangle_2$  states can be connected by an interaction respecting HQSS. For instance, in the context of models based on the exchange of vector mesons, these contributions necessarily involve a  $D^*$ , instead of a  $\rho$ -meson, that will induce the transfer of charm between the baryon-baryon and meson-meson vertices.

#### 6.4.1 $\text{SU}(6)_{\text{lsf}} \times \text{SU}(2)_{\text{HQSS}}$

To illustrate the discussion on the HQSS structure of the  $\Lambda_c(2595)$  and  $\Lambda_c(2625)$  within molecular descriptions, we will focus on the model derived in Refs. [86, 172]. There, the isoscalar interaction,  $\hat{V}$ , used as kernel of the BSE in the  $J^P = 1/2^-$  and  $J^P = 3/2^-$  sectors respects HQSS (Eq. (6.6)) and it leads to<sup>8</sup>

$$\langle 1 || \hat{V} || 1 \rangle_{1^-} = -4f(s), \quad \langle 2 || \hat{V} || 2 \rangle_{1^-} = 0, \quad \langle 1 || \hat{V} || 2 \rangle_{1^-} = \sqrt{2}f(s), \quad \langle 2 || \hat{V} || 2 \rangle_{0^-} = -12f(s), \quad (6.7)$$

<sup>8</sup>Note that the order baryon-meson, instead of meson-baryon, is used in Refs. [86, 172]. This induces a minus sign for off diagonal elements involving the  $D^*N$  pair in the  $J = 1/2$  sector. In addition, there exists a minus sign of difference between the conventions of [86, 172] and those adopted here for the  $\Sigma_c^*$ .



when the coupled-channels space is truncated to that generated by the  $\pi\Sigma_c^{(*)}$  and  $D^{(*)}N$  pairs. Besides,  $f(s)$  is a function of the meson-baryon Mandelstam variable  $s$ . Note that  $\langle 1|\widehat{V}|1\rangle_{1^-}$  is determined by the isoscalar  $\pi\Sigma_c^{(*)} \rightarrow \pi\Sigma_c^{(*)}$  transition, which is approximated in [86, 172] by the LO WT chiral interaction. This fixes  $f(s)$  to

$$f(s) = \frac{\sqrt{s} - M}{2f_\pi^2} \frac{E + M}{2M} \quad (6.8)$$

using the normalizations of these works. In the above equation,  $M(E)$  is the common mass (center-of-mass energy) of the  $\Sigma_c^{(*)}$  baryons and  $f_\pi \sim 92$  MeV is the pion decay constant<sup>9</sup>. Coming back to Eq. (6.7), we see a large attraction for the  $j_q^P = 0^-$  *ldof* configuration, which is constructed out of the  $DN$  and  $D^*N$  pairs, since the *ldof* in the  $s$ -wave  $\pi\Sigma_c$  channel can be only  $j_q^P = 1^-$ . Indeed, the  $j_q^P = 0^-$  eigenvector of the matrix  $\widehat{V}$  is

$$v_0^{\text{atr}} \equiv |S_Q^P = 1/2^+ j_q^P = 0^-; J^P = 1/2^-\rangle_2. \quad (6.9)$$

On the other hand, diagonalizing  $\widehat{V}$  in the  $j_q^P = 1^-$  *ldof* subspace, we find additional attractive and slightly repulsive eigenvalues  $\lambda_1^{\text{atr}} = -2 - \sqrt{6} \sim -4.45$  and  $\lambda_1^{\text{rep}} = -2 + \sqrt{6} \sim 0.45$ , respectively, to be compared to  $\lambda_0 = -12$  obtained in the  $j_q^P = 0^-$  sector. The corresponding eigenvectors are  $v_1^{\text{atr}} \sim (1, \sqrt{2} - \sqrt{3})$  and  $v_1^{\text{rep}} \sim (\sqrt{3} - \sqrt{2}, 1)$  in the  $|j_q^P = 1^-\rangle_\alpha$ ,  $\alpha = 1, 2$  basis. Taking normalized vectors, we find for  $J^P = 1/2^-$

$$\|v_1^{\text{atr}}\|_{1/2^-}^2 = \underbrace{0.91}_{\pi\Sigma_c} + \underbrace{0.07}_{DN} + \underbrace{0.02}_{D^*N}, \quad \|v_1^{\text{rep}}\|_{1/2^-}^2 = \underbrace{0.09}_{\pi\Sigma_c} + \underbrace{0.68}_{DN} + \underbrace{0.23}_{D^*N}, \quad \|v_0^{\text{atr}}\|_{1/2^-}^2 = \underbrace{0.25}_{DN} + \underbrace{0.75}_{D^*N}, \quad (6.10)$$

while for  $J^P = 3/2^-$ , we have

$$\|v_1^{\text{atr}}\|_{3/2^-}^2 = \underbrace{0.91}_{\pi\Sigma_c^*} + \underbrace{0.09}_{D^*N}, \quad \|v_1^{\text{rep}}\|_{3/2^-}^2 = \underbrace{0.09}_{\pi\Sigma_c^*} + \underbrace{0.91}_{D^*N} \quad (6.11)$$

In light of these results, we could easily explain some features of the results found in Refs. [86, 172] for the lowest-lying odd-parity  $\Lambda_c^*$  states. There, a narrow  $J^P = 1/2^-$   $\Lambda_{c(n)}^{\text{MOL}}(2595)$  resonance ( $\Gamma \sim 1$  MeV) is reported, mostly generated from the extended WT  $DN - D^*N$  coupled-channels dynamics. The modulus square of the couplings of this resonance to  $DN$  and  $D^*N$  are approximately in the ratio 1 to 2.4, which does not differ much from the 1 to 3, that one would expect from the decomposition of  $\|v_0^{\text{atr}}\|_{1/2^-}^2$

<sup>9</sup>In the approach of Refs. [86, 172] sizable flavor symmetry breaking terms are included. Actually, the symmetry-pattern exhibited by the reduced matrix elements in Eq. (6.7) is modified, by computing the function  $f(s)$  using physical hadron masses and decay constants (see for instance, Eq. (7) of Ref. [86]). This induces mostly SU(4)-flavor breaking corrections, since the charmed-hadrons masses and decay constants follow in good approximation the HQSS-predictions, which do not significantly alter the discussion that follows.

in Eq. (6.10). Besides, this state has a small coupling to the  $\pi\Sigma_c$  channel, which further supports a largely dominant  $0^-$  *ldof* attractive configuration in its structure. Moreover, the detailed analysis carried out in [86] reveals that this narrow resonance stems from a **21**  $SU(6)_{\text{lsf}}$  irreducible representation (irrep), where the light quarks –three quarks and anti-quark– behave (do not behave) as an isoscalar spin-singlet (triplet) diquark–symmetric spin-flavor state–.

The RS adopted in Ref. [86, 172], proposed in [170, 171], plays an important role in enhancing the influence of the  $D^*N$  channel in the dynamics of the narrow  $\Lambda_{c(n)}^{\text{MOL}}(2595)$  state. Furthermore, this RS also produces a reduction in the mass of the resonance of around 200 MeV, which thus appears in the region of 2.6 GeV, instead of in the vicinity of the  $DN$  threshold. The RS establishes that all loop functions are set to zero at a common point (see Section 3.2.2 and Eq. (3.97)), regardless of the total angular momentum  $J$  of the sector. However, we should point out that such RS might not be fully consistent with HQSS.

In addition, there appears a second  $J^P = 1/2^-$  pole [ $\Lambda_{c(b)}^{\text{MOL}}(2595)$ ] in the 2.6 GeV region [86, 172]. Although it is placed relatively close to the  $\pi\Sigma_c$  threshold, this resonance is broad ( $\Gamma \sim 70 - 90$  MeV) thanks to its sizable coupling to this open channel, which in this case is larger than those to  $DN$  and  $D^*N$ . The study of Ref. [86] associates this isoscalar resonance to a **15**  $SU(6)_{\text{lsf}}$  irrep, where the *ldof* effectively behave as an isoscalar spin-triplet diquark (antisymmetric spin-flavor configuration). Thus, it is quite reasonable to assign a dominant  $j_q^P = 1^-$  configuration to the *ldof* in this second pole. However, the ratios of  $\pi\Sigma_c, DN$  and  $D^*N$  couplings of this second resonance do not follow the pattern inferred from  $\|v_1^{\text{atr}}\|_{1/2^-}^2$  in Eq. (6.10) as precisely as in the case of the narrow state. Actually, the couplings of this broad state to the  $DN$  and  $D^*N$  pairs, though smaller, turn out to be comparable (absolute value) in magnitude to the  $\pi\Sigma_c$  one (1.6, 1.4 and 2.3, respectively [86]). This points to the possibility that this second pole might also have a sizable component of the  $1^-$  repulsive configuration, for which we should expect  $DN$  and  $D^*N$  couplings much larger than the  $\pi\Sigma_c$  one (likely in proportion 9 to 1 for the squares of the absolute values, just opposite to what is expected from the  $1^-$  attractive eigenvector in Eq. (6.10)). Indeed, the fact that the  $\Lambda_{c(b)}^{\text{MOL}}(2595)$  is located above the  $\pi\Sigma_c$  threshold reinforces this picture, where there would be a significant mixing among the attractive and repulsive  $1^-$  configurations, provoked by the flavor breaking corrections incorporated in the model of Refs. [86, 172]. These symmetry breaking terms affect the kernel  $f(s)$  of the BSE, the meson-baryon loops and the renormalization of the UV behaviour of the latter to render finite the unitarized amplitudes. The large difference between the actual  $\pi\Sigma_c$  and  $D^{(*)}N$  thresholds, which are supposed to be degenerate to obtain the results of Eq. (6.10), should certainly play an important role. The mass breaking effects were less relevant for the narrow  $\Lambda_{c(n)}^{\text{MOL}}(2595)$  resonance, because in that case i) the  $\pi\Sigma_c$  channel had little influence in the dynamics of the state, and ii) the

dominant  $DN$  and  $D^*N$  thresholds turn out to be relatively close, thanks to HQSS. In addition, other higher channels like  $\eta\Lambda_c$ ,  $K\Xi_c^{(\prime)}$ ,  $D_s\Lambda$ ,  $\rho\Sigma_c$ , ... which are considered in [86, 172], have not been included here in the simplified analysis that leads to the results of Eq. (6.10). Finally, one should neither discard a small  $0^-$   $ldof$  component in the  $\Lambda_{c(b)}^{\text{MOL}}(2595)$  wave-function that will also change the couplings of this broad state to the different channels.

Note that the total angular momentum and parity of the  $ldof$  are neither really conserved in the  $SU(6)_{\text{lsf}} \times SU(2)_{\text{HQSS}}$  model, nor in the real physical world because the charm quark mass is finite. Hence, both the narrow and broad  $\Lambda_{c(n,b)}^{\text{MOL}}(2595)$  resonances reported in [86, 172] will have an admixture of the  $0^-$  and  $1^-$  configurations<sup>10</sup> in their inner structure. More importantly, the physical  $\Lambda_c(2595)$  and the second resonance, if it exists, will also contain both type of  $ldof$  in their wave-function. As stressed in the Introduction, a non-negligible  $0^-$  component in the  $\Lambda_c(2595)$  or a double-pole structure have not been considered in the theoretical analyses of the exclusive semileptonic  $\Lambda_b$  decays into  $\Lambda_c(2595)$  carried out in Refs. [316, 317, 319]. One of the main objectives of this work is precisely the study of how these non-standard features affect the  $\Lambda_b \rightarrow \Lambda_c^*$  transitions.

Finally, the lowest-lying  $J^P = 3/2^-$  isoscalar resonance found in Refs. [86, 172] is clearly the HQSS partner of the broad  $J^P = 1/2^-$   $\Lambda_{c(b)}^{\text{MOL}}(2595)$  state, with quantum number  $j_q^P = 1^-$  for the  $ldof$ . It is located above the  $\pi\Sigma_c^*$  threshold, with a width of around 40-50 MeV, and placed in the **15**  $SU(6)_{\text{lsf}}$  irrep [86], as the broad  $\Lambda_{c(b)}^{\text{MOL}}(2595)$  resonance. Moreover, the complex coupling of this  $J^P = 3/2^-$  pole to the  $\pi\Sigma_c^*$  channel is essentially identical to that of the  $\Lambda_{c(b)}^{\text{MOL}}(2595)$  to  $\pi\Sigma_c$ . In turn, the square of the absolute value of its coupling to  $D^*N$  compares reasonably well with the sum of the squares of the couplings of the  $\Lambda_{c(b)}^{\text{MOL}}(2595)$  to  $DN$  and  $D^*N$ , as one would expect from Eqs. (6.10) and (6.11). This  $J^P = 3/2^-$  isoscalar resonance is identified with the  $d$ -wave  $\Lambda_c(2625)$  in Refs. [86, 172]. In these works, it is argued that a small change in the renormalization subtraction constant could easily move the resonance down by 40 MeV to the nominal position of the physical state, and that in addition, this change of the mass would considerably reduce the width, since its position would get much closer to the threshold of the only open channel  $\pi\Sigma_c^*$ .

Thus, within the  $SU(6)_{\text{lsf}} \times SU(2)_{\text{HQSS}}$  model, the  $\Lambda_c(2625)$  turns out to be the HQSS partner of the second broad  $\Lambda_{c(b)}^{\text{MOL}}(2595)$  pole instead of the narrow  $\Lambda_{c(n)}^{\text{MOL}}(2595)$  resonance, as commonly assumed in the theoretical analyses of the exclusive semileptonic  $\Lambda_b$  decays into  $\Lambda_c(2595)$ . This picture clearly contradicts the predictions of the CQMs where first, there is not a second 2595 pole, and second, the  $\Lambda_c(2625)$  and the

<sup>10</sup>However, the previous discussion has allowed us to reasonably identify the dominant one in each case. The existence of a certain mixing is out of doubt, thus for instance, the narrow state can decay into  $\pi\Sigma_c$  through its  $1^-$  small component.

narrow  $\Lambda_c(2595)$  are HQSS siblings, produced by a  $\lambda$ -mode excitation of the ground  $1/2^+$   $\Lambda_c$  baryon.

### 6.4.2 Extended local hidden gauge (ELHG)

Within the model of Ref. [85], the dynamics of the lowest-lying odd-parity  $\Lambda_c^*$  is mostly governed by the  $DN$ ,  $D^*N$  and  $\pi\Sigma_c$  interactions ( $V^{\text{HG}}$ ). They are constructed using an SU(4) extension of the local hidden gauge formalism derived for the light meson sector [134–136], that in a first stage respects HQSS. It gives rise to reduced matrix elements

$$\begin{aligned} \langle 1||V^{\text{HG}}||1\rangle_{1^-} &= -4f(s), & \langle 2||V^{\text{HG}}||2\rangle_{1^-} &= -3f(s), & \langle 1||V^{\text{HG}}||2\rangle_{1^-} &= 0, \\ & & \langle 2||V^{\text{HG}}||2\rangle_{0^-} &= -3f(s), & & \end{aligned} \quad (6.12)$$

in the isoscalar sector. The flavor symmetry of the WT function  $f(s)$  is broken in the meson-baryon space by the use of physical masses. At first,  $D^*$ -exchange driven interaction terms connecting  $|j_q^P = 1^-; J^P\rangle_1$  and  $|j_q^P = 1^-; J^P\rangle_2$  states are neglected, as well as  $DN \rightarrow D^*N$  coupled-channel interactions in the  $J^P = 1/2^-$  sector.

In a second stage, some additional contributions driven by the  $D^*D\pi$  coupling, that formally vanish in the infinitely heavy quark mass limit, are considered in the kernels (potentials) of the BSE. These new terms provide:

- First,  $DN \rightarrow \pi\Sigma_c$  transitions in the  $J^P = 1/2^-$  sector, which would give rise to  $\langle 1||V^{\text{HG}}||2\rangle_{1^-} = \sqrt{2}f(s)/4$ . The factor  $1/4$  roughly accounts for the ratio  $(m_\rho/m_{D^*})^2$ , which one would expect to suppress the diagrams induced by the  $t$ -channel exchange of charmed vector mesons compared to those mediated by members of the light  $\rho$ -octet [338]. This assumes a universal KSFR vector-meson coupling. However, the effects due to  $\langle 1||V^{\text{HG}}||2\rangle_{1^-} \neq 0$  are, inconsistently with HQSS, not considered in the  $J^P = 3/2^-$  sector, and thus  $D^*N$  and  $\pi\Sigma_c^*$  channels are not connected<sup>11</sup> in the formalism of Ref. [85]. Actually, the isoscalar  $\pi\Sigma_c^*$  pair is separately treated as a single channel. We will come back to this point below.
- Second,  $D^{(*)}N \rightarrow DN$  transitions in the  $J^P = 1/2^-$  sector obtained from box diagrams, which also generate contributions to the  $DN \rightarrow DN$  and  $D^*N \rightarrow D^*N$  diagonal interaction-terms. In the  $J^P = 3/2^-$  sector, modifications of the

<sup>11</sup>We should also point out that the  $D^*N \rightarrow \pi\Sigma_c$  transition in the  $J^P = 1/2^-$  sector is also set to zero in [85]. This is also inconsistent with HQSS, since this symmetry relates this off diagonal term of the interaction with the  $DN \rightarrow \pi\Sigma_c$  one (a factor  $1/\sqrt{3}$ ).

$D^*N \rightarrow D^*N$  potential induced by box-diagrams constructed out, in this case, of the anomalous  $D^*D^*\pi$  coupling are also taken into account in [85].

In addition, other higher channels like  $\eta\Lambda_c$ ,  $\rho\Sigma_c$ , ... are considered in [85], though they have a little influence in the lowest-lying  $\Lambda_c^*$  states. After fine tuning some UV cutoffs to reproduce the masses of the experimental narrow  $\Lambda_c(2595)$  and  $\Lambda_c(2625)$ , the authors of Ref. [85] found that the latter resonance is essentially a  $D^*N$  state, while the former one couples strongly both to  $DN$  and  $D^*N$  and has a quite small coupling to  $\pi\Sigma_c$ . In addition, a state at 2611 MeV and a width of around 100 MeV, which couples mostly to  $\pi\Sigma_c$  is also dynamically generated, confirming the double pole structure predicted in the  $SU(6)_{\text{lsf}} \times SU(2)_{\text{HQSS}}$  model of Refs. [86, 172]. Note also that the narrow  $\Lambda_c(2595)$  state found in [85] has similar  $DN$  and  $D^*N$  couplings, from where one can conclude that it should have an important  $0^-$  *ldof* configuration.

On the other hand, in the  $J^P = 3/2^-$  sector the isoscalar  $\pi\Sigma_c^*$  is treated as a single channel in [85]. It gives rise to a further broad state ( $\Gamma \sim 100$  MeV) in the region of 2675 MeV, which is not related to the  $\Lambda_c(2625)$  in that reference.

Finally, we should mention that the box-diagrams interaction terms evaluated in this ELHG model break HQSS at the charm scale, and it becomes difficult to identify any HQSS resonance doublet among the results reported in [85].

### 6.4.3 SU(4) flavor $t$ -channel exchange of vector mesons

As already mentioned in this kind of models [170, 338], the BSE potentials are calculated from the zero-range limit of  $t$ -channel exchange of vector mesons between pseudoscalar mesons and baryons. Chiral symmetry is preserved in the light meson sector, while the interaction is still of the WT type. Thus, the  $J = 1/2$  lowest-lying odd-parity  $\Lambda_c^*$  resonances are mostly generated from  $DN, \pi\Sigma_c$  coupled-channels dynamics. SU(4) flavor symmetry is used to determine the  $DN \rightarrow DN$  and  $DN \rightarrow \pi\Sigma_c$  interactions, which could be also derived assuming that the KSFR coupling relation holds also when charm hadrons are involved. The flavor symmetry is broken by the physical hadron masses, and in particular the large mass of the  $D^*$  suppresses the off diagonal matrix element  $DN \rightarrow \pi\Sigma_c$ , as compared to the diagonal ones that are driven by  $\rho$ -meson exchange (see also the discussion in the previous subsection about the factor 1/4 included in the ELHG approach of Ref. [85]). These approaches do not include the  $D^*N \rightarrow D^*N, DN, \pi\Sigma_c$  transitions, and therefore are not consistent with HQSS. Nevertheless, a  $J^P = 1/2^-$  narrow resonance close to the  $\pi\Sigma_c$  threshold, which can be readily identified with the  $\Lambda_c(2595)$ , is generated. It couples strongly to  $DN$ , and its nature is therefore very different from those obtained in the  $SU(6)_{\text{lsf}} \times SU(2)_{\text{HQSS}}$  and in the ELHG models, for which the  $D^*N$  channel plays a crucial role. The reason why these SU(4) models can generate the  $\Lambda_c(2595)$  is that the

lack of the  $D^*N$  in the  $J^P = 1/2^-$  sector is compensated by the enhanced strength in the  $DN$  channel. For instance, the  $DN$  coupling in the approaches of Refs. [170, 338] turned out to be of the same magnitude as that of the narrow  $\Lambda_{c(n)}^{\text{MOL}}(2595)$  to  $D^*N$  in the  $\text{SU}(6)_{\text{lsf}} \times \text{SU}(2)_{\text{HQSS}}$  model of Refs. [86, 172]. On the other hand, the  $\pi\Sigma_c$  coupling, though still small, was found twice larger in Refs. [170, 338]. By construction, the resonance described in [170, 338] will mix  $J_q^P = 0^-$  and  $1^-$   $ldof$  configurations. The gross features of this dynamically generated state are similar to those of the resonance reported in Ref. [337], where the similarity between the  $DN$  and  $\bar{K}N$  systems, once the strange quark in the later is replaced by a charm quark, was exploited.

In addition, the models based on the  $t$ -channel exchange of vector mesons, when the unitarized amplitudes are renormalized as suggested in [170, 171], produce also a second  $J^P = 1/2^-$  broad resonance ( $\Gamma \sim 100$  MeV) above 2600 MeV, with  $\pi\Sigma_c$  (largest) and  $DN$  couplings similar to those found in the  $\text{SU}(6)_{\text{lsf}} \times \text{SU}(2)_{\text{HQSS}}$  and in the ELHG approaches (see Table XIV of Ref. [172] and the related discussion for an update of the results of the model used in [338]). Therefore, this type of molecular models might also predict a double pole structure for the  $\Lambda_c(2595)$ , in analogy with what happens in the unitary chiral descriptions of the  $\Lambda(1405)$ . We should, however, note that this second broad state is not generated when a RS based on an UV hard-cutoff is used [338, 339].

In the isoscalar  $J^P = 3/2^-$  sector, the chiral  $\pi\Sigma_c^*$  WT interaction, driven by  $\rho$ -exchange, leads to a resonance with some resemblances to that reported in Refs. [86, 172], and that it is identified in [171] with the  $\Lambda_c(2625)$ , despite being located above 2660 MeV and having a width of the order of 50 MeV. Actually, this pole corresponds to that found in the single channel  $\pi\Sigma_c^*$  analysis of Ref. [85], where it was, however, not associated to the physical  $\Lambda_c(2625)$  state.

#### 6.4.4 Chiral isoscalar $\pi\Sigma_c^{(*)}$ molecules

The chiral interactions between the ground-state singly charmed baryons and the Goldstone bosons lead to scenarios [171, 336, 340] where  $\pi\Sigma_c$  and  $\pi\Sigma_c^*$  isoscalar molecules naturally emerge in the  $J^P = 1/2^-$  and  $J^P = 3/2^-$  sectors, respectively. These states will form a  $1^-$  HQSS doublet, whose masses and widths depend on the details of the used RS. The works of Refs. [171, 336] found  $J^P = 1/2^-, 3/2^-$  resonances of around 50 MeV of width and masses in the 2660 MeV region using a RS, inspired in the success of Refs. [33, 69, 327] to describe the chiral  $\text{SU}(3)$  meson-baryon  $J^P = 1/2^-$  and  $J^P = 3/2^-$  sectors, later also employed in the  $\text{SU}(6)_{\text{lsf}} \times \text{SU}(2)_{\text{HQSS}}$  model of Refs. [86, 172]<sup>12</sup>. The  $\pi\Sigma_c^*$  pole found in the ELHG scheme followed in [85] clearly

<sup>12</sup>As we discussed above, the consideration of the  $DN$  and  $D^*N$  channels in [86, 172] strongly modifies the  $J^P = 1/2^-$  sector, leading to a quasi-bound  $D^*N$  state.

matches the results of Ref. [171], though it was not identified with the  $\Lambda_c(2625)$  in the work of Ref. [85].

In sharp contrast, subtraction constants or UV cutoffs were fine-tuned in Ref. [340] in such a way that the  $\Lambda_c(2595)$  and  $\Lambda_c(2625)$  experimental masses were reproduced, leading to weakly  $\pi\Sigma_c$  and  $\pi\Sigma_c^*$  bound states. Thus, the needed UV cutoffs turned out to be slightly higher than expected, 1.35 and 2.13 GeV, respectively. This could indicate some degrees of freedom that are not considered in the approach, such that CQM states or  $D^{(*)}N$  components, and that could play a certain role, being their effects effectively accounted for the fitted real parts of the unitarity loops [352, 353]. The importance that the CQM degrees of freedom can have on the behavior of these resonances will be studied in Chapter 7.

## 6.5 Weinberg compositeness condition

In section 3.2.3 we discussed the Weinberg compositeness condition (Eq. (3.117a)), which can be used to determine the relevance of hadron components in molecular states. For the particular case of the  $\Lambda_c(2595)$ , the situation is a bit unclear. For instance, it was shown in Ref. [354] that the  $\Lambda_c(2595)$  is not predominantly a  $\pi\Sigma_c$  molecular state using the effective range expansion. A similar conclusion was reached in Ref. [355], using a generalized effective range expansion including Castillejo-Dalitz-Dyson pole contributions. In this latter work, the effects of isospin breaking corrections are also taken into account and the extended compositeness condition for resonances developed in Ref. [45] was applied to calculate the component coefficients. Furthermore, although in the unitary approaches, the  $\Lambda_c(2595)$  is found to be of molecular nature [85, 86, 170, 172, 336–338, 340], there is no general agreement on its dominant meson-baryon components yet.

In general, one can conclude that the compositeness of the  $\Lambda_c(2595)$  depends on the number of considered coupled channels, and on the particular regularization scheme adopted in the unitary approaches and, therefore, would be model dependent [341].

## 6.6 Semileptonic $\Lambda_b \rightarrow \Lambda_c^* \ell \bar{\nu}_\ell$ decays

The differential decay width for the semileptonic  $b \rightarrow c$  transition shown in Fig. 6.1 is given by

$$\frac{d\Gamma}{d\omega} = \Gamma_0 \frac{96 M_{\Lambda_c^*}^3}{\pi M_{\Lambda_b}^5} \sqrt{\omega^2 - 1} \mathcal{L}^{\alpha\beta}(q) \mathcal{H}_{\alpha\beta}(P, P'), \quad \Gamma_0 = |V_{cb}|^2 \frac{G_F^2 M_{\Lambda_b}^5}{192\pi^3} \quad (6.13)$$

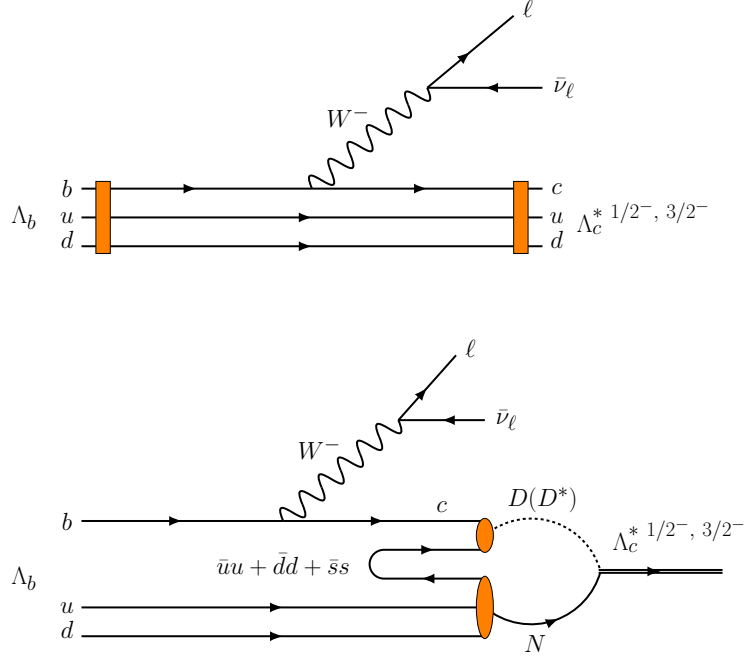


Figure 6.1: Above: Diagrammatic representation of the  $\Lambda_b \rightarrow \Lambda_c^* \ell \bar{\nu}_\ell$  decay. Bellow: Hadronization creating  $q\bar{q}$  pairs, together with the pictorial representation of the mechanism to produce a  $\Lambda_c^*$  resonance, through an intermediate propagation of  $DN$  and  $D^*N$  pairs.

where  $|V_{cb}|$  is the modulus of the Cabibbo–Kobayashi–Maskawa (CKM) matrix element for the  $b \rightarrow c$  transition,  $G_F = 1.16638 \times 10^{-11} \text{ MeV}^{-2}$  is the Fermi decay constant,  $P^\mu, M_{\Lambda_b}$  ( $P'^\mu, M_{\Lambda_c^*}$ ) are the four-momentum and mass of the initial (final) baryon,  $q^\mu = P^\mu - P'^\mu$ . In the decay,  $\omega$  ranges from  $\omega = 1$ , corresponding to zero recoil of the final baryon, to a maximum value given, neglecting the antineutrino mass, by  $\omega = \omega_{\max} = \frac{M_{\Lambda_b}^2 + M_{\Lambda_c^*}^2 - m_\ell^2}{2M_{\Lambda_b}M_{\Lambda_c^*}}$ , where  $m_\ell$  is the final charged lepton mass. In addition,  $\mathcal{L}^{\alpha\beta}(q)$  is the leptonic tensor after integrating in the lepton momenta

$$\begin{aligned} \mathcal{L}^{\alpha\beta}(q) &= \int \frac{d^3k}{2|\vec{k}|} \frac{d^3k'}{2\sqrt{m_\ell^2 + \vec{k}'^2}} \left( k'^\alpha k^\beta + k'^\beta k^\alpha - g^{\alpha\beta} \vec{k} \cdot \vec{k}' + i\epsilon^{\alpha\beta\rho\sigma} k'_\rho k_\sigma \right) \delta^4(q - k - k') \\ &= -\frac{\pi}{6q^2} (q^2 - m_\ell^2) \left\{ \left( q^2 - \frac{m_\ell^2}{2} - \frac{m_\ell^4}{2q^2} \right) g^{\alpha\beta} - \left( q^2 + m_\ell^2 - 2\frac{m_\ell^4}{q^2} \right) \frac{q^\alpha q^\beta}{q^2} \right\} \quad (6.14) \end{aligned}$$



where  $k$  and  $k'$  are the four-momenta of the outgoing antineutrino and charged lepton [in our convention, we take  $\epsilon_{0123} = +1$  and the metric  $g^{\mu\mu} = (+, -, -, -)$ ]. Besides,  $\mathcal{H}_{\alpha\beta}(P, P')$  is the hadronic tensor given by

$$\mathcal{H}^{\alpha\beta}(P, P') = \frac{1}{2} \sum_{r, r'} \langle \Lambda_c^*, r' \vec{P}' | J_{bc}^\alpha(0) | \Lambda_b, r \vec{P} \rangle \langle \Lambda_c^*, r' \vec{P}' | J_{bc}^\beta(0) | \Lambda_b, r \vec{P} \rangle^* \quad (6.15)$$

with  $|\Lambda_b, r \vec{P}\rangle$  ( $|\Lambda_c^*, r' \vec{P}'\rangle$ ) the initial (final) baryon state with three-momentum  $\vec{P}$  ( $\vec{P}'$ ) and helicity  $r$  ( $r'$ ), and normalized such that

$$\langle B, r' \vec{P}' | B, r \vec{P} \rangle = (2\pi)^3 \frac{E}{M} \delta_{rr'} \delta^3(\vec{P} - \vec{P}'), \quad B = \Lambda_b, \Lambda_c^* \quad (6.16)$$

with  $E$  and  $M$ , the baryon energy for three-momentum  $\vec{P}$  and its mass, respectively. Finally,  $J_{bc}^\mu(0)$  is the  $b \rightarrow c$  charged weak current

$$J_{bc}^\mu(0) = \bar{\Psi}_c(0) \gamma^\mu (1 - \gamma_5) \Psi_b(0) \quad (6.17)$$

with  $\Psi_{b,c}$ , Dirac fields, with dimensions of mass to the 3/2. Hadronic matrix elements can be parameterized in terms of form factors [317]. For  $\frac{1}{2}^+ \rightarrow \frac{1}{2}^-$  transitions the form factor decomposition reads

$$\begin{aligned} \langle \Lambda_c^{*1/2-}, r' \vec{P}' | J_{bc}^\mu(0) | \Lambda_b, r \vec{P} \rangle = & \bar{u}_{\Lambda_c^*}(\vec{P}', r') \left\{ \gamma^\mu [F_1 \gamma_5 - G_1] + v^\mu [F_2 \gamma_5 - G_2] \right. \\ & \left. + v'^\mu [F_3 \gamma_5 - G_3] \right\} u^{\Lambda_b}(\vec{P}, r) \end{aligned} \quad (6.18)$$

The  $u_r$  are dimensionless Dirac spinors ( $\bar{u}_{r'} u_r = \delta_{rr'}$ ),  $v^\mu, v'^\mu$  are the four velocities of the initial and final baryons and the three vector (axial)  $F_1, F_2, F_3$  ( $G_1, G_2, G_3$ ) form factors are functions of  $\omega$  or equivalently of  $q^2$ . For  $\frac{1}{2}^+ \rightarrow \frac{3}{2}^-$  decays we write

$$\begin{aligned} \langle \Lambda_c^{*3/2-}, r' \vec{P}' | J_{bc}^\mu(0) | \Lambda_b, r \vec{P} \rangle = & \bar{u}_{\Lambda_c^*}^{\alpha}(\vec{P}', r') \Gamma^{\alpha\mu} u^{\Lambda_b}(\vec{P}, r) \\ \Gamma^{\alpha\mu} = & v^\alpha \left\{ \gamma^\mu [l_{V_1} - l_{A_1} \gamma_5] + v^\mu [l_{V_2} - l_{A_2} \gamma_5] + v'^\mu [l_{V_3} - l_{A_3} \gamma_5] \right\} \\ & + g^{\alpha\mu} [l_{V_4} - l_{A_4} \gamma_5] \end{aligned} \quad (6.19)$$

Here  $u_{\alpha r'}^{\Lambda_c^*}$  is the Rarita-Schwinger spinor of the final spin 3/2 baryon normalized such that  $(\bar{u}_{\alpha r'}^{\Lambda_c^*}) u_r^{B' \alpha} = -\delta_{rr'}$ , and we have four vector ( $l_{V_{1,2,3,4}}(\omega)$ ) and four axial ( $l_{A_{1,2,3,4}}(\omega)$ ) form factors.

## 6.7 Infinite heavy quark mass limit

The large spin invariance in the  $m_Q \rightarrow \infty$  limit leads to considerable simplifications [322, 356]. In particular, the semileptonic decay of the ground state  $\Lambda_b$  into either  $\Lambda_c^*$  in the  $j_q^P = 1^-$  heavy doublet is described by an universal form-factor [313]. In this limit, the bottom quark carries all of the angular momentum of the  $\Lambda_b$ , where the  $ldof$  are coupled to  $j_q^P = 0^+$ . As discussed in Section 2.5.1, the  $\Lambda_b$  is accounted by a Dirac spinor  $u_b(v)$ , with  $v$  the velocity of the  $\Lambda_b$  (and of its heavy point-like constituent), satisfying Eq. (2.68). The charm  $j_q^P = 1^-$  doublet of baryons, with four velocity  $v'$ , are represented by the multiplet-spinor  $\mathcal{W}_c^\mu(v')$ , which obeys Eqs. (2.77) and (2.78), where the spin 1/2 and spin 3/2 members of this doublet are written as the Dirac  $u_c^{1/2}(v')$  and the Rarita-Schwinger spinors  $u_c^{3/2\mu}(v')$ , respectively.

Under a Lorentz transformation,  $\Lambda$ , and  $b$  and  $c$  quark spin transformations  $\widehat{S}_b$  and  $\widehat{S}_c$ , the above spinor wave functions transform as  $S(\Lambda)u_b$ ,  $\Lambda_v^\mu S(\Lambda)\mathcal{W}_c^\nu$  and  $\widehat{S}_b u_b$  and  $\widehat{S}_c \mathcal{W}_c^\mu$ , respectively, with  $S(\Lambda) = \exp\{-i\sigma_{\mu\nu}S^{\mu\nu}/4\}$ , the usual spinor representation. Note that  $\widehat{S}_b$  and  $\widehat{S}_c$  are also of the form  $S(\widehat{\Lambda})$ , but with  $\widehat{\Lambda}$  restricted to spatial rotations and affecting only to the heavy quark spinor.

In addition in the  $m_Q \rightarrow \infty$  limit, under heavy quark spin rotations, the  $b \rightarrow c$  flavor changing current transforms as  $J_{bc}^\mu \rightarrow \widehat{S}_c J_{bc}^\mu \widehat{S}_b^\dagger$ . From Eq. (2.91), we get that the most general form for the matrix element respecting HQSS is [313, 317]

$$\langle \Lambda_c^{*1/2^-, 3/2^-}; j_q^P = 1^- | J_{bc}^\mu(0) | \Lambda_b \rangle = \sigma(\omega)v_\lambda \bar{\mathcal{W}}_c^\lambda(v') \gamma^\mu (1 - \gamma_5) u_b(v) + \mathcal{O}(1/m_{b,c}), \quad (6.20)$$

Here  $\sigma(\omega)$  is the (real) dimensionless leading IW function for the transition to this excited doublet. It follows  $\sqrt{3}F_1/(\omega - 1) = \sqrt{3}G_1/(\omega + 1) = -\sqrt{3}F_2/2 = -\sqrt{3}G_2/2 = l_{V_1} = l_{A_1} = \sigma$  and  $F_3 = G_3 = l_{V_{2,3,4}} = l_{A_{2,3,4}} = 0$ . In Ref. [317],  $\sigma(\omega)$  was predicted in the large  $N_c$  limit,

$$\sigma(\omega) = 1.2[1 - 1.4(\omega - 1)] \quad (6.21)$$

where subleading  $1/N_c$  corrections are neglected.

The matrix element in Eq. (6.20) vanishes at zero recoil, where  $v = v'$ , and it trivially leads to<sup>13</sup>

$$\begin{aligned} \mathcal{H}_{3/2^-}^{\alpha\beta}[j_q^P = 1^-] &= 2\mathcal{H}_{1/2^-}^{\alpha\beta}[j_q^P = 1^-] = \frac{2\sigma^2(\omega)}{3}(\omega^2 - 1) \left( v^\alpha v'^\beta + v^\beta v'^\alpha - \omega g^{\alpha\beta} \right. \\ &\quad \left. - i\epsilon^{\alpha\beta\rho\sigma} v_\rho v'_\sigma \right) + \mathcal{O}(1/m_{b,c}) \end{aligned} \quad (6.22)$$

<sup>13</sup>The sum over the initial and final polarizations in the definition of the hadronic tensor in Eq. (6.15) can be written as trace in the Dirac space, with the help of the spin 1/2 and 3/2 projectors. These latter operators are given in Eq. (2.76).

the antisymmetric term does not contribute to  $d\Gamma/d\omega$  since the leptonic tensor, after integrating in the lepton momenta, becomes symmetric. Thus in the  $m_Q \rightarrow +\infty$  limit,  $d\Gamma_{\Lambda_c^{*3/2}}/d\omega = 2d\Gamma_{\Lambda_c^{*1/2}}/d\omega$  since both members of the  $j_q^P = 1^-$  doublet are degenerate. Furthermore, one easily deduces that  $\Lambda_b$  decays to excited  $\Lambda_c^{*3/2^-}$  with helicity  $\pm 3/2$  are forbidden by HQSS in the IW limit, since the component of the  $ldof$  total angular momentum along the decay axis is conserved, and equal to zero.

On the other hand, for the ground-state  $\Lambda_b$  transition to the  $J^P = 1/2^-$  charmed baryon with  $j_Q^P = 0^-$   $ldof$ , one can use for the latter a spinor  $u_c(v')$ , but the form-factors must be pseudoscalar and therefore involve a Levi-Civita tensor [323]. At leading order in the  $1/m_Q$  expansion, there are not enough vectors available to contract with the indices of the epsilon tensor so these unnatural<sup>14</sup> parity matrix elements vanish [316, 317].

A different way to understand why the  $\Lambda_b[1/2^+, j_q^P = 0^+] \rightarrow \Lambda_c^*[1/2^-, j_q^P = 0^-]$  is forbidden in the IW limit is adopting the picture introduced in Refs. [224, 321]. In the heavy-quark limit, the weak transition occurs on the  $b$  quark, which turns into a  $c$  quark and a  $W^-$  boson, as shown in the lower panel of Fig. 6.1. Since we will have a  $1/2^-$  or  $3/2^-$  state at the end, and the  $u, d$  quarks are spectators, remaining in a  $0^+$  spin-parity configuration, the final charm quark must carry negative parity and hence must be in an  $L = 1$  level. This corresponds to an orbital angular momentum excitation between the heavy quark and the isoscalar  $u, d$  diquark as a whole, which maintains the same spin-parity quantum numbers,  $0^+$ , as in the initial  $\Lambda_b$ , leading to a non-zero  $ldof$  wave-function overlap. Within this picture, the total angular momentum and parity of the light subsystem will be  $j_q^P = 1^- [= 0^+ \otimes (L = 1)]$ , and the transition will be described by the matrix element in Eq. (6.20), that will go through  $p$ -wave, giving rise to the  $(\omega^2 - 1)$  factor in Eq. (6.22). In sharp contrast, the  $(j_q^P = 0^-, J^P = 1/2^-)$  final baryon contains a  $p$ -wave excitation inside the brown muck and a realignment of the light quarks spins to construct a spin triplet state. That requires going beyond the spectator approximation of Fig. 6.1, involving dynamical changes in the QCD dressing of the heavy baryon during the transition, which are  $1/m_Q$ -suppressed. Thus in the heavy quark limit, the initial and final  $ldof$  overlap for the unnatural  $0^+ \rightarrow 0^-$  transition vanishes. It would be parametrized by a pseudoscalar form-factor, involving the Levi-Civita tensor. As mentioned above, at leading order in the  $1/m_Q$  expansion, there are not enough vectors available to contract with the indices of the epsilon tensor.

<sup>14</sup>A semileptonic baryonic transition is unnatural if it involves transitions between tensor  $(0^+, 1^-, 2^+, \dots)$  to pseudo-tensor  $(0^-, 1^+, 2^-, \dots)$ , or vice-versa,  $j_q^P$   $ldof$  quantum numbers.

## 6.8 $\mathcal{O}(\Lambda_{\text{QCD}}/m_c)$ corrections

Corrections of order  $1/m_Q$  to  $d\Gamma(\Lambda_b \rightarrow \Lambda_c^{*3/2}[j_q^P = 1^-])/d\omega$  and  $d\Gamma(\Lambda_b \rightarrow \Lambda_c^{*1/2}[j_q^P = 1^-])/d\omega$  distributions were studied in [317] and shown to be quite large, specially in the  $J^P = 1/2^-$  case (see Fig. 1 of that reference).

Neglecting  $\mathcal{O}(\Lambda_{\text{QCD}}/m_b)$  terms, this is to say keeping still the invariance of the weak matrix element under arbitrary  $b$ -quark spin rotations, the general forms of the semileptonic matrix elements are

$$\langle \Lambda_c^{*1/2^-} | \mathbf{J}_{bc}^\mu(0) | \Lambda_b \rangle = \frac{1}{\sqrt{3}} \bar{u}_c(v') [(\not{v} - \omega)\Delta_1 - \Delta_2] \gamma^\mu (1 - \gamma_5) u_b(v) + \mathcal{O}(1/m_b), \quad (6.23)$$

$$\langle \Lambda_c^{*3/2^-} | \mathbf{J}_{bc}^\mu(0) | \Lambda_b \rangle = \bar{u}_c^\lambda(v') v_\lambda [\Omega_1 - (\not{v} - \omega)\Omega_2] \gamma^\mu (1 - \gamma_5) u_b(v) + \mathcal{O}(1/m_b), \quad (6.24)$$

where  $\Delta_{1,2}$  and  $\Omega_{1,2}$  are form factors function of  $\omega$  that are used to construct independent linear combinations of the identity and  $\not{v}$  matrices. For semileptonic transitions to  $\Lambda_c^{*1/2^-}$ , we find  $\sqrt{3}F_1 = (\omega - 1)\Delta_1 + \Delta_2$ ,  $\sqrt{3}G_1 = (\omega + 1)\Delta_1 + \Delta_2$ ,  $F_2 = G_2 = -2\Delta_1/\sqrt{3}$  and  $F_3 = G_3 = 0$ . Similarly for  $\Lambda_c^{*3/2^-}$ , we find  $l_{V_1} = \Omega_1 + (\omega + 1)\Omega_2$ ,  $l_{A_1} = \Omega_1 + (\omega - 1)\Omega_2$ ,  $l_{V_2} = l_{A_2} = -2\Omega_2$  and  $l_{V_{3,4}} = l_{A_{3,4}} = 0$ .

If  $\Delta_1 = \Omega_1 = \sigma$  and  $\Delta_2 = \Omega_2 = 0$ , the IW limit of Eq. (6.22) is recovered for transitions to  $\Lambda_c^{*3/2^-, 1/2^-}[j_q^P = 1^-]$  states<sup>15</sup>.

The differential decay widths deduced from the general matrix elements of Eqs. (6.23) and (6.24) are given by

$$\begin{aligned} \frac{d\Gamma[\Lambda_b \rightarrow \Lambda_c^*(J^P)]}{d\omega} &= C_J \frac{8\Gamma_0}{3} \left( \frac{M_{\Lambda_c^*}}{M_{\Lambda_b}} \right)^3 \left( 1 - \frac{m_\ell^2}{q^2} \right)^2 (\omega^2 - 1)^J \left\{ \alpha_J^2 \left[ 3\omega \frac{q^2 + m_\ell^2}{M_{\Lambda_b}^2} \right. \right. \\ &+ 2 \frac{M_{\Lambda_c^*}}{M_{\Lambda_b}} (\omega^2 - 1) \left( 1 + \frac{2m_\ell^2}{q^2} \right) \left. \right] + 2(\omega^2 - 1) [\alpha_1(\omega)\alpha_2(\omega)]_J \left[ \frac{2q^2 + m_\ell^2}{M_{\Lambda_b}^2} \right. \\ &\left. \left. + \left( 1 - \frac{M_{\Lambda_c^*}^2}{M_{\Lambda_b}^2} \right) \left( 1 + \frac{2m_\ell^2}{q^2} \right) \right] \right\} + \mathcal{O}(1/m_b), \end{aligned} \quad (6.25)$$

with  $J^P = 1/2^-, 3/2^-$ ,  $C_J = (2J + 1)$  and

$$\alpha_{J=1/2}^2(\omega) = \Delta_2^2(\omega) + (\omega^2 - 1)\Delta_1^2(\omega), \quad \alpha_1(\omega)\alpha_2(\omega)|_{J=1/2} = \Delta_1(\omega)\Delta_2(\omega) \quad (6.26)$$

$$\alpha_{J=3/2}^2(\omega) = \Omega_1^2(\omega) + (\omega^2 - 1)\Omega_2^2(\omega), \quad \alpha_1(\omega)\alpha_2(\omega)|_{J=3/2} = \Omega_1(\omega)\Omega_2(\omega) \quad (6.27)$$

At order  $\mathcal{O}(\Lambda_{\text{QCD}}/m_Q)$ , there are corrections originating from the matching of the  $b \rightarrow c$  flavor changing current onto the heavy quark effective theory and from order

<sup>15</sup>Note that for the  $1/2^-$  member of the  $j_q^P = 1^-$  multiplet, we have  $v_\lambda [(\gamma^\lambda + v'^\lambda)\gamma_5 u_c^{1/2}(v')]^\dagger \gamma^0 = \bar{u}_c^{1/2}(v')(\not{v} - \omega)\gamma_5$  and  $\gamma_5\gamma^\mu(1 - \gamma_5) = \gamma^\mu(1 - \gamma_5)$ .

$\Lambda_{\text{QCD}}/m_Q$  corrections to the effective Lagrangian [72, 316, 317, 357, 358]. Following the discussion of Ref. [317], for  $\Lambda_b$  decays, they have a quite different physiognomy depending on the total angular momentum and parity of the *ldof* in the daughter charm excited baryon. In particular,

- $j_q^P = 1^-$ : Neglecting  $1/m_b$  corrections and QCD short-range logarithms [317],

$$\Delta_1(\omega) = \sigma(\omega) + \frac{1}{2m_c} \left( \phi_{\text{kin}}^{(c)}(\omega) - 2\phi_{\text{mag}}^{(c)}(\omega) \right), \quad \Delta_2(\omega) = \frac{1}{2m_c} \left( 3(\omega\bar{\Lambda}' - \bar{\Lambda})\sigma(\omega) + 2(1 - \omega^2)\sigma_1(\omega) \right) \quad (6.28)$$

$$\Omega_1(\omega) = \sigma(\omega) + \frac{1}{2m_c} \left( \phi_{\text{kin}}^{(c)}(\omega) + \phi_{\text{mag}}^{(c)}(\omega) \right), \quad \Omega_2(\omega) = \frac{\sigma_1(\omega)}{2m_c} \quad (6.29)$$

with  $m_c \sim 1.4$  GeV, the charm quark mass, and  $\bar{\Lambda} \sim 0.8$  GeV [ $\bar{\Lambda}' \sim (1 \pm 0.1)$  GeV] the energy of the *ldof* in the  $m_Q \rightarrow \infty$  limit in the  $\Lambda_b$  [ $\Lambda_c^*$  ( $j_q^P = 1^-$ )] baryon. The  $\sigma_1(\omega)$  form-factor determines, together with  $\bar{\Lambda}$  and  $\bar{\Lambda}'$ , the  $1/m_c$  corrections stemming from the matching of the QCD and effective theory currents. This sub-leading IW function is unknown and in Ref. [317], it was varied in the range  $\pm 1.2[1 - 1.6(\omega - 1)]$  GeV. In addition,  $\phi_{\text{kin}}^{(c)}$  and  $\phi_{\text{mag}}^{(c)}$  account for the time ordered product of the dimension-five kinetic energy and chromomagnetic operators in the effective Lagrangian. The chromomagnetic term is neglected in [317], because it is argued that it should be small relative to  $\Lambda_{\text{QCD}}$ . In addition, the kinetic energy correction is estimated in the large  $N_c$  limit,  $\phi_{\text{kin}}^{(c)} = -\frac{\bar{\Lambda}}{8} \sqrt{\frac{\bar{\Lambda}^3}{\kappa}} (\omega^2 - 1) \sigma(\omega)$ , with  $\kappa = (0.411 \text{ GeV})^3$  [317].

The Eqs. (6.28) and (6.29) can be re-derived from

$$\begin{aligned} \langle \Lambda_c^{*1/2^-, 3/2^-}; j_q^P = 1^- | J_{bc}^\mu(0) | \Lambda_b \rangle &= \mathcal{U}_c^\lambda(v') \{ v_\lambda [\beta_1 + (\omega - \psi)\beta_2] \\ &+ \gamma_\lambda \beta_3 / 3 \} \gamma^\mu (1 - \gamma_5) u_b(v) + \mathcal{O}(1/m_b), \end{aligned} \quad (6.30)$$

where the  $\mathcal{O}(1/m_c)$   $\beta_2$  and  $\beta_3$  form-factors and the sub-leading term of  $\beta_1$  depend on  $J$ . Thus, we have

$$\begin{aligned} \beta_1(\omega)|_J &= \sigma(\omega) + \frac{1}{2m_c} \left( \phi_{\text{kin}}^{(c)}(\omega) + c_J \phi_{\text{mag}}^{(c)}(\omega) \right) \\ \beta_2(\omega)|_J &= \frac{c_J}{2m_c} \sigma_1(\omega), \quad \beta_3(\omega) = 3 \frac{(\omega\bar{\Lambda}' - \bar{\Lambda})}{2m_c} \sigma(\omega) \end{aligned} \quad (6.31)$$

with  $c_{J=1/2} = -2$  and  $c_{J=3/2} = 1$ , which correspond to the eigenvalues of the operator  $2\vec{S}_c \cdot \vec{J}_q$

$$c_J = J(J+1) - \frac{1}{2} \left( \frac{1}{2} + 1 \right) - 1(1+1), \quad (6.32)$$

for  $j_q = 1$  and  $S_c = 1/2$ , and

$$\Omega_1 = \beta_1(\omega)|_{J=3/2}, \quad \Delta_1 = \beta_1(\omega)|_{J=1/2}, \quad \Omega_2 = \beta_2(\omega)|_{J=3/2}, \quad \Delta_2 = \beta_3(\omega) + \beta_2(\omega)|_{J=1/2}. \quad (6.33)$$

The  $1/m_b$  contributions, not taken into account, are much smaller than the theoretical uncertainties induced by the errors on  $(\bar{\Lambda} - \bar{\Lambda}')$  and the  $\sigma_1(\omega)$  form-factor. Hence, the form-factors of Eqs. (6.28) and (6.29) provide an excellent approximation to the results reported in Ref. [317].

Two final remarks to conclude this discussion: i) The  $(\omega\bar{\Lambda}' - \bar{\Lambda})$  difference in  $\Delta_2$  [ $\gamma_\lambda$  form-factor in Eq. (6.30)] provides a  $s$ -wave  $W^- \Lambda_c^*(1/2^-)$  term that should scale as  $\sqrt{\omega^2 - 1}$ , and hence should dominate this differential rate at zero recoil. ii) The kinetic operator correction is the only  $1/m_c$  term that does not break HQSS.

- $j_q^P = 0^-$ : For the case of this unnatural transition, the matrix elements of the  $1/m_Q$  current and kinetic energy operator corrections are zero for the same reason that the leading form factor vanished [317]. The time ordered products involving the chromomagnetic operator lead to non-zero contributions, which however vanish at zero recoil [317] and can be cast in a  $\Delta_1$ -type form factor. At order  $1/m_Q$  the corresponding  $\Delta_2$  form-factor is zero.

From the above results, we conclude that the  $\Lambda_b$  semileptonic decay to a  $J^P = 1/2^-$ -daughter charm excited baryon with a  $j_q^P = 0^-$   $ldof$ -configuration can be visible only if HQSS is severely broken and higher  $(1/m_Q)^n$  corrections are sizable.

## 6.9 Decays to molecular $\Lambda_c^{\text{MOL}}$ states

Following the spectator image of Fig. 6.1, the  $c$  quark created in the weak transition must carry negative parity and hence must be in a relative  $p$ -wave. The parity and total angular momentum of the final resonance are those of the intermediate system before hadronization. Since the molecular  $\Lambda_c^{\text{MOL}}$  states come from meson-baryon interaction in our picture, we must hadronize the final state including a  $u\bar{u} + d\bar{d} + s\bar{s}$  state as in the upper panel of Fig. 6.1. The  $c$  quark must be involved in the hadronization, because it is originally in an  $L = 1$  state, but after the hadronization produces the  $D^{(*)}N$  state, and the  $c$  quark in the  $D^{(*)}$  meson is in an  $L = 0$  state. Neglecting hidden-strange contributions, the hadronization results in isoscalar  $s$ -wave  $DN$  and  $D^*N$  pairs, but does not produce  $\pi\Sigma_c^{(*)}$  states [224, 321].

The production of  $J^P = 1/2^-, 3/2^-$  resonances ( $R_J$ ) is done after the created  $DN$  and  $D^*N$  in the first step couple into the resonance, as shown in the upper panel of

Fig. 6.1. The transition matrix,  $t_{R_J}$ , for such mechanism leads to

$$\overline{\sum} \sum |t_{R_J}|^2 = \sum_M \mathcal{C}(\frac{1}{2}1J|M0M)^2 |\varphi(\omega)|^2 \left| C_J^{DN} g_{R_J}^{DN} G_{DN} + C_J^{D^*N} g_{R_J}^{D^*N} G_{D^*N} \right|^2, \quad (6.34)$$

where the sums are over the spins of the initial and final particles, and the bar over the sum denotes the average over initial spins. The Clebsch-Gordan coefficient accounts for the coupling of spin and orbital angular momentum of the  $c$ -quark to the total angular momentum  $J$  of the intermediate system, composed by the charm quark and the spectator isoscalar  $0^+ ud$  diquark (see Fig. 6.1). Because angular momentum conservation, the spin of the resonance, produced after hadronization and meson-baryon re-scattering, will be  $J$  as well. The important point is that the third component of the orbital angular momentum of the  $c$ -quark must be zero [148, 149] (see also the discussion at the beginning of Subsec. 6.7). Let us note for future purposes that  $\mathcal{C}(\frac{1}{2}1\frac{3}{2}|M0M)^2 / \mathcal{C}(\frac{1}{2}1\frac{1}{2}|M0M)^2 = 2$ ,  $M = \pm 1/2$ .

The function  $\varphi(\omega)$  accounts for some  $\omega$  dependences induced by the hadronization process and by the matrix element between the initial  $s$ -wave  $b$ -quark, the outgoing  $W$ -plane wave and the  $p$ -wave  $c$ -quark created in the intermediate hadronic state. This latter factor should scale like  $|\vec{q}| \propto \sqrt{\omega^2 - 1}$  close to zero recoil [224, 321]. In the heavy quark limit assumed in the mechanism depicted in Fig. 6.1, one expects  $\varphi(\omega)$  to be independent of the angular momentum,  $J$ , of the final resonance.

The  $C_J^{D^{(*)}N}$  coefficients account for different overlaps between  $DN$  and  $D^*N$   $s$ -wave pairs and the intermediate hadronic state, whose wave-function is determined by a excitation among the heavy quark and the brown muck (*ldof*) as a whole. This is a  $\lambda$ -excited state in the framework of CQM's, and it has  $j_q^P = 1^-$  quantum-numbers for the brown muck. The values of  $C_J^{D^{(*)}N}$  can be readily obtained from Eq. (6.5),

$$C_J^{D^{(*)}N} = \langle D^{(*)}N; J | S_Q^P = 1/2^+ j_q^P = 1^-; J \rangle_2 \quad (6.35)$$

Finally,  $G_{D^{(*)}N}$  is the loop function for the  $D^{(*)}N$  propagation<sup>16</sup> and  $g_{R_J}^{D^{(*)}N}$  is the dimensionless coupling of the resonance  $R_J$  to the  $D^{(*)}N$  channel in isospin zero. They are defined for instance in Eqs. (15) and (18) of Ref. [172], and we compute them at the resonance position in the complex plane. Note that the couplings  $g_{R_J}^{D^{(*)}N}$ , obtained from the residues of the coupled-channels meson-baryon  $T$ -matrix, contain effects from intermediate  $\pi\Sigma_c^{(*)}$  loops.

<sup>16</sup>We are assuming that  $G_{D^{(*)}N}$  is the same both for  $J = 1/2$  and  $J = 3/2$ . This is correct as long as the renormalization of the UV divergences of this loop function does not depend on the angular momentum, as in the  $SU(6)_{\text{lsf}} \times SU(2)_{\text{HQSS}}$  and ELHG models of Refs. [86, 172] and [85], respectively.

With all these ingredients close to zero recoil, we find

$$\frac{d\Gamma/d\omega[\Lambda_b \rightarrow \Lambda_c^*(1/2^-)]}{d\Gamma/d\omega[\Lambda_b \rightarrow \Lambda_c^*(3/2^-)]}\Big|_{\text{MOL}} = \frac{1}{2} \frac{\left| \frac{\sqrt{3}}{2} g_{R_{J=1/2}}^{DN} G_{DN} + \frac{1}{2} g_{R_{J=1/2}}^{D^*N} G_{D^*N} \right|^2}{\left| g_{R_{J=3/2}}^{D^*N} G_{D^*N} \right|^2} \quad (6.36)$$

where the factor 1/2 comes from the ratio of Clebsch-Gordan coefficients. In this way, we recover the main result of Ref. [321]. It shows that the above ratio of differential decay widths is very sensitive to the couplings of the  $\Lambda_c^*$  resonances to the  $DN$  and  $D^*N$  channels. We could expect Eq. (6.36) to hold also in good approximation for the ratio of integrated rates since the available phase space is quite small

In the infinite heavy quark mass limit, the degeneracy of the  $D$  and  $D^*$  masses implies  $G_{DN} = G_{D^*N}$ . In addition for  $1^-$  and  $0^-$   $ldof$  quantum numbers, the couplings of  $DN$  and  $D^*N$  to  $\Lambda_c^*$  are related

$$j_q^P = 1^- \Rightarrow \frac{2}{\sqrt{3}} g_{\Lambda_c^*(1/2^-)}^{DN} = 2g_{\Lambda_c^*(1/2^-)}^{D^*N} = g_{\Lambda_c^*(3/2^-)}^{D^*N} \quad (6.37)$$

$$j_q^P = 0^- \Rightarrow \sqrt{3} g_{\Lambda_c^*(1/2^-)}^{DN} = -g_{\Lambda_c^*(1/2^-)}^{D^*N}, \quad (6.38)$$

as inferred from Eq. (6.5). Hence, we re-obtain the  $m_Q \rightarrow \infty$  results of Subsec. 6.7,

$$\frac{d\Gamma/d\omega[\Lambda_b \rightarrow \Lambda_c^*(1/2^-)]_{j_q^p=1^-}}{d\Gamma/d\omega[\Lambda_b \rightarrow \Lambda_c^*(3/2^-)]_{j_q^p=1^-}} = \frac{1}{2}, \quad \frac{d\Gamma/d\omega[\Lambda_b \rightarrow \Lambda_c^*(1/2^-)]_{j_q^p=0^-}}{d\Gamma/d\omega[\Lambda_b \rightarrow \Lambda_c^*(3/2^-)]_{j_q^p=1^-}} = 0 \quad (6.39)$$

For molecular states, we might have deviations from the above IW limit predictions, and in particular visible widths for a charm  $J^P = 1/2^-$  excited baryon with significant  $0^-$   $ldof$  components. This could happen if the meson-baryon interactions, which generate the molecular state, induce important  $(1/m_Q)^n$  corrections, bigger than would be expected from the discussion in Subsec. 6.8.

## 6.10 $\Lambda_b \rightarrow \Lambda_c^* \pi^-$ decay

Looking again at the diagram depicted in the lower panel of Fig. 6.1, the  $\Lambda_b \rightarrow \Lambda_c^* \pi^-$  decay could proceed through the mechanism of external emission [305], where the gauge  $W^-$  boson couples to  $\pi^-$  instead of to the  $(\ell^- \bar{\nu}_\ell)$  lepton pair. This is the factorization approximation, which should be accurate for processes that involve a heavy hadron and multiple light mesons in the final state, provided the light mesons are all highly collinear and energetic [359]. Actually for  $\Lambda_b \rightarrow \Lambda_c^* \pi^-$  decay, corrections are expected to be of the order  $\Lambda_{\text{QCD}}/E_\pi$ , with  $E_\pi$  the energy of the pion in the center of mass frame. There exist also some small strong coupling logarithmic corrections stemming from the matching of full QCD with the effective heavy quark theory.



The  $\Lambda_b \rightarrow \Lambda_c^* \pi^-$  width is related to the differential decay rate  $d\Gamma_{\text{sl}}/d\omega$  at  $q^2 = m_\pi^2$  [ $\omega = (M_{\Lambda_b}^2 + M_{\Lambda_c^*}^2 - m_\pi^2)/2M_{\Lambda_b}M_{\Lambda_c^*}$ ] for the analogous semileptonic decay [317],

$$\Gamma_\pi[\Lambda_b \rightarrow \Lambda_c^* \pi^-] \propto |V_{ud}|^2 f_\pi^2 \left. \frac{d\Gamma_{\text{sl}}[\Lambda_b \rightarrow \Lambda_c^* e^- \bar{\nu}_e]}{d\omega} \right|_{q^2=m_\pi^2} \quad (6.40)$$

with  $m_\pi$  and  $f_\pi$ , the pion mass and decay constant, respectively. In the case of decays into  $\Lambda_c^*$  molecular states, we find again that the ratio of  $gG$  factors of Eq. (6.36) provides an estimate for  $\left. \frac{\Gamma_\pi[\Lambda_b \rightarrow \Lambda_c^*(1/2^-)]}{\Gamma_\pi[\Lambda_b \rightarrow \Lambda_c^*(3/2^-)]} \right|_{\text{MOL}}$ . However, the kinematics now is significantly different to that of zero recoil. In the  $M_{\Lambda_b}$  rest frame, the recoil three momentum is of the order of 2.2 GeV, even larger than the charm quark mass. Hence, the approximation of neglecting the effects of operators like  $\vec{S}_c \cdot \vec{j}_q$  in the weak transition becomes inappropriate, since factors proportional to  $|\vec{q}|/m_c$  can be large in this kinematics [ $(\omega^2 - 1) \sim 0.7$ ]. This type of operators couples the charm quark spin and the angular momentum of the  $ldof$  and induces dependences on  $J$ , the total angular momentum of the created hadron. In this situation, it can not be guaranteed that the function  $\varphi(\omega)$ , introduced in Eq. (6.34), is independent of  $J$ . In fact, in Ref. [224] and in addition to the quotient of  $gG$  coefficients, a factor  $(\vec{q}^2 + E_\pi^2)/E_\pi^2 \sim 2$  was found that increased the value of the  $\left. \frac{\Gamma_\pi[\Lambda_b \rightarrow \Lambda_c^*(1/2^-)]}{\Gamma_\pi[\Lambda_b \rightarrow \Lambda_c^*(3/2^-)]} \right|_{\text{MOL}}$  ratio. We will also use here this result, with some precautions, and we will multiply by a factor of 2 the estimates for the latter ratio deduced from the  $gG$  factors.

## 6.11 Results

### 6.12 Semileptonic ( $\mu^- \bar{\nu}_\mu$ or $e^- \bar{\nu}_e$ ) and pion $\Lambda_b \rightarrow \Lambda_c^*$ decays

In Table 6.2, we show results for the ratios of semileptonic ( $\mu^- \bar{\nu}_\mu$  or  $e^- \bar{\nu}_e$ ) and pion  $\Lambda_b$  decays into odd parity  $J = 1/2$  and  $3/2$  charm baryons, obtained within the molecular schemes of Refs. [86, 172] ( $\text{SU}(6)_{\text{lsf}} \times \text{SU}(2)_{\text{HQSS}}$ ) and [85] (ELHG). As commented in Subsec. 6.4, a double pole structure for the  $\Lambda_c(2595)$  is found in these approaches, with clear similarities to the situation for the  $\Lambda(1405)$ , and hence we give results for both, the narrow ( $n$ ) and ( $b$ ) broad  $\Lambda_c^{\text{MOL}}(2595)$  states. In Table 6.2, we also show experimental estimates for these ratios deduced from branching fractions given in the RPP [21]. We have considered that the reconstructed  $\Lambda_c(2595)$  resonance observed in the decays corresponds to the molecular narrow resonance. In addition,  $m_Q \rightarrow \infty$  limit results ( $\text{IW}_\infty$ ) and predictions obtained incorporating the subleading corrections ( $\text{IW}_{\mathcal{O}(1/m_Q)}$ ) discussed in Ref. [317] are also shown in Table 6.2. In this latter work, it is assumed that the  $\Lambda_c(2595)$  and  $\Lambda_c(2625)$  form the lowest-lying  $j_q^P = 1^-$

	$\text{IW}_\infty$	$\text{IW}_{\theta(1/m_q)}$	$\text{SU}(6)_{\text{sf}} \times \text{SU}(2)_{\text{HQSS}}$	ELHG	RPP
$\Gamma_{\text{sl}}[\Lambda_b \rightarrow \Lambda_{c^{(n)}}(2595)]/\Gamma_{\text{sl}}[\Lambda_b \rightarrow \Lambda_c(2625)]$	0.5	$1.4^{+1.7}_{-1.0}$	0.14	0.39–0.48	$0.6^{+0.4}_{-0.3}$
$\Gamma_{\text{sl}}[\Lambda_b \rightarrow \Lambda_{c^{(b)}}(2595)]/\Gamma_{\text{sl}}[\Lambda_b \rightarrow \Lambda_c(2625)]$	—	—	0.39	$\sim 0.02$	—
$\Gamma_\pi[\Lambda_b \rightarrow \Lambda_{c^{(n)}}(2595)]/\Gamma_\pi[\Lambda_b \rightarrow \Lambda_c(2625)]$	0.5	$1.4^{+3.3}_{-1.1}$	0.14–0.28	0.76–0.91	$1.0 \pm 0.6$
$\Gamma_\pi[\Lambda_b \rightarrow \Lambda_{c^{(b)}}(2595)]/\Gamma_\pi[\Lambda_b \rightarrow \Lambda_c(2625)]$	—	—	0.39–0.78	$\sim 0.02$	—

Table 6.2: Ratios of semileptonic ( $\mu^- \bar{\nu}_\mu$  or  $e^- \bar{\nu}_e$ ) and pion  $\Lambda_b$  decays into odd parity  $J = 1/2$  and  $3/2$  charm baryons. We show predictions obtained from the molecular schemes of Refs. [86, 172] ( $\text{SU}(6)_{\text{sf}} \times \text{SU}(2)_{\text{HQSS}}$ ) and [85] (ELHG), together with the  $m_q \rightarrow \infty$  limit ( $\text{IW}_\infty$ ) ratios, and those found including the subleading corrections [ $\text{IW}_{\theta(1/m_q)}$ ] derived in Ref. [317] for the case of a  $j_q^P = 1^-$  HQSS doublet. The ELHG results for the narrow  $\Lambda_c(2595)$  are taken from Refs. [224, 321]. In the case of molecular approaches, the  $gG$  factors that enter in Eq. (6.36) are compiled in Table 6.3. The ranges quoted for the  $\text{SU}(6)_{\text{sf}} \times \text{SU}(2)_{\text{HQSS}}$  pion-mode ratios account for the factor of two introduced at the end of Sec. 6.10, suggested by the findings of Ref. [224]. We also show in the last column experimental estimates for these ratios obtained from branching fractions given in the RPP [21]. See the text for more details.

	$\text{SU}(6)_{\text{sf}} \times \text{SU}(2)_{\text{HQSS}}$		ELHG	
	$g_{R_J}^{DN} G_{DN}$	$g_{R_J}^{D^*N} G_{D^*N}$	$g_{R_J}^{DN} G_{DN}$	$g_{R_J}^{D^*N} G_{D^*N}$
$\Lambda_{c^{(n)}}^{\text{MOL}}(2595)$	$-10.54 + 0.02 i$	$11.65 - 0.42 i$	$13.88 - 1.06 i$	$26.51 + 2.10 i$
$\Lambda_{c^{(b)}}^{\text{MOL}}(2595)$	$3.16 - 3.45 i$	$4.14 + 0.17 i$	$-0.68 + 3.13 i$	$-4.66 + 3.42 i$
$\Lambda_c^{\text{MOL}}(2625)$	—	$-5.82 + 2.58 i$	—	29.10

Table 6.3: Values (MeV) of the factors  $g_{R_J}^{D^{(*)N}} G_{D^{(*)N}}$  from Refs. [172] ( $\text{SU}(6)_{\text{sf}} \times \text{SU}(2)_{\text{HQSS}}$ ) and [85] (ELHG). The signs of  $g_{R_J}^{D^*N} G_{D^*N}$  are changed with respect to Ref. [85], as discussed in [224]. The values quoted for the  $\text{SU}(6)_{\text{sf}} \times \text{SU}(2)_{\text{HQSS}}$   $g_{R_J}^{D^*N} G_{D^*N}$  take into account the order meson-baryon used in this work to couple the spins (see footnote 8).

HQSS doublet, and the values quoted in the table follow mostly from Eqs. (2.26) and (2.28) of that reference. To the error budget deduced from these equations, we have added in quadrature the effects due to the uncertainty ( $\pm 0.1$  GeV) on the  $\bar{\Lambda}'$  parameter in Eq. (6.28), which produces variations in the ratios of about 25%–30% [317]. The errors on the  $\text{IW}_{\mathcal{O}(1/m_Q)}$  ratios are largely dominated by the uncertainties on the subleading  $\sigma_1$  form-factor. It leads to opposite effects for  $\Lambda_c(2595)$  or  $\Lambda_c(2625)$  final states [317], as can be inferred here from Eqs. (6.31) and (6.32). The biggest (smallest)  $\Gamma_{\text{sl},\pi}^{\Lambda_{1/2}}/\Gamma_{\text{sl},\pi}^{\Lambda_{3/2}}$  values correspond to  $\sigma_1(1) = -1.2$  ( $+1.2$ ) GeV, while the central values are obtained for  $\sigma_1(\omega) = 0$ . The  $\Gamma_{\text{sl}}^{\Lambda_{1/2}}$  rate, depending on  $\sigma_1$ , could be significantly enhanced (around a factor 2.5 for  $\sigma_1 = 0$ ) compared to the infinite mass prediction ( $\sim 0.020\Gamma_0$ ), while  $1/m_Q$  effects are much smaller for  $\Gamma_{\text{sl}}^{\Lambda_{3/2}}$ . Predictions for the pion decay widths depend on  $d\Gamma_{\text{sl}}/d\omega$  at  $q^2 = m_\pi^2$ , and turn out to be quite uncertain due to  $\sigma_1$ . We see that  $\text{IW}_{\mathcal{O}(1/m_Q)}$  predictions and experimental estimates for the  $\Gamma^{\Lambda_{1/2}}/\Gamma^{\Lambda_{3/2}}$  ratios agree, within errors, for both semileptonic and pion  $\Lambda_b$  decay modes. A certain tendency is observed in the central values, for which the theoretical estimations are greater than the experimental ones, in particular in the semileptonic mode. However, it would not be really significant due to the great uncertainties.

Concerning the ELHG ratios for the narrow molecular  $\Lambda_c(2595)$  state, we give in Table 6.2 the ranges quoted in the original works of Refs. [224, 321]. The lowest ratios can be found using the  $gG$  coefficients compiled in Table 6.3, while the highest values account for corrections due to the contribution of hidden-strange ( $D_s^{(*)}\Lambda$ ) channels in the hadronization. Within the ELHG scheme the broad  $\Lambda_c(2595)$  ratios are negligible. This is because in this approach, the  $J^P = 3/2^-$   $\Lambda_c(2625)$  is a quasi-bound  $D^*N$  state with a large coupling to this channel, whose absolute value is around five times bigger than that of the broad  $\Lambda_c(2595)$  resonance to  $D^*N$  or  $DN$  [224]. The narrow ELHG  $\Lambda_c(2595)$  molecule has  $DN$  and  $D^*N$  couplings (in absolute value) similar to  $g_{\Lambda_c(2625)}^{D^*N}$ , and its  $\Gamma_{\text{sl},\pi}^{\Lambda_{1/2}}/\Gamma_{\text{sl},\pi}^{\Lambda_{3/2}}$  ratios are larger and about 0.4 and 0.8, respectively, compatible within errors with the experimental expectations. It should be also noted that after renormalization, the  $DN$  loop function is almost a factor of two smaller than the  $D^*N$  one, which produces a significant source of HQSS breaking in the ELHG approach of Ref. [224].

Finally, we see that the  $\text{SU}(6)_{\text{lsf}} \times \text{SU}(2)_{\text{HQSS}}$  ratios for the narrow molecular  $\Lambda_c(2595)$  resonance, though small (0.14 – 0.28), are neither negligible, nor totally discarded by the available data. As we expected, they are suppressed because within this approach this state has a large  $j_q^P = 0^-$   $ldof$  component. Semileptonic decays into the broad  $\Lambda_c(2595)$  resonance are about a factor of three larger, but the  $\Gamma_{\text{sl},\pi}^{1/2(b)}/\Gamma_{\text{sl},\pi}^{3/2}$  ratios are still below 1/2, the  $m_Q \rightarrow \infty$  prediction, and well below the  $\text{IW}_{\mathcal{O}(1/m_Q)}$  central values obtained in [317] (see Fig. 6.2). Both sets of results point to important  $(1/m_Q)^n$  corrections, induced by the meson-baryon interactions that generate the

molecular states. On the other hand, we do not expect large variations from the consideration of hidden strange channels as intermediate states. From the couplings reported in Refs. [86, 172], only  $\Lambda D_s$  and  $\Lambda D_s^*$  might be important through their coupling to the narrow  $\Lambda_c(2595)$  state, but the respective thresholds are located (around 3.1 and 3.2 GeV) well above the resonance position, and it is not reasonable to claim for large effects produced by these high energy physics contributions. Actually, we have checked that the ratios given in Table 6.2 for the  $SU(6)_{\text{lsf}} \times SU(2)_{\text{HQSS}}$  model hardly change if the large number of coupled-channels used in Refs. [86, 172] is reduced only to  $D^{(*)}N$  and  $\pi\Sigma_c^{(*)}$ .

The predictions for the ratios in molecular schemes are very sensitive to the interference and relative weights of the  $DN$  and  $D^*N$  contributions [224, 321], and thus future accurate measurements of these ratios will shed light on the nature of the  $\Lambda_c(2595)$ , allowing us to address issues as the existence of two poles or the importance of the  $D^*N$  channel in the formation of the resonance(s). Such studies will also help to understand the interplay between CQM and hadron-scattering degrees of freedom [22, 165, 360–363] in the dynamics of the  $\Lambda_c(2595)$  and  $\Lambda_c(2625)$ .

Note that in other molecular schemes, like the  $SU(4)$  flavor  $t$ -channel exchange of vector mesons of Refs. [170, 338, 339] or those based on the chiral isoscalar  $\pi\Sigma_c^{(*)}$  interactions [171, 336, 340], where the  $D^*N$  channel is not included, the  $\Gamma_{\text{sl}}[\Lambda_b \rightarrow \Lambda_c(2625)]$  and  $\Gamma_{\pi}[\Lambda_b \rightarrow \Lambda_c(2625)]$  widths will be zero or highly suppressed. This is because the  $\pi\Sigma_c^*$  pair, that dynamically generates the  $\Lambda_c(2625)$  resonance in these models, can be only produced by going beyond the spectator approximation implicit in the mechanism of Fig. 6.1. This places an additional limitation on the validity of these approaches, which already have some problems to describe the mass and width of the  $\Lambda_c(2625)$  (see the related discussion in Subsecs. 6.4.3 and 6.4.4).

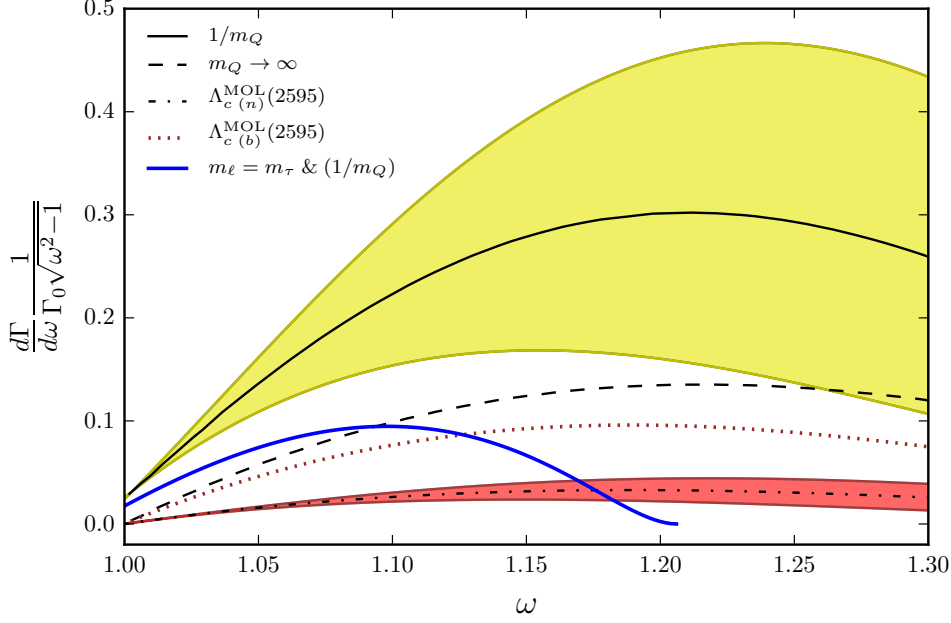


Figure 6.2: Differential  $\Lambda_b \rightarrow \Lambda_c^*(1/2^-)\tau\bar{\nu}_\tau$  (solid blue line) and  $\Lambda_b \rightarrow \Lambda_c^*(1/2^-)e\bar{\nu}_e$  rates calculated using different approaches. The black dashed and solid lines, together with the error bands of the latter, are taken from Fig.1a of Ref. [317], where the final baryon is treated as the  $J^P = 1/2^-$  member of the lowest-lying  $j_q^P = 1^-$  HQSS doublet. The dashed line shows the  $m_Q \rightarrow \infty$  prediction, Eqs. (6.21) and (6.22), while the solid line include  $1/m_Q$  effects for  $\sigma_1(\omega) = 0$ . The bands account for the changes in the differential decay rate when  $\sigma_1(1)$  is varied in the range  $[-1.2, 1.2]$  GeV. The spectrum of the  $\tau$ -mode, which ends around  $\omega \sim 1.2$ , is calculated using Eq. (6.25) with  $\Delta_{1,2}$  given in Eq. (6.28), and taking  $\sigma_1(\omega) = 0$ . (Further details on the  $\mathcal{O}(1/m_c)$  corrections for  $\tau$ -decays can be found in Table 6.4). On the other hand, the lowest dotted and dashed-dotted curves, together with the error bands of the latter, stand for the decay into the broad  $[\Lambda_{c(b)}^{\text{MOL}}(2595)]$  and narrow  $[\Lambda_{c(n)}^{\text{MOL}}(2595)]$  molecular resonances found in the  $\text{SU}(6)_{\text{lsf}} \times \text{SU}(2)_{\text{HQSS}}$  model of Refs. [86, 172]. These differential rates have been obtained multiplying the corresponding molecular  $gG$  ratios given in Table 6.2 by the  $\mathcal{O}(1/m_Q)$  improved  $\Lambda_b \rightarrow \Lambda_c^*(3/2^- [j_q^P = 1^-])e\bar{\nu}_e$  distribution displayed in Fig.1b of Ref. [317]. Central values have been evaluated using the black solid line of this latter figure. The bands, depicted for the decay into the narrow  $\Lambda_c(2595)$  molecular state, show the impact in the spectrum of the uncertainties on the  $\mathcal{O}(1/m_Q)$  corrections, and have been calculated using the shaded region shown in Fig.1b of Ref. [317].

### 6.13 $\Lambda_b \rightarrow \Lambda_c(2595)\tau \bar{\nu}_\tau$ and $\Lambda_b \rightarrow \Lambda_c(2625)\tau \bar{\nu}_\tau$ decays

Let us now pay attention to  $\Lambda_b$  semileptonic decays with a  $\tau$  lepton in the final state. At the LHC, a large number of ground-state  $\Lambda_b$  baryons are produced [364], and its decays into charmed baryons can be used to constrain violations of LFU. These decays are of interest in light of the  $R(D^{(*)})$  puzzle in the semileptonic  $\bar{B} \rightarrow D^{(*)}\tau \bar{\nu}_\tau$  decays (see for instance the discussion in [17], and references therein). Decays involving the ground state charmed baryon,  $\Lambda_c$ , have been already studied in lattice QCD [365] and beyond the Standard Model [366]. On the other hand, the LHCb collaboration has reported large samples of  $\Lambda_c(2595)$  and  $\Lambda_c(2625)$  baryons in  $\Lambda_b$  semileptonic decays [367], which makes meaningful to investigate the LFU ratios [319, 320]

$$R[\Lambda_c^*] = \frac{\mathcal{B}(\Lambda_b \rightarrow \Lambda_c^* \tau \bar{\nu}_\tau)}{\mathcal{B}(\Lambda_b \rightarrow \Lambda_c^* \mu \bar{\nu}_\mu)} \quad (6.41)$$

with  $\Lambda_c^* = \Lambda_c(2595)$  or  $\Lambda_c(2625)$ , due to the good prospects that LHCb can measure them in the short term. Results are shown in Table 6.4.

We have used Eq. (6.25) to compute  $\Gamma[\Lambda_b \rightarrow \Lambda_c(2595) \tau \bar{\nu}_\tau]$  and  $\Gamma[\Lambda_b \rightarrow \Lambda_c(2625) \tau \bar{\nu}_\tau]$ , assuming that the  $\Lambda_c(2595)$  and  $\Lambda_c(2625)$  form the lowest-lying  $j_q^P = 1^-$  HQSS doublet, and have taken the  $\mathcal{O}(1/m_c)$  improved form factors given in Eq. (6.31). Therefore, spin symmetry in the  $b$ -quark sector is conserved, which implies neglecting terms of order  $\Lambda_{\text{QCD}}/m_b$ . This is an excellent approximation, and we reproduce within a 5% the  $\Lambda_c(2595)$  differential and integrated rates reported in Ref. [317]. The approximation works even better for the  $\Lambda_c(2625)$ , and moreover it leads to simple expressions for the  $\omega$ -differential widths, including full finite-lepton mass contributions that are necessary for testing LFU. Note that the calculations of Ref. [317] were made in the  $m_\ell \rightarrow 0$  limit.

Predictions for semileptonic  $\tau$ -decays are relatively stable against the uncertainties on the  $\mathcal{O}(1/m_c)$  corrections, because in this case  $\omega_{\text{max}} \sim 1.2$ , and the largest contributions to the integrated width come from regions relatively close to zero recoil (see blue solid line of Fig. 6.2). However, there are still some uncertainties associated with the lack of information about the form factor  $\sigma_1(\omega)$ , although they are significantly smaller than those shown in Table 6.2 for the case of massless leptons. The  $\sigma_1$  term produces, also for  $\tau$ -decays, opposite effects for  $\Lambda_c(2595)$  or  $\Lambda_c(2625)$  final states (see Eqs. (6.31) and (6.32)). Uncertainties partially cancel in the  $R[\Lambda_c(2595)]$  and  $R[\Lambda_c(2625)]$  ratios, which are predicted in Table 6.4 with moderate errors. We expect these ratios to be comprised in the intervals [0.10, 0.15] and [0.10, 0.13], respectively. These estimates compare rather well with those obtained in the covariant confined quark model employed in Ref. [320].

Next we discuss the  $\Gamma_{\text{sl};\tau}^{1/2}/\Gamma_{\text{sl};\tau}^{3/2}$  ratio, for which theoretical errors are larger. The central value of this ratio compares rather well with that quoted in Table 6.2 for light

leptons ( $\mu$  or  $e$ ), though its errors for the  $\tau$  mode are slightly smaller.

The  $\Gamma_{sl;\tau}^{1/2}/\Gamma_{sl;\tau}^{3/2}$  ratio would drastically change if the final charmed baryons turned out to be predominantly hadronic molecules. In that situation, we would obtain the same values as in Table 6.2 from the  $gG$  factors compiled in Table 6.3. We should point out that because the available phase space is smaller for the  $\tau$  mode, the decay most likely occurs near the zero-recoil point where the approximations that lead to the quotient of  $gG$  factors in Eq. (6.36) are more precise. The predicted ratios would depend on the molecular scheme, and on the member of the double pole structure of the  $\Lambda_c(2595)$  involved in the decay. However, in all cases, we would obtain values below 0.5, at least one-sigma away from the predictions collected in Table 6.4, based on the hypothesis that the  $\Lambda_c(2595)$  and  $\Lambda_c(2595)$  form the lowest-lying  $1^-$  HQSS multiplet of excited charm-baryons. This latter picture also discards the existence of a second  $J^P = 1/2^-$  (broad) resonance in the 2.6 GeV region.

It is not clear how the  $R[\Lambda_c(2595)]$  and  $R[\Lambda_c(2625)]$  ratios would be affected if any of the resonances has a large molecular component, since this will also affect the decay widths into light leptons that appear in the denominators of these ratios. Therefore, one might think that they would not be significantly modified with respect to the values given in Table 6.4, that mostly account for the reduction of phase space. Nevertheless, it is difficult to be more quantitative. However,  $R[\Lambda_c(2595)]$  may be affected by a new source of potentially large systematic errors, if in the  $\tau$  and  $\mu$  or  $e$  modes, the same  $\Lambda_c(2595)$  molecular state is not observed. This confusion would produce large numerical variations that would suggest false violations of LFU.

Finally, in Table 6.5 we collect several predictions [320,368–372] of the LFU ratios for the  $\Lambda_b$  semileptonic decay into the ground-state  $\Lambda_c$  ( $1/2^+$ ).

Comparing the ratios of Tables 6.4 and 6.5, we see that  $R[\Lambda_c]$  is predicted to be significantly larger than  $R[\Lambda_c^*]$ . (Note, however, that the result of Ref. [372] is considerably smaller than those given by the other authors.)

## 6.14 Conclusions

In this chapter, we have studied the  $\Lambda_b \rightarrow \Lambda_c^* \ell \bar{\nu}_\ell$  and  $\Lambda_b \rightarrow \Lambda_c^* \pi^-$  [ $\Lambda_c^* = \Lambda_c(2595)$  and  $\Lambda_c(2625)$ ] decays, paying special attention to the implications that can be derived from HQSS. We have critically reviewed different molecular descriptions of these charm excited baryons, and have discussed in detail the main features of those schemes that predict a two-pole pattern for the  $\Lambda_c(2595)$ , in analogy to the case of the similar  $\Lambda(1405)$  resonance in the strange sector.

We have calculated the ratios  $\Gamma(\Lambda_b \rightarrow \Lambda_c(2595)\pi^-)/\Gamma(\Lambda_b \rightarrow \Lambda_c(2625)\pi^-)$  and  $\Gamma(\Lambda_b \rightarrow \Lambda_c(2595)\ell\bar{\nu}_\ell)/\Gamma(\Lambda_b \rightarrow \Lambda_c(2625)\ell\bar{\nu}_\ell)$ , and have shown that molecular schemes are very sensitive to the interference and relative weights of the  $DN$  and  $D^*N$  contri-

butions, as firstly pointed out in Refs. [224, 321]. Actually, we have re-derived some of the results of these latter works using a manifest Lorentz and HQSS invariant formalism. In this context, we have argued that future accurate measurements of the above ratios will shed light on the nature of the  $\Lambda_c(2595)$ , allowing us to address issues as the existence of two poles or the importance of the  $D^*N$  channel in the formation of the resonance(s).

We have also investigated the LFU ratios  $R[\Lambda_c^*] = \mathcal{B}(\Lambda_b \rightarrow \Lambda_c^* \tau \bar{\nu}_\tau) / \mathcal{B}(\Lambda_b \rightarrow \Lambda_c^* \mu \bar{\nu}_\mu)$ . We have computed  $\Gamma[\Lambda_b \rightarrow \Lambda_c(2595) \tau \bar{\nu}_\tau]$  and  $\Gamma[\Lambda_b \rightarrow \Lambda_c(2625) \tau \bar{\nu}_\tau]$  assuming that the  $\Lambda_c(2595)$  and  $\Lambda_c(2625)$  form the lowest-lying  $j_q^P = 1^-$  HQSS doublet, and have taken  $\mathcal{O}(1/m_c)$  improved form factors [317]. We have used a scheme that preserves spin-symmetry in the  $b$ -quark sector, which implies neglecting corrections of order  $\Lambda_{\text{QCD}}/m_b$ . This is an excellent approximation that leads to simple expressions for the  $\omega$ -differential widths, including full finite-lepton mass contributions that are necessary for testing LFU. Finally, we have pointed out that the  $R[\Lambda_c(2595)]$  ratio may be affected by a new source of potentially large systematic errors if there are two  $\Lambda_c(2595)$  poles.

At the LHC, a large number  $\Lambda_b$  baryons are produced, and the LHCb collaboration has reported large samples of  $\Lambda_c(2595)$  and  $\Lambda_c(2625)$  baryons in its semileptonic decays. Hence, there are good prospects that LHCb can measure in the near future some of the ratios discussed in this chapter.







# Chapter 7

## The nature of the $\Lambda_c(2595)$ and $\Lambda_c(2625)$ resonances

### 7.1 Introduction

Constituent quark models (CQMs) find a nearly degenerate pair of  $p$ -wave  $\Lambda_c^*$  excited states, with spin-parity  $J^P = 1/2^-$  and  $3/2^-$ , and masses similar to those of the isoscalar odd-parity  $\Lambda_c(2595)$  and  $\Lambda_c(2625)$  resonances [74, 309–312]. Taking into account the two different excitation-modes generally considered (the  $\lambda$ - and  $\rho$ -modes), the  $\Lambda_c^{\text{CQM}}(2595)$  and  $\Lambda_c^{\text{CQM}}(2625)$  resonances should correspond to the members of the HQSS-doublet associated to  $(\ell_\lambda = 1, \ell_\rho = 0)$ , with total spin  $S_q = 0$  for the  $ldof$ . The total spins of these states are the result of coupling the orbital-angular momentum  $\ell_\lambda$  of the  $ldof$ -with respect to the heavy quark- with  $S_Q$ , spin of the heavy quark. Therefore, both  $\Lambda_c^{\text{CQM}}(2595)$  and  $\Lambda_c^{\text{CQM}}(2625)$  states will be connected by a simple rotation of the heavy-quark spin, and these resonances will be degenerate in the  $m_Q \rightarrow \infty$  limit.

Since the total angular momentum and parity of the  $ldof$  in the  $s$ -wave  $\Sigma_c\pi$  and  $\Sigma_c^*\pi$  pairs are  $1^-$ , as in the CQM  $\Lambda_c(2595)$  and  $\Lambda_c(2625)$  resonances, the  $\Lambda_c^{\text{CQM}}(2595, 2625) \rightarrow \pi \Sigma_c^{(*)} \rightarrow \pi \pi \Lambda_c$  decays respect HQSS, and hence one could expect sizable widths for these resonances, unless these transitions are kinematically suppressed. This turns out to be precisely the case [21], and as it is shown in Refs. [314, 315], the use of the actual resonance masses leads to widths for the CQM  $(\ell_\lambda = 1, \ell_\rho = 0)$  states ( $j_q^P = 1^-$ ) predicted in [312] consistent with data.

Within CQM schemes, it is nevertheless unclear why the role played by the  $\Sigma_c^{(*)}\pi$  baryon-meson pairs in the generation of the  $\Lambda_c(2595)$  and  $\Lambda_c(2625)$  resonances can be safely ignored, especially in the  $\Lambda_c(2595)$  case, since it is located very close to the  $\Sigma_c\pi$  threshold (1 MeV below or four MeV above depending on the charged channel). This

observation leads us naturally to consider molecular descriptions of these lowest-lying odd parity charmed baryon states, which should show up as poles in coupled-channel  $T$ -matrices, fulfilling exact unitarity.

As already mentioned in the previous chapter, the first molecular studies [336, 337] of the  $\Lambda_c(2595)$  and  $\Lambda_c(2625)$  were motivated by the appealing similitude of these resonances to the  $\Lambda(1405)$  and  $\Lambda(1520)$  in the strange sector. In particular the two isoscalar  $s$ -wave  $\Lambda(1405)$  and  $\Lambda_c(2595)$  resonances have several features in common. The mass of the former lies in between the  $\Sigma\pi$  and  $N\bar{K}$  thresholds, to which it couples strongly. In turn, the  $\Lambda_c(2595)$  lies below the  $ND$  and just slightly above the  $\Sigma_c\pi$  thresholds, and substituting the  $c$  quark by a  $s$  quark, one might expect the interaction of  $ND$  to play a role in the dynamics of the  $\Lambda_c(2595)$  similar to that played by  $N\bar{K}$  in the strange sector. The first works had some clear limitations. The  $J^P = 1/2^-$  sector was studied in [336], where the amplitudes obtained from the scattering of Goldstone-bosons off  $1/2^+$  heavy-light baryons were unitarized. Despite the interactions being fully consistent with chiral symmetry, neither the  $ND$ , nor the  $ND^*$  channels were considered<sup>1</sup>. The work of Ref. [337] also studied the  $\Lambda_c(2595)$  and there, the interactions were obtained from chirally motivated Lagrangians upon replacing the  $s$  quark by the  $c$  quark. Though in this way, the  $ND$  channel was accounted for, the HQSS counterpart  $ND^*$  was not considered. Subsequent works [170, 171, 338, 339] introduced some improvements, but they failed to provide a scheme fully consistent with HQSS. In all cases, the  $\Lambda_c(2595)$ , or the  $\Lambda_c(2625)$  when studied, could be dynamically generated after a convenient tuning of the low energy constants (LEC) needed to renormalize the ultraviolet (UV) divergences resulting from the baryon-meson loops. As mentioned before, none of these works were consistent with HQSS since none of them considered the  $ND^*$  channel [172]. Heavy pseudoscalar and vector mesons should be treated on equal footing, since they are degenerated in the heavy quark limit, and are connected by a spin-rotation of the heavy quark that leaves unaltered the QCD Hamiltonian in that limit.

The first molecular description of the  $\Lambda_c(2595)$  and  $\Lambda_c(2625)$  resonances, using interactions fully consistent with HQSS, was proposed in Refs. [86, 172]. In these works a consistent  $SU(6)_{\text{lsf}} \times SU(2)_{\text{HQSS}}$  extension of the chiral WT  $\pi N$  Lagrangian, was derived. Two states with  $J^P = 1/2^-$  were dynamically generated in the region of 2595 MeV. The first one, identified with the  $\Lambda_c(2595)$  resonance, was narrow and it strongly coupled to  $ND$  and especially to  $ND^*$ , with a small coupling to the open  $\Sigma_c\pi$  channel. Its wave-function had a large  $j_q^P = 0^-$  component that coupled to the spin ( $S_Q = \frac{1}{2}$ ) of the charm quark gives a total  $J^P = \frac{1}{2}^-$  for the  $\Lambda_c(2595)$ . Since the

<sup>1</sup>A detailed treatment of the interactions between the ground-state  $1/2^+$  and  $3/2^+$  singly charmed and bottomed baryons and the pseudo-Nambu-Goldstone bosons, discussing also the effects of the next-to-leading-order chiral potentials, can be found in [340].

transition of the dominant  $j_q^P = 0^-$  term of the  $\Lambda_c(2595)$  to the final  $\Sigma_c\pi$  state is forbidden by HQSS, this mechanism will act in addition to any possible kinematical suppression.

The second  $J^P = 1/2^-$  state found in [86, 172] was quite broad since it had a sizable coupling to the  $\Sigma_c\pi$  channel, and reproduced, in the charm-sector, the chiral two-pole structure of the  $\Lambda(1405)$  [24, 32, 34, 35, 64, 69, 324]. On the other hand, a  $J^P = 3/2^-$  state is generated mainly by the  $(ND^* - \Sigma_c^*\pi)$  coupled-channel dynamics. It would be the charm counterpart of the  $\Lambda(1520)$ , and it was argued that could be identified with the  $\Lambda_c(2625)$  resonance.

Several  $\Lambda_c^*$  poles were also obtained in the approach followed in Ref. [85]. There, the interaction of  $ND$  and  $ND^*$  states, together with their coupled channels are considered by using an extension of the SU(3) local hidden gauge formalism from the light meson sector [134–136] to four flavours. The scheme also respects LO HQSS constraints [349] and, as in Refs. [86, 172], a two-pole structure for the  $\Lambda_c(2595)$  was also found, with the  $ND^*$  channel playing a crucial role in its dynamics. This is a notable difference to the situation in the strange sector, where the analog  $N\bar{K}^*$  channel is not even considered in most of the studies of the  $\Lambda(1405)$ , because of the large  $\bar{K}^* - \bar{K}$  mass splitting. We will refer to this model as ELHG for the rest of this Chapter.

However neither the  $SU(6)_{\text{lsf}} \times SU(2)_{\text{HQSS}}$  model, nor the ELHG consider the interplay between  $\Sigma_c^{(*)}\pi - ND^{(*)}$  baryon-meson degrees of freedom and bare  $p$ -wave  $c\bar{u}d$  quark-model states. This is unjustified, in the same way, it was also unjustified the neglect of baryon-meson effects in the CQM approaches.

The CQM approach of Ref. [312] finds isoscalar  $J^P = 1/2^-$  and  $3/2^-$  states at 2628 and 2630 MeV, respectively. Given the proximity of these bare three-quarks states to the  $\Lambda_c(2595)$  and  $\Lambda_c(2625)$ , it is reasonable to expect a significant influence of the CQM degrees of freedom on the dynamics of the physical states. This seems to be specially true for the  $\Lambda_c(2625)$ , for which the CQM prediction almost matches its mass. CQM degrees of freedom can be taken into account in hadron scattering schemes by considering an additional energy dependent interaction [257, 363, 373], driven by a pole in the baryon-meson tree-level amplitudes located at the bare mass,  $\overset{\circ}{M}_{\text{CQM}}$ , of the CQM state. At energies far enough from  $\overset{\circ}{M}_{\text{CQM}}$ , the contribution of the CQM degrees of freedom can be possibly accounted for an appropriate LEC (induced by the UV regulator of the loops) in the unitarized baryon-meson amplitude. However, such contribution becomes more important for energies approaching  $\overset{\circ}{M}_{\text{CQM}}$ , and its energy dependence might then not be safely ignored.

In this chapter we will study the structure of the  $\Lambda_c(2595)$  and  $\Lambda_c(2625)$  resonances in the framework of an effective theory consistent with heavy quark spin and chiral symmetries, incorporating for the very first time the interplay between

$\Sigma_c^{(*)}\pi - ND^{(*)}$  baryon-meson degrees of freedom and bare  $p$ -wave  $c\bar{u}d$  quark-model states. For simplicity, we will use the  $SU(6)_{\text{lsf}} \times \text{HQSS}$  baryon-meson amplitudes, though the most important conclusions extracted here do not depend on the particular hadron scattering model employed.

The chapter is based on the findings of Ref. [4] and it is organized as follows. After this Introduction, the used formalism is briefly revised in Sect. 7.2, that is split in several subsections dealing with the  $SU(6)_{\text{lsf}} \times \text{HQSS}$  hadron amplitudes, their renormalization and structure in the complex plane, with the inclusion of the CQM degrees of freedom and finally with the evaluation of the  $\Lambda_c^*(1/2^-, 3/2^-) \rightarrow \Lambda_c(1/2^+) \pi\pi$  three-body decays. The results of this research are presented and discussed in Sect. 7.3, first neglecting CQM effects (Subsec. 7.3.1) and next coupling CQM and baryon-meson degrees of freedom (Subsec. 7.3.2). Finally, the main conclusions of this chapter are summarized in Sect. 7.4.

## 7.2 Formalism

### 7.2.1 $SU(6)_{\text{lsf}} \times \text{HQSS}$ amplitudes and renormalization

The building-blocks considered in [86, 172, 347] in the  $C = 1$  sector are the pseudoscalar ( $D_s, D, K, \pi, \eta, \bar{K}, \bar{D}, \bar{D}_s$ ) and vector ( $D_s^*, D^*, K^*, \rho, \omega, \bar{K}^*, \bar{D}^*, \bar{D}_s^*, \phi$ ) mesons, the spin-1/2 octet and the spin-3/2 decuplet of low-lying light baryons, in addition to the spin-1/2 ( $\Lambda_c, \Sigma_c, \Xi_c, \Xi'_c, \Omega_c$ ), and spin-3/2 ( $\Sigma_c^*, \Xi_c^*, \Omega_c^*$ ) charmed baryons. All baryon-meson pairs with ( $C = 1, S = 0, I = 0$ ) quantum numbers span the coupled-channel space for a given total angular momentum  $J$  and odd parity. The  $s$ -wave tree level amplitudes between two channels are given by the  $SU(6)_{\text{lsf}} \times \text{HQSS}$  WT kernel

$$V_{ij}^J(s) = D_{ij}^J \frac{2\sqrt{s} - M_i - M_j}{4f_i f_j} \sqrt{\frac{E_i + M_i}{2M_i}} \sqrt{\frac{E_j + M_j}{2M_j}}, \quad (7.1)$$

with  $s$  the baryon-meson Mandelstam variable,  $M_i$  and  $m_i$ , the masses of the baryon and meson in the  $i$  channel, respectively, and  $E_i$ , the center-of-mass energy of the baryon in the same channel. The hadron masses and meson decay constants,  $f_i$ , have been taken from Ref. [86]. The  $D_{ij}^J$  matrices are determined by the underlying  $SU(6)_{\text{lsf}} \times \text{HQSS}$  group structure of the interaction. Tables for all of them can be found in the Appendix B of Ref. [86]. Here, we truncate the coupled-channels space to that generated by the  $\Sigma_c \pi$ ,  $ND$  and  $ND^*$  and  $\Sigma_c^* \pi$  and  $ND^*$  in the  $J^P = 1/2^-$  and  $3/2^-$  sectors, respectively. Other higher channels like  $\Lambda_c \eta$ ,  $\Lambda_c \omega$ ,  $\Xi_c^{(\prime,*)} K^{(*)}$ ,  $\Lambda D_s^{(*)}$ ,  $\Sigma_c^{(*)} \rho, \dots$  are little relevant for the dynamics of the  $\Lambda_c(2595)$  and  $\Lambda_c(2625)$  resonances [86, 172], and have not been considered in the analysis carried out in this Chapter.

The matrices  $D^J$  are given in [86] in a basis of  $s$ -wave baryon-meson states. They become, however, diagonal when states with well defined  $ldof$  total angular momentum,  $j_q$ , are used. For the latter states, HQSS constrains are straightforward because of the symmetry that QCD acquires, in the infinite quark mass limit, under arbitrary rotations of the spin of the heavy quark [70–72]. In both bases, the total angular momentum of the baryon-meson pair is defined, and both sets of states are related by a Racah rotation [3, 349] (see also Chapter 6). In the  $(\Sigma_c^{(*)}\pi, ND^{(*)})$  truncated space, these matrices read

$$D^{J=1/2} = \begin{pmatrix} \Sigma_c\pi & ND & ND^* \\ -4 & \sqrt{3/2} & -1/\sqrt{2} \\ \sqrt{3/2} & -3 & -3\sqrt{3} \\ -1/\sqrt{2} & -3\sqrt{3} & -9 \end{pmatrix} \quad D^{J=3/2} = \begin{pmatrix} \Sigma_c^*\pi & ND^* \\ -4 & -\sqrt{2} \\ -\sqrt{2} & 0 \end{pmatrix} \quad (7.2)$$

with eigenvalues  $\lambda_0 = -12$ ,  $\lambda_1^{\text{atr}} = -2 - \sqrt{6}$  and  $\lambda_1^{\text{rep}} = -2 + \sqrt{6}$ , and  $\lambda_1^{\text{atr}}$  and  $\lambda_1^{\text{rep}}$ , for  $J^P = 1/2^-$  and  $J^P = 3/2^-$ , respectively, as was seen in Chapter 6. Actually, the  $SU(6)_{\text{lsf}} \times SU(2)_{\text{HQSS}}$  extension of the WT  $\pi N$  interaction proposed in [86, 172, 347] leads to a large attraction ( $\lambda_0$ ) in the subspace where the total angular-momentum-parity quantum numbers of the  $ldof$  are  $j_q^P = 0^-$ . This latter configuration does not occur for  $J = 3/2$ , when only  $s$ -wave interactions are considered, and the  $ldof$  are necessarily coupled to  $j_q^P = 1^-$ . In the  $j_q^P = 1^-$ -subspace, there exist both attractive ( $\lambda_1^{\text{atr}}$ ) and repulsive ( $\lambda_1^{\text{rep}}$ ) components, and HQSS relates the  $D^{J=1/2}$  and  $D^{J=3/2}$  matrices.

In this chapter, for the two-body loop function, we will use two renormalization schemes. First, dimensional regularization using Lutz prescription, found in Eq. (3.98) (which we shall call  $\mu$ -RS), and then a sharp-cutoff, using the loop function in Eq. (3.103) (this scheme we shall call  $\Lambda$ -RS).

For the  $\mu$ -RS, we use the prescription adopted in Ref. [86], where the subtraction points,  $\mu$ , are chosen to be independent of the total angular momentum  $J$ , common for all channels in a given  $CSI$  sector, and equal to

$$\mu = \alpha\mu_m, \quad (7.3)$$

with  $\mu_m$  defined in Eq. (3.97) (see Eq. (3.95)). In addition,  $\alpha$  is a parameter that can be slightly adjusted to data [172]. Also, for the  $\Lambda$ -RS, note that there are no cutoff effects in the finite  $\overline{G}_i(s)$ -loop function, as it would happen if the two-body propagator would have been directly calculated using the UV cutoff  $\Lambda$ .

## 7.2.2 Interplay between bare CQM and baryon-meson degrees of freedom

Within the quark model approach of Ref. [312], odd-parity  $\Lambda^*$  states are obtained at 2628 and 2630 MeV for  $J = 1/2$  and  $3/2$ , respectively. The  $ldof$  are coupled to angular momentum–parity quantum numbers  $j_q^P = 1^-$  ( $\lambda$ -mode) in both cases, which explains their approximate degeneracy. Higher excited states appear at 2.9 GeV ( $\rho$ -mode), far from the  $\Lambda_c(2595)$  and  $\Lambda_c(2625)$  narrow resonances, and will not be considered in the present analysis. However, the low-lying  $\lambda$ -mode states, given their proximity to the  $\Lambda_c(2595)$  and  $\Lambda_c(2625)$ , might significantly influence the dynamics of the physical states. This seems to be specially truth for the  $\Lambda_c(2625)$ , since the prediction of Ref. [312] for its mass is only 2 MeV higher than the experimental one [(2628.11  $\pm$  0.19) MeV [21]].

Bare CQM-states effects on the baryon-meson dynamics can be effectively considered by means of an energy dependent interaction [22, 165, 363]

$$V_{\text{ex}}^J(s) = 2 \overset{\circ}{M}_{\text{CQM}} \frac{[V_{\text{CQM}}^J]^\dagger \cdot [V_{\text{CQM}}^J]}{s - (\overset{\circ}{M}_{\text{CQM}})^2}, \quad V_{\text{CQM}}^{J=1/2} = \begin{pmatrix} d_1 & \sqrt{3}c_1/2 & -c_1/2 \\ \Sigma_c\pi & ND & ND^* \end{pmatrix}$$

$$V_{\text{CQM}}^{J=3/2} = \begin{pmatrix} -d_1 & c_1 \\ \Sigma_c^*\pi & ND^* \end{pmatrix} \quad (7.4)$$

where  $d_1$  and  $c_1$  are undetermined dimensionless parameters that control the strength of the baryon-meson-CQM-state vertex. Note that  $[V_{\text{CQM}}^J]^\dagger \cdot [V_{\text{CQM}}^J]$  gives rise to  $3 \times 3$  and  $2 \times 2$  matrices in the  $J^P = 1/2^-$  and  $3/2^-$  sectors, respectively. The relation between  $ND$  and  $ND^*$  in  $V_{\text{CQM}}^{J=1/2}$  and  $ND^*$  in  $V_{\text{CQM}}^{J=1/2}$  was obtained using Eq. (6.4). The above interaction accounts for the contribution to baryon-meson scattering of the exchange of an intermediate odd-parity CQM  $\lambda$ -mode state. It does not obviously affect the  $j_q^P = 0^-$ -subspace of the  $J^P = 1/2^-$  sector, and it is consistent with HQSS in the  $j_q^P = 1^-$ -subspace of the  $J^P = 1/2^-$  and  $J^P = 3/2^-$  sectors, which are related by a spin rotation of the heavy quark.

Note that  $V_{\text{ex}}^J(s)$  introduces a pole in the baryon-meson tree-level amplitudes located at the bare mass value,  $\sqrt{s} = \overset{\circ}{M}_{\text{CQM}}$ . It should be interpreted as the mass of the CQM state in the limit of vanishing coupling to the baryon–meson-pairs ( $d_1, c_1 \rightarrow 0$ ), and therefore it is not an observable. The interaction with the baryon-meson cloud dresses the CQM state through loops, renormalizing its mass, and the dressed state might also acquire a finite width, when it is located above threshold. A priori,  $\overset{\circ}{M}_{\text{CQM}}$  is a free parameter of the present approach, and moreover it depends on the renormalization scheme [363]. This is because, in the effective theory, the UV regulator is finite, and the difference between the bare and the physical resonance masses is



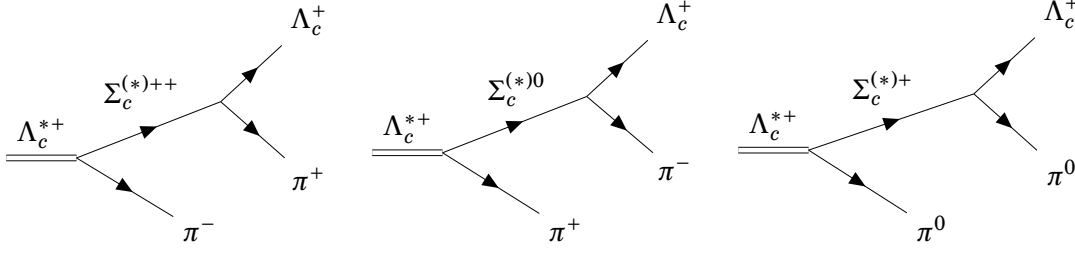


Figure 7.1: Diagrams for  $\Lambda_c(2595)$  or  $\Lambda_c(2625)$  decay into  $\Lambda_c^+$  and two pions, mediated by the  $\Sigma_c$  or  $\Sigma_c^*$  resonances, respectively.

a finite renormalization that depends on the adopted scheme. The value of the bare mass, which is thus a free parameter, can either be indirectly fitted to experimental observations, or obtained from schemes that ignore the coupling to baryon-meson pairs, such as some CQMs. In this latter case, the issue certainly would be to set the UV regulator to match the quark model and the baryon-meson scattering approaches [363]. For simplicity, and consistently with HQSS, we take a common bare mass for both  $J = 1/2$  and  $J = 3/2$ , which is fixed to the average of masses reported in the quark model of Ref. [312] ( $\overset{\circ}{M}_{\text{CQM}} = 2629$  MeV). We will explore different values of the renormalization scheme-dependent bare couplings  $d_1$  and  $c_1$  to elucidate the robustness of our results.

At energies far enough from  $\overset{\circ}{M}_{\text{CQM}}$ , the contribution of  $V_{\text{ex}}$  can be regarded as a small contact interaction that can be accounted for by means of a LEC. However, the exchange contribution becomes more important for energies approaching  $\overset{\circ}{M}_{\text{CQM}}$ , and it may not be safe to ignore its energy dependence. One might expect such situation in the  $J = 3/2$  sector, where  $V_{\text{ex}}$  should provide a sizable attraction (repulsion) for energies slightly below (above)  $\overset{\circ}{M}_{\text{CQM}}$ , relevant in the dynamics of the  $\Lambda_c(2625)$ . We expect a less relevant role in the case of the  $\Lambda_c(2595)$ , since this resonance is located furthest from  $\overset{\circ}{M}_{\text{CQM}}$ .

### 7.2.3 The $\Lambda_c^*(1/2^-, 3/2^-) \rightarrow \Lambda_c(1/2^+) \pi \pi$ three-body decays through the $\pi \Sigma_c^{(*)}$ intermediate state

Isospin conservation forbids single pion transitions between the  $\Lambda_c^*$  and  $\Lambda_c$ , and hence the  $\Lambda_c^*(1/2^-, 3/2^-)$  decay into  $\Lambda_c$  and two pions. The decays proceed via an intermediate  $I = 1$  baryon-state down to a  $\Lambda_c \pi$  pair. The relatively small masses of the  $\Lambda_c^*$ 's above  $\Lambda_c$  kinematically restrict the outgoing pion energies, making feasible a chiral derivative expansion [150]. There are two different final states,  $\Lambda_c^+ \pi^- \pi^+$  and  $\Lambda_c^+ \pi^0 \pi^0$ , and we will consider here only the resonant term driven by the exci-

tation of the  $\Sigma_c^{(*)}$  and its subsequent decay into  $\Lambda_c\pi$ , as shown in Fig. 7.1. This is by large the dominant contribution to the  $\Lambda_c(2595)$  width, while it becomes significantly smaller for the  $\Lambda_c(2625)$  one, since the virtual  $\Sigma_c^*$  intermediate state is very much off-shell [150,374]. Indeed the ARGUS Collaboration reported a ratio [375]  $R = \Gamma[\Lambda_c(2625) \rightarrow \Lambda_c^+\pi^+\pi^- (\text{non-resonant})]/\Gamma[\Lambda_c(2625) \rightarrow \Lambda_c^+\pi^+\pi^- (\text{total})] = 0.54 \pm 0.14$ .

The  $\Lambda_c(2595)$  or  $\Lambda_c(2625)$  decay width into the charged-pions mode<sup>2</sup>, at lowest order in chiral perturbation theory and in the heavy mass limit, is given in the resonance rest frame (LAB) by [150]

$$\begin{aligned} \frac{d\Gamma_{\pi^-\pi^+}}{ds_{12}ds_{23}} &= \Gamma_0 \left\{ E_3^2 \vec{p}_2^2 \left| G_{\Sigma_c^{(*)}}(s_{12}) \right|^2 + E_2^2 \vec{p}_3^2 \left| G_{\Sigma_c^{(*)}}(s_{13}) \right|^2 + 2E_2 E_3 \right. \\ &\quad \left. \times \text{Re} \left[ G_{\Sigma_c^{(*)}}^*(s_{12}) G_{\Sigma_c^{(*)}}(s_{13}) \right] \vec{p}_2 \cdot \vec{p}_3 \right\} \quad (7.8) \\ \Gamma_0 &= \frac{g_D^2 g_{R\Sigma_c^{(*)}\pi}^2}{144 f_\pi^2 \pi^3} \frac{M_{\Lambda_c} M_{\Sigma_c^{(*)}}^2}{M_R^2 (M_R - M_{\Sigma_c^{(*)}})^2} \quad G_{\Sigma_c^{(*)}}(s) = \frac{1}{s - M_{\Sigma_c^{(*)}}^2 + i M_{\Sigma_c^{(*)}} \Gamma_{\Sigma_c^{(*)}}(s)} \\ \Gamma_{\Sigma_c^{(*)}}(s) &= \frac{g_D^2}{6\pi f_\pi^2} \frac{M_{\Lambda_c}}{M_{\Sigma_c^{(*)}}} |\vec{p}_{\Lambda_c\pi}|^3, \quad |\vec{p}_{\Lambda_c\pi}| = \frac{\lambda^{\frac{1}{2}}(s, M_{\Lambda_c}^2, m_\pi^2)}{2\sqrt{s}}, \\ s_{13} &= M_R^2 + 2m_\pi^2 + M_{\Lambda_c}^2 - s_{12} - s_{23}, \quad E_3 = \sqrt{m_\pi^2 + \vec{p}_3^2} = \frac{M_R^2 + m_\pi^2 - s_{12}}{2M_R}, \end{aligned}$$

<sup>2</sup>The  $\Lambda(2595)$  and  $\Lambda(2625)$  amplitudes read

$$\begin{aligned} T_{\pi^-\pi^+}^{J=1/2} &= -\frac{g_D g_{R\Sigma_c\pi}}{3f_\pi} \frac{2M_{\Sigma_c}}{(M_R - M_{\Sigma_c})} \bar{u}_{\Lambda_c} \left\{ (v p_{\pi^-}) G_{\Sigma_c}(s_{12}) (\not{p}_{\pi^+} + v p_{\pi^+}) \gamma_5 \frac{1+\not{v}}{2} + (v p_{\pi^+}) G_{\Sigma_c}(s_{13}) \right. \\ &\quad \left. \times (\not{p}_{\pi^-} + v p_{\pi^-}) \gamma_5 \frac{1+\not{v}}{2} \right\} u_R \quad (7.5) \end{aligned}$$

$$T_{\pi^-\pi^+}^{J=3/2} = \frac{g_D g_{R\Sigma_c\pi}}{3f_\pi} \frac{2M_{\Sigma_c}}{(M_R - M_{\Sigma_c})} \left[ (v p_{\pi^-}) G_{\Sigma_c}(s_{12}) p_{\pi^+}^\mu + (v p_{\pi^+}) G_{\Sigma_c}(s_{13}) p_{\pi^-}^\mu \right] \bar{u}_{\Lambda_c} P_{\mu\nu}(v) u_R^\nu \quad (7.6)$$

where  $v$  is the common velocity of all involved charmed hadrons, which remains unaltered in the heavy quark limit. It satisfies  $v^2 = 1$  and  $\not{v} u_R^{(\nu)} = u_R^{(\nu)}$  and  $\not{v} u_{\Lambda_c} = u_{\Lambda_c}$ , with  $u$  and  $u^\nu$  mass-dimensions Dirac and Rarita-Schwinger spinors, respectively. The spin 3/2 projector is

$$P^{\mu\nu}(v) = \left( -g^{\mu\nu} + v^\mu v^\nu + \frac{1}{3} (\gamma^\mu + v^\mu) (\gamma^\nu - v^\nu) \right) \frac{1+\not{v}}{2} \quad (7.7)$$

with metric  $(+, -, -, -)$ , and the sum over fermion polarizations is given by  $u\bar{u} = 2M(1+\not{v})/2$  and  $u^\mu \bar{u}^\nu = 2MP^{\mu\nu}$ .

$$E_2 = \sqrt{m_\pi^2 + \vec{p}_2^2} = \frac{M_R^2 + m_\pi^2 - s_{13}}{2M_R}, \quad \vec{p}_2 \cdot \vec{p}_3 = E_2 E_3 + m_\pi^2 - s_{23}/2$$

with  $M_R$  the resonance mass,  $\lambda(x, y, z) = x^2 + y^2 + z^2 - 2xy - 2xz - 2yz$ . In addition,  $s_{12}$  (invariant mass square of  $\Lambda_c \pi^+$ ) varies between  $(M_{\Lambda_c} + m_\pi)^2$  and  $(M_R - m_\pi)^2$ , while the limits of  $s_{23}$  (invariant mass square of the  $\pi^+ \pi^-$  pair) are

$$\begin{aligned} s_{23}^{\max, \min} &= (E_{\pi^+}^* + E_{\pi^-}^*)^2 - (p_{\pi^+}^* \mp p_{\pi^-}^*)^2, \quad E_{\pi^+}^* = \frac{s_{12} + m_\pi^2 - M_{\Lambda_c}^2}{2\sqrt{s_{12}}}, \\ E_{\pi^-}^* &= \frac{M_R^2 - m_\pi^2 - s_{12}}{2\sqrt{s_{12}}} \end{aligned} \quad (7.9)$$

with  $p_{\pi^\pm}^{*2} = E_{\pi^\pm}^{*2} - m_\pi^2$ . The expression of Eq. (7.8) corresponds to the square of the sum of amplitudes associated to the first two diagrams of Fig. 7.1. The processes occur so close to threshold, specially the  $\Lambda_c(2595)$  decay, that the available phase space might depend significantly on the small isospin-violating mass differences between members of the pion and  $\Sigma_c^{(*)}$ -multiplets. We have used  $m_\pi = m_{\pi^\pm}$ ,  $M_{\Sigma_c^{(*)}} = (M_{\Sigma_c^{++(*)}} + M_{\Sigma_c^{0(*)}})/2$ ,  $M_{\Lambda_c(2595)} = 2592.25$  MeV and  $M_{\Lambda_c(2625)} = 2628.11$  MeV. The errors on the masses of the  $\Lambda_c^*$  resonances quoted in the RPP [21] are 0.28 MeV and 0.19 MeV, respectively, and turn out to be relevant only for the  $\Lambda_c(2595)$  width, but even in that case, it induces variations of the order of 1%. In addition  $g_D/f_\pi = 0.0074$  MeV<sup>-1</sup>, which leads to  $\Gamma[\Sigma_c \rightarrow \Lambda_c \pi] = 1.9$  MeV and  $\Gamma[\Sigma_c^* \rightarrow \Lambda_c \pi] = 14.4$  MeV, and we take the dimensionless coupling  $g_{R\Sigma_c^{(*)}\pi}$  from the residue at the resonance-pole of the  $\Sigma_c^{(*)}\pi$  channel (*s*-wave) that we choose to be real, by an appropriate redefinition of the overall phases of the meson and baryon fields.

The rates for the neutral-pions channel can be obtained by adding a symmetry factor 1/2 to avoid double counting the two identical bosons in the final state and using  $m_\pi = m_{\pi^0}$ ,  $M_{\Sigma_c^{(*)}} = M_{\Sigma_c^{+(*)}}$ .

Adding the contribution of neutral and charged pion modes, we find that the  $\Sigma_c^{(*)}$ -resonant contribution to the  $\Lambda_c(2595)$  and  $\Lambda_c(2625)$  decays into  $\Lambda_c^+$  and two pions are

$$\begin{aligned} \Gamma[\Lambda_c(2595) \rightarrow \Lambda_c \pi \pi] &= 1.84 \times g_{\Lambda_c(2595)\Sigma_c \pi}^2 \text{ [MeV]}, \\ \Gamma[\Lambda_c(2625) \rightarrow \Lambda_c \pi \pi] &= 0.27 \times g_{\Lambda_c(2625)\Sigma_c^* \pi}^2 \text{ [MeV]} \end{aligned} \quad (7.10)$$

with the  $\pi^0 \pi^0$  channel being the 81.5% and 45.0% of the total for the  $\Lambda_c(2595)$  and  $\Lambda_c(2625)$  partial widths, respectively. In the exact isospin limit, the two-neutral-pions partial width is a factor of two smaller than the  $\pi^+ \pi^-$  one. The experimental width of the  $\Lambda_c(2595)$  is  $2.6 \pm 0.6$  MeV (nearly 100% saturated by the two  $\Lambda_c \pi \pi$  modes), while there exists an upper bound of 0.97 MeV for the  $\Lambda_c(2625)$  [21]. Hence,

the experimental  $\Gamma[\Lambda_c(2595)]$  provides a direct measurement of the  $s$ -wave coupling constant  $g_{\Lambda_c(2595)\Sigma_c\pi}^2$ , assuming that a possible  $D$ -wave contribution is negligible [376]. The bound on  $\Gamma[\Lambda_c(2625)]$ , on the other hand, puts upper limits on the coupling in  $s$ -wave of this resonance to the  $\Sigma_c^*\pi$  pair, but one should bear in mind that in this case, the resonant contribution does not saturate the decay width.

The interference term in Eq. (7.8) for the charged mode, and the equivalent one in the case of  $\pi^0\pi^0$ , gives a small contribution to the integrated width. In particular for the  $\Lambda_c(2595)$ , it is of the order of  $-1\%$  and  $-0.2\%$  for the  $\pi^+\pi^-$  and  $\pi^0\pi^0$  channels, respectively. For the  $\Lambda_c(2625)$ , it becomes larger around  $-5\%$  and  $-4\%$ , respectively, but it is still quite small. This can be easily understood by changing the  $s_{12}$  and  $s_{23}$  integration variables to  $E_3$  and  $\cos\theta_{23}$ , with  $\theta_{23}$  the angle formed by the two pions in the resonance rest-frame. The energy  $E_2$  (or equivalently  $s_{13}$ ) depends on  $\cos\theta_{23}$  through the conservation of energy equation,  $M_R = E_3(\vec{p}_3) + E_2(\vec{p}_2) + E_{\Lambda_c}(\vec{p}_2 + \vec{p}_3)$ . In the infinite charm limit, the recoiling  $\Lambda_c$  baryon carries off momentum but not kinetic energy, and hence the approximation [150]

$$E_2 \sim M_R - M_{\Lambda_c} - E_3 \quad (7.11)$$

turns out to be quite accurate, specially for the  $\Lambda_c(2595)$  where the energy released by the decaying resonance is very small. Within this approximation, the only dependence of the differential decay rate on  $\cos\theta_{23}$  comes from the scalar product  $\vec{p}_2 \cdot \vec{p}_3$  in the interference term, that would vanish in the integrated width, since  $\cos\theta_{23}$  covers almost totally the  $[-1, 1]$  range for all  $E_3$  allowed values. Indeed, we recover Eq. (3.5), up to a factor 1/2, of Ref. [150] from the expression of Eq. (7.8) by neglecting the interference term and adopting the approximation of Eq. (7.11), using that  $ds_{12} = 2M_R dE_3$  and taking into account that the integration over  $ds_{23}$  gives  $4p_{\pi^+}^* p_{\pi^-}^* \sim 4\sqrt{E_3^2 - m_\pi^2}\sqrt{E_2^2 - m_\pi^2}$ , approximating in the propagators ( $s_{12(13)} - M_{\Sigma_c^{(*)}}^2$ ) by  $2M_{\Sigma_c^{(*)}}(M_R - E_{3(2)} - M_{\Sigma_c^{(*)}})$ , and finally identifying  $g_D^2 = h_1^2/2$  and  $g_{R\Sigma_c^{(*)}\pi}^2 = 3h_2^2(M_R - M_{\Sigma_c^{(*)}})^2/(2f_\pi^2)$ , with  $h_{1,2}$  used in Ref. [150]. The factor 1/2 introduced in this latter work does not hold for the  $\pi^+\pi^-$  decay mode, though should be included for the neutral mode<sup>3</sup>.

Finally, we would like to mention that the three-body  $\Lambda_c(2595) \rightarrow \Lambda_c\pi\pi$  decay rate can be approximated by using the narrow width approximation of the  $\Sigma_c^{(*)}$ -propagators,

$$|G_{\Sigma_c}(s)|^2 \sim \frac{\pi}{M_{\Sigma_c}\Gamma_{\Sigma_c}(s)}\delta(s - M_{\Sigma_c}^2) = \frac{6\pi f_\pi^2}{M_{\Lambda_c}|\vec{p}_\pi^{\Lambda_c\pi}|^3}\delta(s - M_{\Sigma_c}^2) \quad (7.12)$$

<sup>3</sup>Note, however, that the expression for the  $\Lambda_c\pi^0\pi^0$  partial width used by the CDF Collaboration in Ref. [376] is wrong by a factor of two. The 1/2 in Eq. (13) for the amplitude in that reference should be replaced by  $1/\sqrt{2}$ .

which leads to

$$\Gamma_{\pi^- \pi^+} \sim (\Gamma_{\Lambda_c(2595) \rightarrow \Sigma_c^{++} \pi^-} + \Gamma_{\Lambda_c(2595) \rightarrow \Sigma_c^0 \pi^+}), \quad \Gamma_{\pi^0 \pi^0} \sim \Gamma_{\Lambda_c(2595) \rightarrow \Sigma_c^+ \pi^0} \quad (7.13)$$

$$\Gamma_{\Lambda_c(2595) \rightarrow \Sigma_c^a \pi^b} = \frac{g_{\Lambda_c(2595)\Sigma_c\pi}^2}{6\pi} \frac{M_{\Sigma_c^a}}{M_{\Lambda_c(2595)}} |\vec{p}_\pi|, \quad |\vec{p}_\pi| = \frac{\lambda^{\frac{1}{2}}(M_{\Lambda_c(2595)}^2, M_{\Sigma_c^a}^2, m_{\pi^b}^2)}{2M_{\Lambda_c(2595)}} \quad (7.14)$$

for the charge-combinations  $(a, b) = (++, -), (0, +)$  and  $(+, 0)$ , which correspond to the square of the amplitudes of each of the three diagrams depicted in Fig. 7.1. To obtain Eq. (7.13) from Eq. (7.8), using the approximation of Eq. (7.12), we have neglected the interference contributions, have approximated the LAB energy of the non-resonant pion and the momentum of the resonant one by  $(M_{\Lambda_c(2595)} - M_{\Sigma_c})$  and  $|\vec{p}_\pi|$ , respectively, and in addition, we have made use that the momentum of the non-resonant pion in the  $\Sigma_c$ -rest frame is  $M_{\Lambda_c(2595)}|\vec{p}_\pi|/M_{\Sigma_c}$ . The two body  $s$ -wave-widths limit of Eq. (7.13) works well when the intermediate  $\Sigma_c$  is nearly on-shell. The value used here for  $M_{\Lambda_c(2595)}$  is 1.2 (4.6) MeV below (above) the  $\Sigma_c^{+,0} m_{\pi^\mp}$  ( $\Sigma_c^+ m_{\pi^0}$ ) threshold. We find that  $\Gamma_{\pi^0 \pi^0}$  and  $\Gamma_{\Lambda_c(2595) \rightarrow \Sigma_c^+ \pi^0}$  differ only in  $0.19 g_{\Lambda_c(2595)\Sigma_c\pi}^2$  [MeV], this is to say, the latter width is just 2.5% greater than the former one. The  $\Sigma_c^{++}$  and  $\Sigma_c^0$  cannot be put on shell for this mass of the  $\Lambda_c(2595)$ , but clearly the differential decay width of Eq. (7.8) is strongly dominated by the contribution of two well separated peaks that correspond to the first two mechanisms shown in Fig. 7.1 [150].

Finally, we should acknowledge that we have neither considered direct two pion emission processes mediated by heavier  $\Sigma_c^{(*)}$ -resonances, nor  $\pi\pi$  or  $\pi\Lambda_c$  final state-interactions (FSI) effects. In the case of the  $\Lambda_c(2595)$ , the decay is dominated by the intermediate  $\Sigma_c(2455)$ -mechanism [21]. Indeed, the ARGUS Collaboration reported a value of  $0.66_{-0.16}^{+0.13} \pm 0.07$  for the ratio of resonant contribution to width and total width [377], while the results of the E687 Collaboration are consistent with this ratio being 100% [378]. Other mechanisms are then expected to be significantly smaller. We should bear in mind that we only use the three body decays of the  $\Lambda_c(2595)$  and  $\Lambda_c(2625)$  to limit the acceptable values of the couplings of these resonances to the  $\Sigma_c^{(*)}\pi$  pairs, and thus considering only the intermediate  $\Sigma_c(2455)$ -contribution is sufficiently accurate for our purposes. On the other hand, pions are produced almost at threshold and hence one should expect small effects from their FSI. The  $\pi\Lambda_c$  FSI are however large, and are dominated by the production of the  $\Sigma_c(2455)$ , which effects are explicitly taken into account thanks to the complex propagator of this intermediate resonance. For the  $\Lambda_c(2625)$  case, contact two pion emission processes can be more relevant. However, the strongest bound for  $g_{\Lambda_c(2625)\Sigma_c^*\pi}^2$  comes from the  $\Sigma_c^*(2520)$  resonant contribution measured by the ARGUS Collaboration [375], which is precisely what we compute here using the mechanisms depicted in Fig. 7.1.

## 7.3 Results and discussion

### 7.3.1 $SU(6)_{\text{lsf}} \times \text{HQSS}$ hadron molecules: dependence on the renormalization scheme

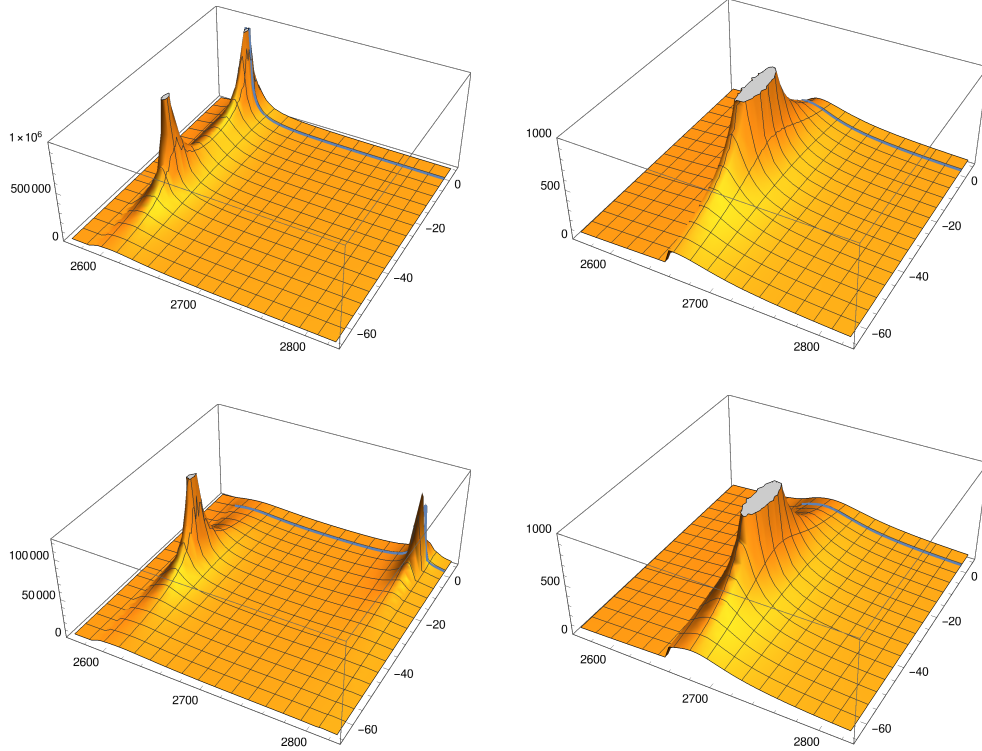


Figure 7.2: Absolute value of the determinant of the  $T$ -matrix ( $\text{AVD-}T$ ) in the  $J^P = 1/2^-$  (left) and  $J^P = 3/2^-$  (right) sectors using two UV renormalization schemes:  $\mu$ -RS with  $\alpha = 0.95$  [SC- $\mu$  in the figure] and a cutoff of 650 MeV in the top and bottom panels respectively. We display the  $\text{AVD-}T$  for both the FRS ( $\text{Im}(E) > 0$ ) and the SRS ( $\text{Im}(E) < 0$ ) [fm] of the unitarized amplitudes as a function of the complex energy  $E$  [MeV]. We also show the scattering line (blue solid curve) in all the cases. Bare CQM exchange interactions are set to zero ( $d_1 = c_1 = 0$  in Eq. (7.4)). In the  $z$ -axis we have  $\text{AVD-}T$ , in the  $x$ -axis we have  $\text{Re}(E)$  and in the  $y$ -axis we have  $\text{Im}(E)$ .

First we present in Fig. 7.2 the dynamically generated resonances (poles in the SRS of the amplitudes) that are obtained, when the effects produced by the exchange of CQM bare states are neglected. We show both the  $J = 1/2$  and  $J = 3/2$  sectors, and consider the two renormalization schemes introduced in Subsec. 7.2.1. The numerical positions of the poles and residues are given in the first row of Tables 7.1 and 7.2.

The  $\mu$ -RS results found here, working with the reduced  $ND^{(*)} - \Sigma_c^{(*)}\pi$  coupled-

		$\Lambda = 650 \text{ MeV}$				$\mu\text{-RS } (\alpha = 0.95)$			
$d_1$	$c_1$	$M - i\Gamma/2$	Type	$ g_{\Sigma_c^*\pi} $	$ g_{ND^*} $	$M - i\Gamma/2$	Type	$ g_{\Sigma_c^*\pi} $	$ g_{ND^*} $
0	0	(2680.4 - i33.0)	1 <sup>-</sup>	2.0	2.5	(2662.6 - i27.2)	1 <sup>-</sup>	2.3	2.4
-0.8	0	(2704.0 - i31.5)	1 <sup>-</sup>	1.7	2.2	(2688.8 - i28.4)	1 <sup>-</sup>	1.8	1.9
-0.8	0	2615.8	CQM	1.0	0.6	2617.5	CQM	1.1	0.5
-0.8	-1	(2706.8 - i30.2)	1 <sup>-</sup>	1.7	2.6	(2681.1 - i27.0)	1 <sup>-</sup>	1.8	2.4
-0.8	-1	2614.9	CQM	1.1	0.2	2617.7	CQM	1.0	0.5
-0.8	1	(2701.4 - i32.4)	1 <sup>-</sup>	1.8	1.8	(2695.5 - i30.6)	1 <sup>-</sup>	1.8	1.5
-0.8	1	2620.9	CQM	0.9	1.5	2612.9	CQM	1.2	1.4

Table 7.1: Properties of the CQM and molecular  $J^P = 3/2^-$  poles for different renormalization schemes and values of the  $d_1$  and  $c_1$  LECs, which determine the interplay between CQM and baryon-meson pair degrees of freedom. The angular momentum-parity quantum numbers of the  $ldof$  are always 1<sup>-</sup>, and masses and widths are given in MeV units.

		$\Lambda = 650 \text{ MeV}$					$\mu\text{-RS } (\alpha = 0.95)$				
$d_1$	$c_1$	$M - i\Gamma/2$	Type	$ g_{\Sigma_c^* \pi} $	$ g_{ND} $	$ g_{ND^*} $	$M - i\Gamma/2$	Type	$ g_{\Sigma_c^* \pi} $	$ g_{ND} $	$ g_{ND^*} $
0	0	(2609.9 - $i$ 28.8)	$1^-$	2.0	2.3	0.7	(2608.9 - $i$ 38.6)	$1^-$	2.3	2.0	1.9
0	0	(2798.7 - $i$ 2.0)	$0^-$	0.3	1.8	4.1	(2610.2 - $i$ 1.2)	$0^-$	0.5	3.9	6.2
-0.8	0	2590.0	$1^-$	1.1	1.0	0.3	2591.1*	$1^-$	1.3	1.5	0.5
-0.8	0	(2799.0 - $i$ 2.2)	$0^-$	0.3	1.8	4.1	(2611.6 - $i$ 0.4)	$0^-$	0.3	3.5	6.2
-0.8	0	(2659.1 - $i$ 17.3)	CQM	1.3	1.6	0.3	(2652.8 - $i$ 22.2)	CQM	1.5	0.8	1.7
-0.8	-1	2589.3	$1^-$	1.2	0.5	0.2	(2589.4 - $i$ 8.6)*	$1^-$	2.6	1.7	0.7
-0.8	-1	(2800.7 - $i$ 2.3)	$0^-$	0.3	1.7	4.1	(2610.1 - $i$ 0.0)	$0^-$	0.0	3.8	5.9
-0.8	-1	(2657.2 - $i$ 15.8)	CQM	1.2	2.3	0.5	(2642.3 - $i$ 19.4)	CQM	1.5	1.1	2.5
-0.8	1	2591.0	$1^-$	0.9	1.2	0.4	2590.3	$1^-$	1.1	1.7	0.5
-0.8	1	(2798.8 - $i$ 1.9)	$0^-$	0.3	1.8	4.1	(2612.6 - $i$ 0.7)	$0^-$	0.4	3.2	6.3
-0.8	1	(2660.0 - $i$ 18.9)	CQM	1.3	1.1	0.2	(2659.6 - $i$ 26.8)	CQM	1.6	0.7	1.2

Table 7.2: Properties of the CQM and molecular  $J^P = 1/2^-$  poles for different renormalization schemes and values of the  $d_1$  and  $c_1$  LECs, which determine the interplay between CQM and baryon-meson pair degrees of freedom. Molecular states are labeled according to their dominant  $Idof$  configuration,  $0^-$  or  $1^-$ , and masses and widths are given in MeV units. \*: Virtual state placed in the 100 sheet below the  $\Sigma_c^* \pi$  threshold.



channels space, reproduce reasonably well the most important features reported in the original works of Refs. [86, 172]. Indeed, we choose  $\alpha = 0.95$  to better account for some of the effects produced by the channels that have not been considered in the current approach. We see that a narrow  $J^P = 1/2^- \Lambda_{c(n)}^{0^-}(2595)$  resonance ( $\Gamma \sim 2$  MeV) is produced. This is mostly generated from the extended WT  $ND - ND^*$  coupled-channels dynamics in the  $j_q^P = 0^-$  subspace. This state has a small coupling to the ( $j_q^P = 1^-$ )  $\Sigma_c \pi$  channel which, in addition to the proximity to the open threshold, explains its small width. There appears a second  $J^P = 1/2^-$  pole [ $\Lambda_{c(b)}^{1^-}(2595)$ ] in the 2.6 GeV region. Although it is placed relatively close to the  $\Sigma_c \pi$  threshold, this resonance is broad ( $\Gamma \sim 75$  MeV) because of its sizable coupling to the latter open channel. Nevertheless, as seen in Fig. 7.2, this second wide state will not produce visible effects on the baryon-meson  $s$ -wave cross sections, since its possible impact for real values of  $s$  will be shadowed by the narrow  $\Lambda_{c(n)}^{0^-}$  that is located at a similar mass and much closer to the scattering line. Thus, this double pattern structure would be difficult to be confirmed experimentally, and it will not certainly show up in the  $\Lambda_c \pi \pi$  spectrum, where the evidences of the  $\Lambda_c(2595)$  have been reported [376, 377, 379]. However, it has been argued that exclusive semileptonic  $\Lambda_b$  ground-state decays into excited charmed  $\Lambda_c^*$  baryons could unravel the two  $\Lambda_c(2595)$  states [3, 321], if they exist.

In the  $J^P = 3/2^-$  sector, we find a resonance that clearly is the HQSS partner of the broad  $J^P = 1/2^- \Lambda_{c(b)}^{1^-}(2595)$  state, with quantum numbers  $1^-$  for  $j_q^P$ . It is located above the  $\Sigma_c^* \pi$  threshold, with a width of around 55 MeV. Furthermore, the coupling of this  $J^P = 3/2^-$  pole to the  $\Sigma_c^* \pi$  channel is essentially identical to that of the  $\Lambda_{c(b)}^{1^-}(2595)$  to  $\Sigma_c \pi$ . This  $J^P = 3/2^-$  isoscalar resonance might be identified with the  $D$ -wave  $\Lambda_c(2625)$ , although its mass and width significantly differ from those of the physical state. In Refs. [172] and [86], it is argued that a change in the renormalization subtraction constant could move the resonance down by 40 MeV to the nominal position of the physical state, and that in addition, this change of the mass would considerably reduce the width, since the state might even become bound below the  $\Sigma_c^* \pi$  threshold. Thus, within the  $SU(6)_{\text{lsf}} \times SU(2)_{\text{HQSS}}$  model, the  $\Lambda_c(2625)$  would turn out to be the HQSS partner of the second broad  $\Lambda_{c(b)}^{1^-}(2595)$  pole instead of the narrow  $\Lambda_{c(n)}^{0^-}(2595)$  resonance<sup>4</sup>. This is in sharp contrast to the predictions of the CQMs, where there is no a second 2595 pole, and the  $\Lambda_c(2625)$  and the narrow  $\Lambda_c(2595)$  are HQSS siblings, produced by a  $\lambda$ -mode excitation of the ground  $1/2^+$   $\Lambda_c$  baryon.

The  $\mu$ -RS plays an important role in enhancing the influence of the  $ND^*$  channel in the dynamics of the narrow  $\Lambda_{c(n)}^{0^-}(2595)$  state. Indeed, this scheme also produces a

<sup>4</sup>A more detailed discussion, incorporating some elements of group theory, can be found in [86] and in Subsection 6.4.1 of Chapter 7.

reduction in the mass of the resonance of around 200 MeV, which thus appears in the region of 2.6 GeV, instead of in the vicinity of the  $ND$  threshold. Indeed, we see also in Fig. 7.2 and Table 7.2 that if the UV behaviour of the amplitudes is renormalized by means of a common momentum cutoff of 650 MeV, the position of the  $j_q^P = 0^-$  pole in the  $J^P = 1/2^-$  sector moves up drastically, and it now appears at 2.8 GeV with little chances to be identified with the physical  $\Lambda_c(2595)$  state. It is still narrow, because HQSS prevents its coupling to  $\Sigma_c\pi$  to become large. However, the main features of the broad  $J^P = 3/2^-$  resonance and the  $j_q^P = 1^-$  one in the  $J = 1/2$  sector are not much affected by the change of renormalization scheme. The mass position of the latter resonance can be moved down to the vicinity of the  $\Sigma_c\pi$  threshold using cutoffs of the order of 750 MeV, still reasonable. At the same time its width also decreases since the available phase space for the decay becomes smaller. However, to obtain masses for the  $3/2^-$ -state of around 2625 MeV, significantly larger cutoffs of the order of 1200 MeV are needed. This might hint the existence of some further contributions to those induced for the baryon-meson unitarity loops, and that are effectively accounted for the somehow unnatural UV regulator. In this context, we will discuss in the next subsection effects produced by CQM degrees of freedom. In addition, the coupling  $|g_{\Sigma_c^*\pi}|$  would take values of around 1.6 leading to  $\Gamma[\Lambda_c(2625) \rightarrow \Lambda_c\pi\pi] \sim 0.7$  MeV from Eq. (7.10), 30% below the upper bound on the total width of the resonance. However, taking into account that the  $\Sigma_c^*$ -resonant contribution measured by the ARGUS Collaboration is  $(46 \pm 14)\%$  [375] of the total, we find that 0.7 MeV is around two sigmas above the inferred upper bound for the resonant mechanism. Note that using Eq. (7.10), the upper bound on the  $\Sigma_c^*$ -resonant contribution to the  $\Lambda_c(2625)$  width leads to

$$|g_{\Sigma_c^*\pi}| < 1.3 \pm 0.2 \quad (7.15)$$

We end up this discussion by studying the relation between cutoff and  $\mu$ -RS UV renormalization schemes. Results obtained in  $\mu$ -RS are recovered by using appropriate channel-dependent cutoffs as detailed in Eq. (3.102). These are 459 MeV, 544 MeV, 905 MeV and 1044 MeV for  $\pi\Sigma_c$ ,  $\pi\Sigma_c^*$ ,  $ND$  and  $ND^*$ , respectively. We see that the cutoff for  $ND^*$  is large and it enhances the importance of this channel in the dynamics of the narrow  $\Lambda_{c(n)}^{0^-}(2595)$  resonance found in the  $\mu$ -RS.

### 7.3.2 CQM and baryon-meson degrees of freedom

As mentioned in Subsec. 7.2.2, the quark model of Ref. [312] predicts a ( $J^P = 1/2^-, 3/2^-$ ) HQSS doublet of states, almost degenerate and with  $\overset{\circ}{M}_{\text{CQM}} \sim 2629$  MeV. Though with some precautions, because the CQM bare mass is not an observable and the matching procedure between the quark model and the effective hadron theory is not well defined, it seems natural to think that the bare CQM states should have an important

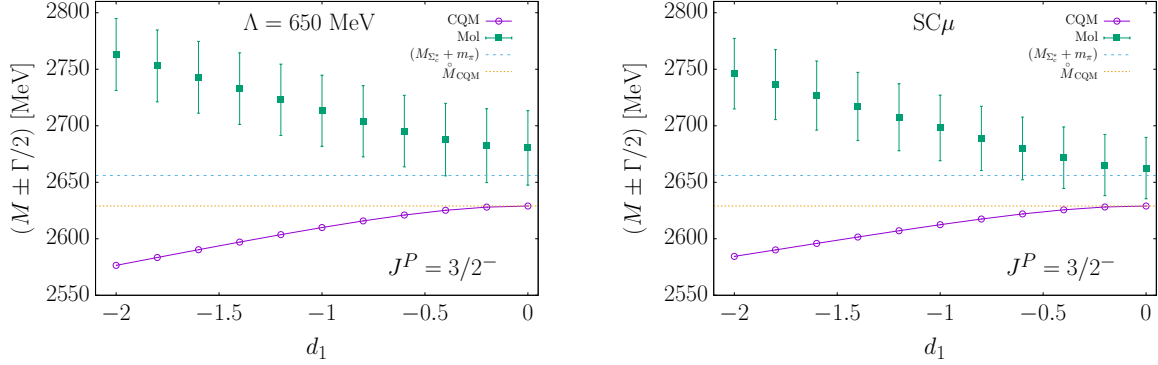


Figure 7.3: Dependence of the  $J^P = 3/2^-$  CQM and molecular pole positions as a function of the LEC  $d_1$ , for  $c_1 = 0$ . We show results for both, the cutoff and  $\mu$ -RS ( $\alpha = 0.95$ ) [SC- $\mu$  in the figure] renormalization schemes, and the values of the bare CQM mass and the  $\Sigma_c^* \pi$  threshold energy.

influence in the dynamics of the  $\Lambda_c(2595)$  and  $\Lambda_c(2625)$  resonances, which are located so close. Indeed, the baryon-meson interactions of Eq. (7.4), driven by the exchange of the CQM state, have a strong energy dependence close to  $\overset{\circ}{M}_{\text{CQM}} \sim 2629$  that might be difficult to accommodate by just modifying the real part of the unitarity loops. The LECs  $c_1$  and  $d_1$ , that control the interplay between bare CQM and baryon-meson degrees of freedom, are unknown. They are also renormalization scheme-dependent, and once the scheme is fixed, they should be inferred from data. The hope is that in this way, some theoretical predictions could become renormalization independent, at least in some energy window around the experimental inputs.

### The $\Lambda_c(2625)$

First we pay attention to the  $J^P = 3/2^-$  sector. In Figs. 7.3, 7.4 and 7.5, we show results obtained using  $\mu$ -RS ( $\alpha = 0.95$ ) or a common UV cutoff of 650 MeV for different CQM & baryon-meson couplings. In principle one expects that  $d_1$  should be more relevant than  $c_1$  because the  $\Sigma_c^* \pi$ -threshold is closer to  $\overset{\circ}{M}_{\text{CQM}}$  than the  $ND^*$  one. Thus, in a first stage we set  $c_1$  to zero and start varying  $d_1$ . Results are depicted in Fig. 7.3 (note that in this situation, the irreducible amplitudes depend on  $d_1^2$ ). There are now two poles in both renormalization schemes. The lightest one is located below the  $\Sigma_c^* \pi$ -threshold and it tends to  $\overset{\circ}{M}_{\text{CQM}}$  when  $d_1 \rightarrow 0$ . Its coupling to  $\Sigma_c^* \pi$ ,  $|g_{\Sigma_c^* \pi}|$ , grows from zero, when  $d_1 = 0$ , to values of around 1.8 or 1.9, when  $d_1 = -2$ , for the UV cutoff or  $\mu$ -RS renormalization schemes, respectively. The upper bound of Eq. (7.15) is not satisfied above  $|d_1| > 1.2(1.0)$  for the  $\Lambda = 650$  MeV ( $\mu$ -RS) scheme.

On the other hand, the second pole, located a higher masses, is a broad resonance,

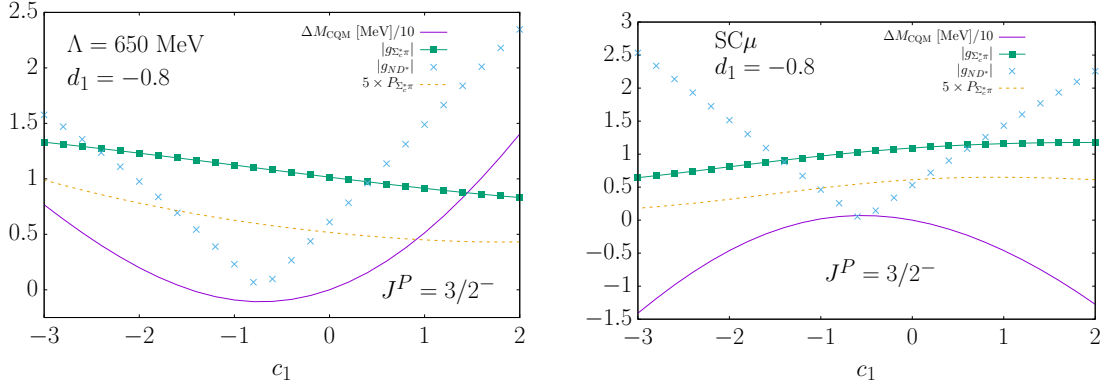


Figure 7.4: Dependence of the couplings, mass and  $\Sigma_c^* \pi$ -molecular probability of the  $J^P = 3/2^-$  dressed CQM pole as a function of the LEC  $c_1$ , for  $d_1 = -0.8$ . We show results for both, the cutoff and  $\mu$ -RS ( $\alpha = 0.95$ ) [SC- $\mu$  in the figure] renormalization schemes. In addition,  $\Delta M_{\text{CQM}} = [M_{\text{CQM}}(d_1) - M_{\text{CQM}}(d_1 = -0.8)]$ , with  $M_{\text{CQM}}(d_1 = -0.8) = 2615.81$  MeV and 2617.49 MeV for the left and right panels, respectively.

with a width of around 60 MeV and little sensitivity to  $d_1$ . Indeed, as can be seen in the figure, the width varies less than 2 (8) MeV in the UV cutoff ( $\mu$ -RS) scheme, when  $d_1$  changes from 0 to  $-2$ . The mass of this second resonance is more affected by  $d_1$ , and gets bigger when  $d_1^2$  increases, since the CQM exchange interaction is repulsive for energies above  $\overset{\circ}{M}_{\text{CQM}}$ . The pole matches the  $\text{SU}(6)_{\text{lsf}} \times \text{HQSS}$  molecular one discussed in Subsec. 7.3.1, when the coupling between CQM and baryon-meson degrees of freedom is switched off.

Within the non-relativistic CQM used in Ref. [315], the LEC  $d_1$  is predicted to be  $-0.8$ . With all cautions, already mentioned, about the matching between quark-models and hadron-hadron based images of the problem, and the dependence on the renormalization procedure, we will fix  $d_1$  to the latter value, and study the dependence of the previous results on  $c_1$ . We let this latter parameter vary in the range  $-3$  to  $2$  in Fig. 7.4, where the  $|g_{\Sigma_c^* \pi}|$  and  $|g_{ND^*}|$  couplings, the mass and  $\Sigma_c^* \pi$ -molecular probability of the  $J^P = 3/2^-$  dressed CQM pole are shown as a function of  $c_1$ . The molecular probability is defined through the Weinberg's compositeness, given by Eq. (3.114), which here we write as  $P_i$ , with  $i$  the channel. As can be seen in the left panel of the figure, the variation of the mass of the CQM pole with  $c_1$  is quite mild within the cutoff scheme. It changes only about 3 MeV,  $M_{\text{CQM}} \in [2614.7, 2617.8]$  MeV, when  $c_1$  varies in the  $[-2.0, 0.5]$  interval and, at most,  $M_{\text{CQM}}$  reaches values close to 2630 MeV for the largest positive values of  $c_1$  shown in the figure. At the same time  $|g_{\Sigma_c^* \pi}|$  goes from 1.3 down to 0.8 when  $c_1$  varies from  $-3$  to  $2$ . Hence, one can accommodate the experimental mass in the region of 2628 MeV, consistently

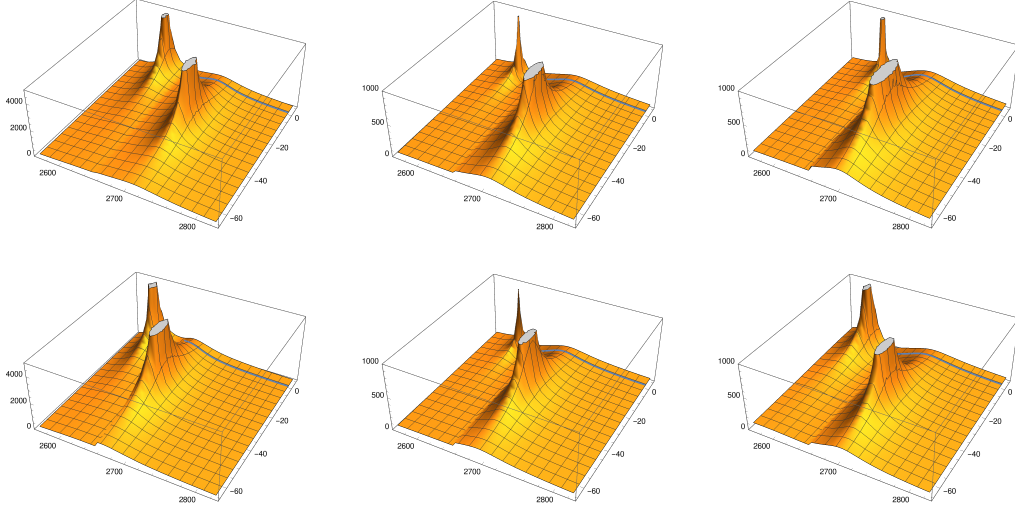


Figure 7.5: AVD- $T$  in the  $J^P = 3/2^-$  sector using two UV renormalization schemes :  $\mu$ -RS ( $\alpha = 0.95$ ) and a cutoff of 650 MeV in the bottom and top panels, respectively, for different CQM & baryon-meson pair couplings (from left to right):  $(c_1 = -3, d_1 = -0.8)$ ,  $(c_1 = 0, d_1 = -0.8)$  and  $(c_1 = 2, d_1 = -0.8)$ . We display the AVD- $T$  for both the FRS ( $\text{Im}(E) > 0$ ) and the SRS ( $\text{Im}(E) < 0$ ) [fm] of the unitarized amplitudes as a function of the complex energy  $E$  [MeV]. We also show the scattering line (blue solid curve) in all the cases. Axes are defined as in Fig. 7.2.

with the upper bound on the  $\Sigma_c^*$ -resonant contribution to the width discussed in Eq. (7.15). The molecular probability of this state would be small since  $P_{\Sigma_c^* \pi} \sim 0.1$ , reaching maximum values of about 0.2, when  $c_1$  is close to  $-3$ . Moreover, for this latter value of  $c_1$ ,  $P_{ND^*}$  is of the order of 0.04. When  $c_1$  increases,  $P_{ND^*}$  (not shown in the plot) continues decreasing and it becomes zero close to  $c_1 = 0.2$ . From this point,  $P_{ND^*}$  starts growing to reach values of the order of 0.08 for  $c_1 = 2$ . The coupling  $|g_{ND^*}|$ , displayed in the figure, follows a similar pattern, as expected.

Results obtained within the  $\mu$ -RS, shown in the right panel of Fig. 7.4, differ from those discussed above, but some qualitative features are similar. The  $P_{ND^*}$  and  $|g_{ND^*}|$  patterns, the small molecular probability and the mild dependence of  $M_{\text{CQM}}$  and  $|g_{\Sigma_c^* \pi}|$  on  $c_1$ . The maximum values obtained for the mass ( $\sim 2618$ ) of the state are found for  $c_1$  in the region of  $-0.8$ . Note however that the possible tension with the experimental mass of 2628.11 MeV is not really significant, since the agreement can be likely improved by changing the renormalization parameter  $\alpha$ .

In Table 7.1, we present together the properties of CQM and molecular  $J^P = 3/2^-$  poles, for  $d_1 = -0.8$  and  $c_1 = 0, 1$  and  $-1$ , and both renormalization schemes. The dressed CQM results of the table were already discussed in Fig. 7.4. The properties of the molecular state, that would have  $j_q^P = 1^-$  quantum-numbers, hardly depend

on  $c_1$  and both renormalization schemes predict a new state around 2.7 GeV and 60 MeV of width. The emergence of this new resonance, that would not be the  $\Lambda_c(2625)$ , can be clearly seen in the FRS and SRS plots of Fig. 7.5, where larger values of  $|c_1|$  than in Table 7.1 have been considered.

Hence, we conclude that the physical  $\Lambda_c(2625)$  finds naturally its origin in the CQM bare state obtained in Ref. [312], while we predict the existence of a molecular baryon, moderately broad, with a mass of about 2.7 GeV and sizable couplings to both  $\Sigma_c^* \pi$  and  $ND^*$ .

This latter pole will not show up in the experimental  $\Lambda_c \pi \pi$  spectrum, dominated by the physical resonance. Furthermore this state, mistakenly associated with the  $\Lambda_c(2625)$  in the previous  $SU(6)_{\text{lsf}} \times \text{HQSS}$  studies of Refs. [86, 172] where the coupling to CQM degrees of freedom was not considered, will be similar to that found in the chiral approach of Ref. [171] or to the  $\Sigma_c^* \pi$  pole reported in the ELHG scheme followed<sup>5</sup> in [85]. The  $SU(3)$  chiral approach of Ref. [340] reduces the mass of this molecular state down to that of the  $\Lambda_c(2625)$  by using a large UV cutoff of 2.13 GeV. This points out, following the arguments given in [352, 353], to the existence of some relevant degrees of freedom (CQM states and/or  $ND^*$  components) that are not properly accounted for in [340].

### The $\Lambda_c(2595)$

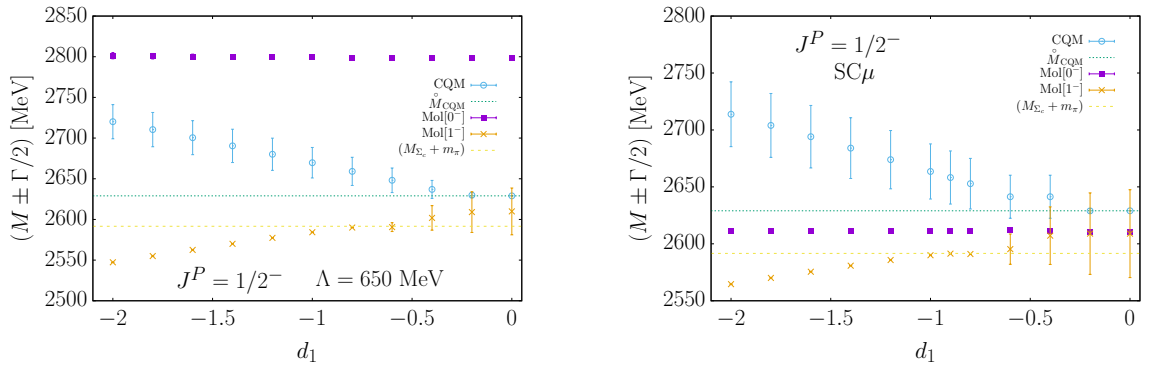


Figure 7.6: Dependence of the  $J^P = 1/2^-$  CQM and molecular pole positions as a function of the LEC  $d_1$ , for  $c_1 = 0$ . We show results for both, the cutoff and  $\mu$ -RS ( $\alpha = 0.95$ ) [SC- $\mu$  in the figure] renormalization schemes, and the values of the bare CQM mass and the  $\Sigma_c \pi$  threshold energy. Molecular states are labeled according to their dominant  $ldof$  configuration,  $0^-$  or  $1^-$ .

<sup>5</sup>In that work, it was not identified with the  $\Lambda_c(2625)$  resonance, which is generated there as a  $ND^*$  state, after modifying the ELHG  $ND^* \rightarrow ND^*$  potential including box-diagrams constructed out of the anomalous  $D^* D^* \pi$  coupling, and fitting the UV cutoffs to reproduce its mass.

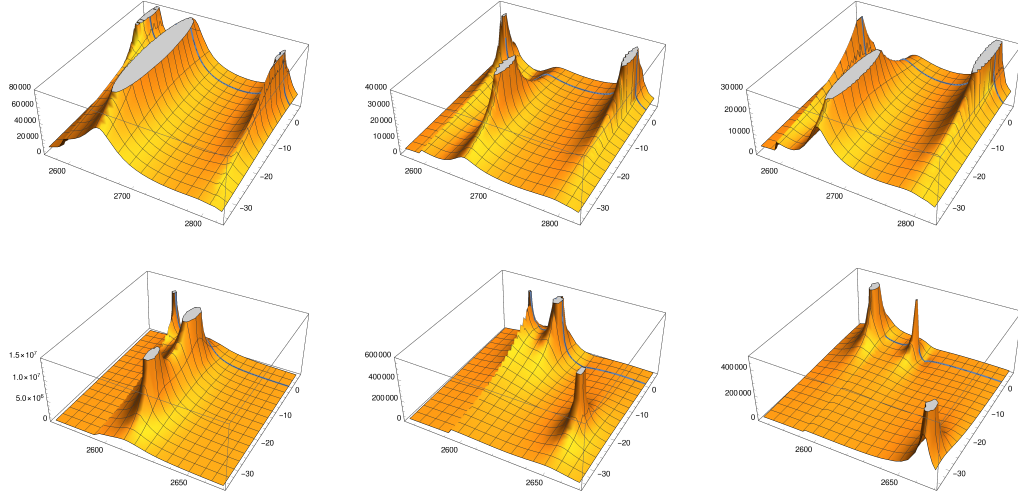


Figure 7.7: AVD- $T$  in the  $J^P = 1/2^-$  sector using two UV renormalization schemes :  $\mu$ -RS ( $\alpha = 0.95$ ) [SC- $\mu$  in the figure] and a cutoff of 650 MeV in the bottom and top panels, respectively, for different CQM & baryon-meson pair couplings (from left to right):  $(c_1 = -3, d_1 = -0.8)$ ,  $(c_1 = 0, d_1 = -0.8)$  and  $(c_1 = 2, d_1 = -0.8)$ . We display the AVD- $T$  for both the FRS ( $\text{Im}(E) > 0$ ) and the SRS ( $\text{Im}(E) < 0$ ) [fm] of the unitarized amplitudes as a function of the complex energy  $E$  [MeV]. We also show the scattering line (blue solid curve) in all the cases. Note that the range of  $\text{Re}(E)$  is much larger in the top panels than in the bottom ones. Axes are defined as in Fig. 7.2.

Now, we turn the discussion into the  $J^P = 1/2^-$  sector. As we did before, in a first stage we set  $c_1$  to zero and start varying  $d_1$ . Results are depicted in Fig. 7.6. There appear now three poles for both renormalization schemes considered in this Chapter. As compared to the case in the left panels of Fig. 7.2, where the coupling between CQM and baryon-meson degrees of freedom was switched off, there is an extra state which has its origin in the  $j_q^P = 1^-$  CQM bare state. The mass and the width of the narrow state at 2800 MeV ( $\Lambda = 650$  MeV) or 2610 MeV ( $\mu$ -RS) are practically unaltered by  $d_1$ . This is a trivial consequence of the largely dominant  $j_q^P = 0^-$  configuration of these states, since HQSS forbids their coupling to the  $j_q^P = 1^-$  CQM bare state.

The location of the second broad molecular state,  $[\Lambda_{c(b)}^{1^-}(2595)]$ , observed in Fig. 7.2 is strongly influenced by the quark-model state that produces an attraction that grows with  $d_1^2$ . Thus, for  $d_1 < -0.6$  or  $-0.7$ , depending of the renormalization procedure, it moves below the  $\Sigma_c\pi$  threshold and becomes a bound state. Within the  $\mu$ -RS, this  $j_q^P = 1^-$  molecular state would not be, however, identified with the physical  $\Lambda_c(2595)$  resonance, that would be reproduced by the narrow  $\Lambda_{c(n)}^{0^-}(2595)$  pole

at 2610-2611 MeV, with small  $|g_{\Sigma_c\pi}|$  coupling<sup>6</sup> and large  $|g_{ND}|$  and  $|g_{ND^*}|$  ones, especially the latter ( $\geq 6.2$ ). The situation is different in the UV cutoff scheme, since the  $j_q^P = 0^-$  narrow resonance is placed at 2800 MeV, and it is precisely the  $j_q^P = 1^-$  molecular state, the best candidate to describe the physical  $\Lambda_c(2595)$ .

In addition, we see in Fig. 7.6 that the bare CQM state is modified due to the baryon-meson loop effects, and it is moved to the complex plane acquiring also a finite width that obviously grows with  $d_1^2$ . The quantitative details, nevertheless, depend on renormalization scheme.

As in the  $\Lambda_c(2625)$  subsection, we fix  $d_1 = -0.8$  from the CQM of Ref. [315], and study in Table 7.2 and Fig. 7.7, the dependence of the spectrum of states on the LEC  $c_1$ . As expected, the mass position of the  $j_q^P = 0^-$  pole is hardly affected, while its small width depends much more on  $c_1$ . As mentioned above, within the  $\mu$ -RS scheme the physical  $\Lambda_c(2595)$  is identified with the  $\Lambda_{c(n)}^{0^-}(2595)$ . We see that the pole might have a coupling to the  $\Sigma_c\pi$ -pair smaller than 1, and thus it would be smaller than needed to reproduce the experimental width from Eq. (7.10). In the UV cutoff approach, instead, there would be a molecular narrow state close to the  $ND$  threshold, strongly coupled to it and that might provide some visible signatures in processes involving final state interactions of this baryon-meson pair (see bottom panels of Fig. 7.7). In this latter renormalization scheme, the  $\Lambda_c(2595)$  is described by the  $j_q^P = 1^-$  hadron molecule located below threshold at around 2590 MeV, little affected by  $c_1$ , and with  $|g_{\Sigma_c\pi}| \sim 1$ . Thus from Eq. (7.10), the  $\Lambda_c(2595) \rightarrow \Lambda\pi\pi$  width will be predicted to be around 1.8, in good agreement with experiment ( $2.6 \pm 0.6$ ). Nevertheless, the  $\Lambda_c(2595)$ , despite of having  $1^-$  quantum numbers for the  $ldof$ , would not be the HQSS partner of the  $\Lambda_c(2625)$  either in this case, because the predominantly quark-model structure of the latter. Indeed, the  $\Lambda_c(2595)$  would have a large molecular content,  $P_{\Sigma_c^*\pi} = 0.6 - 0.7$ .

Note that the  $j_q^P = 1^-$  state in the  $\mu$ -RS scheme will be irrelevant, since its effects will be completely overcome by those produced by the  $\Lambda_{c(n)}^{0^-}(2595)$  (see Fig. 7.7), independently it is placed below the  $\Sigma_c\pi$  threshold or it becomes a broad resonance.

The different inner structure of the  $\Lambda_c(2595)$  within the UV cutoff and  $\mu$ -RS schemes, and the dependence of this structure on  $c_1$  will lead to differences in  $ND$  and  $ND^*$  couplings that would produce different predictions for the exclusive semileptonic  $\Lambda_b \rightarrow \Lambda_c(2595)$  decay [3, 321].

Finally, we see that in both renormalization schemes we obtain the dressed CQM pole at masses around 2640–2660 MeV and with a width of the order of 30-50 MeV, depending on the chosen regulator and on  $c_1$ , though for moderate variations, one should not expect a large dependence on  $c_1$  because the  $ND$  and  $ND^*$  thresholds are not too close. This is a prediction of the present work, and this state should provide

<sup>6</sup>It decreases with  $d_1^2$  and it varies from 0.5 for  $d_1 = 0$  down to 0.04 for  $d_1 = -2$ .



signatures in the open channel  $\Sigma_c\pi$  since its coupling to this pair is sizable, well above one. As seen in Fig. 7.7, for large negative values<sup>7</sup> of  $c_1$  in the  $\mu$ -RS case, it could be, however, be shadowed by the  $\Lambda_{c(n)}^{0-}$ (2595) resonance.

### 7.3.3 Further comments

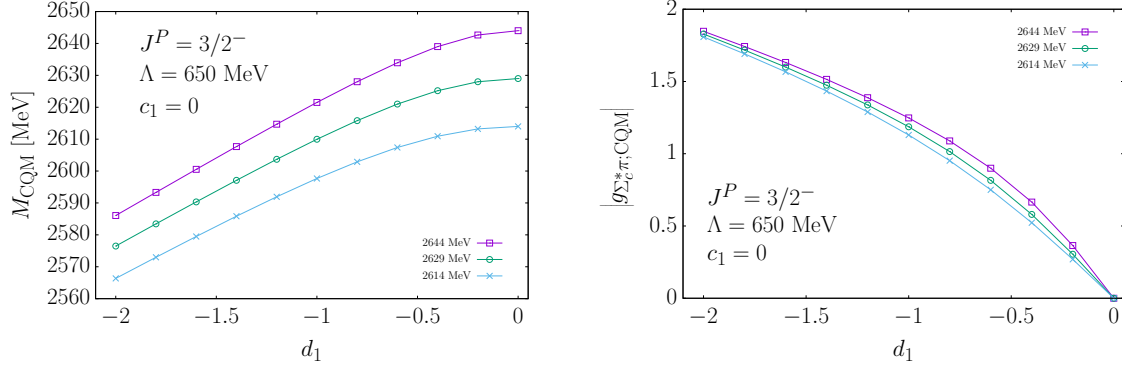


Figure 7.8: Mass (left) and coupling to  $\Sigma_c^*\pi$  (right) of the dressed CQM state as a function of the LEC  $d_1$ , for three different values of the mass of the bare CQM state,  $\bar{M}_{\text{CQM}} = 2544, 2529$  and  $2514$  MeV, in the  $J^P = 3/2^-$  sector. In addition, the LEC  $c_1$  has been fixed to zero. We show results obtained with the cutoff renormalization scheme.

Here, we briefly revisit and summarize some of the features/assumptions of the current approach that induce ambiguities in the main conclusions of this Chapter, which we will be collected in the next section. We also suggest, when possible, how the model dependence can be fixed by future measurements.

- The regularization of the loop function determines the off-shell behaviors of the amplitudes and leads to a model dependence, as we have put here of manifest by comparing the  $SC\mu$  and UV cutoff results. This source of systematic errors is ignored in most of the molecular approaches available in the literature. The existence of a narrow  $J^P = 1/2^-$  state close to the  $ND$  threshold would disentangle between these two renormalization schemes, since it will definitely favor the UV cutoff scheme. This state would show up in the  $\Sigma_c\pi$  spectrum through virtual  $ND$  and  $ND^*$  loops.
- The LECs  $c_1$  and  $d_1$ , that control the interplay between the bare CQM and the baryon-meson degrees of freedom are uncertain and are UV renormalization

<sup>7</sup>What it is really relevant is that the product  $c_1 d_1$  is positive.

scheme dependent parameters. Nevertheless, the results displayed in Fig. 7.3 for the  $J^P = 3/2^-$  higher mass resonance constrain considerably  $d_1$  (coupling between the bare CQM state and  $\Sigma_c\pi$ ). We find a sizable dependence of the mass of this state on  $d_1$  that can serve to fix this LEC in both renormalization schemes employed in this Chapter. Interestingly, we also observe that the mass and the width of this resonance do not depend drastically on the regularization method. We note that the range of values considered in Fig. 7.3 for  $|d_1|$  is sufficiently large, given that it is estimated to be around 0.8 in Ref. [315], using a framework compatible with the CQM employed in [312] from which we have taken  $\overset{\circ}{M}_{\text{CQM}}$ . Hence, we end up with a reasonably robust prediction for the existence of a  $J^P = 3/2^-$  molecular baryon, moderately broad ( $\Gamma \sim 60$  MeV), with a mass of about 2.7 GeV and sizable couplings to both  $\Sigma_c^*\pi$  and  $ND^*$ . The future observation of this resonance, additional to the  $\Lambda_c(2625)$ , would greatly limit the possible values of  $d_1$ .

The results shown in Fig. 7.3 were obtained for  $c_1 = 0$ , i.e. a vanishing coupling between the bare CQM state and the  $j_q^P = 1^-$ -component of the  $ND^*$  pair. Nevertheless, moderate non-zero values of this LEC do not modify appreciably the mass and the width of the higher  $J^P = 3/2^-$  resonance, as seen in Table 7.1. This is because this state is placed significantly far from the  $ND^*$  threshold. Indeed, most of the results found in this Chapter are little sensitive to  $c_1$ , because the  $ND$  and  $ND^*$  thresholds are far from  $\overset{\circ}{M}_{\text{CQM}}$ , mass of the bare three-quark state with  $j_q^P = 1^-$ , and in addition, the former meson-baryon pairs feel the strongest interaction in the  $j_q^P = 0^-$  channel, as discussed in Subsec. 7.2. This reduced dependence on  $c_1$  certainly make our results more robust<sup>8</sup>.

- The CQM  $j_q^P = 1^-$  bare mass,  $\overset{\circ}{M}_{\text{CQM}}$ , is also an UV renormalization scheme dependent parameter in our approach. We have fixed it to the value obtained in the state of the art CQM calculation of Ref. [312]. There, single- and double-heavy baryons were studied, with model parameters fixed by the strange baryon spectra, finding that the predictions for the masses of the observed charmed and bottomed baryons turned out to be in a fairly good agreement with experiment. The predictions for the  $\Lambda_c(2625)$  are the most sensitive to the choice of  $\overset{\circ}{M}_{\text{CQM}}$ , but even in this case, the properties of this resonance are reasonably stable in front of moderate variations of the mass of the bare CQM state, as can be seen in Fig. 7.8. In this latter figure, we show the produced changes in the mass (left) and coupling to  $\Sigma_c^*\pi$  (right) of the dressed  $J^P = 3/2^-$  CQM

<sup>8</sup>In any case as we mentioned, the position of the  $J^P = 1/2^-$  poles show certain dependence for very large values of  $c_1$  (see Fig. 7.7), which might be used to constrain this LEC.

state, as a function of the LEC  $d_1$ , when  $\overset{\circ}{M}_{\text{CQM}}$  is shifted by  $\pm 15$  MeV with respect to the value of 2529 MeV used here and taken from [312]. We see that as  $|d_1|$  increases the effect on the mass of the dressed state decreases. The  $J^P = 3/2^-$  higher mass resonance, located in the region of 2.7 GeV, is much less affected and for the largest  $|d_1| = 2$  coupling, its mass changes only at the level of 5 MeV, while it becomes 2-3 MeV wider (narrower) when  $\overset{\circ}{M}_{\text{CQM}} = 2614(2644)$  MeV is employed. These variations are comparable to those produced by  $c_1$ , as mentioned above.

## 7.4 Conclusions

We have shown that the  $\Lambda_c(2595)$  and the  $\Lambda_c(2625)$  are probably not HQSS partners. The  $J^P = 3/2^-$  resonance should be viewed mostly as a quark-model state naturally predicted to lie very close to its nominal mass [312]. This contradicts a large number of molecular scenarios suggested for this resonance in the literature. In addition, there will exist a molecular baryon, moderately broad, with a mass of about 2.7 GeV and sizable couplings to both  $\Sigma_c^* \pi$  and  $ND^*$ , that will fit into the expectations of being a  $\Sigma_c^* \pi$  molecule generated by the chiral interaction of this pair.

The  $\Lambda_c(2595)$  is predicted, however, to have a predominant molecular structure. This is because, it is either the result of the chiral  $\Sigma_c \pi$  interaction, which threshold is located much closer than the mass of the bare three-quark state, or because the  $ldof$  in its inner structure are coupled to the unnatural  $0^-$  quantum-numbers. The latter scenario is what happens in the  $\mu$ -RS renormalization scheme that enhances the influence of the  $ND^*$  channel in the dynamics of this narrow resonance. Attending to the three-body  $\Lambda_c(2595) \rightarrow \Lambda \pi \pi$  decay width, the  $\mu$ -RS scenario is slightly disfavored, and it looks more natural to assign a  $1^-$  configuration to the  $ldof$  content of the physical  $\Lambda_c(2595)$  state, as found when an UV cutoff is employed.

We also obtain a further  $J^P = 1/2^-$  resonance that is the result of dressing with baryon-meson loops the bare CQM pole. It would have a mass of around 2640–2660 MeV and a width of the order of 30-50 MeV. Finally, within the UV cutoff renormalization scheme, we also find a narrow state at 2800 MeV close to the  $ND$  threshold. This state has large  $ND$  and  $ND^*$  couplings and it should provide some visible signatures in processes involving final state interactions of the  $ND$  and  $ND^*$  pairs.

The spectrum found in this chapter cannot be easily understood in terms of HQSS, despite having used interactions that respect this symmetry. This is because the bare quark-model state and the  $\Sigma_c \pi$  threshold are located extraordinarily close to the  $\Lambda_c(2625)$  and  $\Lambda_c(2595)$ , respectively, and hence they play totally different roles in each sector. Note that  $(M_{\Sigma_c^*} - M_{\Sigma_c}) \sim 65$  MeV is around a factor of two larger than the  $\Lambda_c(2625) - \Lambda_c(2595)$  mass splitting. This does not fit well into a molecular picture

of these two resonances generated by  $\Sigma_c^{(*)}\pi$  chiral forces, and in addition the splitting found in the CQM study of Ref. [312] is only of 2 MeV, much smaller than any of the mass differences quoted above. Moreover, the  $\mu$ -RS renormalization scheme leads to an unexpected enhancing of the importance of the  $j_q^P = 0^-$  components of the  $SU(6)_{\text{sf}} \times \text{HQSS}$  interaction in the  $J^P = 1/2^-$  sector, which are driven by  $ND - ND^*$  coupled-channels interactions. This is not the case when an UV cutoff is employed.

# Chapter 8

## $\Xi_b$ and $\Xi_c$ as molecular states from extended Local Hidden Gauge

### 8.1 Introduction

In the present chapter we study, with the extended local hidden gauge formalism, in detail the  $\Xi_c$  and  $\Xi_b$  states from the molecular point of view. There are many  $\Xi_c$  states reported in the PDG [21] corresponding to excited states. One of the  $\Xi_c$  states,  $\Xi_c(2930)$ , first reported by the BaBar Collaboration [380], was recently confirmed with more statistics by the Belle Collaboration [381]. On the other hand, for  $\Xi_b$ , apart from the  $J^P = 1/2^+$  ground states,  $\Xi_b$ ,  $\Xi'_b$ , and the  $J^P = 3/2^+$   $\Xi_b^*$ , there are no states reported in the PDG [21]. Yet, the LHCb Collaboration has recently reported one such state, the  $\Xi_b(6227)$  [382], which we shall also investigate in the present work.

Recent studies of such states using QCD sum rules can be found in Refs. [383–386], where also reference to works on this particular issue is done, mostly on quark models. As to molecular states of this type we refer to the work of Ref. [86].

The experimental finding of five new excited  $\Omega_c$  states by the LHCb Collaboration [348] (see also Ref. [387]) stimulated new work along the molecular line and in Ref. [351] a study was done of coupled channels interaction using an extension to SU(4) of the chiral Lagrangians. The interesting result from this work was that two states could be interpreted as  $1/2^-$  resonances and the mass and width were well reproduced. This is a non trivial achievement since in other approaches mostly masses are studied and not widths. Some quark models go one step forward and using the  $^3P_0$  model also evaluate widths, as in Ref. [78]. The fact that the widths obtained are quite different than in the molecular model is a positive sign that the study of the widths, and partial decay widths of these resonances, carry valuable information

concerning their nature.

The work of Ref. [351], with vector meson exchange in an extension to SU(4) of the chiral Lagrangians, got a boost from Ref. [388], where it was shown that the relevant matrix elements of the interaction can be obtained considering the exchange of light vector mesons in an extension of the local hidden gauge approach [134–138], where the heavy quarks were mere spectators, such that there was no need to invoke SU(4) and one could make a mapping of the SU(3) results where the local hidden gauge approach was developed. Like in Ref. [351], in Ref. [388] the same two states were obtained with similar widths, and in addition there was another state reproduced with  $3/2^-$ , which was not addressed in [351]. Similar results were then obtained in Ref. [6] with a continuation of the work of Ref. [86] with parameters adjusted to input from the experiment of Ref. [348].

The former results stimulated further work along these lines with predictions for  $\Omega_b$  states in Ref. [350], for which there are not yet experimental counterparts. Encouraged by the success in the  $\Omega_c$  states, in the present work we follow this line of research to study  $\Xi_c$  and  $\Xi_b$  states. In the first case there are several states to compare with our predictions, and in the second case only one excited state, such that many of the states found will be predictions to be tested with future experiments.

Related to these works is the study of the  $\Xi_{cc}$  molecular states in Ref. [389], stimulated by the new measurement of the  $\Xi_{cc}$  by the LHCb Collaboration, with a mass of 3621 MeV [390]. This value is higher than that previously measured by the SELEX Collaboration [391, 392]. However, this first measurement by SELEX was not confirmed by the FOCUS [393], Belle [394], BABAR [395] and the LHCb [396] Collaborations. Using the value of the new measurement of the LHCb Collaboration [390], molecular  $\Xi_{cc}$  states were studied in Ref. [389], where excited bound states were found above 4000 MeV and broad  $\Xi_{cc}\pi$  and  $\Xi_{cc}^*\pi$  resonances were found around 3837 and 3918 MeV, respectively.

With all this recent experimental activity there is much motivation to make predictions with different models which can serve as potential guide for experimental set ups and finally to deepen our understanding of the nature of the baryon resonances.

This chapter is based on Ref. [5].

## 8.2 Formalism

Recently two new resonances, the  $\Xi_c(2930)$  ( $J=?^?$ ) and the  $\Xi_b(6227)$  ( $J=?^?$ ), have been measured by the Belle [381] and LHCb [382] Collaborations, respectively. Besides these, there is also an abundance of other unexplained resonances in the charm sector [21]:  $\Xi_c(2790)$  ( $J = 1/2^-$ ),  $\Xi_c(2815)$  ( $J = 3/2^-$ ),  $\Xi_c(2970)$  ( $J=?^?$ ),  $\Xi_c(3055)$  ( $J=?^?$ ),  $\Xi_c(3080)$  ( $J=?^?$ ) and  $\Xi_c(3123)$  ( $J=?^?$ ). The objective of this work is to shed some

light into the nature of these states and to explain at least some of them within the hadronic molecular picture. For that, we shall use an extension of the chiral unitary approach with coupled channels outlined in Ref. [388], since as we shall see, only the light quarks play a relevant role in the interaction. As in Ref. [388], we will separate the interaction into pseudoscalar meson-baryon( $1/2^+$ ) ( $PB$ ), vector meson-baryon( $1/2^+$ ) ( $VB$ ) and pseudoscalar meson-baryon( $3/2^+$ ) ( $PB^*$ ). One should mention that in this theory, these three sectors do not decay into each other, because that would require the exchange of pseudoscalar mesons, and those transitions are momentum-dependent and small compared to the ones with a vector meson exchange [349,388]. Analyzing the spin-parity of each sector, we find that for the states that arise from  $PB$  we have  $J^P = 0^- \otimes 1/2^+ = 1/2^-$ , for  $VB$  we have degenerate states  $J^P = 1^- \otimes 1/2^+ = 1/2^-, 3/2^-$  and for  $PB^*$  we have  $J^P = 0^- \otimes 3/2^+ = 3/2^-$ . In Tables 8.1 to 8.3 we show, for the charm sector, the channels chosen for the  $PB$ ,  $VB$  and  $PB^*$  sectors. To get the channels for the beauty sector, one needs only to substitute the  $c$  quark by a  $b$  quark, and we show the results in tables 8.4 to 8.6.

$\Xi_c\pi$	$\Xi'_c\pi$	$\Lambda_c\bar{K}$	$\Sigma_c\bar{K}$	$\Lambda D$	$\Xi_c\eta$	$\Sigma D$	$\Xi'_c\eta$	$\Omega_c K$	$\Xi D_s$
2607	2716	2782	2949	2983	3017	3060	3126	3191	3287

Table 8.1: Charm sector channels with  $J^P = 1/2^-$  and respective thresholds (in MeV).

$\Lambda D^*$	$\Lambda_c\bar{K}^*$	$\Sigma D^*$	$\Xi_c\rho$	$\Xi_c\omega$	$\Sigma_c\bar{K}^*$
3124	3182	3202	3245	3252	3349

Table 8.2: Charm sector channels with  $J^P = 1/2^-, 3/2^-$  and respective thresholds (in MeV).

$\Xi_c^*\pi$	$\Sigma_c^*\bar{K}$	$\Xi_c^*\eta$	$\Sigma^*D$	$\Omega_c^*K$
2784	3014	3194	3252	3262

Table 8.3: Charm sector channels with  $J^P = 3/2^-$  and respective thresholds (in MeV).

$\Xi_b\pi$	$\Xi'_b\pi$	$\Lambda_b\bar{K}$	$\Sigma_b\bar{K}$	$\Lambda\bar{B}$	$\Xi_b\eta$	$\Sigma\bar{B}$	$\Xi'_b\eta$	$\Omega_b K$	$\Xi B_s$
5931	6073	6115	6309	6395	6341	6473	6483	6542	6685

Table 8.4: Beauty sector channels with  $J^P = 1/2^-$  and respective thresholds (in MeV).

In this work, the kernel will be calculated using an extension of the local hidden gauge approach (LHG), which produces Feynman diagrams of the type shown in

$\Lambda\bar{B}^*$	$\Lambda_b\bar{K}^*$	$\Sigma\bar{B}^*$	$\Xi_b\rho$	$\Xi_b\omega$	$\Sigma_b\bar{K}^*$
6440	6515	6518	6568	6576	6709

Table 8.5: Beauty sector channels with  $J^P = 1/2^-, 3/2^-$  and respective thresholds (in MeV).

$\Xi_b^*\pi$	$\Sigma_b^*\bar{K}$	$\Xi_b^*\eta$	$\Sigma^*\bar{B}$	$\Omega_b^*K$
6091	6329	6500	6664	6567

Table 8.6: Beauty sector channels with  $J^P = 3/2^-$  and respective thresholds (in MeV).

Fig. 8.1, that is, the initial meson baryon pair goes into the final pair through the exchange of a vector meson in the  $t$ -channel.

In the  $PB$  case, the meson-meson interaction (the upper vertex in Fig. 8.1) is given by the  $VPP$  Lagrangian in Eq. (2.33), where here the matrices  $\Phi$  and  $V^\mu$  are the SU(4) pseudoscalar meson and vector meson flavor matrices, respectively. Note that the original  $\mathcal{L}_{VPP}$  interaction obeys SU(3) flavor symmetry, but just like in Ref. [388], we extend it to SU(4) to take into account the  $c$  ( $b$ ) quark. The meson matrices are thus

$$\Phi = \begin{pmatrix} \frac{1}{\sqrt{2}}\pi^0 + \frac{1}{\sqrt{3}}\eta + \frac{1}{\sqrt{6}}\eta' & \pi^+ & K^+ & \bar{D}^0 \\ \pi^- & -\frac{1}{\sqrt{2}}\pi^0 + \frac{1}{\sqrt{3}}\eta + \frac{1}{\sqrt{6}}\eta' & K^0 & D^- \\ K^- & \bar{K}^0 & -\frac{1}{\sqrt{3}}\eta + \sqrt{\frac{2}{3}}\eta' & D_s^- \\ D^0 & D^+ & D_s^+ & \eta_c \end{pmatrix}, \quad (8.1)$$

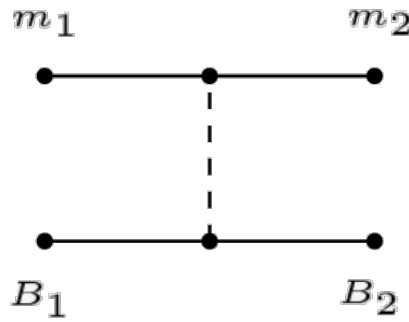


Figure 8.1: Example of a type of diagram that arises from the LHG.



and

$$V = \begin{pmatrix} \frac{1}{\sqrt{2}}\rho^0 + \frac{1}{\sqrt{2}}\omega & \rho^+ & K^{*+} & \bar{D}^{*0} \\ \rho^- & -\frac{1}{\sqrt{2}}\rho^0 + \frac{1}{\sqrt{2}}\omega & K^{*0} & \bar{D}^{*-} \\ K^{*-} & \bar{K}^{*0} & \phi & D_s^{*-} \\ D^{*0} & D^{*+} & D_s^{*+} & J/\Psi \end{pmatrix}. \quad (8.2)$$

The use of SU(4) here is a formality. We shall see later that the dominant terms are due to the exchange of light vectors, where the heavy quark are spectators. Then Eq. (2.33) automatically projects over SU(3). The terms with the exchange of a heavy vector are very suppressed, as we shall see. In principle, in this case one would be using explicitly SU(4), however, as seen in Ref. [397], since the matrices  $\phi$  and  $V$  stand for  $q\bar{q}$ , Eq. (2.33) actually only measures the quark overlap of  $\phi$  and  $V$  and possible  $q$  vector structure, hence, the role of SU(4) is just a final counting of the number of quarks. The lower vertex  $V^\mu BB$  does not rely on SU(4) either, as we see below.

Now, for the lower vertex in Fig. 8.1, the interaction in SU(3) can be described by the following Lagrangian [296]

$$\mathcal{L}_{VBB} = g \left( \bar{B} \gamma_\mu [V^\mu, B] + \langle \bar{B} \gamma_\mu B \rangle \langle V^\mu \rangle \right), \quad (8.3)$$

where  $B$  is the SU(3) baryon matrix, and  $V$  the  $3 \times 3$  part of  $V$  in Eq. (8.2) containing  $\rho$ ,  $\omega$ ,  $K^*$ ,  $\phi$ . Here we do a non-relativistic approximation, which consists in substituting  $\gamma^\mu \rightarrow \gamma^0$ . The extension to the charm or bottom sectors is done without relying on SU(4) as explained below. As discussed in Refs. [388, 389], it can be shown that the same interaction in SU(3) of Eq. (8.3) can be obtained considering an operator at the quark level, such that Eq. (8.3) becomes

$$\mathcal{L}_{VB_f B_i} = g \langle B_f | V_{ql} | B_i \rangle, \quad (8.4)$$

where  $|B_i\rangle$ ,  $|B_f\rangle$  are the initial and final baryon spin-flavor wave functions with the following structure,

$$|B\rangle = |\phi_{\text{flavor}}\rangle \otimes |\chi_{\text{spin}}\rangle, \quad (8.5)$$

and  $V_{ql}$  is the quark operator of the exchanged vector meson, which, for example, for the diagonal ones in Eq. (8.2) is

$$\rho^0 = \frac{1}{\sqrt{2}}(u\bar{u} - d\bar{d}), \quad (8.6a)$$

$$\omega = \frac{1}{\sqrt{2}}(u\bar{u} + d\bar{d}), \quad (8.6b)$$

$$\phi = s\bar{s}. \quad (8.6c)$$

The states described by Eq. (8.5) are constructed using only SU(3) symmetry, taking the heavy quark as a spectator, which implies that all diagonal terms are described through the exchange of light vectors, respecting heavy quark spin symmetry.

The states that we will be using in the  $PB$  sector are constructed using the method outlined in Ref. [208], but with the necessary changes in phases in order to obey the sign notation in Ref. [8,306], which is consistent with the chiral matrices. Doing this we obtain the following states:

$$|\Xi_c^+\rangle = \left| \frac{1}{\sqrt{2}} c(us - su) \right\rangle |\chi_{MA}\rangle, \quad |\Xi_c^0\rangle = \left| \frac{1}{\sqrt{2}} c(ds - sd) \right\rangle |\chi_{MA}\rangle, \quad (8.7a)$$

$$|\Xi_c'^+\rangle = \left| \frac{1}{\sqrt{2}} c(us + su) \right\rangle |\chi_{MS}\rangle, \quad |\Xi_c'^0\rangle = \left| \frac{1}{\sqrt{2}} c(ds + sd) \right\rangle |\chi_{MS}\rangle, \quad (8.7b)$$

$$|\Lambda_c^+\rangle = \left| \frac{1}{\sqrt{2}} c(ud - du) \right\rangle |\chi_{MA}\rangle, \quad |\Sigma_c^{++}\rangle = |cuu\rangle |\chi_{MS}\rangle, \quad (8.7c)$$

$$|\Sigma_c^+\rangle = \left| \frac{1}{\sqrt{2}} c(ud + du) \right\rangle |\chi_{MS}\rangle, \quad |\Sigma_c^0\rangle = |c\bar{d}d\rangle |\chi_{MS}\rangle, \quad (8.7d)$$

$$|\Lambda^0\rangle = \frac{1}{\sqrt{2}} (|\phi_{MS}\rangle |\chi_{MS}\rangle + |\phi_{MA}\rangle |\chi_{MA}\rangle),$$

$$|\phi_{MS}\rangle = \frac{1}{2} (|dus\rangle + |dsu\rangle - |uds\rangle - |usd\rangle),$$

$$|\phi_{MA}\rangle = \frac{1}{2\sqrt{3}} (|u(ds - sd)\rangle + |d(su - us)\rangle - 2|s(ud - du)\rangle), \quad (8.7e)$$

$$|\Sigma^+\rangle = \frac{1}{\sqrt{2}} (|\phi_{MS}\rangle |\chi_{MS}\rangle + |\phi_{MA}\rangle |\chi_{MA}\rangle),$$

$$|\phi_{MS}\rangle = -\frac{1}{\sqrt{6}} (|u(us + su)\rangle - 2|suu\rangle),$$

$$|\phi_{MA}\rangle = \frac{1}{\sqrt{2}} |u(su - us)\rangle, \quad (8.7f)$$

$$|\Sigma^0\rangle = \frac{1}{\sqrt{2}} (|\phi_{MS}\rangle |\chi_{MS}\rangle + |\phi_{MA}\rangle |\chi_{MA}\rangle),$$

$$|\phi_{MS}\rangle = \frac{1}{2\sqrt{3}} (|u(ds + sd)\rangle + |d(su + us)\rangle - 2|s(du + ud)\rangle),$$

$$|\phi_{MA}\rangle = \frac{1}{2} (|u(ds - sd)\rangle - |d(su - us)\rangle), \quad (8.7g)$$

$$|\Sigma^-\rangle = \frac{1}{\sqrt{2}} (|\phi_{MS}\rangle |\chi_{MS}\rangle + |\phi_{MA}\rangle |\chi_{MA}\rangle),$$

$$|\phi_{MS}\rangle = \frac{1}{\sqrt{6}} (|d(ds + sd)\rangle - 2|sdd\rangle),$$

$$|\phi_{MA}\rangle = \frac{1}{2}|d(ds - sd)\rangle, \quad (8.7h)$$

$$|\Omega_c^0\rangle = |css\rangle|\chi_{MS}\rangle, \quad (8.7i)$$

$$|\Xi^0\rangle = \frac{1}{\sqrt{2}}(|\phi_{MS}\rangle|\chi_{MS}\rangle + |\phi_{MA}\rangle|\chi_{MA}\rangle),$$

$$|\phi_{MS}\rangle = \frac{1}{\sqrt{6}}(|s(us + su)\rangle - 2|uss\rangle),$$

$$|\phi_{MA}\rangle = -\frac{1}{2}|s(us - su)\rangle, \quad (8.7j)$$

$$|\Xi^-\rangle = \frac{1}{\sqrt{2}}(|\phi_{MS}\rangle|\chi_{MS}\rangle + |\phi_{MA}\rangle|\chi_{MA}\rangle),$$

$$|\phi_{MS}\rangle = -\frac{1}{\sqrt{6}}(|s(ds + sd)\rangle - 2|dss\rangle),$$

$$|\phi_{MA}\rangle = \frac{1}{2}|s(ds - sd)\rangle. \quad (8.7k)$$

Here, the  $|\chi_{MS}\rangle$  and  $|\chi_{MA}\rangle$  are the mixed-symmetric and mixed-antisymmetric spin states, respectively, which, together with the symmetric,  $|\chi_S\rangle$ , and antisymmetric,  $|\chi_A\rangle$ , states, form an orthogonal basis, such that

$$\langle\chi_i|\chi_j\rangle = \delta_{ij}. \quad (8.8)$$

Now we need to go from the charge basis to the isospin basis. When calculating the isospin states, one needs to pay attention to the phases that come from the following isospin multiplets:

$$\begin{aligned} \Xi &= \begin{pmatrix} \Xi^0 \\ -\Xi^- \end{pmatrix}; & \pi &= \begin{pmatrix} -\pi^+ \\ \pi^0 \\ \pi^- \end{pmatrix}; \\ \bar{K} &= \begin{pmatrix} \bar{K}^0 \\ -K^- \end{pmatrix}; & \Sigma &= \begin{pmatrix} -\Sigma^+ \\ \Sigma^0 \\ \Sigma^- \end{pmatrix}; \\ D &= \begin{pmatrix} D^+ \\ -D^0 \end{pmatrix}; & \rho &= \begin{pmatrix} -\rho^+ \\ \rho^0 \\ \rho^- \end{pmatrix}. \end{aligned}$$

Then, for the isospin states we obtain:

1.  $|\Xi_c \pi\rangle = \sqrt{\frac{2}{3}}|\Xi_c^0 \pi^+\rangle + \sqrt{\frac{1}{3}}|\Xi_c^+ \pi^0\rangle,$
2.  $|\Xi'_c \pi\rangle = \sqrt{\frac{2}{3}}|\Xi'^0_c \pi^+\rangle + \sqrt{\frac{1}{3}}|\Xi'^+_c \pi^0\rangle,$
3.  $|\Lambda_c \bar{K}\rangle = |\Lambda^+_c \bar{K}^0\rangle,$
4.  $|\Sigma_c \bar{K}\rangle = -\left(\sqrt{\frac{2}{3}}|\Sigma^{++}_c \bar{K}^-\rangle + \sqrt{\frac{1}{3}}|\Sigma^+_c \bar{K}^0\rangle\right),$
5.  $|\Lambda D\rangle = |\Lambda^0 D^+\rangle,$
6.  $|\Xi_c \eta\rangle = |\Xi^+_c \eta\rangle,$
7.  $|\Sigma D\rangle = \sqrt{\frac{2}{3}}|\Sigma^+ D^0\rangle - \sqrt{\frac{1}{3}}|\Sigma^0 D^+\rangle,$
8.  $|\Xi'_c \eta\rangle = |\Xi'^+_c \eta\rangle,$
9.  $|\Omega_c \eta\rangle = |\Omega^0_c K^+\rangle,$
10.  $|\Xi D_s\rangle = |\Xi^0 D^+_s\rangle.$

For the  $VB$  sector, the upper vertex of the three vector meson interaction is given by Eq. (2.36) and for the lower vertex we again use Eq. (8.4).

Finally, for the  $PB^*$  sector, for the upper vertex we will use again the  $VPP$  interaction given by Eq. (2.33). Since from Eq. (8.3) to Eq. (8.4) we have made the approximation that  $\gamma^\mu \rightarrow \gamma^0$ , this makes Eq. (8.4) spin independent and as such, we can still use it for the  $VB^*B^*$  vertices. Additionally, we have, for the  $B^*$  baryons, the following spin-flavor states:

1.  $|\Xi_c^{*+}\rangle = \left|\frac{1}{\sqrt{2}}c(us + su)\right\rangle|\chi_S\rangle,$
2.  $|\Xi_c^{*0}\rangle = \left|\frac{1}{\sqrt{2}}c(ds + sd)\right\rangle|\chi_S\rangle,$
3.  $|\Omega_c^*\rangle = |css\rangle|\chi_S\rangle,$
4.  $|\Sigma_c^{*++}\rangle = |cuu\rangle|\chi_S\rangle,$
5.  $|\Sigma_c^{*+}\rangle = \left|\frac{1}{\sqrt{2}}c(ud + du)\right\rangle|\chi_S\rangle,$
6.  $|\Sigma_c^{*0}\rangle = |cdd\rangle|\chi_S\rangle,$
7.  $|\Sigma^{*+}\rangle = \frac{1}{\sqrt{3}}|u(su + us) + suu\rangle|\chi_S\rangle,$
8.  $|\Sigma^{*0}\rangle = \frac{1}{\sqrt{6}}|s(du + ud) + d(su + us) + u(sd + ds)\rangle|\chi_S\rangle,$
9.  $|\Sigma^{*-}\rangle = \frac{1}{\sqrt{3}}|d(sd + ds) + sdd\rangle|\chi_S\rangle.$

The isospin states for the  $VB$  and  $PB^*$  cases are similar to the ones of the  $PB$  case.

All these Lagrangians will give the WT kernels of Eq. (3.42) [296, 388]. Here, we define  $D_{ij} = -C_{ij}$ , and also  $f \rightarrow f_\pi = 93$  MeV. In the case of the  $VB$  interaction we get the same kernel, even though the  $VVV$  vertex is described by a different Lagrangian. Actually the meson baryon chiral lagrangians [398, 399] can be obtained from the local hidden gauge approach neglecting the  $(p/m_V)^2$  term in the exchanged vectors [139]. Then, the kernel will be the same as in Eq. (3.42) with an extra  $\vec{\epsilon} \cdot \vec{\epsilon}'$  factor, due to the polarizations of the initial and final vector mesons, which can be factorized in the Bethe-Salpeter equation. This means that the equation is spin independent, and that is why we find degenerate states with  $J^P = 1/2^-$  and  $J^P = 3/2^-$  with this interaction [349]. Because of this we can just omit that factor.

One can also add relativistic corrections to Eq. (3.42) using Eq. (3.41).

Finally, the  $D_{ij}$  coefficients are calculated using the interactions in Eqs. (2.33) and (8.4), and the obtained results are illustrated in Tables 8.7, 8.8 and 8.9 for  $PB$ ,  $VB$  and  $PB^*$  sectors respectively.

$J_B = 1/2$	$\Xi_c \pi$	$\Xi'_c \pi$	$\Lambda_c \bar{K}$	$\Sigma_c \bar{K}$	$\Lambda D$	$\Xi_c \eta$	$\Sigma D$	$\Xi'_c \eta$	$\Omega_c K$	$\Xi D_s$
$\Xi_c \pi$	-2	0	$-\sqrt{\frac{3}{2}}$	0	$\frac{1}{2\sqrt{2}}\lambda$	0	$-\frac{1}{2\sqrt{2}}\lambda$	0	0	0
$\Xi'_c \pi$		-2	0	$-\frac{1}{\sqrt{2}}$	$-\frac{3}{2\sqrt{6}}\lambda$	0	$-\frac{1}{2\sqrt{6}}\lambda$	0	$-\sqrt{3}$	0
$\Lambda_c \bar{K}$			-1	0	$-\frac{1}{\sqrt{3}}\lambda$	$\frac{2}{\sqrt{3}}$	0	0	0	0
$\Sigma_c \bar{K}$				-3	0	0	$-\frac{1}{\sqrt{3}}\lambda$	-2	0	0
$\Lambda D$					-1	$-\frac{1}{6}\lambda$	0	$\frac{1}{2\sqrt{3}}\lambda$	0	$-\frac{\sqrt{6}}{2}$
$\Xi_c \eta$						0	$-\frac{1}{2}\lambda$	0	0	$\frac{1}{\sqrt{6}}\lambda$
$\Sigma D$							-3	$-\frac{1}{2\sqrt{3}}\lambda$	0	$-\sqrt{\frac{3}{2}}$
$\Xi'_c \eta$								0	$-\frac{2\sqrt{6}}{3}$	$-\frac{1}{3\sqrt{2}}\lambda$
$\Omega_c K$									-2	$-\frac{1}{\sqrt{3}}\lambda$
$\Xi D_s$										-2

Table 8.7:  $D_{ij}$  coefficients for the  $PB$  states coupling to  $J^P = 1/2^-$ .

$J_B = 1/2$	$\Lambda D^*$	$\Lambda_c \bar{K}^*$	$\Sigma D^*$	$\Xi_c \rho$	$\Xi_c \omega$	$\Sigma_c \bar{K}^*$
$\Lambda D^*$	-1	$-\frac{1}{\sqrt{3}}\lambda$	0	$\frac{1}{2\sqrt{2}}\lambda$	$-\frac{1}{2\sqrt{6}}\lambda$	0
$\Lambda_c \bar{K}^*$		-1	0	$-\sqrt{\frac{3}{2}}$	$\frac{1}{\sqrt{2}}$	0
$\Sigma D^*$			-3	$-\frac{1}{2\sqrt{2}}\lambda$	$-\frac{1}{2\sqrt{6}}\lambda$	$-\frac{1}{\sqrt{3}}\lambda$
$\Xi_c \rho$				-2	0	0
$\Xi_c \omega$					0	0
$\Sigma_c \bar{K}^*$						-3

Table 8.8:  $D_{ij}$  coefficients for the  $VB$  states coupling to  $J^P = 1/2^-, 3/2^-$ .

$J_B = 3/2$	$\Xi_c^* \pi$	$\Sigma_c^* \bar{K}$	$\Xi_c^* \eta$	$\Sigma^* D$	$\Omega_c^* K$
$\Xi_c^* \pi$	-2	$-\frac{1}{\sqrt{2}}$	0	$-\frac{1}{\sqrt{6}}\lambda$	$-\sqrt{3}$
$\Sigma_c^* \bar{K}$		-3	-2	$\frac{1}{\sqrt{3}}\lambda$	0
$\Xi_c^* \eta$			0	$-\frac{1}{\sqrt{3}}\lambda$	$-\frac{2\sqrt{6}}{3}$
$\Sigma^* D$				-3	0
$\Omega_c^* K$					-2

Table 8.9:  $D_{ij}$  coefficients for the  $PB^*$  states coupling to  $J^P = 3/2^-$ .

Note the factor  $\lambda$  in some of the nondiagonal terms. This factor was added to the terms in the interaction that have an exchange of a heavy vector meson. One can understand this by looking at the propagator of the vector meson ( $V_H$ ) when, in

Fig. 8.1, the upper vertex is of the type  $LV_H H$ , with  $H$ ,  $V_H$  heavy mesons, and  $L$  a light meson (see Fig. 8.2). Then, the propagator will be,

$$\Delta \sim \frac{1}{q^2 - m_{V_H}^2}, \quad (8.9)$$

with  $q$  the transferred momentum. Since  $V_H$  is heavy, we can take  $\vec{q} \simeq 0$  and

$$\Delta \sim \frac{1}{(q^0)^2 - m_{V_H}^2} \simeq \frac{1}{(m_H - m_L)^2 - m_{V_H}^2}, \quad (8.10)$$

where we also have used that  $\vec{p}_H \simeq 0$  and  $\vec{p}_L \simeq \vec{q} \simeq 0$ . In the calculation of the amplitudes in Eq. (3.42), we end up with a factor, which is relative to the exchange of the light vector

$$\lambda = -m_V^2 \Delta \simeq \frac{-m_V^2}{(m_H - m_L)^2 - m_{V_H}^2}, \quad (8.11)$$

with  $m_V = 800 \text{ MeV}$ . In the case of heavy vector exchange, because  $m_{V_H} > m_V$ , the  $\lambda$  will be smaller and of the order of  $\lambda \simeq 1/4$  [338, 388]. We can check that, for the case of  $\bar{K} \rightarrow D$  with  $D_s^*$  exchange, one gets  $\lambda \simeq 0.25$ . For more details on how to calculate the kernel of the interaction we refer the reader to the Appendix of Ref. [389].

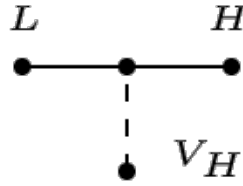


Figure 8.2: Diagram of  $L \rightarrow H$  vertex with  $V_H$  emission, where  $L$  is a light meson,  $H$  a heavy meson and  $V_H$  a heavy vector meson.

Since the  $\Xi_c$  and  $\Xi_b$  states are heavy quark states, one should comment on how our model deals with HQSS. For that, one should note that, with the exception of the vertices with the  $\lambda$ , in all other vertices the heavy quark behaves as a spectator, which guarantees that the dominant terms (in the  $1/m_Q$  counting) obey HQSS rules. In the terms where that does not happen, their influence is scaled down because of the introduction of the  $\lambda$  parameter, which is a small number.

Finally, the same process can be repeated for the beauty sector, where one only needs to substitute the  $c$  quark by a  $b$  quark. Then, the  $D_{ij}$  coefficients will be equal to the ones in the charm sector case, the only difference being that now  $\lambda = 0.1$  [350], because the heavy vector mesons will now be  $B^*$  and  $B_s^*$  instead of  $D^*$  and  $D_s^*$ .

## 8.3 Results

The cutoff scheme is used here to regularize the loop integration. The cutoff regularization avoids potential pathologies of the dimensional regularization in the charm sector or beauty sector, where the real part of  $G$  can become positive below the threshold and artificial poles can be found in the  $T$ -matrix, which can lead to the production of the bound states with a repulsive potential [400]. Also, in order to respect the rules of the heavy quark symmetry in bound states, the same cutoff has to be taken for all channels as it was shown in Refs. [340, 401, 402]. The explicit form for the loop function  $G$  was given in Eq. (3.93).

### 8.3.1 Molecular $\Xi_c$ states generated from meson-baryon states

First, we will start with the  $PB$  states, which will lead us to the states with  $J^P = 1/2^-$ . The poles that appear in this sector are illustrated in Table 8.10, where we vary the value of the cutoff  $q_{max}$  from 600 MeV to 800 MeV.

It can be seen in Table 8.10 that we can always obtain six poles in the range of the masses observed experimentally, and the reason we vary the value of  $q_{max}$  is to adjust the pole position to the experimental data. In this way, it can be seen clearly that if we take  $q_{max}$  to be 700 MeV, we get two poles that are in a good agreement with the experimental data. One is located at 2791.30 MeV, the other at 2937.15 MeV. They are found to agree very well with the first and the third resonances of  $\Xi_c$ ,  $\Xi_c(2790)$  and  $\Xi_c(2930)$ , which were first reported in Refs. [403, 404] and [380] respectively. Although some of the poles in Table 8.10 are relatively sensitive to the variation of  $q_{max}$ , obtaining a good agreement with two resonances simultaneously, while adjusting only one parameter, is very reasonable. Furthermore, if we look at the imaginary parts of these two poles we get their widths, 7.26 MeV and 14.62 MeV, which are very close to the experimental data,  $8.9 \pm 0.6 \pm 0.8$  MeV and  $36 \pm 7 \pm 11$  MeV respectively, within errors. On top of that, it is also important to look at the couplings to various channels as well as the product  $g_i G_i^{II}$ . As shown in Tables 8.11, the 2791.30 MeV resonance has a large contribution from the  $\Sigma D$  component. However, there are only three open channels where this resonance can decay into, and we can see that one of these open channels ( $\Xi_c' \pi$ ) is exactly the same channel where the state  $\Xi_c(2790)$  was discovered in the first place [404, 405]. Apart from that, although the couplings are considerably smaller than some to closed channels (for example,  $\Sigma D$ ), the coupling constant to  $\Xi_c' \pi$  is the dominant one among all the open channels, which is consistent with the experimental observation. Predictions on the decay widths to the open channels can be made precisely using the couplings obtained in Table 8.11 and the

formula of Ref. [10], which has the form

$$\Gamma_a = \frac{1}{2\pi} \frac{M_a}{M_R} g_a^2 p_a, \quad (8.12)$$

with

$$p_a = \frac{\lambda^{1/2}(M_R^2, M_a^2, m_a^2)}{2M_R}, \quad (8.13)$$

where  $M_a$  and  $m_a$  stand for the masses of the  $a$ th-channel baryon and meson respectively, and  $M_R$  is the mass of the resonance (the real part of the pole). In Table 8.13, we give the partial decay widths of the pole in Table 8.11, and it can be clearly seen that the state decays mostly to  $\Xi'_c \pi$ , as expected.

Similarly, for the state located at 2937.15 MeV, we can see that the resonance has a large contribution from the  $\Lambda D$  channel. Also, we have the same open channels as the ones in Table 8.13. We can see that the coupling constant to the channel  $\Xi'_c \pi$  becomes smaller than before as shown in Table 8.12. However, the couplings to the channels  $\Xi_c \pi$  and  $\Lambda_c \bar{K}$  are bigger, yet, there is more phase space for decay for  $\Xi_c \pi$  and  $\Xi'_c \pi$ , but altogether the final width to these three channels are comparable as one can see in Table 8.14. The  $\Lambda_c \bar{K}$  channel accounts for about 1/3 of the total width and this is the channel where the BaBar Collaboration observed the state  $\Xi_c(2930)$  [380].

On the other hand, for the  $VB$  channels, in Table 8.15, we obtain four poles for all the cutoffs, and in order to be consistent with the  $J^P = 1/2^-$  sector, we stick with the same cutoff  $q_{max} = 700$  MeV, which leads us to three poles that can be selected as possible candidates for  $\Xi_c(2970)$ ,  $\Xi_c(3055)$  or  $\Xi_c(3080)$ , and  $\Xi_c(3123)$  states.

As shown in Table 8.16, we present the couplings of the first three poles for  $q_{max} = 700$  MeV. For the first state, 2973.76 MeV, it couples very strongly to  $\Sigma D^*$  and almost nothing to the rest of the channels, thus it can be considered as a  $\Sigma D^*$  bound state. The second state, located at 3068.21 MeV, couples to both  $\Lambda_c \bar{K}^*$  and  $\Xi_c \rho$ , with similar values for the coupling as well as  $gG^{II}$ . The situation of the third state, 3109.04 MeV, is similar to what we found in the first state, where it practically only couples to  $\Lambda D^*$ , and the product  $gG^{II}$  is also significantly larger than for the rest of the channels. Moreover, we notice that all these three poles are below thresholds, so they do not decay to any of the coupled states shown in Table 8.16, instead it may decay into the pseudoscalar-baryon ones.

Now we study the  $PB^*$  states with  $J^P = 3/2^-$ . All the poles obtained in this sector are given in Table 8.17. One can see from the poles with  $q_{max} = 700$  MeV, two of them are relatively close to the experimental observed states,  $\Xi_c(2930)$  and  $\Xi_c(3055)$ . It is noteworthy that the first one,  $2912.78 + i19.94$ , which agrees rather well with the experimental data, is similar to the pole  $(2937.15 + i7.31)$  found in the  $J^P = 1/2^-$  sector in Table 8.10, since the  $J^P$  of  $\Xi_c(2930)$  has not been measured, it can be either one of



these two poles. Although the mass of the state, 2912.78 MeV, may be slightly smaller than the observed state  $\Xi_c(2930)$ , the width (which is 39.88 MeV) is remarkably close to the data fit ( $36 \pm 7 \pm 11$  MeV) by the BaBar Collaboration [380]. Similarly, for the other pole obtained at the position 3015.18 MeV, its width (2.74 MeV) is a few MeV below the value of  $7.8 \pm 1.2 \pm 1.5$  MeV reported in Refs. [21, 406]. Apart from that, in Table 8.18, we present our results on the couplings of these two poles to various channels, where we can see that for the first pole only the channel  $\Xi_c^* \pi$  is open for decay, and the width of this state decaying to  $\Xi_c^* \pi$  is found to be 56.92 MeV using Eq. (8.12). On the other hand, for the pole at 3015.18 MeV, both channels  $\Xi_c^* \pi$  and  $\Sigma_c^* \bar{K}$  are open for decay. We can see that the state at 3015.18 MeV couples mostly to the channel  $\Sigma^* D$ , and the coupling constants to the open channels are both very small, but the strengths of the wave functions at the origin are considerable for these open channels, and clearly,  $gG^{II}$  for the former channel is bigger than the latter one, which can also be seen in the widths obtained, 2.65 MeV and 0.08 MeV, for the channels  $\Xi_c^* \pi$  and  $\Sigma_c^* \bar{K}$ , respectively.

### 8.3.2 Molecular states for $\Xi_b$ generated from meson-baryon states

In this subsection, we follow closely the calculations in the previous one. It starts with the  $J^P = 1/2^-$  sector, where we also have ten coupled channels similar to the ones we considered for  $\Xi_c$ , only with the  $c$  quark replaced by a  $b$  quark in each channel. The poles from the  $PB$  interaction are given in Table 8.19, where we obtain six poles for each cutoff. Taking into account the uncertainty caused by the variation of the cutoff, we can associate the pole, 6220.30 MeV with  $q_{max} = 650$  MeV, to the state  $\Xi_b(6226)$  recently observed by the LHCb Collaboration [382]. The newly observed state  $\Xi_b(6226)$  is reported with the values  $6226.9 \pm 2.0 \pm 0.3 \pm 0.2$  MeV/ $c^2$  and  $18.1 \pm 5.4 \pm 1.8$  MeV/ $c^2$  for its mass and width, respectively. We can see that the mass obtained is merely a few MeV below the experimental data, and the width (25.20 MeV) is also in very good agreement with the data. Moreover, for the couplings of this pole we can look at the results in Table 8.20, where we can see that the main contribution comes from the  $\Sigma_b \bar{K}$  channel. Also, we see that it has only three open channels, and it should be noted that two of these channels, the  $\Xi_b \pi$  and  $\Lambda_b \bar{K}$ , are the ones where the state  $\Xi_b(6226)$  has been observed [382]. However, according to our findings, it couples mostly to the  $\Xi_b' \pi$  among the open channels, which suggests that it would be easier to find the state  $\Xi_b(6226)$  in the  $\Xi_b' \pi$  channel instead of the other two, which can be confirmed by future experiments.

The decay widths of the pole of Table 8.20 are given in Table 8.24, where we can

obtain the ratio of branching fractions of state 6220.30 MeV as follows

$$\frac{\mathcal{B}(6220.30 \rightarrow \Lambda_b \bar{K})}{\mathcal{B}(6220.30 \rightarrow \Xi_b \pi)} = 0.5, \quad (8.14)$$

which is relatively close to the results  $(1 \pm 0.5)$  presented in Ref. [382] given its uncertainty.

On the other hand, for the  $VB$  interaction, we observed four poles for each cut-off, but none of these poles for  $q_{max} = 650$  MeV can be associated to any known  $\Xi_b$  states with negative parity, since there are not enough data available for  $\Xi_b$  states. Furthermore, almost all of the poles found in this sector are below their respective thresholds, which makes it more plausible that these channels could qualify as bound states rather than resonances.

Moving on to the  $J^P = 3/2^-$  sector, we also get four poles for each cutoff, which are given in Table 8.21, where we also find a possible candidate for  $\Xi_b(6227)$ . The state 6240.21 MeV agrees really well with the experimental data [382], as both mass and width are within acceptable ranges. For the couplings as well as  $g_i G_i^{II}$ , shown in Table 8.22, it can be seen that the state at 6240.21 MeV couples mostly to  $\Sigma_b^* \bar{K}$  and  $\Xi_b^* \eta$ , and only slightly to the rest of the channels. However, when we look at the magnitude of  $g G^{II}$ , we can see that not only the channel  $\Sigma_b^* \bar{K}$  is significantly bigger than the others, also the only open channel  $\Xi_b^* \pi$  is considerably large compared to the other channels. Besides, the decay width of this particular pole to  $\Xi_b^* \pi$  is 34.3851 MeV, which is similar to the value of the width for at 6220.30 MeV decaying to  $\Xi_b' \pi$ , in Table 8.24, because they have almost the same phase space for decay.

$q_{max}$	600	650	700	750	800
	2684.23+i89.72	2679.71+i76.48	2673.49+i64.54	2666.24+i54.01	2658.68+i44.52
	2800.72+i100.03	2801.80+i86.16	2803.28+i72.06	2803.31+i57.77	2794.76+i31.06
	2880.76+i10.31	2842.47+i10.13	<b>2791.30+i3.63</b>	2738.46+i1.36	2685.56+i0.89
	2896.57+i1.34	2870.10+i10.64	2850.70+i16.38	2830.84+i23.17	2817.77+i40.45
	2969.50+i3.30	2955.62+i5.10	<b>2937.15+i7.31</b>	2913.82+i10.03	2886.31+i13.46
	3171.55+i32.48	3160.12+i37.77	3148.11+i41.88	3135.67+i44.96	3125.96+i47.18

Table 8.10: Poles in the  $J^P = 1/2^-$  sector from pseudoscalar-baryon interaction (all units are in MeV). The bold numbers indicate the poles that can be associated with the experimental data.

	$\Xi_c\pi$	$\Xi'_c\pi$	$\Lambda_c\bar{K}$	$\Sigma_c\bar{K}$	$\Lambda D$
<b>2791.30+i3.63</b>					
$g_i$	-0.01-i0.03	0.39-i0.44	-0.09-i0.05	1.05-i0.47	1.91-i0.09
$g_i G_i^{II}$	0.78+i0.53	-3.98+i14.85	2.70+i0.73	-11.27+i4.95	-7.45+i0.27
	$\Xi_c\eta$	$\Sigma D$	$\Xi'_c\eta$	$\Omega_c\bar{K}$	$\Xi D_s$
$g_i$	0.23+i0.03	<b>8.82+i0.38</b>	0.49-i0.17	0.21-i0.26	5.44+i0.20
$g_i G_i^{II}$	-2.00-i0.26	<b>-29.16-i1.48</b>	-3.53+i1.19	-1.42+i1.74	-11.96-i0.49

Table 8.11: The coupling constants to various channels and  $g_i G_i^{II}$  for the pole at 2191.30 +i3.63 MeV in the  $J^P = 1/2^-$  sector with  $q_{max} = 700$  MeV (all units are in MeV). The bold numbers indicate the channel with largest coupling.

	$\Xi_c\pi$	$\Xi'_c\pi$	$\Lambda_c\bar{K}$	$\Sigma_c\bar{K}$	$\Lambda D$
<b>2937.15+i7.31</b>					
$g_i$	-0.29+i0.10	0.03-i0.32	0.28-i0.22	0.27+i0.08	<b>3.96-i0.29</b>
$g_i G_i^{II}$	0.83-i9.44	6.42+i6.63	0.31+i10.35	-5.40-i1.98	<b>-27.75+i0.73</b>
	$\Xi_c\eta$	$\Sigma D$	$\Xi'_c\eta$	$\Omega_c\bar{K}$	$\Xi D_s$
$g_i$	-0.07+i0.39	-2.44+i0.10	0.09+i0.04	-0.12-i0.26	3.55-i0.13
$g_i G_i^{II}$	1.11-i5.19	12.15-i0.15	-0.85-i0.40	0.98+i2.23	-9.83+i0.23

Table 8.12: The coupling constants to various pseudoscalar-baryon channels and  $g_i G_i^{II}$  for the pole at 2937.15 MeV in the  $J^P = 1/2^-$  sector with  $q_{max} = 700$  MeV (all units are in MeV). The bold numbers indicate the channel with largest coupling.

Channel	$\Xi_c\pi$	$\Xi'_c\pi$	$\Lambda_c\bar{K}$
$\Gamma_i$	0.04	8.00	0.12

Table 8.13: The widths of pole 2791.30+i3.63 decaying to various channels (all units are in MeV).

Channel	$\Xi_c\pi$	$\Xi'_c\pi$	$\Lambda_c\bar{K}$
$\Gamma_i$	5.22	4.45	5.88

Table 8.14: The widths of pole 2937.15+i7.31 decaying to various channels (all units are in MeV).

$q_{max}$	600	650	700	750	800
	3055.63	3016.46	<b>2973.76</b>	2928.28	2880.75
	3117.37	3094.39	<b>3068.21</b>	3040.89	3013.14
	3121.75	3115.67	<b>3109.04</b>	3100.55	3090.16
	3234.03+i0.22	3204.98	3174.50	3143.09	3111.43

Table 8.15: The poles in the  $J^P = 1/2^-, 3/2^-$  sector from the vector-baryon interaction (all units are in MeV). The bold numbers indicate the poles that can be associated with the experimental data.

<b>2973.76</b>	$\Lambda D^*$	$\Lambda_c\bar{K}^*$	$\Sigma D^*$	$\Xi_c\rho$	$\Xi_c\omega$	$\Sigma_c\bar{K}^*$
$g_i$	0	0.07	<b>9.30</b>	0.33	0.30	0.55
$g_i G_i^{II}$	0	-0.48	<b>-31.85</b>	-2.29	-2.02	-2.87
<b>3068.21</b>	$\Lambda D^*$	$\Lambda_c\bar{K}^*$	$\Sigma D^*$	$\Xi_c\rho$	$\Xi_c\omega$	$\Sigma_c\bar{K}^*$
$g_i$	0.37	<b>3.08</b>	-0.26	<b>3.57</b>	-0.85	-0.04
$g_i G_i^{II}$	-2.33	<b>-30.22</b>	1.20	<b>-30.89</b>	7.19	0.22
<b>3109.04</b>	$\Lambda D^*$	$\Lambda_c\bar{K}^*$	$\Sigma D^*$	$\Xi_c\rho$	$\Xi_c\omega$	$\Sigma_c\bar{K}^*$
$g_i$	<b>3.05</b>	0.05	0.03	-0.51	0.09	0.01
$g_i G_i^{II}$	<b>-26.23</b>	-0.60	-0.17	5.04	-0.81	-0.05

Table 8.16: The coupling constants to various vector-baryon channels and  $g_i G_i^{II}$  for the poles in the  $J^P = 1/2^-, 3/2^-$  sector with  $q_{max} = 700\text{MeV}$  (all units are in MeV). The bold numbers indicate the channels with largest couplings.

$q_{max}$	600	650	700	750	800
	2868.84+i101.02	2869.69+i87.71	2870.00+i71.15	2871.12+i55.04	2888.93+i43.98
	2950.39+i11.19	2932.11+i15.01	<b>2912.78+i19.94</b>	2891.71+i27.88	2855.31+i26.46
	3099.36+i0.55	3059.03+i0.89	<b>3015.18+i1.37</b>	2968.69+i2.98	2918.23+i7.32
	3243.94+i32.64	3233.36+i38.32	3222.35+i42.93	3211.05+i46.56	3199.61+i49.32

Table 8.17: The poles in the  $J^P = 3/2^-$  sector from the pseudoscalar-baryon interaction (all units are in MeV). The bold numbers indicate the poles that can be associated with the experimental data.

185

	$\Xi_c^* \pi$	$\Sigma_c^* \bar{K}$	$\Xi_c^* \eta$	$\Sigma^* D$	$\Omega_c^* K$
<b>2912.78+i19.94</b>					
$g_i$	0.41-i1.28	<b>3.78-i0.47</b>	1.87-i0.12	-1.09-i0.83	0.16-i0.85
$g_i G_i^{II}$	11.65+i36.25	<b>-48.53+i2.60</b>	-14.80+i0.42	3.17+i2.60	-1.34+i6.20
<b>3015.18+i1.37</b>					
	$\Xi_c^* \pi$	$\Sigma_c^* \bar{K}$	$\Xi_c^* \eta$	$\Sigma^* D$	$\Omega_c^* K$
$g_i$	0.03-i0.24	0.11+i0.07	0.42+i0.03	<b>8.94-i0.04</b>	-0.04-i0.20
$g_i G_i^{II}$	4.82+i5.04	-3.19-i1.64	-4.18-i0.34	<b>-33.36+i0.03</b>	0.31+i1.72

Table 8.18: The coupling constants to various pseudoscalar-baryon channels and  $g_i G_i^{II}$  for the poles in the  $J^P = 3/2^-$  sector with  $q_{max} = 700$  MeV (all units are in MeV). The bold numbers indicate the channels with largest couplings.

$q_{max}$	600	650	700	750	800
	6002.21+i81.90	5997.45+i69.73	5991.25+i58.74	5984.13+i49.02	5976.61+i40.29
	6152.19+i91.66	6152.17+i78.48	6152.24+i64.42	6150.40+i48.36	6137.15+i27.48
	6237.52+i11.30	<b>6220.30+i12.60</b>	6201.74+i19.00	6183.11+i27.85	6175.03+i40.45
	6263.48+i0.07	6205.08+i2.94	6141.06+i1.73	6073.96+i0.17	6004.35+i0.44
	6359.89+i0.82	6338.97+i1.44	6312.50+i2.42	6280.97+i3.77	6244.54+i5.65
	6513.45+i29.56	6501.26+i33.87	6488.63+i37.17	6482.88+i39.75	6482.86+i41.90

Table 8.19: The poles in the  $J^P = 1/2^-$  sector from the pseudoscalar-baron interaction (all units are in MeV). The bold number indicates the pole that can be associated with the experimental data.

	$\Xi_b\pi$	$\Xi'_b\pi$	$\Lambda_b\bar{K}$	$\Sigma_b\bar{K}$	$\Lambda\bar{B}$
<b>6220.30+i12.60</b>					
$g_i$	0.01+i0.02	0.34-i0.91	-0.01-i0.01	<b>3.53-i0.14</b>	-1.03+i0.61
$g_i G_i^{II}$	-0.60+i0.05	10.08+i25.84	0.42+i0.15	<b>-44.85-i0.67</b>	1.47-i0.78
	$\Xi_b\eta$	$\Sigma\bar{B}$	$\Xi'_b\eta$	$\Omega_b\bar{K}$	$\Xi B_s$
$g_i$	-0.00+i0.04	-2.09+i4.72	1.80+i0.02	0.09-i0.65	-1.93+i2.81
$g_i G_i^{II}$	0.02-i0.38	2.54-i5.25	-13.14-i0.55	-0.74+i4.33	1.45-i2.02

Table 8.20: The coupling constants to various pseudoscalar-baryon channels and  $g_i G_i^{II}$  for the poles in the  $J^P = 1/2^-$  sector with  $q_{max} = 650$  MeV (all units are in MeV). The bold numbers indicate the channel with largest coupling.

$q_{max}$	600	650	700	750	800
	<b>6169.97+i192.88</b>	<b>6169.85+i180.29</b>	<b>6168.88+i66.55</b>	<b>6166.89+i49.80</b>	<b>6155.48+i29.00</b>
	<b>6258.53+i10.88</b>	<b>6240.21+i14.65</b>	<b>6221.49+i19.71</b>	<b>6203.04+i27.94</b>	<b>6193.81+i39.67</b>
	6474.16+i0.14	6424.37+i0.20	6369.22+i0.34	6309.51+i0.68	6245.85+i2.08
	6538.85+i30.15	6527.01+i34.64	6514.86+i38.05	6502.41+i40.62	6500.43+i42.56

Table 8.21: The poles in the  $J^P = 3/2^-$  sector from the pseudoscalar-baron interaction (all units are in MeV). The bold number indicates the pole that can be associated with the experimental data.

	$\Xi_b^* \pi$	$\Sigma_b^* \bar{K}$	$\Xi_b^* \eta$	$\Sigma^* \bar{B}$	$\Omega_b^* K$
$g_i$	0.23-i0.93	<b>3.39-i0.36</b>	1.74-i0.10	-0.78-i0.36	0.03-i0.65
$g_i G_i^{II}$	13.03+i24.31	<b>-43.16+i1.85</b>	-12.78+i0.27	0.63+i0.30	-0.29+i4.27

Table 8.22: The coupling constants to various pseudoscalar-baryon channels and  $g_i G_i^{II}$  for the poles in the  $J^P = 3/2^-$  sector with  $q_{max} = 650$  MeV (all units are in MeV). The bold numbers indicate the channel with largest coupling.

$q_{max}$	600	650	700	750	800
	<b>6342.09</b>	<b>6295.86</b>	<b>6244.94</b>	<b>6190.01</b>	<b>6131.80</b>
	6425.22	6407.58	6379.79	6351.13	6322.26
	6434.39	6417.24	6406.58	6393.82	6378.88
	6579.47+i0.05	6548.79+i0.03	6516.72	6484.01	6451.25

Table 8.23: The poles in the  $J^P = 1/2^-, 3/2^-$  sector from the vector-baron interaction (all units are in MeV).

Channel	$\Xi_b \pi$	$\Xi_b' \pi$	$\Lambda_b \bar{K}$
$\Gamma_i$	0.02	35.01	0.01

Table 8.24: The widths of pole 6220.30+i12.60 decaying to various channels (all units are in MeV).

## 8.4 Conclusions

Motivated by the experimental findings of  $\Xi_c$  and  $\Xi_b$  states, we use the BSE coupled channel formalism to study the  $\Xi_{c(b)}$  states dynamically generated from the extended LHG meson-baryon interaction, considering three types of interactions ( $PB$ ,  $VB$  and  $PB^*$ ), for both the charm and beauty sectors. We search for poles with different cutoffs in the SRS once the scattering matrix is evaluated. In addition, the couplings of the poles to various channels are also calculated. With that, we are able to assess the strength at the origin of the wave function and further evaluate the decay widths to the open channels.

The only free parameter in our study is the ultraviolet regulator in the meson-baryon loop function, where we employ the cutoff regularization scheme, and we have taken different values for the cutoff in the charm and beauty sectors.

We obtain multiple  $\Xi_c$  excited states, with some of them agreeing significantly well with the experimental data. For example, the lowest state we observe in the charm sector is at 2791.30 MeV (with a width of 7.26 MeV) generated from the  $PB$  interaction. This resonance has the same  $J^P$  quantum numbers as the state  $\Xi_c(2790)$  (with width  $8.9 \pm 0.6 \pm 0.8$  MeV), also it can be seen that there is a very good agreement in their masses and widths. On top of that, we also obtain states at 2937.15 MeV (2912.78 MeV), 2973.76 MeV, 3068.21 MeV (3015.18 MeV) and 3109.04 MeV (the numbers in the brackets implying the second option), which can be associated to the experimentally observed states  $\Xi_c(2930)$ ,  $\Xi_c(2970)$ ,  $\Xi_c(3055)$  and  $\Xi_c(3080)$ , respectively. On the other hand, we found two poles in the  $b$  sector, at 6220.30 MeV (with width 25.20 MeV) and 6240.21 MeV (with width 29.30 MeV) and  $J^P = 1/2^-$  and  $3/2^-$ , respectively. We see that both their masses and widths agree well with the recent observed state  $\Xi_b(6227)$  with width  $18.1 \pm 5.4 \pm 1.8$  MeV.

Overall, the states obtained in this chapter agree well with some of the already observed resonances in both charm and beauty sectors, and it would be interesting to see the further measurements of spin and parity of these states to see if they also agree with our predictions. Furthermore, with the increased luminosity in future runs, the comparisons of the predictions made here and the experimental measurements will shed light on the nature of these hadrons.



# Chapter 9

## $\Omega_c$ , $\Xi_c$ and $\Xi_b$ molecular states within a $SU(6)_{\text{lsf}} \times \text{HQSS}$ model

### 9.1 Introduction

The study of heavy baryons with charm or bottom content has been the subject of much interest over the past years in view of newly discovered states [21]. In particular, there has been a tremendous effort to understand the nature of the experimental states within conventional quarks models, QCD sum-rules frameworks, QCD lattice analysis or molecular baryon-meson models (see Refs. [13, 98–102] for recent reviews).

The attention has been recently revived by the experimental observation of several excited states. Recent detections have been reported by the LHCb Collaboration regarding five  $\Omega_c$  excited states in the  $\Xi_c^+ K^-$  spectrum in  $pp$  collisions [348], and the excited  $\Xi_b(6227)$  state in  $\Lambda_b^0 K^-$  and  $\Xi_b^0 \pi^-$  invariant mass spectra also in  $pp$  collisions [382], as already mentioned in the previous chapter. Moreover, the Belle Collaboration has confirmed the observation of four of the excited  $\Omega_c$  states [387], and detected the  $\Xi_c(2930)$  state in its decay to  $\Lambda_c^+ K^-$  in  $B^- \rightarrow K^- \Lambda_c^+ \bar{\Lambda}_c^-$  decays [381].

Earlier predictions for such states have been reported within conventional quark models [73–75, 77, 79, 310–312, 384, 407–409]. The experimental discovery of the five  $\Omega_c$  states has triggered a large activity in the field, and thus some quark models have been revisited in view of the new results [410–416], suggestions as pentaquarks have been advocated [417–421], models based on QCD sum-rules have been put to test [383, 422–427], or quark-soliton models have been employed [428]. Also, Lattice QCD has reported results on the spectroscopy of  $\Omega_c$  states [429].

Within molecular models, there have been previous predictions on  $\Omega_c$  states [86, 170, 172, 339]. In Ref. [170] several resonant states were obtained with masses much

below 3 GeV, by employing a zero-range exchange of vector mesons as the bare interaction for the  $s$ -wave baryon-meson scattering. Similar qualitative results were obtained in Ref. [339], where finite range effects were considered. Lately the work of Ref. [351] has revisited Ref. [170], finding that, after modifying the regularization scheme with physically motivated parameters, two  $\Omega_c$  resonant states were generated at 3050 MeV and 3090 MeV with spin-parity  $J^P = 1/2^-$ , reproducing the masses and widths of two of the experimental states. More recently, the  $\Omega_c$  states have been also investigated using an extended local hidden gauge (LHG) approach [388]. Within this scheme, low-lying  $1/2^+$  and  $3/2^+$  baryons, as well as pseudoscalar and vector mesons, are considered to construct the baryon-meson coupled channel space. In this manner, two  $\Omega_c$  states of  $J^P = 1/2^-$  and one  $\Omega_c^*$   $J^P = 3/2^-$  can be identified, the first two in good agreement with the results of [351] and the third one fairly well.

With regards to  $\Xi_c$ , the theoretical analysis based on the extended LHG formalism of Chapter 8 has shown that not only the  $\Xi_c(2930)$  can have a molecular interpretation, but also other  $\Xi_c$  states around 3 GeV reported in the PDG [21]. In particular, the  $\Xi_c(2790)$  would be a  $J^P = 1/2^-$  molecular state, whereas  $\Xi_c(2930)$ ,  $\Xi_c(2970)$ ,  $\Xi_c(3055)$  and  $\Xi_c(3080)$  could be described as molecules with either  $1/2^-$  or  $3/2^-$ . On the other hand, the same model has produced two states for  $\Xi_b(6227)$  with masses close to the experimental one with similar widths, being the spin-parity assignment either  $1/2^-$  or  $3/2^-$ . The  $\Xi_b$  state has been also studied within a unitarized model that uses the leading-order chiral Lagrangian in Refs. [340, 430], identifying the  $\Xi_b(6227)$  state as a  $s$ -wave  $\Sigma_b \bar{K}$  molecule, with a preferred  $1/2^-$  spin-parity assignment [430].

The leading order terms of the extended hidden-gauge formalism are consistent with HQSS [349], which, as we have seen, is an accurate symmetry of QCD when the quark masses become larger than the typical confinement scale. Aiming to incorporate explicitly HQSS, a scheme was developed in Refs. [83, 86, 172, 347, 431] that implements an extension of the Weinberg-Tomozawa (WT) interaction that is consistent with the  $SU(6)_{\text{lsf}} \times SU(2)_{\text{HQSS}}$  symmetry group. Indeed, the works of Refs. [86, 172] are the first meson-baryon molecular studies, fully consistent with HQSS, of the well-established odd-parity  $\Lambda_c(2595)$  [ $J = 1/2$ ] and  $\Lambda_c(2625)$  [ $J = 3/2$ ] resonances.

Within this framework, it has been identified a two-pole pattern for the  $\Lambda_c(2595)$  resonance<sup>1</sup> [86, 172], similar to the  $\Lambda(1405)$  [32, 35, 288]. The same scheme has also generated dynamically the  $\Lambda_b(5912)$  and  $\Lambda_b(5920)$  narrow resonances, discovered by LHCb [346], which turn out to be HQSS partners, naturally explaining their approximate mass degeneracy [83].

In the  $SU(6)_{\text{lsf}} \times SU(2)_{\text{HQSS}}$  work of Ref. [86] five  $\Omega_c$  states were found, three

<sup>1</sup>The details of this double pole structure, generated by the  $\Sigma_c \pi$ ,  $ND$  and  $ND^*$  coupled-channels dynamics, depend strongly on the adopted renormalization scheme, which could considerably enhance the role played by the two latter channels around the resonance energy. This was discussed in great detail in Chapter 7.

$J = 1/2$  and the two  $J = 3/2$  bound states, the positions being shown in Table VI of that reference or in Table 9.1 in the present chapter. These states come from the most attractive  $SU(6)_{\text{lsf}} \times \text{HQSS}$  representations. Attending to the breaking pattern of the spin-flavor  $SU(8)$  symmetry discussed in Ref. [86], the two lowest-lying  $\Omega_c$  and  $\Omega_c^*$  states (**a** and **b**) and the  $\Lambda_c(2595)$  would be members of the same **21**  $SU(6)_{\text{lsf}}$  multiplet, while both, the third  $\Omega_c$  (**c**) and the  $\Lambda_c(2625)$  resonances would be in the **15**  $SU(6)_{\text{lsf}}$ - irreducible representation (irrep), if one assumes that the  $\Lambda_c(2625)$  is the HQSS partner of the  $\Lambda_c(2595)$  (see Chapter 7 for arguments against that). Finally, the two heaviest  $\Omega_c$  and  $\Omega_c^*$  states (**d** and **e**) reported in [86] would not be directly related to the  $\Lambda_c(2595)$  and  $\Lambda_c(2625)$  resonances, since they would stem originally from a different  $SU(8)$  representation. These five odd-parity  $\Omega_c, \Omega_c^*$  states, coming from the most attractive  $SU(6)_{\text{lsf}} \times \text{HQSS}$  representations, have masses below 2.98 GeV, and cannot be easily identified with any of the LHCb resonances, located all of them above 3 GeV. Predicted masses, however, depend not only on the baryon-meson interactions, but also on the adopted renormalization scheme (RS), as revealed for the  $\Lambda_c(2595)$  and  $\Lambda_c(2625)$  resonance sectors in Chapter 7. In the present chapter, we review the RS used in [86], and its impact in the generation of the  $\Omega_c^{(*)}$  states. We show how the pole positions can be moved up by implementing a different RS, making then feasible the identification of at least three states with the observed  $\Omega_c^{(*)}$  states by LHCb.

Furthermore, with the discovery of the  $\Xi_c(2930)$  and  $\Xi_b(6227)$  we can follow a similar procedure and study the possible molecular interpretation of those states, revisiting the previous  $SU(6)_{\text{lsf}} \times SU(2)_{\text{HQSS}}$  works on the  $\Xi_c$  [86] and  $\Xi_b$  [83] sectors. We can then compare these results with the ones obtained in Chapter 8 within the LHG formalism, showing the assigned spin-parity  $J^P$  (when possible) as well as masses, widths, and decay channels. Hence, this study is a first step to quantify the systematic uncertainties associated with the use of different models for the BSE interaction kernels involving charmed pseudoscalar and vector mesons and  $J^P = 1/2^+$  and  $J^P = 3/2^+$  baryons. We also pay in this context a special attention to the depen-

Name	$M_R$ (MeV)	$\Gamma_R$ (MeV)	$J$
<b>a</b>	2810.9	0	1/2
<b>b</b>	2814.3	0	3/2
<b>c</b>	2884.5	0	1/2
<b>d</b>	2941.6	0	1/2
<b>e</b>	2980.0	0	3/2

Table 9.1:  $\Omega_c$  and  $\Omega_c^*$  states, reported in Ref. [86], coming from the most attractive  $SU(6)_{\text{lsf}} \times \text{HQSS}$  representations. We label those states from **a** to **e**, according to their position in energy.

dence on the RS as well as to the flavor-symmetry content of the  $SU(6)_{\text{lsf}} \times \text{HQSS}$  model, as we determine the possible HQSS partners and siblings among the experimental states while predicting new ones. We are able to unambiguously identify the corresponding multiplets among the resonances generated dynamically. At the same time, we are also able to assign approximate heavy  $SU(8)$  and light  $SU(6)$  spin-flavor multiplet labels to the states.

This part of the thesis is based on Refs. [6, 7] and it is organized as follows. In Sec. 9.2 we briefly present the  $SU(6)_{\text{lsf}} \times SU(2)_{\text{HQSS}}$  extension of the WT interaction. Next, in Sec. 9.3 we show the results obtained in this chapter. The section is divided into three subsections, Subsecs. 9.3.1, 9.3.2 and 9.3.3 for the  $\Omega_c^{(*)}$ ,  $\Xi_c^{(*)}$  and  $\Xi_b^{(*)}$  states, respectively. Finally, in Sec. 9.4 we present our conclusions.

## 9.2 Formalism

We will consider the  $C = 1$  charmed sectors with strangeness  $S = -2$  and isospin  $I = 0$  quantum numbers, where the  $\Omega_c^{(*)}$  excited states are located, and with  $S = -1$  and  $I = 1/2$ , where the  $\Xi_c(2930)$  resonance has been observed by the Belle Collaboration [381]. Also, we examine the bottom ( $B = -1, S = -1, I = 1/2$ ) sector, where the  $\Xi_b(6227)$  has been found [382]. We will revise the results of Refs. [83, 86] for the  $\Omega_c$  and  $\Xi_c$  resonances, and the  $\Xi_b$  states, respectively.

The building-blocks in the ( $C = 1, S = -2, I = 0$ ) sector are the pseudoscalar and vector

$$\begin{aligned} D_s, D, K, \pi, \eta, \bar{K}, \bar{D}, \bar{D}_s \\ D_s^*, D^*, K^*, \rho, \omega, \bar{K}^*, \bar{D}^*, \bar{D}_s^*, \phi \end{aligned} \quad (9.1)$$

mesons, the spin-1/2 octet and the spin-3/2 decuplet of low-lying light baryons, in addition to the spin-1/2 ( $\Lambda_c, \Sigma_c, \Xi_c, \Xi'_c, \Omega_c$ ), and spin-3/2 ( $\Sigma_c^*, \Xi_c^*, \Omega_c^*$ ) charmed baryons [86, 347]. In the case of ( $C = 1, S = -1, I = 1/2$ ) sector, the building-blocks are the pseudoscalar ( $D_s, D, K, \pi, \eta, \bar{K}$ ) and vector ( $D_s^*, D^*, K^*, \rho, \omega, \bar{K}^*, \phi$ ) mesons, and the spin-1/2 ( $\Lambda, \Sigma, \Xi, \Lambda_c, \Sigma_c, \Xi_c, \Xi'_c, \Omega_c$ ), and spin-3/2 ( $\Sigma_c^*, \Xi_c^*, \Omega_c^*$ ) charmed baryons [86, 172]. For bottom ( $B = -1, S = -1, I = 1/2$ ) states, one can substitute the  $c$  quark by a  $b$  quark, and we have the spin-1/2 ( $\Lambda, \Sigma, \Xi, \Lambda_b, \Sigma_b, \Xi_b, \Xi'_b, \Omega_b$ ), and spin-3/2 ( $\Sigma_b^*, \Xi_b^*, \Omega_b^*$ ) baryons, and the pseudoscalar ( $\bar{B}_s, \bar{B}, K, \pi, \eta, \bar{K}$ ) and vector ( $\bar{B}_s^*, \bar{B}^*, K^*, \rho, \omega, \bar{K}^*, \phi$ ) mesons [83]. All baryon-meson pairs with ( $C = 1$  or  $B = -1, S, I$ ) quantum numbers span the coupled-channel space for a given total angular momentum ( $J$ ). The  $s$ -wave tree level amplitudes between two channels are given by the  $SU(6)_{\text{lsf}} \times \text{HQSS}$  WT interactions shown in Eq. (7.1). The hadron masses and meson decay constants,  $f_i$ , have been taken from Ref. [86]. The  $D_{ij}^J$  matrices are determined by the underlying

$SU(6)_{\text{lsf}} \times \text{HQSS}$  group structure of the interaction. Tables for all of them can be found in Refs. [86] and [83] for the charm and bottom sectors, respectively.

We then solve the BSE in coupled-channels using the HQSS WT interactions as kernels of the non-perturbative re-summation (see Sec. 3.2). We look for poles both in the FRS and SRS of the complex amplitudes, and as in the previous Chapter 7, we compare results from the subtraction constant,  $\mu$ -RS, and the sharp cutoff,  $\Lambda$ -RS, schemes. In order to analyze the contribution of each baryon-meson channel, since we will be dealing with resonances, we shall also use here Eq. (3.118), to estimate the wave function of each channel at the origin of the coordinate space [177].

## 9.3 Results

### 9.3.1 $\Omega_c$ excited states

The LHCb experiment has analyzed the  $\Xi_c^+ K^-$  spectrum using  $pp$  collisions and five new narrow excited  $\Omega_c^0$  states have been observed: the  $\Omega_c^0(3000)$ ,  $\Omega_c^0(3050)$ ,  $\Omega_c^0(3066)$ ,  $\Omega_c^0(3090)$  and the  $\Omega_c^0(3119)$ , the last three also seen in the  $\Xi_c^+ K^-$  decay. Moreover, a sixth broad structure around 3188 has also been found in the  $\Xi_c^+ K^-$  spectrum.

Name	$M_R$ (MeV)	$\Gamma_R$ (MeV)	$J$	$M_R^{exp}$	$\Gamma_R^{exp}$
<b>a</b>	2922.2	0	1/2	—	—
<b>b</b>	2928.1	0	3/2	—	—
<b>c</b>	2941.3	0	1/2	—	—
<b>d</b>	2999.9	0.06	1/2	3000.4	4.5
<b>e</b>	3036.3	0	3/2	3050.2	0.8

Table 9.2:  $\Omega_c$  and  $\Omega_c^*$  states obtained using  $\alpha = 1.16$

As mentioned, the unitarized coupled-channel model of Ref. [86], based on a  $SU(6)_{\text{lsf}} \times \text{HQSS}$ - extended WT interaction, predicted five excited odd-parity  $\Omega_c$  states with spins 1/2 and 3/2 and masses below 3 GeV (Table 9.1). In Fig. 9.1, the positions of the three  $\Omega_c$  states (upper panel) and the two  $\Omega_c^*$  (lower panel) are shown. We see that all masses are below 2.98 GeV, which makes difficult to identify any of them with any of the LHCb resonances. Masses and widths of other five resonances above 3 GeV are also displayed in Fig. 9.1. These resonances were not discussed in Ref. [86], and are much more uncertain, as they result from less attractive  $SU(6)_{\text{lsf}} \times \text{HQSS}$  multiplets related to the exotic **4752**  $SU(8)$  irrep.

All these states have been dynamically generated by solving a coupled-channel BSE using a  $SU(6)_{\text{lsf}} \times \text{HQSS}$ -extended WT interaction as a kernel. The baryon-meson loops have been renormalized implementing one-substraction with  $\alpha = 1$  (the

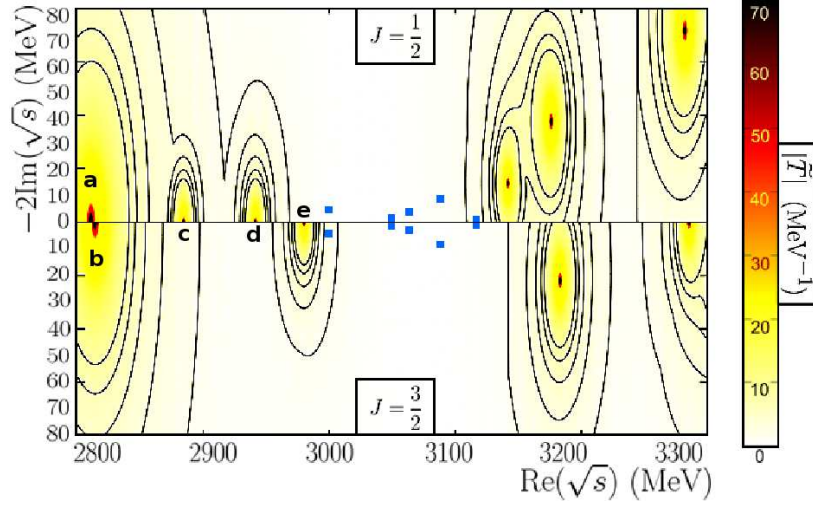


Figure 9.1:  $\Omega_c(J = 1/2)$  and  $\Omega_c^*(J = 3/2)$  odd-parity states, reported in Ref. [86], coming from the most attractive  $SU(6)_{\text{lsf}} \times \text{HQSS}$  representations. These five states, denoted as in Table 9.1, are located below 3 GeV for  $J = 1/2$  (upper plot) and  $J = 3/2$  (lower plot), while the five heavier resonant states above 3 GeV, also shown, come from less attractive  $SU(6)_{\text{lsf}} \times \text{HQSS}$  multiplets, stemming from the exotic **4752**  $SU(8)$  representation. Since the dynamically generated states may couple differently to their baryon-meson components, we show the  $ij$ -channel independent quantity  $|\tilde{T}(z)|_J$  defined in Eq. (3.111), which allows us to identify all the resonances within a  $J$ -sector at once. The blue dots correspond to the experimentally observed states. We display them both in the upper and lower plots because their spin is not determined.

one used in Eqs. (3.95) and (3.97)). This RS was chosen following the works of Refs. [170, 171], where it was claimed that such a choice guarantees an approximate crossing symmetry<sup>2</sup>. Moreover it also allowed for a successful description of the  $\Lambda_c(2595)$  and  $\Lambda_c(2625)$  resonances, with almost<sup>3</sup> no-free parameters [172].

However, it is possible to allow for some freedom and slightly modify the choice of the subtraction point by changing the value of  $\alpha$ . In this way, we might move up in energy the states found in Ref. [86] and compiled in Table 9.1, and try to identify some of them with the experimentally observed  $\Omega_c^{(*)}$  states. We concentrate our study on those states as they are the ones most likely to exist since they originate from the most attractive  $SU(6)_{\text{lsf}} \times \text{HQSS}$  representations.

Masses become higher when  $\alpha$  becomes greater than one. Allowing for just moderately changes, we find that for  $\alpha = 1.16$  the two last states, labeled with **d** and **e** in Table 9.1, are now located near the experimental  $\Omega_c(3000)$  and  $\Omega_c(3050)$ , with masses 2999.9 MeV and 3036.3 MeV, respectively, while their widths are almost zero.

<sup>2</sup>Note that exact crossing symmetry is only achieved where the loop function is equal to zero.

<sup>3</sup>The  $\alpha$  parameter in Eq. (7.3) was slightly reduced from the default value of 1 advocated in Ref. [170, 171].

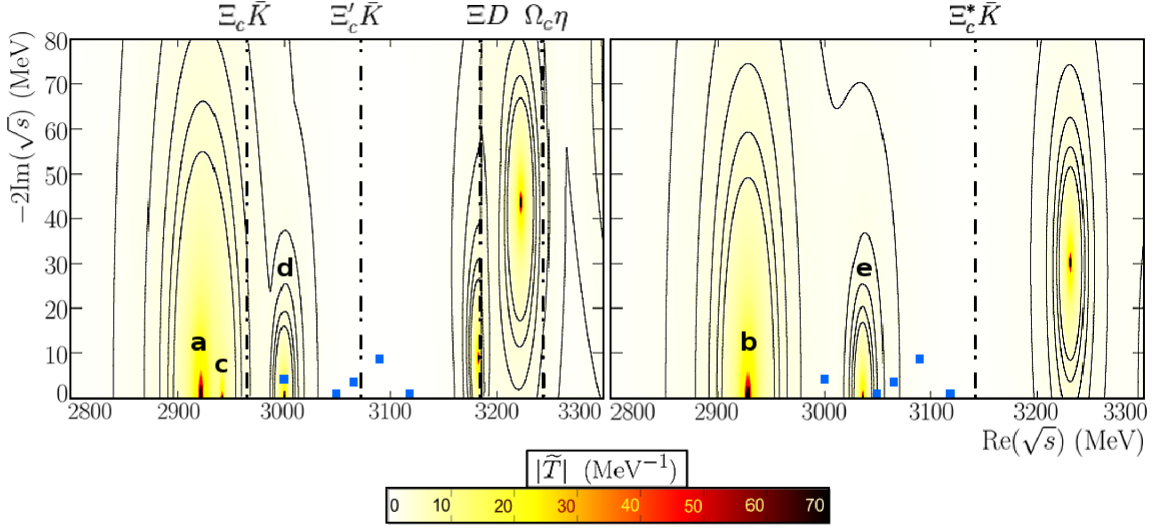


Figure 9.2:  $\Omega_c$  and  $\Omega_c^*$  states obtained within the scheme of Ref. [86] using  $\alpha = 1.16$ . The left (right) plot shows the states dynamically generated for  $J = \frac{1}{2}$  ( $J = \frac{3}{2}$ ). The dotted blue points are the experimental observations, while some baryon-meson thresholds (dashed-dotted lines) are displayed for completeness. The function  $|\tilde{T}(z)|_J$  is defined as in Fig. 9.1.

The poles found with this new value of  $\alpha$  are compiled in Table 9.2 and displayed in Fig. 9.2. Moreover, the analysis of the product of the coupling times the loop function at the pole,  $g_i G_i(s_R)$ , of Table 9.3 allows us to study the importance of the different baryon-meson channels in the dynamical generation of the  $\Omega_c$  and  $\Omega_c^*$  states. In particular, the state at 2999.9 MeV is mainly a  $\Xi_c'^+ \bar{K}$  molecular state that also couples strongly to  $\Omega_c \eta$ ,  $\Xi D$  and  $\Xi_c \bar{K}^*$ . As for the state at 3036.3 MeV, the dominant  $\Xi_c^* \bar{K}$  channel can be reconciled with the experimentally seen decay  $\Xi_c^+ K^-$ , if one allows for the  $\Xi_c^* \bar{K} \rightarrow \Xi_c \bar{K}$   $d$ -wave transition, that does not involve the exchange of the charm-quark.

In view of the previous results, we now explore a different RS in order to evaluate the impact of the renormalization procedure in the predictions of the  $\Omega_c$  and  $\Omega_c^*$  low-lying odd parity states, aiming at providing an alternative description for some of the states observed by LHCb. Thus, we allow for a variation of the subtraction constants in each channel different to that imposed within the  $\mu$ -RS, but still in a controlled way. For that purpose, we use the relation between the subtraction constants and the  $\Lambda$ -RS, and employ a common UV cutoff for all baryon-meson loops within reasonable limits (we refer the reader to Subsec 3.2.2 for details). In this way, on the one hand, we avoid any fictitious reduction of any baryon-meson channel by

using a small value of the cutoff and, on the other hand, we prevent an arbitrary variation of the subtraction constants<sup>4</sup>, since we correlate all of them to a reasonable value of the UV cutoff, while still keeping the full analyticity of the baryon-meson loops.

To identify our five dynamically generated  $\Omega_c$  and  $\Omega_c^*$  states of Table 9.1 using the new subtraction constants, we first need to determine how the masses (and widths) of our generated states change as we adiabatically vary the values of the subtraction constants. This can be done by

$$G_i(s) = \bar{G}_i(s) - (1-x)\bar{G}_i(\mu^2) + xG_i^\Lambda(s_{i+}), \quad (9.2)$$

where  $x$  is a parameter that changes slowly from 0 to 1,  $\mu^2 = (m_{th}^2 + M_{th}^2)$  and  $G_i^\Lambda(s_{i+})$  is the divergent part of the loop function regularized with a sharp-cutoff (given by Eq. (3.101)). In this manner, we can follow in the complex energy plane the original  $\Omega_c$  and  $\Omega_c^*$  as we modified our prescription to use a common cutoff for the computation of the subtraction constants.

Our results for the  $\Omega_c$  and  $\Omega_c^*$  are shown in Table 9.4 for a fixed cutoff of  $\Lambda = 1090$  MeV. In this case, we find that three poles (those previously named **c**, **b** and **d**) can be identified with the three experimental states at 3000 MeV, 3050 MeV and 3119 or 3090 MeV. The identification is possible not only due to the closeness in energy to the experimental ones but also because of the dominant contribution of the experimental  $\Xi_c \bar{K}$  and  $\Xi_c' \bar{K}$  channels to their dynamical generation. The contribution is measured by the product  $gG$  at the pole, as reported in Table 9.5 for  $J = 1/2$  and Table 9.6 for  $J = 3/2$ . For the  $J = 1/2$  state at 2994 MeV (pole **c**), we observe a significant contribution of the  $\Xi_c' \bar{K}$  and  $\Xi_c \bar{K}$  channels, while  $\Omega_c \eta$  is also relevant. We identify this state with  $\Omega_c(3000)$ . As for the  $J = 1/2$  state at 3117 MeV (pole **d**), the dominant contribution comes from  $\Xi D$  but also from  $\Xi_c \bar{K}^*$ ,  $\Xi D^*$  and  $\Xi_c \bar{K}$ . Thus, we can identify this state with  $\Omega_c(3119)$  or the  $\Omega_c(3090)$  given its proximity in mass. Moreover, a sizable width of  $8.7 \pm 1.0 \pm 0.8$  MeV is reported for the latter state in Ref. [348] to be compared with the one around 4 MeV found here for the state **d**. Finally, the  $J = 3/2$  state at 3049 MeV (pole **b**) could be identified with  $\Omega_c(3050)$  as it couples strongly to  $\Xi_c^* \bar{K}$  and  $\Xi_c \bar{K}^*$ , channels connected to  $\Xi_c \bar{K}$  by  $d$ -wave transitions, while having also an important contribution from  $\Omega_c^* \eta$ . In summary, two  $J = 1/2$  and one  $J = 3/2$  can be identified experimentally for a cutoff of  $\Lambda = 1090$  MeV.

In order to assess the dependence of our results on the cutoff, we have examined lower and higher values. As indicated before, the variation in the cutoff scale changes the value of the subtraction constant. This variation is related to the change of the size of higher order corrections in the meson-baryon scattering amplitude that are not known and not fixed by unitarization. Below 800 MeV, all resonances become

<sup>4</sup>This will induce an enormous freedom difficult to fix with the scarce available data.



heavier and much wider than the observed LHCb states. Actually, a clear identification between our results and some of the experimental states is not possible until a value of  $\Lambda \sim 1000$  MeV. For cutoffs bigger than 1300–1350 MeV, the  $\Omega_c$  and  $\Omega_c^*$  states coming from the most attractive  $SU(6)_{\text{lsf}} \times \text{HQSS}$  representations appear well below 3 GeV, and we can neither make an identification between those states and the LHCb spectrum. In Fig. 9.3, we show the obtained pole positions for  $\Lambda = 1090$  MeV (Table 9.4) and two additional cutoffs, around 100 MeV smaller and bigger, respectively, than this central one. It can be seen that for  $\Lambda = 1090$  MeV and  $\Lambda = 1200$  MeV, a maximum number of three states can be identified. As compared to the  $\Lambda = 1090$  MeV case previously discussed, for  $\Lambda = 1200$  MeV we can identify two  $\Omega_c^*$  states with  $J = 3/2$  at 3000 MeV and 3090 MeV, whereas a  $J = 1/2$   $\Omega_c$  is seen at 3050 MeV. The  $J = 1/2$  state at 3050 MeV corresponds now to the **d** state, that for  $\Lambda = 1090$  MeV was identified with the  $\Omega_c(3119)$  or  $\Omega_c(3090)$  resonances, and it has a dominant  $\Xi D$  component. It might still be the  $\Omega_c(3090)$ . The  $J = 1/2$  **c** pole now moves well below 3 GeV and this makes difficult its identification with any of the LHCb states. In the  $J = 3/2$  sector, the resonance that appears at 3000 MeV is the pole **b** and strongly couples to  $\Xi_c^* \bar{K}$  and  $\Xi_c \bar{K}^*$ , as already mentioned above. The additional  $J = 3/2$  state at 3090 MeV is the pole **e** in the nomenclature used in Table 9.4 for  $\Lambda = 1090$  MeV, and as it can be seen there, it has a large  $\Xi D^*$  molecular component, and it could be associated to the  $\Omega_c(3119)$  or  $\Omega_c(3090)$  LHCb resonances. In all three cases and in order to make the experimental identification possible, a significant coupling to the  $\Xi_c \bar{K}$  channel could be obtained, often via  $\Xi_c^* \bar{K}$  and  $\Xi_c \bar{K}^*$  allowing for the  $d$ -wave transitions. In summary we see that by changing the UV cutoff, the pole positions of the dynamically generated states are modified making more plausible different identifications between some of these states and those observed by LHCb.

As mentioned in the introduction of the chapter, the molecular nature of the five  $\Omega_c$  narrow states has been recently analyzed in Refs. [351, 388] as well as the observed broad structure around 3188 MeV in Ref. [432]. In Ref. [351] the interaction of the low-lying mesons (pseudoscalar and vector mesons separately) with the ground-state  $1/2^+$  baryons in the  $C = +1$ ,  $S = -2$  and  $I = 0$  sector has been built from  $t$ -channel vector meson exchanges. Two  $J = 1/2$  baryon-meson molecular states could be identified with the experimental  $\Omega_c(3050)$  and  $\Omega_c(3090)$ , mostly having the state at 3050 MeV a  $\Xi_c' \bar{K}$  component with an admixture of  $\Omega_c \eta$ , while the 3090 MeV would be a  $\Xi D$  molecule. These results have been reproduced in the  $J = 1/2$  sector in Ref. [388], within a LHG approach extended to the charm sector that also incorporates baryon  $3/2^+$ -pseudoscalar meson components. This is because the diagonal terms in the interaction kernel are the same in both models and these two  $\Omega_c$  states do not couple to baryon  $1/2^+$ -vector meson channels in Refs. [351, 388]. Furthermore, by incorporating baryon  $3/2^+$ -pseudoscalar meson states, a  $J = 3/2$  baryon-meson molecular state has been also identified in Ref. [388] with the experimental  $\Omega_c(3119)$ . This state

would be a baryon  $3/2^+$ - pseudoscalar meson molecule with large couplings to  $\bar{K}\Xi_c^*$  and  $\Omega_c^*\eta$ .

For  $\Lambda = 1090$  MeV, we have also obtained in the present analysis three baryon-meson molecular states that couple predominantly to  $\bar{K}\Xi_c'$ ,  $D\Xi$  and  $\bar{K}\Xi_c^*$ , respectively, but with a different experimental assignment of masses, that is,  $J = 1/2$   $\Omega_c(3000)$  and  $J = 1/2$   $\Omega_c(3119)$  or  $\Omega_c(3090)$ , and  $J = 3/2$   $\Omega_c(3050)$ , which correspond to poles **c** and **d**, and **b**, respectively. However, the  $g_i G_i(s_R)$  strengths for the dominant channels found in this work are in reasonable good agreement with those given in Ref. [388]. As we have illustrated in Fig. 9.3, our predictions for masses are subjected to sizable uncertainties, which might lead to confusions in the assignments to the LHCb states proposed in this work.

Nevertheless we should highlight that, we use here a different regularization scheme of the loop functions and different interaction matrices than in the works of Refs. [351, 388] that should explain the differences found. Note that the matrix elements involving the interaction of Goldstone-bosons and heavy-baryons are fixed by chiral symmetry and should agree in the three approaches. The differences come from channels involving  $D$ ,  $D^*$  and light-vector mesons, where HQSS does not completely fix the interactions. Furthermore, in the models of Refs. [351, 388] some HQSS breaking terms suppressed by the heavy-quark-mass are accepted. In addition, we incorporate the mixing of channels involving pseudoscalar mesons with channels involving vector mesons, while such mixings are claimed to be negligible in the case of Ref. [388]. Our model also incorporates the contribution of baryon-meson states of higher mass than those included in Refs. [351, 388], though, those heavier baryon-meson channels do not give any relevant contribution to the generation of the low-lying  $\Omega_c$  and  $\Omega_c^*$  states.

In Ref. [432] the broad structure observed by the LHCb Collaboration around 3188 MeV has been analyzed as the superposition of two  $D\Xi$  bound states within the Bethe-Salpeter formalism in the ladder and instantaneous approximation. As can be seen in Fig. 9.3. we also generate resonances in this region, but it is difficult to reach any conclusion since most likely, we would have to consider also some states from less attractive  $SU(6)_{\text{lf}} \times \text{HQSS}$  multiplets, stemming from the exotic **4752**  $SU(8)$  representation [86]. A candidate of a loosely bound molecular state with a large  $\Xi_c^* \bar{K}$  component and a mass around 3140 MeV is also predicted in Ref. [89]. It results from  $\Xi_c^* \bar{K} / \Xi_c \bar{K}^* / \Xi_c' \bar{K}^*$  coupled-channel dynamics using a one-boson-exchange potential. It is difficult to associate such state with any of the predictions obtained here from the scheme of Ref. [86], since the work of Ref. [89] does not consider  $\Xi^{(*)} D^{(*)}$  channels.

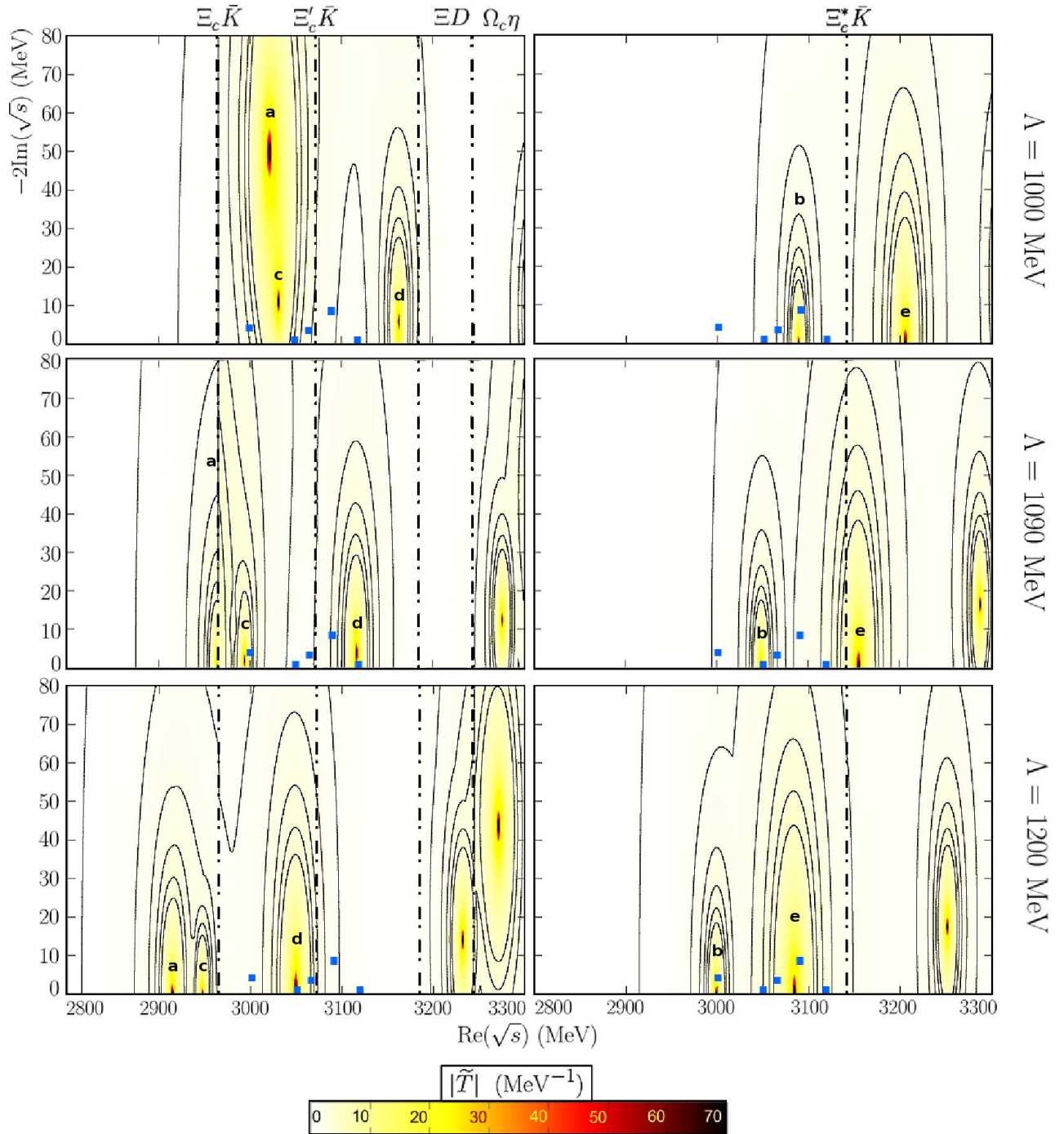
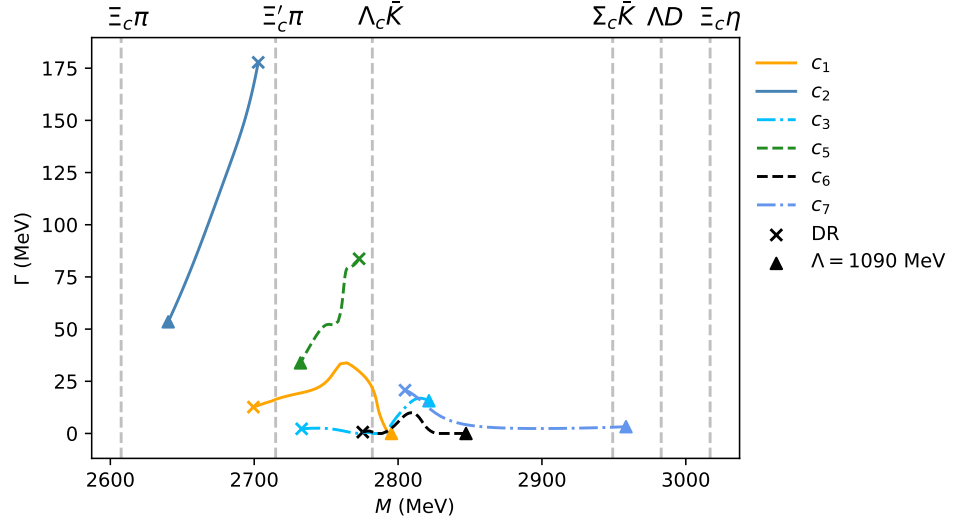
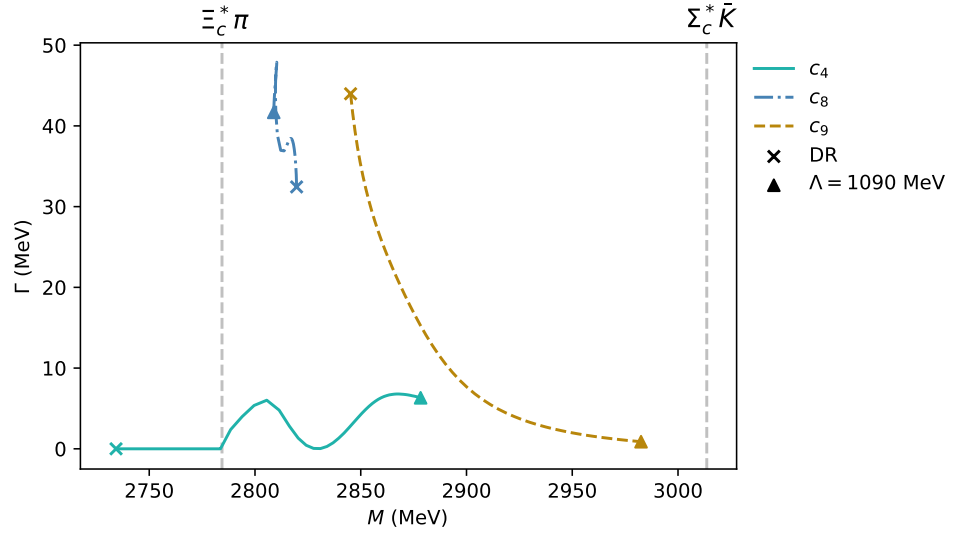


Figure 9.3:  $\Omega_c$  and  $\Omega_c^*$  states for different UV cutoffs. The blue squares indicate the experimental points. Dashed-dotted lines represent the closest baryon-meson thresholds. The left plots are for  $J = \frac{1}{2}$  and the right ones for  $J = \frac{3}{2}$ , while the function  $|\tilde{T}(z)|_J$  is defined as in Fig. 9.1. For the two largest values of  $\Lambda$ , some resonant states from less attractive  $\text{SU}(6)_{\text{lf}} \times \text{HQSS}$  multiplets, stemming from the exotic  $\mathbf{4752}$   $\text{SU}(8)$  representation, are also visible in the region of higher masses.

### 9.3.2 $\Xi_c$ excited states



(a)  $J = 1/2$



(b)  $J = 3/2$

Figure 9.4: Evolution of the masses and widths of the dynamically generated  $\Xi_c$  states as we vary the renormalization scheme from using a subtraction constant to a common cutoff of  $\Lambda = 1090$  MeV. The cross symbolizes the position of the states in the subtraction constant scheme (or dimensional regularization (DR)) [86], while the triangle indicates the mass and width of the same states for the cutoff scheme.

As already pointed out, the first observation of the  $\Xi_c(2930)$  state was reported by the Belle Collaboration in Ref. [381]. This state was observed through its decay to  $\Lambda_c^+ K^-$  with no assigned quantum numbers. Besides this recently discovered state, there are other three  $\Xi_c$  excited states with energies below 3 GeV [21]. As seen in Table 9.7, the  $1/2^-$   $\Xi_c(2790)$  state decays into  $\Xi_c' \pi$ , whereas the  $3/2^-$   $\Xi_c(2815)$  decays into  $\Xi_c' \pi$  and has also the decay chain  $\Xi_c^* \pi$ , followed by  $\Xi_c^* \rightarrow \Xi_c \pi$  [403]. Also, a  $\Xi_c(2970)$  with unknown quantum numbers has been observed decaying into  $\Lambda_c^+ \bar{K} \pi$ ,  $\Sigma_c \bar{K}$ ,  $\Xi_c 2\pi$ ,  $\Xi_c' \pi$  and  $\Xi_c^* \pi$ .

We again start by revising the results Ref. [86] in the  $\Xi_c$  sector in order to understand whether the experimental states can be accommodated in our model. We perform in this sector an analysis similar to that carried out in the previous subsection for the  $\Omega_c^*$  states. In view of these latter results, we will only attempt to vary here the UV cutoff  $\Lambda$  and not the subtraction parameter  $\alpha$  of the  $\mu$ -RS (Eqs. (3.95),(3.97) and (7.3)). The widths of our  $\Xi_c$  states as a function of their masses in the  $J = 1/2$  and  $J = 3/2$  sectors are shown in the upper and lower plots of Fig. 9.4, respectively, together with different baryon-meson thresholds, to which they can couple. The dynamically generated states of Ref. [86] are displayed with a cross and the "DR" legend, as those have been obtained using one subtraction at certain scale or dimensional regularization. In what follows, we label the states as  $c_1 \dots c_9$ , and they correspond to those given in Table V of Ref. [86]. They have either  $J^P = 1/2^-$  or  $J^P = 3/2^-$  and are ordered by their mass position. Hence,  $c_1$  ( $c_9$ ) corresponds to the lightest (heaviest) state of mass 2699.4 MeV (2845.2 MeV), among those quoted in the mentioned table, where their SU(6) and SU(3) quantum numbers are also given. We observe that the masses of our  $\Xi_c$  states using one subtraction constant (DR) are below or close to the experimental  $\Xi_c(2790)$  or  $\Xi_c(2815)$  states, while being far below in mass with respect to  $\Xi_c(2930)$  or  $\Xi_c(2970)$ .

Again, we slowly evolve in Eq. (9.2)  $x$  from 0 to 1 while following the evolution of the states, as seen in Fig. 9.4, to a sharp cutoff. Here we choose  $\Lambda = 1090$  MeV, which was the preferred cutoff for the  $\Omega_c$  excited states studied in the previous subsection. The  $c_1$  to  $c_9$  states for a  $\Lambda = 1090$  MeV are shown with a triangle. We find that most of these states move to higher energies, except for  $c_2$ ,  $c_5$  and  $c_8$ , whereas getting closer to the experimental values. Note that for this cutoff, the  $J^P = 1/2^-$   $c_1$  state become virtual above the  $\Lambda_c \bar{K}$  threshold.

Once we have identified our  $\Xi_c$  states in the cutoff scheme, we can assess the dependence of our results on this regulator, as well as their possible experimental identification. In Fig. 9.5 we show the evolution of the  $c_1$  to  $c_9$  states as we vary the cutoff from 1 GeV (triangles) to 1.2 GeV (crosses), and we also display different two-body thresholds. Moreover, in Table 9.8 we show masses and widths of the  $c_1$  to  $c_9$  states with  $J = 1/2$  or  $J = 3/2$ , together with the couplings to the dominant baryon-meson channels ( $g > 1$ ) and the couplings to the decay channels reported

experimentally for the  $\Xi_c$  states. All these results are obtained for  $\Lambda = 1150$  MeV. In this table we also indicate the  $SU(6)_{\text{lsf}} \times \text{HQSS}$ ,  $SU(6)$  and  $SU(3)$  irreps, to which the  $c_1$  to  $c_9$  states belong (see Ref. [86] for group-structure details).

As we evolve the cutoff value from  $\Lambda = 1000$  MeV to  $\Lambda = 1200$  MeV, that is, from the right to left in Fig. 9.5, we observe that some of our dynamically generated resonances can be identified with the experimental states attending to the complex energy position. In the  $J^P = 1/2^-$  sector, we observe that the  $\Xi_c(2790)$  could be one of the  $c_1$ ,  $c_3$ ,  $c_6$  or even the  $c_5$  states. The identification with the  $\Xi_c(2790)$  is possible because these states couple to  $\Xi'_c \pi$ , although this baryon-meson channel is not the dominant one for their dynamical generation, as seen in Table 9.8 for a  $\Lambda = 1150$  MeV, except for  $c_5$ . Indeed, this latter feature of  $c_5$  disfavors its identification with the  $\Xi_c(2790)$ . This is because it would become too broad ( $\Gamma \geq 70$  MeV) for UV cutoffs of around 1 GeV, that would lead the  $c_5$  resonance to have masses closer to the experimental one, as seen in Fig. 9.5. In addition in the DR scheme, the mass of the  $c_5$  state is close to 2790 MeV, but its width is approximately of 84 MeV [86] (see also Fig. 9.4), while experimentally  $\Gamma_{\Xi_c(2790)} \sim 10$  MeV.

Looking at the behavior of the  $c_1$ ,  $c_3$ ,  $c_6$  poles with the UV cutoff in Fig. 9.5, it seems natural to assign the  $\Xi_c(2790)$  to the  $c_1$  pole. This state has a width of the order of 10 MeV for UV cutoffs in the region of 1.2 GeV, where it is located below the  $\Lambda_c \bar{K}$  threshold. At the same time, the state has large  $\Lambda_c \bar{K}$  and small  $\Xi'_c \pi$  couplings (see Table 9.8), respectively, which explains its small experimental width despite being placed well above the latter threshold, and it is natural to think that the  $\Lambda_c \bar{K}$  channel should play an important role in the dynamics of the  $\Xi_c(2790)$  given its proximity to that threshold. Note that the light degrees of freedom (*ldof*) in the inner structure of the  $c_1$  are predominantly coupled to  $j_q^P = 0^-$  spin-parity quantum numbers (see Chapter 7). Thus with this identification, this first odd parity excited  $\Xi_c$  state would not have a dominant configuration consisting of a spinless light diquark and a unit of angular momentum between it and the heavy quark, as argued for instance in the Belle paper [403]. This is to say, the  $\Xi_c(2790)$  will not be a constituent quark model  $\lambda$ -mode excited state (see Ref. [312] and Chapter 7) with  $j_q^P = 1^-$  and hence it will not form part of any HQSS doublet, thus making the assignment to  $c_3$  unlikely. Actually, if the spin-parity quantum numbers for the *ldof* in the  $\Xi_c(2790)$  were predominantly  $1^-$ , one would expect a larger width for this resonance, since its decay to the open channel  $\Xi'_c \pi$  is HQSS allowed. This is precisely the situation for the  $c_3$  that is broader than the experimental state. In summary, we conclude a large molecular  $\Lambda_c \bar{K}$  component for the  $\Xi_c(2790)$  that will have then a dominant  $j_q^P = 0^-$  configuration. The  $\Xi_c(2790)$  identification with the  $c_1$  pole differs from the previous assignments in Ref. [86], where the  $\Xi_c$  states were obtained using the one subtraction RS. There, the  $c_7$  state was assigned to  $\Xi_c(2790)$  due to its closeness in energy and the sizable  $\Xi'_c \pi$  coupling within the DR scheme.

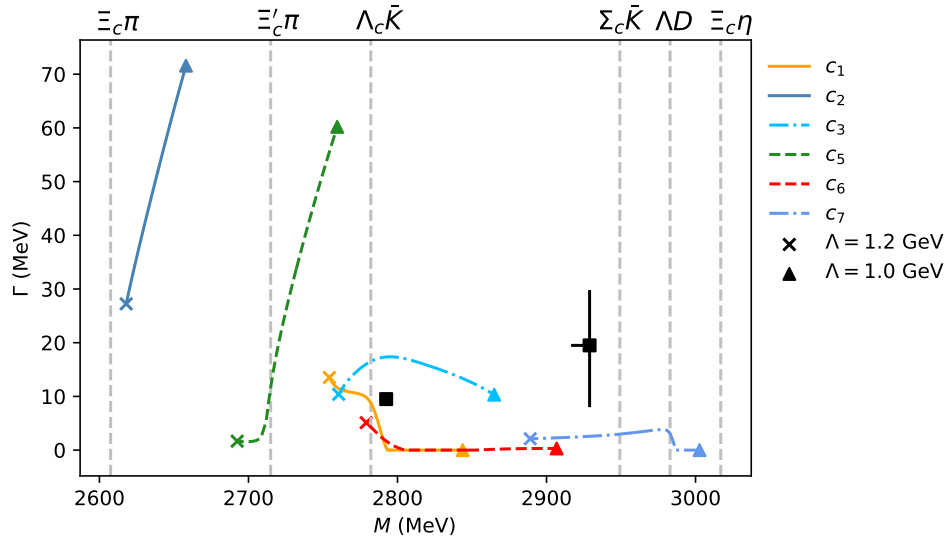
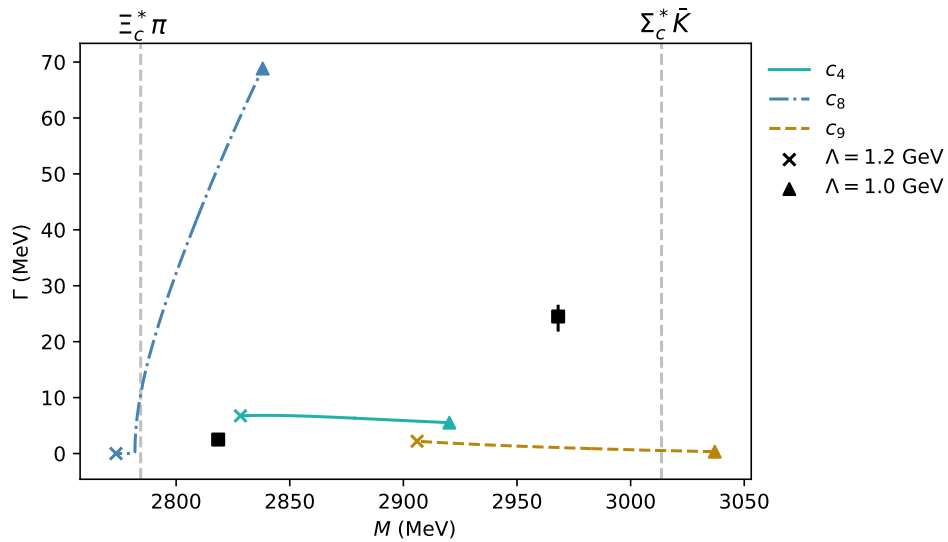
(a)  $J = 1/2$ (b)  $J = 3/2$ 

Figure 9.5: Evolution of the masses and widths of the dynamically generated  $\Xi_c$  states, as we vary the cutoff from  $\Lambda = 1$  GeV (triangles) to  $\Lambda = 1.2$  GeV (crosses). In Fig. 9.5a (Fig. 9.5b), the  $c_1$  ( $c_8$ ) state becomes virtual above (below) the  $\Lambda_c \bar{K}$  ( $\Xi_c^* \pi$ ) threshold. The squares and their associated errorbars show the masses and widths of the experimental  $\Xi_c(2790)$  and  $\Xi_c(2930)$  (Fig. 9.5a) and  $\Xi_c(2815)$  and  $\Xi_c(2970)$  (Fig. 9.5b) together with their experimental errors. The spin-parity of both  $\Xi_c(2930)$  and  $\Xi_c(2970)$  resonances are not experimentally determined [21], and we have displayed them here just for illustrative purposes.

With regards to the recently discovered  $\Xi_c(2930)$ , if we assume that this state has  $J^P = 1/2^-$ , we could identify it either with our  $c_6$  or  $c_7$  states, as they both couple to the  $\Lambda_c \bar{K}$  channel, although not dominantly as seen in Table 9.8 for a  $\Lambda = 1150$  MeV. The assignment to the  $c_6$  pole is, however, disfavored because of the mass difference between this state and the experimental  $\Xi_c(2930)$ . As for  $c_7$ , the small  $\Lambda_c \bar{K}$  coupling of this state makes also somehow doubtful its identification with the  $\Xi_c(2930)$ . In the case of our  $c_2$  and  $c_5$  states, we should mention that we do not have any clear experimental candidate at this point for the  $c_5$  dynamically generated  $J = 1/2$  state, whereas the  $c_2$  state becomes broad and appears below 2650 MeV, thus not allowing for any reasonable experimental assignment.

For  $J^P = 3/2^-$ , the analysis of the evolution of the different states in Fig. 9.5 allows for the identification of the experimental  $\Xi_c(2815)$  with  $c_4$  or  $c_8$ . These states couple to  $\Xi_c^* \pi$  in  $s$ -wave, although for  $c_4$ , couplings to other baryon-meson states ( $\Sigma_c^* \bar{K}$ ,  $\Lambda_c \bar{K}^*$  or  $\Sigma_c^* \bar{K}^*$ ) are larger as seen in Table 9.8. The experimental  $\Xi_c(2815)$  is quite narrow,  $\Gamma_{\Xi_c(2815)} \sim 2 - 3$  MeV, despite the  $\Xi_c^* \pi$  threshold being around 30 MeV below its mass. This hints to a subdominant  $\Xi_c^* \pi$  molecular component in the inner structure of this resonance. Moreover, looking at the dependence of the  $J^P = 3/2^-$  pole masses and widths with the UV cutoff displayed in Fig. 9.5, it seems reasonable to assign the  $c_4$  state to the  $\Xi_c(2815)$  resonance.

As for  $\Xi_c(2970)$ , assuming that it has  $J = 3/2^-$ , we could identify it with the  $c_9$  state for values of the cutoff around  $\Lambda \simeq 1.1$  GeV. In this case, we have to take into account that this state couples to  $\Lambda_c \bar{K}^*$  and  $\Sigma_c^* \bar{K}$ , and  $\Xi_c^* \pi$  (though not dominantly), and those baryon-meson channels can decay into  $\Lambda_c \bar{K} \pi$  and  $\Xi_c \pi \pi$ , respectively. Nevertheless, the predicted width would be significantly smaller than the range of 20-30 MeV quoted in the PDG [21] and shown in Table 9.7. Compared to the results of Ref. [86], the  $\Xi_c(2815)$  was identified there with  $c_9$ , assuming that  $\Xi_c(2790)$  and  $\Xi_c(2815)$  were the  $c_7$  and  $c_9$  HQSS partners.

In fact, we observe several HQSS partners among our states as well as possible siblings within the same SU(3) representation. The  $\Xi_c(2790)$  resonance belongs to an  $J = 1/2$  SU(3) antitriplet irrep, and it would be the  $SU(6)_{\text{lsf}} \times \text{HQSS}$  (see Table 9.8) partner of a narrow  $\Lambda_c^*$  state discussed in Refs. [86, 172] and Chapter 7. This latter state has large (small)  $ND$  and  $ND^*$  ( $\Sigma_c \pi$ ) couplings, and depending on the renormalization scheme (one-subtraction or UV cutoff), it is part of a double pole pattern for the  $\Lambda_c(2595)$ , similar to that found for the  $\Lambda(1405)$  within unitarized chiral models [24, 32, 34, 35, 64, 69, 292, 324] (see related review in [21]), or it is located in the region of 2.8 GeV close to the  $ND$  threshold (see Chapter 7).

On the other hand, the  $c_3$  pole belonging to  $(\mathbf{168}, \mathbf{21}, \mathbf{6}_2)$  representation and the  $c_4$  of the  $(\mathbf{168}, \mathbf{21}, \mathbf{6}_4)$  form a  $(j_q^P = 1^-)$ -HQSS doublet. As mentioned earlier, the  $c_4$  can be identified with the  $\Xi_c(2815)$ , but we note that the  $\Xi_c(2815)$  is not the sibling of the  $\Lambda_c(2625)$  because of the different coupling strengths to  $\Xi_c^* \pi$  and  $\Sigma_c^* \pi$ , respectively.



Whereas  $\Xi_c(2815)$  weakly couples to  $\Xi_c^*\pi$ , the  $\Lambda_c(2625)$  strongly does to  $\Sigma_c^*\pi$ . However, this latter state is narrow because the  $\Sigma_c^*\pi$  channel is closed (located around 30 MeV above the mass of the resonance). Indeed, recently it has been argued that the  $\Lambda(2625)$  is probably a constituent three quark state (see [312] and Chapter 7).

As for the  $J = 1/2$   $c_5$  and the  $J = 3/2$   $c_8$  states, those form part of a SU(6) **15**-plet, belonging to the SU(6)<sub>1sf</sub>× HQSS (**168, 15, 3<sub>2</sub>**) and (**168, 15, 3<sub>4</sub>**) irreps [86]. They form a HQSS doublet with  $j_q^P = 1^-$  and hence have large couplings to  $\Xi_c'\pi$  and  $\Xi_c^*\pi$ , respectively. Indeed, as a good approximation, they are dynamically generated by the charmed baryon–Goldstone boson interactions. These moderately broad states are in the SU(3)<sub>2J+1</sub> **3<sub>2</sub>**\* and **3<sub>4</sub>**\* irreps, which should be completed by one  $J = 1/2$  and one  $J = 3/2$   $\Lambda_c$  resonances stemming from the  $\Sigma_c\pi$  and  $\Sigma_c^*\pi$  chiral interactions (see Ref. [340] and Chapter 7), neglecting higher energy channels. The  $J = 3/2$  sibling is, however, not the  $\Lambda_c(2625)$ . As mentioned before, the  $\Lambda_c(2625)$  is probably a quark model ( $\lambda$ -mode excitation) state (see Ref. [312] and Chapter 7). Another resonance with mass and width of around 2.7 GeV and 60 MeV (see Ref. [340] and Chapter 7), that has not been discovered yet, would then be the SU(3) sibling of the  $c_8$  state.

The features of the  $J = 1/2$  counterpart of  $c_5$  in the  $\Lambda_c$  sector are much more uncertain and depend on both the employed renormalization scheme and on the interplay between quark-model and baryon-meson degrees of freedom (see Chapter 7). Thus, for instance neglecting the latter, it would appear around 2.6 GeV with a large width of 60–80 MeV because its sizable coupling to the  $\Sigma_c\pi$  pair. Within the UV cutoff RS, this state can be easily moved below the  $\Sigma_c\pi$  threshold and be identified with the narrow  $\Lambda_c(2595)$  [340]. In the DR scheme advocated in Ref. [86], this broad state, together with the  $j_q^P = 0^-$  narrow state mentioned above in the discussion of the  $\Xi_c(2790)$ , gives rise to a double pole structure for the  $\Lambda_c(2595)$ .

Within the UV cutoff renormalization scheme examined here, the ( $c_7, c_9$ ) HQSS-doublet might correspond to the experimental  $\Xi_c(2930)$  and  $\Xi_c(2970)$  states. The  $c_7$  state, that we have tentatively assigned to the  $\Xi_c(2930)$ , exhibits (Table 9.8) moderate couplings to  $\Xi_c\pi$  and  $\Lambda_c\bar{K}$ , small ones to  $\Xi_c'\pi$  and  $\Sigma_c\bar{K}$ , and finally large couplings to  $\Lambda D^{(*)}$ ,  $\Sigma D^{(*)}$  and  $\Sigma^*D^*$ . It belongs to a SU(3) sextet, where there is also a  $\Omega_c$  state. The latter corresponds to the one labeled as **d** in the previous subsection, where it was tentatively assigned either to the  $\Omega_c(3090)$  or the  $\Omega_c(3119)$  observed by the LHCb Collaboration in the  $\Xi_c\bar{K}$  mode [348]. This is in fact consistent with what one might expect from its  $c_7$ -sibling couplings. Assuming the *equal spacing rule* we could predict the possible existence of a  $J = 1/2^-$   $\Sigma_c$  state around 2800 MeV that will complete the sextet. The  $\Sigma_c(2800)$  clearly fits into this picture since it is observed in the  $\Lambda_c\pi$  channel [21].

Recently there has been an analysis of the  $\Xi_c$  sector within a baryon-meson molecular model based on LHG that implements the interaction between the  $1/2^+$  and  $3/2^+$  ground-state baryons with  $0^-$  and  $1^-$  mesons (see Chapter 8). The authors

have found that five of their dynamically generated  $\Xi_c$  states can be identified with the experimental  $\Xi_c(2790)$ ,  $\Xi_c(2930)$ ,  $\Xi_c(2970)$ ,  $\Xi_c(3055)$  and  $\Xi_c(3080)$ . Whereas the  $\Xi_c(2790)$  would be a  $1/2^-$  state, the  $\Xi_c(2930)$ ,  $\Xi_c(2970)$ ,  $\Xi_c(3055)$  and  $\Xi_c(3080)$  could be either  $1/2^-$  or  $3/2^-$  ones. Compared to this approach, our model identifies the experimental  $\Xi_c(2790)$  and  $\Xi_c(2930)$  as  $1/2^-$  states, and the  $\Xi_c(2815)$  and  $\Xi_c(2970)$  as  $3/2^-$ . The different assignment is mainly due the distinct renormalization scheme used in the two approaches as well as the fact the interactions involving  $D$  and  $D^*$  and light vector mesons with baryons are not completely fixed by HQSS or chiral symmetries, thus allowing for different assumptions.

### 9.3.3 $\Xi_b$ excited states

With regards to the bottom sector, the  $\Xi_b(6227)$  resonance has been recently measured by the LHCb experiment [382], with  $\Gamma_{\Xi_b(6227)} \sim 18$  MeV. Its quantum numbers, though, remain unknown, whereas the observed decay channels are  $\Lambda_b^0 K^-$  and  $\Xi_b^0 \pi^-$  (see Table 9.7).

We start again by revising the previous results of Ref. [83] with  $B = -1$ ,  $S = -1$ ,  $I = 1/2$  ( $\Xi_b$  sector). Masses and widths of the dynamically generated states within our model using the DR scheme, together with their irreps, spins and couplings to the dominant baryon-meson channels as well those for the experimental decay channels of  $\Xi_b(6227)$  are shown in Table 9.9. We obtain nine states, which are the bottom counterparts of the  $\Xi_c$  ones discussed in the previous subsection. Compared to Ref. [83], we report here five more poles, since in that reference only SU(3) flavor partners of  $\Lambda_b$  states were searched (members of antitriplet irreps). Also, two of them, the state at 6035 MeV with  $J = 1/2$  and the one at 6043 MeV with  $J = 3/2$  were wrongly assigned in Ref. [83] to the SU(6) **15** representation. Instead, they should belong to the SU(6) **21** representation, as seen in Table 9.9. Moreover, there is a state at 6073 MeV in Table IV in Ref. [83] that does not appear in our present calculation. The differences between of them are due to the difficulty in determining the number of states and their representations as we break the  $SU(6)_{\text{lf}} \times \text{HQSS}$  symmetry to SU(3) in the bottom sector, as almost all states have zero width and states with widths closer to zero are more difficult to follow in the complex energy plane.

As in the  $\Xi_c$  sector, our  $b_1$  to  $b_9$  states using one-subtraction renormalization are too low in energy so as to assign any of them to the experimental  $\Xi_b(6227)$  state. Thus, we proceed as in the previous subsection and vary the renormalization scheme from one-subtraction to cutoff. In this manner, we identify our  $b_1$  to  $b_9$  states using one-subtraction renormalization with the ones within the cutoff scheme, and we study their evolution as we change the value of the cutoff.

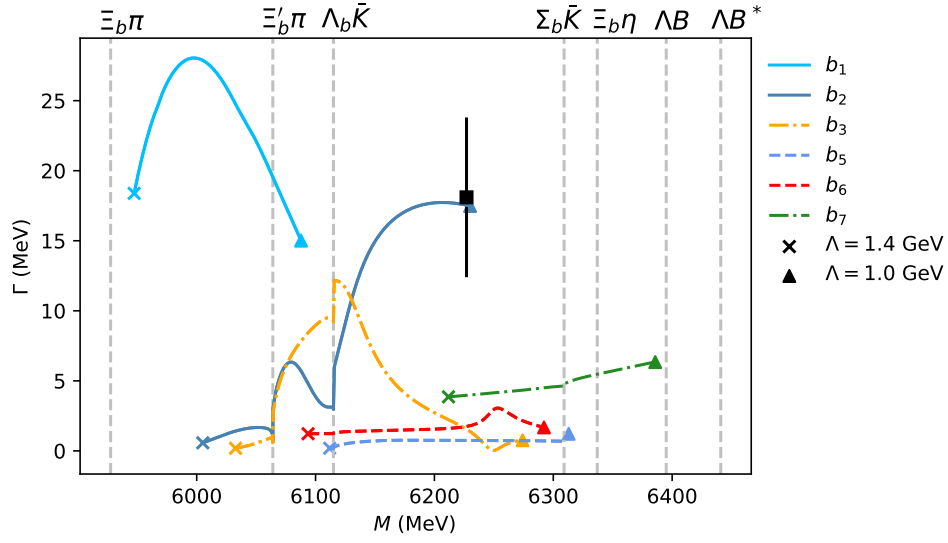
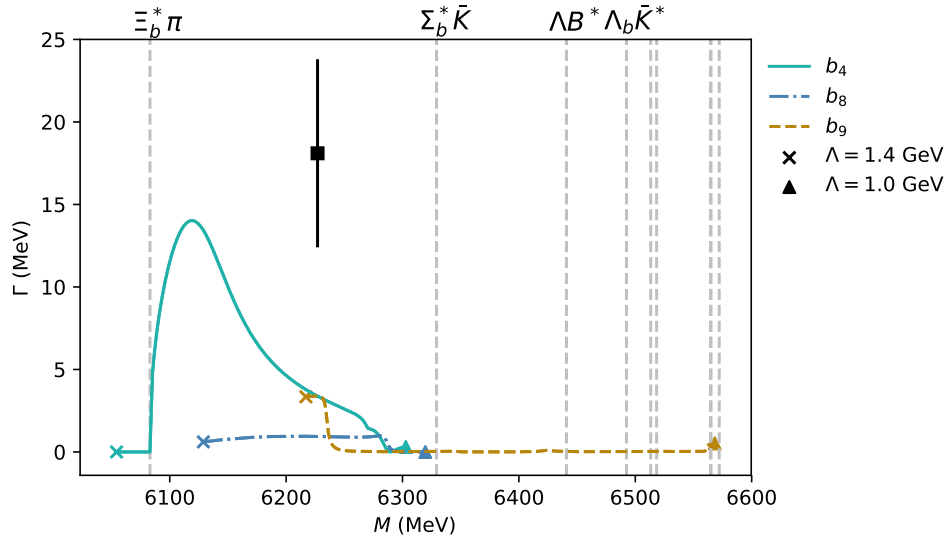
(a)  $J = 1/2$ (b)  $J = 3/2$ 

Figure 9.6: Evolution of the masses and widths of the dynamically generated  $\Xi_b$  states, as we vary the cutoff from  $\Lambda = 1000$  MeV (triangles) to  $\Lambda = 1400$  MeV (crosses), with  $J = 1/2$  (upper panel) and  $J = 3/2$  (lower panel). The square and its bars represent the position of the  $\Xi_b(6227)$  resonance, and its errors in mass and width, respectively. We show the experimental result for both values of  $J$  due to its unknown quantum numbers. In Fig. 9.6b, the last five thresholds (not labelled in the figure because they are too close to each other) are:  $\Xi_b^* \eta$  (6492.45 MeV),  $\Sigma B^*$  (6518.35 MeV),  $\Omega_b K$  (6564.68 MeV),  $\Xi_b \rho$  (6565.04 MeV) and  $\Xi_b \omega$  (6572.12 MeV).

In Fig. 9.6 we display the evolution of the masses and widths of the dynamically generated  $\Xi_b$  states as we vary the cutoff from  $\Lambda = 1000$  MeV (triangles) to  $\Lambda = 1400$  MeV, for  $J = 1/2$  (upper plot) and  $J = 3/2$  (lower plot). The square and its bar represent the position of the  $\Xi_b(6227)$  resonance, and the error for its mass and width, respectively. We show the experimental result ( $\Xi_b(6227)$ ) for both  $J = 1/2$  and  $J = 3/2$  because its quantum numbers have not been determined yet. Additionally, in Table 9.10, we collect the masses and the widths of the  $b_1$  to  $b_9$  states with  $J = 1/2$  or  $J = 3/2$ , together with the couplings to the dominant baryon-meson channels and the couplings to the decay channels of the  $\Xi_b(6227)$ , for  $\Lambda = 1150$  MeV as in the charm sector. We also indicate the  $SU(6)_{\text{HSF}} \times \text{HQSS}$ ,  $SU(6)$  and  $SU(3)$  irreducible representations of these states.

We might try now to assign the experimental  $\Xi_b(6227)$  to any of our states, while determining the negative parity baryons with  $B = -1$  belonging to the same  $\mathbf{3}^*$  and  $\mathbf{6}$   $SU(3)$  representations. The observed decay modes,  $\Lambda_b^0 K^-$ ,  $\Xi_b^0 \pi^-$  [382], of the resonance support that this state should have  $1/2^-$  spin-parity, assuming  $s$ -wave. Moreover, the  $j_q^P = 0^-$  component should be also quite relevant, which according to the couplings collected in Table 9.10 makes plausible its identification either with the  $b_1$  or  $b_2$  states. The evolution displayed in the upper plot of Fig. 9.6 leads us to assign the  $\Xi_b(6227)$  to the  $b_2$  state. The  $b_2$  pole would stem from a  $SU(6)$   $\mathbf{15}$ -plet, composed of  $J = 1/2$  and  $J = 3/2$   $SU(3)$  antitriplets and of a  $J = 1/2$   $SU(3)$  sextet, where the  $\Xi_b(6227)$  would be accommodated. The  $J = 1/2^-$   $\Lambda_b(5912)$  and  $J = 3/2^-$   $\Lambda_b(5920)$  (LHCb [346]) would be part of the  $\mathbf{3}_2^*$  and  $\mathbf{3}_4^*$  multiplets forming a HQSS-doublet [83]. These antitriplets should be completed by another HQSS-doublet of  $\Xi_b$  and  $\Xi_b^*$  states,  $b_5$  and  $b_8$ , that according to Fig. 9.6 and Table 9.10 should have masses around 6250 MeV and could be seen in the  $\Sigma_b^{(*)} \bar{K}$  and  $\Xi_b^{(*)} \pi$  modes.

Coming back to the  $\Xi_b(6227)$ , it belongs to a  $j_q^P = 0^-$  sextet that should be completed by  $J = 1/2$   $\Sigma_b$  and  $\Omega_b$  states. The recent  $\Sigma_b(6097)$  resonance seen by the LHCb Collaboration [433] in the  $\Lambda_b \pi$  channel nicely fits in this multiplet. Relying again in the *equal spacing rule*, we could foresee the existence of a  $J = 1/2$   $\Omega_b$  odd parity state with a mass of around 6360 MeV that should be observed in the  $\Xi_b \bar{K}$  channel. Some molecular  $\Omega_b$  states were predicted previously in Ref. [350], but all of them above 6.4 GeV.

Previous works based on molecular approaches have also found the  $\Xi_b(6227)$  as a dynamically-generated state. In Refs. [340, 430] a unitarized model using the leading-order chiral Lagrangian found the  $\Xi_b(6227)$  as a  $s$ -wave  $\Sigma_b \bar{K}$  molecule, with a preferred  $1/2^-$  spin-parity assignment [430]. In our present model the  $\Lambda \bar{B}^*$ ,  $\Sigma \bar{B}$  and  $\Lambda \bar{B}$  are the dominant channels in the generation of the  $\Xi_b(6227)$ , though it also couples (weakly) to  $\Sigma_b \bar{K}$ . The main difference between models comes from the fact that our scheme has a more extensive number of channels, whereas the antitriplet

and sextet multiplets of ground-state baryons mix when constructing the interaction matrices. Also, in Chapter 8 we have also analyzed the  $\Xi_b$  sector. There we have found two poles with masses close to the  $\Xi_b(6227)$  and widths  $\sim 25 - 30$  MeV, close to the experimental one, with  $1/2^-$  and  $3/2^-$  spin-parity. In this chapter, we identify the  $\Xi_b(6227)$  as a  $1/2^-$  state and, again, the difference arises because of the renormalization scheme and the interaction matrices involving  $D$ ,  $D^*$  and light vector mesons.



Figure 9.7: Bottom baryon states classified within the  $J = 1/2$  (left diagram) and  $J = 3/2$  (right diagram)  $SU(3) \mathbf{3}^*$  irreps. The question mark indicates states predicted in this work.



Figure 9.8: Charm and bottom resonances classified within  $SU(3) \mathbf{6}$  irreps with  $J = 1/2$ , which however stem from different  $SU(6)_{\text{sf}} \times \text{HQSS}$  irreps:  $(\mathbf{120}, \mathbf{21}, \mathbf{6}_2)$  and  $(\mathbf{168}, \mathbf{15}, \mathbf{6}_2)$ , respectively. The question mark indicates states predicted in this work.

$J = 1/2$			pole <b>d</b>		$J = 3/2$			
channel	$ g $	$gG$ (MeV)	channel	$ g $	$gG$ (MeV)	channel	$ g $	pole <b>e</b>
$\Xi_c \bar{K}$	0.1	$-1.4 + 0.3j$	$\Xi_c^* \bar{K}$	1.9	$-26.6 - 0.1j$	$\Xi_c \bar{K}^*$	1.6	$-14$
$\Xi_c' \bar{K}$	1.8	$-27.1$	$\Omega_c^* \eta$	1.7	16.3	$\Xi_c' \bar{K}^*$	0.6	$-4.9$
$\Xi D$	1.7	10.4	$\Xi D^*$	1.6	$-8.5$	$\Omega_c \omega$	0	0.3
$\Omega_c \eta$	1.7	15.7	$\Xi_c \bar{K}^*$	1.6	$-14$	$\Xi_c^* \bar{K}^*$	1.3	$-8.9$
$\Xi D^*$	0.8	$-3.5 - 0.1j$	$\Xi_c^* D$	0.5	$-2.7$	$\Xi_c^* \bar{K}^*$	0.6	$-2.4$
$\Xi_c \bar{K}^*$	1.3	10.1	$\Xi_c' \bar{K}^*$	0.6	$-4.9$	$\Omega_c^* \omega$	0.1	0.4
$\Xi_c' \bar{K}^*$	1.1	$-7.3 - 0.2j$	$\Omega_c \omega$	0	0.3	$\Xi_c^* \bar{K}^*$	1.3	$-8.9$
$\Omega_c \omega$	0.1	0.7	$\Xi_c^* \bar{K}^*$	1.3	$-8.9$	$\Xi_c^* D^*$	0.6	$-2.4$
$\Xi_c^* \bar{K}^*$	0.6	$3.6 - 0.2j$	$\Xi_c^* D^*$	0.6	$-2.4$	$\Omega_c^* \omega$	0.1	0.4
$\Xi_c^* D^*$	0.7	$-2.6$	$\Omega_c^* \omega$	0.1	0.4	$\Omega D_s$	0.8	$-3.3$
$\Omega_c^* \omega$	0	0	$\Omega D_s$	0.8	$-3.3$	$\Omega_c \phi$	0.6	3.5
$\Omega_c \eta'$	0.5	2.5	$\Omega_c \phi$	0.6	3.5	$\Omega_c^* \eta'$	0.5	2.8
$\Omega_c \phi$	1.1	$5.4 + 0.1j$	$\Omega_c^* \eta'$	0.5	2.8	$\Omega D_s^*$	1	$-3.4$
$\Omega D_s^*$	1.2	$-3.7$	$\Omega D_s^*$	1	$-3.4$	$\Omega_c^* \phi$	1.2	6.5
$\Omega_c^* \phi$	0.6	$-2.9 + 0.1j$	$\Omega_c^* \phi$	1.2	6.5			

Table 9.3: Properties of the  $\Omega_c(2999.9)$  an  $\Omega_c(3036.3)$  states, labeled as poles **d** and **e**, respectively, obtained using  $\alpha = 1.16$ . The first column displays the different baryon-meson channels coupled to  $\Omega_c(2999.9)$ , ordered by their threshold energies, in the  $J = 1/2$  sector. The second and third columns show the absolute value of the coupling and the product of the coupling times the loop function at the pole position, respectively, for all baryon-meson coupled states. The fourth, fifth and sixth columns are equivalent to the first three columns but for  $\Omega_c^*(3036.3)$  in the  $J = 3/2$  sector

Name	$M_R$ (MeV)	$\Gamma_R$ (MeV)	$J$	$M_R^{exp}$	$\Gamma_R^{exp}$
<b>a</b>	2963.95	0.0	1/2	—	—
<b>c</b>	2994.26	1.85	1/2	3000.4	4.5
<b>b</b>	3048.7	0.0	3/2	3050.2	0.8
<b>d</b>	3116.81	3.72	1/2	3119.1/ 3090.2	1.1/ 8.7
<b>e</b>	3155.37	0.17	3/2	—	—

Table 9.4:  $\Omega_c$  and  $\Omega_c^*$  states calculated using the subtraction constants associated to a cutoff of  $\Lambda = 1090$  MeV. We identify experimentally two  $J = 1/2$  and one  $J = 3/2$  states.

channel	pole <b>a</b>		pole <b>c</b>		pole <b>d</b>	
	$ g $	$gG$ (MeV)	$ g $	$gG$ (MeV)	$ g $	$gG$ (MeV)
$\Xi_c \bar{K}$	0.9	$-33.0 - 0.1j$	0.3	$-10.2 + 6.0j$	0.3	$-11.7 + 2.2j$
$\Xi'_c \bar{K}$	0.4	$-7.3$	1.7	$39.1 + 0.9j$	0.0	$-0.6 + 0.1j$
$\Xi D$	1.8	10.1	1.0	$-6.4 - 2.1j$	2.3	$-26.9 - 1.1j$
$\Omega_c \eta$	0.4	4.1	1.9	$-22.7 - 0.5j$	0.3	$-4.6$
$\Xi D^*$	1.7	3.6	1.4	$3.5 - 0.9j$	2.2	$12.5 - 0.8j$
$\Xi_c \bar{K}^*$	0.0	$-0.1$	1.8	$-8.7 + 0.2j$	1.8	$17.4 + 0.1j$
$\Xi'_c \bar{K}^*$	0.9	0.4	1.4	$1.8 - 0.3j$	0.2	$-0.7 - 0.6j$
$\Omega_c \omega$	0.5	$-0.4$	0.6	$-1.0 + 0.2j$	0.3	$1.7 + 0.1j$
$\Xi_c^* \bar{K}^*$	1.2	$-2.0$	0.3	$0.1 + 0.2j$	1.5	$3.8 - 0.4j$
$\Xi^* D^*$	0.2	0.4	0.9	$1.7 - 0.1j$	2.5	$0.4 - 0.1j$
$\Omega_c^* \omega$	0.4	0.5	0.1	$0.0+$	0.9	$-2.7 + 0.1j$
$\Omega_c \eta'$	0.1	$-0.6$	0.2	$1.0 + 0.1j$	0.6	$0.8$
$\Omega_c \phi$	0.4	2.6	1.1	$7.2 - 0.6j$	0.1	$0.2 - 0.3j$
$\Omega D_s^*$	0.3	2.0	0.1	$-0.8 - 0.4j$	1.9	$-9.2 - 0.2j$
$\Omega_c^* \phi$	0.8	6.5	0.4	$-2.8 - 1.2j$	0.6	$3.4 - 0.5j$

Table 9.5:  $J = 1/2$   $\Omega_c$  states, labeled as poles **a**, **c** and **d**, calculated using the subtraction constants determined by a unique UV cutoff  $\Lambda = 1090$  MeV [see Eq. (3.103)]. The first column displays the different baryon-meson coupled channels, ordered by their threshold energies. The subsequent columns show the absolute value of the coupling and the product of the coupling times the loop function at the pole for all baryon-meson coupled states for pole **a** at 2963.95 MeV (second and third columns), pole **c** at 2994.26 MeV (fourth and fifth columns) and pole **d** at 3116.81 MeV (sixth and seventh columns). Poles **c** at 2994.26 MeV and **d** at 3116.81 MeV might be identified with the experimental  $\Omega_c(3000)$  and the  $\Omega_c(3119)$  or  $\Omega_c(3090)$ , respectively.

channel	pole <b>b</b>		pole <b>e</b>	
	$ g $	$gG$ (MeV)	$ g $	$gG$ (MeV)
$\Xi_c^* \bar{K}$	1.8	$-38.8 - 0.1j$	0.1	$-4.3 + 0.1j$
$\Omega_c^* \eta$	1.8	20.1	0.8	$13.3 - 0.3j$
$\Xi D^*$	0.8	-3.0	3.6	-24.4
$\Xi_c \bar{K}^*$	2.1	-14.0	0.9	$10.5 + 0.2j$
$\Xi^* D$	0.9	1.9	2.2	-10.7
$\Xi_c' \bar{K}^*$	0.5	-1.3	0.1	$-0.6 + 0.1j$
$\Omega_c \omega$	0.3	1.0	0.4	-2.9
$\Xi_c^* \bar{K}^*$	1.2	-0.7	0.6	$2.4 + 0.1j$
$\Xi^* D^*$	1.1	-1.2	2.4	-2.3
$\Omega_c^* \omega$	0.4	0.4	0.2	-1.0
$\Omega D_s$	0.1	-0.4	1.4	2.1
$\Omega_c \phi$	0.5	-2.6	0.2	-0.4
$\Omega_c^* \eta'$	0.1	-0.5	0.8	-2.0
$\Omega D_s^*$	0.2	-1.1	1.9	8.1
$\Omega_c^* \phi$	1.1	-7.6	0.1	0.4

Table 9.6:  $J = 3/2$   $\Omega_c^*$  states, labeled as poles **b** and **e**, calculated using the subtraction constants determined by a unique UV cutoff  $\Lambda = 1090$  MeV [see Eq. (3.103)]. The first column displays the different baryon-meson coupled channels, ordered by their threshold energies, for  $J = 3/2$ . The subsequent columns show the absolute value of the coupling and the product of the coupling with the loop function at the pole for all baryon-meson coupled states for pole **b** at 3048.7 MeV (second and third columns) and pole **e** at 3155.37 MeV (fourth and fifth columns). Pole **b** at 3048.7 MeV might be identified with the experimental  $\Omega_c(3050)$ .



<b>Baryon</b>	$J^P$	<b>M (MeV)</b>	$\Gamma$ (MeV)	<b>Decay channels</b>
$\Xi_c(2790)^+/\Xi_c(2790)^0$	$1/2^-$	$2792.4 \pm 0.5 / 2794.1 \pm 0.5$	$8.9 \pm 1.0 / 10.0 \pm 1.1$	$\Xi_c'\pi$
$\Xi_c(2815)^+/\Xi_c(2815)^0$	$3/2^-$	$2816.73 \pm 0.21 / 2820.26 \pm 0.27$	$2.43 \pm 0.26 / 2.54 \pm 0.25$	$\Xi_c'\pi, \Xi_c^*\pi$
$\Xi_c(2930)^+/\Xi_c(2930)^0$	?	$2942 \pm 5 / 2929.7^{+2.8}_{-5.0}$	$15 \pm 9 / 26 \pm 8$	$\Lambda_c^+K^-, \Lambda_c^+K_S^0$
$\Xi_c(2970)^+/\Xi_c(2970)^0$	?	$2969.4 \pm 0.8 / 2967.8^{+0.9}_{-0.7}$	$20.9^{+2.4}_{-3.5} / 28.1^{+3.4}_{-4.0}$	$\Lambda_c^+\bar{K}\pi, \Sigma_c\bar{K}, \Xi_c2\pi,$ $\Xi_c'\pi, \Xi_c^*\pi$
$\Xi_b(6227)$	?	$6226.9 \pm 2$	$18 \pm 6$	$\Lambda_b^0K^-, \Xi_b^0\pi^-$

Table 9.7: Excited  $\Xi_c$  states below 3 GeV and the excited  $\Xi_b$  state found experimentally [21]. We show the assigned  $J^P$  (when possible), the mass M and width  $\Gamma$ , as well as the decay channels.

Irreps	State	M (MeV)	$\Gamma$ (MeV)	J	Couplings	
(168, 21 <sub>2,1</sub> , 3 <sub>2</sub> <sup>*</sup> )	c <sub>1</sub>	2773.59	10.52	1/2	$g_{\Xi_c\pi} = 0.5, g_{\Xi_c'\pi} = 0.3, g_{\Lambda_c\bar{K}} = 1.3, g_{\Sigma_c\bar{K}} = 0.9,$	
					$g_{\Lambda D} = 1.6, g_{\Sigma D} = 1.5, g_{\Lambda D^*} = 2.9, g_{\Sigma D^*} = 1.0,$	$g_{\Xi_c'\rho} = 1.0, g_{\Lambda_c\bar{K}^*} = 0.2$
(168, 15 <sub>2,1</sub> , 6 <sub>2</sub> )	c <sub>2</sub>	2627.5	38.84	1/2	$g_{\Xi_c\pi} = 1.8, g_{\Xi_c'\pi} = 0.04, g_{\Lambda_c\bar{K}} = 1.2, g_{\Sigma_c\bar{K}} = 0.1,$	
					$g_{\Lambda_c\bar{K}^*} = 0.04, g_{\Sigma D} = 1.2, g_{\Lambda D^*} = 1.0, g_{\Sigma D^*} = 1.9$	
(168, 21 <sub>2,1</sub> , 6 <sub>2</sub> )	c <sub>3</sub>	2790.99	16.09	1/2	$g_{\Xi_c\pi} = 0.3, g_{\Xi_c'\pi} = 0.8, g_{\Lambda_c\bar{K}} = 0.2, g_{\Sigma_c\bar{K}} = 1.7,$	
					$g_{\Lambda D} = 2.6, g_{\Lambda D^*} = 2.2, g_{\Xi_c'\eta} = 1.1, g_{\Lambda_c\bar{K}^*} = 1.0,$	$g_{\Sigma D^*} = 2.3, g_{\Sigma_c\bar{K}^*} = 1.1, g_{\Xi D_s^*} = 1.7$
(168, 21 <sub>2,1</sub> , 6 <sub>4</sub> )	c <sub>4</sub>	2850.89	6.76	3/2	$g_{\Xi_c^*\pi} = 0.6, g_{\Sigma_c^*\bar{K}} = 2.2, g_{\Lambda_c\bar{K}^*} = 1.5, g_{\Xi_c^*\eta} = 1.1,$	
					$g_{\Sigma^*D} = 1.1, g_{\Sigma^*D^*} = 1.5, g_{\Sigma_c^*\bar{K}^*} = 1.8$	
(168, 15 <sub>2,1</sub> , 3 <sub>2</sub> <sup>*</sup> )	c <sub>5</sub>	2715.23	12.28	1/2	$g_{\Xi_c\pi} = 0.2, g_{\Xi_c'\pi} = 1.8, g_{\Lambda_c\bar{K}} = 0.5, g_{\Sigma_c\bar{K}} = 1.2,$	
					$g_{\Lambda D} = 3.1, g_{\Lambda_c\bar{K}^*} = 0.1, g_{\Sigma D} = 1.5$	
(120, 21 <sub>2,1</sub> , 3 <sub>2</sub> <sup>*</sup> )	c <sub>6</sub>	2807	1.82	1/2	$g_{\Xi_c\pi} = 0.1, g_{\Xi_c'\pi} = 0.1, g_{\Lambda_c\bar{K}} = 0.2, g_{\Sigma_c\bar{K}} = 1.4,$	
					$g_{\Sigma D} = 1.6, g_{\Lambda D^*} = 1.1, g_{\Sigma D^*} = 4.3, g_{\Xi D_s} = 1.1,$	$g_{\Sigma_c\bar{K}^*} = 1.4, g_{\Xi D_s^*} = 1.9$
(120, 21 <sub>2,1</sub> , 6 <sub>2</sub> )	c <sub>7</sub>	2922.5	2.48	1/2	$g_{\Xi_c\pi} = 0.2, g_{\Xi_c'\pi} = 0.03, g_{\Lambda_c\bar{K}} = 0.2, g_{\Sigma_c\bar{K}} = 0.1,$	
					$g_{\Lambda D} = 1.8, g_{\Sigma D} = 1.4, g_{\Lambda D^*} = 1.7, g_{\Lambda_c\bar{K}^*} = 1.2,$	$g_{\Sigma D^*} = 1.5, g_{\Xi_c\rho} = 1.2, g_{\Sigma^*D^*} = 3.7, g_{\Sigma_c\bar{K}^*} = 1.1,$
(168, 15 <sub>2,1</sub> , 3 <sub>4</sub> <sup>*</sup> )	c <sub>8</sub>	2792.06	22.79	3/2	$g_{\Xi_c^*\pi} = 1.7, g_{\Sigma_c^*\bar{K}} = 1.0, g_{\Lambda D^*} = 2.4, g_{\Sigma D^*} = 1.2,$	
					$g_{\Lambda_c\bar{K}^*} = 0.2$	
(120, 21 <sub>2,1</sub> , 6 <sub>4</sub> )	c <sub>9</sub>	2942.05	1.46	3/2	$g_{\Xi_c^*\pi} = 0.2, g_{\Sigma_c^*\bar{K}} = 0.2, g_{\Lambda_c\bar{K}^*} = 0.4, g_{\Lambda D^*} = 2.7,$	
					$g_{\Sigma D^*} = 2.2, g_{\Sigma^*D} = 2.8, g_{\Sigma^*D^*} = 3.4, g_{\Xi^*D_s} = 1.4,$	$g_{\Xi^*D_s^*} = 1.8$

Table 9.8: Masses and widths of the  $c_1$  to  $c_9$  states with  $J = 1/2$  or  $J = 3/2$  and odd parity in the  $C = 1, S = -1$  and  $I = 1/2$  sector, together with the couplings (in modulus) to the dominant baryon-meson channels ( $g > 1$ ) and the couplings to the decay channels reported experimentally for the  $\Xi_c$  states. All results have been obtained for  $\Lambda = 1150$  MeV. We also indicate the  $SU(6)_{\text{flavor}} \times \text{HQSS}, SU(6)$  and  $SU(3)$  irreducible representations of these states. We use the notation  $\mathbf{R}_{2J_C+1,C}$ , where  $\mathbf{R}$  is the  $SU(6)$  irreducible representation (irrep) label (for which we use the dimension),  $J_C$  is the spin carried by the quarks with charm ( $1/2$  in all cases) and  $C$  the charm content (1 in all cases). In addition, we also use  $\mathbf{r}_{2J+1}$ , where  $\mathbf{r}$  is the  $SU(3)$  irrep, with  $J$  the total angular momentum of the state (see Ref. [86] for details).

Irreps	State	$M_R$ (MeV)	$\Gamma_R$ (MeV)	$J$	Couplings
(168, 21 <sub>2,1</sub> , 3 <sub>2</sub> <sup>*</sup> )	$b_1$	5873.98	0	1/2	$g_{\Lambda\bar{B}} = 1.3, g_{\Sigma\bar{B}} = 4.4, g_{\Lambda\bar{B}^*} = 2.3, g_{\Sigma\bar{B}^*} = 7.3,$ $g_{\Xi\bar{B}_s} = 2.6, g_{\Xi_b\eta'} = 1.0, g_{\Xi\bar{B}_s^*} = 4.5$
(168, 15 <sub>2,1</sub> , 6 <sub>2</sub> )	$b_2$	5940.85	35.59	1/2	$g_{\Xi_b\pi} = 1.8, g_{\Lambda\bar{B}} = 3.7, g_{\Lambda\bar{B}^*} = 6.2, g_{\Sigma\bar{B}^*} = 1.6,$ $g_{\Xi\bar{B}_s} = 1.1, g_{\Xi\bar{B}_s^*} = 1.9$
(168, 21 <sub>2,1</sub> , 6 <sub>2</sub> )	$b_3$	5880.76	0	1/2	$g_{\Lambda\bar{B}} = 2.5, g_{\Sigma\bar{B}} = 2.4, g_{\Lambda\bar{B}^*} = 1.3, g_{\Sigma\bar{B}^*} = 1.6,$ $g_{\Xi\bar{B}_s} = 1.7, g_{\Sigma^*\bar{B}^*} = 8.0, g_{\Xi_b'\eta'} = 1.0, g_{\Xi^*\bar{B}_s^*} = 4.9$
(168, 21 <sub>2,1</sub> , 6 <sub>4</sub> )	$b_4$	5880.27	0	3/2	$g_{\Lambda\bar{B}^*} = 2.8, g_{\Sigma\bar{B}^*} = 2.8, g_{\Sigma^*\bar{B}} = 5.0, g_{\Sigma^*\bar{B}^*} = 6.3,$ $g_{\Xi\bar{B}_s^*} = 1.8, g_{\Xi^*\bar{B}_s} = 3.1, g_{\Xi^*\eta'} = 1.0, g_{\Xi^*\bar{B}_s^*} = 3.9$
(168, 15 <sub>2,1</sub> , 3 <sub>2</sub> <sup>*</sup> )	$b_5^*$	5949.93	0.7	1/2	$g_{\Xi_b'\pi} = 1.4, g_{\Lambda\bar{B}} = 6.2, g_{\Lambda\bar{B}^*} = 3.8, g_{\Sigma^*\bar{B}^*} = 1.6,$ $g_{\Xi^*\bar{B}_s^*} = 2.2$
(120, 21 <sub>2,1</sub> , 3 <sub>2</sub> <sup>*</sup> )	$b_6$	6034.80	28.8	1/2	$g_{\Xi_b\pi} = 1.0, g_{\Lambda_b\bar{K}} = 2.0, g_{\Lambda\bar{B}} = 1.0, g_{\Lambda\bar{B}^*} = 2.1,$ $g_{\Sigma\bar{B}^*} = 1.1, g_{\Xi\bar{B}_s} = 1.3, g_{\Xi\bar{B}_s^*} = 2.1$
(120, 21 <sub>2,1</sub> , 6 <sub>2</sub> )	$b_7$	6035.39	0.02	1/2	$g_{\Sigma_b\bar{K}} = 2.3, g_{\Lambda\bar{B}} = 1.0, g_{\Sigma\bar{B}} = 4.5, g_{\Sigma\bar{B}^*} = 2.8,$ $g_{\Xi_b\omega} = 1.2, g_{\Sigma^*\bar{B}^*} = 2.3$
(168, 15 <sub>2,1</sub> , 3 <sub>4</sub> <sup>*</sup> )	$b_8^*$	5958.20	0	3/2	<b>- R.S. not connected -</b>
(120, 21 <sub>2,1</sub> , 6 <sub>4</sub> )	$b_9$	6043.28	0	3/2	$g_{\Sigma_b^*\bar{K}} = 2.3, g_{\Lambda\bar{B}^*} = 1.1, g_{\Sigma\bar{B}^*} = 5.5, g_{\Sigma^*\bar{B}} = 1.5,$ $g_{\Xi_b\omega} = 1.2, g_{\Sigma^*\bar{B}^*} = 1.7$

Table 9.9: Masses and widths of the  $b_1$  to  $b_9$  states with  $J = 1/2$  or  $J = 3/2$  in the  $B = -1, S = -1$  and  $I = 1/2$  sector, together with the couplings to the dominant baryon-meson channels and the couplings to the experimental decay channels of the  $\Xi_b(6227)$ , using one-subtraction renormalization, as in Table IV of Ref. [83]. We also indicate the  $SU(6)_{\text{lf}} \times \text{HQSS}, SU(6)$  and  $SU(3)$  irreducible representations of these states, as in Table 9.8. States with \* are virtual states. Note that the  $b_8^*$  lies in the real axis, but in a sheet that is not connected to the physical sheet, thus we are not showing the couplings indicating "R.S (real sheet) not connected".

Irreps	State	$M_R$ (MeV)	$\Gamma_R$ (MeV)	J	Couplings
(168, 21 <sub>2,1</sub> , 3 <sub>2</sub> <sup>*</sup> )	$b_1$	6025.46	25.88	1/2	$g_{\Xi_b\pi} = 0.94$ , $g_{\Lambda_b\bar{K}} = 1.4$ , $g_{\Xi_b\eta} = 2.1$ , $g_{\Sigma\bar{B}} = 1.4$ ,
					$g_{\Sigma\bar{B}^*} = 2.6$ , $g_{\Xi\bar{B}^*} = 1.3$
(168, 15 <sub>2,1</sub> , 6 <sub>2</sub> )	$b_2$	6152.61	15.29	1/2	$g_{\Xi_b\pi} = 0.33$ , $g_{\Lambda_b\bar{K}} = 0.51$ , $g_{\Sigma_b\bar{K}} = 0.40$ , $g_{\Lambda\bar{B}} = 1.9$ , $g_{\Sigma\bar{B}} = 2.1$ , $g_{\Lambda\bar{B}^*} = 7.3$ , $g_{\Xi\bar{B}_s} = 1.6$
(168, 21 <sub>2,1</sub> , 6 <sub>2</sub> )	$b_3$	6179.4	3.81	1/2	$g_{\Xi_b\pi} = 0.05$ , $g_{\Lambda_b\bar{K}} = 0.1$ , $g_{\Lambda\bar{B}} = 1.08$ , $g_{\Sigma\bar{B}} = 1.92$ ,
					$g_{\Lambda\bar{B}^*} = 1.87$ , $g_{\Omega_b K} = 2.26$ , $g_{\Xi\bar{B}_s} = 5.13$ , $g_{\Xi\bar{B}_s^*} = 2.65$ , $g_{\Xi_b\phi} = 2.29$ , $g_{\Omega_b K^*} = 1.04$ , $g_{\Xi_b'\phi} = 1.15$
(168, 21 <sub>2,1</sub> , 6 <sub>4</sub> )	$b_4$	6202.73	4.48	3/2	$g_{\Lambda\bar{B}^*} = 2.3$ , $g_{\Sigma\bar{B}^*} = 1.5$ , $g_{\Omega_b K} = 2.2$ , $g_{\Xi\bar{B}_s^*} = 5.5$ ,
					$g_{\Xi_b\phi} = 2.3$ , $g_{\Omega_b\bar{K}^*} = 1.2$ , $g_{\Xi_b^*\phi} = 1.3$
(168, 15 <sub>2,1</sub> , 3 <sub>2</sub> <sup>*</sup> )	$b_5$	6243.02	0.74	1/2	$g_{\Xi_b\pi} = 0.02$ , $g_{\Lambda_b\bar{K}} = 0.12$ , $g_{\Sigma_b\bar{K}} = 0.48$ , $g_{\Sigma\bar{B}} = 1.8$ , $g_{\Sigma\bar{B}^*} = 6.9$
(120, 21 <sub>2,1</sub> , 3 <sub>2</sub> <sup>*</sup> )	$b_6$	6212.26	1.6	1/2	$g_{\Xi_b\pi} = 0.05$ , $g_{\Lambda_b\bar{K}} = 0.01$ , $g_{\Sigma_b\bar{K}} = 1.2$ , $g_{\Lambda\bar{B}} = 1.3$ ,
					$g_{\Sigma\bar{B}} = 4.9$ , $g_{\Lambda\bar{B}^*} = 2.3$ , $g_{\Xi_b'\eta} = 1.6$
(120, 21 <sub>2,1</sub> , 6 <sub>2</sub> )	$b_7$	6327.28	5.29	1/2	$g_{\Xi_b\pi} = 0.01$ , $g_{\Lambda_b\bar{K}} = 0.02$ , $g_{\Lambda\bar{B}} = 1.4$ , $g_{\Sigma\bar{B}} = 1.3$ ,
					$g_{\Lambda\bar{B}^*} = 1.2$ , $g_{\Lambda_b\bar{K}^*} = 1.9$ , $g_{\Sigma\bar{B}^*} = 1.3$ , $g_{\Xi_b\rho} = 1.5$ , $g_{\Sigma^*\bar{B}^*} = 2.2$
(168, 15 <sub>2,1</sub> , 3 <sub>4</sub> <sup>*</sup> )	$b_8$	6240.82	0.92	3/2	$g_{\Xi_b^*\pi} = 0.15$ , $g_{\Sigma_b^*\bar{K}} = 1.3$ , $g_{\Lambda\bar{B}^*} = 2.0$ , $g_{\Xi_b^*\eta} = 1.5$ ,
					$g_{\Sigma\bar{B}^*} = 4.8$
(120, 21 <sub>2,1</sub> , 6 <sub>4</sub> )	$b_9$	6459.42	0.02	3/2	$g_{\Xi^*\bar{B}_s} = 4.5$ , $g_{\Omega_b K^*} = 2.2$ , $g_{\Xi_b'\phi} = 3.0$ , $g_{\Xi^*\bar{B}_s^*} = 3.0$ ,
					$g_{\Omega_b\bar{K}^*} = 1.0$ , $g_{\Xi_b^*\phi} = 1.3$

Table 9.10: As Table 9.8, but for the  $\Xi_b$  sector ( $\Lambda = 1150$  MeV).

## 9.4 Conclusions

In this chapter we have explored the possible molecular interpretation of several experimental excited  $\Omega_c$ ,  $\Xi_c$  and  $\Xi_b$  states. We have used a coupled-channel unitarized model, that is based on a  $SU(6)_{\text{lsf}} \times \text{HQSS}$ -extended WT baryon-meson interaction, within the on-shell approximation for the BSE. We have paid special attention to the dependence of our predictions on the renormalization scheme, so as to assess the robustness of our results.

In the  $(C = 1, S = -2, I = 0)$  sector, where five  $\Omega_c$  states have been recently observed by the LHCb Collaboration [348], we have firstly reviewed the previous results of Ref. [86]. There, the BSE is renormalized using a one-subtraction RS at fixed scale for all channels, as advocated in Refs. [170, 171]. Five odd-parity  $\Omega_c, \Omega_c^*$  states, coming from the most attractive  $SU(6)_{\text{lsf}} \times \text{HQSS}$  representations, are dynamically generated, but with masses below 2.98 GeV that cannot be easily identified with any of the LHCb resonances, located all of them above 3 GeV. Predicted masses can be moved up by implementing a different RS. We have explored two different scenarios, introducing at most only one additional undetermined parameter in the scheme. In the first one, the common energy-scale used in [86] to perform the subtractions is modified allowing for moderate variations. In the second one, a common UV cutoff is used to render finite the UV divergent loop functions in all channels. In both cases, we could move two or three states in the region between 3 and 3.1 GeV, where the LHCb resonances lie. In particular, when we use  $\Lambda = 1090$  MeV, we obtain three baryon-meson molecular states (poles **c** and **d**, and **b**) that couple predominantly to  $\bar{K}\Xi_c', D\Xi$  and  $\bar{K}\Xi_c^*$ , and can be easily related to the LHCb resonances and to results of Refs. [351, 388]. For the dominant channels, we obtain strengths for the wave function at the origin in a reasonable good agreement with those found in Ref. [388]. There exist, however, some disagreements in the predictions for the masses, which need to be taken with some caution. At least, our predictions for masses are subjected to sizable uncertainties, which might lead also to confusions in the assignments to the LHCb states proposed in this work. Nevertheless, we can conclude that some (probably at least three) of the states observed by LHCb [348] will have odd parity and spins  $J = 1/2$  and  $J = 3/2$ . Moreover, those associated to the poles **b** with  $J = 3/2$  and **c** with  $J = 1/2$  would belong to the same  $SU(6)_{\text{lsf}} \times \text{HQSS}$  multiplets [83, 86] that the strangeness-less  $\Lambda_c(2595)$  and  $\Lambda_c(2625)$ , and  $\Lambda_b(5912)$  and  $\Lambda_b(5920)$  resonances in the charm and bottom sectors, respectively. We should, however, warn the reader about the effects produced by quark model states, which might significantly alter the actual wave-function of the  $\Lambda_c(2595)$  and  $\Lambda_c(2625)$  resonances, as it was discussed in Chapter 7.

In the  $(C = 1, S = -1, I = 1/2)$  and  $(B = -1, S = -1, I = 1/2)$  sectors, we have also presented molecular interpretations for the experimental  $\Xi_c(2790)$ ,  $\Xi_c(2815)$ ,  $\Xi_c(2930)$ ,

$\Xi_c(2970)$  and  $\Xi_b(6227)$  states, and have predicted the spin-parity quantum numbers of the latter three resonances. We have found that the  $\Xi_c(2790)$  state has a large molecular  $\Lambda_c\bar{K}$  component, with a dominant  $j_q^P = 0^-$  configuration, and discussed the differences between the  $3/2^-$   $\Lambda_c(2625)$  and  $\Xi_c(2815)$  states, finding that they cannot be SU(3) siblings. We have also predicted the existence of other  $\Xi_c$ -states, not yet experimentally detected, being two of them siblings of the two poles that might form the  $\Lambda_c(2595)$ , assuming that such a pattern exists. Interestingly, the recently discovered  $\Xi_c(2930)$  and  $\Xi_c(2970)$  are found to be HQSS partners.

The flavor-symmetry content of the framework has also allowed us to understand the nature of the  $\Sigma_c(2800)$  and  $\Sigma_b(6097)$  states, for which we have determined their spin-parity. Moreover, we have predicted several states, some of them displayed in Figs. 9.7 and 9.8 (marked with a ? symbol). Among them, we stress the  $\Omega_b(6360)$  state, with a dominant  $\Xi_b\bar{K}$  contribution, in the sextet where the  $\Sigma_b(6097)$  and  $\Xi_b(6227)$  are located, together with the  $\Xi_b(6240)$  and  $\Xi_b^*(6240)$  states, partners of the HQSS doublet  $\Lambda_b(5912)$  and  $\Lambda_b(5920)$  discussed in [83].

Comparison of the results of this chapter with those obtained in Ref. [388] and Chapter 8 with the LHG formalism, for the  $\Omega_c$  and  $\Xi_{b,c}$  molecular states, represents a first step to quantify the systematic uncertainty due to the use of different models for the BSE interaction kernels involving charmed pseudoscalar and vector mesons, which are not constrained by chiral symmetry. However, it should also be noted that some differences are also produced by the renormalization procedure adopted to make finite the UV divergent loops.

# Chapter 10

## Predictions for $\Xi_b^- \rightarrow \pi^- (D_s^-) \Xi_c^*$ and $\Xi_b^- \rightarrow \bar{\nu}_l l \Xi_c^*$ decays, with $\Xi_c^* = \Xi_c^0(2790)$ and $\Xi_c^0(2815)$

### 10.1 Introduction

The introduction of chiral dynamics in the study of meson-baryon interactions [399, 434] has allowed a rapid development in this field. A qualitative step forward was given by introducing unitarity in coupled channels, using the chiral Lagrangians as a source of the interaction [24, 30–32, 34]. In many cases the interaction is strong enough to generate bound states in some channels, which decay into the open states considered in the coupled channel formalism. The most renowned case is the one of the two  $\Lambda(1405)$  states [32,34,35,65]. The original works considered the interaction of pseudoscalar mesons with baryons, but the extension to vector mesons with baryons was soon done in Refs. [31, 334]. The extension to vector mesons finds its natural framework in the use of the local hidden gauge Lagrangians [135–137], which extend the chiral Lagrangians and accommodate vector mesons.

The mixing of pseudoscalar-baryon ( $PB$ ) and vector-baryon ( $VB$ ) channels in that framework was done in Ref. [297] in the light sector, and was extended to the charm sector in Refs. [85, 435]. An alternative approach to this mixing was used in Chapters 7 and 9 to describe the  $\Lambda_c^*$  and the new  $\Omega_c^*$  and  $\Xi_{c,b}^*$  states, respectively. Within this framework, the chiral Weinberg-Tomozawa  $SU(3)$  meson-baryon interaction is extended to four flavors, including vector meson and  $J^P = 3/2^+$  baryon degrees of freedom, as well. The model implements leading order HQSS constraints, and full details can be found in Ref. [86].

The study described in this part of the thesis is similar to the one carried out

in Chapter 6, but in this case for the sector with charm and strangeness. However, while in Chapter 6 we emphasized the HQSS constraints derived for transitions, here we take the perspective that the  $\Xi_c^0(2790)$  and  $\Xi_c^0(2815)$  resonances are dynamically generated from the pseudoscalar-baryon and vector-baryon interactions, and pay special attention to effects of these latter channels on the considered non-leptonic and semileptonic  $\Xi_b^-$  decays. There is the further assumption that these two resonances form a  $j_q^P = 1^-$  (spin-parity of the light degrees of freedom) HQSS doublet. Actually, the present analysis is an extension of the similar ones in Refs. [224, 321] for the corresponding  $\Lambda_b$  decays. Thus in the present chapter, based on Ref. [8], we retake the ideas of Refs. [224, 321] and apply them to the study of the  $\Xi_b^- \rightarrow \pi^- \Xi_c^0(2790)(\frac{1}{2}^-)$ ,  $\Xi_b^- \rightarrow \pi^- \Xi_c^0(2815)(\frac{3}{2}^-)$ ,  $\Xi_b^- \rightarrow D_s^- \Xi_c^0(2790)$ ,  $\Xi_b^- \rightarrow D_s^- \Xi_c^0(2815)$ ,  $\Xi_b^- \rightarrow \bar{\nu}_l l \Xi_c^0(2790)$  and  $\Xi_b^- \rightarrow \bar{\nu}_l l \Xi_c^0(2815)$  decays. The  $\Xi_c^0(2790)(\frac{1}{2}^-)$  and  $\Xi_c^0(2815)(\frac{3}{2}^-)$  play an analogous role to the  $\Lambda_c(2595)(\frac{1}{2}^-)$  and  $\Lambda_c(2625)(\frac{3}{2}^-)$ , substituting the  $u$ -quark by an  $s$ -quark. For the couplings of the  $\Xi_c^0(2790)$  and  $\Xi_c^0(2815)$  to the different coupled channels, we will use results from the  $SU(6)_{\text{isf}} \times \text{HQSS}$  model of Ref. [86], which has been described in Chapters 7 and 9. We will adapt the formalism developed in Refs. [224, 321] to the present case and will make predictions for these partial decay modes, which are not yet measured.

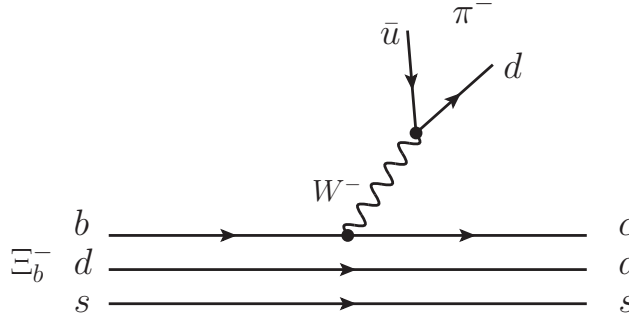
## 10.2 Formalism

We follow the steps of Ref. [212] for the weak decay of  $B$  mesons leading to hadronic resonances in the final state, generalized to the weak decay of  $\Lambda_b$  baryons into baryonic resonances in Ref. [436]. In this latter study, the  $\Lambda_b \rightarrow J/\psi K^- p$  and  $\Lambda_b \rightarrow J/\psi \pi \Sigma$  reactions in the region of the  $\Lambda(1405)$  resonance were studied, and predictions were made for the  $K^- p$  invariant mass distribution, which were confirmed by experiment later in the LHCb work disclosing pentaquark states [119]. The analysis of Ref. [436] also predicted that the  $K^- p$  and  $\pi \Sigma$  would be produced with isospin  $I = 0$ , which was also confirmed in Ref. [119] since their partial wave analysis only gave  $J/\psi$  and  $\Lambda^*$  states. Work along the same lines as Ref. [436] was done in Ref. [63] in the decay of  $\Lambda_c$  leading to  $\Lambda(1405)$  and  $\Lambda(1670)$ , and in Ref. [437] in the  $\Lambda_b \rightarrow J/\psi K \Xi$  reaction. The scheme of Ref. [436] applied to the present case proceeds as depicted in Fig. 10.1.

The first point to take into account is that in the  $\Xi_b^-$  baryon, the  $ds$  pair has spin  $S = 0$ . Symmetry of the wave function requires the flavour combination  $ds - sd$ , and color provides the antisymmetry. The next step is the hadronization of the final  $c ds$  state into meson-baryon pairs.

We must consider some basic facts:



Figure 10.1: Diagrammatic representation of the weak decay  $\Xi_b^- \rightarrow \pi^- \Xi_c^*$ .

1. The  $ds$  quarks are spectators in the process. They have  $S = 0$  and come in the combination  $\frac{1}{\sqrt{2}}(ds - sd)$ .
2. We will consider only final  $\Xi_c^*$  resonances with negative parity, and generated from the meson-baryon interaction in  $s$ -wave. Since the pair  $ds$  has positive parity, the  $c$  quark must carry the negative parity and hence it will be produced in  $p$ -wave ( $L = 1$ ) in the weak interaction diagram depicted in Fig. 10.1.
3. The  $c$  quark will be incorporated into a final  $D(D^*)$  meson and thus will go back to its ground state. Hence, the hadronization, introducing  $(\bar{u}u + \bar{d}d + \bar{s}s)$  with the quantum numbers of the vacuum, must involve the  $c$  quark.

With these constraints, the hadronization proceeds as shown in Fig. 10.2.

Technically the hadronization is implemented as follows: The  $\Xi_b^-$  state has a flavor function

$$|\Xi_b^- \rangle \equiv \frac{1}{\sqrt{2}} |b(ds - sd)\rangle, \quad (10.1)$$

and after the weak decay, the  $b$  quark is substituted by a  $c$  quark and we will have a state

$$|H\rangle = \frac{1}{\sqrt{2}} |c(ds - sd)\rangle. \quad (10.2)$$

With the hadronization, we will have now

$$|H'\rangle = \frac{1}{\sqrt{2}} \sum_{i=1}^3 |cq_i(ds - sd)\rangle. \quad (10.3)$$

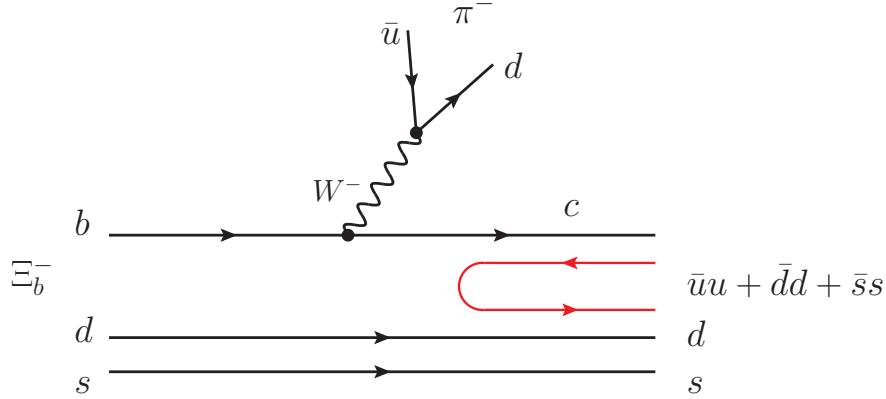


Figure 10.2: Hadronization after the weak process in Fig. 10.1 to produce a meson-baryon pair in the final state.

Next we write the  $q\bar{q}$  matrix in terms of the physical mesons given by Eq. (8.1),

$$|H'\rangle = \frac{1}{\sqrt{2}} \sum_{i=1}^3 |\Phi_{4i} q_i (ds - sd)\rangle. \quad (10.4)$$

Then we can write

$$|H'\rangle = \frac{1}{\sqrt{2}} [ |D^0 u (ds - sd)\rangle + |D^+ d (ds - sd)\rangle + |D_s^+ s (ds - sd)\rangle ]. \quad (10.5)$$

The last state in Eq. (10.5) contains two extra  $s$  quarks and corresponds to a more massive component that we omit in our study.

Next we see that we have a mixed antisymmetric component for the baryonic states of three quarks. If we evaluate the overlap with the mixed antisymmetric representations of the  $\Sigma^-$ ,  $\Sigma^0$ ,  $\Lambda^0$  states [438], we find

$$|H'\rangle = \frac{1}{\sqrt{2}} |D^0 \Sigma^0\rangle + |D^+ \Sigma^-\rangle - \frac{1}{\sqrt{6}} |D^0 \Lambda\rangle. \quad (10.6)$$

Yet, we have to be careful here with the phase conventions. By looking at the phase convention of Ref. [438] and the one inherent in the baryon octet matrix given by Eq. (2.37), which is used in the chiral Lagrangians, one can see that one must change the phases of  $\Sigma^+$ ,  $\Lambda$ ,  $\Xi^0$  from Ref. [438] to agree with the chiral Lagrangians<sup>1</sup>.

<sup>1</sup>One way to see this is to take the singlet baryon state of Ref. [438] with a minus sign, introduce the hadronization with  $\bar{u}u + \bar{d}d + \bar{s}s$  as we have done before and see the meson-baryon content. The relative phases are deduced by comparing this result with the SU(3) singlet  $\text{Tr}(B \cdot \phi)$ , obtained with

With this clarification about the phases, the state that we obtain consistent with the chiral convention is:

$$|H'\rangle = \frac{1}{\sqrt{2}} |D^0 \Sigma^0\rangle + |D^+ \Sigma^-\rangle + \frac{1}{\sqrt{6}} |D^0 \Lambda\rangle. \quad (10.7)$$

We also mention the phase convention for mesons in terms of isospin states, where  $|\pi^+\rangle = -|1, 1\rangle$ ,  $|K^-\rangle = -|\frac{1}{2}, -\frac{1}{2}\rangle$ ,  $|D^0\rangle = -|\frac{1}{2}, -\frac{1}{2}\rangle$ , and for baryons  $|\Sigma^+\rangle = -|1, 1\rangle$ ,  $|\Xi^-\rangle = -|\frac{1}{2}, -\frac{1}{2}\rangle$ .

In terms of isospin,  $|H'\rangle$  can be written as

$$|H'\rangle = -\sqrt{\frac{3}{2}} \left| \Sigma D(J = \frac{1}{2}) \right\rangle + \frac{1}{\sqrt{6}} \left| \Lambda D(J = \frac{1}{2}) \right\rangle. \quad (10.8)$$

For  $D^*$  production the flavour counting is the same and we would have the same combination substituting  $D$  by  $D^*$ .

### 10.3 The weak vertex

One must evaluate the weak transition matrix elements. For this we follow the approach in Ref. [224]. The vertex  $W^- \rightarrow \pi^-$  is of the type [229, 306]

$$\mathcal{L}_{W\pi} \sim W^\mu \partial_\mu \phi, \quad (10.9)$$

while the  $bcW$  vertex is of the type

$$\mathcal{L}_{qWq} \propto \bar{q}_{\text{fin}} W_\mu \gamma^\mu (1 - \gamma_5) q_{\text{in}}. \quad (10.10)$$

Since we are dealing with heavy quarks, as in Ref. [224] we keep the dominant terms in a non-relativistic expansion:  $\gamma^0$  and  $\gamma^i \gamma^5$  ( $i = 1, 2, 3$ ). Thus, combining the two former vertices we obtain a structure for the weak transition at the quark level of the type

$$V_P \sim q^0 + \vec{\sigma} \cdot \vec{q}, \quad (10.11)$$

with  $q^\mu$  the four-momentum of the pion.

In Ref. [224] the operator in Eq. (10.11), which acts at the quark level between the  $b$  and  $c$  quarks, was converted into an operator acting over the  $\Lambda_c^*$  and  $\Lambda_b$  at the macroscopical level with the result

$$V_P \sim \left\{ \left( i \frac{q^0}{q} \vec{\sigma} \cdot \vec{q} + iq \right) \delta_{J, \frac{1}{2}} - i \frac{q^0}{q} \sqrt{3} \vec{S}^+ \cdot \vec{q} \delta_{J, \frac{3}{2}} \right\} \text{ME}(q), \quad (10.12)$$

the nonet of mesons in Eq. (8.1) for  $\phi$  (taking only the  $3 \times 3$  part of the matrix), and Eq. (2.37) for  $B$ . The matrix  $\phi$  contains also a singlet of mesons, the octet matrix is the same putting in the diagonal  $\left( \frac{\pi^0}{\sqrt{2}} + \frac{\eta_8}{\sqrt{6}}, -\frac{\pi^0}{\sqrt{2}} + \frac{\eta_8}{\sqrt{6}}, -\frac{2\eta_8}{\sqrt{6}} \right)$ . Two alternative derivations are done in the Appendix of Ref. [306] with the same conclusions.

where  $\vec{S}^+$  is the spin transition operator from spin  $\frac{1}{2}$  to spin  $\frac{3}{2}$  normalized such that

$$\langle M' | S_\mu^+ | M \rangle = \mathcal{C}(\frac{1}{2}, 1, \frac{3}{2}; M, \mu, M'), \quad (10.13)$$

with  $\mu$  in the spherical basis and  $\mathcal{C}(\frac{1}{2}, 1, \frac{3}{2}; M, \mu, M')$  the Clebsch-Gordan coefficients. In addition,  $\text{ME}(q)$  is the quark matrix element involving the radial wave functions (here we do the same as in Ref. [224], but the macroscopic states are  $\Xi_c^*$  and  $\Xi_b$  respectively),

$$\text{ME}(q) = \int dr r^2 j_1(qr) \phi_{\text{in}}(r) \phi_{\text{fin}}^*(r), \quad (10.14)$$

where  $j_1(qr)$  is a spherical Bessel function and  $\phi_{\text{in}}(r)$  is the radial wave function of the  $b$  quark in  $\Xi_b^-$  and  $\phi_{\text{fin}}(r)$  the radial wave function of the  $c$  quark, prior to the hadronization, which is in an excited  $L = 1$  state.

Since we require ratios of production rates, the matrix element  $\text{ME}(q)$  cancels in the ratio and what matters to differentiate the cases with spin  $\frac{1}{2}$  and  $\frac{3}{2}$  is the operator in Eq. (10.12). One should note that the presence of the factor  $j_1(qr)$  in Eq. (10.14) is due to the fact that the  $c$  quark is created with  $L = 1$  as we discussed previously.

In Sect. 10.7, we will improve on the non-relativistic approximation of Eq. (10.11), but we already advance that the ratios of rates only change at the level of 1% with respect to this non-relativistic approximation.

## 10.4 The spin structure in the hadronization

The next issue is to see how the hadronization affects the cases of  $DB$  or  $D^*B$  (with  $B = \Sigma, \Lambda$ ) production in spin  $J = \frac{1}{2}$  or  $\frac{3}{2}$ . For this we follow again the approach of Ref. [224]. The calculation proceeds in a similar way as in Sec. 5.2 for the hadronization process shown in Fig. 5.2:

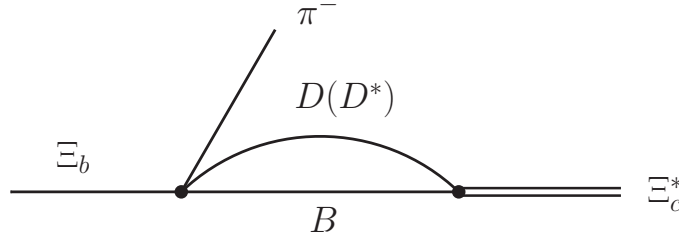
1. The  $\bar{q}q$  pair is created with  $J^P = 0^+$ . Since the  $\bar{q}$  has negative intrinsic parity we need  $L = 1$  in the quarks to restore the positive parity and this forces the  $\bar{q}q$  pair to come with spin  $S = 1$  to give  $J = 0$ . This is the essence of the  ${}^3P_0$  model.
2. Since what we want is to elaborate on the spin dependence of the matrix elements, we assume a zero range interaction, as is also done in similar problems like the study of pairing in nuclei [439, 440].
3. Since the  $d, s$  quarks are spectators and carry  $J = 0$ , the total angular momentum of the  $\Xi_c^*$  is the same as the angular momentum of the  $c$  quark after the weak production.

$\mathcal{C}(j, J)$	$J = \frac{1}{2}$	$J = \frac{3}{2}$
(pseudoscalar) $j = 0$	$\frac{1}{4\pi} \frac{1}{2}$	0
(vector) $j = 1$	$\frac{1}{4\pi} \frac{1}{2\sqrt{3}}$	$-\frac{1}{4\pi} \frac{1}{\sqrt{3}}$

Table 10.1:  $\mathcal{C}(j, J)$  coefficients in Eq. (5.9).

4. The angular momentum of the  $c$  quark and the  $\bar{q}q$  pair are recombined to give  $L' = 0$ , since all quarks are in their ground state in the  $D\Sigma$ ,  $D^*\Sigma$ ,  $D\Lambda$ , and  $D^*\Lambda$  final states. The total angular momentum of the  $c$  quark and that of the  $\bar{q}$  of the  $\bar{q}q$  pair are recombined to give  $j = 0, 1$ , for the  $D$  or  $D^*$  production. The total angular momentum of the  $q$  from the  $\bar{q}q$  pair determines the spin of the baryon  $\Xi_c^*$  since the  $ds$  quarks carry spin zero. The Clebsch-Gordan coefficients appearing in the different combinations are recombined to give a Racah coefficient [230] and the final result is given by Eq. (5.9), substituting  $|00; ud\rangle_{\text{spectator}}$  by  $|00; ds\rangle$  with the coefficients  $\mathcal{C}(j, J)$  given in Table 10.1.

What we have done so far is to obtain the angular structure of the mechanism for  $DB(D^*B)$  production, but we finally want to have the production of the resonances  $\Xi_c^0(2790)$  and  $\Xi_c^0(2815)$ . The way to produce these dynamically generated resonances is depicted in Fig. 10.3. It involves the amplitudes for  $\Xi_b \rightarrow \pi^- D(D^*)B$  production studied before, together with the  $D(D^*)B$  loop functions and the couplings of the  $\Xi_c^*$  resonance to these meson-baryon components. The width for the  $\Xi_b \rightarrow \pi^- \Xi_c^*$  decay is

Figure 10.3: Mechanism for the production of the  $\Xi_c^*$  resonances by re-scattering of  $D(D^*)\Sigma(\Lambda)$  and coupling of the meson-baryon components to  $\Xi_c^*$ .

given by

$$\Gamma_{\Xi_b \rightarrow \pi^- \Xi_c^*} = \frac{1}{2\pi} \frac{M_{\Xi_c^*}}{M_{\Xi_b}} q \sum \sum |t|^2, \quad (10.15)$$

with  $q$  the momentum of the pion in the  $\Xi_b$  rest frame.

By combining Eqs. (10.8), (10.12), (5.9), we obtain

$$J = \frac{1}{2} : \overline{\Sigma} \Sigma |t|^2 = C^2 (q^2 + \omega_\pi^2) \left| \frac{1}{2} \left( -\sqrt{\frac{3}{2}} \right) g_{R,\Sigma D} G_{\Sigma D} + \frac{1}{2} \frac{1}{\sqrt{6}} g_{R,\Lambda D} G_{\Lambda D} \right. \\ \left. + \frac{1}{2\sqrt{3}} \left( -\sqrt{\frac{3}{2}} \right) g_{R,\Sigma D^*} G_{\Sigma D^*} + \frac{1}{2\sqrt{3}} \frac{1}{\sqrt{6}} g_{R,\Lambda D^*} G_{\Lambda D^*} \right|^2 \quad (10.16)$$

and

$$J = \frac{3}{2} : \overline{\Sigma} \Sigma |t|^2 = C^2 2\omega_\pi^2 \left| \frac{1}{\sqrt{3}} \left( -\sqrt{\frac{3}{2}} \right) g_{R,\Sigma D^*} G_{\Sigma D^*} + \frac{1}{\sqrt{3}} \frac{1}{\sqrt{6}} g_{R,\Lambda D^*} G_{\Lambda D^*} \right|^2, \quad (10.17)$$

where  $\omega_\pi$  is the pion energy  $\sqrt{m_\pi^2 + q^2}$ , and  $G_{BD}$ ,  $G_{BD^*}$  are the loop functions for the propagator of  $BD$  ( $BD^*$ ) in the resonance formation mechanism of Fig. 10.3, and  $g_{R,BD(BD^*)}$  the coupling of the resonance  $\Xi_c^*$  to any of the states  $BD$  ( $BD^*$ ).  $C$  in Eqs. (10.16) (10.17) is a factor that contains the matrix element  $\text{ME}(q)$  and constants of the weak interaction. Since the mass of the two  $\Xi_c^*$  that we investigate are not very different, then we assume  $C$  to be a constant that cancels in the ratio of the rates for the production of the two resonances. In this case we find

$$R_1 \equiv \frac{\Gamma_{\Xi_b \rightarrow \pi^- \Xi_c(1)}}{\Gamma_{\Xi_b \rightarrow \pi^- \Xi_c(2)}} = \frac{M_{\Xi_c(1)} p_\pi(1) \overline{\Sigma} \Sigma |t|^2(1)}{M_{\Xi_c(2)} p_\pi(2) \overline{\Sigma} \Sigma |t|^2(2)}, \quad (10.18)$$

where 1,2 refer to the  $\Xi_c(2790)$  and  $\Xi_c(2815)$  respectively.

The case of  $D_s^-$  production instead of  $\pi^-$  is identical. Instead of the  $\bar{u}d$  coupling to the gauge boson  $W$ , we now have that of the  $\bar{c}s$  pair, which is equally Cabbibo favoured and is proportional to  $\cos\theta_C$  in both cases, with  $\theta_C$  the Cabbibo angle. The only difference in this case is that the momentum of the  $D_s^-$  is smaller than that in the case of pion production. The momenta of  $D_s^-$  in the cases  $\Xi_c(2790)$  and  $\Xi_c(2815)$  are very similar and, hence, by analogy to Eq. (10.18) we can write

$$R_2 \equiv \frac{\Gamma_{\Xi_b \rightarrow D_s^- \Xi_c(1)}}{\Gamma_{\Xi_b \rightarrow D_s^- \Xi_c(2)}} = \frac{M_{\Xi_c(1)} p_{D_s^-}(1) \overline{\Sigma} \Sigma |t|^2(1)}{M_{\Xi_c(2)} p_{D_s^-}(2) \overline{\Sigma} \Sigma |t|^2(2)}, \quad (10.19)$$

with  $p_{D_s^-}(1,2)$  evaluated for the  $\Xi_c(2790)$  and  $\Xi_c(2815)$  respectively, and  $\overline{\Sigma} \Sigma |t|^2(1,2)$  have to be reevaluated with the new momentum.

If we assume that  $\text{ME}(q)$  is not very different in the case of  $\pi^-$  or  $D_s^-$  production we can also write

$$R_3 \equiv \frac{\Gamma_{\Xi_b \rightarrow D_s^- \Xi_c(1)}}{\Gamma_{\Xi_b \rightarrow \pi^- \Xi_c(1)}} = \frac{p_{D_s^-}(1) \overline{\Sigma} \Sigma |t|^2(1, D_s^-)}{p_{\pi^-}(1) \overline{\Sigma} \Sigma |t|^2(1, \pi^-)}. \quad (10.20)$$

We expect this equation to hold only at the qualitative level since  $\text{ME}(q)$  is not necessarily the same for these two different values of  $q$ .

## 10.5 Semileptonic decay

The semileptonic processes,  $\Xi_b \rightarrow \bar{\nu}_l l \Xi_c^0(2790)$  and  $\Xi_b \rightarrow \bar{\nu}_l l \Xi_c^0(2815)$  proceed in a similar way but instead of a  $\pi^-$  we have  $\bar{\nu}_l l$  production. The semileptonic decays of  $BD$  hadrons along the lines described here have been studied in Refs. [253,441]. The weak decay of  $\Lambda_c \rightarrow \bar{\nu}_l l \Lambda(1405)$  is addressed in Ref. [442] and the  $\Lambda_b \rightarrow \bar{\nu}_l l \Lambda_c(2595)$  and  $\Lambda_b \rightarrow \bar{\nu}_l l \Lambda_c(2625)$  in Ref. [321]. The first step for the  $\Xi_b \rightarrow \bar{\nu}_l l \Xi_c^*$  reaction is shown in Fig. 10.4a.

The only difference with the nonleptonic decay studied in the former sections is the coupling of  $W$  to  $\bar{\nu}_l l$ . Following Ref. [253] we have, for the combined  $W\bar{\nu}_l l$  and  $Wcb$  vertices,

$$t' = -iG_F \frac{V_{bc}}{\sqrt{2}} L^\alpha Q_\alpha, \quad (10.21)$$

with  $G_F$  the Fermi coupling constant,  $V_{bc}$  the Cabbibo-Kobayashi-Maskawa matrix element for the  $b \rightarrow c$  transition, and  $L^\alpha$ ,  $Q_\alpha$  the leptonic and quark currents:

$$L^\alpha = \bar{u}_l \gamma^\alpha (1 - \gamma_5) u_{\nu_l}, \quad (10.22a)$$

$$Q_\alpha = \bar{u}_c \gamma_\alpha (1 - \gamma_5) u_b. \quad (10.22b)$$

Once again we retain  $\gamma^0$  and  $\gamma^i \gamma_5$  from the quark matrix elements, which are the leading terms in a non-relativistic reduction. Actually the  $\bar{\nu}_l l$  pair comes out with a large momentum [321] and the momenta of the baryons are small.

The first step in Fig. 10.4a produces a different structure from Eq. (10.11) in the nonleptonic case, and one finds (see Eqs. (5),(6),(14) of Ref. [321])

$$\sum_{\text{lepton pol.}} L^\alpha L^{\dagger\beta} Q_\alpha Q_\beta^\dagger = \frac{8}{m_\nu m_l} p_\nu p_l, \quad (10.23)$$

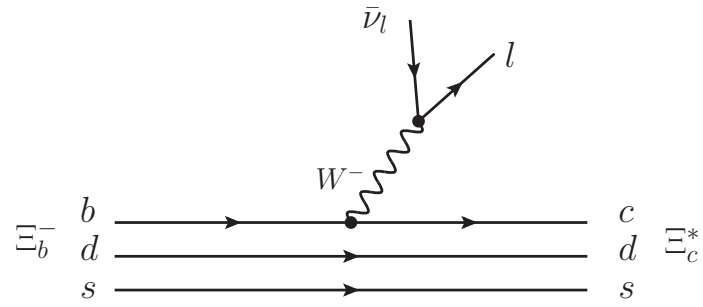
where  $p_\nu, p_l$  are the neutrino and lepton momenta in the  $\Xi_b$  rest frame, and  $m_\nu, m_l$  their masses. Note that we are using the field normalization of Mandl and Shaw [216] and  $\sum_\lambda u_\lambda(p) \bar{u}_\lambda(p) = (\not{p} + m)/2m$ . The masses  $m_\nu, m_l$  in Eq. (10.23) get canceled in the formula of the width, Eq. (10.26), and there are no problems even in the limit of small or zero neutrino mass. In Ref. [321] it was shown that by constructing the hadron states from the quark-model ones and summing over the initial and final polarizations of the hadrons (see Eq. (16) of Ref. [321]) one obtains,

$$\overline{\sum} \sum L^\alpha L^{\dagger\beta} Q_\alpha Q_\beta^\dagger \rightarrow A_J \frac{8}{m_\nu m_l} p_\nu p_l, \quad (10.24)$$

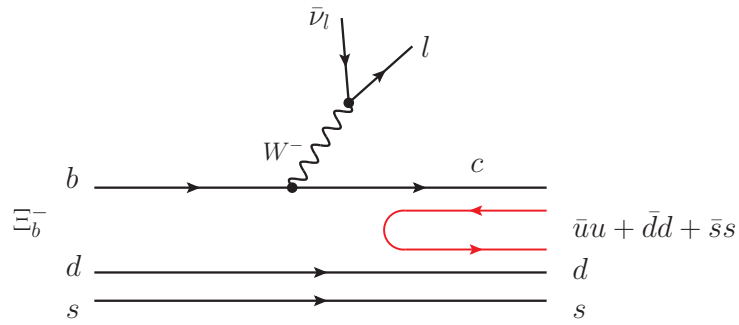
with

$$A_{1/2} = 1, \quad (10.25a)$$

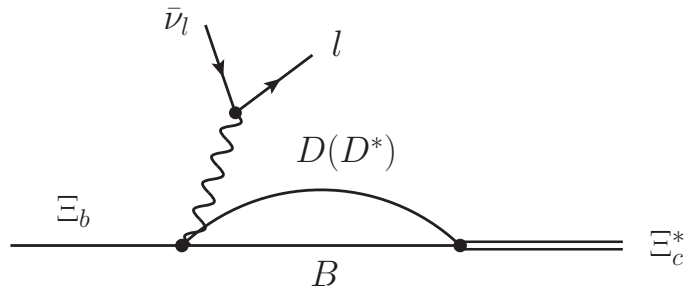
$$A_{3/2} = 2. \quad (10.25b)$$



(a) First step at quark level.



(b) Hadronization to produce  $D(D^*)B$ .



(c) Propagation of  $D(D^*)B$  and coupling to the  $\Xi_c^*$ .

Figure 10.4: Different steps of  $\Xi_c^*$  production in the  $\Xi_b^- \rightarrow \bar{\nu}_l l \Xi_c^*$  process.



The rest of the work needed is identical to the one in the nonleptonic case of the former sections. One can also do an angle integration analytically in the evaluation of  $\Gamma$  and one finally obtains

$$\frac{d\Gamma}{dM_{\text{inv}}(\bar{\nu}_l l)} = \frac{M_{\Xi_c^*}}{M_{\Xi_b}} 2m_\nu 2m_l \frac{1}{(2\pi)^3} p_{\Xi_c^*} \tilde{p}_l \bar{\Sigma} \Sigma |t'|^2, \quad (10.26)$$

where  $p_{\Xi_c^*}$  is the  $\Xi_c^*$  momentum in the  $\Xi_b$  rest frame and  $\tilde{p}_l$  the lepton momentum in the  $\bar{\nu}_l l$  rest frame, and  $\bar{\Sigma} \Sigma |t'|^2$  is given by [321]

$$\bar{\Sigma} \Sigma |t'|^2 = C'^2 \frac{8}{m_\nu m_l} \frac{1}{M_{\Xi_b}^2} \left( \frac{M_{\text{inv}}}{2} \right)^2 \left[ \tilde{E}_{\Xi_b}^2 - \frac{1}{3} \tilde{p}_{\Xi_b}^2 \right] A_J V_{\text{had}}(J), \quad (10.27)$$

with

$$J = \frac{1}{2} : A_J V_{\text{had}}(J) = \left| \frac{1}{2} \left( -\sqrt{\frac{3}{2}} \right) g_{R,\Sigma D} G_{\Sigma D} + \frac{1}{2} \frac{1}{\sqrt{6}} g_{R,\Lambda D} G_{\Lambda D} \right. \\ \left. + \frac{1}{2\sqrt{3}} \left( -\sqrt{\frac{3}{2}} \right) g_{R,\Sigma D^*} G_{\Sigma D^*} + \frac{1}{2\sqrt{3}} \frac{1}{\sqrt{6}} g_{R,\Lambda D^*} G_{\Lambda D^*} \right|^2, \quad (10.28)$$

and

$$J = \frac{3}{2} : A_J V_{\text{had}}(J) = 2 \left| \frac{1}{\sqrt{3}} \left( -\sqrt{\frac{3}{2}} \right) g_{R,\Sigma D^*} G_{\Sigma D^*} + \frac{1}{\sqrt{3}} \frac{1}{\sqrt{6}} g_{R,\Lambda D^*} G_{\Lambda D^*} \right|^2, \quad (10.29)$$

where  $G_{BD}$ ,  $G_{BD^*}$  and  $g_{R,BD}$ ,  $g_{R,BD^*}$  are the same as in the nonleptonic decay and  $C'$  is again a factor that contains the matrix element  $\text{ME}(q)$  evaluated at the proper value of  $q$ . A novelty here is that  $q$  is not constant when one integrates  $\frac{d\Gamma}{dM_{\text{inv}}}$  over  $M_{\text{inv}}$ . However, the fact that  $M_{\text{inv}}$  peaks around the maximum allowed in the Dalitz plot [321], as we show in Fig. 10.5 for the present case, allows us to consider  $C'$  constant over the whole range of  $M_{\text{inv}}$ .

The magnitudes  $\tilde{E}_{\Xi_b}$  and  $\tilde{p}_{\Xi_b}$  in Eq. (10.26) are the energies of  $\Xi_b$  and its momentum in the rest frame of the  $\bar{\nu}_l l$  pair which are given by [253]

$$\tilde{E}_{\Xi_b} = \frac{M_{\Xi_b}^2 + M_{\text{inv}}^2 - M_{\Xi_c^*}^2}{2M_{\text{inv}}}, \quad (10.30a)$$

$$\tilde{p}_{\Xi_b} = \frac{\lambda^{\frac{1}{2}} \left( M_{\Xi_b}^2, M_{\text{inv}}^2, M_{\Xi_c^*}^2 \right)}{2M_{\text{inv}}}. \quad (10.30b)$$

An approximate value for the ratio of the semileptonic production for the two resonances is given by

$$R = \frac{\Gamma_{\Xi_b \rightarrow \bar{\nu}_l l} \Xi_c(2790)}{\Gamma_{\Xi_b \rightarrow \bar{\nu}_l l} \Xi_c(2815)} = \frac{A_{\frac{1}{2}} V_{\text{had}} \left( \frac{1}{2} \right)}{A_{\frac{3}{2}} V_{\text{had}} \left( \frac{3}{2} \right)}. \quad (10.31)$$

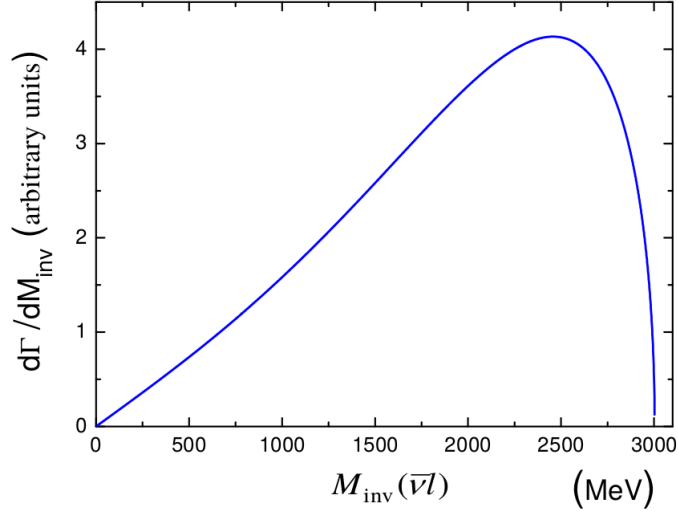


Figure 10.5: The invariant mass distribution for  $\bar{\nu}_l l$  in the  $\Xi_b \rightarrow \bar{\nu}_l l \Xi_c(2790)$ . The one for the  $\Xi_b \rightarrow \bar{\nu}_l l \Xi_c(2815)$  decay is very similar.

	$\Sigma D$	$\Sigma D^*$	$\Lambda D$	$\Lambda D^*$
$g$	$-1.178 - i0.101$	$0.777 + i0.285$	$-1.396 + i0.892$	$0.569 - i0.601$
$gG$	$6.544 + i0.239$	$-3.372 - i1.067$	$8.277 - i5.921$	$-2.45 + i2.844$

Table 10.2: Values of  $g$  and  $gG$  for the different channels for the resonance  $\Xi_c^0(2790)(\frac{1}{2}^-)$ .

	$\Lambda D^*$	$\Sigma D^*$
$g$	$2.346 - i0.599$	$0.791 + i0.49$
$gG$	$-12.297 + i4.213$	$-4.148 - i2.15$

Table 10.3: Values of  $g$  and  $gG$  for the different channels for the resonance  $\Xi_c^0(2815)(\frac{3}{2}^-)$ .

## 10.6 Results

We use the values of  $g_{R,\Sigma D}$ ,  $g_{R,\Sigma D^*}$ ,  $g_{R,\Lambda D}$ ,  $g_{R,\Lambda D^*}$  and of the  $G_{\Sigma D}$ ,  $G_{\Sigma D^*}$ ,  $G_{\Lambda D}$ ,  $G_{\Lambda D^*}$  from Ref. [86] which we have redone in order to evaluate the complex couplings and the  $G$  functions since only the modulus of  $g_{R,i}$  were given there and the values of  $G_i$  were not tabulated. We give all this information in Tables 10.2 and 10.3. The overall procedure is equivalent to what was done in Chapters 7 and 9 for the  $\Lambda_c^{(*)}$  and  $\Omega_c^{(*)}$  and  $\Xi_{c,b}^{(*)}$  states, respectively (see Ref. [86] for some more details).

	$R_1$	$R_2$	$R_3$
$g_{R,\Sigma D^*} = 0$	0.84	0.596	0.686
$g_{R,\Lambda D^*} = 0$	0.205	0.145	0.686
$g_{R,\Sigma D^*} \rightarrow -g_{R,\Sigma D^*}$	0.481	0.341	0.686
$g_{R,\Lambda D^*} \rightarrow -g_{R,\Lambda D^*}$	0.071	0.05	0.686

Table 10.4: Values of  $R_1, R_2, R_3$  obtained by both changing the sign of the  $g_{R,BD^*}$  couplings or setting them to zero.

Using the values in Tables 10.2 and 10.3 and Eq. (10.18) we obtain

$$R_1 = \frac{\Gamma_{\Xi_b \rightarrow \pi^- \Xi_c^0(2790)}}{\Gamma_{\Xi_b \rightarrow \pi^- \Xi_c^0(2815)}} = 0.384, \quad (10.32)$$

and from Eq. (10.19)

$$R_2 = \frac{\Gamma_{\Xi_b \rightarrow D_s^- \Xi_c^0(2790)}}{\Gamma_{\Xi_b \rightarrow D_s^- \Xi_c^0(2815)}} = 0.273. \quad (10.33)$$

Similarly we can obtain from Eq. (10.20)

$$R_3 = \frac{\Gamma_{\Xi_b \rightarrow D_s^- \Xi_c^0(2790)}}{\Gamma_{\Xi_b \rightarrow \pi^- \Xi_c^0(2790)}} = 0.686. \quad (10.34)$$

In order to see how sensitive these rates are to the values of the  $D^*B$  couplings we reevaluate them by first setting them to zero or changing their sign. The results we obtain are shown in Table 10.4.

As we can see, the results shown in Table 10.4 tell us the relevance of the  $D^*B$  components in the production of these resonances.

As for the sector of the semileptonic decay rates corresponding to Eq. (10.31) we find that

$$R = \frac{\Gamma_{\Xi_b \rightarrow \bar{\nu}_l l \Xi_c(2790)}}{\Gamma_{\Xi_b \rightarrow \bar{\nu}_l l \Xi_c(2815)}} = 0.191, \quad (10.35)$$

and if we integrate Eq. (10.26) we find

$$R = 0.197. \quad (10.36)$$

As we can see, the numbers are essentially the same.

Once again, if the couplings to  $D^*B$  states are changed we obtain different results, shown in Table 10.5.

	$R$
$g_{R,\Sigma D^*} = 0$	0.430
$g_{R,\Lambda D^*} = 0$	0.105
$g_{R,\Sigma D^*} \rightarrow -g_{R,\Sigma D^*}$	0.246
$g_{R,\Lambda D^*} \rightarrow -g_{R,\Lambda D^*}$	0.036

Table 10.5: Values of  $R$  of the semileptonic decay, obtained by both changing the sign of the  $g_{R,BD^*}$  couplings or setting them to zero.

## 10.7 Relativistic Effects

The evaluation of rates presented in the previous section was based in a non relativistic approximation to the operator in Eq. (10.10), given by Eq. (10.11). This could look as a very drastic approximation since in the  $\Xi_b^- \rightarrow \pi^- \Xi_c^0(2790)$  decay, the momentum of the  $\Xi_c^0(2790)$  is  $\sim 2223 \text{ MeV}/c$ , not much smaller than its mass. Yet, the difference between the relativistic and non relativistic energies is only 12%. But the effect of some neglected terms in the matrix element of Eq. (10.10) could be bigger. Actually this is the case, and in Ref. [321] the relativistic effects were considered in the  $\Lambda_b \rightarrow \bar{\nu}_l l \Lambda_c(2595)(\Lambda_c(2625))$  semileptonic decays and the effect was an increase in about 30% of the individual decay rates. Yet, when the ratios of rates were taken, the effects amounted to only about 1%. Here we will do this exercise again for the semileptonic decay and extend it to the nonleptonic case. Let us begin by this latter one.

Let us start from the full relativistic amplitude obtained from Eqs. (10.9), (10.10),

$$t_{\text{rel}} \propto q_\mu \bar{q}_{\text{fin}} \gamma^\mu (1 - \gamma_5) q_{\text{in}} \equiv q^\mu Q_\mu. \quad (10.37)$$

Considering the  $b$  and  $c$  quarks as free particles, for the purpose of estimating the effect of the relativistic terms, and summing and averaging over the spin third components (hence, also neglecting the separation into the  $PB$  and  $VB$  baryon components that we have done), we can write (see Eq. (8) of Ref. [253])

$$\begin{aligned} & \overline{\sum} \sum |t_{\text{rel}}|^2 \\ &= q^\mu q^\nu \frac{p_{b\mu} p_{c\nu} + p_{c\mu} p_{b\nu} - p_b \cdot p_c g_{\mu\nu} - i \epsilon_{\rho\mu\sigma\nu} p_b^\rho p_c^\sigma}{m_b m_c} \\ &= \frac{2(q \cdot p_b)(q \cdot p_c) - q^2(p_b \cdot p_c)}{m_b m_c}. \end{aligned} \quad (10.38)$$

At this point we make use of the heavy-quark symmetry approximate relations

$$\frac{p_b^\mu}{m_b} \sim \frac{p_{\Xi_b}^\mu}{M_{\Xi_b}}, \quad \frac{p_c^\mu}{m_c} \sim \frac{p_R^\mu}{M_R}, \quad (10.39)$$

where  $R$  stands for the  $\Xi_c^*$  final baryon resonance produced. These relationships are obtained neglecting the internal relative three momenta of the quarks in the heavy baryons versus their masses, and are commonly used in heavy hadron dynamics. Then Eq. (10.38) can be approximately written as

$$\overline{\sum} \sum |t_{\text{rel}}|^2 = \frac{2(q \cdot p_{\Xi_b})(q \cdot p_{\Xi_c^*}) - q^2(p_{\Xi_b} \cdot p_{\Xi_c^*})}{M_{\Xi_b} M_{\Xi_c^*}}. \quad (10.40)$$

We can see that if we make the non relativistic reduction  $p_{\Xi_c^*} \simeq (M_{\Xi_c^*}, \vec{0})$ , then we get  $\overline{\sum} \sum |t_{\text{rel}}|^2 = q^{02} + \vec{q}^2$ , which is the  $(|\vec{q}|^2 + \omega_\pi^2)$  factor that we find in Eq. (10.16) for  $J = 1/2$ . For  $J = 3/2$  the factor is  $2\omega_\pi^2$ . There is only 0.2% difference between these two magnitudes, but we can take just the first term in the numerator of Eq. (10.40),  $\frac{2(q \cdot p_{\Xi_b})(q \cdot p_{\Xi_c^*})}{M_{\Xi_b} M_{\Xi_c^*}}$ , as the relativistic form for the case of spin 3/2, replacing  $2\omega_\pi^2$ . The terms in Eq. (10.40) are trivially evaluated since

$$\begin{aligned} q^2 &= m_\pi^2, & 2q \cdot p_{\Xi_c^*} &= M_{\Xi_b}^2 - m_\pi^2 - M_{\Xi_c^*}^2, \\ 2q \cdot p_{\Xi_b} &= M_{\Xi_b}^2 + m_\pi^2 - M_{\Xi_c^*}^2, \\ 2p_{\Xi_b} \cdot p_{\Xi_c^*} &= M_{\Xi_b}^2 + M_{\Xi_c^*}^2 - m_\pi^2. \end{aligned}$$

When we make these replacements in the individual rates we obtain the following results:

$$\frac{\Gamma_{\Xi_b^- \rightarrow \pi^- \Xi_c^0}^{(\text{rel})}(2790)}{\Gamma_{\Xi_b^- \rightarrow \pi^- \Xi_c^0}^{(\text{nonrel})}(2790)} = 2.07, \quad (10.41a)$$

$$\frac{\Gamma_{\Xi_b^- \rightarrow \pi^- \Xi_c^0}^{(\text{rel})}(2815)}{\Gamma_{\Xi_b^- \rightarrow \pi^- \Xi_c^0}^{(\text{nonrel})}(2815)} = 2.05. \quad (10.41b)$$

As we can see, the relativistic corrections are important and increase the individual rates in about a factor of two. Yet, since the ratios of rates is the only thing that we determine, we have now, replacing  $R_1$  of Eq. (10.32),

$$R_1^{(\text{rel})} = \frac{\Gamma_{\Xi_b^- \rightarrow \pi^- \Xi_c^0}^{(\text{rel})}(2790)}{\Gamma_{\Xi_b^- \rightarrow \pi^- \Xi_c^0}^{(\text{rel})}(2815)} = 0.389, \quad (10.42)$$

while before  $R_1$  was 0.384. Hence, the change in the ratio is a mere 1%. Similarly we

evaluate

$$\frac{\Gamma_{\Xi_b^- \rightarrow D_s^- \Xi_c^0}^{(\text{rel})}}{\Gamma_{\Xi_b^- \rightarrow D_s^- \Xi_c^0}^{(\text{nonrel})}} = 1.64, \quad (10.43a)$$

$$\frac{\Gamma_{\Xi_b^- \rightarrow D_s^- \Xi_c^0}^{(\text{rel})}}{\Gamma_{\Xi_b^- \rightarrow D_s^- \Xi_c^0}^{(\text{nonrel})}} = 1.52. \quad (10.43b)$$

We can see that because of the larger mass of the  $D_s^-$  with respect to the one of the pion, the  $\Xi_c^0$  momentum is smaller and the relativistic effects are also smaller. Once again we look at the ratio  $R_2$  of Eq. (10.33) and we obtain now

$$R_2^{(\text{rel})} = \frac{\Gamma_{\Xi_b^- \rightarrow D_s^- \Xi_c^0}^{(\text{rel})}}{\Gamma_{\Xi_b^- \rightarrow D_s^- \Xi_c^0}^{(\text{rel})}} = 0.295, \quad (10.44)$$

replacing the non-relativistic value of 0.273. The effects in this ratio are of the order of 8%.

Finally, we look into the ratio  $R_3$  of Eq. (10.34) and we find now

$$R_3^{(\text{rel})} = \frac{\Gamma_{\Xi_b^- \rightarrow D_s^- \Xi_c^0}^{(\text{rel})}}{\Gamma_{\Xi_b^- \rightarrow \pi^- \Xi_c^0}^{(\text{rel})}} = 0.543, \quad (10.45)$$

replacing the non-relativistic value of 0.686. In this case the change is of the order of 20%, because of the larger relativistic effects in the case of the  $\pi^-$  emission compared to the one of  $D_s^-$  emission.

In order to estimate the relativistic effects of the semileptonic decay we follow the steps of Ref. [321]. We do not repeat the steps here but, using the results of Section VI of Ref. [321], we replace in Eq. (10.23)

$$p_\nu p_l \rightarrow \frac{(p_{\Xi_b} \cdot p_\nu)(p_{\Xi_c^*} \cdot p_l)}{M_{\Xi_b} M_{\Xi_c^*}}, \quad (10.46)$$

or, equivalently (see Eq. (35) of Ref. [321]) replacing the angle integrated value of  $p_\nu p_l$

$$\begin{aligned} p_\nu p_l &\equiv \frac{1}{M_{\Xi_b}^2} \left( \frac{M_{\text{inv}}}{2} \right)^2 \left[ \tilde{E}_{\Xi_b}^2 - \frac{1}{3} \tilde{p}_{\Xi_b}^2 \right] \\ &\rightarrow \frac{1}{M_{\Xi_b} M_{\Xi_c^*}} \left( \frac{M_{\text{inv}}}{2} \right)^2 \left[ \tilde{E}_{\Xi_b} \tilde{E}_{\Xi_c^*} - \frac{1}{3} \tilde{p}_{\Xi_b}^2 \right], \end{aligned} \quad (10.47)$$

where  $M_{\text{inv}}$  is the  $\bar{\nu}l$  invariant mass and the energies and momenta with tilde refer to the rest frame of the  $\bar{\nu}l$ , given by [321]

$$\tilde{p}_{\Xi_b} = \tilde{p}_{\Xi_c^*} = \frac{\lambda^{1/2}(M_{\Xi_b}^2, M_{\text{inv}}^2, M_{\Xi_c^*}^2)}{2M_{\text{inv}}}, \quad (10.48)$$

and  $\tilde{E}_{\Xi_b} = \sqrt{\tilde{p}_{\Xi_b}^2 + M_{\Xi_b}^2}$ ,  $\tilde{E}_{\Xi_c^*} = \sqrt{\tilde{p}_{\Xi_c^*}^2 + M_{\Xi_c^*}^2}$ . When we make these replacements in the semileptonic decays we find the following results:

$$\frac{\Gamma_{\Xi_b^- \rightarrow \bar{\nu}_l l \Xi_c^0(2790)}^{(\text{rel})}}{\Gamma_{\Xi_b^- \rightarrow \bar{\nu}_l l \Xi_c^0(2790)}^{(\text{nonrel})}} = 1.46, \quad (10.49a)$$

$$\frac{\Gamma_{\Xi_b^- \rightarrow \bar{\nu}_l l \Xi_c^0(2815)}^{(\text{rel})}}{\Gamma_{\Xi_b^- \rightarrow \bar{\nu}_l l \Xi_c^0(2815)}^{(\text{nonrel})}} = 1.45, \quad (10.49b)$$

and the ratio  $R$  of Eqs. (10.35), (10.36) becomes now

$$R = \frac{\Gamma_{\Xi_b^- \rightarrow \bar{\nu}_l l \Xi_c^0(2790)}^{(\text{rel})}}{\Gamma_{\Xi_b^- \rightarrow \bar{\nu}_l l \Xi_c^0(2815)}^{(\text{rel})}} = 0.198, \quad (10.50)$$

replacing the non-relativistic value of 0.197 of Eq. (10.36), less than 1% change. The smaller relativistic effects in the case of the semileptonic decay can be traced back to the large invariant mass of the  $\bar{\nu}_l l$  pair (see Fig. 10.5) with respect to the  $\pi^-$  or even the  $D_s^-$  mass.

## 10.8 Estimation of absolute values for the rates and uncertainties

The evaluation of the absolute values for the rates would require the knowledge of the form factor of Eq. (10.14) for which we do not have enough information, particularly for the excited  $c$  quark of  $\phi_{\text{fin}}(r)$ . This is the reason why we have calculated ratios where this matrix element will cancel. In order to evaluate absolute values for the decay rates, we shall construct ratios with respect to a related process for which there are experimental data. The ideal one is the decay  $\Lambda_b \rightarrow \pi^- \Lambda_c(2595)$  ( $\Lambda_c(2625)$ ). In the case of the  $\pi^- \Lambda_c(2595)$  the momentum of the  $\Lambda_c$  is  $q = 2208 \text{ MeV}/c$ . This value only differs in  $15 \text{ MeV}/c$  from the one of the  $\Xi_b \rightarrow \pi^- \Xi_c(2790)$ , less than 1% difference. Thus, since the transition  $b \rightarrow \pi^- c$  is the same in both cases and the  $ds$  or  $ud$

quarks are spectators in the  $\Xi_b$  and  $\Lambda_b$  decays respectively, we can simply assume the matrix  $\text{ME}(q)$  of Eq. (10.14) to be the same in both reactions. In that case, we have

$$\frac{BR(\Xi_b \rightarrow \pi^- \Xi_c^*)}{BR(\Lambda_b \rightarrow \pi^- \Lambda_c^*)} = \frac{M_{\Xi_c^*}}{M_{\Xi_b}} \frac{M_{\Lambda_b}}{M_{\Lambda_c^*}} \frac{q \bar{\Sigma} \Sigma |t|^2 \Big|_{\Xi_b}}{q \bar{\Sigma} \Sigma |t|^2 \Big|_{\Lambda_b}} \cdot \frac{\Gamma_{\Lambda_b}}{\Gamma_{\Xi_b}}, \quad (10.51)$$

where  $\bar{\Sigma} \Sigma |t|^2 \Big|_{\Xi_b}$  is given by Eqs. (10.16), (10.17) and  $\bar{\Sigma} \Sigma |t|^2 \Big|_{\Lambda_b}$  by Eqs. (41), (42) of Ref. [224] which we write below

$$J = \frac{1}{2}: \quad \bar{\Sigma} \Sigma |t|^2 \Big|_{\Lambda_b} = (q^2 + w_\pi^2) \left| \frac{1}{2} g_{R,DN} G_{DN} + \frac{1}{2\sqrt{3}} g_{R,D^*N} G_{D^*N} \right|^2, \quad (10.52)$$

$$J = \frac{3}{2}: \quad \bar{\Sigma} \Sigma |t|^2 \Big|_{\Lambda_b} = 2w_\pi^2 \left| \frac{1}{\sqrt{3}} G_{D^*N} g_{R,D^*N} \right|^2. \quad (10.53)$$

In Eq. (10.51), we could take [110],

$$\frac{\Gamma_{\Lambda_b}}{\Gamma_{\Xi_b}} = \frac{\tau_{\Xi_b}}{\tau_{\Lambda_b}} = 1.08 \pm 0.19. \quad (10.54)$$

Using the following ratios [110]

$$BR[\Lambda_b \rightarrow \pi^- \Lambda_c(2595)] = \frac{(3.4 \pm 1.5) \times 10^{-4}}{BR[\Lambda_c(2595) \rightarrow \Lambda_c \pi^+ \pi^-]}, \quad (10.55)$$

$$BR[\Lambda_b \rightarrow \pi^- \Lambda_c(2625)] = \frac{(3.3 \pm 1.3) \times 10^{-4}}{BR[\Lambda_c(2625) \rightarrow \Lambda_c \pi^+ \pi^-]}, \quad (10.56)$$

with  $BR[\Lambda_c^* \rightarrow \Lambda_c \pi^+ \pi^-] = 0.67$  [110], we obtain

$$BR[\Xi_b \rightarrow \pi^- \Xi_c(2790)] = (7 \pm 4) \times 10^{-6}, \quad (10.57)$$

$$BR[\Xi_b \rightarrow \pi^- \Xi_c(2815)] = (13 \pm 7) \times 10^{-6}, \quad (10.58)$$

where the 50% relative error is obtained summing in quadratures the relative errors in Eqs. (10.54), (10.55), (10.56) and an error of the order of 20% affecting to the  $\Lambda_b \rightarrow \pi^- \Lambda_c^*$  decay, as discussed in Ref. [224]. It estimates the effects produced by the  $D_s \Lambda$  and  $D_s^* \Lambda$  channels neglected in the approach followed in that work (see discussion in Section 6 of that reference).

As for the semileptonic decay, we would equally have

$$\frac{BR(\Xi_b \rightarrow \bar{\nu}_l l \Xi_c^*)}{BR(\Lambda_b \rightarrow \bar{\nu}_l l \Lambda_c^*)} = \frac{\int dM_{\text{inv}} \frac{d\Gamma}{dM_{\text{inv}}} \Big|_{\Xi_b}}{\int dM_{\text{inv}} \frac{d\Gamma}{dM_{\text{inv}}} \Big|_{\Lambda_b}} \cdot \frac{\Gamma_{\Lambda_b}}{\Gamma_{\Xi_b}}, \quad (10.59)$$



where  $\frac{d\Gamma}{dM_{\text{inv}}}\Big|_{\Xi_b}$  is given by Eq. (10.26) and  $\frac{d\Gamma}{dM_{\text{inv}}}\Big|_{\Lambda_b}$  by Eq. (27) of Ref. [321], which we reproduce below, with

$$\frac{d\Gamma}{dM_{\text{inv}}}\Big|_{\Lambda_b} = \frac{M_{\Lambda_c^*}}{M_{\Lambda_b}} 2m_\nu 2m_l \frac{1}{(2\pi)^3} p_{\Lambda_c^*} \tilde{p}_l \overline{\sum} \sum |T|^2 \Big|_{\Lambda_b} \quad (10.60)$$

with  $p_{\Lambda_c^*}$  the  $\Lambda_c^*$  momentum in the  $\Lambda_b$  rest frame and  $\tilde{p}_l$  the lepton momentum in the  $\bar{\nu}l$  rest frame, and

$$\overline{\sum} \sum |T|^2 \Big|_{\Lambda_b} = C'^2 \frac{8}{m_\nu m_l} p_\nu p_l A_J V_{\text{had}}(J) \quad (10.61)$$

with

$$A_J V_{\text{had}}(J) \equiv \begin{cases} \left| \frac{1}{2} g_{R,DN} G_{DN} + \frac{1}{2\sqrt{3}} g_{R,D^*N} G_{D^*N} \right|^2, & \text{for } J = 1/2 \\ 2 \left| \frac{1}{\sqrt{3}} g_{R,D^*N} G_{D^*N} \right|^2, & \text{for } J = 3/2 \end{cases} \quad (10.62)$$

The experimental branching ratios are [110]

$$BR[\Lambda_b \rightarrow \bar{\nu}_l l \Lambda_c(2595)] = (7.9_{-3.5}^{+4.0}) \times 10^{-3}, \quad (10.63)$$

$$BR[\Lambda_b \rightarrow \bar{\nu}_l l \Lambda_c(2625)] = (13.0_{-5.0}^{+6.0}) \times 10^{-3}, \quad (10.64)$$

from where we obtain

$$BR[\Xi_b \rightarrow \bar{\nu}_l l \Xi_c(2790)] = (1.0_{-0.5}^{+0.6}) \times 10^{-4}, \quad (10.65)$$

$$BR[\Xi_b \rightarrow \bar{\nu}_l l \Xi_c(2815)] = (3.3_{-1.6}^{+1.8}) \times 10^{-4}, \quad (10.66)$$

where the 50-60% relative error comes from summing in quadratures the relative errors of Eq. (10.54), Eqs. (10.63), (10.64) and an extra 20% from the consideration of the  $D_s \Lambda$ ,  $D_s^* \Lambda$  channels in Ref. [321].

We have also estimated uncertainties in the magnitudes that we have calculated, related to uncertainties in the model. For this, we have used the freedom that we have in the cut off, or subtraction constant in dimensional regularization, employed to regularize the loops. We have allowed small changes that induce a change of about 6 MeV in the mass of the  $\Xi_c^{0*}$  states (about double than the empirical errors). With this we find the uncertainties:

$$\begin{aligned} \frac{\delta R_1}{R_1} &\simeq 0.35, & \frac{\delta R_2}{R_2} &\simeq 0.35, \\ \frac{\delta R_3}{R_3} &\simeq 0, & \frac{\delta R}{R} &\simeq 0.35. \end{aligned}$$

As to the absolute values in Eqs. (10.57) (10.58) (10.65) (10.66) we find uncertainties also of the order of 25% from this source, which summed in quadratures to the existing errors, do not change much the errors that we already associated to these numbers and discussed above. It might be surprising that the errors in the ratios are bigger than in the absolute values of the rates from this source. This is because an increase in the subtraction constant decreases the rate for the  $\Xi_c(2790)$  and increases the rate for the  $\Xi_c(2815)$  both in the nonleptonic and the semileptonic decays.

We want to note that the smaller absolute numbers obtained for the present decay, compared to those of the  $\Lambda_b$  stem from the large cancellations between the terms in Eqs. (10.16) (10.17) and (10.28) (10.29), between the  $\Sigma D$  and  $\Lambda D$  contributions. We should also warn that to estimate the absolute rates we have used two different theoretical models for the  $DN$ ,  $D^*N$  and  $D\Sigma$ ,  $D^*\Sigma$ ,  $D\Lambda$ ,  $D^*\Lambda$  interactions from Ref. [435] and Ref. [86] respectively. One should expect some systematic errors from this source, more difficult to evaluate, but we think that, with the large uncertainties that we already have, these new uncertainties would also be accommodated.

## 10.9 Conclusion

We have studied the nonleptonic  $\Xi_b^- \rightarrow M + \Xi_c^*$ , with  $M = \pi^-$ ,  $D_s^-$  and  $\Xi_c^* = \Xi_c^0(2790)[\frac{1}{2}^-]$ ,  $\Xi_c^0(2815)[\frac{3}{2}^-]$ . We have assumed that the  $\Xi_c^*$  resonances are dynamically generated from the  $PB$  and  $VB$  interactions, as done in Ref. [86], and that they form a  $j_q^P = 1^-$  HQSS doublet. We saw that the present decays only involved the  $D\Lambda$ ,  $D\Sigma$ ,  $D^*\Lambda$ ,  $D^*\Sigma$  channels and we took the needed couplings from that work. Given the fact that the momentum of the meson  $M$  is very similar for the case of the production of the two resonances (since their masses are very close) we could eliminate in the ratio of widths the matrix element at the quark level involving the wave functions of the  $b$  and  $c$  quarks. Then, only factors related to the spin structure of the channels and the couplings of the hadronic model for the resonances were relevant, which tells us that the measurement of these partial decay widths are relevant to learn details on the nature of the  $\Xi_c^*$  resonances. With more uncertainty we were able to also predict the ratio of  $\Xi_b^- \rightarrow \pi^- \Xi_c^*$  and  $\Xi_b^- \rightarrow D_s^- \Xi_c^*$  for the same resonance.

We also evaluated the semileptonic rates. In this case we can only evaluate one ratio, the one of the semileptonic decay  $\Xi_b \rightarrow \bar{\nu}_l l \Xi_c^*$  for the  $\Xi_c^0(2790)$  and  $\Xi_c^0(2815)$  resonances. Once again, the predictions will be valuable when these partial decay widths can be measured. We should stress that both the nonleptonic and semileptonic decay widths are measured for the case of  $\Lambda_b \rightarrow \pi^- \Lambda_c(2595)$ ,  $\Lambda_b \rightarrow \pi^- \Lambda_c(2625)$  and  $\Lambda_b \rightarrow \bar{\nu}_l l \Lambda_c(2595)$  and  $\Lambda_b \rightarrow \bar{\nu}_l l \Lambda_c(2625)$  and the method used here gave results in agreement with experiment [224, 321], so we are confident that the predictions done here are fair. We also estimated the absolute branching ratios of

---

all these decays from the ratios to the related  $\Lambda_b \rightarrow \pi^- \Lambda_c(2595)(\Lambda_c(2625))$ ,  $\Lambda_b \rightarrow \bar{\nu}_l l \Lambda_c(2595)(\Lambda_c(2625))$  reactions and the experimental rates for these latter decays. The branching ratios obtained are well within measurable range, where branching ratios of  $\Xi_b^-$  of the order of  $10^{-7}$  have already been observed [110]. In any case the experimental result could test the accuracy of the model of Ref. [86], which is one of the possible ways to address the molecular states, with a particular dynamics consistent with HQSS.

We also checked that the results were sensitive to the couplings of the  $D^*B$  components and confirmation of this feature by experiment could give a boost to the relevance of the mixing of pseudoscalar-baryon and vector-baryon components in the building up of the molecular baryonic states, a subject which is catching up in the hadronic community [85, 86, 297, 332, 435, 443, 444].



**Part IV**

**Triangle Singularities**



# Chapter 11

## Triangle Singularities in non-leptonic $B^- \rightarrow D^{*0}$ decays

### 11.1 Introduction

In this chapter, based on Ref. [9], we investigate the  $B^- \rightarrow D^{*0}\pi^-\pi^0\eta$  and  $B^- \rightarrow D^{*0}\pi^-\pi^+\pi^-$  decays via  $a_0$  and  $f_0$  formation. The process of  $B^- \rightarrow D^{*0}K^-K^{*0}$  followed by the  $K^{*0}$  decay into  $\pi^-K^+$  and the merging of the  $K^+K^-$  into  $a_0$  or  $f_0$  (see Fig. 11.1) generate a singularity, which would appear around 1418 MeV in the invariant mass of  $\pi^-a_0$  or  $\pi^-f_0$ , as calculated using Eq. (3.134). In this study, these  $a_0$  and  $f_0$  states appear as the dynamically generated states of  $\pi\pi$ ,  $K\bar{K}$ ,  $\eta\eta$ , and  $K\bar{K}$ ,  $\pi^0\eta$  in the  $I = 0$  and  $I = 1$  channels, respectively, as studied in Refs. [122, 166].

The mechanism proposed here, without the indication of how the  $K^*\bar{K}$  could be formed, and without a quantitative evaluation of the process, was suggested in

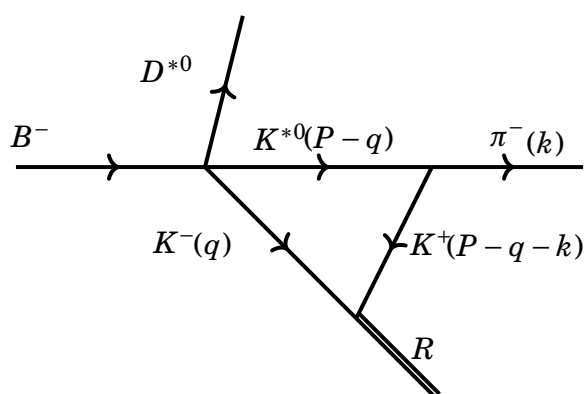


Figure 11.1: Diagram for the decay of  $B^-$  into  $D^{*0}$ ,  $\pi^-$  and  $R$ , where  $R = a_0(980)$  or  $f_0(980)$ .

Ref. [106]. We provide here a realistic example of a physical process where this can occur, which also allows us to perform a quantitative calculation of the amplitudes involved.

Weak decays of heavy hadrons are turning into a good laboratory to find many triangle singularities. Apart from the work of Ref. [128], the  $B_c \rightarrow B_s \pi \pi$  reaction has been suggested, where  $B_c^+ \rightarrow \bar{K}^{*0} B^+$ ,  $\bar{K}^{*0} \rightarrow \pi^0 \bar{K}^0$  and  $\bar{K}^0 B^+ \rightarrow \pi B_s^0$  [127]. Yet, there are large uncertainties quantizing the  $\bar{K}^0 B^+ \rightarrow \pi B_s^0$  amplitude and the  $B_c^+ \rightarrow \bar{K}^{*0} B^+$  weak decay.

In the present case we rely upon the well known  $K\bar{K} \rightarrow \pi\pi$  ( $K\bar{K} \rightarrow \pi\eta$ ) amplitudes, and the  $B^- \rightarrow D^{*0} \bar{K}^{*0} K^-$  vertex can be obtained from experiment. Hence, we are able to quantize the decay rates of the mechanism proposed and we find that the mass distribution of these decay processes shows a peak associated with the triangle singularity, and finally find the branching fractions  $\text{Br}(B^- \rightarrow D^{*0} \pi^- a_0; a_0 \rightarrow \pi^0 \eta) = (1.66 \pm 0.45) \times 10^{-6}$  and  $\text{Br}(B^- \rightarrow D^{*0} \pi^- f_0; f_0 \rightarrow \pi^+ \pi^-) = (2.82 \pm 0.75) \times 10^{-6}$ .

## 11.2 Formalism

We will analyze the effect of triangle singularities in the following decays:  $B^- \rightarrow D^{*0} \pi^- \eta \pi^0$  and  $B^- \rightarrow D^{*0} \pi^- \pi^+ \pi^-$ . The complete Feynman diagram for these decays, with the triangle mechanism through the  $a_0$  or  $f_0$  mesons, is shown in Fig. 11.2.

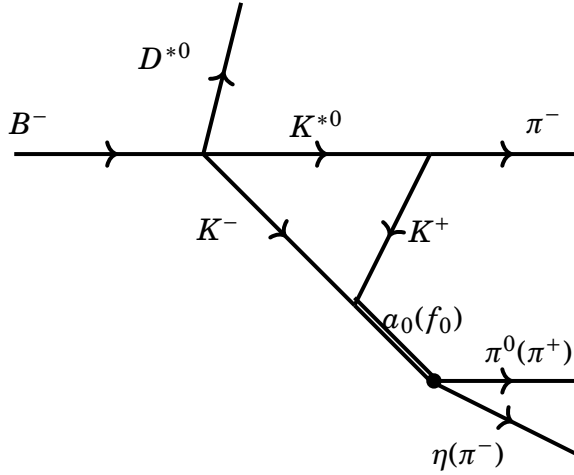


Figure 11.2: Diagram for the decay of  $B^- \rightarrow D^{*0} \pi^- \eta \pi^0 (\pi^+ \pi^-)$ .

At first, we evaluate the  $B^- \rightarrow D^* \pi R$  ( $R = a_0, f_0$ ). This then produces the triangle diagram shown in Fig. 11.1. From Eq. (3.124), the  $T$  matrix  $t_{B \rightarrow D^* \pi R}$  will have the



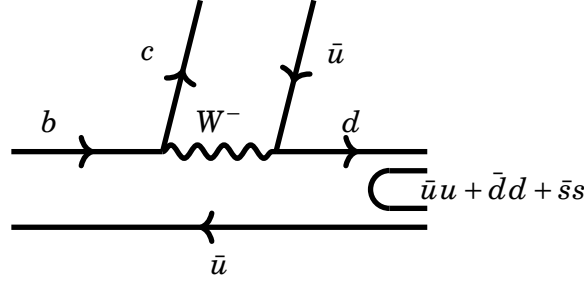


Figure 11.3: Diagram for the decay of  $B^-$  into  $D^{*0}$ ,  $K^{*0}$  and  $K^-$  as seen through the quark constituents of the hadrons.

following form,

$$-it_{B^- \rightarrow D^{*0} \pi R} = i \sum_{\text{pol. of } K^*} \int \frac{d^4 q}{(2\pi)^4} \frac{i t_{B^- \rightarrow D^{*0} K^{*0} K^-}}{q^2 - m_K^2 + i\epsilon} \frac{i t_{K^* K^+ \pi^-}}{(P-q)^2 - m_{K^*}^2 + i\epsilon} \frac{i t_{K^+ K^-, R}}{(P-q-k)^2 - m_K^2 + i\epsilon}. \quad (11.1)$$

The amplitude in Eq. (11.1) is evaluated in the center-of-mass (CM) frame of  $\pi R$ . Now we need to calculate the three vertices,  $t_{B^- \rightarrow D^{*0} K^{*0} K^-}$ ,  $t_{K^* K^+ \pi^-}$  and  $t_{K^+ K^-, R}$ , in Eq. (11.1).

First, we discuss the  $B^- \rightarrow D^{*0} K^- K^{*0}$  vertex. At the quark level, the Cabibbo-allowed vertex is formed through an internal emission of a  $W$  boson [305] (as can be seen in Fig. 11.3), producing a  $c\bar{u}$  that forms the  $D^{*0}$ , with the remaining  $d\bar{u}$  quarks hadronizing and producing the  $K^-$  and  $K^{*0}$  mesons with the selection of the  $\bar{s}s$  pair from a created vacuum  $\bar{u}u + \bar{d}d + \bar{s}s$  state<sup>1</sup>. Since both  $D^{*0}$  and  $K^{*0}$  have  $J^P = 1^-$ , the interaction in the  $B^- \rightarrow D^{*0} K^- K^{*0}$  vertex can proceed via  $s$ -wave and we take the amplitude of the form,

$$t_{B^- \rightarrow D^{*0} K^{*0} K^-} = C \epsilon_\mu(K^*) \epsilon^\mu(D^*). \quad (11.2)$$

Given that we know that the branching ratio of this decay is  $\text{Br}(B^- \rightarrow D^{*0} K^{*0} K^-) = (1.5 \pm 0.4) \times 10^{-3}$  [110, 445], we can determine the constant  $C$  by calculating the width of this decay,

$$\frac{d\Gamma_{B^- \rightarrow D^{*0} K^{*0} K^-}}{dM_{\text{inv}}(K^* D^*)} = \frac{1}{(2\pi)^3} \frac{|\vec{p}_{K^-}| |\vec{p}_{K^*}|}{4M_B^2} \overline{\sum \sum} |t_{B^- \rightarrow D^{*0} K^{*0} K^-}|^2, \quad (11.3)$$

where  $\vec{p}_{K^-}$  is the momentum of  $K^-$  in the  $B^-$  rest frame, and  $\vec{p}_{K^*}$  is the momentum of  $K^{*0}$  in the  $K^{*0} D^{*0}$  CM frame. The absolute values of both momenta are given

<sup>1</sup>In weak decays of  $B$  mesons, there is always a  $bc$  transition (could be  $bu$ ) which is Cabibbo suppressed. It is then customary to refer to Cabibbo allowed or suppressed processes by looking at the second weak vertex.

by

$$|\vec{p}_{K^-}| = \frac{\lambda^{1/2}(M_B^2, m_{K^-}^2, M_{\text{inv}}^2(K^* D^*))}{2M_B}, \quad (11.4a)$$

$$|\vec{p}_{K^*}| = \frac{\lambda^{1/2}(M_{\text{inv}}^2(K^* D^*), m_{K^*}^2, m_{D^*}^2)}{2M_{\text{inv}}(K^* D^*)}. \quad (11.4b)$$

Now, if we square the  $T$  matrix in Eq. (11.2) and sum over the polarizations, we get

$$\overline{\sum} \sum |t_{B^- \rightarrow D^{*0} K^{*0} K^-}|^2 \quad (11.5)$$

$$= C^2 \sum_{\text{pol}} \epsilon_\mu(K^*) \epsilon_\nu(K^*) \epsilon^\mu(D^*) \epsilon^\nu(D^*) \quad (11.6)$$

$$= C^2 \left( 2 + \frac{(p_{K^*} \cdot p_{D^*})^2}{m_{K^*}^2 m_{D^*}^2} \right) \quad (11.7)$$

$$= C^2 \left( 2 + \frac{(M_{\text{inv}}^2(K^* D^*) - m_{K^*}^2 - m_{D^*}^2)^2}{4m_{K^*}^2 m_{D^*}^2} \right). \quad (11.8)$$

where we used the fact that  $(p_{K^*} + p_{D^*})^2 = M_{\text{inv}}^2(K^* D^*)$ , *i.e.*,  $p_{K^*} \cdot p_{D^*} = \frac{1}{2}(M_{\text{inv}}^2(K^* D^*) - m_{K^*}^2 - m_{D^*}^2)$ .

Then, using this last equation in Eq. (11.3), we get

$$\frac{C^2}{\Gamma_{B^-}} = \frac{\text{Br}(B^- \rightarrow D^{*0} K^{*0} K^-)}{\int dM_{\text{inv}}(K^* D^*) \frac{1}{(2\pi)^3} \frac{|\vec{p}_{K^-}| |\vec{p}_{K^*}|}{4M_B^2} \left( 2 + \frac{(M_{\text{inv}}^2(K^* D^*) - m_{K^*}^2 - m_{D^*}^2)^2}{4m_{K^*}^2 m_{D^*}^2} \right)}, \quad (11.9)$$

where the integral has the limits  $M_{\text{inv}}(K^* D^*)|_{\text{min}} = m_{D^*} + m_{K^*}$  and  $M_{\text{inv}}(K^* D^*)|_{\text{max}} = M_B - m_K$ .

Now we calculate the contribution of the vertex  $K^{*0} \rightarrow \pi^- K^+$  using the local hidden gauge formalism. Performing the matrix operations and the trace we get

$$\mathcal{L}_{K^* K \pi} = -ig K^{*0\mu} (K^- \partial_\mu \pi^+ - \pi^+ \partial_\mu K^-). \quad (11.10)$$

So, for the  $t$  matrix we get,

$$-it_{K^* K^+ \pi^-} = -ig \epsilon_{K^*}^\mu (p_{K^+} - p_\pi)_\mu \quad (11.11)$$

$$\simeq -ig \vec{\epsilon}_{K^*} \cdot (\vec{p}_\pi - \vec{p}_{K^+}), \quad (11.12)$$

with  $\vec{p}_{K^+}$  and  $\vec{p}_\pi$  calculated in the CM frame of  $\pi R$ . At the energy where the triangle singularity appears ( $M_{\text{inv}}(\pi R) = 1418$  MeV), the momentum of  $K^*$  is about

150 MeV/c, which is small enough, compared with the mass of  $K^*$ , to omit the zeroth component of the polarization vector in Eq. (11.11).

Finally we only need the  $R \rightarrow K^+K^-$  coupling before we can analyze the triangle diagram. The coupling of  $R$  with  $\pi^0\eta$  or  $\pi^+\pi^-$  proceeds in  $s$ -wave. Then, the vertex is written simply as a constant,

$$t_{K^+K^-,R} = g_{K^-K^+,R}. \quad (11.13)$$

We shall use this coupling only formally, since its product with the  $g_{R,\pi^+\pi^-}$  ( $g_{R,\pi^0\eta}$ ) coupling will be traded off in favor of the  $K\bar{K} \rightarrow \pi^+\pi^-$  ( $\pi^0\eta$ ) scattering amplitude. We can now analyze the effect of the triangle singularity on the  $B^- \rightarrow D^*\pi R$  decay. Substituting Eqs. (11.2), (11.12) and (11.13) for Eq. (11.1), the decay amplitude  $t_{B^- \rightarrow D^*\pi R}$  is written as

$$t_{B^- \rightarrow D^*\pi R} = -ig_{K^-K^+,R} g_C \sum_{\text{pol. of } K^*} \int \frac{d^4q}{(2\pi)^4} \frac{\vec{\epsilon}_{D^*} \cdot \vec{\epsilon}_{K^*}}{q^2 - m_K^2 + i\epsilon} \frac{\vec{\epsilon}_{K^*} \cdot (\vec{p}_\pi - \vec{p}_{K^+})}{(P-q)^2 - m_{K^*}^2 + i\epsilon} \\ \times \frac{1}{(P-q-k)^2 - m_K^2 + i\epsilon}, \quad (11.14)$$

where for  $t_{B^- \rightarrow D^*0K^*0K^-}$  we have also the spatial components of the polarization vectors, and  $\vec{p}_{K^+}$ ,  $\vec{p}_{K^+}$  are taken in the CM frame of  $\pi R$ . As we have mentioned below Eq. (11.12), the momentum of the  $K^{*0}$  around the triangle peak is small compared with the mass, and we can omit the zeroth component of the polarization vector of the  $K^{*0}$  [128].

Now we only need to calculate the width  $\Gamma$  associated with the diagram in Fig. 11.1. Right away we see that since

$$\sum_{\text{pol. of } K^*} \epsilon_{K^*}^i \epsilon_{K^*}^j = \delta_{ij}, \quad (11.15)$$

Eq. (11.14) reduces to

$$t_{B^- \rightarrow D^*\pi R} = g_{K^-K^+,R} g_C i \int \frac{d^4q}{(2\pi)^4} \frac{\vec{\epsilon}_{D^*} \cdot (\vec{p}_{K^+} - \vec{p}_\pi)}{q^2 - m_K^2 + i\epsilon} \frac{1}{(P-q)^2 - m_{K^*}^2 + i\epsilon} \frac{1}{(P-q-k)^2 - m_K^2 + i\epsilon}, \quad (11.16)$$

where  $\vec{p}_{K^+} = \vec{P} - \vec{q} - \vec{k} = -(\vec{q} + \vec{k})$  and  $\vec{p}_\pi = \vec{k}$ .

Defining  $f(\vec{q}, \vec{k})$  as a product of the three propagators in Eq. (11.16), we can use the formula,

$$\int d^3q q_i f(\vec{q}, \vec{k}) = k_i \int d^3q \frac{\vec{q} \cdot \vec{k}}{|\vec{k}|^2} f(\vec{q}, \vec{k}), \quad (11.17)$$

which follows from the fact that the  $\vec{k}$  is the only vector not integrated in the integrand of Eq. (11.16). Then, Eq. (11.16) becomes

$$t_{B^- \rightarrow D^* \pi R} = -\vec{e}_{D^*} \cdot \vec{k} g_{K^- K^+, R} g^C t_T, \quad (11.18)$$

with

$$t_T = i \int \frac{d^4 q}{(2\pi)^4} \left( 2 + \frac{\vec{q} \cdot \vec{k}}{|\vec{k}|^2} \right) \frac{1}{q^2 - m_K^2 + i\epsilon} \frac{1}{(P - q)^2 - m_{K^*}^2 + i\epsilon} \frac{1}{(P - q - k)^2 - m_K^2 + i\epsilon}. \quad (11.19)$$

Squaring and summing over the polarizations of  $D^*$ , Eq. (11.18) becomes

$$\sum_{\text{pol}} |t_{B^- \rightarrow D^* \pi R}|^2 = |\vec{k}|^2 g_{K^- K^+, R}^2 g^2 C^2 |t_T|^2, \quad (11.20)$$

The analytical integration of  $t_T$  in Eq. (11.19) over  $q^0$  leads to (see Eq. (3.125)),

$$t_T = \int \frac{d^3 q}{(2\pi)^3} \left( 2 + \frac{\vec{q} \cdot \vec{k}}{|\vec{k}|^2} \right) \frac{1}{8\omega^* \omega \omega'} \frac{1}{k^0 - \omega' - \omega^*} \frac{1}{P^0 + \omega + \omega' - k^0} \frac{1}{P^0 - \omega - \omega' - k^0 + i\epsilon} \times \frac{\{2P^0 \omega + 2k^0 \omega' - 2[\omega + \omega'][\omega + \omega' + \omega^*]\}}{P^0 - \omega^* - \omega + i\epsilon}, \quad (11.21)$$

with  $\omega^*(\vec{q}) = \sqrt{m_{K^*}^2 + |\vec{q}|^2}$ ,  $\omega'(\vec{q}) = \sqrt{m_K^2 + |\vec{q} + \vec{k}|^2}$  and  $\omega(\vec{q}) = \sqrt{m_K^2 + |\vec{q}|^2}$ . To regularize the integral in Eq. (11.21) we use the same cutoff of the meson loop that will be used to calculate  $t_{K^+ K^- \rightarrow \pi^0 \eta}$  and  $t_{K^+ K^- \rightarrow \pi^+ \pi^-}$  (which are calculated using the BSE),  $\theta(q_{\text{max}} - |q^*|)$ , where  $\vec{q}^*$  is the  $K^-$  momentum in the  $R$  rest frame [123].

From Eq. (3.134) we can determine that the singularity will appear at around  $M_{\text{inv}}(\pi R) = 1418$  MeV.

For the three body decay of  $B^- \rightarrow D^{*0} \pi^- R$  in Fig. 11.1, the mass distribution is given by

$$\frac{d\Gamma}{dM_{\text{inv}}(\pi R)} = \frac{1}{(2\pi)^3} \frac{|\vec{p}_{D^*}| |\vec{p}_\pi|}{4M_B^2} \sum_{\text{pol.}} |t_{B^- \rightarrow D^* \pi R}|^2, \quad (11.22)$$

with

$$|\vec{p}_{D^*}| = \frac{\lambda^{1/2}(M_B^2, m_{D^*}^2, M_{\text{inv}}^2(\pi R))}{2M_B}, \quad (11.23a)$$

$$|\vec{p}_\pi| = |\vec{k}| = \frac{\lambda^{1/2}(M_{\text{inv}}^2(\pi R), m_\pi^2, M_R^2)}{2M_{\text{inv}}(\pi R)} \quad (11.23b)$$

With Eq. (11.18) and a factor  $1/\Gamma_{B^-}$ , the mass distribution of  $B^-$  decaying into  $D^* \pi R$  is written as

$$\frac{1}{\Gamma_{B^-}} \frac{d\Gamma}{dM_{\text{inv}}(\pi R)} = \frac{C^2}{\Gamma_{B^-}} \frac{g^2}{(2\pi)^3} \frac{|\vec{p}_{D^*}||\vec{k}|}{4M_B^2} |\vec{k}|^2 \cdot |t_T \times g_{K^-K^+,R}|^2, \quad (11.24)$$

where  $\frac{C^2}{\Gamma_{B^-}}$  is given in Eq. (11.9).

To take into account the fact that  $a_0$  and  $f_0$  are resonances that have a width and can decay to  $\pi^0 \eta$  and  $\pi^+ \pi^-$ , respectively, we proceed as done in Eq. (4.68) and do a convolution of the mass distribution,

$$\frac{d\Gamma}{dM_{\text{inv}}(\pi R)} = \frac{1}{(2\pi)^3} \int dM_{\text{inv}}^2(R) \left(-\frac{1}{\pi} \text{Im}D\right) |g_{K^-K^+,R}|^2 \frac{|\vec{p}_{D^*}||\vec{p}_\pi|}{4M_B^2} \overline{\sum} \sum |\tilde{t}_{B^-,D^*\pi R}|^2, \quad (11.25)$$

where

$$D = \frac{1}{M_{\text{inv}}^2(R) - M_R^2 + iM_R\Gamma_R}, \quad (11.26)$$

with  $\tilde{t}_{B^-,D^*\pi R} = t_{B^- \rightarrow D^* \pi R} / g_{K^-K^+,R}$  and  $R = a_0$  and  $f_0$ . What Eq. (11.25) is accomplishing is a convolution of Eq. (11.22) with the mass distribution of the  $R$  resonance given by its spectral function. Note that the mass distributions of the  $f_0(980)$ ,  $a_0(980)$  states follow a Flatté distribution rather than the Breit Wigner, but the use of Eq. (11.26) is only formal to arrive to an expression that uses the scattering amplitudes  $t_{K^+K^-, \pi^+\pi^-(\pi^0\eta)}$ , which are calculated with the chiral unitary approach and automatically incorporate the Flatté form and the usual requirements of analyticity and unitarity.

Evaluating explicitly the imaginary part of  $D$ , Eq. (11.25) becomes

$$\begin{aligned} \frac{d\Gamma}{dM_{\text{inv}}(\pi R)} &= \frac{1}{(2\pi)^3} \int dM_{\text{inv}}^2(R) \frac{1}{\pi} |g_{K^-K^+,R}|^2 \frac{|\vec{p}_{D^*}||\vec{p}_\pi|}{4M_B^2} \overline{\sum} \sum |\tilde{t}_{B^-,D^*\pi R}|^2 \\ &\quad \times \frac{M_R\Gamma_R}{(M_{\text{inv}}^2(R) - M_R^2)^2 + (M_R\Gamma_R)^2}. \end{aligned} \quad (11.27)$$

Now, for the case of  $a_0(980)$ , we only have the decay  $a_0 \rightarrow \pi^0 \eta$  (we neglect the small  $K\bar{K}$  decay fraction), and thus,

$$\Gamma_{a_0} = \frac{1}{8\pi} \frac{|g_{a_0 \rightarrow \pi^0 \eta}|^2}{M_{\text{inv}}^2(\pi^0 \eta)} |\vec{q}_\eta|, \quad (11.28)$$

with

$$|\vec{q}_\eta| = \frac{\lambda^{1/2}(M_{\text{inv}}^2(\pi^0\eta), m_\pi^2, m_\eta^2)}{2M_{\text{inv}}(\pi^0\eta)}. \quad (11.29)$$

Then Eq. (11.27) becomes

$$\begin{aligned} \frac{d\Gamma}{dM_{\text{inv}}(\pi a_0)} &= \frac{1}{(2\pi)^3} \int dM_{\text{inv}}^2(\pi^0\eta) \frac{|\vec{p}_{D^*}||\vec{p}_\pi|}{4M_B^2} \overline{\sum} \sum |\tilde{t}_{B^-, D^* \pi R}|^2 \\ &\times \frac{M_{a_0} |g_{a_0 \rightarrow \pi^0 \eta}|^2 |g_{K^- K^+ \rightarrow a_0}|^2}{(M_{\text{inv}}^2(\pi^0\eta) - M_{a_0}^2)^2 + (M_{a_0} \Gamma_{a_0})^2} \frac{1}{8\pi^2} \frac{|\vec{q}_\eta|}{M_{\text{inv}}^2(\pi^0\eta)}. \end{aligned} \quad (11.30)$$

But since for the resonance we have formally,

$$\frac{|g_{a_0 \rightarrow \pi^0 \eta}|^2 |g_{K^- K^+ \rightarrow a_0}|^2}{(M_{\text{inv}}^2(\pi^0\eta) - M_{a_0}^2)^2 + (M_{a_0} \Gamma_{a_0})^2} = |t_{K^+ K^- \rightarrow \pi^0 \eta}|^2, \quad (11.31)$$

Eq. (11.30) reduces to

$$\frac{d^2\Gamma}{dM_{\text{inv}}(\pi a_0) dM_{\text{inv}}(\pi^0\eta)} = \frac{1}{(2\pi)^5} \frac{|\vec{p}_{D^*}||\vec{k}||\vec{q}_\eta|}{4M_B^2} \overline{\sum} \sum |t_{B^-, D^* \pi R} \times t_{K^+ K^- \rightarrow \pi^0 \eta}|^2, \quad (11.32)$$

where we have approximated a factor  $M_{a_0}/M_{\text{inv}}(\pi^0\eta)$  to unity. For the case of  $f_0(980)$ ,  $f_0 \rightarrow \pi^+\pi^-$  is not the only possible decay and as such  $\Gamma_{f_0 \rightarrow \pi^+\pi^-}$  will not be the same as the  $\Gamma_R$  in Eq. (11.26). However, when we put  $|t_{K^+ K^- \rightarrow \pi^+\pi^-}|^2$  in the end, we already select the  $\pi\pi$  part of the  $f_0$  decay. Thus, for the case of  $f_0$  we just need to substitute, in Eq. (11.32),  $t_{K^+ K^- \rightarrow \pi^0 \eta} \rightarrow t_{K^+ K^- \rightarrow \pi^+\pi^-}$ ,  $M_{\text{inv}}(\pi a_0) \rightarrow M_{\text{inv}}(\pi f_0)$ ,  $M_{\text{inv}}(\pi^0\eta) \rightarrow M_{\text{inv}}(\pi^+\pi^-)$ , and  $|\vec{q}_\eta| \rightarrow |\vec{q}_\pi|$ , with

$$|\vec{q}_\pi| = \frac{\lambda^{1/2}(M_{\text{inv}}^2(\pi^+\pi^-), m_{\pi^+}^2, m_{\pi^-}^2)}{2M_{\text{inv}}(\pi^+\pi^-)}. \quad (11.33)$$

The amplitudes  $t_{K^+ K^- \rightarrow \pi^0 \eta}$  and  $t_{K^+ K^- \rightarrow \pi^+\pi^-}$  themselves are calculated based on the chiral unitary approach, where the  $a_0$  and  $f_0$  appear as dynamically generated states [122, 166], with a sharp cutoff of  $q_{\text{max}} = 600$  MeV for the reproduction of the  $a_0$  and  $f_0$  peaks which appear around 980 MeV in the invariant mass of  $\pi^0\eta$  or  $\pi^+\pi^-$  [212, 213].

Finally, we substitute everything we have calculated into Eq. (11.32) and obtain,

$$\frac{1}{\Gamma_{B^-}} \frac{d^2\Gamma}{dM_{\text{inv}}(\pi R) dM_{\text{inv}}(R)} = \frac{g^2}{(2\pi)^5} \frac{|\vec{p}_{D^*}||\vec{q}_\eta||\vec{k}|^3}{4M_B^2} |t_T \times t_{K^+ K^- \rightarrow \pi^0 \eta(\pi^+\pi^-)}|^2 \frac{C^2}{\Gamma_{B^-}}. \quad (11.34)$$

### 11.3 Results

Let us begin by showing in Fig. 11.4 the contribution of the triangle loop (defined in Eq. (11.21)) to the total amplitude. We plot the real and imaginary parts of  $t_T$ , as well as the absolute value with  $M_{\text{inv}}(R)$  fixed at 980 MeV. As can be observed, there is a peak around 1420 MeV, as predicted in Eq. (3.134).

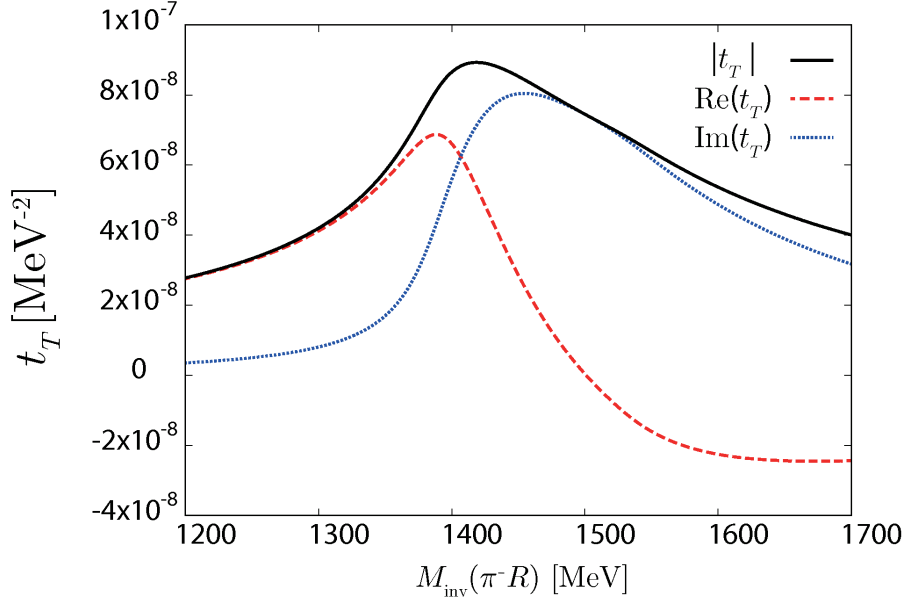


Figure 11.4: Triangle amplitude  $t_T$  for the decay  $B^- \rightarrow D^{*0}\pi R$ . We take  $M_{\text{inv}}(R) = 980$  MeV.

In Figs. 11.5 and 11.6 we plot Eq. (11.34) for both  $B^- \rightarrow D^{*0}\pi^- \eta \pi^0$  and  $B^- \rightarrow D^{*0}\pi^- \pi^+ \pi^-$ , respectively, by fixing  $M_{\text{inv}}(\pi R) = 1418$  MeV, which is the position of the triangle singularity, and varying  $M_{\text{inv}}(R)$ . We can see a strong peak around 980 MeV and consequently we see that most of the contribution to our width  $\Gamma$  will come from  $M_{\text{inv}}(R) = M_R$ . For Fig. 11.5 the dispersion is bigger, we have strong contributions for  $M_{\text{inv}}(\pi^0 \eta) \in [880, 1080]$ . However, for Fig. 11.6 most of the contribution comes from  $M_{\text{inv}}(\pi^+ \pi^-) \in [940, 1020]$ . The conclusion is that when we calculate the mass distribution  $\frac{d\Gamma}{dM_{\text{inv}}(\pi a_0)}$ , we can restrict the integral in  $M_{\text{inv}}(R)$  to the limits already mentioned.

When we integrate over  $M_{\text{inv}}(R)$  we obtain  $\frac{d\Gamma}{dM_{\text{inv}}(\pi R)}$  which we show in Fig. 11.7. We see a clear peak of the distribution around 1420 MeV, for  $f_0$  and  $a_0$  production. However, we also see that the distribution stretches up to large values of  $M_{\text{inv}}(\pi R)$  where the phase space of the reaction finishes. This is due to the  $|\vec{k}|^3$  factor in Eq. (11.34) that contains a  $|\vec{k}|$  factor from phase space and a  $|\vec{k}|^2$  factor from the dynamics of the process, as we can see in Eq. (11.20). Yet, a clear peak in  $M_{\text{inv}}(\pi^- R)$

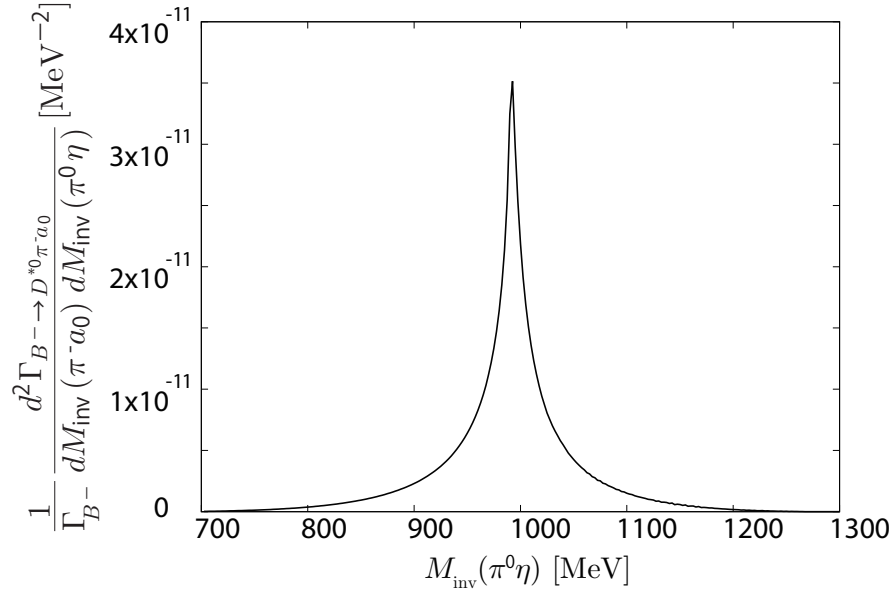


Figure 11.5: The derivative of the mass distribution of  $B^- \rightarrow D^{*0} \pi^- \pi^0 \eta$  with regards to  $M_{\text{inv}}(a_0)$ .

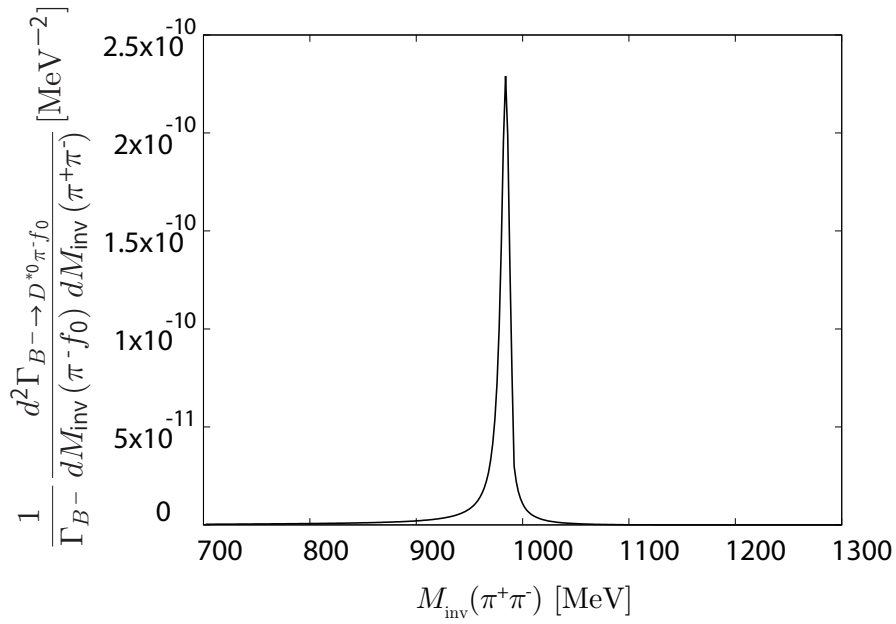


Figure 11.6: The derivative of the mass distribution of  $B^- \rightarrow D^{*0} \pi^- \pi^+ \pi^-$  with regards to  $M_{\text{inv}}(f_0)$ .

can be seen for both the  $B^- \rightarrow D^{*0} \pi^- f_0$  and  $B^- \rightarrow D^{*0} \pi^- a_0$  reactions.

Integrating now  $\frac{d\Gamma}{dM_{\text{inv}}(\pi a_0)}$  and  $\frac{d\Gamma}{dM_{\text{inv}}(\pi f_0)}$  over the  $M_{\text{inv}}(\pi a_0)$  ( $M_{\text{inv}}(\pi f_0)$ ) masses in



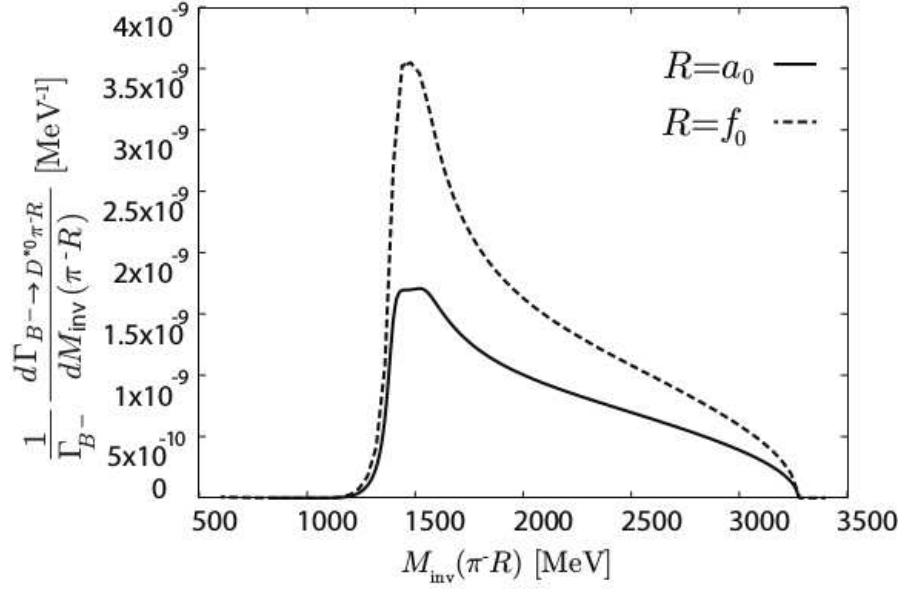


Figure 11.7: The mass distribution of  $B^- \rightarrow D^{*0} \pi^- \pi^0 \eta$  (full line) and  $B^- \rightarrow D^{*0} \pi^- \pi^+ \pi^-$  (dashed line).

Fig. 11.7, we obtain the branching fractions

$$\text{Br}(B^- \rightarrow D^{*0} \pi^- a_0; a_0 \rightarrow \pi^0 \eta) = (1.66 \pm 0.45) \times 10^{-6}, \quad (11.35a)$$

$$\text{Br}(B^- \rightarrow D^{*0} \pi^- f_0; f_0 \rightarrow \pi^+ \pi^-) = (2.82 \pm 0.75) \times 10^{-6}. \quad (11.35b)$$

These numbers are within measurable range. The errors come from the experimental errors in the branching ratio of  $B^- \rightarrow D^{*0} K^{*0} K^-$ . Another source of uncertainty would come from the  $t_{K^+ K^-, \pi^+ \pi^- (\pi^0 \eta)}$  matrices, but the errors in  $|t_{K^+ K^-, \pi^+ \pi^- (\pi^0 \eta)}|^2$  are smaller than 10% from the study of many reactions, which summed in quadrature to those of the experimental branching ratio, are essentially negligible.

Note that we have assumed all the strength of  $\pi^0 \eta$  from 880 MeV to 1080 MeV to be part of the  $a_0$  production, but in an experimental analysis one might associate part of this strength to a background. We note this in order to make proper comparison with these results when the experiment is performed.

The shape of  $t_T$  in Fig. 11.4 requires some extra comment. We see that  $\text{Im}(t_T)$  peaks around 1420 MeV, where the triangle singularity is expected. However  $\text{Re}(t_T)$  also has a peak around 1390 MeV. This picture is not standard. Indeed, in Ref. [446], where a triangle singularity is disclosed for the process  $N(1835) \rightarrow \pi N(1535)$ ,  $t_T$  has the real part peaking at the place of the triangle singularity and  $\text{Im}(t_T)$  has no peak. In Ref. [286], a triangle singularity develops in the  $\gamma p \rightarrow p \pi^0 \eta \rightarrow \pi^0 N(1535)$  process and there  $\text{Im}(t_T)$  has a peak at the expected energy of the triangle singularity while the  $\text{Re}(t_T)$  has no peak. Similarly, in the study of  $N(1700) \rightarrow \pi \Delta$  in Ref. [447] a trian-

gle singularity develops and here  $\text{Im}(t_T)$  has a peak but  $\text{Re}(t_T)$  has not. However, the two peaks in the real and imaginary parts of  $t_T$  are also present in the study of the  $B^- \rightarrow K^- \pi D_{s_0}^+$  reaction in Ref. [128]. This latter work has a loop with  $D^0 K^{*0} K^+$ , and by taking  $\Gamma_{K^*} \rightarrow 0$ ,  $\epsilon \rightarrow 0$  the peak of  $\text{Im}(t_T)$  was identified with the triangle singularity while the peak in the  $\text{Re}(t_T)$  was shown to come from the threshold of  $D^0 K^{*0}$ . In the present case the situation is similar: The peak of  $\text{Im}(t_T)$  at about 1420 MeV comes from the triangle singularity while the one just below 1400 MeV comes from the threshold of  $K^{*0} K^-$  in the diagram of Fig. 11.1, which appears at 1386 MeV. Yet, by looking at  $|t_T|$  in Fig. 11.4 and the region of the peak of  $\frac{d\Gamma}{dM_{\text{inv}}}$  in Fig. 11.7, we can see that this latter peak comes mostly from the triangle singularity.

## 11.4 Conclusions

We have performed the calculations for the reactions  $B^- \rightarrow D^{*0} \pi^- a_0(980); a_0 \rightarrow \pi^0 \eta$  and  $B^- \rightarrow D^{*0} \pi^- f_0(980); f_0 \rightarrow \pi^+ \pi^-$ . The starting point is the reaction  $B^- \rightarrow D^{*0} K^{*0} K^-$ , which is a Cabibbo favored process and for which the rates are tabulated in the PDG [110] and are relatively large. Then we allow the  $K^{*0}$  to decay into  $\pi^- K^+$  and the  $K^+ K^-$  fuse to give the  $f_0(980)$  or the  $a_0(980)$ . Both of them are allowed, since the  $K^{*0} K^-$  state does not have a particular isospin. The triangle diagram corresponding to this mechanism develops a singularity at about 1420 MeV in the invariant masses of  $\pi^- f_0$  or  $\pi^- a_0$ , and makes the strength of the process studied relatively large.

We evaluate  $\frac{d^2\Gamma}{dM_{\text{inv}}(\pi^- a_0) dM_{\text{inv}}(\pi^0 \eta)}$ , and  $\frac{d^2\Gamma}{dM_{\text{inv}}(\pi^- f_0) dM_{\text{inv}}(\pi^+ \pi^-)}$  and see clear peaks in the  $M_{\text{inv}}(\pi^0 \eta)$ ,  $M_{\text{inv}}(\pi^+ \pi^-)$  distributions, showing clearly the  $a_0(980)$  and  $f_0(980)$  shapes. Integrating over  $M_{\text{inv}}(\pi^0 \eta)$  and  $M_{\text{inv}}(\pi^+ \pi^-)$  we obtain  $\frac{d\Gamma}{dM_{\text{inv}}(\pi a_0)}$  and  $\frac{d\Gamma}{dM_{\text{inv}}(\pi f_0)}$  respectively, and these distributions show a clear peak for  $M_{\text{inv}}(\pi a_0)$ ,  $M_{\text{inv}}(\pi f_0)$  around 1420 MeV. This peak is a consequence of the triangle singularity, and in this sense the work done here should be a warning not to claim a new resonance when this peak is seen in a future experiment. On the other hand, the results make predictions for an interesting effect of a triangle singularity in an experiment that is feasible in present experimental facilities. The rates obtained are also within measurable range. Finding new cases of triangle singularities is of importance also, because their study will give incentives to update present analysis tools to take into account such possibility when peaks are observed experimentally, avoiding the natural tendency to associate those peaks to resonances.

# Chapter 12

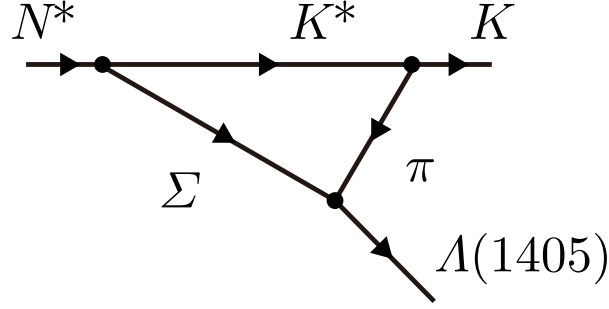
## Triangle Singularities in $\Lambda(1405)$ production in $\pi p$ and $pp$ reactions

### 12.1 Introduction

In Ref. [54], the role of the triangle singularity (TS) on the angle and the energy dependence of the  $\Lambda(1405)$  photo-production was studied. The strength of the triangle peak is tightly connected with the coupling strength of the two hadrons merging into a third one. For example, in the study of the  $B^-$  decay into  $K^- \pi^- D_{s0}^+ (D_{s1}^+)$  [128], the  $DK$  ( $D^*K$ ) in the triangle loop goes into  $D_{s0}$  ( $D_{s1}$ ), which is dynamically generated from the  $DK$  ( $D^*K$ ) and has a large coupling to this channel [448,449]. Then, the observation of the peak from the triangle mechanism would give an additional support for the hadronic molecular picture of these states.

For further understanding of the nature of the  $\Lambda(1405)$  and triangle mechanisms, in this chapter, based on Ref. [10], we investigate the  $\pi^- p \rightarrow K^0 \pi \Sigma$  and  $pp \rightarrow p K^+ \pi \Sigma$  processes including a triangle diagram. In both processes, the triangle diagram is formed by a  $N^*$  decay into  $K^* \Sigma$  followed by the decay of  $K^*$  into  $\pi K$  and the fusion of the  $\pi \Sigma$  to form the  $\Lambda(1405)$ , which finally decays into  $\pi \Sigma$ . In this process, the  $K^* \pi \Sigma$  loop generates a triangle singularity around 2140 MeV in the invariant mass of  $K \Lambda(1405)$  from the formula given by Eq. (3.134). The corresponding diagram is shown in Fig. 12.1. The  $N^*$  resonance which strongly couples to  $K^* \Sigma$  is obtained in Ref. [139] based on the hidden local symmetry and the chiral unitary approach, and the analysis of the  $K \Sigma$  photo-production off nucleon around the  $K^* \Lambda$  threshold energy suggests that the resonance is responsible for the observed cross section [450].

As the result of our calculation, we found a peak in the  $K \Lambda(1405)$  mass distribution around 2100 MeV in both reactions, which is lowered with respect to the 2140 MeV given by the TS master formula, Eq. (3.134), by the initial  $N^*$  resonance

Figure 12.1: Triangle diagram for the  $\Lambda(1405)$  production from a  $N^*$  resonance.

which peaks around 2030 MeV. The experimental study on the  $\Lambda(1405)$  production from the  $\pi^- p$  is reported in Refs. [325,451], but the energy is too small for the triangle singularity from the  $K^* \pi \Sigma$  loop to be observed. The production of the  $\Lambda(1405)$  from the proton-proton collision is studied in Refs. [452–454]. The future observation of the inevitable peak from the triangle mechanism induced by the  $\Lambda(1405)$  would give further support for the molecular nature of the  $\Lambda(1405)$ .

## 12.2 Formalism

### 12.2.1 $\pi^- p \rightarrow K^0 \pi \Sigma$

In this subsection we will study the effects of the triangle loop in the following decays:  $\pi^- p \rightarrow K^0 \pi^+ \Sigma^-$ ,  $\pi^- p \rightarrow K^0 \pi^0 \Sigma^0$  and  $\pi^- p \rightarrow K^0 \pi^- \Sigma^+$ . The diagrams where the triangle singularity can appear for those reactions are shown in Fig. 12.2. To evaluate the differential cross section associated with this diagram we will use

$$\frac{d\sigma_{K^0 \pi \Sigma}}{dm_{\text{inv}}} = \frac{M_p M_\Sigma}{2(2\pi)^3 s} \frac{|\vec{k}| |\vec{p}_\pi|}{|\vec{p}_\pi|} \sum \sum |t_{\pi^- p \rightarrow K^0 \pi \Sigma}|^2, \quad (12.1)$$

with  $m_{\text{inv}}$  the invariant mass of the final  $\pi \Sigma$ ,

$$|\vec{p}_\pi| = \frac{\lambda^{\frac{1}{2}}(s, m_\pi^2, M_N^2)}{2\sqrt{s}}, \quad (12.2)$$

the momentum of the initial  $\pi^-$  in the  $\pi^- p$  center-of-mass frame (CM),

$$|\vec{k}| = \frac{\lambda^{\frac{1}{2}}(s, m_K^2, m_{\text{inv}}^2)}{2\sqrt{s}}, \quad (12.3)$$

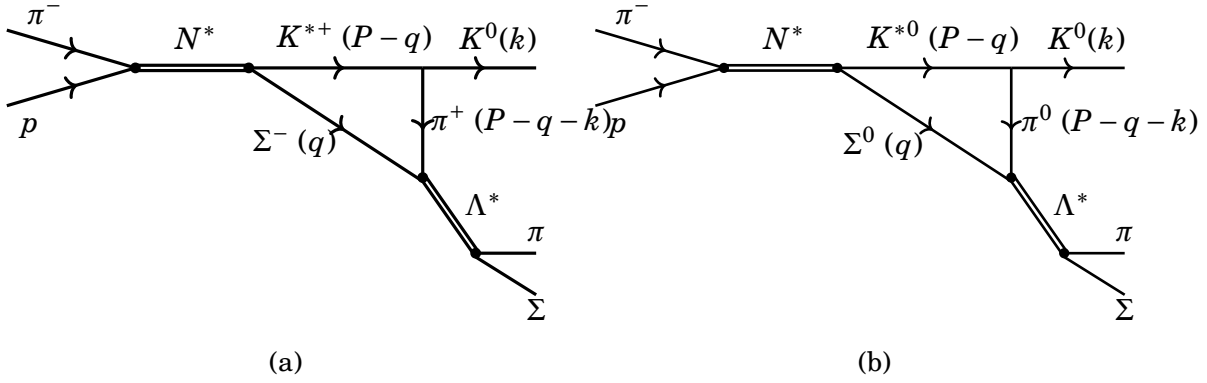


Figure 12.2: Diagrams for the reaction  $\pi^- p \rightarrow K^0 \pi \Sigma$  that contain the triangle mechanism, where  $\pi \Sigma$  can be  $\pi^- \Sigma^+$ ,  $\pi^0 \Sigma^0$  and  $\pi^+ \Sigma^-$ .

the momentum of the final  $K^0$  in the  $\pi^- p$  CM, and

$$|\vec{p}_\pi| = \frac{\lambda^{\frac{1}{2}}(m_{\text{inv}}^2, m_\pi^2, M_\Sigma^2)}{2m_{\text{inv}}}, \quad (12.4)$$

the momentum of the final  $\pi$  in the  $\pi \Sigma$  CM.

The resonance  $N^*(2030)$  studied in Ref. [139] from the vector-baryon interaction, mediated by the exchange of vector mesons, appears there as spin degenerate in  $J^P = 1/2^-$  and  $3/2^-$ . The degeneracy can be broken by mixing with states of pseudoscalar-baryon and connecting these by pion exchange as done in Ref. [297]. There should be then two states near degenerate at the end. We conduct our study with the  $J^P = 1/2^-$  state.

The case of spin  $3/2^-$  is discussed at the end of this subsection. For the moment it is sufficient to mention that the structure and conclusions for that term are the same as for the  $1/2^-$  state.

In the isospin basis the  $\pi^- p \rightarrow N^*$  vertex has then the form

$$-it_{\pi N, N^*} = -ig_{\pi N, N^*}^{I=\frac{1}{2}}. \quad (12.5)$$

To estimate the  $g_{\pi N, N^*}^{I=\frac{1}{2}}$  we assume that  $\Gamma_{N^*, \pi N}$  is of the order of 70 MeV and then use the formula,

$$\Gamma_{N^*, \pi N} = \frac{1}{2\pi} \frac{M_\Sigma}{M_{N^*}} (g_{\pi N, N^*}^{I=\frac{1}{2}})^2 |\vec{p}_\pi| \quad (12.6)$$

with  $M_{N^*}$  the mass of  $N^*(2030)$ . Here,  $|\vec{p}_\pi|$  is the momentum of  $\pi$  that results from the decay of  $N^*$  and is evaluated using Eq. (12.2),  $s = M_{N^*}^2$ . Finally, we obtain  $g_{\pi N, N^*}^{I=\frac{1}{2}} \simeq 1.1$ .

The value of  $\Gamma_{N^*,\pi N} = 70$  MeV is just an estimate. We should warn here that we are not so much interested in the strength of the cross section, which we cannot evaluate accurately in this formalism. One reason is precisely that  $\Gamma_{N^*,\pi N}$  is not known. Yet, the important thing is the shape of the invariant mass distribution, and as we shall see later on, we also prove that the triangle mechanism is more important than tree-level mechanisms. The estimate of 70 MeV is based on values that we get from the old version of the PDG [455], for two states  $N^*(2080)(3/2^-)$  and  $N^*(2090)(1/2^-)$  and the original papers of Refs. [456,457] and Ref. [458], playing with very large errors in both experiments.

Since we will have different amplitudes if we change the charge of the intermediate  $\pi\Sigma$  particles, it is convenient to go from the isospin basis ( $I, I_3$ ) to the charge basis. Although a formalism using the different  $\pi\Sigma$  isospin channels is possible, we find it convenient to work in the charge basis. Using the Clebsch-Gordan coefficients, we have

$$|\pi^- p\rangle = \sqrt{\frac{1}{3}} \left| \frac{3}{2}, -\frac{1}{2} \right\rangle - \sqrt{\frac{2}{3}} \left| \frac{1}{2}, -\frac{1}{2} \right\rangle. \quad (12.7)$$

This means that the coupling of  $\pi^- p$  to  $N^*$  will be

$$g_{\pi^- p, N^*} = -\sqrt{\frac{2}{3}} g_{\pi N, N^*}^{I=\frac{1}{2}} \quad (12.8)$$

For the  $N^*(2030) \rightarrow K^* \Sigma$  process in  $s$ -wave, as shown in the appendix for spin  $J = 1/2$ , we have

$$-it_{N^*, K^* \Sigma} = -i \frac{1}{\sqrt{3}} g_{N^*, \Sigma K^*} \vec{\sigma} \cdot \vec{\epsilon}_{K^*}. \quad (12.9)$$

From Ref. [139], we get  $g_{N^*, K^* \Sigma}^{I=\frac{1}{2}} = 3.9 + i0.2$ , and since we have both  $\Sigma^- K^{*+}$  and  $\Sigma^0 K^{*0}$  (Figs. 12.2a and 12.2b respectively), then, using

$$|\Sigma^0 K^{*0}\rangle = \sqrt{\frac{2}{3}} \left| \frac{3}{2}, -\frac{1}{2} \right\rangle + \sqrt{\frac{1}{3}} \left| \frac{1}{2}, -\frac{1}{2} \right\rangle, \quad (12.10a)$$

$$|\Sigma^- K^{*+}\rangle = \sqrt{\frac{1}{3}} \left| \frac{3}{2}, -\frac{1}{2} \right\rangle - \sqrt{\frac{2}{3}} \left| \frac{1}{2}, -\frac{1}{2} \right\rangle, \quad (12.10b)$$

we get

$$g_{N^*, \Sigma^0 K^{*0}} = \sqrt{\frac{1}{3}} g_{N^*, \Sigma K^*}^{I=\frac{1}{2}} \quad (12.11a)$$

$$g_{N^*, \Sigma^- K^{*+}} = -\sqrt{\frac{2}{3}} g_{N^*, \Sigma K^*}^{I=\frac{1}{2}} \quad (12.11b)$$

Then, for the amplitude of the  $\pi^- p \rightarrow \Sigma K^*$  reaction through  $N^*$  (2030), we have

$$t_{\pi^- p, \Sigma^0 K^{*0}} = \frac{1}{\sqrt{3}} \frac{g_{\pi^- p, N^*} g_{N^*, \Sigma^0 K^{*0}}}{\sqrt{s} - M_{N^*} + i \frac{\Gamma_{N^*}}{2}} \vec{\sigma} \cdot \vec{\epsilon}_{K^*}, \quad (12.12a)$$

$$t_{\pi^- p, \Sigma^- K^{*+}} = \frac{1}{\sqrt{3}} \frac{g_{\pi^- p, N^*} g_{N^*, \Sigma^- K^{*+}}}{\sqrt{s} - M_{N^*} + i \frac{\Gamma_{N^*}}{2}} \vec{\sigma} \cdot \vec{\epsilon}_{K^*}. \quad (12.12b)$$

The  $K^{*+} \rightarrow K^0 \pi^+$  vertex can be calculated using the local hidden gauge lagrangians,

$$-it_{K^{*+}, K^0 \pi^+} = -ig \epsilon_{K^*}^\mu (p_{K^0} - p_{\pi^+})_\mu \quad (12.13)$$

$$= ig \epsilon_{K^*}^\mu (P - q - 2k)_\mu \quad (12.14)$$

$$\simeq ig \vec{\epsilon}_{K^*} \cdot (\vec{q} + 2\vec{k}), \quad (12.15)$$

where in the last step we made a non-relativistic approximation, neglecting the  $\epsilon_{K^*}^0$  component. This is very accurate when the momentum of the  $K^*$  is small compared to its mass. We shall evaluate the triangle diagram in the  $\Sigma K^*$  CM, where the on-shell momentum of the  $K^*$  is about 250 MeV/c at  $M_{\text{inv}}(\Sigma K^*) \simeq 2140$  MeV where the triangle singularity appears. In Ref. [128] it is shown that the effect of neglecting the  $\epsilon^0$  component goes as  $(p_{K^*}/m_{K^*})^2$ , with a coefficient in front that renders this correction negligible.

Similarly, for  $K^{*0} \rightarrow K^0 \pi^0$  we get

$$-it_{K^{*0}, K^0 \pi^0} = -i \frac{1}{\sqrt{2}} g \vec{\epsilon}_{K^*} \cdot (\vec{q} + 2\vec{k}). \quad (12.16)$$

The last amplitude,  $t_{\Sigma\pi, \Sigma\pi}$ , can be calculated using the BSE with the kernel of Eq. (3.42). For the evaluation of the  $t$  matrix, we use the momentum cutoff  $q_{\text{max}} = 630$  MeV for the loop function  $G$ , and  $f = 1.15f_\pi$  with the pion decay constant  $f_\pi = 93$  MeV as done in Ref. [31].

Thus, the amplitude associated with the diagram in Fig. 12.2a, that we call  $t_1$ , is given by

$$t_1 = -i \frac{2}{3\sqrt{3}} \frac{g_{\pi N, N^*}^{I=\frac{1}{2}} g_{N^*, \Sigma K^*}^{I=\frac{1}{2}}}{\sqrt{s} - M_{N^*} + i \frac{\Gamma_{N^*}}{2}} g \sum_{\text{pol. of } K^*} \int \frac{d^4 q}{(2\pi)^4} \frac{2M_\Sigma \vec{\sigma} \cdot \vec{\epsilon}_{K^*}}{q^2 - M_\Sigma^2 + i\epsilon} \frac{(2\vec{k} + \vec{q}) \cdot \vec{\epsilon}_{K^*}}{(P - q)^2 - m_{K^*}^2 + i\epsilon} \times \frac{t_{\Sigma^- \pi^+, \Sigma\pi}}{(P - q - k)^2 - m_\pi^2 + i\epsilon}. \quad (12.17)$$

Again, using Eq. (11.17), in the non-relativistic approximation,

$$\sum_{\text{pol.}} \epsilon_{K^* i} \epsilon_{K^* j} = \delta_{ij},$$

Eq. (12.17) becomes

$$t_1 = -\frac{4M_\Sigma}{3\sqrt{3}} \frac{g_{\pi N, N^*}^{I=\frac{1}{2}} g_{N^*, \Sigma K^*}^{I=\frac{1}{2}}}{\sqrt{s} - M_{N^*} + i\frac{\Gamma_{N^*}}{2}} g \vec{\sigma} \cdot \vec{k} t_T t_{\Sigma^- \pi^+, \Sigma \pi}, \quad (12.18)$$

with  $t_T$  given by Eq. (11.19) (with the appropriate substitutions for the different particles). Again we integrate  $t_T$  over  $q^0$ , to get Eq. (11.21), where now  $P^0 = \sqrt{s}$ ,  $\omega^*(\vec{q}) = \sqrt{m_{K^*}^2 + |\vec{q}|^2}$ ,  $\omega'(\vec{q}) = \sqrt{m_\pi^2 + |\vec{q} + \vec{k}|^2}$  and  $\omega(\vec{q}) = \sqrt{M_\Sigma^2 + |\vec{q}|^2}$ . We regularize the integral in Eq. (11.21) by using the same cutoff used to calculate the amplitude  $t_{\Sigma \pi, \Sigma \pi}$ .

For the case when  $N^*(2030) \rightarrow K^{*+} \Sigma^-$ ,  $t_2$ , we have

$$t_2 = -\frac{2M_\Sigma}{3\sqrt{3}} \frac{g_{\pi N, N^*}^{I=\frac{1}{2}} g_{N^*, \Sigma K^*}^{I=\frac{1}{2}}}{\sqrt{s} - M_{N^*} + i\frac{\Gamma_{N^*}}{2}} g \vec{\sigma} \cdot \vec{k} t_T t_{\Sigma^0 \pi^0, \Sigma \pi}. \quad (12.19)$$

Thus, the total amplitude in Eq. (12.1) associated with  $\pi^- p \rightarrow K^0 \pi \Sigma$  becomes

$$t_{\pi^- p \rightarrow K^0 \pi \Sigma} = t_1 + t_2 = C \vec{\sigma} \cdot \vec{k} t_T (t_{\Sigma^- \pi^+, \Sigma \pi} + \frac{1}{2} t_{\Sigma^0 \pi^0, \Sigma \pi}), \quad (12.20)$$

with

$$C = -\frac{2}{3\sqrt{3}} g_{\pi N, N^*}^{I=\frac{1}{2}} g_{N^*, \Sigma K^*}^{I=\frac{1}{2}} g \frac{2M_\Sigma}{\sqrt{s} - M_{N^*} + i\frac{\Gamma_{N^*}}{2}}. \quad (12.21)$$

Here, the  $t_T$  associated with the diagrams in Figs. 12.2a and 12.2b are the same because we use the isospin averaged mass and width of the hadrons in  $t_T$ .

Calculating the square of the amplitude and summing and averaging over the spins we get

$$\overline{\sum} \sum |t_{\pi^- p \rightarrow K^0 \pi \Sigma}|^2 = |C|^2 |\vec{k}|^2 |t_T|^2 |t_{\Sigma^- \pi^+, \Sigma \pi} + \frac{1}{2} t_{\Sigma^0 \pi^0, \Sigma \pi}|^2 \quad (12.22)$$

Finally, using Eq. (12.22) in Eq. (12.1) we can calculate the  $\frac{d\sigma_{K^0 \pi \Sigma}}{dm_{\text{inv}}}$  associated with the diagrams in Fig. 12.2.

In order to incorporate the contribution of spin 3/2, we follow the appendix Eq. (B.11) and (B.14) and we see that instead of

$$\sum_{K^* \text{ pol.}} \frac{1}{3} \vec{\sigma} \cdot \vec{\epsilon}_{K^*} \vec{\epsilon}_{K^*} \cdot \vec{k} \quad (12.23)$$

we get

$$\sum_{K^* \text{ pol.}} \sigma_3 \epsilon_{K^* 3} \vec{\epsilon}_{K^*} \cdot \vec{k}. \quad (12.24)$$



Hence, after summing over the  $K^*$  polarizations

$$\frac{1}{3}\vec{\sigma}\cdot\vec{k}\rightarrow\sigma_3k_3 \quad (12.25)$$

and upon squaring it for  $|t|^2$  and summing and averaging over the baryon spins we get

$$\frac{1}{9}|\vec{k}|^2\rightarrow k_3^2\rightarrow\frac{1}{3}|\vec{k}|^2 \quad (12.26)$$

where the last step considers the angle integration over  $\vec{k}$  in  $d\sigma/M_{\text{inv}}$ .

The conclusion is that the sum of the spin 1/2 and 3/2 is three times bigger than the contribution of  $J = 1/2$  alone, or equivalently, the  $J = 3/2$  contributes twice the amount of  $J = 1/2$ . This is logical since in the diagram of Fig. B.2, one is summing over two third components of the  $R$  for  $J = 1/2$  and over four for  $J = 3/2$ . For practical reasons we can evaluate the whole contribution using the  $J = 1/2$  formalism removing the factor  $1/\sqrt{3}$  in Eq. (12.9) and this is what we shall do in what follows.

### 12.2.2 $pp \rightarrow pK^+\pi\Sigma$

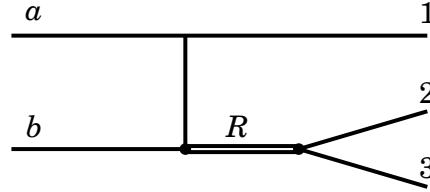


Figure 12.3: Diagram of  $a b \rightarrow 1 R \rightarrow 1 2 3$ .

Now we will study the effects of the triangle loop in the following decays:  $pp \rightarrow pK^+\pi^+\Sigma^-$ ,  $pp \rightarrow pK^+\pi^0\Sigma^0$  and  $pp \rightarrow pK^+\pi^-\Sigma^+$ . For this, we will first start analyzing the diagram in Fig. 12.3. For this diagram, the differential cross section is calculated using the formula in Ref. [111],

$$\frac{d^2\sigma}{dt dM_{\text{inv}}} = \frac{\Pi_F(2M_F)}{32p_a^2s(2\pi)^3} |\vec{p}_2| \overline{\sum} \sum |t_{ab \rightarrow 123}|^2, \quad (12.27)$$

with  $t = (p_a - p_1)^2$ ,  $M_{\text{inv}}$  the invariant mass of particles 2 and 3,  $\vec{p}_2$  the momentum of particle 2 in the 23 CM, such that

$$|\vec{p}_2| = \frac{\lambda^{\frac{1}{2}}(M_{\text{inv}}^2, m_2^2, m_3^2)}{2M_{\text{inv}}}, \quad (12.28)$$

$p_a$  the momentum of the particle  $a$  in the initial state,

$$p_a = \frac{\lambda^{\frac{1}{2}}(s, M_a^2, M_b^2)}{2\sqrt{s}}, \quad (12.29)$$

and  $\Pi_F (2M_F)$  means that we multiply  $2M_F$  for each fermion in Fig. 12.3, where  $M_F$  is the mass of the respective fermion. This factor appears because we use the normalization of Ref. [216].

The complete diagrams for our reaction are shown in Fig. 12.4. The triangle part of the diagrams is very similar to the last case, except that because of charge conservation the particles in the loop will be different. Thus, instead of Eqs. (12.10a) and (12.10b), we will have

$$|\Sigma^+ K^{*0}\rangle = -\sqrt{\frac{1}{3}} \left| \frac{3}{2}, \frac{1}{2} \right\rangle - \sqrt{\frac{2}{3}} \left| \frac{1}{2}, \frac{1}{2} \right\rangle, \quad (12.30a)$$

$$|\Sigma^0 K^{*+}\rangle = \sqrt{\frac{2}{3}} \left| \frac{3}{2}, \frac{1}{2} \right\rangle - \sqrt{\frac{1}{3}} \left| \frac{1}{2}, \frac{1}{2} \right\rangle, \quad (12.30b)$$

where, to match the sign convention of the  $\Phi$  and  $B$  matrices, we used  $|\Sigma^+\rangle = -|1\ 1\rangle$ .

Then, we get  $g_{N^*, \Sigma^+ K^{*0}} = -\sqrt{2/3} g_{N^*, \Sigma K^*}^{I=\frac{1}{2}}$  and  $g_{N^*, \Sigma^0 K^{*+}} = -\sqrt{1/3} g_{N^*, \Sigma K^*}^{I=\frac{1}{2}}$ .

The vertices  $K^{*0} \rightarrow K^+ \pi^-$  and  $K^{*+} \rightarrow K^+ \pi^0$  are calculated using Eq. (2.33), which gives

$$-it_{K^{*0}, K^+ \pi^-} = ig(\vec{q} + 2\vec{k}) \cdot \vec{e}_{K^*}, \quad (12.31a)$$

$$-it_{K^{*+}, K^+ \pi^0} = i \frac{g}{\sqrt{2}} (\vec{q} + 2\vec{k}) \cdot \vec{e}_{K^*} \quad (12.31b)$$

To calculate the cross section for the diagrams in Fig. 12.4, we proceed as done in Ref. [111]. In Fig. 12.3, the  $t$  matrix found in Eq. (12.27) is given by

$$t_{ab \rightarrow 123} = C' \frac{1}{M_{\text{inv}} - M_R + i \frac{\Gamma_R}{2}} g_{R,23}, \quad (12.32)$$

with  $C'$  a parameter that carries the dependence of the amplitude on the variable  $t$  as well as information about the  $pp \rightarrow pR$  transition. Substituting

$$\Gamma_{R,23} = \frac{1}{2\pi} \frac{M_3}{M_{\text{inv}}} g_{R,23}^2 |\vec{p}_2|, \quad (12.33)$$

where particle 3 is assumed to be a baryon, into Eq. (12.27), we get

$$\frac{d^2\sigma}{dt dM_{\text{inv}}} = \frac{\Pi_F(2M_F)}{32p_a^2 s (2\pi)^3} |C'|^2 \left| \frac{1}{M_{\text{inv}} - M_R + i \frac{\Gamma_R}{2}} \right|^2 2\pi \frac{M_{\text{inv}}}{M_3} \Gamma_{R,23}. \quad (12.34)$$

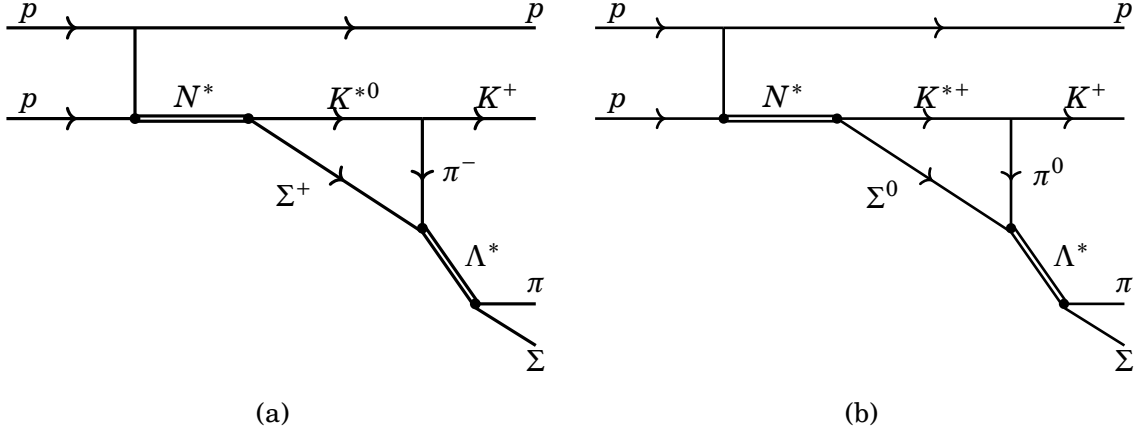


Figure 12.4: Diagrams for the reaction  $pp \rightarrow pK^+\pi\Sigma$  that contain the triangle mechanism, where  $\pi\Sigma$  can be  $\pi^-\Sigma^+$ ,  $\pi^0\Sigma^0$  and  $\pi^+\Sigma^-$ .

Now we can take into account the complete reaction by substituting  $\Gamma_{R,23}$  for  $\Gamma_{N^* \rightarrow K^+\pi\Sigma}$ , where

$$\frac{d\Gamma_{N^* \rightarrow K^+\pi\Sigma}}{dm_{\text{inv}}} = \frac{2M_{N^*}2M_{\Sigma}}{(2\pi)^3 4M_{\text{inv}}^2} |\vec{p}_K| |\vec{p}_\pi| \overline{\sum} \sum |t'|^2, \quad (12.35)$$

with  $|\vec{p}_K|$  the momentum of  $K$  in the rest frame of  $N^*$ ,

$$|\vec{p}_K| = \frac{\lambda^{\frac{1}{2}}(M_{\text{inv}}^2, m_K^2, m_{\text{inv}}^2)}{2M_{\text{inv}}}, \quad (12.36)$$

and  $|\vec{p}_\pi|$  the  $\pi$  momentum in the  $\pi\Sigma$  CM given by Eq. (12.4).

Then, from Eq. (12.34) we obtain

$$\frac{d^3\sigma_{pK^+\pi\Sigma}}{dt dM_{\text{inv}} dm_{\text{inv}}} = \frac{(2M_p)^3 2M_{\Sigma}}{32p_a^2 s (2\pi)^5} |\vec{p}_K| |\vec{p}_\pi| |C'|^2 \left| \frac{1}{M_{\text{inv}} - M_{N^*} + i\frac{\Gamma_{N^*}}{2}} \right|^2 \overline{\sum} \sum |t'|^2. \quad (12.37)$$

The transition amplitude  $t'$  in Eq. (12.37) is

$$t' = \sqrt{\frac{2}{3}} 2M_{\Sigma} g_{N^*, \Sigma K^*}^{I=\frac{1}{2}} g(t_{\Sigma^+\pi^-, \Sigma\pi} + \frac{1}{2} t_{\Sigma^0\pi^0, \Sigma\pi}) \vec{\sigma} \cdot \vec{k} t_T, \quad (12.38)$$

which is constructed in a similar way to what was done in the previous subsection to

obtain Eq. (12.20) but now changing the following variables in Eq. (11.21),

$$P^0 = M_{\text{inv}} \quad (12.39a)$$

$$|\vec{k}| = |\vec{p}_K| = \frac{\lambda^{\frac{1}{2}}(M_{\text{inv}}^2, m_K^2, m_{\text{inv}}^2)}{2M_{\text{inv}}} \quad (12.39b)$$

$$k^0 = \frac{M_{\text{inv}}^2 + m_K^2 - m_{\text{inv}}^2}{2M_{\text{inv}}} \quad (12.39c)$$

Putting Eq. (12.38) into Eq. (12.37) we get

$$\frac{d^3\sigma_{pK^+\pi\Sigma}}{dt dM_{\text{inv}} dm_{\text{inv}}} = C'' \frac{1}{|M_{\text{inv}} - M_{N^*} + i\frac{\Gamma_{N^*}}{2}|^2} |\vec{p}_\pi| |t_{\Sigma^+\pi^-, \Sigma\pi} + \frac{1}{2} t_{\Sigma^0\pi^0, \Sigma\pi}|^2 |\vec{k}|^3 |t_T|^2, \quad (12.40)$$

where  $|\vec{p}_\pi|$  is the  $\pi$  momentum in the  $\pi\Sigma$  CM,

$$|\vec{p}_\pi| = \frac{\lambda^{\frac{1}{2}}(m_{\text{inv}}^2, m_\pi^2, M_\Sigma^2)}{2m_{\text{inv}}}, \quad (12.41)$$

and

$$C'' = \frac{2(2M_p)^3 2M_\Sigma}{3 32p_a^2 s (2\pi)^5} |g_{N^*, \Sigma K^*}^{I=\frac{1}{2}}|^2 g^2 (2M_\Sigma)^2 |C'|^2, \quad (12.42)$$

which is a function of  $s = (p_a + p_b)^2$  and  $t = (p_a - p_1)^2$ .

Using now the relation

$$dt = 2|\vec{p}_a||\vec{p}_1| d\cos\theta, \quad (12.43)$$

which follows from  $t = (p_a - p_1)^2$ , then we obtain

$$\frac{d^3\sigma_{pK^+\pi\Sigma}}{d\cos\theta dM_{\text{inv}} dm_{\text{inv}}} = C'' \frac{2|\vec{p}_a||\vec{p}_1|}{|M_{\text{inv}} - M_{N^*} + i\frac{\Gamma_{N^*}}{2}|^2} |\vec{p}_\pi| |t_{\Sigma^+\pi^-, \Sigma\pi} + \frac{1}{2} t_{\Sigma^0\pi^0, \Sigma\pi}|^2 |\vec{k}|^3 |t_T|^2, \quad (12.44)$$

with

$$|\vec{p}_a| = \frac{\lambda^{\frac{1}{2}}(s, M_p^2, M_p^2)}{2\sqrt{s}}, \quad (12.45a)$$

$$|\vec{p}_1| = \frac{\lambda^{\frac{1}{2}}(s, M_p^2, M_{\text{inv}}^2)}{2\sqrt{s}}. \quad (12.45b)$$

This last step is important to account for the phase space of this process that depends on  $|\vec{p}_1|$ , which is tied to  $M_{\text{inv}}$ .

Finally, we should integrate out the  $\cos\theta$  in Eq. (12.44) but  $C'$  in  $C''$  depend on it. The resultant factor of the  $\cos\theta$  integration is denoted by  $C'''$  and since we do not know the expression for  $C'$ , we take  $C''' = 1$ . This means that from now on we will use arbitrary units (a.u.) for the cross section.

Thus, we end up with

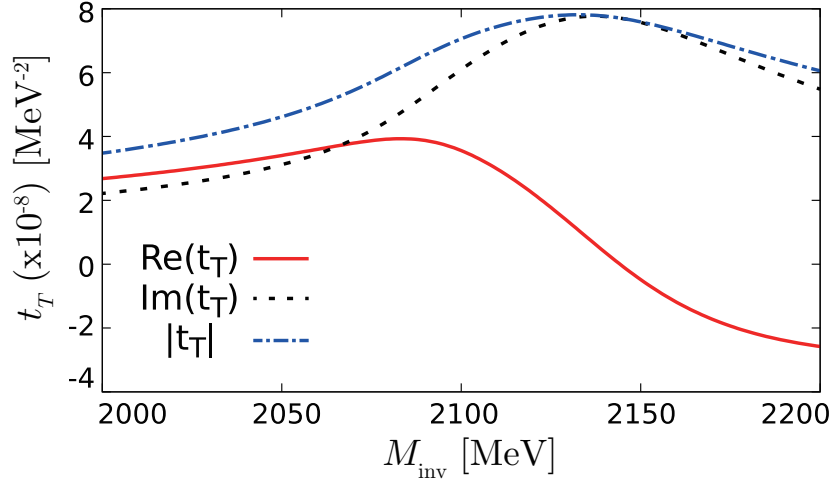
$$\frac{d^2\sigma_{pK^+\pi\Sigma}}{dM_{\text{inv}}dm_{\text{inv}}} = \frac{C'''2|\vec{p}_a||\vec{p}_1|}{|M_{\text{inv}} - M_{N^*} + i\frac{\Gamma_{N^*}}{2}|^2} |\vec{p}_\pi||t_{\Sigma^+\pi^-, \Sigma\pi} + \frac{1}{2}t_{\Sigma^0\pi^0, \Sigma\pi}|^2 |\vec{k}|^3 |t_T|^2. \quad (12.46)$$

## 12.3 Results

In Fig. 12.5, we show the real, imaginary part and absolute value of the amplitude  $t_T$  of Eq. (11.21) as a function of the invariant mass of the  $K\Lambda(1405)$ ,  $M_{\text{inv}}$ , by fixing the invariant mass of  $\pi\Sigma$ ,  $m_{\text{inv}}$ , at 1400 MeV. The absolute value of  $t_T$  has a peak around 2140 MeV as expected from Eq. (3.134), and the peak is dominated by the imaginary part of the amplitude. As mentioned in Ref. [128], the peak of the imaginary part is responsible for the triangle singularity.

In Fig. 12.6, we plot the mass distribution of the  $\pi^-p \rightarrow K^0\pi\Sigma$  scattering process as a function of  $m_{\text{inv}}(\pi^0\Sigma^0)$ ,  $m_{\text{inv}}(\pi^+\Sigma^-)$  and  $m_{\text{inv}}(\pi^-\Sigma^+)$  with a fixed of  $\sqrt{s} = M_{\text{inv}} = 2050, 2100, 2140, 2200, 2230$  MeV. Let us first look at the  $\pi^0\Sigma^0$  mass distribution in Fig. 12.6. At  $M_{\text{inv}} = 2140$  MeV, where a peak associated with the triangle singularity is expected from Eq. (3.134), we can see a clear peak at 1400 MeV associated with  $\Lambda(1405)$  in the  $\pi\Sigma$  invariant mass. As we see in the figure the largest strength is obtained with  $M_{\text{inv}} = 2100$  MeV. A peak is found around 1385 MeV for  $M_{\text{inv}} = 2200, 2230$  MeV with a smaller strength, and the peak position moves towards higher energy a little for  $M_{\text{inv}} = 2050$  MeV. In the case of the  $\pi^+\Sigma^-$  and  $\pi^-\Sigma^+$  final state, while the basic features are shared with the  $\pi^0\Sigma^0$ , the peak positions of the  $\pi^+\Sigma^-$  mass distribution are about 5 MeV less than that of the  $\pi^0\Sigma^0$  mass distribution, and the peak positions in the  $\pi^-\Sigma^+$  mass distribution are about 5 MeV bigger than the values of the  $\pi^0\Sigma^0$  mass distribution with a similar width and strength. Among these processes, the  $\pi^+\Sigma^-$  gives the largest strength. This is roughly because the  $t_{\Sigma^-\pi^+, \Sigma\pi}$  term is twice larger than  $t_{\Sigma^0\pi^0, \Sigma\pi}$  in Eq. (12.22).

As stated before Eq. (12.7), we separate the  $\pi^0\Sigma^0$ ,  $\pi^+\Sigma^-$ , and  $\pi^-\Sigma^+$  channels, although an isospin formalism could be equally implemented. Indeed the  $N^*$  has  $I = 1/2$  and hence the final  $K\pi\Sigma$  state also has  $I = 1/2$ , but the  $\pi\Sigma$  subsystem can be either  $I = 0$  or  $I = 1$ , and the amplitudes  $\pi\Sigma \rightarrow \pi\Sigma$  have a contribution of both  $I = 0$  and  $I = 1$  and even a small one of  $I = 2$ , and these contributions appear with different signs in the charge channels hence leading to different mass distributions. These differences between cross sections of the  $\pi\Sigma$  channels were predicted in the theoretical study

Figure 12.5:  $\text{Re}(t_T)$ ,  $\text{Im}(t_T)$  and  $|t_T|$  of Eq. (11.21).

of the  $\gamma p \rightarrow K^+ \pi \Sigma$  reaction in Ref. [49] and corroborated by experiments done in Refs. [459, 460].

In Fig. 12.7, we show the results of  $\frac{d^2\sigma_{pK^+\pi\Sigma}}{dM_{\text{inv}}dm_{\text{inv}}}$  for the  $pp \rightarrow pK^+\pi\Sigma$  scattering as a functions of  $m_{\text{inv}}(\pi^0\Sigma^0)$ ,  $m_{\text{inv}}(\pi^+\Sigma^-)$  and  $m_{\text{inv}}(\pi^-\Sigma^+)$ , respectively. The total energy of the system  $\sqrt{s}$  is fixed at 3179 MeV which can be accessed experimentally [452–454]. The dependence on  $m_{\text{inv}}$  is similar to that in  $d\sigma_{K^0\pi\Sigma}/dm_{\text{inv}}$ . In the case of the  $\pi^0\Sigma^0$  the peak is located at 1400 MeV by fixing  $M_{\text{inv}} = 2140$  MeV. For  $M_{\text{inv}} = 2200$  and 2230 MeV, the peak positions move towards 1380 MeV and also the widths are broader than that of the 1400 MeV case. Decreasing the value of  $M_{\text{inv}}$  to 2100 MeV, we obtain the peak position around 1405 MeV. The shapes of the results are similar for the  $\pi^+\Sigma^-$  and  $\pi^-\Sigma^+$  mass distributions, but the peak positions are 10 MeV bigger for the case of  $\pi^+\Sigma^-$  and 5 MeV smaller for  $\pi^-\Sigma^+$  mass distribution. In these processes, the  $\pi^-\Sigma^+$  gives the largest strength because of the additional factor two for the  $t_{\Sigma^+\pi^-\Sigma\pi}$  term in Eq. (12.44) compared with  $t_{\Sigma^0\pi^0\Sigma\pi}$ . We should note that the peak with this mechanism appears at lower  $\pi\Sigma$  invariant mass than with the model of Ref. [61], where the peak showed at 1420 MeV. This is due to the fact that with the TS the  $\Lambda(1405)$  is formed by  $\pi\Sigma$ , rather than  $\bar{K}N$ , and this channel couples mostly to the lower mass state of the two  $\Lambda(1405)$  states [35].

For the case of the  $\pi^- p \rightarrow K^0 \pi \Sigma$  reaction, we integrate  $\frac{d\sigma_{K^0\pi\Sigma}}{dm_{\text{inv}}}$  over  $m_{\text{inv}}$  in the range of the  $\Lambda(1405)$  peak,  $m_{\text{inv}} \in (m_\pi + m_\Sigma, 1450 \text{ MeV})$ , with  $m_\pi$  and  $m_\Sigma$  the isospin-averaged mass of  $\pi$  and  $\Sigma$ , and we obtain the cross section of  $\pi^- p \rightarrow K^0 \pi \Sigma$ ,  $\sigma_{K^0\pi\Sigma}$ , as a function of  $M_{\text{inv}}$ . The results are represented in Fig. 12.8. There are peaks around

2100 MeV for all cases, though the expected value of triangular singularity is 2140 MeV. This is because the  $N^*$  resonance in the  $K^*\Sigma$  production has a peak around 2030 MeV (the term  $1/|M_{\text{inv}} - M_{N^*} + i\frac{\Gamma_{N^*}}{2}|^2$  in Eq. (12.44)).

For the case of the  $pp \rightarrow pK^+\pi\Sigma$  reaction, integrating now the  $\frac{d^2\sigma_{pK^+\pi\Sigma}}{dM_{\text{inv}}dm_{\text{inv}}}$  over the  $m_{\text{inv}}$  we obtain  $\frac{d\sigma_{pK^+\pi\Sigma}}{dM_{\text{inv}}}$  which are shown in Fig. 12.9 as a function of  $M_{\text{inv}}$  for  $\pi^0\Sigma^0$ ,  $\pi^+\Sigma^-$  and  $\pi^-\Sigma^+$ . Similarly we get peaks around 2100 MeV for the three cases.

In the  $\pi^-p$  and  $pp$  reactions, the strength is largest for the  $\pi^+\Sigma^-$  and  $\pi^-\Sigma^+$  final state, respectively, reflecting the strength before the integration shown in Figs. 12.6 and 12.7.

We should note that the  $N^*(2030)$  is about 50 MeV below the  $K^*\Sigma$  threshold, but the width of about 125 MeV makes the overlap of the resonance in the region of  $K^*\Sigma$  invariant masses studied still sizable, and the important thing is that this resonance has a large coupling to the  $K^*\Sigma$  channel as we have discussed. We can also rightly question whether the structure found for  $t_T$  is not tied to two-body thresholds rather than to the TS. We can have two thresholds where (in the absence of a  $K^*$  width) two singularities (finite) would appear: the  $K^*\Sigma$  threshold and the  $\Sigma\pi$  threshold. The latter one appears at 1337 MeV but the peaks in the  $\pi\Sigma$  mass distributions show up at about 1400 MeV, related to the  $\Lambda(1405)$ , hence it is not the  $\pi\Sigma$  threshold enhancement what one is seeing there. The  $K^*\Sigma$  threshold appears at 2087 MeV, and the width of the  $K^*$  softens a structure related to this threshold. Actually we see a soft enhancement of  $\text{Re}(t_T)$  in Fig. 12.5 around this energy. This is related to this threshold and a detailed study of the threshold effect and the TS, going to the limit of small width, was conducted in Ref. [128] where a triangle diagram with  $K^*DK$  intermediate states was studied. It was indeed found that  $\text{Re}(t_T)$  had a bump associated with the  $K^*D$  threshold while  $\text{Im}(t_T)$  had a peak stemming from a triangle singularity. Here we have a similar situation where  $\text{Re}(t_T)$  in Fig. 12.5 is influenced by the  $K^*\Sigma$  threshold, while  $\text{Im}(t_T)$  is driven by the TS peaking at higher energy. We see in Fig. 12.5, by looking at  $|t_T|$ , that the peak structure is just provided by  $\text{Im}(t_T)$ , hence it is the TS what is responsible for the peak structure in the cross sections studied.

We should note that our calculations are done without a normalization. In the case of the  $\pi^-p \rightarrow K^0\pi\Sigma$  reaction we made an estimate of the absolute value by assuming a  $N^*(2030)$  decay width to  $\pi N$  of about 70 MeV. This is only a guess of the order of magnitude based on similar decay widths for  $N^*$  resonances in that energy range. It is not possible right now to be more quantitative. In the case of the  $pp \rightarrow pK^+\pi\Sigma$  reaction, we did not even attempt to make an estimate of the absolute value of the cross section. Yet, the results that we find in the next section, where we

show that the triangle mechanism is far more important than the tree-level diagram, give us confidence that the triangle mechanism discussed here is indeed very important and provides a plausible solution to the puzzle of the experimental results of Ref. [453]. At present we would suggest that an experimental exploration is done of the dependence of the cross sections on the  $K^+ \pi \Sigma$  invariant mass to see if the predictions tied to the TS studied here hold or not. A further theoretical study after some extra experimental information from these observables would then be advisable.



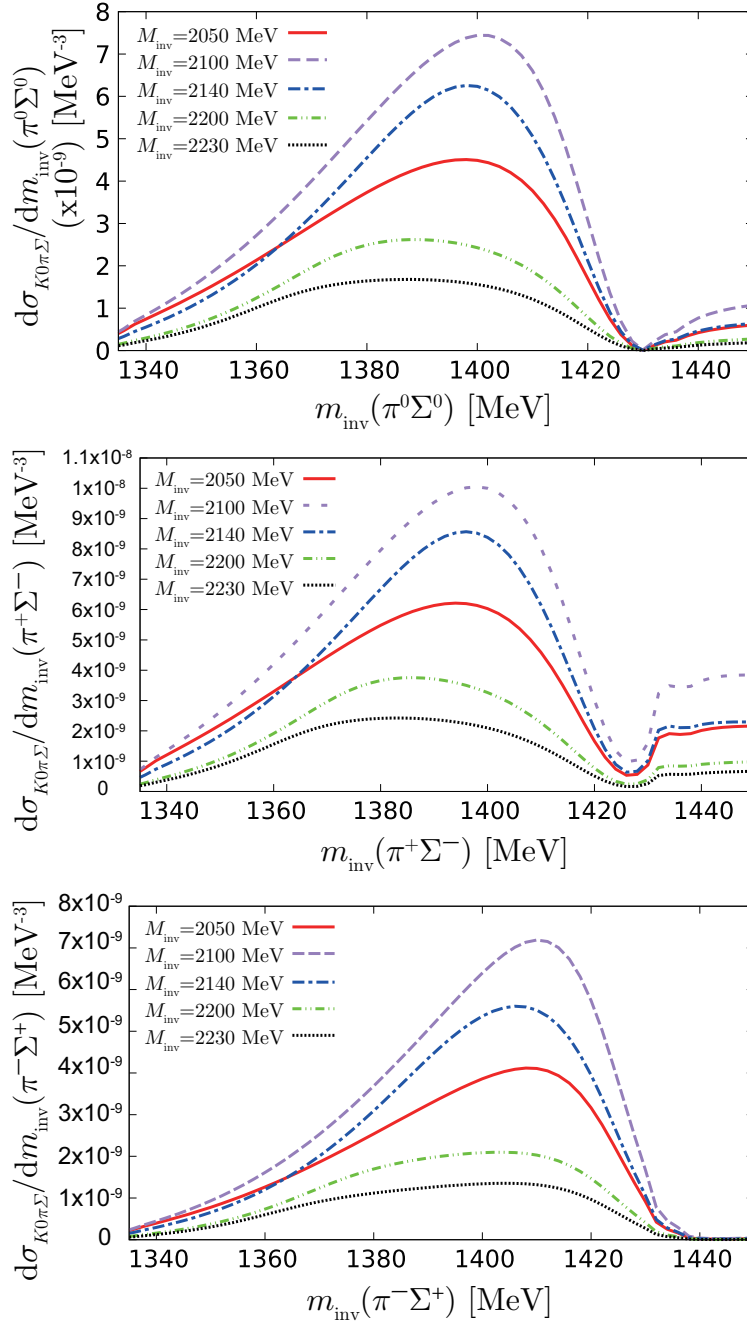


Figure 12.6: The  $\frac{d\sigma}{dm_{\text{inv}}}$  mass distribution as a function of  $m_{\text{inv}}(\pi^0\Sigma^0)$ ,  $m_{\text{inv}}(\pi^+\Sigma^-)$  and  $m_{\text{inv}}(\pi^-\Sigma^+)$  for the  $\pi^- p \rightarrow K^0 \pi \Sigma$  scattering with several fixed values of  $M_{\text{inv}}$ .

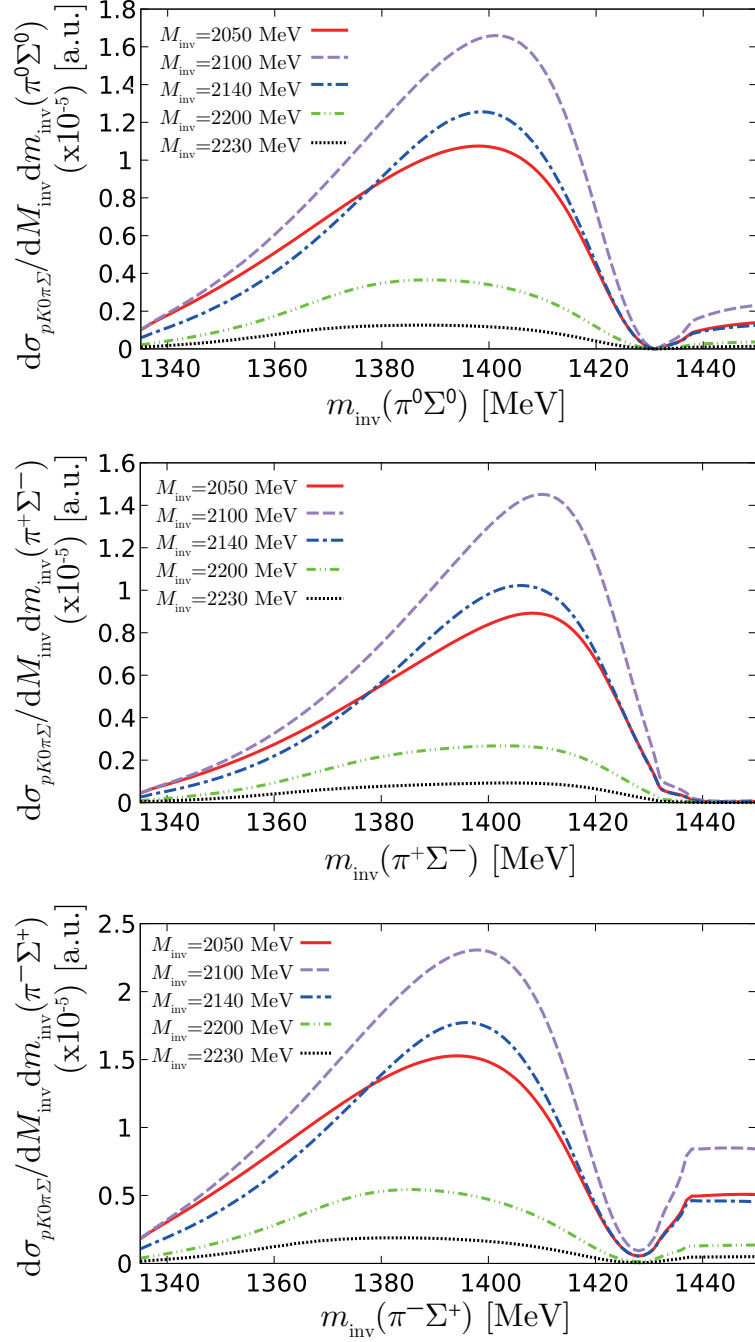


Figure 12.7: The  $\frac{d^2\sigma_{pK^+\pi\Sigma}}{dM_{\text{inv}}dm_{\text{inv}}}$  as a function of  $m_{\text{inv}}(\pi^0\Sigma^0)$ ,  $m_{\text{inv}}(\pi^+\Sigma^-)$  and  $m_{\text{inv}}(\pi^-\Sigma^+)$  for the  $pp \rightarrow pK^+\pi\Sigma$  scattering with several fixed values of  $M_{\text{inv}}$  and  $\sqrt{s} = 3179$  MeV.

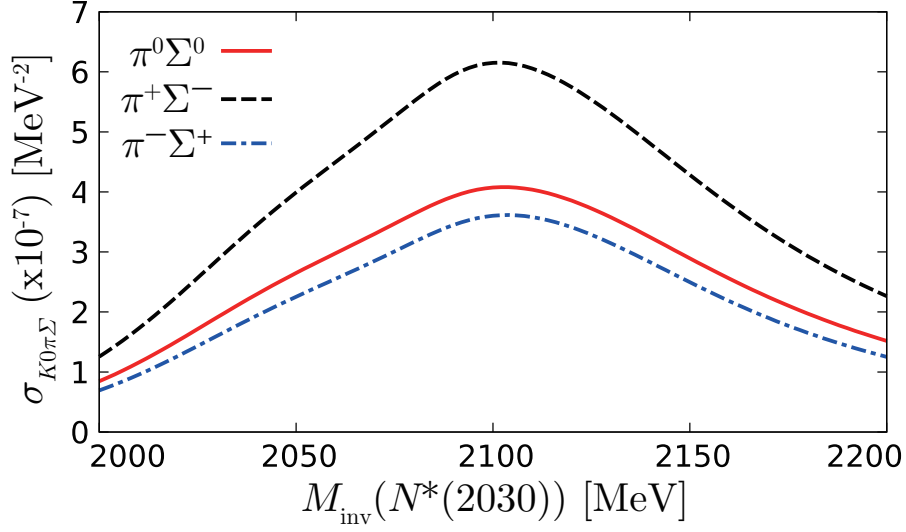


Figure 12.8: The cross section of the  $\pi^- p \rightarrow K^0 \pi \Sigma$  process  $\sigma_{K^0 \pi \Sigma}$  as a function of  $M_{\text{inv}}$  for the  $\pi^- p \rightarrow K^0 \pi \Sigma$  scattering. The red solid line corresponds to the  $\pi^0 \Sigma^0$ , the black dash line the  $\pi^+ \Sigma^-$  and the blue dash-dot line  $\pi^- \Sigma^+$ .

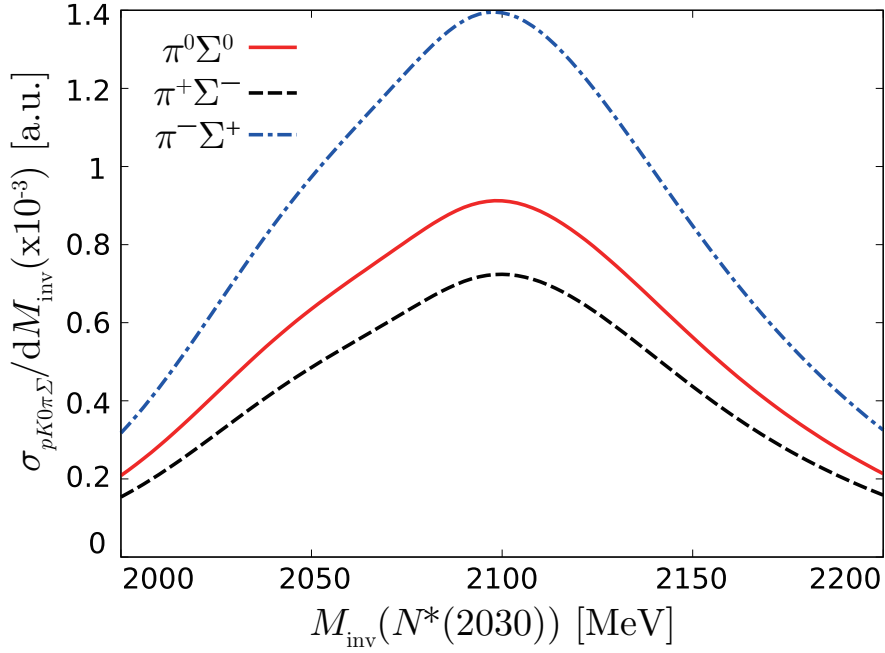


Figure 12.9: The  $\frac{d\sigma_{pK^+\pi\Sigma}}{dM_{\text{inv}}}$  as a function of  $M_{\text{inv}}$  for the  $pp \rightarrow pK^+\pi\Sigma$  scattering with fixed value of  $\sqrt{s} = 3179$  MeV. The red solid line corresponds to the  $\pi^0 \Sigma^0$ , the black dash line the  $\pi^+ \Sigma^-$  and the blue dash-dot line  $\pi^- \Sigma^+$ .

## 12.4 Further considerations

The results obtained so far have relied on a triangle loop with  $K^*\pi\Sigma$  in the intermediate state. We can ask what happens to the related tree-level mechanism with the same final state. Then we can consider the mechanism of Fig. 12.10 for the  $pp \rightarrow pK^+\pi^-\Sigma^+$  reaction. The first thing we realize is that in this mechanism the  $\pi^+\Sigma^-$  are not in a resonant state (the  $\Lambda(1405)$ ) unlike in Fig. 12.4(a). Its contribution will appear as a background that in experiments is removed to get the  $\Lambda(1405)$  signal. Yet, we can make an estimate of this contribution relative to the loop mechanism of Fig. 12.4. We must replace in Eq. (12.46)

$$2M_\Sigma \left( t_{\Sigma^+\pi^-, \Sigma^+\pi^-} + \frac{1}{2} t_{\Sigma^0\pi^0, \Sigma^+\pi^-} \right) \vec{\sigma} \cdot \vec{k} t_T \quad (12.47)$$

by

$$\frac{1}{M_{\text{inv}}^2(\pi^-K^+) - m_{K^*}^2 + im_{K^*}\Gamma_{K^*}} \vec{\sigma} \cdot (\vec{k} - \vec{p}_\pi). \quad (12.48)$$

We have made estimates of these two terms in the region of the peak of  $M_{\text{inv}}(K^{*0}\Sigma^+)$  ( $\sim 2100$  MeV) and the peak of  $M_{\text{inv}}(\pi^-\Sigma^+)$  ( $\sim 1400$  MeV) and we find the tree level small compared to the loop terms, of the order of five times smaller, and out of phase with the other mechanism, which gives rise to a small background below the structure that we have studied.

Next we would like to see what happens if we had a mechanism with  $\bar{K}N$  instead of  $\pi\Sigma$  in the loop. Our argumentation is that by having  $\pi\Sigma$  in the loop we guarantee that the  $\Lambda(1405)$  state of small energy (1385 – 1400 MeV) is produced. However, should there be a mechanism with  $\bar{K}N$  in the loop, then the  $\Lambda(1405)$  state of higher energies ( $\sim 1420$  MeV) would be produced and we would reach different conclusions in the paper. Actually, related to the mechanism that we have we could have the mechanism of Fig. 12.11. The same resonance  $N^*$  that we have discussed also couples to  $\phi N$ . However, as we can see in Fig. 2 of Ref. [139] the strength of the  $N^*$  resonance coupling to  $\phi N$  channel is of the order of 0.25 compared to 7 for the coupling to  $K^*\Sigma$  that we have considered here. This is about a factor 30 smaller than the mechanism we have considered.

We can also see at which  $M_{\text{inv}}(\phi n)$  value one expects the triangle singularity peak, and we find it at  $M_{\text{inv}}(\phi n) = 1970$  MeV (we put the mass of  $\Lambda(1405)$  as 1433 MeV to be above the  $\bar{K}N$  threshold and be able to apply Eq. (3.134)). This energy is lower than the energy of 2100 MeV where the former triangle singularity appeared. This invariant mass is lower than the one reached in the  $\pi^-p \rightarrow K^0\pi\Sigma$  experiments of Refs. [325, 451]. It is at reach in the  $pp \rightarrow pK^+\pi\Sigma$  experiment of Ref. [453]. In addition, the small width of the  $\phi$  makes the TS structure narrower, but the  $p$ -wave

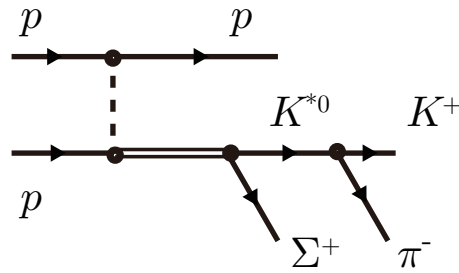


Figure 12.10: Tree-level diagram corresponding to Fig. 12.4(a) with the fixed  $\pi\Sigma$  being  $\pi^-\Sigma^+$ .

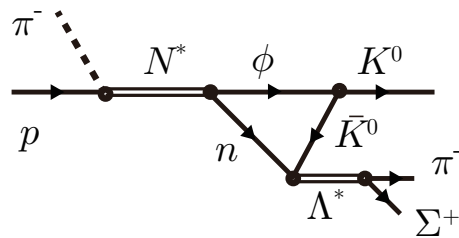


Figure 12.11: Triangle mechanism with  $\phi n\bar{K}^0$  intermediate state.

coupling of  $\phi \rightarrow K\bar{K}$  reduces drastically the strength. Indeed, the  $|\vec{k}|^3$  factor in the cross sections of Eqs. (12.1,12.22) for  $\pi^- p \rightarrow K^0 \pi \Sigma$  and (12.46) for  $pp \rightarrow pK^+ \pi \Sigma$  introduces an extra 0.08 relative reduction factor of the  $\bar{K}N$  triangle mechanism versus the  $K^* \Sigma$  one. The two factors discussed make the  $\phi \bar{K}N$  mechanism negligible versus the  $K^* \pi \Sigma$  one.

On the other hand, one may wonder if there are other  $N^*$  resonances around the 2000 – 2150 MeV that couple strongly to  $\phi N$ , but by looking into the PDG [110] and the older version of the PDG [455], we do not find any resonance with coupling to  $\phi N$ .

We could think of other possible vector mesons and  $N^*$ . The next vector meson is the  $\rho(1450)$ . This mechanism develops a TS at 2614 MeV (the mass of  $\Lambda(1405)$  is again put as 1433 MeV here), which cannot be reached in the experiment of Ref. [453]. In addition the  $\rho(1450) \rightarrow K\bar{K}$  is quoted as “not seen” in the PDG [110] although some searches are quoted there. Furthermore, we do not know of any  $N^*$  resonance around this energy that could have a sizable coupling to  $N\rho(1450)$ .

Finally, we would like to insist that we have not done a determination of the strength of the cross section. For reasons discussed at the beginning we would need information, the  $\pi N$  decay of  $N^*$ , which is not known, and we did estimates. For the case of the  $pp$  reaction we simply give results in arbitrary units. However, the comparison done with the tree level, showing that the strength of the triangle mech-

anism is much more important than the tree level, indicates that the mechanism discussed is relevant for the reaction. Leaving this apart, the shape of the invariant mass distributions is totally given by the mass and width of the particles in the triangle diagram and there is no uncertainty in the shape.

The discussion done above is illustrative and shows the relevant role of the TS with  $K^*\Sigma\pi$  intermediate state, that enhances the excitation of the low-energy  $\Lambda(1405)$  state, providing a plausible explanation of the experimental findings of Ref. [453].

## 12.5 Conclusions

We have carried out a study of contributions of a triangle diagram to the the  $\pi^- p \rightarrow K^0\pi\Sigma$  and  $pp \rightarrow pK^+\pi\Sigma$  processes. In both reactions, the triangle diagram is formed by a  $N^*$  decaying first to  $K^*$  and  $\Sigma$ , the  $K^*$  decays into  $\pi K$ , and then the  $\Sigma$  and the  $\pi$  merge to give  $\Lambda(1405)$ , which finally decays into  $\pi\Sigma$ . In this process, the  $K^*\pi\Sigma$  loop generates a triangle singularity around 2140 MeV in the invariant mass of  $K\Lambda(1405)$  from of Eq. (3.134). We evaluate the real part, imaginary part and absolute value of the amplitude  $t_T$  and find a peak around 2140 MeV. We calculate the  $\frac{d\sigma_{K^0\pi\Sigma}}{dm_{\text{inv}}}$

with some values of  $M_{\text{inv}}$  in the  $\pi^- p \rightarrow K^0\pi\Sigma$  reaction and  $\frac{d^2\sigma_{pK^+\pi\Sigma}}{dM_{\text{inv}}dm_{\text{inv}}}$  with some values of  $M_{\text{inv}}$  and fixed  $\sqrt{s} = 3179$  MeV as a function of  $m_{\text{inv}}(\pi^0\Sigma^0)$ ,  $m_{\text{inv}}(\pi^+\Sigma^-)$  and  $m_{\text{inv}}(\pi^-\Sigma^+)$ . In these distributions, we see peaks around 1400 MeV, representing clearly the  $\Lambda(1405)$ . Integrating over the  $m_{\text{inv}}$  we obtain  $\sigma_{K^0\pi\Sigma}$  and  $\frac{d\sigma_{pK^+\pi\Sigma}}{dM_{\text{inv}}}$  and these distributions show a clear peak for  $M_{\text{inv}}(N^*(2030))$  around 2100 MeV. The peak of the singularity shows up around 2140 MeV. This peak position of the triangular singularity is lowered by the initial  $N^*$  resonance peak around 2030 MeV in the  $K^*\Sigma$  production.

Thus, our results constitute an interesting prediction of the triangle singularity effect in the cross sections of these decays. The work done here could explain why in the experiments of Refs. [453, 454] the invariant mass distribution of  $\pi\Sigma$  for the  $\Lambda(1405)$  are found at lower invariant masses than in other reactions. It would also be interesting to see if the predictions done here concerning the triangle singularity are fulfilled by the experimental data, an issue that has not been investigated so far. This work also can serve as a warning to future experiments that measure these reactions, that they should be careful when associating peaks in this energy region to resonances.

# Chapter 13

## Triangle Singularity and enhancement of the isospin-violating decay

$$\Lambda_c^+ \rightarrow \pi^+ \pi^0 \pi^0 \Sigma^0$$

### 13.1 Introduction

Recent studies suggest that the triangular singularities (TS) can give a significant contribution to isospin-violating processes. In Refs. [115–117], the role of the triangle diagram in the unusually large isospin-violating  $\pi^0 f_0(980)$  production from  $\eta(1405)$  observed in BESIII [118] was studied. The triangular diagrams formed by  $K^{*-} K^+ K^-$  and  $\bar{K}^{*0} K^0 \bar{K}^0$  contribute to this process because of the sensitivity of the triangle singularity to the masses of the particles in the loop diagram, the TS can have a sizable contribution in the isospin-violating process. It is noteworthy that the shape of the  $f_0(980)$  resonance appears narrower than observed in other processes because the resonance shape is modified by the amplitude of the triangle diagram, which gives the width with the order of the charged- and neutral-kaon mass difference. Also, the line shape of the  $\pi\pi$  invariant mass distribution calculated with the triangle diagram agrees with what was observed experimentally [118]. Following these studies, the isospin-violating  $f_0(980)$  productions enhanced by the TS in the  $D_s^+ \rightarrow \pi^+ \pi^0 f_0(980)$  and  $\bar{B}_s^0 \rightarrow J/\psi \pi^0 f_0(980)$  processes were studied in Refs. [461] and [462], respectively.

In this chapter, based on the findings of Ref. [11], we study the isospin-violating  $\Lambda_c^+ \rightarrow \pi^+ \pi^0 \Lambda(1405)$  process with the  $\Lambda(1405)$  decay into  $\pi^0 \Sigma^0$  from the triangle diagram. The triangle diagram is formed by the decay of  $\Lambda_c^+$  into  $\pi^+ K^{*-} p$  ( $\pi^+ \bar{K}^{*0} n$ ) followed by the decay of  $K^{*-} \rightarrow \pi^0 K^-$  ( $\bar{K}^{*0} \rightarrow \pi^0 \bar{K}^0$ ) and the fusion of the  $K^- p$  ( $\bar{K}^0 n$ )

to form  $\Lambda(1405)$ . From Eq. (3.134) one can predict that a singularity from the triangle diagram would appear around 1890 MeV in the  $\pi^0\Lambda(1405)$  invariant mass distribution. The  $\Lambda(1405)$  is successfully described as a hadronic molecule [27–35], and has a large coupling to the  $\bar{K}N$  and the  $\pi\Sigma$  channels (see also Refs. [24, 64] and references therein for the details). The decay of heavy hadrons containing a charm or bottom quark is an exciting field in hadron physics as summarized in Ref. [303], and particularly the  $\Lambda(1405)$  production in the  $\Lambda_c^+$ ,  $\chi_{c0}(1P)$  and  $\Xi_b$  decays was studied in Refs. [63, 301], Ref. [463] and Ref. [464], respectively, where the  $\Lambda(1405)$  affects the  $\pi\Sigma$  or  $\bar{K}N$  mass distribution through the final-state rescattering. Considering the external  $W^+$  emission for the transition of  $\Lambda_c^+$  into  $\pi^+\bar{K}^*N$ , which would give the main contribution to this process, the  $\Lambda(1405)$  production is isospin forbidden. Indeed the  $W$  produces the  $\pi^+$  in one vertex and in the other one includes a  $cs$  transition. We have thus  $\pi^+$  and  $sud$ , with  $ud$  in  $I = 0$ , because there these quarks are spectators. Thus the  $sud$  final state has  $I = 0$  and hadronizes in  $\bar{K}^*N$  (see Fig. 13.3). Meanwhile, the possible effect of the TS on the  $\Lambda(1405)$  production was studied in Refs. [10, 54, 465]. Now, as found in Refs. [115–117, 461, 462] for the  $f_0(980)$  production, we expect that the isospin-violating  $\Lambda(1405)$  production is enhanced by the TS around 1890 MeV in the  $\pi^0\Lambda(1405)$  mass distribution, where the triangle singularity would appear from Eq. (3.134), and that a narrow peak around the  $\Lambda(1405)$  energy in the  $\pi^0\Sigma^0$  mass distribution would appear. The observation of the TS in this isospin-violating  $\Lambda(1405)$  production would give further support to the hadronic molecular picture of the  $\Lambda(1405)$  resonance, and provide us better understanding on the triangle singularity.

## 13.2 Formalism

In the present study, we investigate the  $\Lambda_c^+ \rightarrow \pi^+\pi^0\pi^0\Sigma^0$  decays via  $\Lambda(1405)$  formation. The process of  $\Lambda_c^+ \rightarrow \pi^+K^{*-}p$  followed by the  $K^{*-}$  decay into  $\pi^0K^-$  and the merging of the  $K^-p$  into  $\Lambda(1405)$  (see Fig. 13.1(a)) or  $\Lambda_c^+ \rightarrow \pi^+\bar{K}^{*0}n$  followed by the  $\bar{K}^{*0}$  decay into  $\pi^0\bar{K}^0$  and the merging of the  $\bar{K}^0n$  into  $\Lambda(1405)$  (see Fig. 13.1(b)) generate a singularity, and we will see a signal for the  $\Lambda(1405)$  around 1420 MeV because it comes from  $\bar{K}N$  which couples to the second pole at 1420 MeV in the invariant mass of  $\pi^0\Sigma^0$ . In the study of Ref. [31], the  $\Lambda(1405)$  appears as the dynamically generated state of  $K^-p$ ,  $\bar{K}^0n$ ,  $\pi^0\Lambda$ ,  $\pi^0\Sigma^0$ ,  $\eta\Lambda$ ,  $\eta\Sigma^0$ ,  $\pi^+\Sigma^-$ ,  $\pi^-\Sigma^+$ ,  $K^+\Xi^-$  and  $K^0\Xi^0$  in the coupled-channels calculation.

We will analyze the effect of triangle singularities in the decay of  $\Lambda_c^+ \rightarrow \pi^+\pi^0\pi^0\Sigma^0$ . In this study, we focus on the decay channel of  $\pi^0\Sigma^0$  from  $\Lambda(1405)$ , which does not contain the  $I = 1$  contribution and have small  $I = 2$  one, to focus on the isospin violation. The complete Feynman diagram for the decay with the triangle mechanism



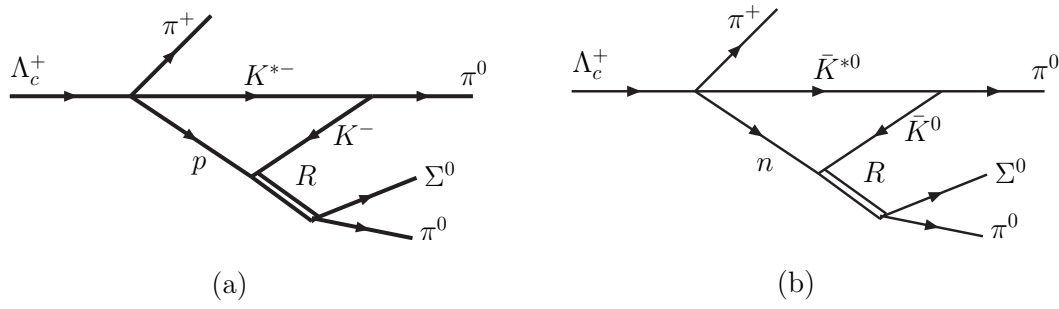
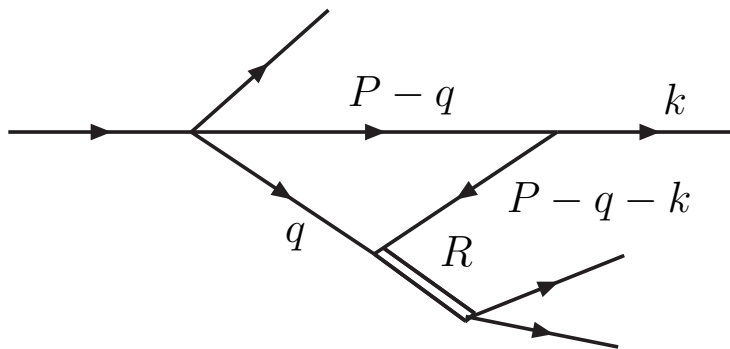
Figure 13.1: Diagram for the decay of  $\Lambda_c^+ \rightarrow \pi^+ \pi^0 \pi^0 \Sigma^0$ 

Figure 13.2: The momenta assignment for the decay process

through the  $\Lambda(1405)$  baryon is shown in Fig. 13.1 and the momenta assignment for the decay process is given in Fig. 13.2.

Now we would like to evaluate the  $\Lambda_c^+ \rightarrow \pi^+ \pi^0 R$  with  $R \rightarrow \pi^0 \Sigma^0$  process which produces the triangle diagram shown in Fig. 13.1, where  $R$  stands for the  $\Lambda(1405)$  resonance. First, let us consider the  $T$  matrix of Fig. 13.1(a), which is given by

$$-it = i \sum_{\text{pol. of } K^*} \int \frac{d^4 q}{(2\pi)^4} \frac{i t_{\Lambda_c^+ \rightarrow \pi^+ K^{*-p}}}{q^2 - M_p^2 + i\epsilon} \frac{i t_{K^{*-} \rightarrow \pi^0 K^-}}{(P-q)^2 - m_{K^{*-}}^2 + i\epsilon} \frac{i t_{K^- p \rightarrow \pi^0 \Sigma^0}}{(P-q-k)^2 - m_{K^-}^2 + i\epsilon}. \quad (13.1)$$

where the amplitude is evaluated in the center-of-mass frame of  $\pi^0 R$ . Thus we need to calculate the three vertices,  $t_{\Lambda_c^+ \rightarrow \pi^+ K^{*-p}}$ ,  $t_{K^{*-} \rightarrow \pi^0 K^-}$  and  $t_{K^- p \rightarrow \pi^0 \Sigma^0}$ , in Eq. (13.1).

### 13.3 Decay mechanism at quark level

Now we look into the  $\Lambda_c^+$  decay mechanism at quark level depicted in Fig. 13.3(a). At the quark level, the Cabibbo-allowed vertex is formed through an external emission of a  $W$  boson [466], which is also color-favored, producing a  $u\bar{d}$  pair that forms the  $\pi^+$ , with the remaining  $sud$  quarks hadronizing from a created vacuum  $\bar{u}u + \bar{d}d + \bar{s}s$  state. Note that  $ud$  in the  $\Lambda_c^+$  are in  $I = 0$  and since they are spectators in the reaction they also have  $I = 0$  in the final state of Fig. 13.3 (a). Performing the hadronization as shown in Fig. 13.3 (b), by writing the  $q\bar{q}$  matrix in terms of physical vector mesons, and looking at the quark content of the octet baryons in Ref. [306] (see table III of that work), one can write the quark states in terms of the hadron states,

$$|H\rangle = K^{*-p} + \bar{K}^{*0} n - \sqrt{\frac{2}{3}} \phi \Lambda. \quad (13.2)$$

However, we will neglect the  $\phi\Lambda$  component since this does not contribute to our triangle singularity mechanism.

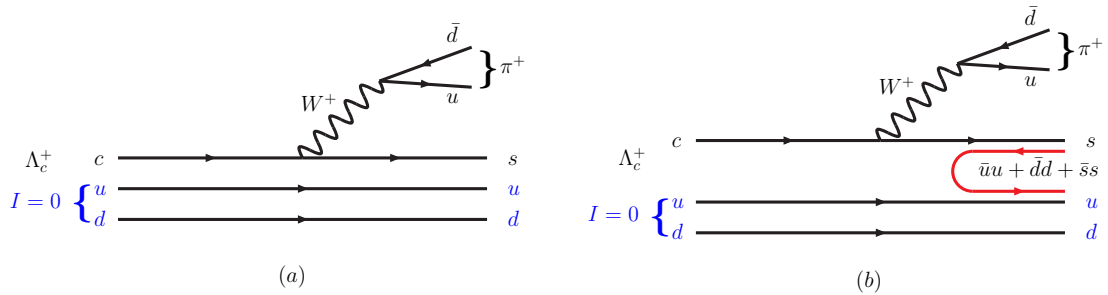


Figure 13.3: (a) Diagram for  $\Lambda_c^+ \rightarrow \pi^+ \pi^0 \pi^0 \Sigma^0$  decay; (b) Hadronization through  $\bar{q}q$  creation with vacuum quantum numbers.

## 13.4 Calculation of the three vertices

### 13.4.1 First vertex

The  $\Lambda_c^+ \rightarrow \pi^+ K^{*-} p$  process can proceed via  $s$ -wave, and we take the amplitude of the process  $t_{\Lambda_c^+ \rightarrow \pi^+ K^{*-} p}$  as

$$t_{\Lambda_c^+ \rightarrow \pi^+ K^{*-} p} = A \vec{\sigma} \cdot \vec{\epsilon}. \quad (13.3)$$

The  $K^{*-} p$  invariant mass distribution of the  $\Lambda_c^+ \rightarrow \pi^+ K^{*-} p$  decay,

$$\frac{d\Gamma_{\Lambda_c^+ \rightarrow \pi^+ K^{*-} p}}{dM_{\text{inv}}(K^{*-} p)} = \frac{1}{(2\pi)^3} \frac{2M_{\Lambda_c^+} 2M_p}{4M_{\Lambda_c^+}^2} p_{\pi^+} \tilde{p}_{K^{*-}} \overline{\sum} \sum |t_{\Lambda_c^+ \rightarrow \pi^+ K^{*-} p}|^2, \quad (13.4)$$

where  $p_{\pi^+}$  is the momentum of  $\pi^+$  in the  $\Lambda_c^+$  rest frame, and  $\tilde{p}_{K^{*-}}$  is the momentum of  $K^{*-}$  in the  $K^{*-} p$  rest frame,

$$p_{\pi^+} = \frac{\lambda^{1/2}(M_{\Lambda_c^+}^2, m_{\pi^+}^2, M_{\text{inv}}^2(K^{*-} p))}{2M_{\Lambda_c^+}}, \quad (13.5a)$$

$$\tilde{p}_{K^{*-}} = \frac{\lambda^{1/2}(M_{\text{inv}}^2(K^{*-} p), m_{K^{*-}}^2, M_p^2)}{2M_{\text{inv}}(K^{*-} p)}. \quad (13.5b)$$

Now, if we square the  $T$  matrix in Eq. (13.3) and sum and average over the polarizations and spins, we get

$$\overline{\sum} \sum |t_{\Lambda_c^+ \rightarrow \pi^+ K^{*-} p}|^2 = 3|A|^2. \quad (13.6)$$

Thus we get

$$\frac{|A|^2}{\Gamma_{\Lambda_c^+}} = \frac{Br(\Lambda_c^+ \rightarrow \pi^+ K^{*-} p)}{\int_{M_{K^{*-}+m_p}^{M_{\Lambda_c^+}-m_{\pi^+}}} \frac{3}{(2\pi)^3} \frac{M_p}{M_{\Lambda_c^+}} p_{\pi^+} \tilde{p}_{K^{*-}} dM_{\text{inv}}(K^{*-} p)}. \quad (13.7)$$

By calculating the width of this decay, using the experimental branching ratio of this decay  $Br(\Lambda_c^+ \rightarrow \pi^+ K^{*-} p) = (1.5 \pm 0.5) \times 10^{-2}$  [110], we can determine the value of the constant  $|A|$ .

### 13.4.2 Second vertex

In a similar way as done in the previous chapter, we calculate the contribution of the vertex  $K^{*-} \rightarrow \pi^0 K^-$  by using the local hidden gauge Lagrangian, and then, for the  $t$  matrix we get,

$$-it_{K^{*-} \rightarrow \pi^0 K^-} = ig \frac{1}{\sqrt{2}} \epsilon_{K^{*-}}^\mu (p_{K^-} - p_{\pi^0})_\mu \quad (13.8)$$

$$\simeq ig \frac{1}{\sqrt{2}} \vec{\epsilon}_{K^{*-}} \cdot (\vec{p}_{\pi^0} - \vec{p}_{K^-}), \quad (13.9)$$

with  $\vec{p}_{K^-}$  and  $\vec{p}_{\pi^0}$  calculated in the center-of-mass frame of  $\pi^0 R$ . At the energy where the triangle singularity appears, compared with the mass of  $K^{*-}$ , the momentum of  $K^{*-}$  is small enough, hence we again omit the zeroth component of the polarization vector in Eq. (13.8).

### 13.4.3 Third vertex

The third vertex corresponds to the mechanism for the production of the  $\pi^0 \Sigma^0$  pair in the final state, after the rescattering of the  $K^- p$  that dynamically generates the  $\Lambda(1405)$  resonance as intermediate state. We will write the vertex as

$$-it_3 = -it_{if} , \quad t_3 \equiv t_{K^- p \rightarrow \pi^0 \Sigma^0} \quad (13.10)$$

where  $t_{if}$  is the  $if$  element of the  $10 \times 10$  scattering matrix  $t$  for the channels  $K^- p$  (1),  $\bar{K}^0 n$  (2),  $\pi^0 \Lambda$  (3),  $\pi^0 \Sigma^0$  (4),  $\eta \Lambda$  (5),  $\eta \Sigma^0$  (6),  $\pi^+ \Sigma^-$  (7),  $\pi^- \Sigma^+$  (8),  $K^+ \Xi^-$  (9), and  $K^0 \Xi^0$  (10), in the coupled-channels calculation. We have  $i = 1$  for the diagrams of Fig. 13.1(a), while the index  $f$  stands for channel 4. The  $t$  matrix is obtained using the BSE, with the chiral Weinberg-Tomozawa kernel. The loop functions for the intermediate states are regularized using the cutoff method and the peak of the  $\Lambda(1405)$  is well reproduced using a cutoff of 630 MeV. We will need this parameter for the next steps of the calculation, being necessary in order to evaluate the loop integral in the diagram of Fig. 13.1.

## 13.5 The total amplitude

Now we obtain the final amplitude of  $\Lambda_c^+ \rightarrow \pi^+ \pi^0 \pi^0 \Sigma^0$  for Fig. 13.1(a),

$$t_{\Lambda_c^+ \rightarrow \pi^+ \pi^0 \pi^0 \Sigma^0} = -A \frac{1}{\sqrt{2}} g \vec{\sigma} \cdot \vec{k} t_{K^- p \rightarrow \pi^0 \Sigma^0} t_T, \quad (13.11)$$

where for simplicity we use  $t_T \equiv t_T(m_{K^{*-}}, M_p, m_{K^-})$  for Fig. 13.1 (a) decay. Here,  $t_T(m_{K^{*-}}, M_p, m_{K^-}) = 2M_p \tilde{t}_T(m_{K^{*-}}, M_p, m_{K^-})$ , with  $\tilde{t}_T$  given by Eq. (11.21), making the appropriate substitutions to account for the different particles. The energy  $k^0$  and momentum  $|\vec{k}|$  of  $\pi^0$  emitted from  $\bar{K}^*$  are given by

$$k^0 = \frac{M_{\text{inv}}^2(\pi^0 \Lambda(1405)) + m_{\pi^0}^2 - M_{\text{inv}}^2(\pi^0 \Sigma^0)}{2M_{\text{inv}}(\pi^0 \Lambda(1405))}, \quad (13.12)$$

$$|\vec{k}| = \frac{\lambda^{1/2}(M_{\text{inv}}^2(\pi^0 \Lambda(1405)), m_{\pi^0}^2, M_{\text{inv}}^2(\pi^0 \Sigma^0))}{2M_{\text{inv}}(\pi^0 \Lambda(1405))}. \quad (13.13)$$

We follow the method of Ref. [9], and obtain the final differential distribution for four particles in the final state,

$$\frac{1}{\Gamma_{\Lambda_c^+}} \frac{d^2\Gamma}{dM_{\text{inv}}(\pi^0\Lambda(1405))dM_{\text{inv}}(\pi^0\Sigma^0)} = \frac{1}{(2\pi)^5} \frac{M_{\Sigma^0}}{M_{\Lambda_c^+}} \tilde{p}_{\pi^+} \tilde{p}_{\pi^0} \tilde{q}_{\Sigma^0} \frac{1}{2} g^2 \frac{A^2}{\Gamma_{\Lambda_c^+}} |\vec{k}|^2 |t_T|^2 \times |t_{K^-p \rightarrow \pi^0\Sigma^0}|^2, \quad (13.14)$$

with

$$\tilde{p}_{\pi^+} = \frac{\lambda^{1/2}(M_{\Lambda_c^+}^2, M_{\text{inv}}^2(\pi^0\Lambda(1405)), m_{\pi^+}^2)}{2M_{\Lambda_c^+}}, \quad (13.15a)$$

$$\tilde{p}_{\pi^0} = |\vec{k}| = \frac{\lambda^{1/2}(M_{\text{inv}}^2(\pi^0\Lambda(1405)), m_{\pi^0}^2, M_{\text{inv}}^2(\pi^0\Sigma^0))}{2M_{\text{inv}}(\pi^0\Lambda(1405))}, \quad (13.15b)$$

$$\tilde{q}_{\Sigma^0} = \frac{\lambda^{1/2}(M_{\text{inv}}^2(\pi^0\Sigma^0), m_{\pi^0}^2, M_{\Sigma^0}^2)}{2M_{\text{inv}}(\pi^0\Sigma^0)}. \quad (13.15c)$$

## 13.6 Isospin-breaking effect

If we use the same masses for  $\bar{K}N$  and  $K^*$  with isospin conservation, we find that the contributions from Fig. 13.1 (a) and Fig. 13.1 (b) will cancel each other. An interesting thing is to investigate the isospin-breaking effect. That means, for the first time, we will precisely look at the  $\Lambda(1405)$  formation in an isospin forbidden mode. We expect that the formation will be driven by a triangle singularity and the shape will be narrower than usual, because it will be tied to the different masses of  $\bar{K}N$ . Therefore, in the following, we will use different masses for  $K^-p$  or  $\bar{K}^0n$ , and also for  $K^{*-}$  and  $\bar{K}^{*0}$ .

Now we consider Fig. 13.1 (b), for the  $\Lambda_c^+ \rightarrow \pi^+ \bar{K}^{*0} n$  followed by  $\bar{K}^{*0} \rightarrow \pi^0 \bar{K}^0$  decay and  $\bar{K}^0 n \rightarrow \pi^0 \Sigma^0$  to see the  $\Lambda(1405)$  formation. We also need to calculate the three vertices,  $t_{\Lambda_c^+ \rightarrow \pi^+ \bar{K}^{*0} n}$ ,  $t_{\bar{K}^{*0} \rightarrow \pi^0 \bar{K}^0}$  and  $t_{\bar{K}^0 n \rightarrow \pi^0 \Sigma^0}$ .

For the first vertex,  $t_{\Lambda_c^+ \rightarrow \pi^+ \bar{K}^{*0} n}$ , we can use the same amplitude in Eq. (13.3)

$$t_{\Lambda_c^+ \rightarrow \pi^+ \bar{K}^{*0} n} = A \vec{\sigma} \cdot \vec{c}. \quad (13.16)$$

As shown in Eq. (13.2), the weight of the production is the same as the  $\pi^+ K^{*-} p$  process with the same sign. Then, we can use the same  $A$  in this case.

The amplitude  $t_{\bar{K}^{*0} \rightarrow \pi^0 \bar{K}^0}$  for the second vertex is written by using Eq. (2.33) as two times as  $K^{*-} \rightarrow \pi^0 K^-$

$$-it_{K^{*0} \rightarrow \pi^0 \bar{K}^0} = -ig \frac{1}{\sqrt{2}} \epsilon_{\bar{K}^{*0}}^\mu (p_{\bar{K}^0} - p_{\pi^0}) \quad (13.17)$$

$$\simeq -ig \frac{1}{\sqrt{2}} \vec{\epsilon}_{\bar{K}^{*0}} \cdot (\vec{p}_{\pi^0} - \vec{p}_{\bar{K}^0}), \quad (13.18)$$

where the amplitude has the opposite sign to the  $\bar{K}^{*-} \rightarrow \pi^0 K^-$  in Eq. (13.9). Finally, the  $\bar{K}^0 n \rightarrow \pi^0 \Sigma^0$  amplitude for the third vertex  $t_3 = t_{if}$  is the component with  $i = 2$  and  $f = 4$ .

The triangle amplitude for the  $\bar{K}^{*0} n \bar{K}^0$  loop, given by  $t_T = t_T(m_{\bar{K}^{*0}}, M_n, m_{\bar{K}^0}) = 2M_n \tilde{t}_T(m_{\bar{K}^{*0}}, M_p, m_{\bar{K}^0})$ , with  $\tilde{t}_T$  given by Eq. (11.21) and replacing the masses and width of the internal particles.

Hence, for the isospin-breaking effect, we get the final differential distributions,

$$\frac{1}{\Gamma_{\Lambda_c^+}} \frac{d^2\Gamma}{dM_{\text{inv}}(\pi^0 \Lambda(1405)) dM_{\text{inv}}(\pi^0 \Sigma^0)} = \frac{1}{(2\pi)^5} \frac{M_{\Sigma^0}}{M_{\Lambda_c^+}} \tilde{p}_{\pi^+} \tilde{q}_{\Sigma^0} \frac{1}{2} g^2 \frac{A^2}{\Gamma_{\Lambda_c^+}} |\vec{k}|^3 \quad (13.19)$$

$$\times \left| t_T(m_{K^{*-}}, M_p, m_{K^-}) t_{K^- p \rightarrow \pi^0 \Sigma^0} - t_T(m_{\bar{K}^{*0}}, M_n, m_{\bar{K}^0}) t_{\bar{K}^0 n \rightarrow \pi^0 \Sigma^0} \right|^2,$$

## 13.7 Results

Let us begin by showing in Fig. 13.4 the contribution of the triangle loop,  $t_T(m_{K^{*-}}, M_p, m_{K^-})$ . We plot the real and imaginary parts of  $t_T(m_{K^{*-}}, M_p, m_{K^-})$ , as well as the absolute value with  $M_{\text{inv}}(R) \equiv M_{\text{inv}}(\pi^0 \Sigma^0)$  fixed at 1420 MeV. It can be observed that the  $\text{Re}(t_T)$  has a peak around 1838 MeV, and  $\text{Im}(t_T)$  has a peak around 1908 MeV, and there is a peak for  $|t_T|$  around 1868 MeV. As discussed in Ref. [128], the peak of the real part is related to the  $K^{*-} p$  threshold and the one of the imaginary part, that dominates for the larger  $\pi^0 R$  invariant masses, to the triangle singularity.

In Fig. 13.5 we plot Eq. (13.19) for  $\Lambda_c^+ \rightarrow \pi^+ \pi^0 \pi^0 \Sigma^0$  by fixing  $M_{\text{inv}}(\pi^0 R) = 1850$  MeV, 1890 MeV, and 1930 MeV and varying  $M_{\text{inv}}(R)$ . We can see that the distribution with largest strength is near  $M_{\text{inv}}(\pi^0 R) = 1890$  MeV. We can also see a strong peak around 1432 MeV for the three different masses of  $M_{\text{inv}}(\pi^0 R)$ . Consequently, we see that most of the contribution to our width  $\Gamma$  will come from  $M_{\text{inv}}(R) = M_R$ , thus we have strong contributions for  $M_{\text{inv}}(\pi^0 \Sigma^0) \in [1390 \text{ MeV}, 1450 \text{ MeV}]$ . The conclusion is that when we calculate the mass distribution  $\frac{d\Gamma}{dM_{\text{inv}}(\pi^0 \Lambda(1405))}$ , we can restrict the integral in  $M_{\text{inv}}(R)$  to the limits already mentioned.

By integrating over  $M_{\text{inv}}(R)$ , we obtain  $\frac{1}{\Gamma_{\Lambda_c^+}} \frac{d\Gamma}{dM_{\text{inv}}(\pi^0 R)}$  which is shown in Fig. 13.6. We see a clear peak of the distribution around 1880 MeV for  $\Lambda(1405)$  production. When performing the integral we observe that the strong contribution comes from  $M_{\text{inv}}(\pi^0 \Sigma^0) \in [1390 \text{ MeV}, 1450 \text{ MeV}]$ . The conclusion is that when we calculate the mass distribution  $\frac{d\Gamma}{dM_{\text{inv}}(\pi^0 \Lambda(1405))}$ , we can restrict the integral in  $M_{\text{inv}}(\pi^0 \Sigma^0)$  to the limits already mentioned.

Integrating now  $\frac{d\Gamma}{dM_{\text{inv}}(\pi^0 \Lambda(1405))}$  over  $M_{\text{inv}}(\pi^0 \Lambda(1405)) \in [1800 \text{ MeV}, 2050 \text{ MeV}]$  in

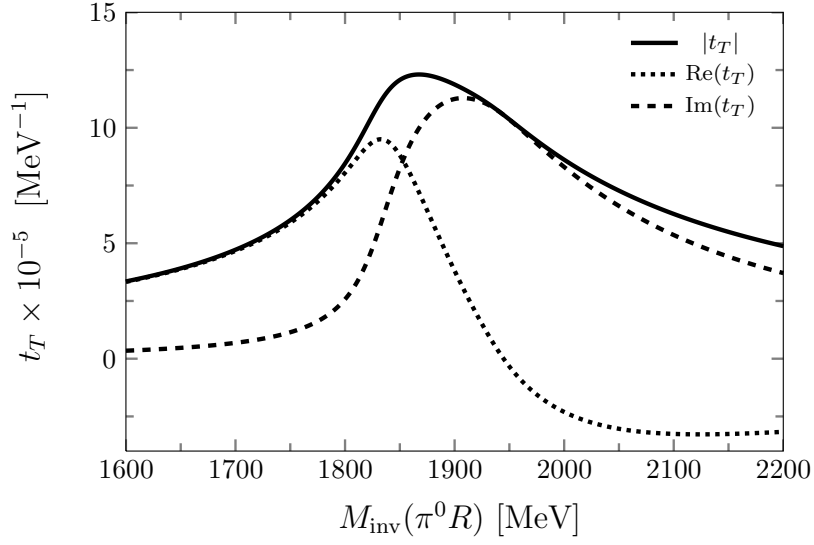


Figure 13.4: Triangle amplitude  $t_T$  for the decay in Fig. 13.1 (a), here taking  $M_{\text{inv}}(R)=1420$  MeV.

Fig. 13.6, we obtain the branching fraction

$$Br(\Lambda_c^+ \rightarrow \pi^+ \pi^0 \Lambda(1405); \Lambda(1405) \rightarrow \pi^0 \Sigma^0) = (4.17 \pm 1.39) \times 10^{-6}. \quad (13.20)$$

This number is within measurable range. The errors come from the experimental errors in the branching ratio of  $Br(\Lambda_c^+ \rightarrow \pi^+ K^{*-} p)$ .

One should stress the most remarkable feature in the distributions of Fig. 13.5: the width of the  $\Lambda(1405)$  produced is a mere 6.5 MeV, remarkably smaller than the nominal widths for the  $\Lambda(1405)$  at 1420 MeV of the order of 30 MeV. As mentioned before, this narrow width is tied basically to the different masses of the  $K^-, \bar{K}^0$  or  $p, n$ . This exceptionally narrow shape has been observed in all the isospin forbidden  $f_0(980)$  production mode. The present reaction would be the first one where the narrow  $\Lambda(1405)$  is seen in an isospin forbidden mode.

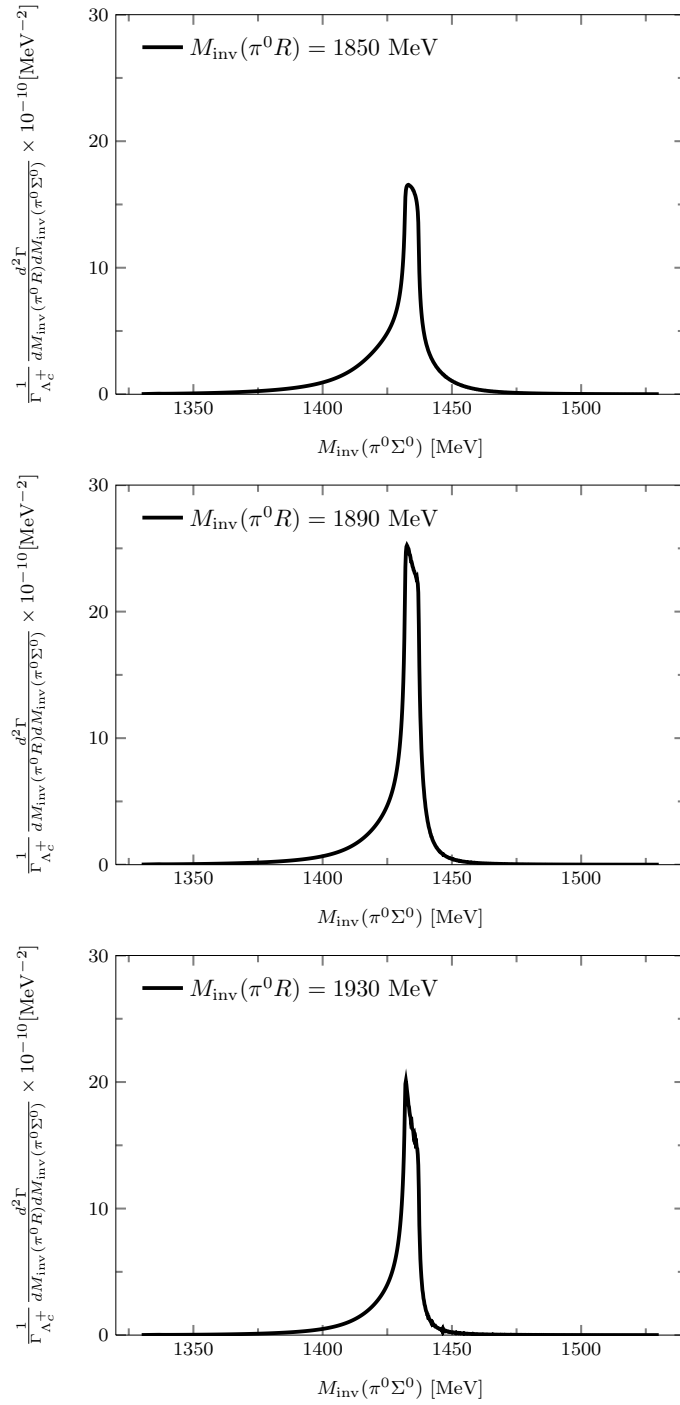


Figure 13.5: The derivative of the mass distribution of  $\Lambda_c^+ \rightarrow \pi^+ \pi^0 \pi^0 \Sigma^0$  with regards to  $M_{\text{inv}}(\Lambda(1405))$ .



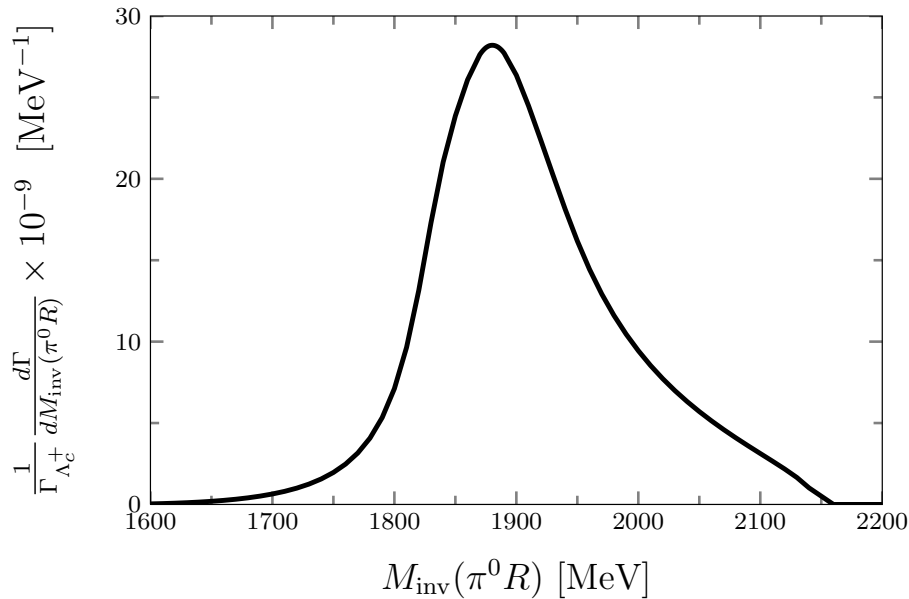


Figure 13.6: The mass distribution of  $\Lambda_c^+ \rightarrow \pi^+ \pi^0 \pi^0 \Sigma^0$ .

## 13.8 Conclusions

The triangle singularities have recently shown to be very effective, enhancing the production of  $f_0(980)$  or  $a_0(980)$  in isospin suppressed modes. These reactions have played a double role. On the first hand they have provided clear examples of triangle singularities, and on the second hand the rates and shapes obtained for the isospin suppressed modes are closely tied to the nature of these resonances and offer extra support to their dynamical origin from the interaction of mesons in coupled channels.

The two states of the  $\Lambda(1405)$ , now already official in the PDG, are another example of dynamical generation from the interaction of meson-baryon in this case. Yet, the resonance has not been observed in an isospin violating reaction so far. The present work provides the first evaluation of the  $\Lambda(1405)$  production in an isospin forbidden reaction. We devised one such reaction, which, as in the case of the  $f_0(980)$  or  $a_0(980)$ , can be enhanced by a triangle singularity. We found such an example in the decay of  $\Lambda_c^+$  into  $\pi^+ \pi^0 \Lambda(1405)$ . The mechanism for the production is given by a first decay of the  $\Lambda_c^+$  into  $\pi^+ \bar{K}^* N$ , then the  $\bar{K}^*$  decays into  $\bar{K} \pi$  and the  $\bar{K} N$  merge to produce the  $\Lambda(1405)$  through a triangle loop containing  $\bar{K}^* N \bar{K}$ , which develops a singularity around 1890 MeV.

The remarkable observation is that a peak tied to the  $\Lambda(1405)$  state of higher

energy (around 1420 MeV) appears in the final  $\pi^0\Sigma^0$  mass spectrum, but peaking even at higher energy, close to the  $\bar{K}N$  threshold of 1432 MeV. It is also remarkably narrow, of the order of 6-7 MeV, and is tied to the difference of masses between the  $K^-$  and  $\bar{K}^0$  and  $p, n$ .

We have shown that the amount of  $\Lambda(1405)$  production has its largest strength at a  $\pi^0\Lambda(1405)$  invariant mass of around 1890 MeV, where the mechanism suggested develops a triangle singularity. The shape and strength obtained are intimately tied to the nature of the  $\Lambda(1405)$  as a dynamically generated resonance from the meson baryon interaction, and in the present case, to its large coupling to the  $\bar{K}N$  component. We found that the strength of the width observed falls within measurable range. The implementation of the reaction would thus bring valuable information on the nature of this resonance, the mechanisms of triangle singularities, plus extra information on the continuously searched for  $\bar{K}N$  interaction.

**Part V**

**Conclusions and Summary**



# Conclusions and Summary

Hadron physics, dealing with the structure and dynamics of strongly interacting systems, has always been the toughest part of particles physics. While QCD is universally admitted as the theory behind it, the intrinsic non-perturbative nature of hadrons made progress slow. The spectrum of hadrons is composed of bound states of quarks and gluons. The distinctive property of confinement in strong interactions prevents quarks and gluons from appearing as free particles. A new generation of dedicated experiments in hadron physics has been proposed with the aim of uncovering properties of strong interactions and specifically the mysteries of confinement.

Indeed, the field has been boosted by the unexpected wealth of data from hadronic physics facilities worldwide. New fields of research in hadron physics opened, in particular on emergence of structures in QCD and the possible formation of exotic states, which did not fit the expectations of the very successful quark model until recently. These discoveries occur especially in the open and hidden charm and bottom hadron sectors, but some of them also occur in the light quark sector. Among various explanations of the internal structure of these excitations, hadronic molecules, being analogues of light nuclei, tetraquarks and glueballs naturally emerge.

The description of hadron molecular exotic states that result from the interaction between two hadrons and the identification of new states from experiments have been the main objectives of this thesis. This work has required the combination of different QCD effective field theories and analytic methods. As sketched in Part I of the thesis, exact and approximate QCD symmetries at the hadron level can be used to construct EFT's, which supplemented with unitarization techniques, are able to describe the low energy hadronic phenomenology.

In addition, triangular singularities and their analytic structure were described 50 years ago, but only now experimental evidences are being reported. We have also investigated various reactions to find out which of the resonances reported by experiments could be just a consequence of these singularities.

In Part II, *Hadrons In The Light Sector*, we have studied different reactions and some excited  $N^*$  states using some of the techniques presented in Part I. In Chapter 4, several reactions of the type  $\tau^- \rightarrow \nu_\tau M_1 M_2$ , with  $M_1 M_2 = PP, PV, VP$  or  $VV$

mesons, were studied. The decay widths of these reactions were compared with their experimental values and, in general, were found to be in good agreement with observation. In the reactions where the agreement was not as optimal, the difference could be justified by the existence of resonance states decaying into the two (final) mesons observed. The importance of  $G$ -parity conservation in reactions that involve only  $u$  and  $d$  quarks was confirmed and, even more surprisingly, we also found that the selection rules of  $G$ -parity have repercussion in reactions with  $K$  and  $K^*$  mesons, where  $G$ -parity cannot be defined. This is a novel and interesting result. We also concluded that  $PP$  reactions proceed through  $p$ -wave interactions, as predicted by  $\chi$ PT, but  $PV$  and  $VV$  reactions must decay through  $s$ -wave interaction. In addition, some mass distributions were successfully compared with experiments, as well.

In Chapter 5, we studied the mass distribution of  $\Lambda_c^+ \rightarrow \bar{K}^0 MB$  decay, with  $MB = \pi N, \eta p$  and  $K\Sigma$ . One of the possible Feynman diagrams for this decay involves the  $N^*(1535)$  as an intermediate state. This resonance is very important for the study of molecular states, since it remains to be well understood outside of the CUA. While effects of the  $N^*(1535)$  and  $N^*(1650)$  are clearly visible in the  $\Lambda_c^+ \rightarrow \bar{K}^0 \pi p (I = 1/2)$  and  $\bar{K}^0 \eta p$  mass distributions, we found that the characteristics are different from those in the meson-baryon amplitude of Ref. [294]. In the mass distributions studied in this chapter, the peak from  $N^*(1535)$  is larger than that from  $N^*(1650)$ , while two peaks with a comparable magnitude are seen in the amplitude of the  $\pi N$  to  $\pi N$  channel obtained in Ref. [294] as well as in data. This is because the  $K\Sigma$  channel which couples more strongly to  $N^*(1650)$  than  $N^*(1535)$  is suppressed in the primary production from  $\Lambda_c^+$  in our treatment of the weak and hadronization processes, and the  $\rho N (I = 1/2)$  and  $K\Lambda$  channels have larger couplings to the  $N^*(1535)$  resonance than to the  $N^*(1650)$  resonance.

We have also revised the study made in Ref. [304], where several methods of calculating this decay through  $N^*(1535)$  were compared, and some discrepancy between CUA and the other methods was found. For this, we used the model developed in Ref. [294] which takes into account  $VB$  channels necessary to generate the  $N^*(1650)$  resonance which adds extra width to the mass distribution, making the discrepancy between CUA and the other models smaller, although still present. The importance of taking into account  $VB$  and  $PB$  channels together is a recurring theme found in this thesis, which was also explored in Chapters 6 and 10.

The fact that the results shown in Part II explained so well the experimental features of the systems studied, served also to establish the effectiveness of the methods used in the light sector and the energy and momentum scales where non-perturbative effects were developed. In Part III, these methods were extended to the heavy sector (baryons with  $c$  and  $b$  quarks). In Chapter 6, we have described  $\Lambda_b \rightarrow \Lambda_c^* R$  transitions, with  $\Lambda_c^* = \Lambda_c(2595)[J^P = 1/2^-]$ ,  $\Lambda_c(2625)[J^P = 3/2^-]$  and  $R = \ell \bar{\nu}_\ell$  or  $\pi$ , using a manifest Lorentz and HQSS invariant formalism, with special emphasis

on the important simplifications/relationships that HQSS imposes on these decays. In the beginning of the chapter, a review was given of the different molecular descriptions of the  $\Lambda_c^*$  excited states which are commonly used in the literature: BSE unitarized amplitudes in coupled channels with kernels obtained from i) the extended local hidden gauge, ii) the  $SU(6)_{\text{lsf}} \times \text{HQSS}$  and iii) the chiral  $SU(3)$  WT Lagrangians. The decay widths for both  $\Lambda_c^*$  states and the ratios between them were calculated, and they could be related to each other assuming that both resonances form a HQSS doublet. A novel result presented in this chapter is the evaluation of  $\Lambda_c(2595)$  and  $\Lambda_c(2625)$  LFU ratios, this is to say ratios of semileptonic decay widths involving  $\tau \bar{\nu}_\tau$  or  $\mu \bar{\nu}_\mu$  final lepton pairs. Furthermore, the possibility of a two pole structure for the  $\Lambda_c(2595)$  –one pole with  $j_q^P = 0^-$  and another one with  $j_q^P = 1^-$  for the light degrees of freedom–, together with the possibility of the unnatural  $\Lambda_b \rightarrow \Lambda_c(2595)[j_q^P = 0^-] \ell \bar{\nu}_\ell$  transition were also studied. The impact of these new ingredients on the LFU ratios is discussed in detail, and it is also argued that the existence of the last  $\Lambda_b$  decay mode would require HQSS will be severely broken. The LHCb collaboration has reported large samples of  $\Lambda_c(2595)$  and  $\Lambda_c(2625)$  baryons, thus there are good chances that LHCb could measure in the near future some of the ratios discussed in this chapter, which can shed light on the nature of these resonances.

Following this line of research, in Chapter 7, we have shown that the  $\Lambda_c(2595)$  and the  $\Lambda_c(2625)$  are very likely not HQSS partners, as the  $J^P = 3/2^-$  resonance was found to be mostly a quark-model state. This finding contradicts a large number of molecular scenarios suggested in the literature, where this resonance is dynamically generated by the  $\Sigma_c^* \pi$  chiral force. We have also predicted a  $J^P = 3/2^-$  state with a mass of about 2.7 GeV and sizable couplings to both  $\Sigma_c^* \pi$  and  $ND^*$ . In turn, the  $\Lambda_c(2595)$  was found to be predominantly a hadron-molecule, with the precise details of its nature depending drastically on the renormalization scheme used. As in the  $J^P = 3/2^-$  sector, for  $J^P = 1/2^-$  we also found an extra resonance, with a mass of around 2640–2660 MeV and a width of the order of 30-50 MeV, that is the result of dressing the bare CQM pole with baryon-meson loops. Finally, for the UV cutoff scheme, we found a narrow state at 2800 MeV with large  $ND$  and  $ND^*$  couplings. In summary, the results found in this chapter could not be easily understood in terms of HQSS. The bare quark-model state and the  $\Sigma_c \pi$  threshold are located very close to the  $\Lambda_c(2625)$  and  $\Lambda_c(2595)$ , respectively, and play completely different roles in both sectors.

In Chapter 8, a study was conducted for several  $\Xi_c$  and  $\Xi_b$  states, using the extended local hidden gauge approach to calculate BSE kernels consistent with HQSS. With only one free parameter (a sharp UV cutoff) several experimentally detected charm and bottom resonances were explained as molecular states, as well as predictions were made that can be confirmed in future experiments. In both Chapters 7 and

8, we have confirmed the versatility of the CUA when extended to the heavy sector, and its ability to explain and predict heavy resonance states. This is further shown in Chapter 9, where we have studied five new  $\Omega_c^*$  states measured by the LHCb collaboration. We use here the CUA with coupled channels, but now extended to the heavy sector by the use of a WT kernel based on the  $SU(6)_{\text{lsf}} \times \text{HQSS}$  symmetry. A detailed study of the effects of the renormalization scheme was done, and results for different sharp cutoff regulators were given. For a cutoff of  $\Lambda = 1090$  MeV, three of the five LHCb  $\Omega_c^*$  resonances could be explained as molecular states and predictions were made for their quantum numbers. We then extended the study to the case of  $\Xi_c$  and  $\Xi_b$  excited states, where we have provided molecular interpretations for several  $-\Xi_c(2790)$ ,  $\Xi_c(2815)$ ,  $\Xi_c(2930)$ ,  $\Xi_c(2970)$  and  $\Xi_b(6227)$ – states, and have predicted the spin-parity quantum numbers of the latter three resonances. In addition, we were also able to predict several new states using the equal spacing rule. The comparison of the results of this chapter with those obtained in Ref. [388] and Chapter 8 with the LHG formalism, for the  $\Omega_c$  and  $\Xi_{b,c}$  molecular states, opens the possibility of estimating systematic uncertainties associated with the use of different models for the interactions of charmed pseudoscalar and vector mesons with baryons.

In Chapter 10, a calculation of ratios of bottom to charm decay widths,  $\Xi_b \rightarrow \Xi_c^* R$  with  $\Xi_c^* = \Xi_c(2790)[J^P = 1/2^-]$ ,  $\Xi_c(2815)[J^P = 3/2^-]$  and  $R = l\bar{\nu}_l, \pi, D_s$ , was done. We show here once again the significant effects of the  $VB$  channels. The vector meson-baryon degrees of freedom appear through the dynamical generation of the  $\Xi_c^*$  within the  $SU(6)_{\text{lsf}} \times \text{HQSS}$  scheme of Ref. [86], and are taken into account in the computation of the ratios by means of the corresponding resonance couplings. An explicit calculation of the decay rates was made, starting from the microscopic quark states and using the  ${}^3P_0$  model to hadronize the quarks and create the  $\Xi_c(2790)$  and  $\Xi_c(2815)$  states. Assuming that both states form a  $j_q^P = 1^-$  HQSS doublet, we could obtain the decay widths to both resonances except for a common unknown factor. This is a matrix element involving the wave functions of both  $b$  and  $c$  quarks, and it cancels out when calculating the ratios. We found that these rates showed a strong dependence on the couplings of the resonances to the  $VB$  states. Finally, predictions were made for the branching ratios of these reactions.

Overall in this Part III, *Hadrons In The Heavy Sector*, we have studied different odd parity charm and bottom resonances, using several models consistent with HQSS. We obtained some interesting results regarding the nature of the  $\Lambda_c(2595)[J^P = 1/2^-]$  and  $\Lambda_c(2625)[J^P = 3/2^-]$  states, explained several  $\Omega_c$ ,  $\Xi_c$  and  $\Xi_b$  resonances and demonstrated the importance of the coupling between  $VB$  and  $PB$  channels. Also, a detailed study of the effects of the renormalization procedure on the model-predictions was made, showing the similarities and distinctions between the schemes, justifying for which cases each of them worked the best.

Finally, in Part IV, we have studied the influence of triangle singularities (TS) in



reactions with both light and heavy hadrons. We have shown how TS can produce signatures in the observed spectra that can look like resonances, or how they can distort some properties of existing states, such as the mass position or width of the peaks. We have also shown how TS can be used to test properties of resonances, since the strength of the triangle diagram strongly depends on the resonance that appears on the lower right vertex. In Chapter 11, we have studied the  $B^- \rightarrow D^{*0} \pi^- a_0(980)$ ;  $a_0 \rightarrow \pi^0 \eta$  and  $B^- \rightarrow D^{*0} \pi^- f_0(980)$ ;  $f_0 \rightarrow \pi^+ \pi^-$  reactions. We have evaluated double mass distributions and saw clear peaks in the  $M_{\text{inv}}(\pi^0 \eta)$  and  $M_{\text{inv}}(\pi^+ \pi^-)$  invariant masses, showing clearly the  $a_0(980)$  and  $f_0(980)$  shapes. Integrating over  $M_{\text{inv}}(\pi^0 \eta)$  and  $M_{\text{inv}}(\pi^+ \pi^-)$ , we have obtained the single mass distributions,  $M_{\text{inv}}(\pi a_0)$  and  $M_{\text{inv}}(\pi f_0)$ , which show a clear peak for around 1420 MeV which is a consequence of the TS. In Chapter 12, we have studied the contributions of a triangle diagram to the  $\pi^- p \rightarrow K^0 \pi \Sigma$  and  $pp \rightarrow p K^+ \pi \Sigma$  processes. Calculating the differential cross sections for the  $\pi^- p \rightarrow K^0 \pi \Sigma$  and the  $pp \rightarrow p K^+ \pi \Sigma$  reactions, we have seen peaks around 1400 MeV for the  $\pi \Sigma$  mass distribution, produced by the  $\Lambda(1405)$ . In addition,  $\sigma_{\pi^- p \rightarrow K^0 \pi \Sigma}$  and  $\frac{d\sigma_{pp \rightarrow p K^+ \pi \Sigma}}{dM_{\text{inv}}(K^+ \pi \Sigma)}$  showed a clear peak around 2100 MeV in the  $K \pi \Sigma$  invariant mass. This signal corresponded to the position of the triangular singularity, lowered by the large influence of the initial  $N^*$  resonance, which peaks around 2030 MeV. These results could explain why in the experiments of Refs. [453, 454] the  $\Lambda(1405)$  was found at lower  $\pi \Sigma$  invariant masses than in other reactions. Finally, in Chapter 13, we have studied the isospin violating decay of  $\Lambda_c^+$  into  $\pi^+ \pi^0 \Lambda(1405)$ , which develops a triangular singularity around 1890 MeV in the  $\pi^0 \Lambda(1405)$  invariant mass distribution. We observed that a peak tied to the octet  $\Lambda(1405)$  state appears in the final  $\pi^0 \Sigma^0$  mass spectrum, showing up at higher energy than usual, close to the  $\bar{K}N$  threshold (1432 MeV). The peak was also found to be quite narrow,  $\sim 6 - 7$  MeV, and it is tied to the difference of masses between the  $K^-$  and  $\bar{K}^0$  and  $p, n$ . We have shown that the shape and strength obtained for the  $\Lambda(1405)$  are largest around a  $\pi^0 \Lambda(1405)$  invariant mass of 1890 MeV, and importantly both features are related to the nature of the  $\Lambda(1405)$  as a dynamically generated resonance from the meson-baryon interaction, in particular to its  $\bar{K}N$  component. We also found that the decay width of this reaction is within measurable range, even though it violates isospin conservation, because of the effects of the triangle singularity.

Overall, we have produced in this thesis many interesting and new results. We have studied light and heavy resonances using the extended CUA with coupled channels and testing the influence of renormalization schemes. We have described several different decays and scattering reactions, studying what the effects of dynamically generated states, HQSS, double pole structure and triangle singularities can be. We have explained many experiments and proposed interesting predictions that can be realistically tested in the near future.



**Part VI**  
**Appendices**



# Appendix A

## Some additional details for the study of the $\tau^- \rightarrow \nu_\tau M_1 M_2$ decays

### A.1 Evaluation of the matrix elements for the operators "1" and $\sigma_i$

We start from Eq. (4.32)

$$\begin{aligned} \text{ME} &= -\frac{1}{\sqrt{3}} \sum_{S_3} \sum_s (-1)^{\frac{1}{2}-s-M'} \mathcal{C} \left( \frac{1}{2} \frac{1}{2} 1; s, S_3 - s, S_3 \right) q Y_{1,-S_3}(\hat{\mathbf{q}}) \mathcal{C} \left( \frac{1}{2} \frac{1}{2} J, M - s, s, M \right) \\ &\times \mathcal{C} \left( \frac{1}{2} \frac{1}{2} J', S_3 - s, M' - S_3 + s, M' \right) \left\{ \begin{array}{l} \langle m | 1 | m' \rangle \\ \langle m | \sigma_\mu | m' \rangle \end{array} \right. \end{aligned} \quad (\text{A.1})$$

where in the case of the "1" operator we have  $m = m' = M - s$  and  $S_3 = M + M'$ , while in the case of  $\sigma_\mu$  we have  $m = M - s$ ,  $m' + \mu = m$ ,  $\mu = M - S_3 + M'$ . In the case of the operator "1" we obtain  $M_0$  and with  $\sigma_\mu, N_\mu$ .

1)  $\mathbf{M}_0$  case

$$\begin{aligned} &-\sqrt{\frac{1}{3}} \sum_s (-1)^{\frac{1}{2}-s-M'} q Y_{1,-(M+M')}(\hat{\mathbf{q}}) \mathcal{C} \left( \frac{1}{2} \frac{1}{2} J; M - s, s, M \right) \\ &\times \mathcal{C} \left( \frac{1}{2} \frac{1}{2} 1; s, M + M' - s, M + M' \right) \mathcal{C} \left( \frac{1}{2} \frac{1}{2} J'; M + M' - s, -M + s, M' \right). \end{aligned}$$

Using the permutation relations in Ref. [230]

$$\begin{aligned} &\mathcal{C} \left( \frac{1}{2} \frac{1}{2} 1; s, M + M' - s, M + M' \right) \\ &= (-1)^{\frac{1}{2}-s} \sqrt{\frac{3}{2}} \mathcal{C} \left( 1 \frac{1}{2} \frac{1}{2}; M + M', -s, M + M' - s \right), \end{aligned} \quad (\text{A.2a})$$

$$\mathcal{C}\left(\frac{1}{2}\frac{1}{2}J; M-s, s, M\right) = \mathcal{C}\left(\frac{1}{2}\frac{1}{2}J; -s, -M+s, -M\right), \quad (\text{A.2b})$$

we obtain:

$$\begin{aligned} M_0 &= -\frac{1}{\sqrt{3}}(-1)^{-M'}\sqrt{\frac{3}{2}}q Y_{1, -(M+M')}(\hat{q}) \sum_s \mathcal{C}\left(1\frac{1}{2}\frac{1}{2}; M+M', -s, M+M'-s\right) \\ &\times \mathcal{C}\left(\frac{1}{2}\frac{1}{2}J'; M+M'-s, -M+s, M'\right) \mathcal{C}\left(\frac{1}{2}\frac{1}{2}J; -s, -M+s, -M\right), \quad (\text{A.3}) \end{aligned}$$

and summing over  $s$ , keeping  $M$  fixed we obtain, using the formulas of Ref. [230],

$$\begin{aligned} M_0 &= -\frac{1}{\sqrt{2}}(-1)^{-M'}\sqrt{2(2J+1)}q Y_{1, -(M+M')}(\hat{q})\mathcal{W}\left(1\frac{1}{2}J'\frac{1}{2}; \frac{1}{2}J\right) \\ &\mathcal{C}(1JJ'; M+M', -M, M'), \quad (\text{A.4}) \end{aligned}$$

in terms of a Racah coefficient,  $\mathcal{W}(\dots)$ .

We can write this in a more symmetrical way by taking

$$\mathcal{C}(1JJ'; M+M', -M, M') = (-1)^{J-M}\sqrt{\frac{2J'+1}{3}}\mathcal{C}(JJ'1; M, M', M+M'), \quad (\text{A.5})$$

such that finally we obtain,

$$\begin{aligned} M_0 &= -(-1)^{J-(M+M')}\frac{1}{\sqrt{3}}\sqrt{(2J+1)(2J'+1)} \\ &\times \mathcal{W}\left(1\frac{1}{2}J'\frac{1}{2}; \frac{1}{2}J\right)\mathcal{C}(JJ'1; M, M', M+M')q Y_{1, -(M+M')}(\hat{q}). \quad (\text{A.6}) \end{aligned}$$

We apply it to the different  $M_1M_2$  cases:

a)  $PP$ :  $J=0, J'=0$

The CGC  $\mathcal{C}(001; \dots)$  is zero, hence:

$$M_0 = 0. \quad (\text{A.7})$$

b)  $PV$ :  $J=0, J'=1$

Using the table in the Appendix of Ref. [230] we find

$$\mathcal{W}\left(1\frac{1}{2}1\frac{1}{2}; \frac{1}{2}0\right) = -\frac{1}{\sqrt{6}}, \quad (\text{A.8})$$

and then, for any  $M'$ ,

$$M_0 = (-1)^{-M-M'}\frac{1}{\sqrt{6}}\delta_{M0}q Y_{1, -(M+M')}(\hat{q}) \quad (\text{A.9})$$

c)  $VP : J = 1, J' = 0$

Now

$$\mathcal{W} \left( 1 \frac{1}{2} 0 \frac{1}{2}; \frac{1}{2} 1 \right) = \frac{1}{\sqrt{6}}, \quad (\text{A.10})$$

and thus we get, for any  $M$ ,

$$M_0 = (-1)^{-M-M'} \frac{1}{\sqrt{6}} \delta_{M'0} q Y_{1, -(M+M')}(\hat{\mathbf{q}}) \quad (\text{A.11})$$

d)  $VV : J = 1, J' = 1$

Now

$$\mathcal{W} \left( 1 \frac{1}{2} 1 \frac{1}{2}; \frac{1}{2} 1 \right) = \frac{1}{3}, \quad (\text{A.12})$$

and thus we get

$$M_0 = (-1)^{-M-M'} \frac{1}{\sqrt{3}} \mathcal{C} (111; M, M', M+M') q Y_{1, -(M+M')}(\hat{\mathbf{q}}). \quad (\text{A.13})$$

2)  $\mathbf{N}_\mu$  case

$$\begin{aligned} N_\mu &= -\frac{1}{\sqrt{3}} \sum_s (-1)^{\frac{1}{2}-s-M'} q Y_{1, \mu-(M+M')}(\hat{\mathbf{q}}) \mathcal{C} \left( \frac{1}{2} \frac{1}{2} J; M-s, s, M \right) \\ &\quad \times \mathcal{C} \left( \frac{1}{2} \frac{1}{2} 1; s, M+M'-\mu-s, M+M'-\mu \right) \\ &\quad \times \mathcal{C} \left( \frac{1}{2} \frac{1}{2} J'; M+M'-\mu-s, -M+\mu+s, M' \right) \sqrt{3} \mathcal{C} \left( \frac{1}{2} 1 \frac{1}{2}; M-s-\mu, \mu, M-s \right) \end{aligned} \quad (\text{A.14})$$

Note that now the variable  $s$  is in the four CGC and we cannot get directly a Racah coefficient. For this we use again formulas of Ref. [230] to decompose two CGC into other two, one of which does not depend on  $s$ . First we use the permutations

$$\begin{aligned} \mathcal{C} \left( \frac{1}{2} \frac{1}{2} 1; s, M+M'-\mu-s, M+M'-\mu \right) &= (-1)^{\frac{1}{2}-s} \\ &\quad \times \sqrt{\frac{3}{2}} \mathcal{C} \left( 1 \frac{1}{2} \frac{1}{2}; M+M'-\mu, -s, M+M'-\mu-s \right), \end{aligned}$$

and

$$\mathcal{C} \left( \frac{1}{2} \frac{1}{2} J; M-s, s, M \right) = \mathcal{C} \left( \frac{1}{2} \frac{1}{2} J; -s, -M+s, -M \right),$$

and we find:

$$\begin{aligned} N_\mu &= -\frac{1}{\sqrt{3}} \sum_s (-1)^{-M'} q Y_{1, \mu-(M+M')}(\hat{\mathbf{q}}) \sqrt{\frac{3}{2}} \mathcal{C} \left( 1 \frac{1}{2} \frac{1}{2}; M+M'-\mu, -s, M+M'-\mu-s \right) \\ &\quad \times \mathcal{C} \left( \frac{1}{2} \frac{1}{2} J'; M+M'-\mu-s, -M+\mu+s, M' \right) \mathcal{C} \left( \frac{1}{2} \frac{1}{2} J; -s, -M+s, -M \right) \\ &\quad \times \sqrt{3} \mathcal{C} \left( \frac{1}{2} 1 \frac{1}{2}; M-s-\mu, \mu, M-s \right). \end{aligned} \quad (\text{A.15})$$

We can write the first two CGC as

$$\begin{aligned} & \mathcal{C}\left(\frac{1}{2}\frac{1}{2}; M+M'-\mu, -s, M+M'-\mu-s\right) \mathcal{C}\left(\frac{1}{2}\frac{1}{2}J'; M+M'-\mu-s, -M+\mu+s, M'\right) \\ &= \sum_{j''} \sqrt{2(2j''+1)} \mathcal{W}\left(\frac{1}{2}J' \frac{1}{2}; \frac{1}{2}j''\right) \mathcal{C}\left(\frac{1}{2}\frac{1}{2}j''; -s, -M+\mu+s, -M+\mu\right) \\ & \quad \times \mathcal{C}\left(1 j'' J'; M+M'-\mu, -M+\mu, M'\right). \end{aligned} \quad (\text{A.16})$$

We use again CGC permutation relations:

$$\begin{aligned} & \mathcal{C}\left(\frac{1}{2}\frac{1}{2}; M-s-\mu, \mu, M-s\right) = -\mathcal{C}\left(\frac{1}{2}\frac{1}{2}; \mu, M-s-\mu, M-s\right), \\ & \mathcal{C}\left(\frac{1}{2}\frac{1}{2}J; -s, -M+s, -M\right) = \mathcal{C}\left(\frac{1}{2}\frac{1}{2}J; M-s, s, M\right), \\ & \mathcal{C}\left(\frac{1}{2}\frac{1}{2}j''; -s, -M+\mu+s, -M+\mu\right) = \mathcal{C}\left(\frac{1}{2}\frac{1}{2}j''; M-\mu-s, s, M-\mu\right). \end{aligned} \quad (\text{A.17})$$

Then summing over  $M-\mu-s$ , keeping  $M-\mu$  fixed, we get for the sum of the three CGC to the right of Eq. (A.17) in Ref. [230]

$$\sqrt{2(2j''+1)} \mathcal{W}\left(\frac{1}{2}J \frac{1}{2}; \frac{1}{2}j''\right) \mathcal{C}\left(1j'' J; \mu, M-\mu, M\right). \quad (\text{A.18})$$

So, finally we get

$$\begin{aligned} N_\mu &= (-1)^{-M'} \sqrt{6} q Y_{1,\mu-(M+M')}(\hat{q}) \sum_{j''} (2j''+1) \mathcal{W}\left(\frac{1}{2}J \frac{1}{2}; \frac{1}{2}j''\right) \mathcal{W}\left(\frac{1}{2}J' \frac{1}{2}; \frac{1}{2}j''\right) \\ & \quad \times \mathcal{C}\left(1j'' J; \mu, M-\mu, M\right) \mathcal{C}\left(1 j'' J'; M+M'-\mu, -M+\mu, M'\right). \end{aligned} \quad (\text{A.19})$$

We apply this equation to the different  $M_1 M_2$  cases and find:

a)  $PP$  :  $J=0, J'=0$

$$\mathcal{C}\left(1j''0; \mu, M-\mu, M\right) = (-1)^{1-\mu} \sqrt{\frac{1}{2j''+1}} \mathcal{C}\left(10j''; \mu, -M, \mu-M\right) \quad (\text{A.20})$$

which implies  $M=0$ , and  $j''=1$ ,

$$\begin{aligned} & \mathcal{C}\left(1j''0; M+M'-\mu, -M+\mu, M'\right) = (-1)^{1-M-M'+\mu} \sqrt{\frac{1}{2j''+1}} \\ & \quad \times \mathcal{C}\left(10j''; M+M'-\mu, -M', M-\mu\right), \end{aligned} \quad (\text{A.21})$$

which also implies that  $M'=0$  and  $j''=1$ . The Racah coefficients are the same as in Eq. (A.10) and we finally get

$$N_\mu = \frac{1}{\sqrt{6}} q Y_{1,\mu}(\hat{q}) \delta_{M0} \delta_{M'0}. \quad (\text{A.22})$$



b)  $PV : J = 0, J' = 1$

We use Eq. (A.20) which implies  $M = 0$  and  $j'' = 1$  and then write

$$\begin{aligned} \mathcal{C}(111; M + M' - \mu, -M + \mu, M') &= (-1)^{1-M-M'+\mu} \\ &\times \mathcal{C}(111; M + M' - \mu, -M', M - \mu). \end{aligned} \quad (\text{A.23})$$

We need the Racah coefficients of Eqs. (A.10) and (A.12), and we get

$$N_\mu = (-1)^{-M} \frac{1}{\sqrt{3}} q Y_{1, \mu - (M+M')}(\hat{\mathbf{q}}) \delta_{M0} \mathcal{C}(111; M' - \mu, -M', -\mu), \quad (\text{A.24})$$

and writing the CGC as  $(-1)^{1-M'} \mathcal{C}(111; M', -\mu, M' - \mu)$  we get finally

$$N_\mu = (-1)^{1-M-M'} \frac{1}{\sqrt{3}} q Y_{1, \mu - M'}(\hat{\mathbf{q}}) \delta_{M0} \mathcal{C}(111; M', -\mu, M' - \mu). \quad (\text{A.25})$$

c)  $VP : J = 1, J' = 0$

We use

$$\begin{aligned} \mathcal{C}(1j''0; M + M' - \mu, -M + \mu, M') &= (-1)^{1-M-M'+\mu} \sqrt{\frac{1}{2j''+1}} \\ &\times \mathcal{C}(10j''; M + M' - \mu, -M', M - \mu), \end{aligned} \quad (\text{A.26})$$

which implies  $M' = 0$  and  $j'' = 1$  and using

$$\mathcal{C}(111; \mu, -M, \mu - M) = \mathcal{C}(111; M, -\mu, M - \mu)$$

we finally find

$$N_\mu = (-1)^{-M} \frac{1}{\sqrt{3}} q Y_{1, \mu - M}(\hat{\mathbf{q}}) \delta_{M'0} \mathcal{C}(111; M, -\mu, M - \mu). \quad (\text{A.27})$$

d)  $VV : J = 1, J' = 1$

We find now

$$\mathcal{W}^2 \left( 1 \frac{1}{2} 1 \frac{1}{2}; \frac{1}{2} j'' \right) = \frac{1}{36} (3 + j'')(2 - j''), \quad (\text{A.28})$$

which means that only  $j'' = 0, j'' = 1$  contribute and for  $j'' = 2$  the coefficient is zero.

i) if  $j'' = 0$  we get

$$N_\mu \rightarrow (-1)^{-M'} \frac{1}{\sqrt{6}} \delta_{M\mu} q Y_{1, \mu - (M+M')}(\hat{\mathbf{q}}). \quad (\text{A.29})$$

ii) if  $j'' = 1$  we write

$$\begin{aligned}\mathcal{C}(111; \mu, M - \mu, M) &= (-1)^{1-\mu} \mathcal{C}(111; M, -\mu, M - \mu), \\ \mathcal{C}(111; M + M' - \mu, -M + \mu, M') &= (-1)^{1-M-M'+\mu} \\ &\times \mathcal{C}(111; M', -M - M' + \mu, -M + \mu),\end{aligned}\quad (\text{A.30})$$

and then

$$\begin{aligned}N_\mu &\rightarrow (-1)^{-M} \sqrt{\frac{2}{3}} q Y_{1,\mu-(M+M')}(\hat{\mathbf{q}}) \mathcal{C}(111; M, -\mu, M - \mu) \\ &\times \mathcal{C}(111; M', -M - M' + \mu, -M + \mu),\end{aligned}\quad (\text{A.31})$$

and for the sum of  $j'' = 0, j'' = 1$  we get the final result

$$\begin{aligned}N_\mu &= \frac{1}{\sqrt{6}} q Y_{1,\mu-(M+M')}(\hat{\mathbf{q}}) \left\{ (-1)^{-M'} \delta_{M\mu} + 2(-1)^{-M} \times \mathcal{C}(111; M, -\mu, M - \mu) \right. \\ &\quad \left. \mathcal{C}(111; M', -M - M' + \mu, -M + \mu) \right\}.\end{aligned}\quad (\text{A.32})$$

## A.2 Evaluation of $\bar{\Sigma} \Sigma |t|^2$

Following the nomenclature  $\bar{L}^{\mu\nu} = \bar{\Sigma} \Sigma L^\mu L^{\nu\dagger}$  adopted before for simplicity, we have for the leptonic sector

$$\bar{L}^{\mu\nu} \equiv \bar{\Sigma} \Sigma L^\mu L^{\nu\dagger} = \frac{1}{m_\tau m_\nu} \left\{ p'^\mu p^\nu + p'^\nu p^\mu - g^{\mu\nu} (p' \cdot p) + i \epsilon^{\alpha\mu\beta\nu} p'_\alpha p_\beta \right\}. \quad (\text{A.33})$$

Thus for the leptonic plus hadronic matrix elements we have

$$\bar{\Sigma} \Sigma |t|^2 = \bar{L}^{00} M_0 M_0^* + \bar{L}^{0i} M_0 N_i^* + \bar{L}^{i0} N_i M_0^* + \bar{L}^{ij} N_i N_j^*. \quad (\text{A.34})$$

We have to take the product of these hadronic components, sum over  $M, M'$  and contract with  $\bar{L}^{\mu\nu}$ . We do that for the different  $M_1 M_2$  cases.

a)  $PP: J = 0, J' = 0$

In this case  $M_0 = 0$  and we only have to calculate  $N_i N_j^*$ .

We use Eq.(A.22) and write

$$q Y_{1,\mu}(\hat{\mathbf{q}}) = \sqrt{\frac{3}{4\pi}} q_\mu = \sqrt{\frac{3}{4\pi}} (\tilde{p}_1 - \tilde{p}_2) = \sqrt{\frac{3}{4\pi}} 2\tilde{p}_1, \quad (\text{A.35})$$

since  $\tilde{\mathbf{p}}_1$  is evaluated in the rest frame of  $M_1 M_2$ . This means that in cartesian coordinates we can write

$$N_i = \frac{1}{\sqrt{6}} \sqrt{\frac{3}{4\pi}} \delta_{M0} \delta_{M'0} 2\tilde{p}_{1i}, \quad (\text{A.36})$$

and then from Eq. (A.34):

$$\overline{\sum} \sum |t|^2 = \sum_{MM'} \frac{1}{m_\tau m_\nu} \frac{1}{2\pi} \{2p_i p_j + \delta_{ij} (\mathbf{p} \cdot \mathbf{p}')\} \tilde{p}_{1i} \tilde{p}_{1j} \delta_{M0} \delta_{M'0}, \quad (\text{A.37})$$

with

$$p_i p_j \tilde{p}_{1i} \tilde{p}_{1j} = (\mathbf{p} \cdot \tilde{\mathbf{p}}_1)^2 = (p \tilde{p}_1)^2 \cos^2 \theta \rightarrow \frac{1}{3} (p \tilde{p}_1)^2, \quad (\text{A.38})$$

where the last step comes from the integral over  $\cos^2 \theta$ . We replace  $\cos^2 \theta$  by  $1/3$  and put the whole phase space later independent on the angles. Then we get, including the weight  $\bar{h}_i$  for the  $N_i$  term

$$\overline{\sum} \sum |t|^2 = \frac{1}{m_\tau m_\nu} \frac{1}{2\pi} \left( E_\tau E_\nu - \frac{1}{3} \mathbf{p}^2 \right) \tilde{p}_1^2 \bar{h}_i^2, \quad (\text{A.39})$$

with

$$\tilde{p}_1 = \frac{\lambda^{1/2} (M_{\text{inv}}^2(M_1 M_2), M_1^2, M_2^2)}{2M_{\text{inv}}(M_1 M_2)}, \quad (\text{A.40})$$

and  $p$  given in Eq. (4.44),

$$p = \frac{\lambda^{1/2} (m_\tau^2, m_\nu^2, M_{\text{inv}}^2(M_1 M_2))}{2M_{\text{inv}}(M_1 M_2)}. \quad (\text{A.41})$$

In Eq. (A.39) and what follows  $E_\tau$ ,  $E_\nu$  are also calculated in the  $M_1 M_2$  rest frame,  $E_\tau = \sqrt{m_\tau^2 + p^2}$ ,  $E_\nu = p$ .

The  $e^{\alpha i \beta j} \tilde{p}_{1i} \tilde{p}_{1j}$  is zero. This term does not contribute in any case, but in some cases the cancellation comes from different terms in the sum over  $M, M'$ . The cancellation of this term when summing over polarizations in semileptonic decays was already found in [253, 442] and we do not elaborate on it further here.

b)  $PV : J = 0, J' = 1$

Now we have

$$M_0 = (-1)^{-M'} \frac{1}{\sqrt{6}} \delta_{M0} q Y_{1,-M'}(\hat{\mathbf{q}}), \quad (\text{A.42a})$$

$$N_\mu = (-1)^{1-M'} \frac{1}{\sqrt{3}} \delta_{M0} q Y_{1,\mu-M'}(\hat{\mathbf{q}}) \mathcal{C}(111; M', -\mu, M' - \mu). \quad (\text{A.42b})$$

First let us see that the  $M_0 N_\mu$  components do not contribute. Indeed we find in the phase space integration

$$\begin{aligned} & \sum_{M'} \int d\Omega Y_{1,-M'} Y_{1,\mu-M'}^* \mathcal{C}(111; M', -\mu, M' - \mu) \\ & = \delta_{\mu 0} \sum_{M'} \mathcal{C}(111; M', -\mu, M' - \mu) = 0. \end{aligned} \quad (\text{A.43})$$

This is again the case also in  $VP$  and  $VV$  and we do not discuss it further.

Thus, we have contributions from:

i)  $M_0 M_0^*$

$$M_0 M_0^* = \frac{1}{6} \delta_{M_0} Y_{1,-M'}(\hat{\mathbf{q}}) Y_{1,-M'}^*(\hat{\mathbf{q}}) q^2. \quad (\text{A.44})$$

In the phase space calculation we shall have

$$\int d\Omega Y_{1,-M'}(\hat{\mathbf{q}}) Y_{1,-M'}^*(\hat{\mathbf{q}}) = 1, \quad (\text{A.45})$$

and then we replace  $Y_1 Y_1^*$  by  $\frac{1}{4\pi}$  evaluating later the phase space for an angle independent amplitude. Thus summing over  $M'$  ( $M = 0$ ) we get

$$\sum_{MM'} M_0 M_0^* = \frac{1}{6} \frac{1}{4\pi} 4\tilde{p}_1^2 \cdot 3 = \frac{1}{2\pi} \tilde{p}_1^2, \quad (\text{A.46})$$

which multiplied by  $\bar{L}^{00}$  gives

$$\bar{\Sigma} \sum |t|^2 = \frac{1}{m_\tau m_\nu} (\mathbf{E}_\tau \mathbf{E}_\nu + \mathbf{p}^2) \frac{1}{2\pi} \tilde{p}_1^2. \quad (\text{A.47})$$

ii)  $\bar{L}^{ij} N_i N_j^*$  For simplicity of the calculation we take  $\mathbf{p}$  in the  $z$  direction. Then

$$\bar{L}^{ij} N_i N_j^* = \frac{1}{m_\tau m_\nu} \left( 2p^2 \delta_{i3} \delta_{j3} N_i N_j^* + (p \cdot p') N_i N_i^* \right), \quad (\text{A.48})$$

but one can see that

$$\sum N_i N_i^* = \sum_\mu N_\mu N_\mu^*. \quad (\text{A.49})$$

Then, from Eq. (A.25)

$$\begin{aligned} \sum_{M,M'} \sum_\mu N_\mu N_\mu^* & = \sum_{M'} \sum_\mu \frac{1}{4\pi} \frac{1}{3} q^2 \int Y_{1,\mu-M'}(\hat{\mathbf{q}}) Y_{1,\mu-M'}^*(\hat{\mathbf{q}}) d\Omega \\ & \quad \times \mathcal{C}(111; M', -\mu, M' - \mu)^2 \\ & = \sum_{\mu,M'} \frac{1}{4\pi} \frac{1}{3} 4\tilde{p}_1^2 \mathcal{C}(111; M', -\mu, M' - \mu)^2 \\ & = \sum_{\mu,M'} \frac{1}{3} \frac{1}{4\pi} \mathcal{C}(111; M', \mu - M', \mu)^2 4\tilde{p}_1^2 = \sum_\mu \frac{1}{4\pi} \frac{4}{3} \tilde{p}_1^2 = \frac{1}{\pi} \tilde{p}_1^2. \end{aligned} \quad (\text{A.50})$$

On the other hand for  $i = 3$ ,  $N_i \equiv N_{\mu=0}$ , and again

$$\begin{aligned} & \sum_{M'} \frac{1}{4\pi} \frac{1}{3} q^2 \int Y_{1,-M'}(\hat{\mathbf{q}}) Y_{1,-M'}^*(\hat{\mathbf{q}}) d\Omega \mathcal{C}(111; M', 0, M')^2 \\ &= \frac{1}{4\pi} \frac{1}{3} 4\tilde{p}_1^2 \sum_{M'} \mathcal{C}(111; M', -M', 0)^2 = \frac{1}{3\pi} \tilde{p}_1^2, \end{aligned} \quad (\text{A.51})$$

and we find for this term

$$\overline{\sum} \sum |t|^2 = \frac{1}{m_\nu m_\tau \pi} \frac{1}{\tilde{p}_1^2} \left( \mathbf{E}_\tau \mathbf{E}_\nu - \frac{1}{3} \mathbf{p}^2 \right). \quad (\text{A.52})$$

Recalling that we have different weights for  $M_0$  and  $N_i$  in each channel we sum the two terms of Eqs. (A.47) and (A.52) to give

$$\overline{\sum} \sum |t|^2 = \frac{1}{m_\tau m_\nu} \frac{1}{2\pi} \tilde{p}_1^2 \left\{ h_i^2 (\mathbf{E}_\tau \mathbf{E}_\nu \mathbf{p}^2) + \bar{h}_i^2 2 \left( \mathbf{E}_\tau \mathbf{E}_\nu - \frac{1}{3} \mathbf{p}^2 \right) \right\}. \quad (\text{A.53})$$

c)  $VP: J = 1, J' = 0$

The evaluation proceeds as before and we obtain the same result.

d)  $VV: J = 1, J' = 1$

From Eqs. (A.13) and (A.32) we have

$$M_0 = (-1)^{-M-M'} \frac{1}{\sqrt{3}} \mathcal{C}(111; M, M', M+M') q Y_{1,-(M+M')}(\hat{\mathbf{q}}), \quad (\text{A.54a})$$

$$\begin{aligned} N_\nu = & \frac{1}{\sqrt{6}} q Y_{1,\mu-(M+M')}(\hat{\mathbf{q}}) \left\{ (-1)^{-M'} \delta_{M\mu} + 2(-1)^{-M} \mathcal{C}(111; M, -\mu, M-\mu) \right. \\ & \left. \times \mathcal{C}(111; M', -M-M'+\mu, -M+\mu) \right\}. \end{aligned} \quad (\text{A.54b})$$

i)  $M_0 M_0^*$

$$\frac{1}{4\pi} \int d\Omega Y_{1,-(M+M')}(\hat{\mathbf{q}}) Y_{1,-(M+M')}^*(\hat{\mathbf{q}}) = \frac{1}{4\pi}, \quad (\text{A.55a})$$

$$\sum_{M, M'} \mathcal{C}(111; M, M', M+M')^2 = \sum_{M, M'} \mathcal{C}(111; M, -M'-M, -M')^2 = \sum_{M'} 1 = 3. \quad (\text{A.55b})$$

Then we get for this term

$$\overline{\sum} \sum |t|^2 = \frac{1}{m_\tau m_\nu \pi} (\mathbf{E}_\tau \mathbf{E}_\nu + \mathbf{p}^2) \tilde{p}_1^2. \quad (\text{A.56})$$

ii)  $\bar{L}^{ij}N_iN_j^*$

We get again in the frame where  $\mathbf{p}$  is in the  $z$  direction

$$\frac{1}{m_\tau m_\nu} \{2\mathbf{p}^2 \delta_{i3} \delta_{j3} + \delta_{ij}(\mathbf{p} \cdot \mathbf{p}')\} N_i N_j^* = \frac{1}{m_\tau m_\nu} \left\{ 2\mathbf{p}^2 N_0 N_0^* + (E_\tau E_\nu - \mathbf{p}^2) \sum_\mu N_\mu N_\mu^* \right\} \quad (\text{A.57})$$

$$\begin{aligned} N_0 N_0^* \rightarrow \frac{1}{6} q^2 \frac{1}{4\pi} \int d\Omega Y_{1,-(M+M')}(\hat{\mathbf{q}}) Y_{1,-(M+M')}^*(\hat{\mathbf{q}}) \left\{ (-1)^{-M'} \delta_{M0} + 2(-1)^{-M} \right. \\ \left. \times \mathcal{C}(111; M, 0, M) \mathcal{C}(111; M', -M - M', -M) \right\} \left\{ (-1)^{-M'} \delta_{M0} \right. \\ \left. + 2(-1)^{-M} \mathcal{C}(111; M, 0, M) \mathcal{C}(111; M', -M - M', -M) \right\}. \end{aligned} \quad (\text{A.58})$$

Now for the  $\delta_{M0} \delta_{M0}$  term we have

$$\sum_{M'} \delta_{M0} \delta_{M0} = 3. \quad (\text{A.59})$$

For the crossed term in Eq. (A.58),  $\delta_{M0} \mathcal{C}(\dots) \mathcal{C}(\dots)$ , we have

$$\delta_{M0} \mathcal{C}(111; M, 0, M) = \mathcal{C}(111; 0, 0, 0) = 0. \quad (\text{A.60})$$

The last term in Eq. (A.58) involves

$$\sum_M \mathcal{C}(111; M, 0, M)^2 \sum_{M'} \mathcal{C}(111; M', -M - M', -M)^2 = 1. \quad (\text{A.61})$$

Hence, altogether the  $N_0 N_0^*$  contribution is

$$\bar{\sum} \sum |t|^2 = \frac{7}{6} \frac{1}{\pi} \tilde{p}_1^2. \quad (\text{A.62})$$

Next we must evaluate  $\sum_\mu N_\mu N_\mu^*$

$$\begin{aligned} \sum_\mu N_\mu N_\mu^* = \frac{1}{6} q^2 \frac{1}{4\pi} \int d\Omega Y_{1,\mu-(M+M')}(\hat{\mathbf{q}}) Y_{1,\mu-(M+M')}^*(\hat{\mathbf{q}}) \sum_\mu \left\{ (-1)^{-M'} \delta_{M\mu} \right. \\ \left. + 2(-1)^{-M} \mathcal{C}(111; M, -\mu, M - \mu) \mathcal{C}(111; M', -M - M' + \mu, -M + \mu) \right\} \\ \times \left\{ (-1)^{-M'} \delta_{M\mu} + 2(-1)^{-M} \mathcal{C}(111; M, -\mu, M - \mu) \right. \\ \left. \times \mathcal{C}(111; M', -M - M' + \mu, -M + \mu) \right\}. \end{aligned} \quad (\text{A.63})$$

The first term involves

$$\sum_{\mu} \delta_{M\mu} \delta_{M\mu} = \delta_{MM}, \quad (\text{A.64a})$$

$$\sum_{M, M'} \delta_{MM} = 9. \quad (\text{A.64b})$$

The crossed term involves

$$\sum_{M'} (-1)^{M'} \mathcal{C}(111; M', -M', 0) = 0, \quad (\text{A.65})$$

and vanishes, and the product of the second terms in Eq. (A.63) gives

$$\begin{aligned} \sum_{M, M'} \frac{1}{6} q^2 \frac{1}{4\pi} \int d\Omega Y_{1, \mu - (M+M')}(\hat{\mathbf{q}}) Y_{1, \mu - (M+M')}^*(\hat{\mathbf{q}}) 4 \sum_{\mu} \mathcal{C}(111; M, -\mu, M - \mu)^2 \\ \times \mathcal{C}(111; M', -M - M' + \mu, -M + \mu)^2. \end{aligned} \quad (\text{A.66})$$

Fixing  $M - \mu$  the sum over  $M$ , and  $M'$  of the CGC coefficients gives 1, and then

$$\sum_{M - \mu} 1 = 3, \quad (\text{A.67})$$

and we get altogether for  $\bar{L}^{ij} N_i N_j^*$ ,

$$\bar{\sum} \sum |t|^2 \rightarrow \frac{1}{m_{\tau} m_{\nu}} \frac{7}{2} \tilde{p}_1^2 \frac{1}{\pi}. \quad (\text{A.68})$$

Summing the  $N_0 N_0^*$  and  $N_{\mu} N_{\mu}^*$  terms we find

$$\begin{aligned} \bar{\sum} \sum |t|^2 &= \frac{1}{m_{\tau} m_{\nu}} \frac{1}{\pi} \tilde{p}_1^2 \left\{ 2 \mathbf{p}^2 \frac{7}{6} + (E_{\tau} E_{\nu} - \mathbf{p}^2) \frac{7}{2} \right\} \\ &= \frac{1}{m_{\tau} m_{\nu}} \frac{1}{\pi} \tilde{p}_1^2 \frac{7}{2} \left\{ E_{\tau} E_{\nu} - \frac{1}{3} \mathbf{p}^2 \right\}, \end{aligned} \quad (\text{A.69})$$

and finally, considering the weights for the  $M_0$  and  $N_i$  parts we get

$$\bar{\sum} \sum |t|^2 = \frac{1}{m_{\tau} m_{\nu}} \frac{1}{\pi} \tilde{p}_1^2 \left\{ h_i^2 \left[ E_{\tau} E_{\nu} + \mathbf{p}^2 \right] + \frac{7}{2} \bar{h}_i^2 \left[ E_{\tau} E_{\nu} - \frac{1}{3} \mathbf{p}^2 \right] \right\}. \quad (\text{A.70})$$





## Appendix B

### Spin 1/2 and 3/2 $N^*$ contributions to the $K^* \Sigma \rightarrow K^* \Sigma$ and $\pi N \rightarrow K^* \Sigma$ reactions

For  $K^* \Sigma \rightarrow K^* \Sigma$ , we have the contribution from vector exchange in Ref. [139] as shown in Fig. B.1. The contribution close to the resonance pole is given by

$$t_{K^* \Sigma, K^* \Sigma} = \frac{g_{K^* \Sigma}^2}{\sqrt{s} - M_R + i\Gamma_R/2} \vec{\epsilon} \cdot \vec{\epsilon}' \equiv t_R \vec{\epsilon} \cdot \vec{\epsilon}', \quad (\text{B.1})$$

where  $\vec{\epsilon}$  and  $\vec{\epsilon}'$  are the polarization vectors of the initial and final vectors. This amplitude contains both spin 1/2 and 3/2. It is easy to split this in spin 1/2 and 3/2. We can write symbolically the amplitude of Fig. B.1 as in Fig. B.2. We can write the vertices corresponding to Fig. B.3 as

$$\tilde{t}_{K^* \Sigma}^{(1/2)} = \frac{1}{\sqrt{3}} g_{K^* \Sigma} \vec{\sigma} \cdot \vec{\epsilon}, \quad (\text{B.2})$$

$$\tilde{t}_{K^* \Sigma}^{(3/2)} = g_{K^* \Sigma} \vec{S} \cdot \vec{\epsilon}, \quad (\text{B.3})$$

where  $\vec{S}$  is the transition operator from spin 3/2 to 1/2, with the properties,

$$\sum_{m_s} \sigma_i |m_s\rangle \langle m_s| \sigma_j = \delta_{ij} + i\epsilon_{ijk} \sigma_k, \quad (\text{B.4})$$

$$\sum_{M_s} S_i |M_s\rangle \langle M_s| S_j^\dagger = \frac{2}{3} \delta_{ij} - \frac{i}{3} \epsilon_{ijk} \sigma_k. \quad (\text{B.5})$$

Each of these operators projects the amplitude of Fig. B.2 over spin 1/2 and 3/2

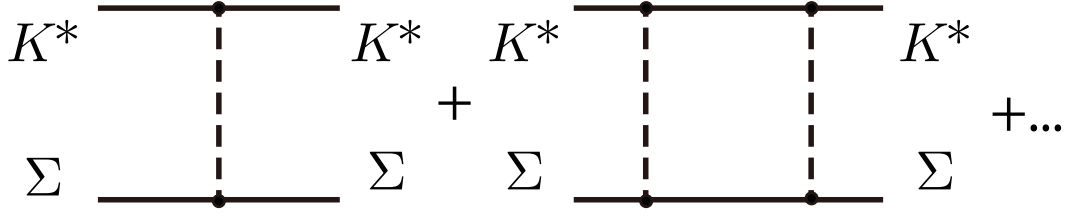
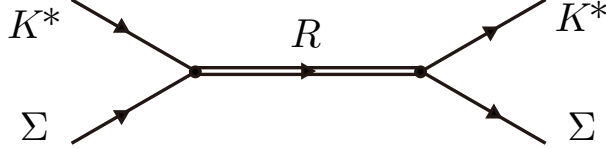

 Figure B.1: Source of  $K^*\Sigma \rightarrow K^*\Sigma$  interaction through vector exchange.


Figure B.2: Representation of Fig. B.1 in terms of the resonance generated by the mechanism of Fig. B.1.

respectively and we have

$$\begin{aligned} t_R^{(1/2+3/2)} &= t_R \left\{ \frac{1}{3} \vec{\sigma} \cdot \vec{\epsilon} \vec{\sigma} \cdot \vec{\epsilon}' + \vec{S} \cdot \vec{\epsilon} \vec{S}^\dagger \cdot \vec{\epsilon}' \right\} \\ &= t_R \vec{\epsilon} \cdot \vec{\epsilon}', \end{aligned} \quad (\text{B.6})$$

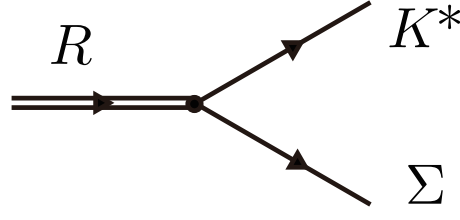
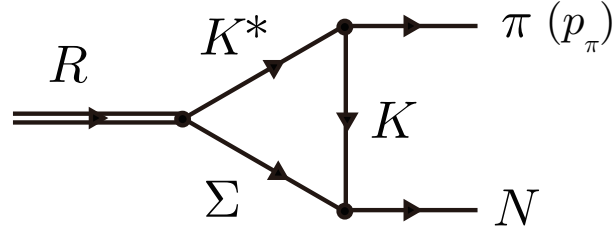
which gives us the proper separation of the amplitude of Fig. B.2 into its spin 1/2 and 3/2 parts. Using the vertices of Eqs. (B.2) and (B.3) it is easy to see that

$$\overline{\Sigma} \Sigma \left| \tilde{t}_{K^*\Sigma}^{(1/2)} \right|^2 = \overline{\Sigma} \Sigma \left| \tilde{t}_{K^*\Sigma}^{(3/2)} \right|^2 = g_{K^*\Sigma}^2, \quad (\text{B.7})$$

which means that by using the form of Eq. (B.1) one has the same width of  $R \rightarrow K^*\Sigma$  for  $J = 1/2$  and  $J = 3/2$  and one can use the coupling  $g_{K^*\Sigma}$  for either case ignoring the spin variables, as done in Ref. [139].

The coupling to  $\pi N$  proceeds via the loop shown in Fig. B.4 [139, 297]. We are only concerned about the ratio between  $J = 1/2$  and  $3/2$ , and thus, we assume the loop of Fig. B.4 dominated by the on shell intermediate  $K^*\Sigma$ . In the limit of small  $K^*$  momentum and separating the product of the  $K^* \rightarrow K\pi$  and  $\Sigma K \rightarrow N$  vertices into  $s$ - and  $d$ -waves (we remove the factor 2 from  $\vec{\epsilon} \cdot (\vec{p}_\pi - \vec{p}_K) = 2\vec{\epsilon} \cdot \vec{p}_\pi$ , for simplicity), we find

$$\vec{\epsilon} \cdot \vec{p}_\pi \vec{\sigma} \cdot \vec{p}_\pi = \epsilon_i \sigma_j \frac{|\vec{p}_\pi|^2}{3} \delta_{ij} + \epsilon_i \sigma_j \left( p_{\pi i} p_{\pi j} - \frac{|\vec{p}_\pi|^2}{3} \delta_{ij} \right), \quad (\text{B.8})$$

Figure B.3: Effective  $R \rightarrow K^* \Sigma$  vertex.Figure B.4: Effective mechanism for  $R \rightarrow \pi N$ .

the couplings of the  $\pi N$  to  $N^*$  with  $J = 1/2$  and  $3/2$  are given by

$$\begin{aligned} \bar{t}_{\pi N}^{(1/2)} &= \sum_{K^* \text{ pol.}} \frac{\tilde{g}}{3} |\vec{p}_\pi|^2 \vec{\sigma} \cdot \vec{\epsilon} \frac{g_{K^* \Sigma}}{\sqrt{3}} \vec{\sigma} \cdot \vec{\epsilon} = \frac{\tilde{g} g_{K^* \Sigma}}{3\sqrt{3}} |\vec{p}_\pi|^2 \vec{\sigma} \cdot \vec{\sigma} \\ &= \frac{1}{\sqrt{3}} \tilde{g} g_{K^* \Sigma} |\vec{p}_\pi|^2; \text{ for } J = 1/2, \end{aligned} \quad (\text{B.9})$$

$$\begin{aligned} \bar{t}_{\pi N}^{(3/2)} &= \sum_{K^* \text{ pol.}} \tilde{g} \epsilon_i \sigma_j \left( p_{\pi i} p_{\pi j} - \frac{1}{3} |\vec{p}_\pi|^2 \delta_{ij} \right) g_{K^* \Sigma} \vec{S} \cdot \vec{\epsilon} \\ &= \tilde{g} g_{K^* \Sigma} \sigma_j S_i \left( p_{\pi i} p_{\pi j} - \frac{1}{3} |\vec{p}_\pi|^2 \delta_{ij} \right); \text{ for } J = 3/2. \end{aligned} \quad (\text{B.10})$$

Next, we look at the  $\pi N \rightarrow K^* \Sigma$  transition of Fig. B.5 and we have

$$\begin{aligned} \bar{t}_{\pi N, K^* \Sigma}^{(1/2)} &= \frac{g_{K^* \Sigma}}{\sqrt{3}} \vec{\sigma} \cdot \vec{\epsilon} \frac{1}{\sqrt{s} - M_R + i\Gamma_R/2} \frac{\tilde{g} g_{K^* \Sigma}}{\sqrt{3}} |\vec{p}_\pi|^2 \\ &\equiv \frac{\tilde{g}}{3} \vec{\sigma} \cdot \vec{\epsilon} |\vec{p}_\pi|^2 t_R, \end{aligned} \quad (\text{B.11})$$

$$\begin{aligned} \bar{t}_{\pi N, K^* \Sigma}^{(3/2)} &= g_{K^* \Sigma} \vec{S} \cdot \vec{\epsilon} \frac{1}{\sqrt{s} - M_R + i\Gamma_R/2} \\ &\quad \cdot \tilde{g} g_{K^* \Sigma} S_i^\dagger \sigma_j \left( p_{\pi i} p_{\pi j} - \frac{1}{3} |\vec{p}_\pi|^2 \delta_{ij} \right) \\ &= \tilde{g} \left( \vec{\sigma} \cdot \vec{p}_\pi \vec{\epsilon} \cdot \vec{p}_\pi - \frac{1}{3} |\vec{p}_\pi|^2 \vec{\sigma} \cdot \vec{\epsilon} \right) t_R. \end{aligned} \quad (\text{B.12})$$

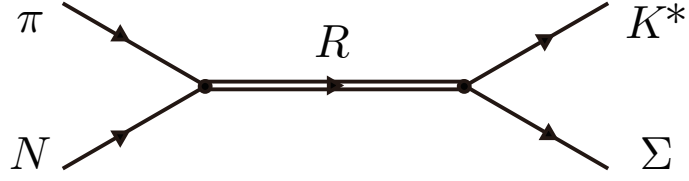


Figure B.5: Mechanism for  $\pi N \rightarrow K^* \Sigma$  combining the vertices of Figs. B.2 and B.4.

In the coupling  $\tilde{g}$  we have included for convenience the result that would come from the loop integration of Fig. B.4, which is common to  $J = 1/2$  and  $J = 3/2$ .

We can sum Eqs. (B.11) and (B.12) to account for both the spin 1/2 and 3/2 (if one adds incoherently the cross sections one obtains the same result, because spin 1/2 and 3/2 do not interfere) and we get

$$\bar{t}_{\pi N, K^* \Sigma}^{(1/2+3/2)} = \tilde{g} \vec{\sigma} \cdot \vec{p}_\pi \vec{\epsilon} \cdot \vec{p}_\pi t_R. \quad (\text{B.13})$$

Since in the scattering  $\vec{p}_\pi$  is in the  $z$  direction we can write

$$\bar{t}_{\pi N, K^* \Sigma}^{(1/2+3/2)} = \tilde{g} |\vec{p}_\pi|^2 \sigma_3 \epsilon_3 t_R. \quad (\text{B.14})$$

In the triangle loop of Fig. 12.1,  $\epsilon_3 \rightarrow k_3$  and then we get a factor  $\sigma_3 k_3$  instead of  $\vec{\sigma} \cdot \vec{k}/3$  using Eq. (B.11) for  $J = 1/2$ .

# Bibliography

- [1] L. R. Dai, R. Pavao, S. Sakai, and E. Oset.  $\tau^- \rightarrow \nu_\tau M_1 M_2$ , with  $M_1, M_2$  pseudoscalar or vector mesons. Eur. Phys. J., A55(2):20, 2019.
- [2] R. Pavao, S. Sakai, and E. Oset. Production of  $N^*(1535)$  and  $N^*(1650)$  in  $\Lambda_c \rightarrow \bar{K}^0 \eta p$  ( $\pi N$ ) decay. Phys. Rev., C98(1):015201, 2018.
- [3] J. Nieves, R. Pavao, and S. Sakai.  $\Lambda_b$  decays into  $\Lambda_c^* \ell \bar{\nu}_\ell$  and  $\Lambda_c^* \pi^-$  [ $\Lambda_c^* = \Lambda_c(2595)$  and  $\Lambda_c(2625)$ ] and heavy quark spin symmetry. Eur. Phys. J., C79(5):417, 2019.
- [4] Juan Nieves and Rafael Pavao. Nature of the lowest-lying odd parity charmed baryon  $\Lambda_c(2595)$  and  $\Lambda_c(2625)$  resonances. Phys. Rev., D101(1):014018, 2020.
- [5] Q. X. Yu, R. Pavao, V. R. Debastiani, and E. Oset. Description of the  $\Xi_c$  and  $\Xi_b$  states as molecular states. Eur. Phys. J., C79(2):167, 2019.
- [6] J. Nieves, R. Pavao, and L. Tolos.  $\Omega_c$  excited states within a  $SU(6)_{\text{lsf}} \times \text{HQSS}$  model. Eur. Phys. J., C78(2):114, 2018.
- [7] J. Nieves, R. Pavao, and L. Tolos.  $\Xi_c$  and  $\Xi_b$  excited states within a  $SU(6)_{\text{lsf}} \times \text{HQSS}$  model. Eur. Phys. J., C80(1):22, 2020.
- [8] R.P. Pavao, W.H. Liang, J. Nieves, and E. Oset. Predictions for  $\Xi_b^- \rightarrow \pi^- (D_s^-) \Xi_c^0(2790) (\Xi_c^0(2815))$  and  $\Xi_b^- \rightarrow \bar{\nu}_l l \Xi_c^0(2790) (\Xi_c^0(2815))$ . Eur.Phys.J., C77:265, 2017.
- [9] R. Pavao, S. Sakai, and E. Oset. Triangle singularities in  $B^- \rightarrow D^{*0} \pi^- \pi^0 \eta$  and  $B^- \rightarrow D^{*0} \pi^- \pi^+ \pi^-$ . Eur.Phys.J., C77:599, 2017.
- [10] M. Bayar, R. Pavao, S. Sakai, and E. Oset. Role of the triangle singularity in  $\Lambda(1405)$  production in the  $\pi^- p \rightarrow K^0 \pi \Sigma$  and  $pp \rightarrow p K^+ \pi \Sigma$  processes. Phys.Rev., C97:035203, 2018.

- [11] L. R. Dai, R. Pavao, S. Sakai, and E. Oset. Anomalous enhancement of the isospin-violating  $\Lambda(1405)$  production by a triangle singularity in  $\Lambda_c \rightarrow \pi^+ \pi^0 \pi^0 \Sigma^0$ . Phys. Rev., D97(11):116004, 2018.
- [12] A. Pich. Chiral perturbation theory. Rept.Prog.Phys., 58:563–610, 1995.
- [13] Feng-Kun Guo, Christoph Hanhart, Ulf-G. Meissner, Qian Wang, Qiang Zhao, and Bing-Song Zou. Hadronic molecules. Rev. Mod. Phys., 90(1):015004, 2018.
- [14] R. Blankenbecler, M. L. Goldberger, S. W. MacDowell, and S. B. Treiman. Singularities of scattering amplitudes on unphysical sheets and their interpretation. Phys. Rev., 123:692–699, Jul 1961.
- [15] S. Godfrey and Nathan Isgur. Mesons in a Relativized Quark Model with Chromodynamics. Phys.Rev., D32:189–231, 1985.
- [16] Simon Capstick and Nathan Isgur. Baryons in a Relativized Quark Model with Chromodynamics. Phys.Rev., D34:2809, 1986.
- [17] A. Cerri et al. Opportunities in Flavour Physics at the HL-LHC and HE-LHC. 2018.
- [18] Murray Gell-Mann. Symmetries of baryons and mesons. Phys. Rev., 125:1067–1084, 1962.
- [19] Murray Gell-Mann. A Schematic Model of Baryons and Mesons. Phys. Lett., 8:214–215, 1964.
- [20] George Zweig. Two Topics in Elementary Particle Physics. Caltech, 1964.
- [21] M. Tanabashi et al. Review of Particle Physics. Phys. Rev., D98(3):030001, 2018.
- [22] Miguel Albaladejo, Pedro Fernandez-Soler, Juan Nieves, and Pablo G. Ortega. Contribution of constituent quark model  $c\bar{s}$  states to the dynamics of the  $D_{s0}^*(2317)$  and  $D_{s1}(2460)$  resonances. Eur. Phys. J., C78(9):722, 2018.
- [23] Stanley M. Flatte. Coupled - Channel Analysis of the pi eta and K anti-K Systems Near K anti-K Threshold. Phys. Lett., 63B:224–227, 1976.
- [24] Tetsuo Hyodo and Daisuke Jido. The nature of the  $\Lambda(1405)$  resonance in chiral dynamics. Prog. Part. Nucl. Phys., 67:55–98, 2012.
- [25] Yan-Rui Liu, Hua-Xing Chen, Wei Chen, Xiang Liu, and Shi-Lin Zhu. Pentaquark and Tetraquark states. Prog. Part. Nucl. Phys., 107:237–320, 2019.

- [26] Nathan Isgur and Gabriel Karl. P Wave Baryons in the Quark Model. Phys.Rev., D18:4187, 1978.
- [27] R.H. Dalitz and S.F. Tuan. A possible resonant state in pion-hyperon scattering. Phys.Rev.Lett., 2:425–428, 1959.
- [28] R.H. Dalitz and S.F. Tuan. The phenomenological description of K-nucleon reaction processes. Annals Phys., 10:307–351, 1960.
- [29] R.H. Dalitz, T.C. Wong, and G. Rajasekaran. Model calculation for  $Y^*(0)$  (1405) resonance state. Phys.Rev., 153:1617–1623, 1967.
- [30] Norbert Kaiser, P.B. Siegel, and W. Weise. Chiral dynamics and the low-energy kaon - nucleon interaction. Nucl.Phys., A594:325–345, 1995.
- [31] E. Oset and A. Ramos. Nonperturbative chiral approach to s wave anti-K N interactions. Nucl. Phys., A635:99–120, 1998.
- [32] J.A. Oller and Ulf G. Meissner. Chiral dynamics in the presence of bound states: Kaon nucleon interactions revisited. Phys.Lett., B500:263–272, 2001.
- [33] M. F. M. Lutz and E. E. Kolomeitsev. Relativistic chiral  $SU(3)$  symmetry, large  $N(c)$  sum rules and meson baryon scattering. Nucl. Phys., A700:193–308, 2002.
- [34] C. Garcia-Recio, J. Nieves, E. Ruiz Arriola, and M.J. Vicente Vacas.  $S = -1$  meson baryon unitarized coupled channel chiral perturbation theory and the  $S(01)$   $\Lambda(1405)$  and  $\Lambda(1670)$  resonances. Phys.Rev., D67:076009, 2003.
- [35] D. Jido, J.A. Oller, E. Oset, A. Ramos, and U.G. Meissner. Chiral dynamics of the two  $\Lambda(1405)$  states. Nucl.Phys., A725:181–200, 2003.
- [36] B. Borasoy, R. Nissler, and W. Weise. Chiral dynamics of kaon-nucleon interactions, revisited. Eur.Phys.J., A25:79–96, 2005.
- [37] Yoichi Ikeda, Tetsuo Hyodo, Daisuke Jido, Hiroyuki Kamano, Toru Sato, and Koichi Yazaki. Structure of  $\Lambda(1405)$  and threshold behavior of  $\pi\Sigma$  scattering. Prog.Theor.Phys., 125:1205–1224, 2011.
- [38] Yoichi Ikeda, Tetsuo Hyodo, and Wolfram Weise. Chiral  $SU(3)$  theory of antikaon-nucleon interactions with improved threshold constraints. Nucl.Phys., A881:98–114, 2012.

- [39] Zhi-Hui Guo and J.A. Oller. Meson-baryon reactions with strangeness -1 within a chiral framework. Phys.Rev., C87:035202, 2013.
- [40] A. Feijoo, V.K. Magas, and A. Ramos. The  $\bar{K}N \rightarrow K\Xi$  reaction in coupled channel chiral models up to next-to-leading order. Phys.Rev., C92:015206, 2015.
- [41] Maxim Mai and Ulf-G. Meißner. Constraints on the chiral unitary  $\bar{K}N$  amplitude from  $\pi\Sigma K^+$  photoproduction data. Eur.Phys.J., A51:30, 2015.
- [42] Jonathan M. M. Hall et al. Lattice QCD Evidence that the  $\Lambda(1405)$  Resonance is an Antikaon-Nucleon Molecule. Phys.Rev.Lett., 114:132002, 2015.
- [43] R. Molina and M. Döring. Pole structure of the  $\Lambda(1405)$  in a recent QCD simulation. Phys.Rev., D94:056010, 2016.
- [44] Takayasu Sekihara, Tetsuo Hyodo, and Daisuke Jido. Comprehensive analysis of the wave function of a hadronic resonance and its compositeness. PTEP, 2015:063D04, 2015.
- [45] Zhi-Hui Guo and J.A. Oller. Probabilistic interpretation of compositeness relation for resonances. Phys.Rev., D93:096001, 2016.
- [46] Yuki Kamiya and Tetsuo Hyodo. Structure of near-threshold quasibound states. Phys.Rev., C93:035203, 2016.
- [47] T. Sekihara, T. Hyodo, and D. Jido. Electromagnetic mean squared radii of  $\Lambda(1405)$  in chiral dynamics. Phys.Lett., B669:133–138, 2008.
- [48] Kenta Miyahara and Tetsuo Hyodo. Structure of  $\Lambda(1405)$  and construction of  $\bar{K}N$  local potential based on chiral SU(3) dynamics. Phys.Rev., C93:015201, 2016.
- [49] J.C. Nacher, E. Oset, H. Toki, and A. Ramos. Photoproduction of the  $\Lambda(1405)$  on the proton and nuclei. Phys.Lett., B455:55–61, 1999.
- [50] J.C. Nacher, E. Oset, H. Toki, and A. Ramos. Radiative production of the  $\Lambda(1405)$  resonance in K- collisions on protons and nuclei. Phys.Lett., B461:299–306, 1999.
- [51] B. Borasoy, P.C. Bruns, Ulf-G. Meissner, and R. Nissler. A Gauge invariant chiral unitary framework for kaon photo- and electroproduction on the proton. Eur.Phys.J., A34:161–183, 2007.



- [52] L. Roca and E. Oset.  $\Lambda(1405)$  poles obtained from  $\pi^0\Sigma^0$  photoproduction data. Phys.Rev., C87:055201, 2013.
- [53] S.X. Nakamura and D. Jido.  $\Lambda(1405)$  photoproduction based on chiral unitary model. PTEP, 2014:023D01, 2014.
- [54] En Wang, Ju-Jun Xie, Wei-Hong Liang, Feng-Kun Guo, and Eulogio Oset. Role of a triangle singularity in the  $\gamma p \rightarrow K^+ \Lambda(1405)$  reaction. Phys.Rev., C95:015205, 2017.
- [55] T. Hyodo, A. Hosaka, E. Oset, A. Ramos, and M.J. Vicente Vacas.  $\Lambda(1405)$  production in the  $\pi - p \rightarrow K^0 \pi \Sigma$  reaction. Phys.Rev., C68:065203, 2003.
- [56] V.K. Magas, E. Oset, and A. Ramos. Evidence for the two pole structure of the  $\Lambda(1405)$  resonance. Phys.Rev.Lett., 95:052301, 2005.
- [57] D. Jido, E. Oset, and T. Sekihara. Kaonic production of  $\Lambda(1405)$  off deuteron target in chiral dynamics. Eur.Phys.J., A42:257–268, 2009.
- [58] K. Miyagawa and J. Haidenbauer. Precise calculation of the two-step process for  $K^- d \rightarrow \pi \Sigma N$  in the Lambda (1405) resonance region. Phys.Rev., C85:065201, 2012.
- [59] Daisuke Jido, Eulogio Oset, and Takayasu Sekihara. The  $K^- d \rightarrow \pi \Sigma n$  reaction revisited. Eur.Phys.J., A49:95, 2013.
- [60] Shota Ohnishi, Yoichi Ikeda, Tetsuo Hyodo, and Wolfram Weise. Structure of the  $\Lambda(1405)$  and the  $K^- d \rightarrow \pi \Sigma n$  reaction. Phys.Rev., C93:025207, 2016.
- [61] L.S. Geng and E. Oset. The Role of the  $\Lambda(1405)$  in the  $pp \rightarrow p K^+ \Lambda(1405)$  reaction. Eur.Phys.J., A34:405–412, 2007.
- [62] Johannes Siebenson and Laura Fabbietti. Investigation of the  $\Lambda(1405)$  line shape observed in  $pp$  collisions. Phys.Rev., C88:055201, 2013.
- [63] Kenta Miyahara, Tetsuo Hyodo, and Eulogio Oset. Weak decay of  $\Lambda_c^+$  for the study of  $\Lambda(1405)$  and  $\Lambda(1670)$ . Phys.Rev., C92:055204, 2015.
- [64] Yuki Kamiya et al. Antikaon-nucleon interaction and  $\Lambda(1405)$  in chiral SU(3) dynamics. Nucl.Phys., A954:41–57, 2016.
- [65] T. Hyodo U.-G, Meissner. Pole Structure of the  $\Lambda(1405)$  Region. C. Patrignani et al. (Particle Data Group), Chin. Phys. C, 40:100001, 2016.

- [66] E. A. Veit, Byron K. Jennings, Anthony William Thomas, and R. C. Barrett. S Wave Meson - Nucleon Scattering in an  $SU(3)$  Cloudy Bag Model. Phys. Rev., D31:1033, 1985.
- [67] K. Tanaka and A. Suzuki. Kaonic hydrogen atom and low-energy anti-K N interaction. Phys. Rev., C45:2068–2078, 1992.
- [68] Y. A. Chao, R. W. Kraemer, D. W. Thomas, and B. R. Martin. Anti-k n data and  $\Lambda(1405)$ . Nucl. Phys., B56:46–51, 1973.
- [69] C. Garcia-Recio, M.F.M. Lutz, and J. Nieves. Quark mass dependence of s wave baryon resonances. Phys.Lett., B582:49–54, 2004.
- [70] Nathan Isgur and Mark B. Wise. Spectroscopy with heavy quark symmetry. Phys.Rev.Lett., 66:1130–1133, 1991.
- [71] Mark B. Wise. Chiral perturbation theory for hadrons containing a heavy quark. Phys.Rev., D45:R2188, 1992.
- [72] Matthias Neubert. Heavy quark symmetry. Phys.Rept., 245:259–396, 1994.
- [73] D. Ebert, R.N. Faustov, and V.O. Galkin. Masses of excited heavy baryons in the relativistic quark model. Phys.Lett., B659:612–620, 2008.
- [74] H. Garcilazo, J. Vijande, and A. Valcarce. Faddeev study of heavy baryon spectroscopy. J.Phys., G34:961–976, 2007.
- [75] D. Ebert, R.N. Faustov, and V.O. Galkin. Spectroscopy and Regge trajectories of heavy baryons in the relativistic quark-diquark picture. Phys.Rev., D84:014025, 2011.
- [76] P.G. Ortega, D.R. Entem, and F. Fernandez. Quark model description of the  $\Lambda_c(2940)^+$  as a molecular  $D^*N$  state and the possible existence of the  $\Lambda_b(6248)$ . Phys.Lett., B718:1381–1384, 2013.
- [77] Zalak Shah, Kaushal Thakkar, Ajay Kumar Rai, and P.C. Vinodkumar. Mass spectra and Regge trajectories of  $\Lambda_c^+$ ,  $\Sigma_c^0$ ,  $\Xi_c^0$  and  $\Omega_c^0$  baryons. Chin.Phys., C40:123102, 2016.
- [78] E. Santopinto et al. The  $\Omega_c$ -puzzle solved by means of spectrum and strong decay amplitude predictions. arXiv:1811.01799, 2018.
- [79] A. Valcarce, H. Garcilazo, and J. Vijande. Towards an understanding of heavy baryon spectroscopy. Eur.Phys.J., A37:217–225, 2008.

- [80] K.C. Bowler et al. Heavy baryon spectroscopy from the lattice. Phys.Rev., D54:3619–3633, 1996.
- [81] Tommy Burch, Christian Hagen, Christian B. Lang, Markus Limmer, and Andreas Schafer. Excitations of single-beauty hadrons. Phys.Rev., D79:014504, 2009.
- [82] Zachary S. Brown, William Detmold, Stefan Meinel, and Kostas Orginos. Charmed bottom baryon spectroscopy from lattice QCD. Phys.Rev., D90:094507, 2014.
- [83] C. Garcia-Recio, J. Nieves, O. Romanets, L.L. Salcedo, and L. Tolos. Odd parity bottom-flavored baryon resonances. Phys.Rev., D87:034032, 2013.
- [84] W.H. Liang, C.W. Xiao, and E. Oset. Baryon states with open beauty in the extended local hidden gauge approach. Phys.Rev., D89:054023, 2014.
- [85] W.H. Liang, T. Uchino, C.W. Xiao, and E. Oset. Baryon states with open charm in the extended local hidden gauge approach. Eur.Phys.J., A51:16, 2015.
- [86] O. Romanets, L. Tolos, C. Garcia-Recio, J. Nieves, L.L. Salcedo, and R.G.E. Timmermans. Charmed and strange baryon resonances with heavy-quark spin symmetry. Phys.Rev., D85:114032, 2012.
- [87] Ming-Zhu Liu, Tian-Wei Wu, Ju-Jun Xie, Manuel Pavon Valderrama, and Li-Sheng Geng.  $D\Xi$  and  $D^*\Xi$  molecular states from one boson exchange. Phys.Rev., D98:014014, 2018.
- [88] Yin Huang, Cheng-jian Xiao, Qi Fang Lü, Rong Wang, Jun He, and Lisheng Geng. Strong and radiative decays of  $D\Xi$  molecular state and newly observed  $\Omega_c$  states. Phys.Rev., D97:094013, 2018.
- [89] Rui Chen, Atsushi Hosaka, and Xiang Liu. Searching for possible  $\Omega_c$ -like molecular states from meson-baryon interaction. Phys.Rev., D97:036016, 2018.
- [90] Yubing Dong, Amand Faessler, Thomas Gutsche, S. Kumano, and Valery E. Lyubovitskij. Radiative decay of  $\Lambda_c(2940)^+$  in a hadronic molecule picture. Phys.Rev., D82:034035, 2010.
- [91] Yubing Dong, Amand Faessler, Thomas Gutsche, and Valery E. Lyubovitskij. Role of the hadron molecule  $\Lambda_c(2940)$  in the  $p\bar{p} \rightarrow pD^0\bar{\Lambda}_c(2286)$  annihilation reaction. Phys. Rev., D90(9):094001, 2014.

- [92] P. G. Ortega, D. R. Entem, and F. Fernández. Hadronic molecules in the open charm and open bottom baryon spectrum. Phys.Rev., D90:114013, 2014.
- [93] Jun He.  $\bar{D}\Sigma_c^*$  and  $\bar{D}^*\Sigma_c$  interactions and the LHCb hidden-charmed pentaquarks. Phys.Lett., B753:547–551, 2016.
- [94] Rui Chen, Atsushi Hosaka, and Xiang Liu. Heavy molecules and one- $\sigma/\omega$ -exchange model. Phys.Rev., D96:116012, 2017.
- [95] Ming-Zhu Liu, Fang-Zheng Peng, Mario Sánchez Sánchez, and Manuel Pavon Valderrama. Heavy-quark symmetry partners of the  $P_c(4450)$  pentaquark. Phys.Rev., D98:114030, 2018.
- [96] J.G. Korner, M. Kramer, and D. Pirjol. Heavy baryons. Prog.Part.Nucl.Phys., 33:787–868, 1994.
- [97] S. Bianco, F.L. Fabbri, D. Benson, and I. Bigi. A Cicerone for the physics of charm. Riv.Nuovo Cim., 26N7:1–200, 2003.
- [98] Eberhard Klempt and Jean-Marc Richard. Baryon spectroscopy. Rev.Mod.Phys., 82:1095–1153, 2010.
- [99] V. Crede and W. Roberts. Progress towards understanding baryon resonances. Rept.Prog.Phys., 76:076301, 2013.
- [100] Hai-Yang Cheng. Charmed baryons circa 2015. Front.Phys.(Beijing), 10:101406, 2015.
- [101] Hua-Xing Chen, Wei Chen, Xiang Liu, and Shi-Lin Zhu. The hidden-charm pentaquark and tetraquark states. Phys.Rept., 639:1–121, 2016.
- [102] Hua-Xing Chen, Wei Chen, Xiang Liu, Yan-Rui Liu, and Shi-Lin Zhu. A review of the open charm and open bottom systems. Rept.Prog.Phys., 80:076201, 2017.
- [103] L. D. Landau. On analytic properties of vertex parts in quantum field theory. Nucl. Phys., 13:181–192, 1959.
- [104] S. Coleman and R. E. Norton. Singularities in the physical region. Nuovo Cim., 38:438–442, 1965.
- [105] C. Adolph et al. Observation of a New Narrow Axial-Vector Meson  $a_1(1420)$ . Phys. Rev. Lett., 115(8):082001, 2015.
- [106] Xiao-Hai Liu, Makoto Oka, and Qiang Zhao. Searching for observable effects induced by anomalous triangle singularities. Phys. Lett., B753:297–302, 2016.

- [107] M. Mikhasenko, B. Ketzner, and Andrey Sarantsev. Nature of the  $\alpha_1(1420)$ . Phys. Rev., D91(9):094015, 2015.
- [108] F. Aceti, L. R. Dai, and E. Oset.  $\alpha_1(1420)$  peak as the  $\pi f_0(980)$  decay mode of the  $\alpha_1(1260)$ . Phys. Rev., D94(9):096015, 2016.
- [109] M. Aghasyan et al. Light isovector resonances in  $\pi^- p \rightarrow \pi^- \pi^- \pi^+ p$  at 190 GeV/c. Phys. Rev., D98(9):092003, 2018.
- [110] C. Patrignani et al. Review of Particle Physics. Chin. Phys., C40(10):100001, 2016.
- [111] V.R. Debastiani, F. Aceti, Wei-Hong Liang, and E. Oset. Revising the  $f_1(1420)$  resonance. Phys.Rev., D95:034015, 2017.
- [112] Ju-Jun Xie, Li-Sheng Geng, and Eulogio Oset.  $f_2(1810)$  as a triangle singularity. Phys.Rev., D95:034004, 2017.
- [113] Qian Wang, Christoph Hanhart, and Qiang Zhao. Decoding the riddle of  $Y(4260)$  and  $Z_c(3900)$ . Phys.Rev.Lett., 111:132003, 2013.
- [114] Xiao-Hai Liu and Gang Li. Exploring the threshold behavior and implications on the nature of  $Y(4260)$  and  $Z_c(3900)$ . Phys.Rev., D88:014013, 2013.
- [115] Jia-Jun Wu, Xiao-Hai Liu, Qiang Zhao, and Bing-Song Zou. The Puzzle of anomalously large isospin violations in  $\eta(1405/1475) \rightarrow 3\pi$ . Phys.Rev.Lett., 108:081803, 2012.
- [116] F. Aceti, W.H. Liang, E. Oset, J.J. Wu, and B.S. Zou. Isospin breaking and  $f_0(980)$ - $a_0(980)$  mixing in the  $\eta(1405) \rightarrow \pi^0 f_0(980)$  reaction. Phys.Rev., D86:114007, 2012.
- [117] Xiao-Gang Wu, Jia-Jun Wu, Qiang Zhao, and Bing-Song Zou. Understanding the property of  $\eta(1405/1475)$  in the  $J/\psi$  radiative decay. Phys.Rev., D87:014023, 2013.
- [118] M. Ablikim et al. First observation of  $\eta(1405)$  decays into  $f_0(980)\pi^0$ . Phys.Rev.Lett., 108:182001, 2012.
- [119] Roel Aaij et al. Observation of  $J/\psi p$  Resonances Consistent with Pentaquark States in  $\Lambda_b^0 \rightarrow J/\psi K^- p$  Decays. Phys.Rev.Lett., 115:072001, 2015.

- [120] R. Aaij et al. Study of the production of  $\Lambda_b^0$  and  $\bar{B}^0$  hadrons in  $pp$  collisions and first measurement of the  $\Lambda_b^0 \rightarrow J/\psi p K^-$  branching fraction. *Chin.Phys.*, C40:011001, 2016.
- [121] Feng-Kun Guo, Ulf-G. Meißner, Wei Wang, and Zhi Yang. How to reveal the exotic nature of the  $P_c(4450)$ . *Phys.Rev.*, D92:071502, 2015.
- [122] J. A. Oller and E. Oset. Chiral symmetry amplitudes in the S wave isoscalar and isovector channels and the  $\sigma$ ,  $f_0(980)$ ,  $a_0(980)$  scalar mesons. *Nucl. Phys.*, A620:438–456, 1997. [Erratum: *Nucl. Phys.*A652,407(1999)].
- [123] Melahat Bayar, Francesca Aceti, Feng-Kun Guo, and Eulogio Oset. A Discussion on Triangle Singularities in the  $\Lambda_b \rightarrow J/\psi K^- p$  Reaction. *Phys. Rev.*, D94(7):074039, 2016.
- [124] Adam P. Szczepaniak. Triangle Singularities and XYZ Quarkonium Peaks. *Phys.Lett.*, B747:410–416, 2015.
- [125] A.E. Bondar and M.B. Voloshin.  $\Upsilon(6S)$  and triangle singularity in  $e^+e^- \rightarrow B_1(5721)\bar{B} \rightarrow Z_b(10610)\pi$ . *Phys.Rev.*, D93:094008, 2016.
- [126] A. Pilloni et al. Amplitude analysis and the nature of the  $Z_c(3900)$ . *Phys.Lett.*, B772:200–209, 2017.
- [127] Xiao-Hai Liu and Ulf-G. Meißner. Generating a resonance-like structure in the reaction  $B_c \rightarrow B_s \pi \pi$ . *Eur.Phys.J.*, C77:816, 2017.
- [128] S. Sakai, E. Oset, and A. Ramos. Triangle singularities in  $B^- \rightarrow K^- \pi^- D_{s0}^+$  and  $B^- \rightarrow K^- \pi^- D_{s1}^+$ . *Eur.Phys.J.*, A54:10, 2018.
- [129] Steven Weinberg. Phenomenological Lagrangians. *Physica*, A96(1-2):327–340, 1979.
- [130] Bastian Kubis. An Introduction to chiral perturbation theory. In *Workshop on Physics and Astrophysics of Hadrons and Hadronic Matter*, 2007.
- [131] Taizo Muta. *Foundations of Quantum Chromodynamics*, volume 78 of *World scientific Lecture Notes in Physics*. World Scientific, Hackensack, N.J., 2010.
- [132] Stefan Scherer and Matthias R. Schindler. A Primer for Chiral Perturbation Theory. *Lect. Notes Phys.*, 830:pp.1–338, 2012.

- [133] A. Bramon, A. Grau, and G. Pancheri. Intermediate vector meson contributions to  $V^0 \rightarrow P^0 P^0 \gamma$  decays. Phys. Lett., B283:416–420, 1992.
- [134] M. Bando, T. Kugo, S. Uehara, K. Yamawaki, and T. Yanagida. Is  $\rho$  Meson a Dynamical Gauge Boson of Hidden Local Symmetry? Phys. Rev. Lett., 54:1215, 1985.
- [135] Masako Bando, Taichiro Kugo, and Koichi Yamawaki. Nonlinear Realization and Hidden Local Symmetries. Phys. Rept., 164:217–314, 1988.
- [136] Ulf G. Meissner. Low-Energy Hadron Physics from Effective Chiral Lagrangians with Vector Mesons. Phys. Rept., 161:213, 1988.
- [137] Masayasu Harada and Koichi Yamawaki. Hidden local symmetry at loop: A New perspective of composite gauge boson and chiral phase transition. Phys. Rept., 381:1–233, 2003.
- [138] H. Nagahiro, L. Roca, A. Hosaka, and E. Oset. Hidden gauge formalism for the radiative decays of axial-vector mesons. Phys. Rev., D79:014015, 2009.
- [139] E. Oset and A. Ramos. Dynamically generated resonances from the vector octet-baryon octet interaction. Eur.Phys.J., A44:445–454, 2010.
- [140] Ken Kawarabayashi and Mahiko Suzuki. Partially conserved axial vector current and the decays of vector mesons. Phys.Rev.Lett., 16:255, 1966.
- [141] Riazuddin and Fayyazuddin. Algebra of current components and decay widths of  $\rho$  and  $K^*$  mesons. Phys.Rev., 147:1071–1073, 1966.
- [142] H. Georgi. Weak Interactions and Modern Particle Theory. Menlo Park, Usa: Benjamin/cummings ( 1984) 165p, 1984.
- [143] A. Krause. Baryon Matrix Elements of the Vector Current in Chiral Perturbation Theory. Helv. Phys. Acta, 63:3–70, 1990.
- [144] M. A. Luty and Martin J. White. Decouplet contributions to hyperon axial vector form-factors. Phys. Lett., B319:261–268, 1993.
- [145] Howard Georgi. Heavy quark effective field theory. In Theoretical Advanced Study Institute in Elementary Particle Physics (TASI 91), pages 0589–630, 1991.
- [146] Aneesh V. Manohar and Mark B. Wise. Heavy quark physics. Camb. Monogr. Part. Phys. Nucl. Phys. Cosmol., 10:1–191, 2000.

- [147] Thomas Mannel, Winston Roberts, and Zbigniew Ryzak. A Derivation of the heavy quark effective Lagrangian from QCD. Nucl. Phys., B368:204–217, 1992.
- [148] Adam F. Falk. Hadrons of arbitrary spin in the heavy quark effective theory. Nucl.Phys., B378:79–94, 1992.
- [149] H.David Politzer. Counting form-factors using the Wisgur symmetry. Phys.Lett., B250:128–129, 1990.
- [150] Peter L. Cho. Strong and electromagnetic decays of two new  $\Lambda_c^*$  baryons. Phys.Rev., D50:3295–3302, 1994.
- [151] A.D. Martin and T.D. Spearman. Elementary particle theory. North-Holland Pub. Co., 1970.
- [152] T. Ericson and W. Weise. Pions and Nuclei (International Series of Monographs on Physics 74). Oxford University Press, USA, 1988.
- [153] Tetsuo Hyodo, Daisuke Jido, and Atsushi Hosaka. Exotic hadrons in s-wave chiral dynamics. Phys. Rev. Lett., 97:192002, 2006.
- [154] Tetsuo Hyodo, Daisuke Jido, and Atsushi Hosaka. Study of exotic hadrons in s-wave scatterings induced by chiral interaction in the flavor symmetric limit. Phys. Rev., D75:034002, 2007.
- [155] Ian J. R. Aitchison. Unitarity, Analyticity and Crossing Symmetry in Two- and Three-hadron Final State Interactions. arXiv:1507.02697, 2015.
- [156] Fokas A. Ablowitz M. Complex variables: Introduction and Applications (2nd Ed.). Cambridge University Press, 2003.
- [157] Thomas Wolkanowski. Master Thesis: Resonances and poles in the second Riemann sheet. hep-ph/1303.4657v5, 2014.
- [158] J. A. Oller and E. Oset. N/D description of two meson amplitudes and chiral symmetry. Phys. Rev., D60:074023, 1999.
- [159] Tetsuo Hyodo, Seung-il Nam, Daisuke Jido, and Atsushi Hosaka. Detailed analysis of the chiral unitary model for meson baryon scatterings with flavor  $SU(3)$  breaking effects. Prog. Theor. Phys., 112:73–97, 2004.
- [160] J. Nieves and E. Ruiz Arriola. The S(11) - N(1535) and - N(1650) resonances in meson baryon unitarized coupled channel chiral perturbation theory. Phys.Rev., D64:116008, 2001.



- [161] Juan Nieves and Enrique Ruiz Arriola. Bethe-Salpeter approach for unitarized chiral perturbation theory. Nucl. Phys., A679:57–117, 2000.
- [162] S. Kondratyuk, A. D. Lahiff, and H. W. Fearing. The Equivalence theorem and the Bethe-Salpeter equation. Phys. Lett., B521:204–210, 2001.
- [163] J. A. Oller, E. Oset, and A. Ramos. Chiral unitary approach to meson meson and meson - baryon interactions and nuclear applications. Prog. Part. Nucl. Phys., 45:157–242, 2000.
- [164] Sourav Sarkar, E. Oset, and M. J. Vicente Vacas. Baryonic resonances from baryon decuplet-meson octet interaction. Nucl. Phys., A750:294–323, 2005. [Erratum: Nucl. Phys.A780,90(2006)].
- [165] Miguel Albaladejo, Pedro Fernandez-Soler, Juan Nieves, and Pablo G. Ortega. Lowest-lying even-parity  $\bar{B}_s$  mesons: heavy-quark spin-flavor symmetry, chiral dynamics, and constituent quark-model bare masses. Eur. Phys. J., C77(3):170, 2017.
- [166] J. A. Oller, E. Oset, and J. R. Pelaez. Meson meson interaction in a nonperturbative chiral approach. Phys. Rev., D59:074001, 1999. [Erratum: Phys. Rev.D75,099903(2007)].
- [167] M. F. M. Lutz and E. E. Kolomeitsev. On meson resonances and chiral symmetry. Nucl. Phys., A730:392–416, 2004.
- [168] Tetsuo Hyodo, Daisuke Jido, and Atsushi Hosaka. Origin of the resonances in the chiral unitary approach. Phys. Rev., C78:025203, 2008.
- [169] Tetsuo Hyodo, Daisuke Jido, and Atsushi Hosaka. Study of exotic hadrons in s-wave chiral dynamics. Prog. Theor. Phys. Suppl., 168:32–35, 2007.
- [170] J. Hofmann and M.F.M. Lutz. Coupled-channel study of crypto-exotic baryons with charm. Nucl.Phys., A763:90–139, 2005.
- [171] J. Hofmann and M.F.M. Lutz. D-wave baryon resonances with charm from coupled-channel dynamics. Nucl.Phys., A776:17–51, 2006.
- [172] C. Garcia-Recio et al. The s-wave charmed baryon resonances from a coupled-channel approach with heavy quark symmetry. Phys.Rev., D79:054004, 2009.
- [173] Steven Weinberg. Elementary particle theory of composite particles. Phys.Rev., 130:776–783, 1963.

- [174] Steven Weinberg. Evidence That the Deuteron Is Not an Elementary Particle. Phys.Rev., 137:B672–B678, 1965.
- [175] V. Baru, J. Haidenbauer, C. Hanhart, Yu. Kalashnikova, and Alexander Evgenyevich Kudryavtsev. Evidence that the  $a_0(980)$  and  $f_0(980)$  are not elementary particles. Phys.Lett., B586:53–61, 2004.
- [176] Martin Cleven, Feng-Kun Guo, Christoph Hanhart, and Ulf-G. Meissner. Bound state nature of the exotic  $Z_b$  states. Eur.Phys.J., A47:120, 2011.
- [177] D. Gamermann, J. Nieves, E. Oset, and E. Ruiz Arriola. Couplings in coupled channels versus wave functions: application to the X(3872) resonance. Phys.Rev., D81:014029, 2010.
- [178] J. Yamagata-Sekihara, J. Nieves, and E. Oset. Couplings in coupled channels versus wave functions in the case of resonances: application to the two  $\Lambda(1405)$  states. Phys.Rev., D83:014003, 2011.
- [179] F. Aceti and E. Oset. Wave functions of composite hadron states and relationship to couplings of scattering amplitudes for general partial waves. Phys.Rev., D86:014012, 2012.
- [180] F. Aceti, L. R. Dai, L. S. Geng, E. Oset, and Y. Zhang. Meson-baryon components in the states of the baryon decuplet. Eur. Phys. J., A50:57, 2014.
- [181] F. Aceti, E. Oset, and L. Roca. Composite nature of the  $\Lambda(1520)$  resonance. Phys.Rev., C90:025208, 2014.
- [182] Tetsuo Hyodo, Daisuke Jido, and Atsushi Hosaka. Compositeness of dynamically generated states in a chiral unitary approach. Phys.Rev., C85:015201, 2012.
- [183] Tetsuo Hyodo. Structure and compositeness of hadron resonances. Int. J. Mod. Phys., A28:1330045, 2013.
- [184] Hideko Nagahiro and Atsushi Hosaka. Elementarity of composite systems. Phys.Rev., C90:065201, 2014.
- [185] C. Garcia-Recio, C. Hidalgo-Duque, J. Nieves, L.L. Salcedo, and L. Tolos. Compositeness of the strange, charm, and beauty odd parity  $\Lambda$  states. Phys.Rev., D92:034011, 2015.
- [186] R. E. Cutkosky. Singularities and discontinuities of Feynman amplitudes. J. Math. Phys., 1:429–433, 1960.

- [187] Christoph Schmid. Final-State Interactions and the Simulation of Resonances. Phys. Rev., 154(5):1363, 1967.
- [188] V. R. Debastiani, S. Sakai, and E. Oset. Considerations on the Schmid theorem for triangle singularities. Eur. Phys. J., C79(1):69, 2019.
- [189] Nathan Isgur, Colin Morningstar, and Cathy Reader. The  $a_1$  in  $\tau$  Decay. Phys. Rev., D39:1357, 1989.
- [190] Johann Heinrich Kuhn and F. Wagner. Semileptonic Decays of the  $\tau$  Lepton. Nucl. Phys., B236:16–34, 1984.
- [191] Johann H. Kuhn and A. Santamaria. Tau decays to pions. Z. Phys., C48:445–452, 1990.
- [192] B. C. Barish and R. Stroynowski. The Physics of the tau Lepton. Phys. Rept., 157:1, 1988.
- [193] Michel Davier, Andreas Hocker, and Zhiqing Zhang. The Physics of hadronic tau decays. Rev. Mod. Phys., 78:1043–1109, 2006.
- [194] Mario Antonelli et al. Flavor Physics in the Quark Sector. Phys. Rept., 494:197–414, 2010.
- [195] Bing An Li.  $U(2)_L \times U(2)_R$  chiral theory of mesons. Phys. Rev., D52:5165–5183, 1995.
- [196] M. K. Volkov and A. B. Arbuzov. Meson production processes in electron-positron collisions and tau-lepton decays within the extended Nambu - Jona-Lasinio model. Phys. Usp., 60(7):643–666, 2017.
- [197] S. Ryu et al. Measurements of Branching Fractions of  $\tau$  Lepton Decays with one or more  $K_S^0$ . Phys. Rev., D89(7):072009, 2014.
- [198] D. Buskulic et al. A Study of  $\tau$  decays involving  $\eta$  and  $\omega$  mesons. Z. Phys., C74:263–273, 1997.
- [199] D. Buskulic et al. Tau hadronic branching ratios. Z. Phys., C70:579–608, 1996.
- [200] R. Barate et al. Three-prong  $\tau$  decays with charged kaons. Eur. Phys. J., C1:65–79, 1998.
- [201] K. Inami et al. Precise measurement of hadronic tau-decays with an eta meson. Phys. Lett., B672:209–218, 2009.

- [202] Kregg E. Arms et al. Study of tau decays to four-hadron final states with kaons. Phys. Rev. Lett., 94:241802, 2005.
- [203] Bernard Aubert et al. Exclusive branching fraction measurements of semileptonic  $\tau$  decays into three charged hadrons,  $\tau^- \rightarrow \phi\pi^- \nu(\tau)$  and  $\tau^- \rightarrow \phi K^- \nu(\tau)$ . Phys. Rev. Lett., 100:011801, 2008.
- [204] P. del Amo Sanchez et al. Studies of  $\tau^- \rightarrow \eta K \nu$  and  $\tau^- \rightarrow \eta\pi^- \nu(\tau)$  at BaBar and a search for a second-class current. Phys. Rev., D83:032002, 2011.
- [205] Yoichiro Nambu and G. Jona-Lasinio. Dynamical Model of Elementary Particles Based on an Analogy with Superconductivity. 1. Phys. Rev., 122:345–358, 1961. 127.
- [206] L. Micu. Decay rates of meson resonances in a quark model. Nucl. Phys., B10:521–526, 1969.
- [207] A. Le Yaouanc, L. Oliver, O. Pene, and J. C. Raynal. Naive quark pair creation model of strong interaction vertices. Phys. Rev., D8:2223–2234, 1973.
- [208] F.E. Close. An Introduction to Quarks and Partons.
- [209] Steven Weinberg. Charge symmetry of weak interactions. Phys. Rev., 112:1375–1379, 1958.
- [210] C. Leroy and J. Pestieau. Tau Decay and Second Class Currents. Phys. Lett., 72B:398–399, 1978.
- [211] A. Martinez Torres, L. S. Geng, L. R. Dai, Bao Xi Sun, E. Oset, and B. S. Zou. Study of the  $J/\psi \rightarrow \phi(\omega)f_2(1270)$ ,  $J/\psi \rightarrow \phi(\omega)f_2'(1525)$  and  $J/\psi \rightarrow K^{*0}(892)\bar{K}_2^{*0}(1430)$  decays. Phys. Lett., B680:310–315, 2009.
- [212] W. H. Liang and E. Oset.  $B^0$  and  $B_s^0$  decays into  $J/\psi f_0(980)$  and  $J/\psi f_0(500)$  and the nature of the scalar resonances. Phys. Lett., B737:70–74, 2014.
- [213] Ju-Jun Xie, Lian-Rong Dai, and Eulogio Oset. The low lying scalar resonances in the  $D^0$  decays into  $K_s^0$  and  $f_0(500)$ ,  $f_0(980)$ ,  $a_0(980)$ . Phys. Lett., B742:363–369, 2015.
- [214] C. Itzykson and J. B. Zuber. Quantum Field Theory. McCraw-Hill, New York, 1980, 1980.
- [215] A. Bohr and B. R. Mottelson. Nuclear Structure, Volume 1. World Scientific, 1998.

- [216] F. Mandl and G. Shae. Quantum Field Theory. John Wiley and sons, 1984.
- [217] Wei-Hong Liang and E. Oset. Pseudoscalar or vector meson production in non-leptonic decays of heavy hadrons. Eur. Phys. J., C78(6):528, 2018.
- [218] L. R. Dai, X. Zhang, and E. Oset. Semileptonic decays of  $B^{(*)}$ ,  $D^{(*)}$  into  $\nu l$  and pseudoscalar or vector mesons. Phys. Rev., D98(3):036004, 2018.
- [219] H. García-Tecocoatzi, R. Bijker, J. Ferretti, and E. Santopinto. Self-energies of octet and decuplet baryons due to the coupling to the baryon-meson continuum. Eur. Phys. J., A53(6):115, 2017.
- [220] J. Ferretti, G. Galatà, and E. Santopinto. Interpretation of the X(3872) as a charmonium state plus an extra component due to the coupling to the meson-meson continuum. Phys. Rev., C88(1):015207, 2013.
- [221] R. Bijker, E. Santopinto, and E. Santopinto. Unquenched quark model for baryons: Magnetic moments, spins and orbital angular momenta. Phys. Rev., C80:065210, 2009.
- [222] Ishrat Asghar, Bilal Masud, E. S. Swanson, Faisal Akram, and M. Atif Sultan. Decays and spectrum of bottom and bottom strange mesons. Eur. Phys. J., A54(7):127, 2018.
- [223] Long-Cheng Gui, Long-Sheng Lu, Qi-Fang Lü, Xian-Hui Zhong, and Qiang Zhao. Strong decays of higher charmonium states into open-charm meson pairs. Phys. Rev., D98(1):016010, 2018.
- [224] Wei-Hong Liang, Melahat Bayar, and Eulogio Oset.  $\Lambda_b \rightarrow \pi^-(D_s^-)\Lambda_c(2595)$ ,  $\pi^-(D_s^-)\Lambda_c(2625)$  decays and  $DN$ ,  $D^*N$  molecular components. Eur.Phys.J., C77:39, 2017.
- [225] Guan-Ying Wang, Shi-Chen Xue, Guan-Nan Li, En Wang, and De-Min Li. Strong decays of the higher isovector scalar mesons. Phys. Rev., D97(3):034030, 2018.
- [226] Li-Ye Xiao, Qi-Fang Lü, and Shi-Lin Zhu. Strong decays of the 1P and 2D doubly charmed states. Phys. Rev., D97(7):074005, 2018.
- [227] Pablo G. Ortega, Jorge Segovia, David R. Entem, and Francisco Fernández. Charmonium resonances in the 3.9 GeV/c<sup>2</sup> energy region and the X(3915)/X(3930) puzzle. Phys. Lett., B778:1–5, 2018.

- [228] J. Gasser and H. Leutwyler. Chiral Perturbation Theory to One Loop. Annals Phys., 158:142, 1984.
- [229] Stefan Scherer. Introduction to chiral perturbation theory. Adv. Nucl. Phys., 27:277, 2003. [,277(2002)].
- [230] M. E. Rose. Elementary theory of angular momentum. Dover publications, 1995.
- [231] J. R. Pelaez. From controversy to precision on the sigma meson: a review on the status of the non-ordinary  $f_0(500)$  resonance. Phys. Rept., 658:1, 2016.
- [232] Matthias Jamin, Antonio Pich, and Jorge Portoles. Spectral distribution for the decay  $\tau \rightarrow \nu(\tau)\pi$ . Phys. Lett., B640:176–181, 2006.
- [233] B. Moussallam. Analyticity constraints on the strangeness changing vector current and applications to  $\tau \rightarrow K\pi\nu(\tau)$ ,  $\tau \rightarrow K\pi\pi\nu(\tau)$ . Eur. Phys. J., C53:401–412, 2008.
- [234] D. M. Asner et al. Resonance structure of  $\tau^- \rightarrow K^- \pi^+ \pi^- \nu(\tau)$  decays. Phys. Rev., D62:072006, 2000.
- [235] L. Roca, E. Oset, and J. Singh. Low lying axial-vector mesons as dynamically generated resonances. Phys.Rev., D72:014002, 2005.
- [236] L. S. Geng, E. Oset, L. Roca, and J. A. Oller. Clues for the existence of two  $K(1)(1270)$  resonances. Phys. Rev., D75:014017, 2007.
- [237] R. Molina, D. Nicmorus, and E. Oset. The  $\rho\rho$  interaction in the hidden gauge formalism and the  $f_0(1370)$  and  $f_2(1270)$  resonances. Phys. Rev., D78:114018, 2008.
- [238] Li-Sheng Geng, Raquel Molina, and Eulogio Oset. On the chiral covariant approach to  $\rho\rho$  scattering. Chin. Phys., C41(12):124101, 2017.
- [239] S. Schael et al. Branching ratios and spectral functions of tau decays: Final ALEPH measurements and physics implications. Phys. Rept., 421:191–284, 2005.
- [240] Markus Wagner and Stefan Leupold. Information on the structure of the  $a(1)$  from tau decay. Phys. Rev., D78:053001, 2008.
- [241] L. R. Dai, L. Roca, and E. Oset.  $\tau$  decay into a pseudoscalar and an axial-vector meson. Phys. Rev., D99(9):096003, 2019.

- [242] L. R. Dai, Q. X. Yu, and E. Oset. Triangle singularity in  $\tau^- \rightarrow \nu_\tau \pi^- f_0(980)$  ( $a_0(980)$ ) decays. Phys. Rev., D99(1):016021, 2019.
- [243] L. R. Dai and E. Oset. Helicity amplitudes in  $B \rightarrow D^* \bar{\nu} l$  decay. Eur. Phys. J., C78(11):951, 2018.
- [244] Matthias Neubert. B decays and CP violation. Int. J. Mod. Phys., A11:4173–4240, 1996.
- [245] Nathan Isgur and Mark B. Wise. Weak Decays of Heavy Mesons in the Static Quark Approximation. Phys. Lett., B232:113–117, 1989.
- [246] Nathan Isgur and Mark B. Wise. WEAK TRANSITION FORM-FACTORS BETWEEN HEAVY MESONS. Phys. Lett., B237:527–530, 1990.
- [247] Irinel Caprini, Laurent Lellouch, and Matthias Neubert. Dispersive bounds on the shape of anti-B  $\rightarrow$  D(\*) lepton anti-neutrino form-factors. Nucl. Phys., B530:153–181, 1998.
- [248] L. R. Dai and E. Oset. Polarization amplitudes in  $\tau^- \rightarrow \nu_\tau VP$  decay beyond the standard model. Eur. Phys. J., A54(12):219, 2018.
- [249] C. Albertus, E. Hernandez, J. Nieves, and J. M. Verde-Velasco. Study of the leptonic decays of pseudoscalar B, D and vector B\*, D\* mesons and of the semileptonic B  $\rightarrow$  D and B  $\rightarrow$  D\* decays. Phys. Rev., D71:113006, 2005.
- [250] Ashutosh Kumar Alok, Dinesh Kumar, Suman Kumbhakar, and S Uma Sankar. D\* polarization as a probe to discriminate new physics in  $\bar{B} \rightarrow D^* \tau \bar{\nu}$ . Phys. Rev., D95(11):115038, 2017.
- [251] Qin Chang, Jie Zhu, Na Wang, and Ru-Min Wang. Probing the effects of new physics in  $\bar{B}^* \rightarrow P \ell \bar{\nu}_\ell$  decays. Adv. High Energy Phys., 2018:7231354, 2018.
- [252] A. A. Pivovarov and O. V. Teryaev. Polarization effects of the  $\tau \rightarrow K^- \pi^0 \nu_\tau$  process in the Nambu–Jona-Lasinio model. JETP Lett., 104(8):523–525, 2016. [Pisma Zh. Eksp. Teor. Fiz.104,no.8,545(2016)].
- [253] Fernando S. Navarra, Marina Nielsen, Eulogio Oset, and Takayasu Sekihara. Testing the molecular nature of  $D_{s0}^*(2317)$  and  $D_0^*(2400)$  in semileptonic  $B_s$  and B decays. Phys. Rev., D92(1):014031, 2015.
- [254] T. E. Coan et al. Decays of  $\tau$  leptons to final states containing  $K_s^0$  mesons. Phys. Rev., D53:6037–6053, 1996.

- [255] R. Barate et al.  $K^0(S)$  production in tau decays. Eur. Phys. J., C4:29–45, 1998.
- [256] J. P. Lees et al. Measurement of the spectral function for the  $\tau^- \rightarrow K^- K_S \nu_\tau$  decay. Phys. Rev., D98(3):032010, 2018.
- [257] J. A. Oller, E. Oset, and J. E. Palomar. Pion and kaon vector form-factors. Phys. Rev., D63:114009, 2001.
- [258] M. K. Volkov and D. G. Kostunin.  $\tau^- \rightarrow \pi^- \pi^0 \nu_\tau$  decay in the extended NJL model. Phys. Part. Nucl. Lett., 10:7–10, 2013.
- [259] L. L. Frankfurt and M. I. Strikman. Hard Nuclear Processes and Microscopic Nuclear Structure. Phys. Rept., 160:235–427, 1988.
- [260] Miguel Albaladejo and Eulogio Oset. Constraints on a possible dibaryon from combined analysis of the  $pn \rightarrow d\pi^+\pi^-$  and  $pn \rightarrow pn\pi^+\pi^-$  cross sections. Phys. Rev., C88:014006, 2013.
- [261] M. K. Volkov and D. G. Kostunin. The decays  $\rho^- \rightarrow \eta\pi^-$  and  $\tau^- \rightarrow \eta(\eta')\pi^- \nu$  in the NJL model. Phys. Rev., D86:013005, 2012.
- [262] M. K. Volkov and A. A. Pivovarov. The decays  $\tau \rightarrow (\eta, \eta')K^- \nu_\tau$  in the extended Nambu-Jona-Lasinio model. JETP Lett., 103(10):613–617, 2016. [Pisma Zh. Eksp. Teor. Fiz.103,no.10,697(2016)].
- [263] M. K. Volkov and A. A. Pivovarov. The decay  $\tau \rightarrow K^- \pi^0 \nu_\tau$  in the Nambu-Jona-Lasinio model. Mod. Phys. Lett., A31(07):1650043, 2016.
- [264] J. E. Palomar. The role of pions and kaons in decays,  $g(\mu)-2$ , the running of  $\alpha(\text{QED})$  and the muonium hyperfine splitting. Nucl. Phys. Proc. Suppl., 121:183–186, 2003. [,183(2002)].
- [265] Henryk Czyz, Agnieszka Grzelinska, and Johann H. Kuhn. Narrow resonances studies with the radiative return method. Phys. Rev., D81:094014, 2010.
- [266] S. Dubnicka and A. Z. Dubnickova. Analyticity in a phenomenology of electro-weak structure of hadrons. Acta Phys. Slov., 60:1–153, 2010.
- [267] M. K. Volkov and A. A. Pivovarov. The decay  $\tau \rightarrow K^0 K^- \nu_\tau$  in the extended Nambu–Jona-Lasinio model. Mod. Phys. Lett., A31(23):1650138, 2016.
- [268] G. Lopez Castro and D. A. Lopez Falcon. VMD description of tau  $\rightarrow$  (omega, phi) pi- tau-neutrino decays and the omega - phi mixing angle. Phys. Rev., D54:4400–4402, 1996.



- [269] M. K. Volkov, K. Nurlan, and A. A. Pivovarov. Production  $\rho(770)$  of Meson Pairs in the Decays  $\rho(1450) \rightarrow \rho(770)\eta$  and  $\tau \rightarrow \rho(770)\eta\nu_\tau$  and in the Process  $e^+e^- \rightarrow \rho(770)\eta$  in the Extended Nambu–Jona-Lasinio Model. JETP Lett., 106(12):771–774, 2017. [Pisma Zh. Eksp. Teor. Fiz.106,no.12,737(2017)].
- [270] M. K. Volkov, A. B. Arbuzov, and D. G. Kostunin. The decay  $\tau \rightarrow \pi\omega\nu$  in the extended NJL model. Phys. Rev., D86:057301, 2012.
- [271] Eberhard Klempt and Alexander Zaitsev. Glueballs, Hybrids, Multiquarks. Experimental facts versus QCD inspired concepts. Phys.Rept., 454:1–202, 2007.
- [272] Simon Capstick and W. Roberts. Quark models of baryon masses and decays. Prog.Part.Nucl.Phys., 45:S241–S331, 2000.
- [273] B.C. Liu and B.S. Zou. Mass and  $K\Lambda$  coupling of  $N^*(1535)$ . Phys.Rev.Lett., 96:042002, 2006.
- [274] L.Ya. Glozman, Willibald Plessas, K. Varga, and R.F. Wagenbrunn. Unified description of light and strange baryon spectra. Phys.Rev., D58:094030, 1998.
- [275] R. Bijker, F. Iachello, and A. Leviatan. Algebraic models of hadron structure. 1. Nonstrange baryons. Annals Phys., 236:69–116, 1994.
- [276] C. Helminen and D.O. Riska. Low lying  $qqq$  anti- $q$  states in the baryon spectrum. Nucl.Phys., A699:624–648, 2002.
- [277] C.S. An and B.S. Zou. The Role of the  $qqqq\bar{q}$  components in the electromagnetic transition  $\gamma^*N \rightarrow N(1535)$ . Eur.Phys.J., A39:195–204, 2009.
- [278] R. Bijker, J. Ferretti, G. Galatà, H. García-Tecocoatzi, and E. Santopinto. Strong decays of baryons and missing resonances. Phys.Rev., D94:074040, 2016.
- [279] Zhen-ping Li. The Eta-prime photoproduction off the nucleon in the quark model. J.Phys., G23:1127–1132, 1997.
- [280] M. Doring, E. Oset, and D. Strottman. Chiral dynamics in the gamma  $p \rightarrow \pi^0 \eta p$  and gamma  $p \rightarrow \pi^0 K^0 \Sigma^+$  reactions. Phys.Rev., C73:045209, 2006.
- [281] Ju-Jun Xie, Bing-Song Zou, and Huan-Ching Chiang. The Role of  $N^*(1535)$  in  $pp \rightarrow pp\phi$  and  $\pi^- p \rightarrow n\phi$  reactions. Phys.Rev., C77:015206, 2008.

- [282] Xu Cao and Xi-Guo Lee. The Role of  $N^*(1535)$  in eta-prime production. Phys.Rev., C78:035207, 2008.
- [283] L.S. Geng, E. Oset, B.S. Zou, and M. Doring. The Role of the  $N^*(1535)$  in the  $J/\psi \rightarrow \bar{p}\eta p$  and  $J/\psi \rightarrow \bar{p}K^+\Lambda$  reactions. Phys.Rev., C79:025203, 2009.
- [284] M. Doring, E. Oset, and B.S. Zou. The Role of the  $N^*(1535)$  resonance and the  $\pi^- p \rightarrow KY$  amplitudes in the OZI forbidden  $\pi N \rightarrow \phi N$  reaction. Phys.Rev., C78:025207, 2008.
- [285] Xu Cao, Ju-Jun Xie, Bing-Song Zou, and Hu-Shan Xu. Evidence of  $N^*(1535)$  resonance contribution in the  $pn \rightarrow d\phi$  reaction. Phys.Rev., C80:025203, 2009.
- [286] V. R. Debastiani, S. Sakai, and E. Oset. Role of a triangle singularity in the  $\pi N(1535)$  contribution to  $\gamma p \rightarrow p\pi^0\eta$ . Phys. Rev., C96(2):025201, 2017.
- [287] Norbert Kaiser, T. Waas, and W. Weise. SU(3) chiral dynamics with coupled channels: Eta and kaon photoproduction. Nucl.Phys., A612:297–320, 1997.
- [288] Tetsuo Hyodo and Wolfram Weise. Effective anti-K N interaction based on chiral SU(3) dynamics. Phys.Rev., C77:035204, 2008.
- [289] Tetsuo Hyodo, Daisuke Jido, and Luis Roca. Structure of the  $\Lambda(1405)$  baryon resonance from its large N(c) behavior. Phys.Rev., D77:056010, 2008.
- [290] T. Inoue, E. Oset, and M.J. Vicente Vacas. Chiral unitary approach to S wave meson baryon scattering in the strangeness  $S = 0$  sector. Phys.Rev., C65:035204, 2002.
- [291] Peter C. Bruns, Maxim Mai, and Ulf G. Meissner. Chiral dynamics of the S11(1535) and S11(1650) resonances revisited. Phys.Lett., B697:254–259, 2011.
- [292] D. Gamermann, C. Garcia-Recio, J. Nieves, and L.L. Salcedo. Odd Parity Light Baryon Resonances. Phys.Rev., D84:056017, 2011.
- [293] K. P. Khemchandani, A. Martinez Torres, H. Nagahiro, and A. Hosaka. Role of vector and pseudoscalar mesons in understanding  $1/2^- N^*$  and  $\Delta$  resonances. Phys. Rev., D88(11):114016, 2013.
- [294] E. J. Garzon and E. Oset. Mixing of pseudoscalar-baryon and vector-baryon in the  $J^P = 1/2^-$  sector and the  $N^*(1535)$  and  $N^*(1650)$  resonances. Phys. Rev., C91(2):025201, 2015.

- [295] Norbert Kaiser, P.B. Siegel, and W. Weise. Chiral dynamics and the  $S_{11}(1535)$  nucleon resonance. Phys.Lett., B362:23–28, 1995.
- [296] E.J. Garzon, J.J. Xie, and E. Oset. Case in favor of the  $N^*(1700)(3/2^-)$ . Phys.Rev., C87:055204, 2013.
- [297] E.J. Garzon and E. Oset. Effects of pseudoscalar-baryon channels in the dynamically generated vector-baryon resonances. Eur.Phys.J., A48:5, 2012.
- [298] K.P. Khemchandani, A. Martinez Torres, H. Kaneko, H. Nagahiro, and A. Hosaka. Coupling vector and pseudoscalar mesons to study baryon resonances. Phys.Rev., D84:094018, 2011.
- [299] K.P. Khemchandani, A. Martinez Torres, H. Nagahiro, and A. Hosaka. Negative parity  $\Lambda$  and  $\Sigma$  resonances coupled to pseudoscalar and vector mesons. Phys.Rev., D85:114020, 2012.
- [300] V. Crede and C.A. Meyer. The Experimental Status of Glueballs. Prog.Part.Nucl.Phys., 63:74–116, 2009.
- [301] Tetsuo Hyodo and Makoto Oka. Determination of the  $\pi\Sigma$  scattering lengths from the weak decays of  $\Lambda_c$ . Phys.Rev., C84:035201, 2011.
- [302] Ju-Jun Xie and Li-Sheng Geng. The  $a_0(980)$  and  $\Lambda(1670)$  in the  $\Lambda_c^+ \rightarrow \pi^+\eta\Lambda$  decay. Eur. Phys. J., C76(9):496, 2016.
- [303] Eulogio Oset et al. Weak decays of heavy hadrons into dynamically generated resonances. Int.J.Mod.Phys., E25:1630001, 2016.
- [304] Ju-Jun Xie and Li-Sheng Geng. Role of the  $N^*(1535)$  in the  $\Lambda_c^+ \rightarrow \bar{K}^0\eta p$  decay. Phys. Rev., D96(5):054009, 2017.
- [305] Ling-Lie Chau. Quark Mixing in Weak Interactions. volume 95, pages 1–94, 1983.
- [306] Kenta Miyahara, Tetsuo Hyodo, Makoto Oka, Juan Nieves, and Eulogio Oset. Theoretical study of the  $\Xi(1620)$  and  $\Xi(1690)$  resonances in  $\Xi_c \rightarrow \pi + MB$  decays. Phys.Rev., C95:035212, 2017.
- [307] En Wang, Hua-Xing Chen, Li-Sheng Geng, De-Min Li, and Eulogio Oset. Hidden-charm pentaquark state in  $\Lambda_b^0 \rightarrow J/\psi p \pi^-$  decay. Phys.Rev., D93:094001, 2016.
- [308] Roel Aaij et al. Observation of the  $\Lambda_b^0 \rightarrow J/\psi p \pi^-$  decay. JHEP, 1407:103, 2014.

- [309] L.A. Copley, Nathan Isgur, and Gabriel Karl. Charmed Baryons in a Quark Model with Hyperfine Interactions. Phys.Rev., D20:768, 1979.
- [310] Sascha Migura, Dirk Merten, Bernard Metsch, and Herbert-R. Petry. Charmed baryons in a relativistic quark model. Eur.Phys.J., A28:41, 2006.
- [311] W. Roberts and Muslema Pervin. Heavy baryons in a quark model. Int.J.Mod.Phys., A23:2817–2860, 2008.
- [312] Tetsuya Yoshida, Emiko Hiyama, Atsushi Hosaka, Makoto Oka, and Katsunori Sadato. Spectrum of heavy baryons in the quark model. Phys.Rev., D92:114029, 2015.
- [313] Nathan Isgur, Mark B. Wise, and Michael Youssefmir. Excited charm baryons in semileptonic  $\Lambda_b$  decay and their contribution to a Bjorken sum rule. Phys.Lett., B254:215–219, 1991.
- [314] Hideko Nagahiro, Shigehiro Yasui, Atsushi Hosaka, Makoto Oka, and Hiroyuki Noumi. Structure of charmed baryons studied by pionic decays. Phys.Rev., D95:014023, 2017.
- [315] A.J. Arifi, H. Nagahiro, and A. Hosaka. Three-Body Decay of  $\Lambda_c^*(2595)$  and  $\Lambda_c^*(2625)$  with consideration of  $\Sigma_c(2455)\pi$  and  $\Sigma_c^*(2520)\pi$  in intermediate States. Phys.Rev., D95:114018, 2017.
- [316] Winston Roberts. Semileptonic decays of heavy Lambda's into excited baryons. Nucl.Phys., B389:549–562, 1993.
- [317] Adam K. Leibovich and Iain W. Stewart. Semileptonic  $\Lambda_b$  decay to excited  $\Lambda_c$  baryons at order  $\Lambda(QCD)/m_Q$ . Phys.Rev., D57:5620–5631, 1998.
- [318] Muslema Pervin, Winston Roberts, and Simon Capstick. Semileptonic decays of heavy lambda baryons in a quark model. Phys.Rev., C72:035201, 2005.
- [319] Philipp Böer, Marzia Bordone, Elena Graverini, Patrick Owen, Marcello Rondono, and Danny Van Dyk. Testing lepton flavour universality in semileptonic  $\Lambda_b \rightarrow \Lambda_c^*$  decays. JHEP, 1806:155, 2018.
- [320] Thomas Gutsche, Mikhail A. Ivanov, Jürgen G. Körner, Valery E. Lyubovitskij, Pietro Santorelli, and Chien-Thang Tran. Analyzing lepton flavor universality in the decays  $\Lambda_b \rightarrow \Lambda_c^{(*)}(\frac{1}{2}^{\pm}, \frac{3}{2}^{\mp}) + \ell \bar{\nu}_\ell$ . Phys.Rev., D98:053003, 2018.

- [321] Wei-Hong Liang, Eulogio Oset, and Zhu-Sheng Xie. Semileptonic  $\Lambda_b \rightarrow \bar{\nu}_l l \Lambda_c(2595)$  and  $\Lambda_b \rightarrow \bar{\nu}_l l \Lambda_c(2625)$  decays in the molecular picture of  $\Lambda_c(2595)$  and  $\Lambda_c(2625)$ . Phys.Rev., D95:014015, 2017.
- [322] Howard Georgi. Comment on heavy baryon weak form-factors. Nucl.Phys., B348:293–296, 1991.
- [323] Thomas Mannel, Winston Roberts, and Zbigniew Ryzak. Baryons in the heavy quark effective theory. Nucl.Phys., B355:38–53, 1991.
- [324] T. Hyodo, S.I. Nam, D. Jido, and A. Hosaka. Flavor SU(3) breaking effects in the chiral unitary model for meson baryon scatterings. Phys.Rev., C68:018201, 2003.
- [325] D.W. Thomas, A. Engler, H.E. Fisk, and R.W. Kraemer. Strange particle production from pi- p interactions at 1.69 gev/c. Nucl.Phys., B56:15–45, 1973.
- [326] S. Prakhov et al.  $K^- p \rightarrow \pi^0 \pi^0 \Sigma^0$  at  $p_{K^-} = 514\text{-MeV}/c$  to  $750\text{-MeV}/c$  mev and comparison with other  $\pi^0 \pi^0$  production. Phys.Rev., C70:034605, 2004.
- [327] E.E. Kolomeitsev and M.F.M. Lutz. On baryon resonances and chiral symmetry. Phys.Lett., B585:243–252, 2004.
- [328] Sourav Sarkar, E. Oset, and M.J. Vicente Vacas. Chiral coupled channel dynamics of the  $\Lambda(1520)$  and the  $K^- p \rightarrow \pi^0 \pi^0 \Lambda$  reaction. Phys.Rev., C72:015206, 2005.
- [329] L. Roca, Sourav Sarkar, V. K. Magas, and E. Oset. Unitary coupled channel analysis of the  $\Lambda(1520)$  resonance. Phys. Rev., C73:045208, 2006.
- [330] T. Hyodo, Sourav Sarkar, A. Hosaka, and E. Oset. The Coupling of anti- $K^*$  N to the  $\Lambda(1520)$ . Phys.Rev., C73:035209, 2006.
- [331] M. Doring, E. Oset, and Sourav Sarkar. Radiative decay of the  $\Lambda(1520)$ . Phys.Rev., C74:065204, 2006.
- [332] C. Garcia-Recio, J. Nieves, and L.L. Salcedo. SU(6) extension of the Weinberg-Tomozawa meson-baryon Lagrangian. Phys.Rev., D74:034025, 2006.
- [333] Hiroshi Toki, Carmen Garcia-Recio, and Juan Nieves. Photon induced  $\Lambda(1520)$  production and the role of the  $K^*$  exchange. Phys.Rev., D77:034001, 2008.
- [334] Sourav Sarkar, Bao-Xi Sun, E. Oset, and M.J. Vicente Vacas. Dynamically generated resonances from the vector octet-baryon decuplet interaction. Eur.Phys.J., A44:431–443, 2010.

- [335] M.F.M. Lutz, G. Wolf, and B. Friman. Scattering of vector mesons off nucleons. Nucl.Phys., A706:431–496, 2002.
- [336] M.F.M. Lutz and E.E. Kolomeitsev. On charm baryon resonances and chiral symmetry. Nucl.Phys., A730:110–120, 2004.
- [337] L. Tolos, J. Schaffner-Bielich, and A. Mishra. Properties of D-mesons in nuclear matter within a self-consistent coupled-channel approach. Phys.Rev., C70:025203, 2004.
- [338] T. Mizutani and A. Ramos. D mesons in nuclear matter: A DN coupled-channel equations approach. Phys.Rev., C74:065201, 2006.
- [339] C.E. Jimenez-Tejero, A. Ramos, and I. Vidana. Dynamically generated open charmed baryons beyond the zero range approximation. Phys.Rev., C80:055206, 2009.
- [340] Jun-Xu Lu, Yu Zhou, Hua-Xing Chen, Ju-Jun Xie, and Li-Sheng Geng. Dynamically generated  $J^P = 1/2^-(3/2^-)$  singly charmed and bottom heavy baryons. Phys. Rev., D92(1):014036, 2015.
- [341] Jun-Xu Lu, Hua-Xing Chen, Zhi-Hui Guo, J. Nieves, Ju-Jun Xie, and Li-Sheng Geng.  $\Lambda_c(2595)$  resonance as a dynamically generated state: The compositeness condition and the large  $N_c$  evolution. Phys.Rev., D93:114028, 2016.
- [342] J.R. Pelaez and G. Rios. Nature of the  $f_0(600)$  from its  $N_c$  dependence at two loops in unitarized Chiral Perturbation Theory. Phys.Rev.Lett., 97:242002, 2006.
- [343] C. Garcia-Recio, J. Nieves, and L.L. Salcedo. Large  $N_c$  Weinberg-Tomozawa interaction and negative parity s-wave baryon resonances. Phys.Rev., D74:036004, 2006.
- [344] J. Nieves and E. Ruiz Arriola. Properties of the rho and sigma Mesons from Unitary Chiral Dynamics. Phys.Rev., D80:045023, 2009.
- [345] J. Nieves, A. Pich, and E. Ruiz Arriola. Large- $N_c$  Properties of the rho and  $f_0(600)$  Mesons from Unitary Resonance Chiral Dynamics. Phys.Rev., D84:096002, 2011.
- [346] R Aaij et al. Observation of excited  $\Lambda_b^0$  baryons. Phys.Rev.Lett., 109:172003, 2012.

- [347] C. Garcia-Recio, J. Nieves, O. Romanets, L.L. Salcedo, and L. Tolos. Hidden charm N and Delta resonances with heavy-quark symmetry. Phys.Rev., D87:074034, 2013.
- [348] Roel Aaij et al. Observation of five new narrow  $\Omega_c^0$  states decaying to  $\Xi_c^+ K^-$ . Phys.Rev.Lett., 118:182001, 2017.
- [349] C.W. Xiao, J. Nieves, and E. Oset. Combining heavy quark spin and local hidden gauge symmetries in the dynamical generation of hidden charm baryons. Phys.Rev., D88:056012, 2013.
- [350] Wei-Hong Liang, J.M. Dias, V.R. Debastiani, and E. Oset. Molecular  $\Omega_b$  states. Nucl.Phys., B930:524–532, 2018.
- [351] Glòria Montaña, Albert Feijoo, and Àngels Ramos. A meson-baryon molecular interpretation for some  $\Omega_c$  excited states. Eur.Phys.J., A54:64, 2018.
- [352] Feng-Kun Guo, Ulf-G. Meißner, and Bing-Song Zou. How the X(5568) challenges our understanding of QCD. Commun.Theor.Phys., 65:593–595, 2016.
- [353] Miguel Albaladejo, Juan Nieves, Eulogio Oset, Zhi-Feng Sun, and Xiang Liu. Can X(5568) be described as a  $B_s\pi$ ,  $B\bar{K}$  resonant state? Phys.Lett., B757:515–519, 2016.
- [354] Tetsuo Hyodo. Structure of Near-Threshold s-Wave Resonances. Phys.Rev.Lett., 111:132002, 2013.
- [355] Zhi-Hui Guo and J.A. Oller. Resonance on top of thresholds: the  $\Lambda_c(2595)^+$  as an extremely fine-tuned state. Phys.Rev., D93:054014, 2016.
- [356] Nathan Isgur and Mark B. Wise. Heavy baryon weak form-factors. Nucl.Phys., B348:276–292, 1991.
- [357] Howard Georgi, Benjamin Grinstein, and Mark B. Wise.  $\Lambda_b$  semileptonic decay form-factors for  $m_c$  does not equal infinity. Phys.Lett., B252:456–460, 1990.
- [358] Thomas Mannel, Winston Roberts, and Zbigniew Ryzak.  $1/m_c$  suppressed semileptonic  $\Lambda_b$  decays. Phys.Lett., B271:421–424, 1991.
- [359] Michael J. Dugan and Benjamin Grinstein. QCD basis for factorization in decays of heavy mesons. Phys.Lett., B255:583–588, 1991.
- [360] P.G. Ortega, J. Segovia, D.R. Entem, and F. Fernandez. Coupled channel approach to the structure of the X(3872). Phys.Rev., D81:054023, 2010.

- [361] Sasa Prelovsek and Luka Leskovec. Evidence for X(3872) from  $DD^*$  scattering on the lattice. Phys.Rev.Lett., 111:192001, 2013.
- [362] A. Martínez Torres, E. Oset, S. Prelovsek, and A. Ramos. Reanalysis of lattice QCD spectra leading to the  $D_{s_0}^*$ (2317) and  $D_{s_1}^*$ (2460). JHEP, 1505:153, 2015.
- [363] E. Cincioglu, J. Nieves, A. Ozpineci, and A.U. Yilmazer. Quarkonium Contribution to Meson Molecules. Eur.Phys.J., C76:576, 2016.
- [364] R. Aaij et al. Measurement of  $b$ -hadron production fractions in 7 TeV pp collisions. Phys.Rev., D85:032008, 2012.
- [365] William Detmold, Christoph Lehner, and Stefan Meinel.  $\Lambda_b \rightarrow p\ell^-\bar{\nu}_\ell$  and  $\Lambda_b \rightarrow \Lambda_c\ell^-\bar{\nu}_\ell$  form factors from lattice QCD with relativistic heavy quarks. Phys.Rev., D92:034503, 2015.
- [366] Alakabha Datta, Saeed Kamali, Stefan Meinel, and Ahmed Rashed. Phenomenology of  $\Lambda_b \rightarrow \Lambda_c\tau\bar{\nu}_\tau$  using lattice QCD calculations. JHEP, 1708:131, 2017.
- [367] Roel Aaij et al. Measurement of the shape of the  $\Lambda_b^0 \rightarrow \Lambda_c^+\mu^-\bar{\nu}_\mu$  differential decay rate. Phys.Rev., D96:112005, 2017.
- [368] Shanmuka Shivashankara, Wanwei Wu, and Alakabha Datta.  $\Lambda_b \rightarrow \Lambda_c\tau\bar{\nu}_\tau$  Decay in the Standard Model and with New Physics. Phys.Rev., D91:115003, 2015.
- [369] Xin-Qiang Li, Ya-Dong Yang, and Xin Zhang.  $\Lambda_b \rightarrow \Lambda_c\tau\bar{\nu}_\tau$  decay in scalar and vector leptoquark scenarios. JHEP, 1702:068, 2017.
- [370] R.N. Faustov and V.O. Galkin. Semileptonic decays of  $\Lambda_b$  baryons in the relativistic quark model. Phys.Rev., D94:073008, 2016.
- [371] K. Azizi and J.Y. Süngü. Semileptonic  $\Lambda_b \rightarrow \Lambda_c\ell\bar{\nu}_\ell$  Transition in Full QCD. Phys.Rev., D97:074007, 2018.
- [372] E. Di Salvo, F. Fontanelli, and Z.J. Ajaltouni. Detailed Study of the Decay  $\Lambda_b \rightarrow \Lambda_c\tau\bar{\nu}_\tau$ . Int.J.Mod.Phys., A33:1850169, 2018.
- [373] V. Baru, C. Hanhart, Yu. S. Kalashnikova, A. E. Kudryavtsev, and A. V. Nefediev. Interplay of quark and meson degrees of freedom in a near-threshold resonance. Eur. Phys. J., A44:93–103, 2010.



- [374] Dan Pirjol and Tung-Mow Yan. Predictions for s wave and p wave heavy baryons from sum rules and constituent quark model. 1. Strong interactions. Phys. Rev., D56:5483–5510, 1997.
- [375] H. Albrecht et al. Observation of a new charmed baryon. Phys. Lett., B317:227–232, 1993.
- [376] T. Aaltonen et al. Measurements of the properties of  $\Lambda_c(2595)$ ,  $\Lambda_c(2625)$ ,  $\Sigma_c(2455)$ , and  $\Sigma_c(2520)$  baryons. Phys. Rev., D84:012003, 2011.
- [377] H. Albrecht et al. Evidence for  $\Lambda_c^+(2593)$  production. Phys. Lett., B402:207–212, 1997.
- [378] P. L. Frabetti et al. Study of higher mass charm baryons decaying to  $\Lambda_c^+$ . Phys. Lett., B365:461–469, 1996.
- [379] K. W. Edwards et al. Observation of excited baryon states decaying to  $\Lambda_c^+\pi^+\pi^-$ . Phys. Rev. Lett., 74:3331–3335, 1995.
- [380] Bernard Aubert et al. A Study of  $\bar{B} \rightarrow \Xi_c \Lambda_c^-$  and  $\bar{B} \rightarrow \Lambda_c^+ \Lambda_c^- \bar{K}$  decays at BABAR. Phys.Rev., D77:031101, 2008.
- [381] Y.B. Li et al. Observation of  $\Xi_c(2930)^0$  and updated measurement of  $B^- \rightarrow K^- \Lambda_c^+ \bar{\Lambda}_c^-$  at Belle. Eur.Phys.J., C78:252, 2018.
- [382] Roel Aaij et al. Observation of a new  $\Xi_b^-$  resonance. Phys.Rev.Lett., 121:072002, 2018.
- [383] Hua-Xing Chen, Qiang Mao, Wei Chen, Atsushi Hosaka, Xiang Liu, and Shi-Lin Zhu. Decay properties of  $P$ -wave charmed baryons from light-cone QCD sum rules. Phys.Rev., D95:094008, 2017.
- [384] Hua-Xing Chen, Qiang Mao, Atsushi Hosaka, Xiang Liu, and Shi-Lin Zhu. D-wave charmed and bottomed baryons from QCD sum rules. Phys.Rev., D94:114016, 2016.
- [385] K. Azizi, Y. Sarac, and H. Sundu. Possible Molecular Pentaquark States with Different Spin and Quark Configurations. Phys.Rev., D98:054002, 2018.
- [386] Zhi-Gang Wang and Jun-Xia Zhang. Possible pentaquark candidates: new excited  $\Omega_c$  states. Eur.Phys.J., C78:503, 2018.
- [387] J. Yelton et al. Observation of Excited  $\Omega_c$  Charmed Baryons in  $e^+e^-$  Collisions. Phys.Rev., D97:051102, 2018.

- [388] V.R. Debastiani, J.M. Dias, W.H. Liang, and E. Oset. Molecular  $\Omega_c$  states generated from coupled meson-baryon channels. Phys.Rev., D97:094035, 2018.
- [389] J.M. Dias, V.R. Debastiani, J. Jun Xie, and E. Oset. Doubly charmed  $\Xi_{cc}$  molecular states from meson-baryon interaction. Phys.Rev., D98:094017, 2018.
- [390] Roel Aaij et al. Observation of the doubly charmed baryon  $\Xi_{cc}^{++}$ . Phys.Rev.Lett., 119:112001, 2017.
- [391] M. Mattson et al. First Observation of the Doubly Charmed Baryon  $\Xi_{cc}^+$ . Phys. Rev. Lett., 89:112001, 2002.
- [392] A. Ocherashvili et al. Confirmation of the double charm baryon  $\Xi_{cc}(3520)$  via its decay to  $p D^+ K^-$ . Phys. Lett., B628:18–24, 2005.
- [393] S.P. Ratti. New results on c-baryons and a search for cc-baryons in FOCUS. volume 115, pages 33–36, 2003.
- [394] Bernard Aubert et al. Search for doubly charmed baryons  $\Xi_{cc}^+$  and  $\Xi_{cc}^{++}$  in BABAR. Phys.Rev., D74:011103, 2006.
- [395] R. Chistov et al. Observation of new states decaying into  $\Lambda_{cc}^+ K^- \pi^+$  and  $\Lambda_{cc}^+ K^0 \pi^-$ . Phys.Rev.Lett., 97:162001, 2006.
- [396] R Aaij et al. Search for the doubly charmed baryon  $\Xi_{cc}^+$ . JHEP, 1312:090, 2013.
- [397] S. Sakai, L. Roca, and E. Oset. Charm-beauty meson bound states from  $B(B^*)D(D^*)$  and  $B(B^*)\bar{D}(\bar{D}^*)$  interaction. Phys.Rev., D96:054023, 2017.
- [398] G. Ecker. Chiral perturbation theory. Prog.Part.Nucl.Phys., 35:1–80, 1995.
- [399] V. Bernard, Norbert Kaiser, and Ulf-G. Meissner. Chiral dynamics in nucleons and nuclei. Int.J.Mod.Phys., E4:193–346, 1995.
- [400] Jia-Jun Wu and B. S. Zou. Prediction of super-heavy  $N^*$  and  $\Lambda^*$  resonances with hidden beauty. Phys. Lett., B709:70–76, 2012.
- [401] A. Ozpineci, C.W. Xiao, and E. Oset. Hidden beauty molecules within the local hidden gauge approach and heavy quark spin symmetry. Phys.Rev., D88:034018, 2013.
- [402] M. Altenbuchinger and Li-Sheng Geng. Off-shell effects on the interaction of Nambu-Goldstone bosons and  $D$  mesons. Phys.Rev., D89:054008, 2014.

- [403] J. Yelton et al. Study of Excited  $\Xi_c$  States Decaying into  $\Xi_c^0$  and  $\Xi_c^+$  Baryons. Phys.Rev., D94:052011, 2016.
- [404] S.E. Csorna et al. Evidence of new states decaying into Xi-prime(c) pi. Phys.Rev.Lett., 86:4243–4246, 2001.
- [405] J.P. Alexander et al. Evidence of new states decaying into Xi(c)\* pi. Phys.Rev.Lett., 83:3390–3393, 1999.
- [406] Y. Kato et al. Studies of charmed strange baryons in the  $\Lambda D$  final state at Belle. Phys.Rev., D94:032002, 2016.
- [407] George Chiladze and Adam F. Falk. Phenomenology of new baryons with charm and strangeness. Phys.Rev., D56:R6738–R6741, 1997.
- [408] J. Vijande, A. Valcarce, T.F. Carames, and H. Garcilazo. Heavy hadron spectroscopy: a quark model perspective. volume E22, page 1330011, 2013.
- [409] Hua-Xing Chen, Wei Chen, Qiang Mao, Atsushi Hosaka, Xiang Liu, and Shi-Lin Zhu. P-wave charmed baryons from QCD sum rules. Phys.Rev., D91:054034, 2015.
- [410] Marek Karliner and Jonathan L. Rosner. Very narrow excited  $\Omega_c$  baryons. Phys.Rev., D95:114012, 2017.
- [411] Kai-Lei Wang, Li-Ye Xiao, Xian-Hui Zhong, and Qiang Zhao. Understanding the newly observed  $\Omega_c$  states through their decays. Phys.Rev., D95:116010, 2017.
- [412] Gabor Andras Almasi, Bengt Friman, and Krzysztof Redlich. Baryon number fluctuations in chiral effective models and their phenomenological implications. Phys.Rev., D96:014027, 2017.
- [413] Bing Chen and Xiang Liu. New  $\Omega_c^0$  baryons discovered by LHCb as the members of  $1P$  and  $2S$  states. Phys.Rev., D96:094015, 2017.
- [414] Ze Zhao, Dan-Dan Ye, and Ailin Zhang. Hadronic decay properties of newly observed  $\Omega_c$  baryons. Phys.Rev., D95:114024, 2017.
- [415] Hai-Yang Cheng and Cheng-Wei Chiang. Quantum numbers of  $\Omega_c$  states and other charmed baryons. Phys.Rev., D95:094018, 2017.
- [416] Wei Wang and Rui-Lin Zhu. Interpretation of the newly observed  $\Omega_c^0$  resonances. Phys.Rev., D96:014024, 2017.

- [417] Gang Yang and Jialun Ping. Dynamical study of  $\Omega_c^0$  in the chiral quark model. Phys.Rev., D97:034023, 2018.
- [418] Hongxia Huang, Jialun Ping, and Fan Wang. Investigating the excited  $\Omega_c^0$  states through  $\Xi_c K$  and  $\Xi_c' K$  decay channels. Phys.Rev., D97:034027, 2018.
- [419] Hyun-Chul Kim, Maxim V. Polyakov, and Michał Praszalowicz. Possibility of the existence of charmed exotica. Phys.Rev., D96:014009, 2017.
- [420] C.S. An and H. Chen. Observed  $\Omega_c^0$  resonances as pentaquark states. Phys.Rev., D96:034012, 2017.
- [421] V.V. Anisovich, M.A. Matveev, J. Nyiri, and A.N. Semenova. Narrow pentaquarks as diquark–diquark–antiquark systems. Mod.Phys.Lett., A32:1750154, 2017.
- [422] S.S. Agaev, K. Azizi, and H. Sundu. On the nature of the newly discovered  $\Omega$  states. Europhys.Lett., 118:61001, 2017.
- [423] S.S. Agaev, K. Azizi, and H. Sundu. Interpretation of the new  $\Omega_c^0$  states via their mass and width. Eur.Phys.J., C77:395, 2017.
- [424] Zhi-Gang Wang. Analysis of  $\Omega_c(3000)$ ,  $\Omega_c(3050)$ ,  $\Omega_c(3066)$ ,  $\Omega_c(3090)$  and  $\Omega_c(3119)$  with QCD sum rules. Eur.Phys.J., C77:325, 2017.
- [425] T.M. Aliev, S. Bilmis, and M. Savci. Are the new excited  $\Omega_c$  baryons negative parity states? 2017.
- [426] Qiang Mao, Hua-Xing Chen, Atsushi Hosaka, Xiang Liu, and Shi-Lin Zhu.  $D$ -wave heavy baryons of the  $SU(3)$  flavor  $\mathbf{6}_F$ . Phys.Rev., D96:074021, 2017.
- [427] S.S. Agaev, K. Azizi, and H. Sundu. Decay widths of the excited  $\Omega_b$  baryons. Phys.Rev., D96:094011, 2017.
- [428] Kai-Lei Wang, Ya-Xiong Yao, Xian-Hui Zhong, and Qiang Zhao. Strong and radiative decays of the low-lying  $s$ - and  $p$ -wave singly heavy baryons. Phys.Rev., D96:116016, 2017.
- [429] M. Padmanath and Nilmani Mathur. Quantum Numbers of Recently Discovered  $\Omega_c^0$  Baryons from Lattice QCD. Phys.Rev.Lett., 119:042001, 2017.
- [430] Yin Huang, Cheng-jian Xiao, Li-Sheng Geng, and Jun He. Strong decays of the  $\Xi_b(6227)$  as a  $\Sigma_b \bar{K}$  molecule. Phys. Rev., D99(1):014008, 2019.

- [431] D. Gamermann, C. Garcia-Recio, J. Nieves, L.L. Salcedo, and L. Tolos. Exotic dynamically generated baryons with negative charm quantum number. Phys.Rev., D81:094016, 2010.
- [432] Chao Wang, Liang-Liang Liu, Xian-Wei Kang, Xin-Heng Guo, and Rui-Wu Wang. Possible open-charmed pentaquark molecule  $\Omega_c(3188)$  - the  $D\Xi$  bound state - in the Bethe-Salpeter formalism. Eur.Phys.J., C78:407, 2018.
- [433] Roel Aaij et al. Observation of Two Resonances in the  $\Lambda_b^0\pi^\pm$  Systems and Precise Measurement of  $\Sigma_b^\pm$  and  $\Sigma_b^{*\pm}$  properties. Phys. Rev. Lett., 122(1):012001, 2019.
- [434] G. Ecker. Progress in Particle and Nuclear Physics, 35:1-80. 1995.
- [435] T. Uchino, Wei-Hong Liang, and E. Oset. Baryon states with hidden charm in the extended local hidden gauge approach. Eur. Phys. J., A52(3):43, 2016.
- [436] Luis Roca, Maxim Mai, Eulogio Oset, and Ulf-G. Meißner. Predictions for the  $\Lambda_b \rightarrow J/\psi \Lambda(1405)$  decay. Eur. Phys. J., C75(5):218, 2015.
- [437] A. Feijoo, V. K. Magas, A. Ramos, and E. Oset.  $\Lambda_b \rightarrow J/\psi K \Xi$  decay and the higher order chiral terms of the meson baryon interaction. Phys. Rev., D92(7):076015, 2015. [Erratum: Phys. Rev.D95,no.3,039905(2017)].
- [438] F.E. Close. An Introduction to Quarks and Partons.
- [439] G.E. Brown. Unified Theory of Nuclear Models and Forces. North-Holland Publishing Company, 1971.
- [440] M. A. Preston and R. K. Bhaduri. Structure of the Nucleus. Addison Wesley Publishing Company, 1975.
- [441] Takayasu Sekihara and Eulogio Oset. Investigating the nature of light scalar mesons with semileptonic decays of D mesons. Phys. Rev., D92(5):054038, 2015.
- [442] N. Ikeno and E. Oset. Semileptonic  $\Lambda_c$  decay to  $\nu l^+$  and  $\Lambda(1405)$ . Phys. Rev., D93(1):014021, 2016.
- [443] K. P. Khemchandani, A. Martinez Torres, H. Nagahiro, and A. Hosaka.  $\Lambda$  and  $\Sigma$  resonances coupled to vector and pseudoscalar mesons. Nucl. Phys., A914:300–304, 2013.

- [444] K. P. Khemchandani, A. Martinez Torres, F. S. Navarra, M. Nielsen, and L. Tolos. A study of the  $KN-K^*N$  coupled systems. Phys. Rev., D91:094008, 2015.
- [445] A. Drutskoy et al. Observation of  $B \rightarrow D^*K^-K^{0*}$  decays. Phys.Lett., B542:171–182, 2002.
- [446] Daris Samart, Wei-hong Liang, and Eulogio Oset. Triangle mechanisms in the build up and decay of the  $N^*(1875)$ . Phys.Rev., C96:035202, 2017.
- [447] L. Roca, E. Oset, and J. Singh. Low lying axial-vector mesons as dynamically generated resonances. Phys.Rev., D72:014002, 2005.
- [448] D. Gamermann, E. Oset, D. Strottman, and M.J. Vicente Vacas. Dynamically generated open and hidden charm meson systems. Phys.Rev., D76:074016, 2007.
- [449] D. Gamermann and E. Oset. Axial resonances in the open and hidden charm sectors. Eur.Phys.J., A33:119–131, 2007.
- [450] A. Ramos and E. Oset. The role of vector-baryon channels and resonances in the  $\gamma p \rightarrow K^0\Sigma^+$  and  $\gamma n \rightarrow K^0\Sigma^0$  reactions near the  $K^*\Lambda$  threshold. Phys.Lett., B727:287–292, 2013.
- [451] A. Engler, H.E. Fisk, R.w. Kraemer, C.M. Meltzer, and J.B. Westgard. Spin of the  $Y_0^*(1405)$ . Phys.Rev.Lett., 15:224, 1965.
- [452] I. Zychor et al. Shape of the  $\Lambda(1405)$  hyperon measured through its  $\Sigma^0\pi^0$  Decay. Phys.Lett., B660:167–171, 2008.
- [453] G. Agakishiev et al. Baryonic resonances close to the  $\bar{K}N$  threshold: the case of  $\Lambda(1405)$  in  $pp$  collisions. Phys. Rev., C87:025201, 2013.
- [454] J. Adamczewski-Musch et al. Inclusive  $\Lambda$  production in proton-proton collisions at 3.5 GeV. Phys.Rev., C95:015207, 2017.
- [455] K. Nakamura et al. Review of particle physics. J. Phys., G37:075021, 2010.
- [456] D. Mark Manley, Richard A. Arndt, Yogesh Goradia, and Vigdor L. Teplitz. An Isobar Model Partial Wave Analysis of  $\pi N \rightarrow \pi\pi N$  in the Center-of-mass Energy Range 1320-MeV to 1930-MeV. Phys. Rev., D30:904, 1984.
- [457] D. M. Manley and E. M. Saleski. Multichannel resonance parametrization of  $\pi N$  scattering amplitudes. Phys. Rev., D45:4002–4033, 1992.

- [458] R. E. Cutkosky, C. P. Forsyth, R. E. Hendrick, and R. L. Kelly. Pion - Nucleon Partial Wave Amplitudes. Phys. Rev., D20:2839, 1979.
- [459] M. Niiyama et al. Photoproduction of  $\Lambda(1405)$  and  $\Sigma^0(1385)$  on the proton at  $E_\gamma = 1.5 - 2.4$ -GeV. Phys. Rev., C78:035202, 2008.
- [460] K. Moriya et al. Differential Photoproduction Cross Sections of the  $\Sigma^0(1385)$ ,  $\Lambda(1405)$ , and  $\Lambda(1520)$ . Phys. Rev., C88:045201, 2013. [Addendum: Phys. Rev.C88,no.4,049902(2013)].
- [461] S. Sakai, E. Oset, and W.H. Liang. Abnormal isospin violation and  $a_0 - f_0$  mixing in the  $D_s^+ \rightarrow \pi^+ \pi^0 a_0(980)(f_0(980))$  reactions. Phys.Rev., D96:074025, 2017.
- [462] Wei-Hong Liang, S. Sakai, Ju-Jun Xie, and E. Oset. Triangle singularity enhancing isospin violation in  $\bar{B}_s^0 \rightarrow J/\psi \pi^0 f_0(980)$ . Chin.Phys., C42:044101, 2018.
- [463] Li-Juan Liu, En Wang, Ju-Jun Xie, Kai-Lan Song, and Jing-Yu Zhu.  $\Lambda(1405)$  production in the process  $\chi_{c0}(1P) \rightarrow \bar{\Lambda} \Sigma \pi$ . Phys.Rev., D98:114017, 2018.
- [464] Kenta Miyahara and Tetsuo Hyodo. Theoretical study of  $\Lambda(1405)$  resonance in  $\Xi_b^0 \rightarrow D^0(\pi \Sigma)$  decay. Phys.Rev., C98:025202, 2018.
- [465] Ju-Jun Xie, Wei-Hong Liang, and Eulogio Oset. Hidden charm pentaquark and  $\Lambda(1405)$  in the  $\Lambda_b^0 \rightarrow \eta_c K^- p(\pi \Sigma)$  reaction. Phys.Lett., B777:447-452, 2018.
- [466] Ling-Lie Chau. Quark Mixing in Weak Interactions. volume 95, pages 1-94, 1983.